Springer Series on Fluorescence 16
Series Editor: Martin Hof

Karel Procházka *Editor*

Fluorescence Studies of Polymer Containing Systems

Springer

16
Springer Series on Fluorescence

Methods and Applications

Series Editor: Martin Hof

Springer Series on Fluorescence

Series Editor: Martin Hof

Recently Published and Forthcoming Volumes

Fluorescence Studies of Polymer Containing Systems
Volume Editor: Karel Procházka
Vol. 16, 2016

Advanced Photon Counting
Volume Editors: Peter Kapusta, Michael Wahl and Rainer Erdmann
Vol. 15, 2015

Far-Field Optical Nanoscopy
Volume Editors: Philip Tinnefeld, Christian Eggeling and Stefan W. Hell
Vol. 14, 2015

Fluorescent Methods to Study Biological Membranes
Volume Editors: Y. Mély and G. Duportail
Vol. 13, 2013

Fluorescent Proteins II
Application of Fluorescent Protein Technology
Volume Editor: G. Jung
Vol. 12, 2012

Fluorescent Proteins I
From Understanding to Design
Volume Editor: G. Jung
Vol. 11, 2012

Advanced Fluorescence Reporters in Chemistry and Biology III
Applications in Sensing and Imaging
Volume Editor: A.P. Demchenko
Vol. 10, 2011

Advanced Fluorescence Reporters in Chemistry and Biology II
Molecular Constructions, Polymers and Nanoparticles
Volume Editor: A.P. Demchenko
Vol. 9, 2010

Advanced Fluorescence Reporters in Chemistry and Biology I
Fundamentals and Molecular Design
Volume Editor: A.P. Demchenko
Vol. 8, 2010

Lanthanide Luminescence
Photophysical, Analytical and Biological Aspects
Volume Editors: P. Hänninen and H. Härmä
Vol. 7, 2011

Standardization and Quality Assurance in Fluorescence Measurements II
Bioanalytical and Biomedical Applications
Volume Editor: Resch-Genger, U.
Vol. 6, 2008

Standardization and Quality Assurance in Fluorescence Measurements I
Techniques
Volume Editor: U. Resch-Genger
Vol. 5, 2008

Fluorescence of Supermolecules, Polymeres, and Nanosystems
Volume Editor: M.N. Berberan-Santos
Vol. 4, 2007

Fluorescence Spectroscopy in Biology
Volume Editor: M. Hof
Vol. 3, 2004

Fluorescence Spectroscopy, Imaging and Probes
Volume Editor: R. Kraayenhof
Vol. 2, 2002

New Trends in Fluorescence Spectroscopy
Volume Editor: B. Valeur
Vol. 1, 2001

More information about this series at http://www.springer.com/series/4243

Fluorescence Studies of Polymer Containing Systems

Volume Editor:
Karel Procházka

With contributions by

J. Duhamel · M. Karayianni · Z. Limpouchová · S. Pispas · K. Procházka · M. Štěpánek · I.K. Voets · D. Wöll

Springer

Volume Editor
Karel Procházka
Faculty of Science
Charles University in Prague
Prague 2, Czech Republic

ISSN 1617-1306 ISSN 1865-1313 (electronic)
Springer Series on Fluorescence
ISBN 978-3-319-26786-9 ISBN 978-3-319-26788-3 (eBook)
DOI 10.1007/978-3-319-26788-3

Library of Congress Control Number: 2016931291

Springer Cham Heidelberg New York Dordrecht London

Printed on acid-free paper

Springer International Publishing AG Switzerland is part of Springer Science+Business Media (www.springer.com)

Series Editor

Prof. Dr. Martin Hof

Academy of Sciences of the Czech Republic
J. Heyrovsky Institute of Physical Chemistry
Department of Biophysical Chemistry
Dolejskova 3
16223 Prague 8
Czech Republic
martin.hof@jh-inst.cas.cz

Aims and Scope

Fluorescence spectroscopy, fluorescence imaging and fluorescent probes are indispensible tools in numerous fields of modern medicine and science, including molecular biology, biophysics, biochemistry, clinical diagnosis and analytical and environmental chemistry. Applications stretch from spectroscopy and sensor technology to microscopy and imaging, to single molecule detection, to the development of novel fluorescent probes, and to proteomics and genomics. The *Springer Series on Fluorescence* aims at publishing state-of-the-art articles that can serve as invaluable tools for both practitioners and researchers being active in this highly interdisciplinary field. The carefully edited collection of papers in each volume will give continuous inspiration for new research and will point to exciting new trends.

Preface

This book outlines and explains the application of fluorescence measurements in polymer research. It shows examples of important studies of complex polymer-containing systems by various fluorescence techniques. The book is not intended to provide an exhaustive survey of all the important fluorescence studies of polymer systems. It outlines several areas in polymer science where the application of fluorescence techniques can successfully contribute to research. The selection of topics and the structure of the book were subject to the following criteria (1) the individual chapters should give the reader an overview of both seminal works and relatively recent studies of polymers using fluorescence techniques; (2) it draws attention to the great potential of fluorescence for investigating complex polymer-containing systems; (3) it accentuates the most important differences between the behavior of low- and high-molar-mass systems and the consequences for the methodology of fluorescence studies of both types of systems; (4) last but not least, the described examples and analyses of their results should be inspiring for a fairly broad community of researchers (both polymer scientists and experts in spectroscopy). It follows that the text is not only a collection of specialized reviews for a relatively narrow group of experts (i.e., for polymer scientists who have been actively using advanced fluorescence techniques for a long time), but its goal is multifold.

First, we would like to address polymer chemists and physicists who plan to employ advanced fluorescence techniques (by themselves or in cooperation) and would like to explore the potential of fluorescence measurements to as great a degree as possible. The pertinent chapters outline the theoretical basis for fluorescence techniques, give hints about which polymer problems are worth studying by fluorescence methods, and draw the attention of the reader to the non-negligible risks associated with incorrect interpretation of the experimental data. Secondly, we would like to help experts in spectroscopy who intend to cooperate with polymer scientists to orient themselves in polymer physics and physical chemistry (at least in several areas of polymer science and technology). The book is intended to facilitate communication among the members of interdisciplinary research teams studying systems containing polymers.

The beginning of the book contains general chapters on the conformational behavior of polymer chains and association processes in polymer solutions. The first chapter on general conformational behavior is presented concisely in an almost textbook-like manner. It summarizes the most important features of conformational behavior. Even though this chapter is only of marginal interest for polymer scientists, it provides useful information for experts in spectroscopy who plan to carry out experimental studies of systems containing polymer components. The chapters devoted to self-assembly are brief up-to-date review articles and may be interesting for both groups of scientists. The middle part (chapter "Theoretical Principles of Fluorescence Spectroscopy" and partly also chapter "Historical Perspective of Advances in Fluorescence Research on Polymer Systems") provides a brief overview on fluorescence techniques and outlines information relevant for studies of both low- and high-molar mass systems. This part can serve as an introductory (textbook-like) chapter for polymer scientists interested in learning more about the theoretical basis of fluorescence spectroscopy. The last part contains several review articles on the application of various fluorescence techniques for studying specific aspects of the behavior of polymer solutions. We would like to stress that the book is focused on synthetic polymers and particularly on their conformational and self-assembling behavior in dilute solutions. We deliberately avoided biopolymer systems. The functional systems of biologically important polymers are very important, and their behavior is in many respects similar to that of the systems of synthetic polymers discussed here. However, other excellent books have already been published on this topic (including in this series).

In summary, the book is intended to attract the interest of polymer scientists, as well as that of experts in fluorescence spectroscopy, to facilitate their communication, help in their cooperation, and provide useful information for both communities.

Prague 2, Czech Republic Karel Procházka

Contents

Conformational and Dynamic Behavior of Polymer and Polyelectrolyte Chains in Dilute Solutions

Karel Procházka

Contents

Abstract This introductory chapter provides a brief (textbook-like) survey of important facts concerning the conformational and dynamic behavior of polymer chains in dilute solutions. The effect of polymer–solvent interactions on the behavior of polymer solutions is reviewed. The physical meanings of the terms good, ϑ-, and poor thermodynamic quality of the solvent are discussed in detail. Basic assumptions of the Kuhn model, which describes the conformational behavior of ideal flexible chains, are outlined first. Then, the correction terms due to finite bond angles and excluded volume of structural units are introduced, and their role is discussed. Special attention is paid to the conformational behavior of polyelectrolytes. The "pearl necklace" model, which predicts the cascade of conformational transitions of "quenched" polymer chains (i.e., of those with fixed position of charges on the chain) in solvents with deteriorating solvent quality, is described and discussed in detail. The incomplete (up-to-date) knowledge of the behavior of "annealed" (i.e., weak) polyelectrolytes and some characteristics of semiflexible chains are addressed at the end of the chapter.

Keywords Ideal polymer chain • Realistic polymer chain • Chain conformations • Solvent quality • Quenched polyelectrolyte • Annealed polyelectrolyte • Pearl necklace model • Persistence length

K. Procházka (✉)
Department of Physical and Macromolecular Chemistry, Faculty of Science, Charles University in Prague, Hlavova 2030, 128 40 Prague 2, Czech Republic
e-mail: karel.prochazka@natur.cuni.cz

K. Procházka (ed.), *Fluorescence Studies of Polymer Containing Systems*, Springer Series on Fluorescence 16, DOI 10.1007/978-3-319-26788-3_1

Before the reader (presumably a scientist engaged in fluorescence studies) starts to read this chapter, he should know the content and purpose of this introductory part to decide whether he needs to refresh his memory about fundamental facts related to the behavior of polymer chains or if he can skip this part. This short (textbook-like) chapter is not aimed at providing an exhausting survey and explanation of the conformational and dynamic behavior of dilute solutions of polymers, copolymers, and polyelectrolytes of various chain architectures. There exist numerous chapters in excellent textbooks explaining the fundamentals of the physical chemistry of polymer solutions [1–5] and very good reviews on this topic [6, 7]. This chapter has a different purpose. Here, we would like to emphasize differences in the behavior of low- and high-molar-mass compounds caused by (i) asymmetry in the sizes of the polymer species with respect to the other components of the mixture, (ii) connectivity of the polymer chains, and (iii) their flexibility. We would like to remind a researcher studying low-molar-mass compounds by fluorescence techniques about what he should be aware of and prepared for when entering the polymer field. We will focus particularly on the aspects of the conformational and dynamic behavior that are important for understanding the results of fluorescence studies on aqueous polyelectrolyte systems. However, first we will outline the basic features of the general behavior of flexible chains in simple solvents.

1 Neutral Chains

The behavior of real polymer chains (homopolymers and copolymers, also including polyelectrolytes) in dilute solutions is a result of an intricate interplay of a number of cooperating and competing forces. The dissolution process reflects both enthalpy and entropy changes in the whole system, i.e., not only those directly connected with polymer chains but also various solvent effects, e.g., rearrangement of the solvent molecules in the solvation shell and counterion effects in polyelectrolyte solutions. Because the most important differences between the properties of high- and low-molar-mass compounds follow from the unique properties of long chains, classical theories of neutral polymer solutions ignore the structure of the solvent and specific solvation effects, as well as tiny details in the chemical composition of the polymer chains, etc. They treat polymer solutions at a simple mean-field level, representing the polymer chain as a sequence of interconnected (relatively short) linear parts (segments). Depending on the level of accuracy of the physical description, the segments represent one or more repeating units and are either freely joined (without any angular limitations) or the arrangement of two or more successive segments is constrained (bond angles, restricted rotation around single bonds, etc.). Furthermore, the simplest models assume that the segments are short lines without excluded volumes and can intersect, while more advanced models employ self-avoiding segments. In polymer thermodynamics, the segment–solvent interactions, w_{PS}, are usually compared with segment–segment, w_{PP}, and solvent–solvent interactions, w_{SS}, which simplifies the description because the

thermodynamic quality of the solvent can be characterized by a single parameter. The commonly used Flory–Huggins parameter [8, 9] (proportional to T^{-1}), $\chi_{FH} = a/T = (z–2)\Delta w/(kT)$, where z is the average number nearest neighbors and k is the Boltzmann constant, is based on the difference between the cross-interaction and the arithmetic average of homo-interactions, $\Delta w = w_{PS}–1/2(w_{PP} + w_{SS})$. It serves as a basis for classification and sorting solvents into two categories: thermodynamically good and bad (poor) solvents. Solvents of the first class dissolve high-molar-mass polymers because the segment–solvent interactions are "reasonably good." The latter category comprises poor or alternatively called thermodynamically bad solvents, which, from the practical point of view, are non-solvents (precipitants). The solvents in a narrow region in between good and bad solvents are often called marginal solvents. The critical marginal solvent in between the two categories of solvents is called the "ϑ-solvent." From a practical point of view, it is necessary to keep in mind that one particular solvent can be good for some polymers and bad for other polymers (depending on the polarity, etc.).

Before we start discussing the physical meaning of the "ϑ-solvent" (and its χ_{FH} value), we would like to briefly mention "favorable" and "unfavorable" interactions. In nonpolar systems of low-molar-mass organic molecules A and B, the cross-term, w_{AB}, can usually be approximated by the geometric average of the w_{AA} and w_{BB} interactions as $w_{AB} = \sqrt{(w_{AA}w_{BB})}$. This means (see any textbook on the physical chemistry of simple liquids or polymers) [10–13] that Δw is positive and the mixing of small nonpolar molecules (without specific interactions) is always endothermic. In other words, the mixing of two nonpolar liquids is an unfavorable process from the point of view of the enthalpy. However, it is also true that an overwhelming number of nonpolar molecules mix spontaneously because their intermixing is accompanied by a considerable increase in entropy. The entropy of mixing of polymer chains with a low-molar-mass solvent is significantly lower than that accompanying the mixing of small mobile molecules. This general feature of polymer solutions can be easily understood when we compare the motion of n_M small monomer molecules dissolved in a solvent before and after polymerization. Assume that this reaction leads to n_P flexible chains, each containing on average N monomers ($n_M = n_P N$). In the first case, i.e., before polymerization, each monomer can move independently in the whole volume and acquires high translational entropy, while, in the latter case, N connected monomer units always have to be close to each other and have to move together, which reduces the entropy of the system considerably (especially if N is high).

The popular and widely used F–H interaction parameter was originally introduced in a successful theory developed independently by Flory [14] and Huggins [8, 15] in the early 1940s to describe the properties of concentrated polymer solutions. Their simple mean-field theory is based on a lattice (Bragg–Williams) model of regular solutions [16] and derives the following expression for the Gibbs energy of mixing a polymer with a solvent:

$$\Delta G = nRT(x_1 \ln\varphi_1 + x_2 \ln\varphi_2 + x_1\varphi_2\chi) \quad (1)$$

where n_i are the numbers of moles ($n = \Sigma n_i$); $x_i = n_i/\Sigma n_i$, the molar fractions; N_i are the degrees of polymerization (number of structural units in the chain: (1) solvent, $N_1 = 1$; (2) polymer, $N_2 >> 1$); and $\varphi_i = N_i n_i/\Sigma N_i n_i$ are the volume fractions of the components. It is obvious that the entropy, i.e., the first two terms in Eq. (1), promotes the dissolution and the enthalpy (the last term) hinders it, but if χ_{FH} is not very positive, the Gibbs function of mixing can be negative and the polymer will dissolve in the solvent. As both the volume fractions, which are present in the two first terms, and the product $x_1\varphi_2\chi$ appearing in the third term, depend on the degree of polymerization, N_2, increasing chain length hinders the dissolution and short chains dissolve in moderately poor solvents while long ones do not dissolve. Focusing on the behavior of infinitely long polymer chains, the theory yields the following value of the interaction parameter for the ϑ-solvent: $(\chi_{FH})_\vartheta = ½$. This value divides the solvents into the two categories described above. The F–H interaction parameters of good solvents theoretically range from 0 to ½. Focusing on nonpolar systems (where the cross-term interaction obeys the geometric average rule), the best solvents (called "athermal" solvents) are those with $\chi_{FH} = 0$, but actual good solvents often have $\chi_{FH} \leq 0$ as a result of specific interactions (sometimes simply because of the high polarity of the components). Poor (bad) solvents are characterized by FH parameters $\chi_{FH} > ½$. The values of the F–H parameter depend on the temperature; the temperature, at which $\chi_{FH} = a/T = ½$, is often called the ϑ-temperature, ϑ (or ϑ-state). The simple F–H theory predicts that the solvent quality for a given polymer will improve with temperature. Above ϑ, chains of any length dissolve, i.e., also the infinitely long ones. At the ϑ-temperature, chains of infinite length start to separate into two liquid phases: a concentrated phase (i.e., the swollen polymer) and a dilute phase (in this case, the pure solvent). The chains of finite lengths start to separate into two phases at lower critical temperatures T_c, depending on the number of segments N_2:

$$a/T_c = ½ + 1/\sqrt{N_2} + 1/(2N_2) \quad (2)$$

and below T_c, both coexisting phases (i.e., also the dilute one) contain finite concentrations of the polymer. The coexistence curves are schematically shown in the lower part of Fig. 1. Because ϑ is the highest critical temperature for a series of coexistence curves for chains differing in length, it is called the upper critical solution temperature (UCST), and the region of critical temperatures for chains of different length is called the UCST region.

The ϑ-temperature has an analogous meaning for polymer–solvent mixtures to the Boyle temperature for gasses: At this temperature, moderately unfavorable interactions between polymer segments and solvent molecules compensate the geometric excluded volume of the segments. The overall excluded volume (which reduces the volume available for the motion of the molecules) [17] drops to zero, and small as well as large molecules move as if the entire volume of the

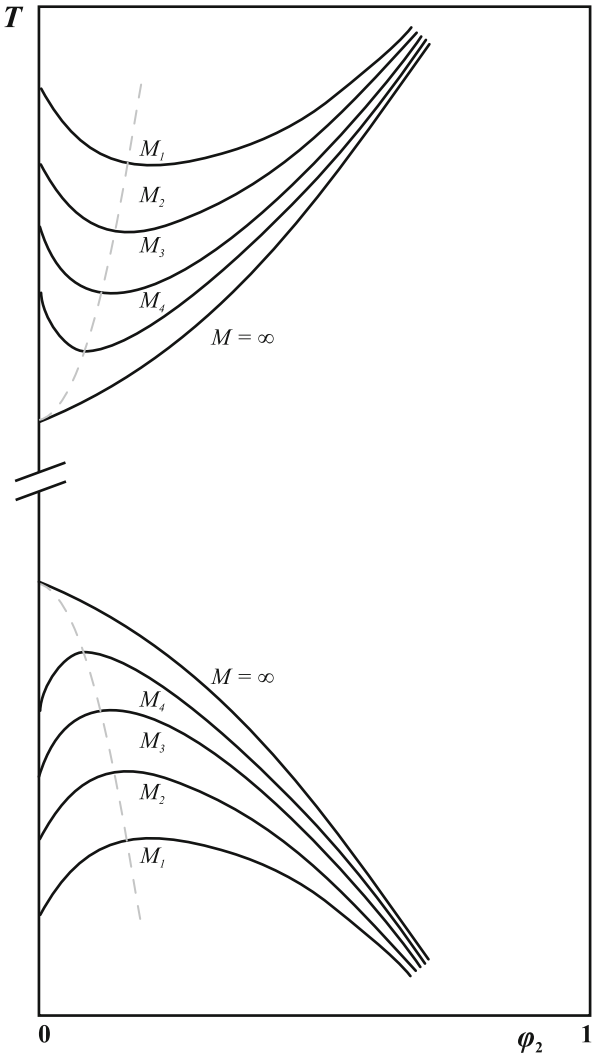

Fig. 1 The coexistence curves. *Upper part*: the LCST region. *Bottom part*: the UCST region. The curves for infinitely long chains ($M = \infty$) separate the homogeneous (one-phase) region from the heterogeneous (two-phase) region

system were available. Hence, the conformations of the polymer chain at the ϑ-temperature are not affected by the excluded volume of the segments, and real self-avoiding chains behave as intersecting random walks.

At the end of this part, we would like to emphasize two important facts: First, because the F–H theory is a theory of regular polymer solutions and the cross-interaction term can be expressed as a geometric average of homo-interactions, the Gibbs function of mixing can be decomposed into parts corresponding to the pure components and to the entropy of mixing. Consequently, it is possible to predict the properties of polymer solutions at a semiquantitative level on the basis of the

properties of the pure components alone (see the appropriate chapters on the solubility parameters in any polymer textbook) [1, 16, 18].

Second, we have seen that the F–H theory predicts an improvement in the solvent quality with temperature. However, at fairly high temperatures above the normal boiling point of the pure solvent (ca. 0.7–0.8 T_{crit}, where T_{crit} is the critical temperature of the pure solvent), i.e., at elevated pressures, the solvent quality starts to deteriorate with increasing temperature, and the polymer solution phase separates upon heating. The worsening of solvent quality for high-molar-mass polymers at high temperatures is a general feature of polymer solutions, reflecting the fact that the thermal expansion of the solvent is significantly greater than that of the polymer. The solvent expands at high temperatures, and the solvent molecules have a quite large free volume for their motion; they move rapidly and acquire high translational entropy. Polymer dissolution requires proper solvation of the segments, which means that part of mobile solvent molecules has to "condense" on the chain. The solvating molecules lose their translational entropy, and since entropy plays an important role at high temperatures, the dissolution of the polymer chains is no longer favorable, and the solution separates into two phases. The coexistence curves are the mirror image of those in the UCST region (see the curves in the upper part of Fig. 1), and the critical temperature for the separation of infinitely long chains, which in this case is the lowest one, is called (somewhat paradoxically) the lower critical solution temperature (LCST). The F–H mean-field theory does not predict LCST and is applicable only in the region of UCST. In some aqueous solutions of neutral water-soluble polymers, LCST behavior is observed at relatively low temperatures because it is caused by specific effects reflecting changes in the water structure in the solvation layer, the formation of hydrogen bonds, etc. (e.g., phase separation occurs below 40 °C in an aqueous solution of polyoxypropylene) [19, 20].

The simplest model for predicting the conformational characteristics of isolated flexible polymer chains was developed by Kuhn and Grün [21] and independently by James and Guth [22]. The chain is approximated by a sequence of segments of the same length l that are interconnected without any geometrical constrains, do not occupy geometrical volume, and do not interact over large distances. The corresponding interpenetrating chain is called an ideal chain. Mathematical treatment yields the distribution function of probability density that the ends of a chain composed of a large number N of segments are separated by distance r in the form (Fig. 2):

$$P(r) = 4\pi \left(\frac{3}{2\pi N l^2}\right)^{\frac{3}{2}} \exp\left(\frac{-3r^2}{2Nl^2}\right) r^2 \tag{3}$$

Note that $P(r)$ is the angularly averaged function and does not depend on the direction of the end-to-end vector. In a narrow region of temperatures close to the ϑ-temperature, real chains behave as interpenetrating ones, and the model provides a qualitatively correct picture of the conformational behavior of flexible chains.

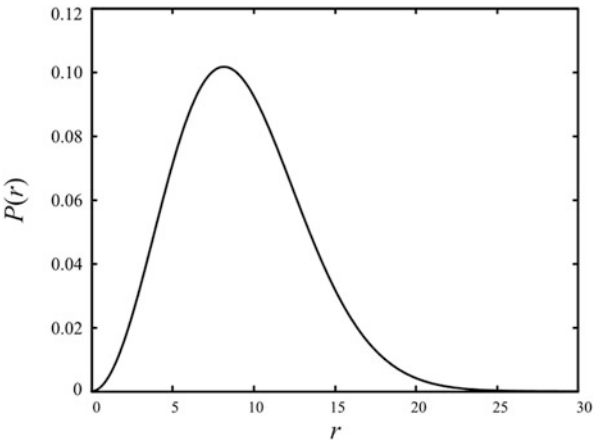

Fig. 2 The distribution function of probability density $P(r)$ that the ends of an ideal chain are separated by distance r

It predicts that (i) the chain adopts a random coil conformation, (ii) it responds to deformation as an entropic spring, and (iii) both the mean-square average end-to-end distance $\sqrt{\langle r^2 \rangle}$ and the radius of gyration R_G of the chain scale with $N^{1/2}$. Scaling exponent ½ means that an ideal 3D polymer chain behaves as a nontrivial fractal object with fractal dimension 2, and its self-similar subunits exhibit the same conformational and scaling behavior as the whole chain. (iv) The conformational behavior of the chains is controlled by the entropy, and the characteristics of the coil depend on the total number of segments N, e.g., the average segment density in the coil domain is proportional to $N^{-1/2}$, which means that longer chains are relatively more expanded (with respect to the unit contour length) and form less dense coils than the shorter ones and (vi) the density profile decreases with the distance from the center of gravity according to the Gaussian function. The Gaussian density profile gave rise to the commonly used name "Gaussian chain." The Monte Carlo and molecular dynamics simulations show that the chain shape fluctuates greatly and that the average ensemble shape is aspherical (the spherical symmetry of the chain characteristics predicted by the simple Kuhn model is derived from the a priori symmetry assumptions used in this theory) and corresponds to an elongated ellipsoid with relative lengths of the axes 1:1.6:3.5 [23].

Various corrections reflecting fixed valence bond angles, hindered rotation around single bonds, and the excluded volume of segments were developed later and are described in detail in textbooks [12, 24]. The scaling behavior of self-avoiding flexible chains was studied by de Gennes [25]. He proposed scaling of $\sqrt{\langle r^2 \rangle}$ and R_G with $r^{0.6}$. Perturbation theories and detailed computer simulations give a value of the scaling exponent of 0.588 and indicate that the average shape of the self-avoiding chain is also reminiscent of an elongated ellipsoid, similar to that representing the interpenetrating coil [26]. The conformational characteristics of real chains with possible rotation around single C–C bonds can be reasonably interpreted using the conclusions drawn from a simple analytical formula (3) without correction terms if we assume that one Kuhn segment represents a short

part of the chain. In this case, rotation around several single bonds ensures that the first and last bonds that connect such an internally flexible segment to the rest of the chain are oriented quite randomly without almost any limitations. The rescaling, i.e., evaluation of the number of Kuhn segments, N_K, and their effective length, l_K, can be based on the contour length, L_C, and the root-mean-square end-to-end distance, $\sqrt{\langle r^2 \rangle}$, because it has to hold that $L_C = Nl = N_K l_K$ and $\sqrt{\langle r^2 \rangle} = N^{1/2} l = N_K^{1/2} l_K$. If the experimental values l_k and the radius of gyration $R_G = (1/\sqrt{6})\sqrt{\langle r^2 \rangle}$ for real chains in ϑ-solvents are used [18], then the angular restrictions and hindered rotation are reasonably accounted for.

Another simple, albeit quite popular, model of flexible linear polymer chains is the rotational isomeric state model (RIS) amply treated by Flory [12, 27]. This model was in fact developed by three independent groups: Volkenstein et al. [28], Lifson [29], and Nagai [30]. Analyzing the hindered internal rotation in butane and in longer alkane chains $(-CH_2-)_n$, the authors of this model realized that the "cis" conformation of four successive bonds (or –CH_2– groups) in the polyethylene chain is very improbable because it is an unstable conformation (characterized by an energy maximum on the energy vs. dihedral angle diagram—see Fig. 3) and its energy is very high (it is ca. 15 kJ/mol larger than that of the stable "trans" conformation characterized by a total energy minimum). Two other low-energy conformations are "+ gauche" and "–gauche" with energy difference of only +3.4 kJ/mol (local minimum) with respect to the "trans" conformation. They are also quite stable because they are separated from the "trans" conformation by high 12.6 kJ/mol barriers. In Fig. 3, which shows the energy diagram of hindered internal rotation in butane, the individual conformations are characterized by dihedral angle Φ between the plane formed by the first, second, and third C atoms and that formed by the second, third, and fourth C atoms in the polyethylene chain: "cis," $\Phi = 0°$; "+gauche," $\Phi = 60°$; "trans," $\Phi = 180°$; and "–gauche," $\Phi = 300°$. The authors considered only three conformations and used statistical thermodynamics to evaluate the partition function and the average conformational characteristics of the ensemble. It may seem that the use of only three stable conformations of the part of

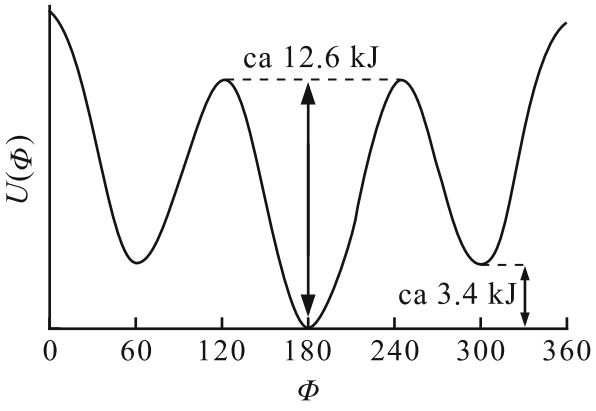

Fig. 3 Schematic energy diagram of hindered internal rotation in butane

the chain containing four C atoms instead of a spectral continuum of a number of conformations depending on the dihedral angle drastically reduces the number of states in the evaluation of the average values of the ensemble. However, the total number of all the considered conformations is 3^{N-1}, which for N ca. 10^3–10^5 yields astronomically high values. The number of possible conformations is in fact less than 3^{N-1}, because the "+g –g" and "–g + g" arrangements of two successive four-member parts of the chain, i.e., C atoms i to $(i+4)$ and $(i+1)$ to $(i+5)$, yield the cyclopentane structure and the next C atom $(i+6)$ would overlap with atom i. Therefore, the + g–g and –g + g arrangements are not allowed, and the corresponding interaction energy is $u(+g–g) = u(-g+g) = \infty$.

Inherently stiff chains which contain multiple bonds, bulky pendant groups, etc., do not obey the predictions of the models developed for flexible chains. They form expanded ellipsoidal or rodlike conformations, depending on the conformational rigidity. The behavior of semiflexible chains can be described by the "wormlike chain" model (WLC) developed by Kratky and Porod [31]. We will neither describe this model nor analyze its predictions, but one conformational characteristic of semiflexible chains based on this model, called the "persistence length," will be briefly mentioned at the end of this chapter. Its physical meaning will be explained and discussed in relation to the behavior of polyelectrolytes, because electrostatic interactions induce an additional stiffening effect in the chain and the highly charged flexible chains thus behave as fairly stiff ones.

The Rouse and the Zimm models are two classical models developed for the description of chain dynamics in the mid-1950s. In addition to dynamic characteristics, they also provide information on the conformational behavior of flexible chains. The Rouse model treats the diffusion of the chain as a collective motion of beads of the same mass connected by elastic springs under the action of randomly fluctuating thermal forces and drag forces [32]. This model neglects both the excluded volume effect and hydrodynamic interactions. It provides correct scaling of size characteristics, but overestimates the decrease in the diffusion coefficient of the chain center of gravity, D, with the length of the chain (number of beads N) predicting the dependence $D \propto 1/N$. The Zimm model [33] is more accurate and assumes both hydrodynamic interactions and excluded volume effects. It predicts the scaling of the diffusion coefficient, $D \propto 1/N^{0.588}$, which is in good agreement with experimental data on self-avoiding chains. Both models neglect solvent effects and the effects of the chemical structure, and hence they predict that the motion of the whole chain can be described by universal formulas, i.e., it depends only on the molar mass of the solvent and friction of the continuous medium in which the chain is immersed (i.e., only on the bulk solvent viscosity). This is a simplification, but the derived formulas describe the dynamic behavior of dilute solutions of nonpolar polymers in nonpolar solvents reasonably well.

To summarize the part devoted to the general behavior of nonpolar polymers in organic solvents, we would like to mention that both linear chains and those with more complicated molecular architectures (stars, brushes, copolymers, etc.) have been intensely studied experimentally, theoretically, and by computer simulations, and their properties are now well understood. The message we would like to convey

is that the fundamental features of the behavior can mostly be adequately explained and understood at a semiquantitative level using the arguments of the simple classical theories outlined above. In the next part, we will concentrate on the more complex and less well-understood conformational and ionization behavior of polyelectrolytes in aqueous media, but would first like to add several general comments on concentrated polymer solutions and polymer melts without going to details.

2 Comments on the Differences Between Dilute and Concentrated Solutions

In dilute solutions, individual polymer chains are relatively far apart and form separated random coils. They move randomly and come into contact from time to time, but are well separated most of the time. The density of the segments, which is proportional to $N^{-1/2}$ in ϑ-solvents, is in fact quite low—it is only several vol.% in most real systems, i.e., the coils are very loose and fairly expanded fractal objects, and the domain of the coil contains a high solvent excess. Good solvents interact favorably with polymer segments, solvate them, and swell the chain—the chain domain expands, and the density of the segments decreases, while the chain contracts in poor solvents. Strictly speaking, dilute polymer solutions are microheterogeneous—they contain separate coil domains immersed in bulk solvent. In a mixture of a good and poor solvents, different interactions (favorable vs. unfavorable) lead to preferential solvation of the chain by the good solvent component, and, in this case, the solvent composition in the domain of the coil may differ from the bulk.

If the concentration increases and the loose coils completely fill the whole volume, they mutually touch and later start to overlap. The "concentration of the first overlap," c^*, separates the regions of dilute and semi-dilute solutions. With a further increase in concentration, the chains interpenetrate, and the viscosity of the polymer solution increases tremendously. However, this does not mean that the dimensions of the individual chains change very much. Because the chains are loose fractal objects, their segments can easily mutually interpenetrate. In concentrated solutions and in polymer melts, the chains are, on average, uniformly intermixed, and, in contrast to dilute solutions, the solution is homogeneous, but the chains still form random coils. Flory predicted theoretically that the dimensions of polymer coils in an amorphous bulk polymer (which behaves as a very viscous "liquid" above the glass transition temperature) are the same as in a dilute solution of a ϑ-solvent [9]. He explained his hypothesis by the following arguments: In bulk polymers, there exists only one type of interaction between polymer segments (which emulates the situation in a good solvent; there is no difference in interactions, and hence χ is theoretically zero), but the trial chain under consideration is squeezed by neighboring chains. This trial chain fills the space delimited by its coil

domain partially by its own segments, which affect the conformations of neighboring chains. The concentration of their segments in this particular place is lower, and the concentration gradient of their segments (i.e., of their chemical potential) generates a force (analogous to that which would cause diffusion in an inhomogeneous solution) which compresses the trial chain to dimensions corresponding to ϑ-conditions. This assumption was later demonstrated experimentally by small-angle X-ray scattering (SAXS) and small-angle neutron scattering (SANS). In the first case [34], a homogeneous melt containing a significant excess of regular polystyrene and a low fraction of its derivative containing one –COOH group at the end of the chain (converted in the $-COO^{-}\ Ag^{+}$ salt) was prepared at a fairly high temperature—well above the glass transition temperature. Both polymers are compatible, i.e., they mix easily ensuring homogeneous intermixing. However, their scattering power for X-rays differs because the presence of heavy Ag^{+} ions increases the scattering power of the minority component. Therefore, the mixture can be studied by small-angle X-ray scattering (SAXS). From the scattering point of view, the mixture behaves as a solution of "optically modified" polystyrene in unmodified polystyrene. Because the so-called contrast, i.e., the difference in the scattering power of the components, can be estimated independently, the characteristics of the dissolved (minority) polymer, such as its molar mass, radius of gyration, etc., could be estimated. For a given molar mass of the modified PS, the measurement yielded a value of the radius of gyration that nicely corresponded to that in a dilute solution in a ϑ-solvent. When viewed from the perspective of later discoveries, this study is slightly problematic, because the presence of ions in a nonpolar polymer matrix can provoke their aggregation and formation of ion clusters (known from later studies of ionomers), which could have influenced the data analysis. However, experimental data suggest that the low fraction of modified polystyrene prevented the formation of ion clusters and the measurement yielded the characteristics of the individual modified chains. SANS was also later used by Cotton et al. [35] and by Kriste et al. [36]. Cotton studied deuterized polystyrene in hydrogenated polystyrene, and Kriste investigated deuterized poly(methyl methacrylate) in the hydrogenated polymer. As deuterium and hydrogen atoms differ strongly in their ability to scatter neutrons and the hydrogenated and deuterized polymer chains of the same chemical structure are fully compatible, both research groups obtained good-quality data and provided persuasive proof of the Flory prediction.

3 Polyelectrolyte Chains

The chains of polyelectrolytes (PEs) contain charged groups. PEs can be divided in two classes: Those with permanently charged groups, e.g., sulfonated polystyrene, are called strong or "quenched" polyelectrolytes. The term "quenched" PE reflects the fact that the positions of the charges are fixed (predetermined by the synthesis). Weak or "annealed" PEs contain ionizable groups that can dissociate in polar

solvents, leaving electric charges on the chain and releasing small mobile counterions in the bulk solvent. In contrast to quenched PE, both the ionization (number of charges on the chain) and the positions of the individual charges are not constant, but depend on the external conditions (pH, temperature, ionic strength). Discrete charges appear and disappear at different positions via reversible association/dissociation processes with a relatively high frequency, and because close approach of charges of the same sign is energetically unfavorable, the spatial distribution of charges is correlated with instantaneous chain conformations and fluctuates (it is an "annealed variable" which gave rise to the term annealed PEs).

Upon dissolution of PEs in polar solvents (most often water), a great majority of the counterions escape into the bulk solvent, which increases the entropy of the system and the thermodynamic stability of PE solutions. However, a certain fraction of them concentrate close to the PE chain and screen (partially neutralize) the multiple charge of the macro-ion. If the linear charge density along the chain exceeds a certain critical value, some counterions actually condense on the chain (Manning condensation) [37–39]. The condition for the onset of the Manning condensation requires that the dimensionless Coulomb coupling strength $\Gamma = \lambda_B/l_{ch}$ be equal to 1. Here, l_{ch} is the linear distance between charges in the chain, and λ_B is the Bjerrum length ($\lambda_B = e^2/(4\pi kT) \approx 0.7$ nm in water; this is the distance between the elementary charges at which the Coulomb interaction energy is the same as the energy of thermal motion), e is the elementary charge, k is the Boltzmann constant, and T is the temperature. Because charges of the same sign on the chain are never fully compensated at short distances by counterions, the highly charged chains adopt stretched conformations. Electric charges on the chain are separated as much as possible, which lowers the spatial charge density and causes electrostatic repulsion. An intrinsically flexible linear PE thus behaves as an effectively stiff chain, because the effective chain flexibility is affected and strongly reduced by electrostatic forces (depending on the charge density and ionic strength of the bulk solution). However, in addition to the direct electrostatic effect, there is a second important reason for stretching the chain. Stretched conformations provide a larger volume for constrained motion of "bound" counterions (which compensate the macro-ion charge) along the chain, which does not reduce their translational entropy (and the overall entropy of the system) as much as in collapsed conformations.

The behavior of an overwhelming majority of practically important PEs in aqueous media is significantly affected by the fact that they contain a fairly hydrophobic backbone (e.g., hydrocarbon chain) and their solubility in aqueous media is due to the presence of charges, either on the chain or on pendant electrolyte groups. In many cases, the presence of pendant ionizable groups (which are usually hydrophilic) weakens the hydrophobicity of the chain, which becomes amphiphilic at short distances. For example, the poly(methacrylic acid), PMAA, is well soluble at high pH values, when the carboxylic groups are highly ionized, but is still fairly well soluble in water at low pH values, where the pendant carboxylic groups are not dissociated. However, the parent poly(isopropylene) backbone, from which PMMA can be derived by attaching a pendant –COOH group at each monomer unit, is an

extremely hydrophobic water-insoluble polymer. In contrast to PMAA, unionized poly(2-vinylpyridine) is fairly hydrophobic and insoluble in neutral buffers, but it is well soluble in acidic media (below pH 5) when the nitrogen atom is protonated and charged. To summarize this paragraph, water is a thermodynamically bad solvent for most PEs.

Experimental studies of PS in poor solvents began in the early 1950s with the paper by Katchalski [40]. Early studies employing viscometry and calorimetry were performed on PMAA and alternating copolymers containing electrolyte and nonpolar hydrophobic monomer units in aqueous buffers [40–43]. The most important achievements were made by Strauss et al. [44–46], Morawetz et al. [47–50], and Ghiggino et al. [51]. It was recognized that the behavior of PMAA differs from that of less hydrophobic PEs, such as poly(acrylic acid), PAA. At that time, PMAA was usually described as a polyelectrolyte similar to polysoaps. Ghiggino was the first to propose the "hypercoiling model" specifically for PMAA on the basis of fluorescence studies more than 10 years before a similar Dobrynin "necklace of pearls model" [52] became a widely used scheme for interpreting the conformational behavior of PEs with hydrophobic backbone in aqueous media.

In the following chapters of this book, we will discuss fluorescence measurements performed mainly on PE solutions in thermodynamically poor solvents. Therefore, the behavior of PEs in poor solvents is our main sphere of interest, but we will first mention the classical Kuhn treatment of polyelectrolytes in ϑ-solvents [53]. The potential energy of a polyelectrolyte chain in a given conformation (described by a set of $\boldsymbol{r}_i$ position vectors of segments) can be written within the framework of the mean-field Debye–Hückel (DH) theory [54] as a sum of three contributions: the energy corresponding to (i) the entropic elasticity of harmonic bonds, U_1, with bond lengths l, which connect the monomers in the polymer chain. This contribution depends on the set of all position vectors, $\{\boldsymbol{r}_i\}$

$$U_1(\{\boldsymbol{r}_i\}) = \frac{3kT}{2l^2}\sum_{i=1}^{N-1}(\boldsymbol{r}_{i+1}-\boldsymbol{r}_i)^2 \tag{4}$$

(ii) the screened electrostatic Coulomb (Yukawa) interaction potential, U_2, between all monomers bearing charges q_i and q_j

$$U_2(\{r_i\}) = kT\sum_{i=1}^{N}\sum_{j<i}\frac{\lambda_\mathrm{B}q_iq_j}{|r_i-r_j|}\exp\left(-\kappa|r_i-r_j|\right) \tag{5}$$

and (iii) the short-range contribution of dispersion forces, U_3, which can be expressed using, e.g., the Lennard-Jones potential, $u_\mathrm{LJ}(r)$, which reasonably approximates the short-range interaction between nonpolar spherical molecules by a power function of their distance r

$$u_{\mathrm{LN}}(r) = 4\varepsilon\left[\left(\frac{\sigma}{r}\right)^{12} - \left(\frac{\sigma}{r}\right)^{6}\right] \tag{6}$$

At the level of the DH approximation, the interaction energy of segment–counterion interactions and added salt–ion interactions does not appear explicitly in the formula and enters indirectly via the concentration dependence of the Debye screening length, $r_{\mathrm{D}}^{-2} = \kappa^2 = 4\pi\lambda_{\mathrm{B}}\sum c_s q_s^2$, where c_{s} and q_{s} are the concentrations of small ions of the s type and their valences, respectively. Kuhn used a model of the chain without short-range interactions (i.e., without U_3) and minimized the expression for the free energy of the system. The crucial rough approximation which he used consisted in the fact that he evaluated the conformational part neglecting the interactions, and the interaction part neglecting the chain connectivity assuming that (i) the charged monomers are distributed uniformly in the chain volume. Taking into account the experimental findings, he further assumed that (ii) electrostatic interactions lead to unidirectional elongation of the chain conformations. He actually postulated that the PE chain adopts the shape of a rotationally symmetrical elongated ellipsoid with one perturbed (electrostatically affected) longitudinal size $R_{\mathrm{E}}^{\mathrm{P}}$ and two unperturbed perpendicular sizes, $R_{\mathrm{E}}^{\mathrm{UP}} = lN^{1/2}$. For $R_{\mathrm{E}}^{\mathrm{P}}$, he obtained the relationship

$$R_{\mathrm{E}}^{\mathrm{P}} = lNu^{1/3}f^{2/3}\left[\ln\left\{eN\left(uf^2\right)^{2/3}\right\}\right]^{1/3} \tag{7}$$

where u is the "interaction parameter" defined as $u = \lambda_{\mathrm{B}}/l$ and f denotes the fraction of charged monomers.

The behavior of PE chains can be analyzed in more detail by the scaling approach based on the concept of thermal and electrostatic blobs. The blob theory assumes that, on small length scales shorter than the "correlation length" ξ_{T} (called also the "blob size"), the energy of random thermal motion counterbalances the excluded volume effect of segments, and short parts of the chain behave as ideal chains. Therefore, it holds that $\xi_{\mathrm{T}}^2 = g_{\mathrm{T}}l^2$, where g_{T} is the number of segments per blob and l is the bond (segment) length. At longer lengths, the effect of the excluded volume dominates the conformational behavior, and the chain behaves as a self-avoiding walk. Taking into account the balance of forces, the size of the thermal blob can be related to the Flory–Huggins interaction parameter, $\xi_{\mathrm{T}} = l/(1-2\chi)$. The electrostatic blob is an extension of the blob concept. The assumption that the conformations inside the electrostatic blob are not perturbed by electrostatic interactions with the corresponding balance of forces yields the relationship between the "interaction parameter" u, the fraction of charged units f, and the parameters that characterize the blob, i.e., the number of segments, $g_{\mathrm{E}} = (uf^2)^{-2/3}$, and the electrostatic correlation length (blob size), $\xi_{\mathrm{E}} = l(uf^2)^{-1/3}$. Application of the scaling approach to the problem of PEs predicts that, on length scales larger than ξ_{E}, the electric charges on the PE chain generate a force which nonuniformly deforms the chain in one direction. This leads to a roughly uniaxial arrangement of electrostatic

blobs in a "string of blobs." The size of the blobs is not constant, but increases toward both ends of the chain. This result is not surprising, because the central section of the chain experiences stronger electrostatic repulsion than the ends of the chain. What is slightly surprising is the finding that the evaluation of the elongated chain size R_E^P yields an identical result to the simple approximate Kuhn model.

Now, we will discuss the behavior of quenched PEs in poor solvents. Experimental studies show that the effective solvent quality depends on a number of factors, namely, the degree of ionization of PE and the ionic strength. A poor solvent for a neutral chain can be a good solvent for the same charged polymer. Sparsely ionized PEs have only low solubility and form compact globular conformations in bad solvents (aqueous buffer), while a polymer of the same chemical nature dissolves well when its chain is strongly ionized and forms a fairly stretched conformation. We should recall that the variable ionization of a quenched PE requires the incorporation of different fractions of permanently charged comonomers in different chains during synthesis, and hence the chemical compositions of chains with different degrees of ionization are not identical. The first attempt to theoretically treat the behavior of quenched PEs in poor solvents was made by Khokhlov [55, 56]. He predicted that a spherically symmetrical globular conformation would deform with increasing charge and would form a prolate ellipsoid. A substantially more detailed description, which is at present generally accepted, was published by Dobrynin, Rubinstein, and Obukhov in 1996 [52]. They combined the scaling approach and Monte Carlo simulation and showed that the transition from the globular to the stretched conformation proceeds as a cascade transition via a series of "pearl necklace" structures (globules formed by collapsed parts of the chain interconnected by relatively short stretched parts) with increasing numbers of pearls of decreasing sizes. The proposed necklace concept was inspired by earlier theoretical works by Kantor and Kardar [57], who explained the formation of globules within one chain by the same physical arguments as used by Rayleigh in 1882 when he studied the instability of charged oil droplets [58]. When an oil droplet is charged, the charge spreads over its surface. Discrete elementary charges of the same sign aim at expanding the surface, because they try to be as far as possible from each other. The corresponding electrostatic potential of repulsive forces is proportional to the square of the total charge and to the reciprocal (average) distance between the charges $\langle r^{-1} \rangle$, which is proportional to the radius of the droplet, R, i.e., $\approx Q^2/(\varepsilon R)$, ε is the dielectric permittivity. The surface energy (proportional to γR^2, γ is the surface tension) tries to minimize the surface and preserve the spherical shape. When the charge increases and exceeds the critical value, at which both terms are equal, the "mother" droplet splits into two smaller "daughter" droplets because the Gibbs energy of the two "daughter" droplets is lower than that of the original "mother" droplet. As both "daughter" droplets contain electric charges of the same sign, they mutually repel and move away from each other.

The formation of pearls on the chain can be explained by analogous arguments. In a poor solvent, minimization of the number of unfavorable interactions between

non-ionized polymer segments and solvent molecules leads to a compact globular arrangement with minimum surface-to-volume area. When the charge on the chain increases, or the solvent quality improves and the effective surface tension decreases, the condition for Rayleigh instability is reached, and the globular conformation splits into two smaller globules. The globules cannot separate due to the chain connectivity and are kept together at a certain distance by a relatively short, albeit fairly stretched part of the chain. From a practical point of view, study of a system with "continuously" increasing charge on the chain assumes synthesis of a series of tailor-made PE samples with increasing numbers of charged groups incorporated into the chain, which is very demanding. It is much easier to vary the solvent quality by changing the temperature, but the range of solvent qualities for temperatures preventing temperature-induced decomposition of the polymer chains is fairly limited. If the chain charge (or temperature) continues to increase, a series of conformation transitions (splitting of globules) will gradually occur. Based on the scaling approach, Dobrynin et al. derived the following formula for the critical charge fraction f_{crit} which corresponds to the Rayleigh instability:

$$f_{\mathrm{crit}} = \left[|\tau|/(N\ u)\right]^{1/2} \tag{8}$$

where $\tau = (1–\vartheta/T)$, ϑ is the theta temperature and N is the total number of segments (monomer units). Theoretical description of the "pearl necklace" structure is relatively complicated because it does not reflect only the Rayleigh instability but also has to take into account other factors. The two charged globules electrostatically repel each other, increasing the energy of the pearl structure. The formation of a string connecting two globules requires that some monomers that were originally hidden inside the large "mother" globule now be exposed to the poor solvent, which is energetically unfavorable. In addition, the string contributes to the overall free energy of the system by its elastic and electrostatic parts. By minimizing the free energy, the authors derived the appropriate formulas for all the relevant parameters that characterize the pearl necklace structure of a chain consisting of n_{b} globules with size (diameter) D_{b} containing m_{b} monomers each. The globules are connected by strings, each having m_{st} monomers, and the total number of monomer units in the PE chain is N. Here, we reproduce only the formula for the total length of the necklace conformation, L_{nec}:

$$L_{\mathrm{nec}} = Nlf\sqrt{\frac{u}{|\tau|}ln\left(\frac{Nuf^2}{|\tau|}\right)} \tag{9}$$

where $\tau = (1–\vartheta/T)$.

The above-described hypothesis was confirmed by many Monte Carlo and molecular dynamics simulations and also by a number of experimental techniques [59–76]. Because the globules are fairly dynamic structures which "move" along the chain, the number of persuasive direct experimental proofs is still limited.

Nevertheless, the above "pearl necklace" scheme is now a generally accepted scheme for the conformational behavior of PEs in poor solvents.

The behavior of annealed PEs in poor solvents is more complex than that of quenched PEs. The probability of dissociation of a particular ionizable group depends, among other factors, on its distances from already ionized neighbor groups. It should be borne in mind that the simultaneous dissociation of two closely spaced ionizable groups is unfavorable, which can be documented by the low ratio of the second-to-first step dissociation constants in oxalic acid, K_2/K_1 approx. 10^{-3}. Hence, the distribution of annealed charges along the chain and its fluctuations are closely related to the instantaneous chain conformations. Therefore, it is not surprising that recent theoretical and computer studies predict different conformational behavior than for quenched PEs.

Conformational transitions in annealed PE solutions have been studied theoretically by Raphael and Joanny [77]. They predicted that annealed PEs should undergo a sudden first-order transition from a highly charged expanded conformation to a collapsed and very little ionized one with a pH-controlled change (decrease) in the degree of ionization. Recent semi-grand canonical Monte Carlo (MC) simulations performed at a constant chemical potential of the charged species indicate some ambiguity and do not support a first-order transition. Several authors observed a first-order transition for annealed PEs only in very poor solvents, while they observed the formation of pearls in marginal poor solvents (close to ϑ-conditions) [68]. Other authors claim that pearl necklace structures are also formed in very poor solvents [63]. At present, the debate concerning the transition from the expanded to the collapsed state is still ongoing, but most researchers believe (or incline to the opinion) that a cascade of pearl necklace transitions proceeds in a broad range of solvent qualities.

4 Comments on Computer Studies of Polymer Conformations and Dynamics

Computer studies (both Monte Carlo and molecular dynamic simulations) have become a very powerful tool for studying the conformational and dynamic behavior of polymer chains. They can be used for testing the predictions of theoretical models concerning the equilibrium properties and moreover they provide information on dynamic characteristics, e.g., on instantaneous fluctuations of chain shapes which is important because most experimental techniques (e.g., scattering techniques) yield the ensemble-average characteristics only. Large numbers of studies have been performed on neutral chains—not only on linear ones but also on stars, combs, etc. [78–85]. The most important advances in understanding the behavior of polyelectrolytes have been made mainly thanks to computer studies. As already mentioned, quenched PEs have been studied both by Monte Carlo [86–89] and by molecular dynamics simulations [59, 63, 71, 73, 87, 90]. Simulation of annealed

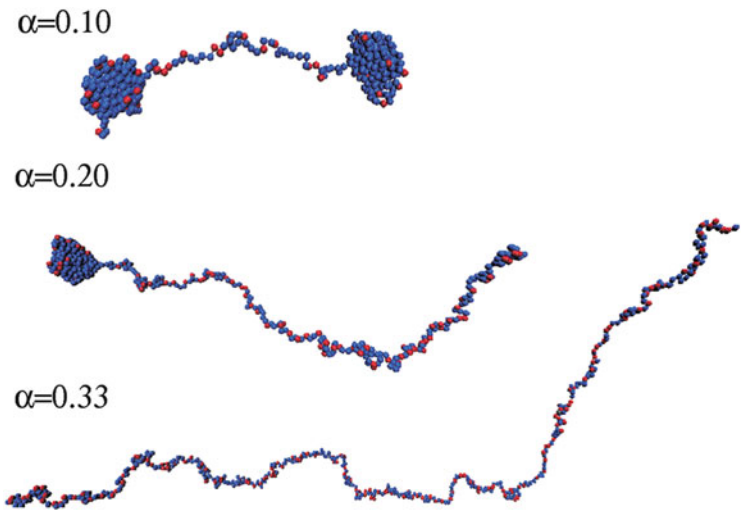

Fig. 4 Simulation snapshots of chain conformations in a bad solvent for three degrees of ionization α. Adapted with kind permission from Collection of Czechoslovak Chemical Communications 73, 2008, 439–458, figure 4, [93]. Copyright 2011

PEs is a very complex and delicate problem, because correct treatment of the dissociation equilibrium at constant pH assumes constant chemical potential of the hydrated protons and other small ions.

So far, almost all computer studies of annealed PEs have been performed by grand canonical Monte Carlo methods (or by reaction ensemble MC), because these simulation variants can treat variable dissociation relatively easily keeping the chemical potentials of small charged species constant [59, 63, 68, 69, 91, 92]. Current molecular dynamics (MD) studies usually use the degree of ionization as an input parameter and cannot correctly treat systems with "mobile charges." However, an interesting MD attempt for annealed PEs was published by Kosovan et al. [93]. The authors combined common molecular dynamics and Monte Carlo methodology. They incorporated a MC exchange of the positions of charges in the chain (submitted to the Metropolis acceptance criterion) [94] in a MD run which made it possible to emulate the appearance and disappearance of mobile charges in different positions on the chain. The authors analyzed the behavior of annealed chains under the condition of a fixed overall degree of ionization using several ensemble-averaged functions: the probability of ionization of monomer units $P(q,i)$ as a function of their position (running number i) in the chain contour and the average bond cosines, i.e., by $\langle \boldsymbol{r}_{i+1} \cdot \boldsymbol{r}_i \rangle / (|\boldsymbol{r}_{i+1}| \cdot |\boldsymbol{r}_i|)$, where $\boldsymbol{r}_i$ is the bond vector i. The ensemble average cosine of the angle between two successive bonds i and $(i+1)$ is a good indicator of the local behavior: It equals zero (or low) in stretched parts of the chain and can increase up to 0.5 in coiled globular parts of the chain. Simulation data for a chain with 500 unimer units and three overall degrees of ionization $\alpha = 0.1$, 0.2, and 0.33 in a bad solvent with the reduced Lennard-Jones interaction parameter $\varepsilon = 1.0$ are shown in Fig. 4. Figure 5 presents the schematics

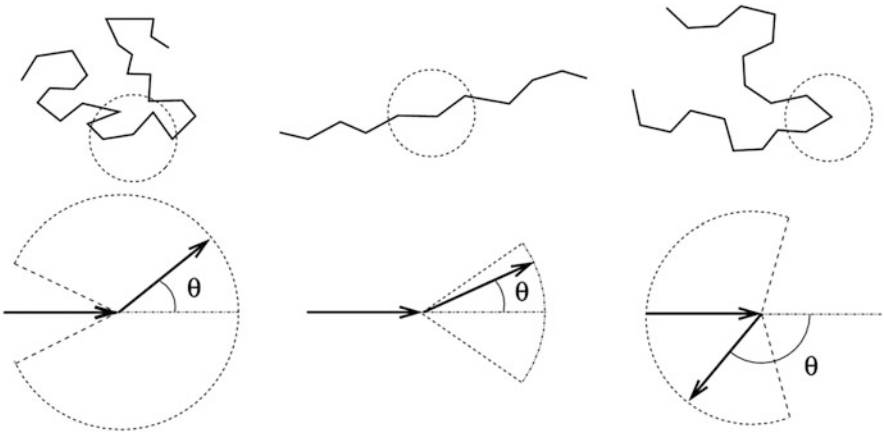

Fig. 5 Schematic illustration of the possible values of bond-angle cosines. Adapted with kind permission from Collection of Czechoslovak Chemical Communications 73, 2008, 439–458, figure 6, [93]. Copyright 2011

explaining the evaluation of bond-angle cosines, Fig. 6 depicts the distribution functions of bond-angle cosines as functions of the position of monomer units in the polymer chain for the above overall degree of ionization, and Fig. 7 shows the probability of ionization of individual beads. Note that $\varepsilon = 0.34$ describes the ϑ-temperature [70]. The data show that the chain forms a pearl necklace structure and the units inside compact globules are considerably less ionized than those exposed to the solvent in the stretched part of the chain.

5 The Persistence Length

In the part devoted to neutral polymers, we mentioned that semiflexible and stiff chains do not obey the behavior predicted by the Kuhn model. Restricted flexibility of the chain can be caused by the presence of stiff units with multiple bonds or bulky pendant groups, but it can be a result of external conditions or stimuli. In the preceding part, it was explained in detail that repulsive interactions together with entropic forces increase the stiffness of PE chains. Hence, a sudden pH change can be used as a stimulus affecting the stiffness of annealed PE chains. The properties of semiflexible polymers are usually treated at the level of the wormlike chain (WLC) model developed by Kratky and Porod [31]. The "persistence length," l_P, is an important parameter strongly related to the WLC model and has been used as the most common characteristic of chain flexibility—in both theoretical and experimental studies. It is used to describe orientational correlations between successive bond vectors in a polymer chain in terms of the normalized orientation correlation function, $C(s) = \langle \boldsymbol{r}_i . \boldsymbol{r}_{i+s} \rangle$. For the WRC model, this function decays exponentially:

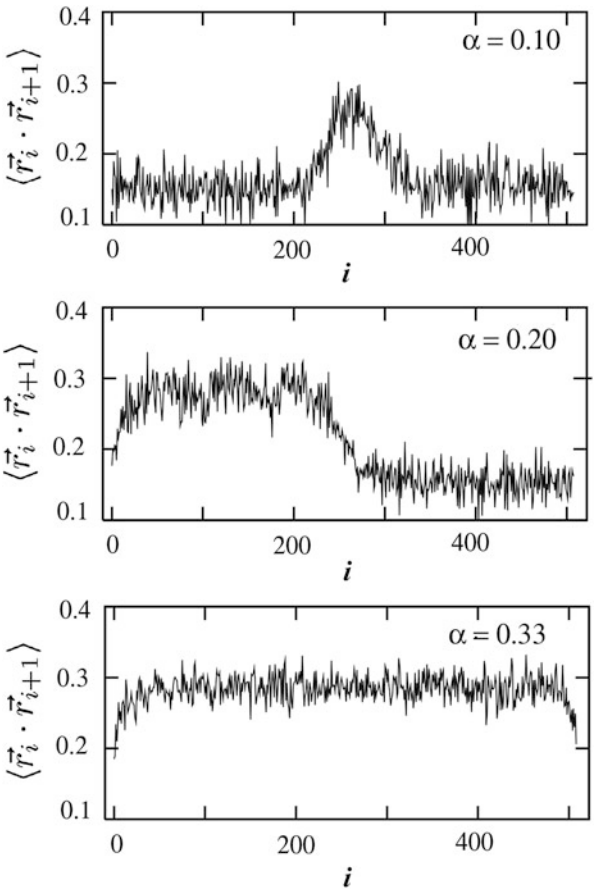

Fig. 6 Average bond-angle cosines as functions of the position of the monomer unit in the polymer chain for the polymer in a bad solvent for three degrees of ionization α. Adapted with kind permission from Collection of Czechoslovak Chemical Communications 73, 2008, 439–458, figure 7, [93]. Copyright 2011

$$C(s) = \exp\left(\frac{-s}{l_P}\right) \tag{10}$$

and the persistence length l_P is related to the bending modulus κ of the chain by $l_P = \kappa/kT$. The persistent length l_P is the length at which the chain "forgets" the orientation of its first segment, i.e., at distances shorter than l_P, short parts of the chain behave like an elastic rod, while at longer distances, the conformational properties can be described statistically by a random walk model. Equation (10) actually describes the rate of decay of the ensemble average cosine of the angle between the orientations of the first and the s-st segment (generally between the n-st and $(n+s)$-st segment) in the chain. From the geometrical point of view, l_P equals the average projection of the end-to-end vector on the tangent to the chain contour at chain end at the limit of infinite length. For the freely jointed chain (Kuhn model), the persistence length is only one half of the segment length, $(1/2)l$.

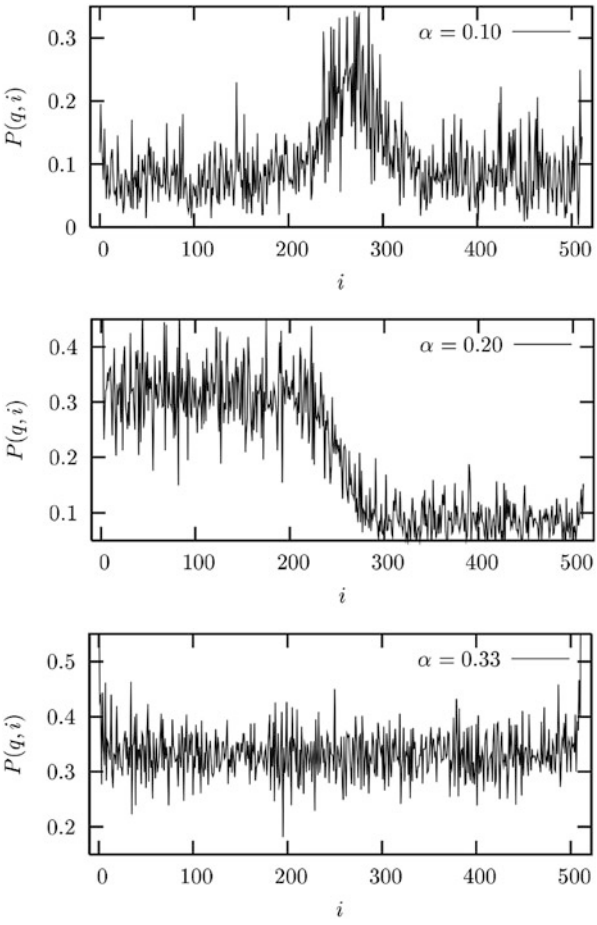

Fig. 7 The probability of charging of individual monomer units $P(q,i)$ for the polymer in a bad solvent as a function of their position in the chain, i, for three degrees of ionization α. Adapted with kind permission from Collection of Czechoslovak Chemical Communications 73, 2008, 439–458, figure 9, [93]. Copyright 2011

The effect of electrostatics on the persistence length of polyelectrolytes has been studied by a number of researchers. The first theoretical model was developed independently by Odijk [95] and by Skolnick and Fixman [96]. They expressed the total persistence length, l_P, as the sum of the natural persistence length, l_0, and the electrostatic persistence length, l_E, i.e., $l_P = l_0 + l_E$. For long chains, they obtained the following formula:

$$l_E = (\alpha N)^2 \lambda_B \lambda_D^2 / 4 \tag{11}$$

where λ_B is the Bjerrum length, λ_D is the Debye screening length, N is the number of monomer units, and α is the normalized linear charge density on the chain. Later, Khokhlov et al. [97] reformulated the problem for a chain of blobs and also obtained the scaling of l_B on λ_D^2. However, there is a strong controversy about the dependence of l_B on λ_D. This problem has been amply studied by computer

simulations [98–100]. Computer simulations suggest that the correlation function of the segment orientations in PE chains cannot be expressed as a single exponential function. The fact that the short-range behavior is dominated by intrinsic stiffness, while the long-range part of orientational correlations is controlled by electrostatics, and that there exists a crossover between these two regimes were suggested originally by Barrat and Joanny [101] and later confirmed by simulations [102]. Gubarev et al. [103] proposed the double-exponential decay of $C(s)$:

$$C(s) = B\exp\left(-\frac{s}{l_1}\right) + (1-B)\exp\left(-\frac{s}{l_2}\right) \tag{12}$$

where l_1 and l_2 are two different decay lengths. Manghi and Netz [104], Dobrynin et al. [103], and others [105] studied the problem in detail and proposed the relation between l_i, l_0, and l_E. They also confirmed that the dependence of l_B on λ_D is more complex than that proposed by Odijk and Skolnick with Fixman.

Acknowledgment This work was supported by the Czech Science Foundation (Grants P106-12-0143 and P106-15-19542S). The authors would like to thank Lucie Suchá and Karel Šindelka for their help with graphics.

References

1. Rubinstein M, Colby R (2003) Polymers physics. Oxford University Press, Oxford
2. Sperling LH (2005) Introduction to physical polymer science. Wiley, Hoboken, NJ
3. Munk P (1989) Introduction to macromolecular science. Wiley, New York
4. Doi M, See H (1996) Introduction to polymer physics. Clarendon, Oxford
5. Kawakatsu T (2004) Statistical physics of polymers: an introduction. Springer, Berlin
6. Lodge TP, Muthukumar M (1996) Physical chemistry of polymers: entropy, interactions, and dynamics. J Phys Chem 100:13275–13292. doi:10.1021/Jp960244z
7. Freire JJ (1999) Conformational properties of branched polymers: theory and simulations. Branched Polym II 143:35–112
8. Huggins ML (1942) Theory of solutions of high polymers. J Am Chem Soc 64(7):1712–1719. doi:10.1021/ja01259a068
9. Flory PJ (1949) The configuration of real polymer chains. J Chem Phys 17(3):303–310. doi:10.1063/1.1747243
10. Flory PJ (1970) Thermodynamics of polymer solutions. Discuss Faraday Soc 49:7
11. Flory PJ (1945) Thermodynamics of dilute solutions of high polymers. J Chem Phys 13 (11):453–465. doi:10.1063/1.1723978
12. Flory PJ (1953) Principles of polymer chemistry. Cornell University Press, Ithaca, NY
13. Flory PJ, Krigbaum WR (1951) Thermodynamics of high polymer solutions. Annu Rev Phys Chem 2:383–402. doi:10.1146/annurev.pc.02.100151.002123
14. Flory PJ (1942) Thermodynamics of high polymer solutions. J Chem Phys 10(1):51–61
15. Huggins ML (1942) Some properties of solutions of long-chain compounds. J Phys Chem 46 (1):151–158. doi:10.1021/j150415a018
16. Teraoka I (2002) Polymer solutions: an introduction to physical properties. Wiley, New York
17. Yamakawa H (1971) Modern theory of polymer solutions. Harper & Row, New York
18. Brandrup J, Immergut EH, Grulke EA, Abe A, Bloch DR (1999) Polymer handbook, vol 89. Wiley, New York

19. Wanka G, Hoffmann H, Ulbricht W (1994) Phase-diagrams and aggregation behavior of poly (oxyethylene)-poly(oxypropylene)-poly(oxyethylene) triblock copolymers in aqueous-solutions. Macromolecules 27(15):4145–4159. doi:10.1021/ma00093a016
20. Attwood D, Collett J, Tait C (1986) Photon correlation studies on the micelles of a poly (oxyethylene)-poly (oxypropylene)-poly (oxyethylene) block copolymer in aqueous solution. In: Surfactants in solution. Springer, pp 419–426
21. Kuhn W, Grun F (1942) Relationships between elastic constants and stretching double refraction of highly elastic substances. Kolloid-Z 101:248
22. James HM, Guth E (1943) Theory of the elastic properties of rubber. J Chem Phys 11 (10):455–481
23. Rudnick J, Gaspari G (1987) The shapes of random-walks. Science 237(4813):384–389. doi:10.1126/science.237.4813.384
24. Tanford C, Huggins ML (1962) Physical chemistry of macromolecules. J Electrochem Soc 109(3):98C
25. De Gennes P-G (1979) Scaling concepts in polymer physics. Cornell University Press, Ithaca, NY
26. Binder K (1995) Monte Carlo and molecular dynamics simulations polymer. Oxford University Press, New York
27. Flory P, Volkenstein M (1969) Statistical mechanics of chain molecules. Wiley, New York
28. Volkenstein MV (1958) The configurational statistics of polymeric chains. J Polym Sci 29 (120):441–454. doi:10.1002/pol.1958.1202912012
29. Lifson S (1959) Neighbor interactions and internal rotations in polymer molecules. 3. Statistics of interdependent rotations and their application to the polyethylene molecule. J Chem Phys 30(4):964–967. doi:10.1063/1.1730136
30. Nagai K, Ishikawa T (1965) Internal rotation and Kerr effect in polymer molecules. J Chem Phys 43(12):4508. doi:10.1063/1.1696725
31. Kratky O, Porod G (1949) Rontgenuntersuchung geloster fadenmolekule. Recueil Des Travaux Chimiques Des Pays-Bas J R Neth Chem Soc 68(12):1106–1122
32. Rouse PE (1953) A theory of the linear viscoelastic properties of dilute solutions of coiling polymers. J Chem Phys 21(7):1272–1280. doi:10.1063/1.1699180
33. Zimm BH (1956) Dynamics of polymer molecules in dilute solution—viscoelasticity, flow birefringence and dielectric loss. J Chem Phys 24(2):269–278. doi:10.1063/1.1742462
34. Krigbaum WR, Godwin RW (1965) Direct measurement of molecular dimensions in bulk polymers. J Chem Phys 43(12):4523. doi:10.1063/1.1696728
35. Cotton JP, Farnoux B, Jannink G, Straziel C (1973) Dilute and semidilute solutions—light and neutron-scattering and osmotic-pressure. J Polym Sci Part C Polym Symp 42:981–985
36. Kirste RG, Schelten J, Kruse WA (1972) Determination of radius of gyration of poly(methyl methacrylate) in glass state by neutron-diffraction. Makromol Chem 162:299
37. Manning GS (1996) Counterion condensation theory constructed from different models. Physica A 231(1–3):236–253. doi:10.1016/0378-4371(95)00452-1
38. Manning GS (1969) Limiting laws and counterion condensation in polyelectrolyte solutions. I. Colligative properties. J Chem Phys 51(3):924. doi:10.1063/1.1672157
39. Manning GS (1969) Limiting laws and counterion condensation in polyelectrolyte solutions II. Self-diffusion of the small ions. J Chem Phys 51(3):934–938
40. Katchalsky A (1951) Solutions of polyelectrolytes and mechanochemical systems. J Polym Sci 7(4):393–412. doi:10.1002/pol.1951.120070403
41. Crescenz V, Delben F, Quadrifo F (1972) Calorimetric investigation of poly(methacrylic acid) and poly(acrylic acid) in aqueous-solution. J Polym Sci Part A 10(2):357. doi:10.1002/pol.1972.160100215
42. Delben F, Quadrifo F, Crescenz V (1972) Enthalpy of dissociation of poly(methacrylic acid) in aqueous-solution. Eur Polym J 8(7):933. doi:10.1016/0014-3057(72)90054-7
43. Arnold R (1957) The titration of polymeric acids. J Colloid Sci 12(6):549–556. doi:10.1016/0095-8522(57)90060-0

44. Strauss UP, Schlesinger MS (1978) Effects of alkyl group-size and counterion type on behavior of copolymers of maleic-anhydride and alkyl vinyl ethers. 2. Fluorescence of dansylated copolymers. J Phys Chem 82(14):1627–1632. doi:10.1021/j100503a011
45. Strauss UP, Vesnaver G (1975) Optical probes in polyelectrolyte studies. 1. Acid–base equilibria of dansylated copolymers of maleic-anhydride and alkyl vinyl ethers. J Phys Chem 79(15):1558–1561. doi:10.1021/j100582a017
46. Strauss UP, Vesnaver G (1975) Optical probes in polyelectrolyte studies. 2. Fluorescence-spectra of dansylated copolymers of maleic-anhydride and alkyl vinyl ethers. J Phys Chem 79 (22):2426–2429. doi:10.1021/j100589a017
47. Bednar B, Morawetz H, Shafer JA (1984) Kinetics of the cooperative complex-formation and dissociation of poly(acrylic acid) and poly(oxyethylene). Macromolecules 17(8):1634–1636. doi:10.1021/ma00138a037
48. Bednar B, Morawetz H, Shafer JA (1985) Kinetics of the conformational transition of poly (methacrylic acid) after changes of its degree of ionization. Macromolecules 18 (10):1940–1944. doi:10.1021/ma00152a024
49. Wang YC, Morawetz H (1986) Study of the equilibrium and the kinetics of the fluorescence enhancement on mixing solutions of auramine-o and poly(methacrylic acid). Macromolecules 19(7):1925–1930. doi:10.1021/ma00161a024
50. Horsky J, Morawetz H (1988) Kinetics of the conformational transition of poly(methacrylic acid) after a ph jump. 2. Studies of nonradiative energy-transfer. Makromol Chem 189 (10):2475–2483
51. Ghiggino K, Tan K, Phillips D (1985) Polymer photophysics. Chapman and Hall, London
52. Dobrynin AV, Rubinstein M, Obukhov SP (1996) Cascade of transitions of polyelectrolytes in poor solvents. Macromolecules 29(8):2974–2979. doi:10.1021/ma9507958
53. Kuhn W, Kunzle O, Katchalsky A (1948) Verhalten polyvalenter fadenmolekelionen in losung. Helv Chim Acta 31(7):1994–2037. doi:10.1002/hlca.19480310716
54. Debye P, Huckel E (1923) The interionic attraction theory of deviations from ideal behavior in solution. Z Phys 24:185
55. Dormidontova EE, Erukhimovich IY, Khokhlov AR (1994) Microphase separation in poor-solvent polyelectrolyte solutions—phase-diagram. Macromol Theory Simul 3(4):661–675. doi:10.1002/mats.1994.040030403
56. Vasilevskaya VV, Khokhlov AR (1992) Swelling and collapse of polymer gel in polymer-solutions and melts. Macromolecules 25(1):384–390. doi:10.1021/ma00027a059
57. Kantor Y, Kardar M (1994) Excess charge in polyampholytes. Europhys Lett 27(9):643–648. doi:10.1209/0295-5075/27/9/002
58. Rayleigh L (1882) On the equilibrium of liquid conducting masses charged with electricity. Philos Mag Ser 5 14(87):184–186. doi:10.1080/14786448208628425
59. Lyulin AV, Dunweg B, Borisov OV, Darinskii AA (1999) Computer simulation studies of a single polyelectrolyte chain in poor solvent. Macromolecules 32(10):3264–3278. doi:10.1021/ma981818w
60. Liao Q, Dobrynin AV, Rubinstein M (2003) Molecular dynamics simulations of polyelectrolyte solutions: nonuniform stretching of chains and scaling behavior. Macromolecules 36 (9):3386–3398. doi:10.1021/ma025995f
61. Liao Q, Dobrynin AV, Rubinstein M (2006) Counterion-correlation-induced attraction and necklace formation in polyelectrolyte solutions: theory and simulations. Macromolecules 39 (5):1920–1938. doi:10.1021/ma052086s
62. Liu B, Dunweg B (2003) Translational diffusion of polymer chains with excluded volume and hydrodynamic interactions by Brownian dynamics simulation. J Chem Phys 118 (17):8061–8072. doi:10.1063/1.1564047
63. Ulrich S, Laguecir A, Stoll S (2005) Titration of hydrophobic polyelectrolytes using Monte Carlo simulations. J Chem Phys 122(9), 094911. doi:10.1063/1.1856923

64. Chodanowski P, Stoll S (1999) Monte Carlo simulations of hydrophobic polyelectrolytes: evidence of complex configurational transitions. J Chem Phys 111(13):6069–6081. doi:10.1063/1.479905
65. Uhlik F, Kosovan P, Limpouchova Z, Prochazka K, Borisov OV, Leermakers FAM (2014) Modeling of ionization and conformations of starlike weak polyelectrolytes. Macromolecules 47(12):4004–4016. doi:10.1021/ma500377y
66. Ou ZY, Muthukumar M (2005) Langevin dynamics of semiflexible polyelectrolytes: rod-toroid-globule-coil structures and counterion distribution. J Chem Phys 123(7):074905. doi:10.1063/1.1940054
67. Yamaguchi T, Kiuchi T, Matsuoka T, Koda S (2005) Multi-pH Monte Carlo simulation of coil-globule transition of weak polyelectrolyte. Bull Chem Soc Jpn 78(12):2098–2104. doi:10.1246/bcsj.78.2098
68. Uyaver S, Seidel C (2004) Pearl-necklace structures in annealed polyelectrolytes. J Phys Chem B 108(49):18804–18814. doi:10.1021/jp0464270
69. Uyaver S, Seidel C (2009) Effect of varying salt concentration on the behavior of weak polyelectrolytes in a poor solvent. Macromolecules 42(4):1352–1361. doi:10.1021/ma801817j
70. Micka U, Holm C, Kremer K (1999) Strongly charged, flexible polyelectrolytes in poor solvents: molecular dynamics simulations. Langmuir 15(12):4033–4044. doi:10.1021/la981191a
71. Limbach HJ, Holm C (2003) Single-chain properties of polyelectrolytes in poor solvent. J Phys Chem B 107(32):8041–8055. doi:10.1021/jp027606p
72. Limbach HJ, Holm C (2001) End effects of strongly charged polyelectrolytes: a molecular dynamics study. J Chem Phys 114(21):9674–9682. doi:10.1063/1.1370077
73. Limbach HJ, Holm C, Kremer K (2002) Structure of polyelectrolytes in poor solvent. Europhys Lett 60(4):566–572. doi:10.1209/epl/i2002-00256-8
74. Kosovan P, Kuldova J, Limpouchova Z, Prochazka K, Zhulina EB, Borisov OV (2010) Molecular dynamics simulations of a polyelectrolyte star in poor solvent. Soft Matter 6 (9):1872–1874. doi:10.1039/b925067k
75. Kosovan P, Kuldova J, Limpouchova Z, Prochazka K, Zhulina EB, Borisov OV (2009) Amphiphilic graft copolymers in selective solvents: molecular dynamics simulations and scaling theory. Macromolecules 42(17):6748–6760. doi:10.1021/ma900768p
76. Kosovan P, Limpouchova Z, Prochazka K (2007) Conformational behavior of comb-like polyelectrolytes in selective solvent: computer simulation study. J Phys Chem B 111 (29):8605–8611. doi:10.1021/jp072894g
77. Raphael E, Joanny JF (1990) Annealed and quenched polyelectrolytes. Europhys Lett 13 (7):623–628. doi:10.1209/0295-5075/13/7/009
78. Binder K, Paul W (2008) Recent developments in Monte Carlo simulations of lattice models for polymer systems. Macromolecules 41(13):4537–4550. doi:10.1021/ma702843z
79. Binder K, Muller M, Virnau P, MacDowell LG (2005) Polymer plus solvent systems: phase diagrams, interface free energies, and nucleation. In: Holm C, Kremer K (eds) Advanced computer simulation approaches for soft matter sciences I, vol 173, Advances in Polymer Science. Springer, Berlin, pp 1–104. doi:10.1007/b99426
80. Baschnagel J, Binder K, Doruker P, Gusev AA, Hahn O, Kremer K, Mattice WL, Muller-Plathe F, Murat M, Paul W, Santos S, Suter UW, Tries V (2000) Bridging the gap between atomistic and coarse-grained models of polymers: status and perspectives. Adv Polym Sci 152:41–156
81. Honeycutt JD (1998) A general simulation method for computing conformational properties of single polymer chains. Comput Theor Polym Sci 8(1–2):1–8. doi:10.1016/s1089-3156(97)00025-1
82. Ahlrichs P, Dunweg B (1999) Simulation of a single polymer chain in solution by combining lattice Boltzmann and molecular dynamics. J Chem Phys 111(17):8225–8239. doi:10.1063/1.480156

83. Havrankova J, Limpouchova Z, Prochazka K (2003) Monte Carlo study of heteroarm star copolymers in good and selective solvents. Macromol Theory Simul 12(7):512–523. doi:10.1002/mats.200350012
84. Viduna D, Limpouchova Z, Prochazka K (2001) Monte Carlo simulation of polymer brushes in narrow pores. J Chem Phys 115(15):7309–7318. doi:10.1063/1.1405444
85. Zhou Z, Daivis PJ (2009) Molecular dynamics study of polymer conformation as a function of concentration and solvent quality. J Chem Phys 130(22), 224904. doi:10.1063/1.3149858
86. Jusufi A, Likos CN (2009) Colloquium: star-branched polyelectrolytes: the physics of their conformations and interactions. Rev Mod Phys 81(4):1753–1772. doi:10.1103/RevModPhys.81.1753
87. Jusufi A, Likos CN, Lowen H (2002) Counterion-induced entropic interactions in solutions of strongly stretched, osmotic polyelectrolyte stars. J Chem Phys 116(24):11011–11027. doi:10.1063/1.1480007
88. Polson JM, Opps SB, Abou Risk N (2009) Theoretical study of solvent effects on the coil-globule transition. J Chem Phys 130(24), 244902. doi:10.1063/1.3153350
89. Rissanou AN, Anastasiadis SH, Bitsanis IA (2009) A Monte Carlo study of the coil-to-globule transition of model polymer chains near an attractive surface. J Polym Sci Part B Polym Phys 47(24):2462–2476. doi:10.1002/polb.21869
90. Limbach HJ, Holm C, Kremer K (2004) Conformations and solution structure of polyelectrolytes in poor solvent. Macromol Symp 211:43–53. doi:10.1002/masy.200450703
91. Ulrich S, Laguecir A, Stoll S (2004) Complex formation between a nanoparticle and a weak polyelectrolyte chain: Monte Carlo simulations. J Nanoparticle Res 6(6):595–603. doi:10.1007/s11051-004-3548-4
92. Nair AKN, Uyaver S, Sun SY (2014) Conformational transitions of a weak polyampholyte. J Chem Phys 141(13):11. doi:10.1063/1.4897161
93. Kosovan P, Limpouchova Z, Prochazka K (2008) Charge distribution and conformations of weak polyelectrolyte chains in poor solvents. Collect Czechoslov Chem Commun 73(4):439–458. doi:10.1135/cccc20080439
94. Allen MP, Tildesley DJ (1987) Computer simulation of liquids. Clarendon, Oxford
95. Odijk T (1977) Polyelectrolytes near the rod limit. J Polym Sci Part B Polym Phys 15(3):477–483. doi:10.1002/pol.1977.180150307
96. Skolnick J, Fixman M (1977) Electrostatic persistence length of a wormlike polyelectrolyte. Macromolecules 10(5):944–948. doi:10.1021/ma60059a011
97. Khokhlov AR, Khachaturian KA (1982) On the theory of weakly charged poly-electrolytes. Polymer 23(12):1742–1750. doi:10.1016/0032-3861(82)90116-1
98. Everaers R, Milchev A, Yamakov V (2002) The electrostatic persistence length of polymers beyond the OSF limit. Eur Phys J E 8(1):3–14. doi:10.1140/epje/i2002-10007-3
99. Nguyen TT, Shklovskii BI (2002) Persistence length of a polyelectrolyte in salty water: Monte Carlo study. Phys Rev E 66(2), 021801. doi:10.1103/PhysRevE.66.021801
100. Ullner M (2003) Comments on the scaling behavior of flexible polyelectrolytes within the Debye-Huckel approximation. J Phys Chem B 107(32):8097–8110. doi:10.1021/jp027381i
101. Barrat JL, Joanny JF (1993) Persistence length of polyelectrolyte chains. Europhys Lett 24(5):333–338. doi:10.1209/0295-5075/24/5/003
102. Micka U, Kremer K (1997) Persistence length of weakly charged polyelectrolytes with variable intrinsic stiffness. Europhys Lett 38(4):279–284. doi:10.1209/epl/i1997-00238-x
103. Gubarev A, Carrillo J-MY, Dobrynin AV (2009) Scale-dependent electrostatic stiffening in biopolymers. Macromolecules 42(15):5851–5860. doi:10.1021/ma9008143
104. Manghi M, Netz RR (2004) Variational theory for a single polyelectrolyte chain revisited. Eur Phys J E 14(1):67–77. doi:10.1140/epje/i2004-10007-3
105. Bacova P, Kosovan P, Uhlik F, Kuldova J, Limpouchova Z, Prochazka K (2012) Double-exponential decay of orientational correlations in semiflexible polyelectrolytes. Eur Phys J E 35(6):53. doi:10.1140/epje/i2012-12053-6

Self-Assembly of Amphiphilic Block Copolymers in Selective Solvents

Maria Karayianni and Stergios Pispas

Contents

Abstract For the last decades, amphiphilic block copolymers have been at the focus of extensive scientific interest, due to their unique properties and numerous potential applications. Their technological potential evolves from their ability to self-assemble into a plethora of morphologically diverse nanostructures such as micelles, polymersomes, cylinders and others. In this chapter, we discuss the basic principles governing amphiphilic block copolymer self-organisation in solutions and the variety of morphologies observed so far, as well as the experimental techniques available for characterising such nanostructures. Some representative examples of self-assembly from nonionic and ionic amphiphilic block copolymers of different macromolecular architectures are also presented.

Keywords Amphiphilic block copolymer • Nanostructures • Micelles • Polymersomes • Morphology • Macromolecular architecture

M. Karayianni • S. Pispas (✉)
Theoretical and Physical Chemistry Institute, National Hellenic Research Foundation, 48 Vasileos Constantinou Avenue, 11635 Athens, Greece
e-mail: pispas@eie.gr

K. Procházka (ed.), *Fluorescence Studies of Polymer Containing Systems*, Springer Series on Fluorescence 16, DOI 10.1007/978-3-319-26788-3_2

Abbreviations

AFM	Atomic force microscopy
AUC	Analytical ultracentrifugation
cmc	Critical micelle concentration
(cryo-)TEM	(cryogenic) Transmission electron microscopy
DLS	Dynamic light scattering
DMF	Dimethylformamide
NMR	Nuclear magnetic resonance
P2VP	Poly(2-vinylpyridine)
P4VP	Poly(4-vinylpyridine)
P4VPDecI	Poly(4-vinylpyridine decyliodide)
P4VPMeI	Poly(4-vinylpyridine methyliodide)
PAA	Poly(acrylic acid)
PAI	Poly(5-(*NN*-diethylaminoisoprene))
PBD	Polybutadiene
PBO	Poly(butylene oxide)
PCL	Poly(ε-caprolactone)
PDEAEMA	Poly(*N*,*N*-diethylaminoethyl methacrylate)
PDMAEMA	Poly(*N*,*N*-dimethylaminoethyl methacrylate)
PDMS	Poly(dimethylsiloxane)
PEE	Poly(ethylethylene)
PEG	Poly(ethylene glycol)
PEHA	Poly(2-ethylhexyl acrylate)
PEO	Poly(ethylene oxide)
PEP	Poly(ethylene-*alt*-propylene)
PSGMA	Poly(sulfonated glycidyl methacrylate)
PI	Polyisoprene
PIB	Poly(isobutylene)
PISC	Poly((sulfamate-carboxylate)isoprene)
PMA	Poly(methyl acrylate)
PMAA	Poly(methacrylic acid)
PMMA	Poly(methyl methacrylate)
PMOXA	Poly(2-methyloxazoline)
P*n*BA	Poly(*n*-butyl acrylate)
P*n*BMA	Poly(*n*-butyl methacrylate)
PPO	Poly(propylene oxide)
PS	Polystyrene
PSS	Poly(styrene sulfonate)
PSSH	Poly(styrene sulfonic acid)
PSSNa	Poly(sodium styrene sulfonate)
P*t*BA	Poly(*tert*-butyl acrylate)
P*t*BMA	Poly(*tert*-butyl methacrylate)
SANS	Small-angle neutron scattering

SAXS	Small-angle X-ray scattering
SEC	Size exclusion chromatography
SEM	Scanning electron microscopy
SLS	Static light scattering
THF	Tetrahydrofuran

1 Introduction

During the last decades, amphiphilic block copolymers have been at the focus of extensive scientific interest, both from an experimental and a theoretical point of view, owing to their unique properties and numerous potential applications involving medicine, biology, biomaterials, microelectronics, photoelectric materials, catalysts, etc. Their most important feature is the ability to self-assemble in solution giving rise to a plethora of resulting morphologies including spherical micelles, cylindrical micelles, lamellae and vesicles and bicontinuous structures, among others. A major contribution to this respect has been the recent development in the synthetic techniques, especially ionic and living radical polymerisation methods, which facilitate the preparation of block copolymers with well-defined compositions, molecular weights, and elaborate architectures. The growing range of available block copolymer architectures includes linear block copolymers, graft copolymers, dendritic polymers, starlike polymers, cyclic polymers and so on, which can self-organise into aggregates of diverse morphologies under certain conditions [1–3].

Among these, the most common and extensively studied systems are those of linear amphiphilic block copolymers which are generally defined as macromolecules consisting of two or more chemically distinct and frequently immiscible blocks linked together by covalent bonds. This immiscibility results in their self-assembly in solutions of a selective solvent of one of the blocks. In particular, when a block copolymer is dissolved in a liquid that is a thermodynamically good solvent for one block and at the same time a precipitant for the other, the copolymer chains associate reversibly thus forming micellar aggregates of nanoscopic dimensions and of various shapes, similar to those obtained from low molecular weight surfactants. The resulting micelles consist of a more or less swollen core of the insoluble blocks surrounded by a flexible corona of the soluble blocks. As far as the micellar morphology is concerned, when the soluble block is predominant, the insoluble block aggregates to form spherical micelles, while cylindrical micelles or vesicles are formed as the length of the soluble block decreases relatively to that of the insoluble block. Nevertheless, for a given copolymer, unusual micelles differing from the spherical morphology can be produced depending on the specific solution conditions [1–3].

As can be expected, the number of studies, both experimental and theoretical, on copolymer self-assembly is vast, and their results have been thoroughly reviewed by various authors including Price [4], Tuzar and Kratochvil [5], Webber et al. [6],

Hamley [7], Alexandridis and Lindman [8], Riess and co-workers [1, 9], Gohy [2], Quémener et al. [10] and Eisenberg et al. [3], to name but a few. In the following, we intend to present a brief overview on the main aspects of micelle formation and morphology, the experimental methods used for their characterisation, as well as theoretical and computer simulation predictions of their structural parameters. Furthermore, representative examples of the main classes of different amphiphilic copolymer-selective solvent systems will be presented, along with possible applications of such systems.

2 Amphiphilic Block Copolymer Micelles

2.1 General Features

It is well established that when an amphiphilic block copolymer is dissolved in a selective solvent at a fixed temperature, above a specific concentration called the critical micelle concentration (cmc), micellisation occurs. Below the cmc, only molecularly dissolved copolymer chains (unimers) are present in the solution, while above the cmc multimolecular micelles are in thermodynamic equilibrium with the unimers. This process is in analogy to classical low molecular weight surfactants, differing in that the cmc is much lower in the case of block copolymers macrosurfactants. The self-assembly arises from the need of the copolymer chains to minimise energetically unfavourable solvophobic interactions. Therefore, micelle formation is dictated by two opposite forces, the attractive force between the insoluble blocks, which leads to aggregation, and the repulsive one between the soluble blocks preventing unlimited growth of the micelle. At the same time, the interaction of the soluble blocks and the solvent is responsible for the stabilisation of the micelles [1, 10].

The morphology of the resulting micellar aggregates is primarily a result of the inherent molecular curvature arising from the relative sizes of the soluble and insoluble domains, and of the way, this influences the packing of the copolymer chains within the aggregates. The dimensionless packing parameter, p, can be used to define the relative size of the insoluble region of a copolymer. The balance between solvophobic and solvophilic interactions gives rise to an optimal surface area, a_0, of the insoluble block at the interface between the soluble and insoluble blocks. This area together with the length, l_c, and the volume, v, of the insoluble block contributes to the packing parameter, which is defined as:

$$p = \frac{v}{a_0 l_c} \tag{1}$$

The packing parameter expresses the ratio of the insoluble chain molecular volume to the volume actually occupied by the copolymer in the assembly, thus usually dictating the most likely self-assembled morphology. As a general rule,

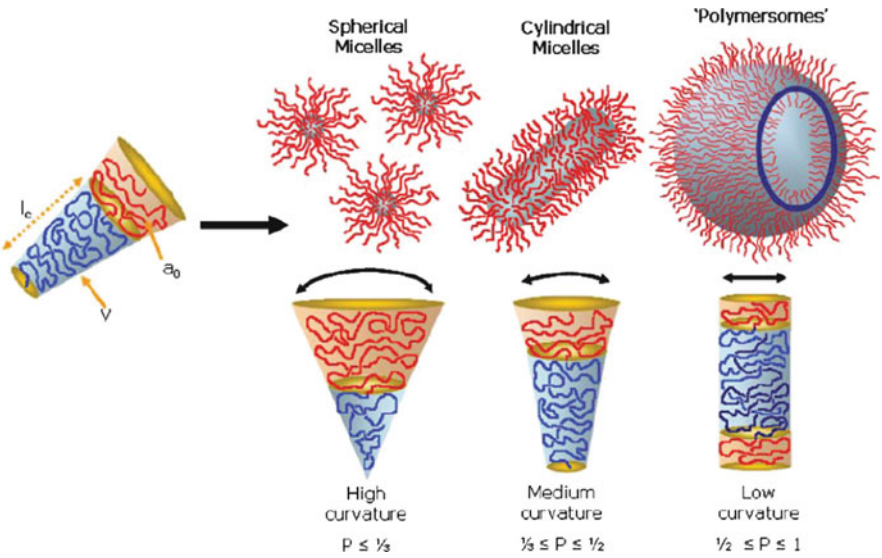

Fig. 1 Various self-assembled structures formed by amphiphilic block copolymers in a block-selective solvent. The type of structure formed is due to the inherent curvature of the molecule, which can be estimated through calculation of its dimensionless packing parameter, p. Reproduced with permission from [12]. Copyright (2009) WILEY-VCH Verlag GmbH & Co. KGaA, Weinheim

spherical micelles are formed when $p \leq 1/3$, cylindrical micelles are formed when $1/3 < p \leq 1/2$ and enclosed membrane structures (vesicles, a.k.a. polymersomes) arise when $1/2 \leq p \leq 1$ [11, 12], as depicted schematically in Fig. 1.

2.2 Micelle Preparation

The preparation of amphiphilic block copolymer micelles is usually achieved by one of the two following methods [1, 2, 5, 13]. The first method is the most straightforward way to prepare a block copolymer micellar solution and consists in the direct dissolution of the bulk sample in a selective solvent for one of the blocks. However, it should be noted that this method is generally suitable for block copolymers with relatively low molecular weight, M_w, and rather short length of the insoluble block. The solubility can be improved by a subsequent annealing processes of the solution such as standing, prolonged stirring, thermal or ultrasound treatments. The main disadvantage of these techniques is that depending on the block copolymer system, an equilibrium situation is not necessarily reached, especially when the insoluble, core-forming block is characterised by a high glass transition temperature (T_g), for example, PS. In this case, the so-called frozen micelles are formed, meaning that a unimer-micelle exchange does not take place

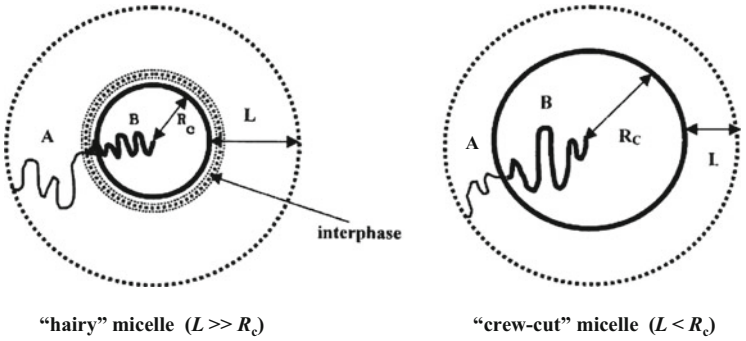

Fig. 2 Schematic representation of AB diblock copolymer micelles in a selective solvent of the A block. R_c, core radius; L, shell (corona) thickness. Adapted from [1]. Copyright (2003) Elsevier

in the solution. The features of these micelles usually depend on the two-phase morphology of the bulk block copolymer sample, as well as on the interactions of the selective solvent and the polymer microphases.

The second method is based on the dissolution of the copolymer in a nonselective solvent, i.e. a common good solvent for both blocks, thus forming molecularly dissolved chains. In order to induce micelle formation, the properties of the solvent are then changed, either by stepwise addition of a selective solvent for one block and precipitant for the other or by changing the temperature or pH of the solution, thus forming stimulus-responsive micelles. In the former case, the initial common solvent can be further eliminated by evaporation or gradually replaced by the selective solvent via a dialysis process. This technique is generally considered the preferred preparation method for micellar systems, mainly in aqueous solutions, since it prevents the formation of large aggregates and allows the formation of micelles from highly asymmetric block copolymers with a large insoluble block. However, it does not always avoid the production of "frozen micelles", due to the formation of a glassy micellar core at a given temperature and/or at a specific common/selective solvent composition. Moreover, if the starting copolymer sample has a polydispersity in composition or M_w, the dialysis process can generate polydisperse micelles regarding to their characteristics.

2.3 Micellar Morphology

2.3.1 Spherical Micelles

The most abundant micellar morphology is that of spherical micelles [1, 10]. The self-assembly of a classical amphiphilic diblock copolymer AB (A and B denote the two different blocks) leads to two different micellar structures, depending on the relative length of the blocks. These two types of spherical micelles are schematically presented in Fig. 2. When the soluble block A is larger than the insoluble

block B, the resulting micelles consist of a small dense core and a very large corona, i.e. the core radius, R_c, is much smaller than the corona thickness, L. These micelles are usually called "hairy", "starlike" or "core-shell" micelles. In the other extremity, if the insoluble block B is larger than the soluble block A, the micelles that are formed are characterised by a large dense core and a rather short highly stretched corona, with $L > R_c$, and the term "crew-cut" micelles is usually used to describe them.

Apart from the core radius and the corona thickness, other characteristic parameters of a micellar system are the aggregation number, N_{agg}, which denotes the average number of polymer chains in a micelle, the radius of gyration, R_g, and the hydrodynamic radius, R_h, of the micelle, as well as the distance between neighbouring blocks at the core/corona interface, called the grafting distance b, with b^2 expressing the area per corona chain on the core surface. These parameters are mainly controlled by the degree of polymerisation of the two blocks, N_A and N_B, and the Flory-Huggins interaction parameter χ. Moreover, the interfacial energy of the core/corona interface, the stretching energy of the block copolymer chains and the repulsion among coronal chains determine the total free energy of the micelle, which must be minimised in order to obtain an equilibrium micellar structure [2].

It is quite evident that both micellar structures can be obtained by the same amphiphilic diblock copolymer system only by changing the structural parameters of the AB copolymer. The relative lengths of the two blocks and the total M_w of the copolymer not only dictate the morphology of the resulting micelles ("hairy" vs. "crew-cut") but also determine the rest of the micellar characteristics (N_{agg}, R_c, b, etc.). Numerous experimental studies have been dedicated to the investigation of this notion, and most typical examples of the studied diblock copolymer systems include PS-PEO, PS-PI, PS-PAA and PPO-PEO among others [1, 2, 10].

Spherical micelles can also result from the self-assembly of triblock copolymers of the ABA type. When these copolymers are dissolved in a selective solvent for the outer A blocks, they form "starlike" micelles, as seen in Fig. 3a. The situation is more complex for the micellisation of ABA copolymers in a selective solvent of the middle B block. If the concentration of the copolymer is low and/or the A blocks have a relatively small M_w, isolated "flower-like" micelles can be assembled, where the B block is looped and the A blocks participate in the same micellar core (Fig. 3b). However, an increase in the concentration of the copolymer or the M_w of the A blocks could lead to micelle association into larger aggregates due to partial conversion from loops to bridges, i.e. the A blocks of the copolymer chain can be located in two different micellar cores (Fig. 3c). Both theoretical [14] and experimental investigations of the self-assembly of ABA triblock copolymers have been carried out, e.g. studies on PAI-PS-PAI copolymers dissolved in DMF [15], as well as PBO-PEO-PBO in water [16, 17].

The introduction of a third block leads to another intriguing class of triblock copolymers that of the ABC type, since it can provide interesting new functionalities and higher diversity of micellar organisations. Depending on the selective solvent, one or two of the triblock copolymer blocks can be insoluble. In the first case, micelles with a compartmentalised corona are formed, while in the second

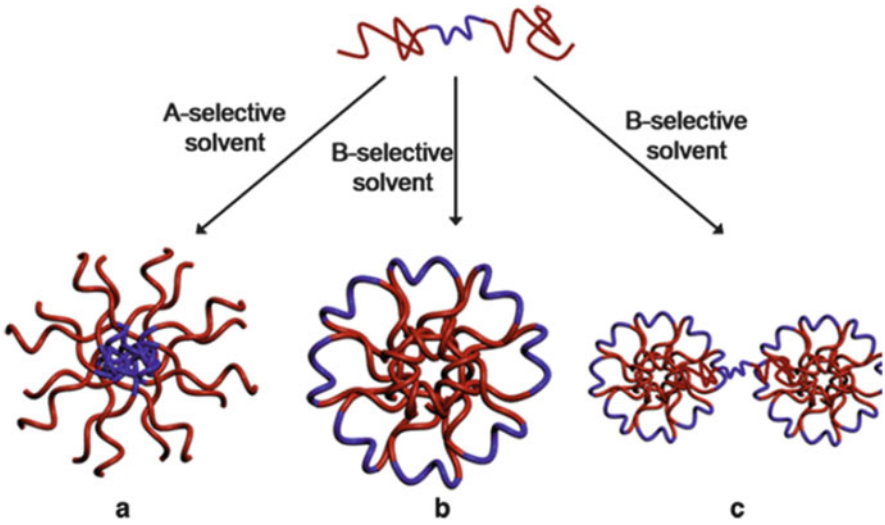

Fig. 3 Self-assembly of ABA triblock copolymers under different conditions. (**a**) "Starlike" micelles. (**b**) "Flower-like" micelles. (**c**) Micelle assembly. Reproduced with permission from [10]. Copyright (2011) Springer-Verlag

case, a compartmentalisation of the core is observed. More specifically, ABC copolymers in a selective solvent for the C block (or equivalently the A block) self-assemble into micelles where the first insoluble A block forms the core, the second insoluble B block is located around the core and the third soluble block C extends in the solution, thus forming the micellar corona. This type of micelles is called "onion", "three-layer" or "core-shell-corona" micelles. When one of the three blocks is insoluble in the specific solvent, the block sequence, i.e. the copolymer architecture, influences the resulting micellar structure. If the insoluble block is located at one extremity of the triblock (A or C block), "core-shell-corona" micelles with a compartmentalised (two-layer) corona are assembled, while when the insoluble block is located between the two soluble ones (B block), "core-corona" micelles are formed. The latter can be further distinguished into two categories: micelles that have a mixed corona and micelles with a laterally compartmentalised corona known as "Janus" micelles. This segregation of the corona in "Janus" micelles usually occurs due to high incompatibility of the two soluble blocks. All the above-mentioned types of micelles are schematically presented in Fig. 4. Characteristic examples of ABC triblock copolymer micellar systems can be found in the review of Gohy et al. [18], including studies of PEHA-PMMA-PAA, PS-P2VP-PEO, PI-P2VP-PEO, PS-PMMA-PAA and so on triblock copolymers in various selective solvents.

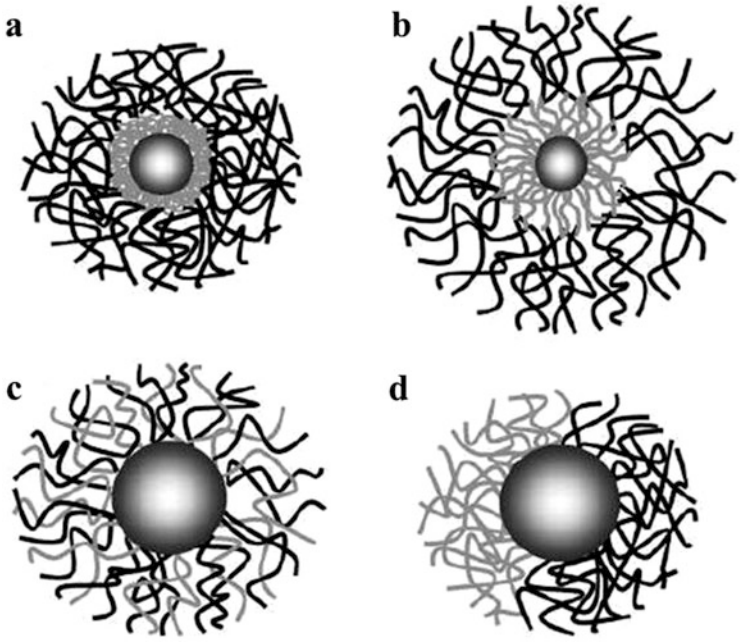

Fig. 4 Schematic representation of different types of micelles formed by ABC triblock copolymers. (**a**) "Core-shell-corona" micelles with insoluble core and shell, (**b**) "core-shell-corona" micelles with radially compartmentalised corona, (**c**) "core-corona" micelles with mixed corona and (**d**) "Janus" micelles with laterally compartmentalised corona. Adapted from [18]. Copyright (2005) Springer-Verlag

2.3.2 Cylindrical Micelles

The second of the three basic micellar morphologies is that of cylindrical micelles, which are often referred to as "worm-like", "rod-like" or even "thread-like" micelles. The fact that this morphology corresponds to the smallest range of packing parameter values ($1/3 < p \leq 1/2$) explains why "worm-like" aggregates are less frequently observed, compared to spherical micelles and polymersomes [19]. A schematic representation of a "worm-like" micelle, along with its characteristic dimensions, i.e. total length L, overall diameter d and core radius R_c, is given in Fig. 5.

In general "worm-like" micelles are classical one-dimensional structures for which the length is several times greater than their cross-sectional diameter. However, they exhibit rich structural polymorphism, in the sense that they can be relatively short (finite length) or very long (reaching the micrometre length scale), while at the same time they can either be rigid or thin and flexible. Thus, relatively short and rigid micelles are usually termed as cylindrical or "rod-like", whereas the ones that are long and thin are called "thread-like" micelles.

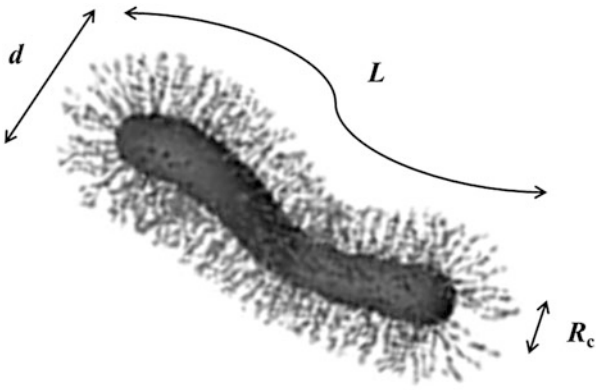

Fig. 5 Schematic representation of a "worm-like" micelle. The characteristic dimensions including total length L, overall diameter d and core radius R_c are shown. Reproduced in part with permission from [20]. Copyright (2003) The Royal Society of Chemistry

From an energetic point of view, infinitely long cylinders are more favourable than shortened cylinders with incorporated end defects, since these structures allow uniform curvature across the entire aggregate. Nevertheless, entropic demands and molecular frustration result in the formation of defects such as end caps and branch points, which are respectively more or less energetically favourable [12, 19, 21]. As a result, a great variety of cylindrical micellar morphologies have been observed, including giant [22] and short [23, 24] "worms", y-junction and end cap defects [25, 26], networks [27, 28] or even toroidal/ring-shaped micelles [29–31], which result when cylindrical structures bend and close up their ends. From these studies, it is evident that all previously mentioned types of amphiphilic copolymers, AB, ABA and ABC, can self-assemble into "worm-like" aggregates, depending on their composition. Finally, because of the cylindrical shape, these micelles provide particularly interesting potential applications in nanotechnology and medicine. For example, a great enhancement of the toughness of epoxy resins was facilitated by the incorporation of PEO-PEP cylinders [32]. In the same manner, cylindrical micelles can orient and stretch in a flowing stream, a fact that makes them ideal for flow-intensive delivery applications such as phage-mimetic drug carriers and micropore delivery agents [33, 34].

2.3.3 Polymersomes

Polymer vesicles or polymersomes constitute an extremely interesting class of macromolecular self-assembly, and since their first observation 20 years ago [35], they have attracted a rapidly increasing degree of scientific attention. This is mainly because of their resemblance to natural cellular membranes, the ability to control their size along with their interactions with the environment, their tailorable membrane properties, as well as their versatile potential applications spanning from (bio-) electronics and catalysis to medical therapy. In the last decade, the

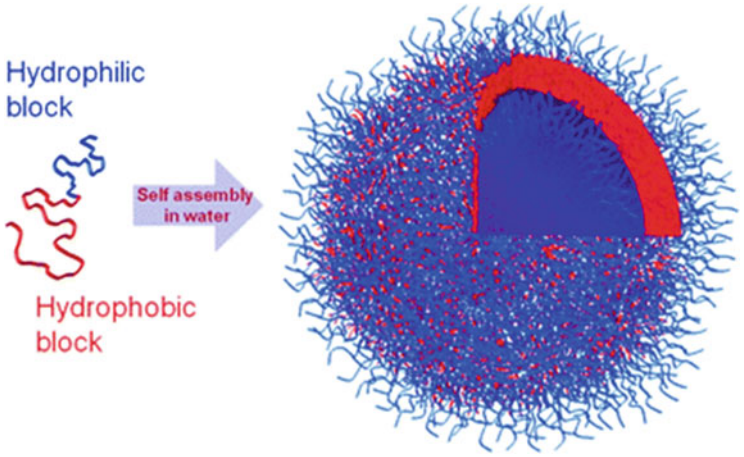

Fig. 6 Schematic representation of a polymer vesicle. Reproduced with permission from [43]. Copyright (2009) The Royal Society of Chemistry

number of studies in this field shows a substantial growth, and a significant amount of reviews on the subject is already available in the literature [12, 36–45].

As mentioned before, if the right hydrophobic/hydrophilic balance is achieved, amphiphilic block copolymers can self-assemble in water into membranes. These membranes usually close, thus forming hollow spheres with an aqueous core, as shown in Fig. 6, with sizes that vary from tens to thousands of nanometres. The resulting structures known as polymer vesicles are commonly referred to as polymersomes in analogy to the lipid-based vesicles which are called liposomes. Contrary to liposomes, polymersomes exhibit enhanced stability and toughness, reduced permeability, restricted chain mobility within the membrane and better resistance to dissolution. These characteristics are attributed to the considerably higher molecular weight of the amphiphilic copolymers compared to that of lipids. Copolymer M_w also determines the vesicular membrane thickness, which can reach up to 50 nm, whereas the liposome bilayer membranes have thicknesses of 3–5 nm. Furthermore, the enhanced mechanical properties of the polymeric vesicle membranes are a consequence of the entanglement and interdigitation that can occur between the hydrophobic chains within the membrane [12, 19].

The chain architecture and chemical composition of the polymersome-forming amphiphilic block copolymers can be either simple or rather complex giving the corresponding polymersomes their peculiar properties. The AB copolymer type, where A and B, respectively, denote the hydrophilic and hydrophobic blocks, is the simplest possible chain architecture, and the majority of polymer vesicles are produced by such copolymers, including PEO-PPO, PS-PAA, PS-PEO, PBD-PAA, PB-PEO and P2VP-PEO among others. Even so, copolymers of more complex linear architecture such as ABA, BAB, ABABA, ABC and ABCA (with C being either hydrophilic or hydrophobic) have also been reported to assemble into polymersomes [43]. A very comprehensive representation of the various membrane

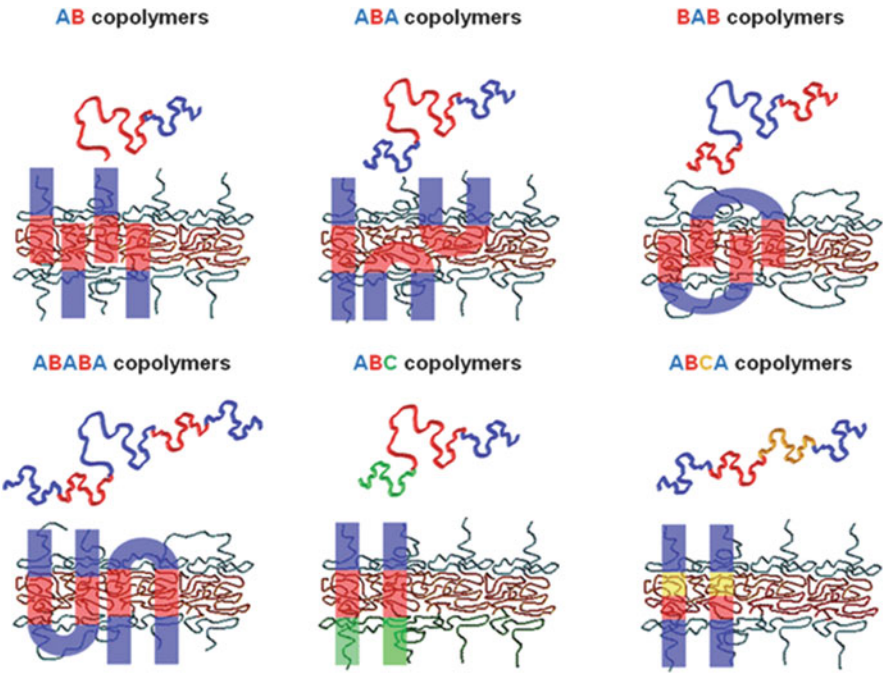

Fig. 7 Membrane conformation of polymersomes formed by diblock, triblock and multiblock copolymers. Reproduced with permission from [43]. Copyright (2009) The Royal Society of Chemistry

conformations of polymersomes formed by diblock, triblock and multiblock amphiphilic copolymers is given in Fig. 7.

Only one membrane conformation is possible for AB copolymers, where the B blocks constitute the hydrophobic layer and the A blocks extend outwards on both sides of the membrane. In the case of the ABA triblocks, the hydrophobic B block either can form a loop so as the hydrophilic A chains are on the same side of the membrane (U shape) or can stretch forming a monolayer with the two A blocks at the opposite sides of the membrane (I shape), while for the BAB type only, the U-shaped conformation is possible since the hydrophobic B chain ends must assemble into a membrane and the hydrophilic A blocks must form a loop. Similar conformations can be anticipated for ABABA pentablock copolymers. The same general rules apply when a third chemically different block is added, and although the overall geometry is the same, multiblock copolymers have an extra level of control over the polymersome structure introduced by the extra interaction between the blocks. Hence, ABC triblock copolymers assemble into asymmetric or "Janus" membranes, and the resulting vesicles are characterised by different external and internal surface chemical properties. Even more interestingly, ABCA tetrablocks (where A is hydrophilic and B and C are both hydrophobic) have been shown to

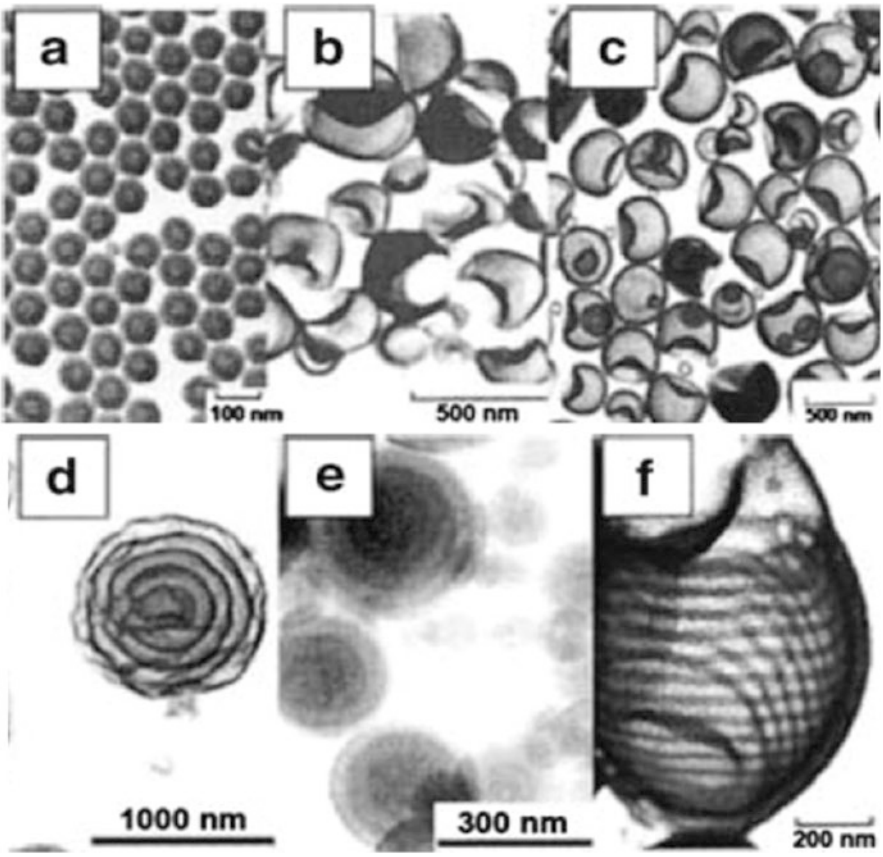

Fig. 8 Micrographs of vesicles with complex morphology. (**a**) Small uniform vesicles, (**b**) large polydisperse vesicles, (**c**) entrapped vesicles, (**d**) hollow concentric vesicles, (**e**) "onion-like" vesicles and (**f**) vesicles with tubes in the wall. Reproduced with permission from [36]. Copyright (2001) WILEY-VCH Verlag GmbH, Weinheim, Fed. Rep. of Germany

form vesicles whose membrane has an internal morphology that changes from lamellae to cylinders upon changing the volume fraction between B and C [46].

Contrary to the ideal notion that polymer vesicles are unilamellar spherical objects with uniform size and shape, in practice, a great variety of vesicular morphologies have been observed. Polymersome morphology is critically influenced by a number of factors such as the nature of the copolymers and their constituent blocks; the presence of ionisable groups or groups capable of hydrogen bonding; the solution conditions, e.g. temperature, concentration and pH; the presence of additives (salts, acids, bases, cosolvents, surfactants); as well as the method of preparation. This fact suggests that the great majority of polymersomes are nonequilibrium structures. As characteristically shown in Fig. 8, Eisenberg and co-workers [36] have managed to produce vesicles with multiple complex

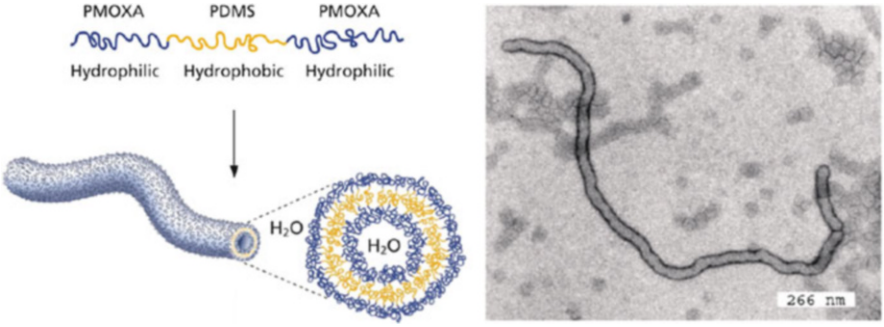

Fig. 9 Self-assembly of ABA triblock copolymers in aqueous solution and TEM image of a polymer nanotube. Reproduced with permission from [47]. Copyright (2004) The Royal Society of Chemistry

morphologies such as small uniform vesicles, large polydisperse vesicles, entrapped vesicles, hollow concentric vesicles, "onion-like" vesicles and vesicles with tubes in the wall, using six different types of polymers (PS-PAA, PS-PEO, PBD-PAA, PS-P4VPMeI, PS-P4VPDecI and PS-PMMA-PAA), only by changing parameters like the copolymer concentration and relative block lengths, the solvent composition, the temperature and the addition of ions to the system. Another interesting morphology is that observed by Grumelard et al. [47] from the self-assembly of an amphiphilic ABA copolymer (PMOXA-PDMS-PMOXA) in water, which led to the formation of a vesicular nanotube seen in Fig. 9.

Apart from their morphological diversity, polymer vesicles have been at the focus of extensive research also because of their potential applications, especially in medical fields. These kinds of applications usually exploit the unique ability of polymersomes to encapsulate hydrophilic compounds within the core and, at the same time, hydrophobic and amphiphilic molecules within the membrane. This feature combined with the enhanced mechanical properties of polymeric membranes renders them ideal delivery devices. As a result, polymer vesicles have been extensively utilised in drug delivery, gene therapy, protein delivery, medical imaging, cancer diagnosis and therapy, etc. [48–54].

2.3.4 Other Morphologies

Although spherical and cylindrical micelles, as well as polymersomes, constitute the majority of structures formed through the self-assembly of amphiphilic copolymers, lately there has been a substantial effort to create new intriguing morphologies, including multicompartment, "disc-like" and bicontinuous micelles. These classes of novel micellar morphology have been recently reviewed by Holder and Sommerdijk [55].

The term multicompartment micelles is used to describe micelles with water-soluble shells and internally segmented cores, where two (or more) separate types

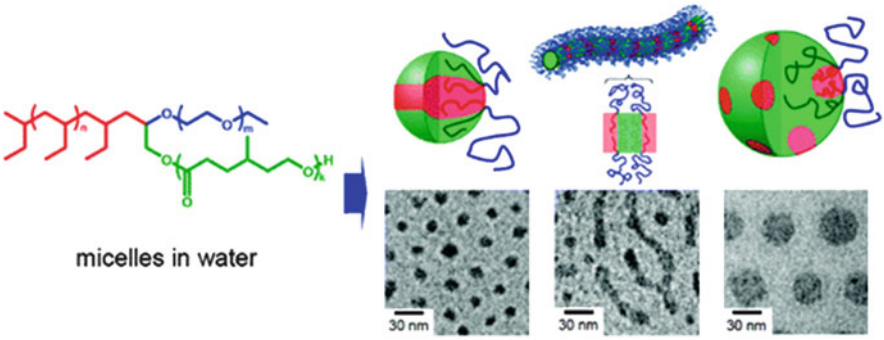

Fig. 10 Structure of a μ-((PEE)-(PEO)-(poly(γ-methyl-ε-caprolactone))) miktoarm block terpolymer, along with schematic representations and cryo-TEM micrographs of the resulting self-assembled micellar structures: "hamburger", segmented "worm-like" and "raspberry" micelles (from *left* to *right*). Reproduced with permission from [56]. Copyright (2008) American Chemical Society

of hydrophobic regions exist. Obviously, this kind of structure provides the advantage of storing two or more incompatible compounds in the different nanocompartments of the core, and it can thus be used in the simultaneous delivery of different types of pharmaceutical and/or bioactive agents which are otherwise incompatible. The overall morphology of such micelles is similar to that of spherical, "worm-like" or even vesicular structures previously discussed, while for their preparation, usually ABC-type copolymers with linear and non-linear (e.g. miktoarm star) chain architecture are used. A characteristic example is that of the self-assembly of a miktoarm star terpolymer with PEE, PEO and poly(γ-methyl-ε-caprolactone) arms (μ-EOC) studied by Lodge, Hillmyer, et al. [56]. Depending on the initial composition of the μ-EOC copolymer, different types of resulting structures with distinct hydrophobic core regions were found, i.e. "hamburger" (where a lamellar region is sandwiched between two other regions), segmented "worm-like" (where the hydrophobic regions alternate along the length of the micelles) or "raspberry" (where one region adopts spherical shapes embedded in the matrix of the other) micelles. A schematic representation of these structures is shown in Fig. 10. Another similar example is that of the multicompartment micelles formed by a linear PISC-PS-PEO triblock terpolymer, where the micellar structure is dictated by the random architecture of the PISC block, which includes hydrophilic and hydrophobic segments [57].

"Disc-like" micelles are relatively rarely observed [58–63], and they are not considered stable equilibrium morphologies, but rather transient intermediate structures which occur under specific circumstances. The latter include (a) extremely strong interfacial tension between the amphiphilic blocks typically manifested by fluoro-containing copolymers, (b) alteration of the interfacial curvature by manipulating the volumes of the core and/or corona regions (usually via the addition of organic or inorganic substances), (c) the presence of "rod-like" corona- and/or core-forming blocks thus leading to parallel arrangement of the chains in the corona/core interface or (d) the presence of crystallisable core-forming blocks which can develop closely packed flat structures [19].

Finally, in limited occasions, self-assembled aggregates with a bicontinuous structure have been reported. For example, in the case of a PS-PAA diblock copolymer in a water/DMF mixture [64], of PEO-PPO-PEO triblock copolymers in water or water/oil mixtures [65–67] and PAA-PMA-PS in water/THF mixture [68], or more complex chain architectures, like a linear-comb [69] and a comb-comb [70] diblock copolymer, are considered.

2.4 Micelle Characterisation: Experimental Techniques

Several experimental techniques are available for the investigation of micellar systems, capable of elucidating different aspects of the micellisation process, as well as the micellar structure and morphology. In a first approach, these techniques can be categorised in three subclasses: microscopy, scattering and spectroscopic techniques. Extensive reviews on the various experimental methods suitable for block copolymer micelle characterisation have been provided [6–8]. Therefore, in this section, our aim is to briefly outline the different methods used and the information they provide, along with some of their main advantages and limitations [1, 2, 71].

2.4.1 Microscopy Techniques

Atomic force, scanning and transmission electron microscopies (AFM, SEM and TEM) have been widely used for the direct visualisation of block copolymer micelles and the determination of micellar size, shape, size distribution and internal structure. All three techniques require deposition of the micelles on a flat substrate and subsequent evaporation of the solvent, while additional coating or staining of the dried samples is usually necessary for SEM or TEM imaging, respectively. Thus, one could argue that the obtained information, especially about the size of the micelles, does not correspond to that in the initial micellar solution, since the surface deposition perturbs in some extend the original micellar size. The more lately developed cryo-TEM technique overcomes these limitations, since the micellar solution is rapidly frozen by liquid nitrogen and the micelles are observed unperturbed in a glassy water phase. This comparative advantage of cryo-TEM has increased its popularity as a standard characterisation technique of macromolecular self-assembly, as highlighted in the recent review of Zhong and Pochan [72].

2.4.2 Scattering Techniques

This subcategory includes static and dynamic light scattering (SLS and DLS), along with small-angle X-ray and neutron scattering (SAXS and SANS) techniques,

which provide information on micellar morphology with the advantage of giving a mean value calculated over a large number of micelles. These are also in situ techniques that produce minimal perturbation in the state of the micelles in solution. Light scattering is a very common technique used for micelle characterisation. SLS allows for the determination of the weight average M_w and thus N_{agg} of the micelles, as well as their R_g, while information about the quality of the solvent for the coronal chains can be obtained through the estimated second virial coefficient, A_2. Moreover, due to its greater sensitivity in larger particles, SLS can be used for the measurement of cmc. The R_h of the micelles can be calculated from their diffusion coefficient obtained through DLS measurements, while at the same time information on the size distribution of the micelles and the relative amounts of individual species in the initial copolymer solution can be extracted. It should also be noted that from the combination of these two techniques, the characteristic ratio $\rho = R_g/R_h$ can be derived, which provides valuable insight on micellar morphology [73].

Small-angle scattering methods rely on the assumption of suitable models for the analysis of scattering data and have been proven very well suited for studying the structure of block copolymer micelles, as well as their interactions or ordering [74]. One of their most important features is that they allow for the independent study of the core or the corona of the micelles. More specifically, SAXS measurements yield parameters like the molecular weight, the overall size and the internal structure of the micelles, while through the appropriate model fitting, additional information on the individual dimensions of the micellar core and corona, as well as on the core/corona interface sharpness, can be acquired. In a similar manner, SANS experiments are usually conducted in deuterated solvents and/or with partially deuterated copolymers, in order to generate a sufficient scattering contrast between the core and the corona of the micelles, thus making possible the determination of their respective dimensions. Of course, the overall micellar characteristics can also be estimated in analogy to SAXS measurements.

2.4.3 Spectroscopic Techniques

From the various available spectroscopic techniques, fluorescence [75, 76] and nuclear magnetic resonance (NMR) [182] spectroscopy have been employed in the study of micellar solutions and are considered especially helpful in the investigation of local phenomena within the micelles. In fluorescence spectroscopy, probe molecules are usually utilised, which either are attached by covalent bonds to specific sites of the copolymer chain or can be easily distributed within the micelle core or corona. Energy transfer, fluorescence quenching and time-dependent fluorescence depolarisation techniques allow for the inspection of the micellar microenvironment. Owing to this local sensitivity determination of very small cmc values, probing the internal viscosity of the micelle core, as well as observation of the solubilisation of low M_w substances into the micelles, is possible. Unimer-micelle equilibrium or chain exchange between micelles can also be studied, by the use of copolymers suitably labelled with fluorophore groups.

Additional information on potential alterations of chain conformations or core/corona interface due to micellisation can also be gained. Similarly, the application of NMR spectroscopy for the study of chain dynamics in micellar systems is based mainly on the fact that block copolymer segment mobility is directly correlated to the intensity of respective NMR spectrum peaks. Thus, when the core of the micelles is formed and the mobility of the insoluble blocks is significantly reduced, the intensity of the corresponding NMR peaks is reduced accordingly.

2.4.4 Other Techniques

Other more or less commonly used experimental methods include analytical ultracentrifugation (AUC), size exclusion chromatography (SEC), viscometry and stop-flow techniques. AUC measures the velocity at which each species in solution is displaced under the influence of a strong centrifugal force [77]. Since the sedimentation velocity depends on the size, M_w and density of the species, as well as on the frictional forces developed by the solvent, information regarding these parameters can be extracted. Furthermore, this method allows for the determination of the weight fraction of micelles and unimers in the solution or even other species such as micelle aggregates. Likewise, SEC has been used to characterise the unimer/micelle distribution in the solution, along with the corresponding hydrodynamic sizes. Nevertheless, it should be noted that perturbation of the unimer-micelle equilibrium is possible during SEC experiments, so this technique is more suited for concentrations far away from the cmc or block copolymer systems that form "frozen" micelles. Viscometry is an extensively used method for the investigation of the hydrodynamic properties of block copolymer micellar solutions, providing information on the hydrodynamic size and the intrinsic viscosity of the micelles, together with an approximate estimation of their compactness. Finally, various stop-flow techniques have been employed in order to investigate the kinetics of micelle formation and dissociation.

2.5 Theoretical Aspects of Micellisation

Numerous theories, models and mathematical approaches have been developed over the years in order to describe the micellisation process and the dependence of fundamental structural parameters of the micelles, like cmc, aggregation number (N_{agg}), overall size (R_m), core radius (R_c) and corona thickness (L), on the molecular characteristics of the block copolymer, with respect to the degrees of polymerisation of the constituent blocks (N_A and N_B), as well as the Flory-Huggins interaction parameters χ between the blocks and between the blocks and the solvent. Some of these approaches use the minimisation of the total free energy of the micellar system so as to extract relations between the copolymer and micelle features, while others are based on the scaling concept of Alexander-de Gennes and

on the proposed mean-field theories [78–81]. Thorough overviews on the thermodynamic background and the different theoretical approaches have been presented by Tuzar and Kratochvil [5], Hamley [7], Linse [82], Riess [1] and Zhulina and Borisov [83].

In scaling theories, two limiting cases have to be considered for a monodisperse AB diblock copolymer in a selective solvent for the A block [82]. These are the "hairy" or "starlike" micelles, with $N_A >> N_B$ and accordingly $L > R_c$, and the "crew-cut" micelles for which $N_B >> N_A$ and $R_c > L$ (see Fig. 2). For the case of "hairy" micelles, based on the star polymer theory of Daoud and Cotton [84], the following scaling relations for N_{agg} and L have been derived:

$$N_{agg} \sim N_B^{4/5} \tag{2}$$

$$L \sim N_{agg}^{1/5} \; N_A^{3/5} \tag{3}$$

Zhulina and Birshtein [85] and Halperin [183] have obtained similar results for N_{agg}, while the corresponding scaling relations for R_c ($\sim N_B^{3/5}$) and L ($\sim N_A^{3/5} N_B^{6/25}$) are in agreement with the ones of Daoud and Cotton. For the total micellar radius, R_m, Halperin found:

$$R_m \sim N_A^{3/5} N_B^{4/25} \tag{4}$$

that demonstrates the predominant contribution of the coronal chains (A block) to the total micelle size.

For "crew-cut" micelles, the theories of Alexander and de Gennes for polymer brushes have been used, assuming micelles with uniformly stretched chains in the core and the corresponding scaling relations are:

$$R_c \sim \gamma^{1/3} N_B^{2/3} \alpha \tag{5}$$

$$N_{agg} \sim \gamma \, N_B \tag{6}$$

where γ is the interfacial tension between the A and B blocks and α is the segment length. These relations demonstrate that in this case, the dependence of the micellar parameters on N_A disappears.

However, scaling theories are not able to predict finite chain effects and polymer-solvent interactions, since they are restricted to long polymer chains in good solvents. More detailed mean-field calculations and molecular simulations are needed in order to complement these models.

Regarding semianalytical mean-field theories, Noolandi and Hong [78] and Leibler et al. [79] derived the micellar characteristics by minimising the free energy of both isolated micelles and the whole micellar system. A further development was achieved by Nagarajan and Ganesh [80], who took into account the molar volumes of the solvent and blocks A and B, the interfacial tension between the B block and the solvent and the interaction parameter between the A block and the solvent. This

way they acquired scaling relations for PPO-PEO micelles in water, which show the strong influence of the coronal block on the micellar characteristics. Specifically:

$$R_c \sim N_A^{-0.17} N_B^{0.73} \tag{7}$$

$$L \sim N_A^{0.74} \; N_B^{0.06} \tag{8}$$

$$N_{agg} \sim N_A^{-0.51} \, N_B^{1.19} \tag{9}$$

In a similar manner, the lattice self-consistent mean-field theory has been used to calculate the effects of the copolymer architecture on the self-assembly behaviour of nonionic and ionic copolymers [82, 86, 87].

Also complementary to the study of block copolymer self-assembly are analytical theories and computational simulations, mainly Monte Carlo-type simulations, as demonstrated by Mattice and Haliloğlu [88] and by Binder et al. [89]. Detailed revisions of simulation studies, along with the background of these techniques, can be found in the reviews of Binder and Muller [90] and Shelley and Shelley [91]. The main advantage of computer simulations is that they are generally straightforward methods with relatively few approximations and without any presumptions of micelle geometry or chain conformation. Moreover, they also provide the possibility to vary intermolecular forces at will in a well-controlled manner. Several aspects of the self-assembly process and basic characteristics of micelles formed by amphiphilic copolymers with different chain architectures, such as AB, ABA, BAB linear and A_2B_2 miktoarm star, have been established and compared [82, 92, 93]. Other aspects including chain-length dependence [89], dynamics of chain exchange [88], formation of surface micelles [94], solubilisation of low molecular weight substances [95, 96], chain density profiles and thickness of the interfacial region [82] have also been considered.

As a closing remark, the universality of the self-assembly mechanism should be noted. Based on experimental results from a series of PS-P4VP block copolymers in toluene, a selective solvent for PS, Förster et al. [97] obtained the following general scaling relation for N_{agg}:

$$N_{agg} = N_{agg,0} \, N_A^{-0.8} N_B^2 \tag{10}$$

When plotted as $N_{agg} N_A^{0.8} / N_{agg,0}$ versus N_B, a master curve (spanning the range of three orders of magnitude for N_B) is produced, which includes data of various diblock, triblock, graft and miktoarm star amphiphilic block copolymers, as well as low molecular weight ionic and nonionic surfactants. Most importantly, $N_{agg,0}$ is related to the surfactant packing parameter and is known for many block copolymer systems, thus allowing tuning of the aggregation number by variations in the molecular masses of the constituent blocks.

3 Representative Amphiphilic Block Copolymer-Selective Solvent Systems

As already mentioned, there has been an extensive amount of studies on the self-assembly of amphiphilic block copolymers in selective solvents over the years. In this section, we will try to give representative examples of these studies divided into two main categories regarding the solvation medium, i.e. amphiphilic copolymers in organic solvents or in aqueous solutions. The latter can be further distinguished in nonionic or ionic containing copolymers. These examples will be limited to the more commonly studied di- and triblock linear copolymers, but concise reviews on the self-assembly of amphiphilic copolymers with more complex non-linear chain architectures can be found elsewhere [98–100].

3.1 Amphiphilic Copolymers in Organic Solvents

Detailed overviews on the micellisation of amphiphilic copolymers in organic solvents are provided in the reviews of Riess [1], Gohy [2], Hamley [7] and Chu et al. [101]. Apparently, a wide range of styrene, acrylate or methacrylate and diene-based block copolymers have been investigated, while AB diblock and ABA triblock architectures have been systematically compared. One of the main conclusions is that the formation of micelles in organic solvents can generally be considered as an entropy-driven process.

Micellisation in organic media leads to the formation of the so-called reverse micelles. These micelles usually contain a polar core formed from PEO, PAA, PMMA or P2VP blocks, surrounded by a less polar corona consisting of PS, PB or PPO chains. Among the most characteristic of such systems are PEO-based di- and triblock copolymers, which have attracted considerable attention. Exemplary studies on the self-assembly of PEO-PPO and PEO-PPO-PEO copolymers in organic solvents, such as formamides, have been conducted by Lindman et al. [102, 103] and Alexandridis and Yang [104, 105]. Due to the ability of PEO to crystallise, the formation of reverse micelles in organic solvents from PEO-based block copolymers is considered in general a more complex process.

This interesting feature of PEO crystallisation has been studied for PS-PEO and PB-PEO micelles by Gervais and Gallot [106] and Gast et al. [107–109], while Wu and Chu [110] and Guo et al. [111] investigated this effect in the case of PEO-PPO-PEO copolymers. These authors have clearly demonstrated that one of the most important parameters in the crystallisation of PEO is the amount of residual water. For instance, Gast et al. [107] showed that PS-PEO copolymers in cyclopentane form micelles with N_{agg} between 17 and 100 depending on the copolymer concentration and on the water content. However, in the absence of water, the chain-folding crystallisation of PEO leads to the formation of lamellar microcrystals or

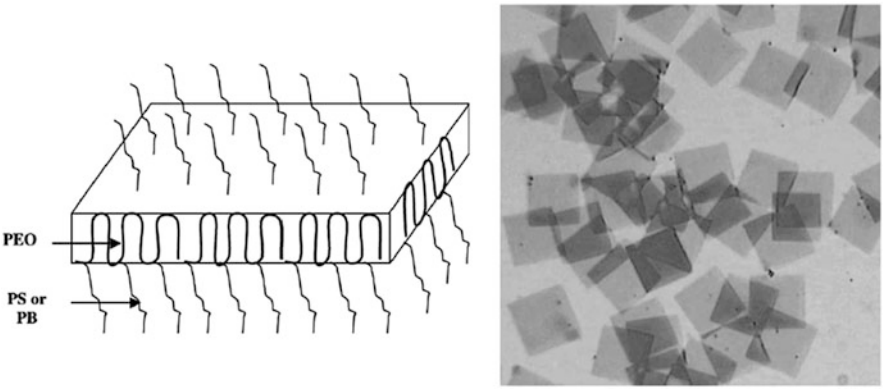

Fig. 11 Schematic structure of lamellar microcrystals or "platelets" formed by the crystallisation of PS-PEO or PB-PEO copolymer micelles in organic solvents, along with a typical micrograph of "platelets" from a PS_{100}-PEO_{2500} copolymer in methylcyclohexane. Reproduced with permission from [1]. Copyright (2003) Elsevier

"shish-kebab" structures. The resulting micelles are known as "platelets" and have an unusual lamellar morphology, as shown in Fig. 11.

Another intriguing study is that of Lodge et al. [24] for an asymmetric PS-PI copolymer in a series of organic solvents. By varying the solvent selectivity for PS, these authors documented the morphological transition of the resulting micelles from spheres to cylinders to vesicles. The various micellar structures were characterised in detail by means of SAXS and cryo-TEM measurements.

Although the majority of the investigations on amphiphilic block copolymers with an ionic block are usually considered in aqueous solutions, some studies of their self-assembly in organic solvents have also been performed. For example, diblock copolymers with a major PS block linked to ionic PAA or PMAA segments have been extensively studied by Eisenberg et al. [112, 113]. In organic solvents, such as toluene, these copolymers formed stable spherical "reverse micelles", consisting of an ionic core and a PS corona. Their characteristic size was systematically investigated by a combination of experimental techniques including TEM, SAXS, DLS and SLS. Similarly, Förster et al. [97] have conducted detailed investigations for PS-P4VP copolymers in toluene, as mentioned in Sect. 2.5. In general, PS-P2VP and PS-P4VP micelles in organic solvents have been widely used as templates for the synthesis of metallic nanoparticles [114–117].

Finally, very few studies have been devoted on the self-assembly of ABC-type amphiphilic triblock copolymers in organic solvents, especially when compared to the corresponding in aqueous media. Tsitsilianis and Sfika [118] studied the formation of spherical micelles from PS-P2VP-PMMA triblocks in toluene, a bad solvent for P2VP, by light scattering, viscometry and TEM. Mixed corona micelles were formed, with their aggregation number and size depending mainly on the molecular characteristics of the three blocks. Comparison with micelles formed from PS-P2VP diblock copolymer of similar composition revealed that the

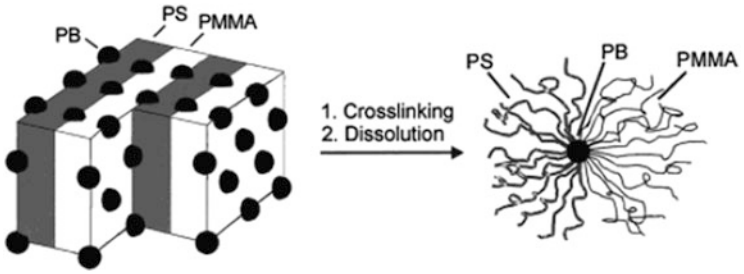

Fig. 12 Schematic representation of the bulk morphology of a PS-PB-PMMA triblock copolymer, along with the resulting "Janus" micelles after PB cross-linking and solubilisation. Reproduced with permission from [120]. Copyright (2001) American Chemical Society

terpolymers form micelles of lower N_{agg} due to the presence of the second end block. In a similar manner, the effect of solvent selectivity on the micellar characteristics of PS-PI-PMMA triblock terpolymers was investigated by Fernyhough et al. [119]. Light scattering and viscosity experiments revealed the formation of spherical mixed corona micelles with high N_{agg} and increased compactness in DMF (a nonselective solvent for PI). The size of the micelles was controlled mainly by the molecular characteristics of the soluble PS and PMMA blocks, but the molecular weight and content of the insoluble PI block also played a role. Another interesting case is that of the formation of "Janus" micelles by cross-linking the PB domains of a PS-PB-PMMA triblock copolymer in the solid state, as seen in the study of Abetz, Müller et al. [120]. The bulk morphology of this copolymer consists of lamellae of the outer PS and PMMA blocks embedding spherical domains of the PB middle block (the so-called lamellae-sphere morphology). When the PB spherical domains are cross-linked and the bulk phase is dissolved in THF, a good solvent for the outer blocks, spherical micelles with two distinct coronal hemispheres of PS and PMMA chains are formed. A schematic representation of the bulk morphology, as well as the resulting "Janus" micelles, is given in Fig. 12.

3.2 Amphiphilic Block Copolymers in Aqueous Solutions

The self-assembly of amphiphilic block copolymers in aqueous solutions has attracted considerable interest not only because of their unique properties but also due to their widespread application possibilities in technical and especially biomedical areas. As far as representative examples of such systems are concerned, a categorisation into nonionic and ionic containing copolymers is feasible.

3.2.1 Nonionic Amphiphilic Block Copolymers

This class of amphiphilic block copolymers typically includes copolymers with a PEO hydrophilic block linked to various hydrophobic blocks like PPO, PBO, PS, PMMA, etc. One of the main advantages of PEO is its non-toxic and non-immunogenic properties, which are the requirements for biomedical use.

The most extensively studied systems are apparently those of PEO-PPO and PEO-PBO di- and triblock copolymers in water. Their micellisation behaviour has been summarised in the review articles of Riess [1], Gohy [2], Hamley [7], Almgren et al. [121], Chu and Zhou [122] and Booth et al. [123, 124]. These studies showed that various micellar morphologies or even physical gels can be formed, depending on parameters such as molecular weight, composition, temperature and concentration. A number of techniques including DLS, SLS, SAXS, SANS and NMR have been utilised in order to characterise these micellar systems. A rather detailed picture of the morphology of spherical micelles formed by PEO-PPO-PEO copolymers has been established by Mortensen and Pedersen [125], who showed that the PPO core is surrounded by a dense layer of PEO segments and an outer corona of flexible PEO chains. Other similar investigations include that of Bahadur et al. [126] who examined the role of various additives on the micellisation behaviour, of Booth and co-workers [127] who were mainly interested in PEO-PBO block copolymers with long PEO sequences and of Hamley et al. [128, 129] who used in situ AFM measurements in water to characterise the morphology of PEO-PPO micelles.

Another well-studied family of PEO-based amphiphilic copolymers is that of PS-PEO diblock and PEO-PS-PEO triblock copolymers, as seen in the works of Riess and co-workers [1]. In summary, the N_{agg} for PS-PEO was found to increase as a function of the copolymer M_w at constant composition, while it decreased with PEO content for a given M_w. Moreover, it was shown that PEO-PS-PEO triblocks had lower N_{agg} than the corresponding PS-PEO diblocks. These types of micelles are generally characterised by two interesting features. The first one is that due to the high T_g of the PS blocks, the resulting micelles belong in the special category of "frozen micelles", i.e. they are nonequilibrium structures with a "glassy" core. Their second feature is that they are prone to secondary aggregation through clustering of the PEO coronal chains, as observed in various cases [130–132]. In the case of highly asymmetric PS-PEO copolymers with short PEO blocks, various "crew-cut" micellar morphologies including spheres, rods, lamellae and vesicles have been observed by Eisenberg et al. [133].

The self-assembly of copolymers containing nonionic hydrophilic PEO blocks and other hydrophobic blocks, such as PI [134] and PB [25], has also been investigated. Of particular interest is the case of PEO-PCL block copolymers, since they are biocompatible and partly biodegradable and they are thus ideal candidates for drug delivery applications [135, 136].

Contrary to AB and ABA type, ABC nonionic amphiphilic copolymers and the corresponding self-assembly studies are rather scarce. One example is that of the

investigation of the micellar properties in water of a PEO-PS-PB copolymer and its fluorinated analogue, which resulted from the selective fluorination of the PB block. The unmodified triblocks formed spherical "core-corona" micelles in aqueous solution, whereas the fluorinated analogues formed "core-shell-corona" oblate elliptical micelles. This behaviour was ascribed to the stronger segregation of the insoluble blocks and the increase in the hydrophobicity of the PB block in the latter case due to fluorination [137].

3.2.2 Ionic Amphiphilic Block Copolymers

Amphiphilic block copolymers with one ionic block constitute an intriguing class of macromolecules, since their self-assembly in aqueous solution usually leads to the formation of spherical micelles with a hydrophobic core and a polyelectrolyte corona. These micelles are particularly interesting because the intrinsic properties of their polyelectrolyte corona are strongly influenced by many parameters like pH, salt concentration, degree of dissociation, polar interactions and so on. Moreover, they can be considered as a model to spherical polyelectrolyte brushes and thus provide a unique opportunity to study polyelectrolyte properties in high concentration conditions. The micellisation behaviour of ionic amphiphilic copolymers has been reviewed by Riess [1], Gohy [2], Eisenberg et al. [112, 113], Förster et al. [138] and Cohen Stuart et al. [139].

Anionic polyelectrolyte block copolymers based on PAA or PMAA ionisable blocks have been extensively studied. Their self-assembly has been examined for a very wide compositional and molecular weight range in aqueous medium, as well as in various water/organic solvent, like dioxane or DMF, mixtures. At high pH, the (meth)acrylic blocks are ionised resulting in stable micelles with extended coronas, due to electrostatic repulsions, which exhibit typical polyelectrolyte behaviour. Characteristic examples of such systems concerning PS-PMAA diblock and PMAA-PS-PMAA triblock copolymers can be found in the studies of Munk, Tuzar, Webber and their co-workers [6, 140–142] and of Procházka et al. [143–146]. Similarly, PS-PAA copolymers have been at the focus of extensive investigations especially by the group of Eisenberg [3, 35, 37, 64, 112, 113], as well as van der Maarel et al. [147–149]. As mentioned before, Eisenberg and co-workers have studied a series of highly asymmetric PS-PAA copolymers with a long PS and a very short PAA block, and their results have been recently reviewed [3]. These copolymers led to the formation of "crew-cut" micelles, whose morphology could be changed from spheres to rods to vesicles and other complex micellar structures by decreasing the PAA/PS ratio in the starting copolymer, by adding salt or by changing the initial common organic solvent. The underlying thermodynamic and kinetic principles explaining the formation of such morphologies have also been thoroughly discussed. Some of the observed intricate morphologies formed from asymmetric PS-PAA copolymers micelles are shown in Fig. 13.

Besides PS, other hydrophobic blocks have been combined with ionic PAA or PMAA sequences as in the cases of P*n*BA-PAA and PIB-PMAA copolymers

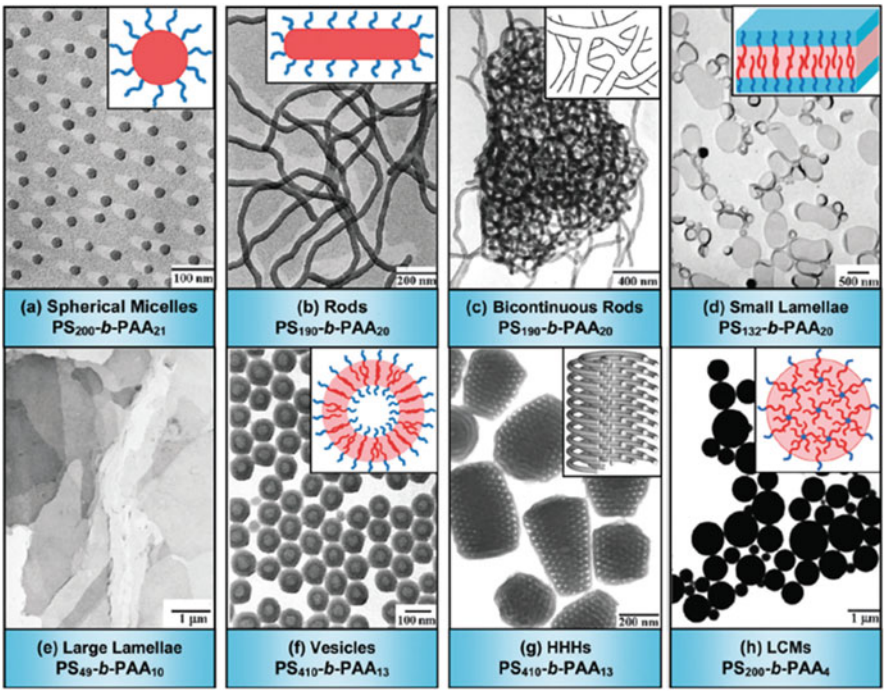

Fig. 13 TEM micrographs and corresponding schematic diagrams of various morphologies formed from amphiphilic PS_m-PAA_n copolymers. *Note*: m and n denote the degrees of polymerisation of PS and PAA, respectively. In the schematic diagrams, red represents hydrophobic PS parts, while blue denotes hydrophilic PAA segments. HHHs, hexagonally packed hollow hoops. LCMs, large compound micelles, in which inverse micelles consist of a PAA core surrounded by PS coronal chains. Reproduced with permission from [3]. Copyright (2012) The Royal Society of Chemistry

studied by Müller et al. [150, 151] or PMMA-PMAA di- and triblocks investigated by Tam et al. [152, 153]. Nevertheless, it should be noted that the ionisation degree of these anionic blocks is strongly dependent on pH and this could be a disadvantage for applications that require pH-independent ionisation behaviour. This drawback can be overcome by the use of anionic polymers derived from strong acids like PSS or PSGMA. PSS-based block copolymer like P*t*BS-PSSNa or PEE-PSSH have been the subject of studies by Guenoun et al. [154, 155] or Förster et al. [156, 157], respectively. In a similar manner, Gohy et al. [158, 159] have examined the micellisation of PSGMA-containing block copolymers like PMMA-PSGMA or P*t*BMA-PSGMA.

As far as cationic polyelectrolyte block copolymers are concerned, the number of studies is considerably smaller. The majority of the works in this area are devoted to quaternised P2VP- or P4VP-containing copolymers like the works of Selb and Gallot [160], Riess et al. [1] and Eisenberg and co-workers [36] on PS-P4VP copolymers or those of Förster et al. on PB-P2VP [138] and Procházka et al. on

P*t*BA-P2VP [161]. Another class of cationic block copolymers is that developed by Armes and co-workers [162–164], who studied the solution properties of various amino-containing poly(methacrylates), such as PDMAEMA and PDEAEMA, which exhibit stimuli responsive properties and were combined together or with other typical hydrophobic blocks.

A significant number of ABC triblock copolymers with at least one ionic block have also been investigated. One of the first examples is that of Patrickios et al. [165–167] who studied a series of triblock copolymers containing mainly PDMAEMA, PMMA and PMAA blocks. By changing the block sequence and the pH of the solution, they observed the formation of either "core-shell-corona" or mixed corona micelles. PEHA-PMMA-PAA and PS-PMMA-PAA triblocks studied by Kříž et al. [168] and Yu and Eisenberg [169], respectively, also formed "core-shell-corona" micelles in water. P2VP-containing ABC triblocks like PS-P2VP-PEO [170–172], PI-P2VP-PEO [173] and PB-P2VP-PEO [1] are the subject of various studies. Gohy and Jérôme [170, 171] showed that an interesting feature of these copolymers is that they form pH-responsive three-layered micelles, with a collapsed (pH > 5) or a swollen (pH < 5) P2VP middle shell, due to the protonation of the pyridine groups.

Less common are the ABC copolymers with one middle polyelectrolyte and two hydrophobic blocks, whose self-assembly in water usually leads to the formation of "flower-like" micelles. Such micelles have been reported by Tsitsilianis et al. in the case of PS-PAA-P*n*BMA [174] or P2VP-PAA-P*n*BMA at pH above 5 [31]. Finally, two more examples of the formation of mixed corona micelles are those observed from the micellisation of a PEO-PS-P4VP triblock copolymer studied by Chen et al. [175] or in the case of PEG-P*n*BA-PDMAEMA triblock investigated by Won et al. [176].

4 Potential Applications and Conclusions

From early on, the unique properties of amphiphilic block copolymers have been exploited in numerous applications, since their surface activity renders them suitable candidates for many industrial and pharmaceutical preparations as dispersants, emulsifiers, wetting agents, foam stabilisers, flocculants, demulsifies, viscosity modifiers, etc. [1, 8].

Among the various possible utilisations of block copolymers, one of the most important categories is that of biomedical applications, as evidenced by the significantly large number of relative studies and reviews [12, 19, 49, 177–181]. Block copolymers in their colloidal form, i.e. micelles or vesicles, have been extensively used as drug delivery systems and carriers of diagnostic agents and in gene therapy. Especially in drug delivery, three major strategies have been developed concerning (a) micelle-forming conjugates of drugs and block copolymers, where the drug is covalently linked to one of the sequences of the copolymer; (b) drugs non-covalently incorporated into the block copolymer, that is, the formation of

the so-called micellar microcontainers; and (c) polyion complex micelles formed between oppositely charged polyelectrolyte block copolymers. The major interest of block copolymers as drug delivery nanosystems stems from the ability to adjust the chemical nature of the blocks along with the molecular characteristics of the copolymer (molecular weight, composition, presence of functional groups for active targeting), thus optimising the performance of the delivery system. Furthermore, block copolymers offer the advantages of tunable dimensions in the range of 10–100 nm, of relatively high cmc and thus enhanced thermodynamic and kinetic stability of the micelles during dilution occurring in biological fluids, of increased targeting efficiency through suitable corona block end-group functionalisation and finally of adjustable distribution, as well as total amount of solubilised drug.

In a similar manner, several nanoparticles have been produced in the presence of block copolymers in selective solvents so as to form micelles that encapsulate particles such as metal salts. Consequently, these micelles are chemically converted to finely disperse colloidal hybrid polymer/metal particles with interesting catalytic, non-linear optic, semiconductor and magnetic properties [1, 20]. Finally, another area of potential application of amphiphilic block copolymers is that involving surface modification through the adsorption of block copolymer micelles or film formation. The use of a suitable micellar system allows for the alteration of specific surface characteristics, such as wetting and biocompatibility, or even enables the dispersion and stabilisation of solid pigment particles in a liquid or solid phase [1, 178].

In conclusion, the self-assembly of amphiphilic block copolymers in selective solvents constitutes a scientific field of ever increasing interest not only from the fundamental understanding point of view but also due to the variety of practical application possibilities. The virtually countless studies that have been devoted in this area so far have revealed a cornucopia of possible self-aggregated structures, from simple spherical micelles and vesicles to sophisticated multicompartment segregated nano-objects. Nevertheless, as our understanding of the basic intramolecular and intermolecular interactions, which govern the self-assembly process, grows and the synthetic capabilities continue to advance, allowing the preparation of copolymers with remarkably diverse architectures and intriguing functionalities, this field of research will always remain active providing new pathways for exploration.

References

1. Riess G (2003) Micellization of block copolymers. Prog Polym Sci 28:1107–1170
2. Gohy J-F (2005) Block copolymer micelles. Adv Polym Sci 190:65–136
3. Mai Y, Eisenberg A (2012) Self-assembly of block copolymers. Chem Soc Rev 41:5969–5985
4. Price C (1982) Colloidal properties of block copolymers. In: Goodman I (ed) Developments in block copolymers. Applied Science, London

5. Tuzar Z, Kratochvil P (1993) Micelles of block and graft copolymers in solution. In: Matijevic E (ed) Surface and colloid science, vol 15. Plenum, New York
6. Webber SE, Munk P, Tuzar Z (eds) (1996) Solvents and self-organization of polymers, NATO ASI series, series E: applied sciences, vol 327. Kluwer, Dordrecht
7. Hamley IW (ed) (1998) The physics of block copolymers. Oxford Science, Oxford
8. Alexandridis P, Lindman B (eds) (2000) Amphiphilic block copolymers: self assembly and applications. Elsevier, Amsterdam
9. Riess G, Dumas PH, Hurtrez G (2002) Block copolymer micelles and assemblies, MML series 5. Citus, London
10. Quémener D, Deratani A, Lecommandoux S (2012) Dynamic assembly of block-copolymers. Top Curr Chem 322:165–192
11. Smart T, Lomas H, Massignani M, Flores-Merino MV, Ruiz Perez L, Battaglia G (2008) Block copolymer nanostructures. Nano Today 3:38–46
12. Blanazs A, Armes SP, Ryan AJ (2009) Self-assembled block copolymer aggregates: from micelles to vesicles and their biological applications. Macromol Rapid Commun 30:267–277
13. Munk P (1996) Equilibrium and nonequilibrium polymer micelles. In: Webber SE, Munk P, Tuzar Z (eds) NATO ASI series, series E: applied sciences, vol 327. Kluwer, Dordrecht
14. Kong W, Li B, Jin Q, Ding D (2010) Complex micelles from self-assembly of ABA triblock copolymers in B-selective solvents. Langmuir 26:4226–4232
15. Giacomelli FC, Riegel IC, Petzhold CL, da Silveria NP, Štěpánek P (2009) Aggregation behavior of a new series of ABA triblock copolymers bearing short outer A blocks in B-selective solvent: from free chains to bridged micelles. Langmuir 25:731–738
16. Zhou Z, Yang Y-W, Booth C, Chu B (1996) Association of a triblock ethylene oxide (E) and butylene oxide (B) copolymer (B(12)E(260)B(12)) in aqueous solution. Macromolecules 29:8357–8361
17. Liu T, Zhou Z, Wu C, Nace VM, Chu B (1998) Dominant factors on the micellization of BnEmBn-type triblock copolymers in aqueous solution. J Phys Chem B 102:2875–2882
18. Fustin C-A, Abetz V, Gohy J-F (2005) Triblock terpolymer micelles: a personal outlook. Eur Phys J E 16:291–302
19. Rangelov S, Pispas S (eds) (2013) Polymer and polymer-hybrid nanoparticles: from synthesis to biomedical applications. CRC Press/Taylor & Francis Group, Boca Raton
20. Förster S, Konrad M (2003) From self-organizing polymers to nano- and biomaterials. J Mater Chem 13:2671–2688
21. Dan N, Safran SA (2006) Junctions and end-caps in self-assembled non-ionic cylindrical micelles. Adv Colloid Interface Sci 123:323–331
22. Won YY, Davis HT, Bates FS (1999) Giant wormlike rubber micelles. Science 283:960–963
23. Won YY, Brannan AK, Davis HT, Bates FS (2002) Cryogenic transmission electron microscopy (cryo-TEM) of micelles and vesicles formed in water by poly(ethylene oxide)-based block copolymers. J Phys Chem B 106:3354–3364
24. Bang J, Jain S, Li Z, Lodge TP, Pedersen JS, Kesselman E, Talmon Y (2006) Sphere, cylinder, and vesicle nanoaggregates in poly(styrene-*b*-isoprene) diblock copolymer solutions. Macromolecules 39:1199–1208
25. Jain S, Bates FS (2003) On the origins of morphological complexity in block copolymer surfactants. Science 300:460–464
26. Jain S, Bates FS (2004) Consequences of nonergodicity in aqueous binary PEO-PB micellar dispersions. Macromolecules 37:1511–1523
27. Jain S, Gong X, Scriven LE, Bates FS (2006) Disordered network state in hydrated block-copolymer surfactants. Phys Rev Lett 96:138304
28. Quémener D, Bonniol G, Phan TNT, Gigmes D, Bertin D, Deratani A (2010) Free-standing nanomaterials from block copolymer self-assembly. Macromolecules 43:5060–5065
29. Pochan DJ, Chen Z, Cui H, Hales K, Qi K, Wooley KL (2004) Toroidal triblock copolymer assemblies. Science 306:94–97

30. Zhu J, Liao Y, Jiang W (2004) Ring-shaped morphology of "crew-cut" aggregates from ABA amphiphilic triblock copolymer in a dilute solution. Langmuir 20:3809–3812
31. Tsitsilianis C, Roiter Y, Katsampas I, Minko S (2008) Diversity of nanostructured self-assemblies from a pH-responsive ABC terpolymer in aqueous media. Macromolecules 41:925–934
32. Dean JM, Verghese NE, Pham HQ, Bates FS (2003) Nanostructure toughened epoxy resins. Macromolecules 36:9267–9270
33. Kim Y, Dalhaimer P, Christian DA, Discher DE (2005) Polymeric worm micelles as nanocarriers for drug delivery. Nanotechnology 16:S484
34. Dalhaimer P, Bates FS, Discher DE (2003) Single molecule visualization of stable, stiffness-tunable, flow-conforming worm micelles. Macromolecules 36:6873–6877
35. Zhang L, Eisenberg A (1995) Multiple morphologies of "crew-cut" aggregates of polystyrene-*b*-poly(acrylic acid) block copolymers. Science 268:1728–1731
36. Burke S, Shen H, Eisenberg A (2001) Multiple vesicular morphologies from block copolymers in solution. Macromol Symp 175:273–283
37. Discher DE, Eisenberg A (2002) Polymer vesicles. Science 297:967–973
38. Antonietti M, Förster S (2003) Vesicles and liposomes: a self-assembly principle beyond lipids. Adv Mater 15:1323–1333
39. Opsteen JA, Cornelissen JJLM, van Hest JCM (2004) Block copolymer vesicles. Pure Appl Chem 76:1309–1319
40. Kita-Tokarczyk K, Grumelard J, Haefele T, Meier W (2005) Block copolymer vesicles–using concepts from polymer chemistry to mimic biomembranes. Polymer 46:3540–3563
41. Hamley IW (2005) Nanoshells and nanotubes from block copolymers. Soft Matter 1:36–43
42. Li M-H, Keller P (2009) Stimuli-responsive polymer vesicles. Soft Matter 5:927–937
43. LoPresti C, Lomas H, Massignani M, Smart T, Battaglia G (2009) Polymersomes: nature inspired nanometer sized compartments. J Mater Chem 19:3576–3590
44. Malinova V, Belegrinou S, de Bruyn Ouboter D, Meier WP (2010) Biomimetic block copolymer membranes. Adv Polym Sci 224:113–165
45. Le Meinsa J-F, Sandre O, Lecommandoux S (2011) Recent trends in the tuning of polymersomes' membrane properties. Eur Phys J E 34:14
46. Brannan AK, Bates FS (2004) ABCA tetrablock copolymer vesicles. Macromolecules 37:8816–8819
47. Grumelard J, Taubert A, Meier W (2004) Soft nanotubes from amphiphilic ABA triblock macromonomers. Chem Commun 13:1462–1463
48. Ahmed F, Photos PJ, Discher DE (2006) Polymersomes as viral capsid mimics. Drug Dev Res 67:4–14
49. Discher DE, Ortiz V, Srinivas G, Klein ML, Kim Y, Christian D, Cai S, Photos P, Ahmed F (2007) Emerging applications of polymersomes in delivery: from molecular dynamics to shrinkage of tumors. Prog Polym Sci 32:838–857
50. Levine DH, Ghoroghchian PP, Freudenberg J, Zhang G, Therien MJ, Greene MI, Hammer DA, Murali R (2008) Polymersomes: a new multi-functional tool for cancer diagnosis and therapy. Methods 46:25–32
51. Christian DA, Cai S, Bowen DM, Kim Y, Pajerowski JD, Discher DE (2009) Polymersome carriers: from self-assembly to siRNA and protein therapeutics. Eur J Pharm Biopharm 71:463–474
52. Onaca O, Enea R, Hughes DW, Meier W (2009) Stimuli-responsive polymersomes as nanocarriers for drug and gene delivery. Macromol Biosci 9:129–139
53. Meng F, Zhong Z, Feijen J (2009) Stimuli-responsive polymersomes for programmed drug delivery. Biomacromolecules 10:197–209
54. Massignani M, Lomas H, Battaglia G (2010) Polymersomes: a synthetic biological approach to encapsulation and delivery. Adv Polym Sci 229:115–154
55. Holder SJ, Sommerdijk NAJM (2011) New micellar morphologies from amphiphilic block copolymers: disks, toroids and bicontinuous micelles. Polym Chem 2:1018–1028

56. Saito N, Liu C, Lodge TP, Hillmyer MA (2008) Multicompartment micelles from polyester-containing ABC miktoarm star terpolymers. Macromolecules 41:8815–8822
57. Uchman M, Štěpánek M, Procházka K, Mountrichas G, Pispas S, Voets IK, Walther A (2009) Multicompartment nanoparticles formed by a heparin-mimicking block terpolymer in aqueous solutions. Macromolecules 42:5605–5613
58. Constancis A, Meyrueix R, Bryson N, Huille S, Grosselin JM, Gulik-Krzywicki T, Soula G (1999) Macromolecular colloids of diblock poly(amino acids) that bind insulin. J Colloid Interface Sci 217:357–368
59. Lodge TP, Hillmyer MA, Zhou ZL, Talmon Y (2004) Access to the superstrong segregation regime with nonionic ABC copolymers. Macromolecules 37:6680–6682
60. Li Z, Chen Z, Cui H, Hales K, Qi K, Wooley KL, Pochan DJ (2005) Disk morphology and disk-to-cylinder tunability of poly(acrylic acid)-*b*-poly(methyl acrylate)-*b*-polystyrene triblock copolymer solution-state assemblies. Langmuir 21:7533–7539
61. Edmonds WF, Li ZB, Hillmyer MA, Lodge TP (2006) Disk micelles from nonionic coil-coil diblock copolymers. Macromolecules 39:4526–4530
62. Cui H, Chen Z, Wooley KL, Pochan DJ (2006) Controlling micellar structure of amphiphilic charged triblock copolymers in dilute solution via coassembly with organic counterions of different spacer lengths. Macromolecules 39:6599–6607
63. Wang W, Liu R, Li Z, Meng C, Wu Q, Zhu F (2010) Synthesis and self-assembly of new double-crystalline amphiphilic polyethylene-*block*-poly[oligo(ethylene glycol) methyl ether methacrylate] coil-brush diblock copolymer. Macromol Chem Phys 211:1452–1459
64. Yu K, Zhang LF, Eisenberg A (1996) Novel morphologies of "crew-cut" aggregates of amphiphilic diblock copolymers in dilute solution. Langmuir 12:5980–5984
65. Zhang K, Khan A (1995) Phase behavior of poly(ethylene oxide)-poly(propylene oxide)-poly (ethylene oxide) triblock copolymers in water. Macromolecules 28:3807–3812
66. Hecht E, Mortensen K, Hoffmann H (1995) L3 phase in a binary block copolymer/water system. Macromolecules 28:5465–5476
67. Alexandridis P, Olsson U, Lindman B (1998) A record nine different phases (four cubic, two hexagonal, and one lamellar lyotropic liquid crystalline and two micellar solutions) in a ternary isothermal system of an amphiphilic block copolymer and selective solvents (water and oil). Langmuir 14:2627–2638
68. Hales K, Chen Z, Wooley KI, Pochan DJ (2008) Nanoparticles with tunable internal structure from triblock copolymers of PAA-*b*-PMA-*b*-PS. Nano Lett 8:2023–2026
69. Parry AL, Bomans PHH, Holder SJ, Sommerdijk N, Biagini SCG (2008) Cryo electron tomography reveals confined complex morphologies of tripeptide-containing amphiphilic double-comb diblock copolymers. Angew Chem Int Ed 47:8859–8862
70. McKenzie BE, Nudelman F, Bomans PHH, Holder SJ, Sommerdijk N (2010) Temperature-responsive nanospheres with bicontinuous internal structures from a semicrystalline amphiphilic block copolymer. J Am Chem Soc 132:10256–10259
71. Pispas S (2003) Dilute solutions of block copolymers in selective solvents. In: Hadjichristidis N, Pispas S, Floudas G (eds) Block copolymers: synthetic strategies, physical properties, and applications. Wiley, Hoboken, NJ
72. Zhong S, Pochan DJ (2010) Cryogenic transmission electron microscopy for direct observation of polymer and small-molecule materials and structures in solution. Polym Rev 50:287–320
73. Schärtl W (2007) Light scattering from polymer solutions and nanoparticles dispersions. Springer, Berlin
74. Pedersen JS, Svaneborg C (2002) Scattering from block copolymer micelles. Curr Opin Colloid Interface Sci 7:158–166
75. Procházka K, Limpouchová Z, Uhlík F, Košovan P, Matějíček P, Štěpánek M, Uchman M, Kuldová J, Šachl R, Humpolíčková J, Hof M (2011) Fluorescence spectroscopy as a tool for investigating the self-organized polyelectrolyte systems. Adv Polym Sci 241:187–249

76. Koynov K, Butt H-J (2012) Fluorescence correlation spectroscopy in colloid and interface science. Curr Opin Colloid Interface Sci 17:377–387
77. Mächtle W, Börger L (2006) Analytical ultracentrifugation of polymers and nanoparticles. Springer, Berlin
78. Noolandi J, Hong KM (1983) Theory of block copolymer micelles in solution. Macromolecules 16:1443–1448
79. Leibler L, Orland H, Wheeler JC (1983) Theory of critical micelle concentration for solutions of block copolymers. J Chem Phys 79:3550–3557
80. Nagarajan R, Ganesh K (1989) Block copolymer self-assembly in selective solvents: theory of solubilization in spherical micelles. Macromolecules 22:4312–4325
81. Hurter PN, Scheutjens JMHM, Hatton TA (1993) Molecular modeling of micelle formation and solubilization in block copolymer micelles. 1. A self-consistent mean-field lattice theory. Macromolecules 26:5592–5601
82. Linse P (2000) Modelling of self-assembly of block copolymers in selective solvent. In: Alexandridis P, Lindman B (eds) Amphiphilic block copolymers: self assembly and applications. Elsevier, Amsterdam
83. Zhulina EB, Borisov OV (2012) Theory of block polymer micelles: recent advances and current challenges. Macromolecules 45:4429–4440
84. Daoud M, Cotton JP (1982) Star shaped polymers: a model for the conformation and its concentration dependence. J Phys (France) 43:531–538
85. Zhulina EB, Birshtein TM (1985) Conformations of block-copolymer molecules in selective solvents (micellar structures). Polym Sci USSR 27:570–578
86. Shusharina NP, Linse P, Khokhlov AR (2000) Lattice mean-field modeling of charged polymeric micelles. Macromolecules 33:8488–8496
87. Monzen M, Kawakatsu T, Doi M, Hasegawa R (2000) Micelle formation in triblock copolymer solutions. Comput Theor Polym Sci 10:275–280
88. Haliloğlu T, Mattice WL (1996) Monte Carlo simulations of self-assembly in macromolecular systems. In: Webber SE, Munk P, Tuzar Z (eds) Solvents and self-organization of polymers, vol 327, NATO ASI series, series E: applied sciences. Kluwer, Dordrecht
89. Milchev A, Bhattacharya A, Binder K (2001) Formation of block copolymer micelles in solution: a Monte Carlo study of chain length dependence. Macromolecules 34:1881–1893
90. Binder K, Muller M (2000) Monte Carlo simulation of block copolymers. Curr Opin Colloid Interface Sci 5:315–323
91. Shelley JC, Shelley MY (2000) Computer simulation of surfactant solutions. Curr Opin Colloid Interface Sci 5:101–110
92. Kim SH, Jo WH (2001) A Monte Carlo simulation for the micellization of ABA- and BAB-type triblock copolymers in a selective solvent. Macromolecules 34:7210–7218
93. Kim KH, Kim SH, Huh J, Jo WH (2002) Micellization of Π-type copolymers in a selective solvent: a Monte Carlo simulation. ACS Polym Prepr (Div Polym Chem) 43:438–439
94. Milchev A, Binder K (1999) Formation of surface micelles from adsorbed asymmetric block copolymers: a Monte Carlo study. Langmuir 15:3232–3241
95. Hurter PN, Alexandridis P, Hatton TA (1995) Solubilization in amphiphilic copolymer solutions. In: Christian SD, Scamehorn JF (eds) Solubilization in surfactant aggregate. Marcel Dekker, New York
96. Chen Y, Shew CY (2001) Monte Carlo simulations for drug carrying capacity of micelles. ACS Polym Prepr (Div Polym Chem) 42:626–627
97. Förster S, Zisenis M, Wenz E, Antonietti M (1996) Micellization of strongly segregated block copolymers. J Chem Phys 104:9956–9970
98. Pitsikalis M, Pispas S, Mays JW, Hadjichristidis N (2001) Nonlinear block copolymer architectures. Adv Polym Sci 135:1–137
99. Hadjichristidis N, Iatrou H, Pitsikalis M, Pispas S, Avgeropoulos A (2005) Linear and non-linear triblock terpolymers. Synthesis, self-assembly in selective solvents and in bulk. Prog Polym Sci 30:725–782

100. Ge Z, Liu S (2009) Supramolecular self-assembly of nonlinear amphiphilic and double hydrophilic block copolymers in aqueous solutions. Macromol Rapid Commun 30:1523–1532
101. Liu T, Liu LZ, Chu B (2000) Formation of amphiphilic block copolymer micelles in nonaqueous solution. In: Alexandridis P, Lindman B (eds) Amphiphilic block copolymers: self assembly and applications. Elsevier, Amsterdam
102. Samii AA, Lindman B, Karlstrom G (1990) Phase behavior of some nonionic polymers in nonaqueous solvents. Prog Colloid Polym Sci 82:280–284
103. Samii AA, Karlstrom G, Lindman B (1991) Phase behavior of poly(ethylene oxide)-poly (propylene oxide) block copolymers in nonaqueous solution. Langmuir 7:1067–1071
104. Alexandridis P, Yang L (2000) Micellization of polyoxyalkylene block copolymers in formamide. Macromolecules 33:3382–3391
105. Yang L, Alexandridis P (2000) Polyoxyalkylene block copolymers in formamide-water mixed solvents: micelle formation and structure studied by SANS. Langmuir 16:4819–4829
106. Gervais M, Gallot B (1977) Influence of the nature of the solvent on the lamellar crystalline structures of block copolymers with an amorphous block and a crystallizable PEO block. Makromol Chem 178:2071–2078
107. Vagberg LJM, Cogan KA, Gast AP (1991) Light scattering study of starlike polymeric micelles. Macromolecules 24:1670–1677
108. Gast AP, Vinson PK, Cogan-Farinas KA (1993) An intriguing morphology in crystallisable block copolymers. Macromolecules 26:1774–1776
109. Lin EK, Gast AP (1996) Semicrystalline diblock copolymer platelets in dilute solution. Macromolecules 29:4432–4441
110. Wu G, Chu B (1994) Light-scattering studies of a block poly(oxyethylene-oxypropylene-oxyethylene) copolymer in water/o-xylene mixtures. Macromolecules 27:1766–1773
111. Guo C, Liu HZ, Chen JY (2000) A fourier transform infrared study on water-induced reverse micelle formation of block copoly(oxyethylene-oxypropylene-oxyethylene) in organic solvent. Colloids Surf A 175:193–202
112. Moffitt M, Zhang L, Khougaz K, Eisenberg A (1996) Micellization of ionic block copolymers in three dimensions. In: Webber SE, Munk P, Tuzar Z (eds) NATO ASI series, series E: applied sciences, vol 327. Kluwer, Dordrecht
113. Zhang L, Khougaz K, Moffitt M, Eisenberg A (2000) Self assembly of block polyelectrolytes. In: Alexandridis P, Lindman B (eds) Amphiphilic block copolymers: self-assembly and applications. Elsevier, Amsterdam
114. Roescher A, Möller M (1995) Extraction of aqueous gold sols with styrene/2-vinylpyridine block copolymers in toluene. Adv Mater 7:151–154
115. Antonietti M, Wenz E, Bronstein LM, Seregina MS (1995) Synthesis and characterization of noble metal colloids in block copolymer micelles. Adv Mater 7:1000–1005
116. Förster S, Antonietti M (1998) Amphiphilic block copolymers in structure-controlled nanomaterial hybrids. Adv Mater 10:195–217
117. Sulman E, Bodrova Y, Matveeva V, Semagina N, Cerveny L, Kurtc V, Bronstein L, Platonova O, Valetsky P (1999) Hydrogenation of dehydrolinalool with novel catalyst derived from Pd colloids stabilized in micelle cores of polystyrene-poly-4-vinylpyridine block copolymers. Appl Catal A 176:75–81
118. Tsitsilianis C, Sfika V (2001) Heteroarm star-like micelles formed from polystyrene-*block*-poly(2-vinyl pyridine)-*block*-poly(methyl methacrylate) ABC copolymers in toluene. Macromol Rapid Commun 22:647–651
119. Fernyhough CM, Pantazis D, Pispas S, Hadjichristidis N (2004) The micellar behavior of linear triblock terpolymers of styrene (S), isoprene (I), and methyl methacrylate (MMA) in selective solvents for PS and PMMA. Eur Polym J 40:237–244
120. Erhardt R, Böker A, Zettl H, Kaya H, Pyckhout-Hintzen W, Krausch G, Abetz V, Müller AHE (2001) Janus micelles. Macromolecules 34:1069–1075

121. Almgren M, Brown W, Hvidt S (1995) Self-aggregation and phase behavior of PEO-PPO-PEO block copolymers in aqueous solution. Colloid Polym Sci 273:2–15
122. Chu B, Zhou Z (1996) Physical chemistry of polyoxyalkylene block copolymer surfactants. In: Nace VM (ed) Nonionic surfactants: polyoxyalkylene block copolymers, Surfactant science series 60. Marcel Dekker, New York
123. Booth C, Yu GE, Nace VM (2000) Block copolymers of ethylene oxide and 1,2-butylene oxide. In: Alexandridis P, Lindman B (eds) Amphiphilic block copolymers: self assembly and applications. Elsevier, Amsterdam
124. Booth C, Attwood D (2000) Effect of block architecture and composition on the association properties of poly(alkylene) copolymers in aqueous solution. Macromol Rapid Commun 21:501–527
125. Mortensen K, Pedersen JS (1996) Structural study on the micelle formation of PEO-PPO-PEO triblock copolymers in aqueous solution. Macromolecules 26:805–812
126. Jain NJ, Aswal VK, Goyal PS, Bahadur P (2000) Salt induced micellization and micelle structures of PEO/PPO/PEO block copolymers in aqueous solution. Colloids Surf A 173:85–94
127. Chaibundit C, Mai SM, Heatley F, Booth C (2000) Association properties of triblock copolymers in aqueous solution: copolymers of ethylene oxide and 1,2-butylene oxide with long E-blocks. Langmuir 16:9645–9652
128. Connell SD, Collins S, Fundin J, Yang Z, Hamley IW (2003) In situ atomic force microscopy imaging of block copolymer micelles adsorbed on a solid substrate. Langmuir 19:10449–10453
129. Hamley IW, Connell SD, Collins S (2004) In situ atomic force microscopy imaging of adsorbed block copolymer micelles. Macromolecules 37:5337–5351
130. Khan TN, Mobbs RH, Price C, Quintana JR, Stubbersfield RB (1987) Synthesis and colloidal behaviour of a polystyrene-b-poly(ethylene oxide) block copolymer. Eur Polym J 23:191–194
131. Xu R, Winnik MA, Riess G, Chu B, Croucher MD (1992) Micellization of polystyrene-poly (ethylene oxide) block copolymers in water. 5. A test of the star and mean-field models. Macromolecules 25:644–652
132. Mortensen K, Brown W, Almdal K, Alami E, Jada A (1997) Structure of PS-PEO diblock copolymers in solution and the bulk state probed using dynamic light-scattering and small-angle neutron-scattering and dynamic mechanical measurements. Langmuir 13:3635–3645
133. Yu K, Eisenberg A (1996) Multiple morphologies in aqueous solutions of aggregates of polystyrene-*block*-poly(ethylene oxide) diblock copolymers. Macromolecules 29:6359–6361
134. Rolland A, O'Mullane JE, Goddard P, Brookman L, Petrak K (1992) Preparation and characterization of PEO-PI-PEO block copolymer aggregates. J Appl Polym Sci 44:1195–1203
135. Luo L, Tam D, Maysinger D, Eisenberg A (2002) Cellular internalization of poly(ethylene oxide)-*b*-poly(ε-caprolactone) diblock copolymer micelles. Bioconjug Chem 13:1259–1265
136. Savić R, Luo L, Eisenberg A, Maysinger D (2003) Micellar nanocontainers distribute to defined cytoplasmic organelles. Science 300:615–618
137. Zhou Z, Li Z, Ren Y, Hillmyer M, Lodge T (2003) Micellar shape change and internal segregation induced by chemical modification of a triptych block copolymer surfactant. J Am Chem Soc 125:10182–10183
138. Förster S, Abetz V, Müller AHE (2004) Polyelectrolyte block copolymer micelles. Adv Polym Sci 166:173–210
139. Cohen Stuart MA, Hofs B, Voets IK, de Keizer A (2005) Assembly of polyelectrolyte-containing block copolymers in aqueous media. Curr Opin Colloid Interface Sci 10:30–36
140. Cao T, Munk P, Ramireddy C, Tuzar Z, Webber SE (1991) Fluorescence studies of amphiphilic poly(methacrylic acid)-*block*-polystyrene-*block*-poly(methacrylic acid) micelles. Macromolecules 24:6300–6305

141. Tian M, Qin A, Ramireddy C, Webber SE, Munk P, Tuzar Z, Procházka K (1993) Hybridization of block copolymer micelles. Langmuir 9:1741–1748
142. Qin A, Tian M, Ramireddy C, Webber SE, Munk P, Tuzar Z (1994) Polystyrene-poly (methacrylic acid) block copolymer micelles. Macromolecules 27:120–126
143. Štěpánek M, Procházka K, Brown W (2000) Time-dependent behavior of block polyelectrolyte micelles in aqueous media studied by potentiometric titrations, QELS and fluorometry. Langmuir 16:2502–2507
144. Matějíček P, Podhájecká K, Humpolíčková J, Uhlík F, Jelínek K, Limpouchová Z, Procházka K, Špírková M (2004) Polyelectrolyte behavior of polystyrene-*block*-poly (methacrylic acid) micelles in aqueous solutions at low ionic strength. Macromolecules 37:10141–10154
145. Milnera M, Štěpánek M, Zusková I, Procházka K (2007) Experimental study of the electrophoretic mobility and effective electric charge of polystyrene-*block*-poly(methacrylic acid) micelles in aqueous media. Int J Polym Anal Charact 12:23–33
146. Procházka K, Matějíček P, Uchman M, Štěpánek M, Humpolíčková J, Hof M, Špírková M (2008) pH-dependent behavior of hydrophobically modified polyelectrolyte shells of polymeric nanoparticles. Macromol Symp 273:95–102
147. Groenewegen W, Egelhaaf SU, Lapp A, van der Maarel JRC (2000) Neutron scattering estimates of the effect of charge on the micelle structure in aqueous polyelectrolyte diblock copolymer solutions. Macromolecules 33:3283–3293
148. Groenewegen W, Lapp A, Egelhaaf SU, van der Maarel JRC (2000) Counterion distribution in the coronal layer of polyelectrolyte diblock copolymer micelles. Macromolecules 33:4080–4086
149. van der Maarel JRC, Groenewegen W, Egelhaaf SU, Lapp A (2000) Salt-induced contraction of polyelectrolyte diblock copolymer micelles. Langmuir 16:7510–7519
150. Eghbali E, Colombani O, Drechsler M, Müller AHE, Hoffmann H (2006) Rheology and phase behavior of poly(*n*-butyl acrylate)-*block*-poly(acrylic acid) in aqueous solution. Langmuir 22:4766–4776
151. Burkhardt M, Martinez-Castro N, Tea S, Drechsler M, Babin I, Grishagin I, Schweins R, Pergushov DV, Gradzielski M, Zezin AB, Müller AHE (2007) Polyisobutylene-*block*-poly (methacrylic acid) diblock copolymers: self-assembly in aqueous media. Langmuir 23:12864–12874
152. Ravi P, Wang C, Tam KC, Gan LH (2003) Association behavior of poly(methacrylic acid)-*block*-poly(methyl methacrylate) in aqueous medium: potentiometric and laser light scattering studies. Macromolecules 36:173–179
153. Yao J, Ravi P, Tam KC, Gan LH (2004) Association behavior of poly(methyl methacrylate-*block*-methacrylic acid) in aqueous medium. Langmuir 20:2157–2163
154. Guenoun P, Davis HT, Tirrell M, Mays JW (1996) Aqueous micellar solutions of hydrophobically modified polyelectrolytes. Macromolecules 29:3965–3969
155. Guenoun P, Davis HT, Doumaux HA, Maldonado A, Mays JW, Talmon Y, Taulier N, Tirrell M, Urbach W, Zheng Y (2000) Polyelectrolyte micelles: self-diffusion and electron microscopy studies. Langmuir 16:4436–4440
156. Förster S, Hermsdorf N, Leube W, Schnablegger H, Regenbrecht M, Akari S, Lindner P, Böttcher C (1999) Fusion of charged block copolymer micelles into toroid networks. J Phys Chem B 103:6657–6668
157. Förster S, Hermsdorf N, Böttcher C, Lindner P (2002) Structure of polyelectrolyte block copolymer micelles. Macromolecules 35:4096–4105
158. Gohy J-F, Antoun S, Jérôme R (2001) Self-aggregation of poly(methyl methacrylate)-*block*-poly(sulfonated glycidyl methacrylate) copolymers. Polymer 42:8637–8645
159. Raviv U, Giasson S, Kampf N, Gohy J-F, Jérôme R, Klein J (2003) Lubrication by charged polymers. Nature 425:163–165
160. Selb J, Gallot Y (1985) Ionic block copolymers. In: Goodman I (ed) Developments in block copolymers, 2nd edn. Elsevier, Amsterdam

161. Procházka K, Martin TJ, Munk P, Webber SE (1996) Polyelectrolyte poly(*tert*-butyl acrylate)-*block*-poly(2-vinylpyridine) micelles in aqueous media. Macromolecules 29:6518–6525
162. Vamvakaki M, Billingham NC, Armes SP (1998) Synthesis of novel block and statistical methacrylate based ionomers containing acid, basic or betaine residues. Polymer 39:2331–2337
163. Bütün V, Vamvakaki M, Billingham NC, Armes SP (2000) Synthesis and aqueous solution properties of novel neutral/acidic block copolymers. Polymer 41:3173–3182
164. Liu S, Armes SP (2001) Recent advances in the synthesis of polymeric surfactants. Curr Opin Colloid Interf Sci 6:249–256
165. Patrickios CS, Hertler WR, Abbott NL, Hatton TA (1994) Diblock, ABC triblock and random methacrylic polyampholytes: synthesis by GTP and solution behavior. Macromolecules 27:930–937
166. Chen W-Y, Alexandridis P, Su C-K, Patrickios CS, Hertler WR, Hatton TA (1995) Effect of block size and sequence on the micellization of ABC triblock methacrylic polyampholytes. Macromolecules 28:8604–8611
167. Patrickios CS, Lowe AB, Armes SP, Billingham NC (1998) ABC triblock methacrylates: group transfer polymerization, synthesis of the ABC, ACB and BAC topological isomers and solution characterization. J Polym Sci Part A Polym Chem 36:617–631
168. Kříž J, Masař B, Pleštil J, Tuzar Z, Pospíšil H, Doskočilová D (1998) Three-layer micelles of an ABC block copolymer: NMR, SANS, and LS study of a poly(2-ethylhexyl acrylate)-*block*-poly(methyl methacrylate)-*block*-poly(acrylic acid) copolymer in D_2O. Macromolecules 31:41–51
169. Yu G, Eisenberg A (1998) Multiple morphologies formed from an amphiphilic ABC triblock copolymer in solution. Macromolecules 31:5546–5549
170. Gohy J-F, Willet N, Varshney S, Zhang J-X, Jérôme R (2001) Core-shell-corona micelles with a responsive shell. Angew Chem Int Ed 40:3214–3216
171. Gohy J-F, Willet N, Varshney SK, Zhang J-X, Jérôme R (2002) pH dependence of the morphology of aqueous micelles formed by polystyrene-*block*-poly(2-vinylpyridine)-*block*-poly(ethylene oxide) copolymers. e-Polymers (35):1–10
172. Štěpánek M, Matějíček P, Humpolíčková J, Procházka K (2005) Reversible aggregation of polystyrene-*block*-poly(2-vinylpyridine)-*block*-poly(ethylene oxide) block copolymer micelles in acidic aqueous solutions. Langmuir 21:10783–10790
173. Koutalas G, Pispas S, Hadjichristidis N (2004) Micelles of poly(isoprene-*b*-2-vinylpyridine-*b*-ethylene oxide) terpolymers in aqueous media and their interaction with surfactants. Eur Phys J E 15:457–464
174. Katsampas I, Tsitsilianis C (2005) Hierarchical self-organization of ABC terpolymer constituted of a long polyelectrolyte end-capped by different hydrophobic blocks. Macromolecules 38:1307–1314
175. Chen X, An Y, Zhao D, He Z, Zhang Y, Cheng J, Shi L (2008) Core-shell-corona Au-micelle composites with a tunable smart hybrid shell. Langmuir 24:8198–8204
176. Sharma R, Lee J-S, Bettencourt RC, Xiao C, Konieczny SF, Won Y-Y (2008) Effects of the incorporation of a hydrophobic middle block into a PEG-polycation diblock copolymer on the physicochemical and cell interaction properties of the polymer-DNA complexes. Biomacromolecules 9:3294–3307
177. Torchilin VP (2001) Structure and design of polymeric surfactant-based drug delivery systems. J Control Release 73:137–172
178. Harada A, Kataoka K (2006) Supramolecular assemblies of block copolymers in aqueous media as nanocontainers relevant to biological applications. Prog Polym Sci 31:949–982
179. Wiradharma N, Zhang Y, Venkataraman S, Hedrick JL, Yang YY (2009) Self-assembled polymer nanostructures for delivery of anticancer therapeutics. Nano Today 4:302–317
180. Tyrrell ZL, Shen Y, Radosz M (2010) Fabrication of micellar nanoparticles for drug delivery through the self-assembly of block copolymers. Prog Polym Sci 35:1128–1143

181. Miyata K, Christie RJ, Kataoka K (2011) Polymeric micelles for nano-scale drug delivery. React Funct Polym 71:227–234
182. Walderhaug H, Söderman O (2009) NMR studies of block copolymer micelles. Curr Opin Colloid Interface Sci 14:171–177
183. Halperin A (1987) Polymeric micelles: a star model. Macromolecules 20:2943–2946

Electrostatically Driven Assembly of Polyelectrolytes

Ilja Karina Voets

Contents

Abstract Screened electrostatic interactions are commonly employed in colloid and polymer science for stabilization in aqueous solutions to avoid macroscopic phase separation, but these are equally versatile as driving force for complexation (or microscopic phase separation) into micelles, vesicles, multilayers and other nanostructured materials. In this introductory chapter, we present an overview of the field of electrostatically driven assembly of polyelectrolytes into nanometre-sized association colloids focusing in particular on the fundamentals followed by a discussion of selected application areas.

Keywords Polyelectrolyte • Co-assembly • Responsive • Complex coacervate • Polyion • Micelle

I.K. Voets (✉)
Department of Chemical Engineering and Chemistry and Institute for Complex Molecular Systems, Eindhoven University of Technology, Eindhoven, The Netherlands
e-mail: I.Voets@tue.nl

K. Procházka (ed.), *Fluorescence Studies of Polymer Containing Systems*,
Springer Series on Fluorescence 16, DOI 10.1007/978-3-319-26788-3_3

1 Electrostatically Driven Self- and Co-assembly

Screened electrostatic interactions are commonly employed in polymer science to avoid macroscopic phase separation by electrostatic stabilization of single polymer chains, micelles and vesicles. Far less investigated but equally versatile is the usage of electrostatic interactions as driving force for complexation into association colloids (such as micelles and vesicles) and other nanostructured materials (such as polyelectrolyte multilayers). Both co-assembly of two oppositely charged polyelectrolytes and self-assembly of polymers comprising oppositely charged blocks (polyampholytes) may lead under the right circumstances to electrostatically driven microphase separation.

In this chapter we aim to introduce the reader to the field of electrostatically driven assembly in aqueous solutions. We focus in particular on micelles comprising two polyelectrolytes, which we denote as 'complex coacervate core micelles', in short C3Ms (Fig. 1). We do not provide an exhaustive overview of the available literature on this topic, but instead, specific examples are highlighted, including the utility of fluorescence-based techniques. First, we discuss the fundamentals of electrostatically driven assembly, after which selected application areas are presented including drug delivery and coating technology. For more information on theoretical aspects, we refer the reader elsewhere [1–14].

1.1 Nomenclature

A series of publications on electrostatically driven assembly in the mid-1990s [15–17] sparked interest in the polymer community since the resulting aggregates showed promise as well-defined nanocarriers for all sorts of charged compounds

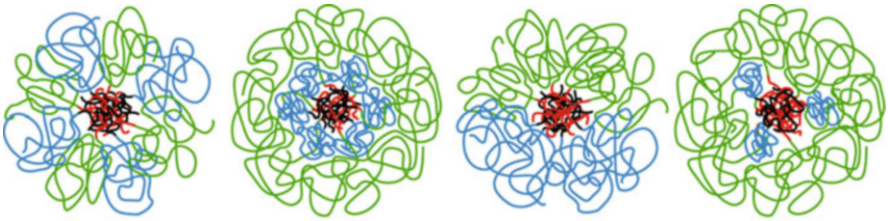

Fig. 1 Schematic representation of co-assembly of two oppositely charged ionic-neutral diblock copolymers in water into complex coacervate core micelles, in short C3Ms, with a core comprising the oppositely charged monomers surrounded by a shell of neutral, water-soluble monomers. The two monomer types in the corona may mix (*left*) or segregate radially (*mid-left*), laterally (*mid-right*) or both radially and laterally (*right*) depending on the chemical composition of the block copolymers and hence the miscibility and differential solvent quality of the neutral monomers. This may lead to the formation of onion-like micelles, also known as core-shell-corona structures (*mid-left*), Janus micelles (*mid-right*) or patchy micelles, also known as raspberry-like micelles (*right*). Figure from Ref. [188]

which cannot easily be transported by micelles of (polymeric) amphiphiles since their hydrophobic interior prevents efficient solubilization. These pioneering studies were followed by numerous papers on the co-assembly in aqueous solution of neutral-ionic (hence double hydrophilic) block, graft and random copolymers with oppositely charged species such as synthetic and biological (co)polymers, supramolecular polymers, multivalent ions, metallic nanoparticles, low molecular weight surfactants (and micelles thereof), polymeric micelles with a polyelectrolyte corona, etc.

Several different terms are in use to describe co-assembled polymeric micelles with a neutral, water-soluble corona surrounding a core of oppositely charged compounds aiming to differentiate these from polymeric micelles with a hydrophobic core self-assembled from amphiphilic polymers. The nomenclatures are: complex coacervate core micelles (C3Ms, used throughout this text), polyion complex (PIC) micelles, block ionomer complex (BIC) micelles and interpolyelectrolyte complex (IPEC) micelles. All names refer to the driving force for association which is interpolyelectrolyte complexation: complexation of positively charged (cationic) polymers with negatively charged (anionic) polymers known as polyelectrolytes, macro-ions, polyions and ionomers.

Strictly speaking, the term C3Ms only applies to micelles with a liquid-like core consisting of a complex coacervate phase and excludes micelles with a solid-like core consisting of a complex precipitate. This follows from the definitions of complex coacervation and complex precipitation by Bungenberg and de Jong who coined the term complex coacervation to describe the associative macrophase separation of two colloids (such as two polyelectrolytes) into two *liquid* phases, of which one phase is enriched and the other phase depleted in both colloids [18]. In practice, however, all four terms—C3/PIC/BIC/IPEC micelle—are used irrespective of the liquid- or solid-like nature of the micellar core which is mostly unknown. A fascinating recent study by Han and co-workers established beyond doubt the liquid-like nature of the interior of network-forming C3Ms [19]. Herein, contrast variation small-angle neutron scattering experiments were performed in combination with electron paramagnetic resonance (EPR) and Overhauser dynamic nuclear polarization (ODNP) experiments to probe the water content and dynamics within coacervate-based terpolymer gels.

Most but not all C3Ms are co-assemblies; furthermore, not all electrostatically driven co-assembly processes lead to C3Ms. Association of polyelectrolytes and oppositely charged spherical micelles with a polyelectrolyte corona generates, for example, layered structures with a hydrophobic core, not with a ‘coacervate’ core [20–24]. Polyampholytes—polymer chains that carry both negatively and positively charged monomers—may form co-assembled C3Ms via interpolyelectrolyte complexation or ‘unimolecular C3Ms’ via intrapolyelectrolyte complexation (i.e. ‘collapse’ of a single polymer chain) [25, 26].

2 Fundamentals of Electrostatically Driven Assembly

Electrostatically driven assembly into complex coacervate core micelles (C3Ms) requires a sufficiently strong interaction between two compounds of opposite charge to overcome (translational) entropy and associate into a composite supramolecular architecture. Each parameter of chemical or of physical nature (molecular weight, monomer type, chain stiffness, ionic strength, p*H*, temperature) that affects the balance between driving and opposing forces tunes assembly. In the following paragraphs, we first discuss the thermodynamics of C3M formation followed by several other fundamental aspects including morphology, stability, formation, dissolution and exchange dynamics.

2.1 Thermodynamics

The thermodynamic framework to describe electrostatically driven micellization naturally builds upon previous work on the micellization of amphiphilic polymers and theories of macro-ion complex formation [1–5, 7, 9, 10, 12, 13, 27, 28]. A full treatise of the state of the art is beyond the scope of this chapter; we here restrict ourselves to a simple description of the free energy of micellization per chain as the sum of several terms which are positive when opposing and negative when driving micellization (Eq. 1).

$$F_{\mathrm{C3M}} = F_{\mathrm{cc}} + F_{\mathrm{surf}} + F_{\mathrm{core}} + F_{\mathrm{corona}} \tag{1}$$

The first term herein, F_{cc}, is related to polyelectrolyte complexation or complex coacervation. This includes enthalpic and entropic terms due to changes in the electrostatic free energy which favour micellization and the entropy of mixing which disfavour C3M formation. The second term, $F_{\mathrm{surf}} = \gamma a_0$, is given by the interfacial tension of the core-corona interface and the area per chain, a_0. Since the density of corona segments is low at the core-corona interface of a micelle, we may use for γ the interfacial tension of the coacervate phase, which can be determined by atomic force spectroscopy [29]. F_{core} is governed by the interaction free energy between core monomers as well as monomer/solvent interactions (since the water volume fraction in the core is non-negligible) and an elastic free energy associated with stretching of core blocks. F_{corona} is associated with an entropic penalty due to the dense packing of monomers in the corona which leads to stretching of the polymer blocks.

Interestingly, this simple equation already reveals that C3Ms form only if the electrostatic interactions between the oppositely charged compounds are sufficiently attractive (negative F_{cc}) to overcome the entropic penalties opposing association, which makes that micelles occur in a limited range of polyelectrolyte concentration, ionic strength, composition and p*H* values. The latter governs the

degree of dissociation α in case of weak polyelectrolytes with a p*H*-dependent degree of dissociation. Micelles will form only in solutions with a composition $f_+ = c_+/(c_+ + c_-)$ close to charge neutrality when $c_-\alpha_- = c_+\alpha_+$. For strong polyelectrolytes with a p*H*-independent α, this simply corresponds to equal concentrations of positively and negatively charged monomers $c_- = c_+$, thus $f_+ = 0.5$, since $\alpha_- = \alpha_+ = 1$ if counterion condensation and specific ion binding are negligible. In case of weak polyelectrolytes, charge stoichiometry depends on the relative monomer concentrations and on p*H*, which determines α. Furthermore, the attractive interaction between oppositely charged polymers diminishes with increasing ionic strength which 'screens' the electrostatic interactions. C3Ms therefore form at low ionic strength and dissociate above a critical ionic strength, I_{cr}, which is dependent on polymer concentration, c_p, f_+, p*H*, and the degree of polymerization of the polyelectrolyte blocks [14, 30, 31].

Whether C3M formation is enthalpically or entropically driven has long been topic of scientific debate. This is because complexation of oppositely charged compounds brings about changes in the electrochemical double layer (EDL) that surrounds the macro-ions, which may be of enthalpic or entropic nature. The EDL is a region around a macro-ion of increased counterion and decreased co-ion concentration relative to their bulk concentration. EDL formation is spontaneous in aqueous solution ($\Delta G < 0$), which means that the enthalpy gain due to a slightly reduced (resp. increased) distance between oppositely (resp. like) charged ions must outweigh the reduced entropy due to translational constraints. Complexation of two macro-ions partially destroys their EDLs, which is entropically favourable if the entropic gain due to counterion release is larger than the macro-ion entropy loss due to configurational and translational restraints. This balance naturally depends on the macro-ion molecular weight and solution ionic strength. Complexation is also enthalpically favourable at low ionic strength upon tight binding of the macro-ions, whereas at high ionic strength $\Delta H > 0$ as the macro-ion complexes are too dilute to outweigh the enthalpic loss due to EDL disintegration. This means that electrostatically driven assembly in weakly charged systems is both enthalpy and entropy-driven at low ionic strength (exothermic), entropy-driven at intermediate ionic strength (endothermic), and prohibited above the critical ionic strength I_{cr} [12, 32]. Complexation is entropically driven below I_{cr} in highly charged systems with considerable counterion condensation [32].

Experimental verification of these theoretical considerations is surprisingly sparse for both macro- and mesoscopic polyelectrolyte complexes [33–38]. Hofs et al. deduced from isothermal titration calorimetry (ITC) experiments at a fixed ionic strength of 50 mM $NaNO_3$ on C3Ms of poly(acrylic acid)-*b*-poly(acrylamide) and poly(*N*,*N*-dimethylaminoethyl methacrylate) that the driving force for complexation of PAA_{42}-*b*-$PAAm_{417}$ and $PDMAEMA_{150}$ into C3Ms comprised both coulombic attraction between the polyelectrolytes and counterion release [34]. Courtois and Berret concluded from the endothermic response in ITC titrations of PAA-*b*-PAAm copolymers with dodecyltrimethylammonium bromide (and vice versa) that PAA-*b*-PAAm/DTAB complexation is driven by counterion entropy [35]. Procházka and co-workers observe stoichiometry-dependent

endothermic and exothermic heat responses upon titration of *N*-dodecylpyridinium chloride into an aqueous solution of poly(methacrylic acid)-*b*-poly(ethylene oxide) [36].

Finally, we note that assembly into C3Ms by weakly charged polyelectrolytes may occur in thermodynamic equilibrium, but this is not always the case. Metastable arrested states may persist when the free energy gain of complexation far exceeds thermal energy k*T*. One facile way to test experimentally if thermodynamic equilibrium is likely reached is to prepare samples in multiplicate following different procedures. Since equilibrium properties are independent of the pathway towards the final state, observable differences in, for example, micellar size and aggregation number arising from differences during sample preparation (e.g. addition of the polycation to the polyanion and vice versa) imply incomplete equilibration [35, 39–41].

2.2 Stoichiometry

Colloidal complexes form upon complexation between oppositely charged macroions if the forces driving and opposing association are properly balanced. Complexation is absent if the driving forces are too weak or the opposing forces too strong and vice versa; macroscopic phase separation occurs if the driving forces are too strong or the opposing forces too weak. In practice, this means that neutral association colloids with a relatively high aggregation number—most often micelles—may form under charge stoichiometric conditions, while smaller, charged complexes are typically abundant at non-stoichiometric compositions [27]. As discussed in the above, charge stoichiometry always corresponds to equal anionic and cationic monomer concentrations, $f_+ = c_+/(c_+ + c_-) = 0.5$ in case of strong polyelectrolytes, since the degree of dissociation $\alpha_- = \alpha_+ = 1$. By contrast, as p*H* influences α for weak polyelectrolytes, charge stoichiometry always corresponds to $c_-\alpha_- = c_+\alpha_+$ but deviates from $f_+ = 0.5$ when $\alpha_- \neq \alpha_+$.

Van der Burgh et al. proposed that a speciation diagram with five components—four charged species, one neutral species—captures the evolution of colloidal complexes as a function of composition f_+ in aqueous solutions of oppositely charged copolymers (Fig. 2) [27]. Let us consider the speciation diagram for a mixture of one ionic-neutral copolymer and a homopolymer with identical polyelectrolyte block length $N_+ = N_-$ and a neutral block length N_n. In such a diagram, the relative abundance of each of the species is shown on the vertical axis as a function of the solution composition f_+ on the horizontal axis. If we consider a titration of a weak polycation to a weak polyanion with identical chain length $N_+ = N_-$ and degree of dissociation $\alpha_- = \alpha_+ = \alpha$, the composition runs from a pure polyanion solution ($f_+ = 0$) to a pure polycation solution ($f_+ = 1$) via a stoichiometric mixture at $f_+ = 0.5$. Initially, at low values of f_+, small, water-soluble complexes (denoted as SCP_) comprising a polycation and a few polyanions coexist with excess polyanions (denoted as dbp). At intermediate f_+ values, these

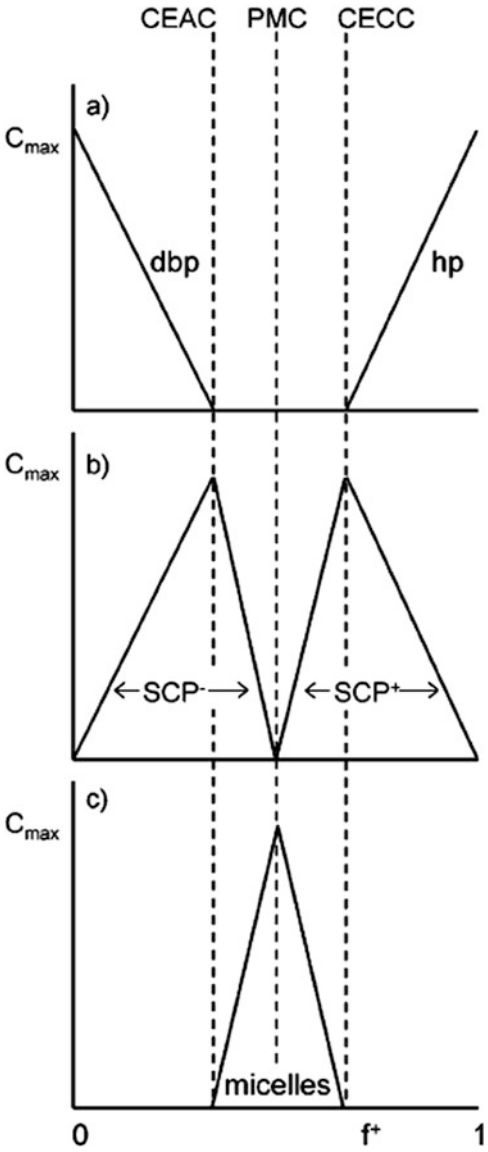

Fig. 2 Speciation diagram as proposed by van der Burgh et al. for the complexation of an ionic-neutral copolymer (dbp) and oppositely charged homopolymer (hp) in aqueous solution. The composition of the mixture, $f_+ = c_+/(c_+ + c_-)$ determines the relative abundance of the five different species: free polymers (dbp, hp), cationic and anionic soluble complex particles ($SCP^{+,-}$), and neutral micelles (C3Ms). The critical excess anionic charge (CEAC), critical excess cationic charge (CECC), and the preferred micellar composition (PMC) are indicated by dotted lines. (**a**) The free polymers are present far off stoichiometry at low f_+ up to the CEAC and at high f_+ above the CECC. (**b**) Soluble complex particles are present at all compositions except $f_+ = 0$, $f_+ = 1$ and at the PMC. The amount of negatively charged SCP increases with increasing f_+ for $0 \leq f_+ \leq$ CEAC and decreases with increasing f_+ for CEAC $\leq f_+ \leq$ PMC. Similarly, the concentration of SCP^+ increases with increasing f_+ for PCM $\leq f_+ \leq$ CECC and decreases with increasing f_+ for CECC $\leq f_+ \leq 1$. (**c**) Micelles (C3Ms) persist only in a narrow region of compositions close to

complexes assemble into charge-neutral micelles with a more or less constant size and aggregation number (denoted as C3Ms), such that the number of SCP^- decreases as the number of micelles increases. The amount of C3Ms passes through a maximum at the preferred micellar composition (here PMC $= f_+ = 0.5$), after which neutral C3Ms dissociate into smaller charged complexes. Whereas the SCPs formed at low f_+ are negatively charged, the SCPs are positively charged at high f_+. When all C3Ms have disappeared and the amount of SCPs (denoted as SCP^+) has passed through a maximum, cationic SCPs coexist with individual polycations until finally the SCPs vanish and only polycations remain at $f_+ = 1$.

Since the majority of research has focused on the stoichiometric complexes, little is known about the structure, composition and relative abundance of the non-stoichiometric complexes [9, 42–47]. Definite proof of the structural evolution proposed by van der Burgh et al. is still lacking, but experimental observations are consistent with the described trends [27]. Recent studies by Procházka and co-workers demonstrate that a combination of experimental techniques such as various scattering methods and ^{1}H NMR spectroscopy may provide valuable insights in this area [36, 46]. The authors demonstrated coexistence of multiple species both on and off stoichiometric mixing fractions. Moreover, the structure of the different species was elucidated, revealing a sequence of morphological transitions from loose aggregates coexisting with free polymer coils at low surfactant-to-polyelectrolyte charge ratios Z to beads-on-a-string nanoparticles followed by core-shell micelles at higher Z coexisting with free surfactant micelles at $Z >> 1$ [46].

2.3 Composition

The chemical composition of neutral C3Ms present at (near-) charge stoichiometric f_+ is generally assumed constant and identical to the overall solution composition at the preferred micellar composition (PMC). These assumptions allow computation of micellar aggregation numbers, P_{agg}, from the average mass determined by, for example, scattering methods. C3Ms are typically smaller than micelles of polymeric amphiphiles of similar block length with aggregation numbers ranging from tens up to a few hundred polymers [11, 34, 48–50]. As added salt reduces the driving force for micellization, P_{agg} is strongly salt-dependent [31, 51, 52]. An almost linear decrease of P_{agg} with increasing c_{salt} is consistent with experimental data [31, 52]. Interestingly, in diblock copolymer/homopolymer C3Ms, the number of encapsulated homopolymers can be precisely controlled by their degree of polymerization, N_{hp} [30, 50]. This is because the size of C3Ms depends critically on the interfacial tension of the coacervate core, γ, and the effective area per corona

Fig. 2 (continued) charge stoichiometry, more specifically, for CEAC $\leq f_+ \leq$ CECC. The amount of C3Ms is maximum at the PMC. Figure from Ref. [27]

chain, a_0. The latter is dependent on the ionic-to-neutral block length ratio of the copolymer but not on N_{hp}. This means that the choice of the diblock copolymer fixes the total amount of charged monomers within the C3M core $n_c = n^+ + n^-$ and thereby the number of homopolymer chains per micelle, n_{hp}, since $n_{hp} = 0.5n_c/N_{hp}$. Consequently, the number of incorporated homopolymers decreases with increasing N_{hp}, until $N_{hp} = 0.5n_c$ when the micelles contain no more than a single homopolymer chain [30, 50].

Whereas micellar aggregation numbers are now routinely determined, we know much less about the water and ion content of the micelles. Estimates of the water content of C3Ms range up to 92 %, similar to values obtained for macroscopic coacervates [19, 53–55]. Several groups have used fluorescent probes, such as auramine O, pyrene and 1,3-di-(1-pyrenyl)-propane (P3P), to assay the polarity and microviscosity of the micellar core and C3V membrane [47, 56, 57]. Estimates of the micro-ion content of microscopic coacervates are lacking. Experimental and theoretical studies on the salt concentration of macroscopic coacervates report at most small differences in ionic strength inside and outside the coacervate phase [7, 8, 58]. Exceptionally, for example, in coacervates of poorly water-soluble polyelectrolytes, there may be larger differences in salt content [7, 8].

Viewing C3Ms as promising nanocarriers, one could consider the ionic-neutral copolymer as the carrier material for the oppositely charged cargo. In the simplest case, C3Ms comprise two types of linear polyelectrolytes. These are H-C3Ms composed of a diblock copolymer/homopolymer pair and D-C3Ms with two diblock copolymers [49]. Recently, increasingly complex polymeric architectures are incorporated, such as star polymers [59], dendritic polymers [60], graft copolymers [56, 61–64], random and gradient copolymers [38, 63], multiblock copolymers [52, 65, 66], dendrimers [50, 67, 68], amphiphilic copolymers [20] and supramolecular polymers [31, 43, 51, 61, 69, 70]. Moreover, one of the polymers may be replaced by inorganic particles [71–75], multivalent ions [73], small complexes [76], surfactants [35, 36, 46, 77–79] or biopolymers, such as DNA and RNA [80], antibodies [81] and enzymes [82–84]. This versatility in loading capacity is a clear advantage of C3Ms, allowing through co-assembly precise control over the encapsulation of a broad range of charged compounds. Recently, C3Ms have also been loaded (or decorated) with additional (charged) components, often with complementary functionality for (multimodal) detection, targeting and treatment [85–87]. Incorporation can be evaluated with fluorescence spectroscopy after covalent coupling or selective binding with a suitable dye [88].

2.4 Morphology

Oppositely charged polyelectrolytes assemble into colloidal aggregates of various morphologies, including spherical micelles, wormlike micelles, vesicles, etc. By far most abundant are spherical C3Ms. The structural data collected to date for spherical core-shell C3Ms is qualitatively consistent with scaling models developed

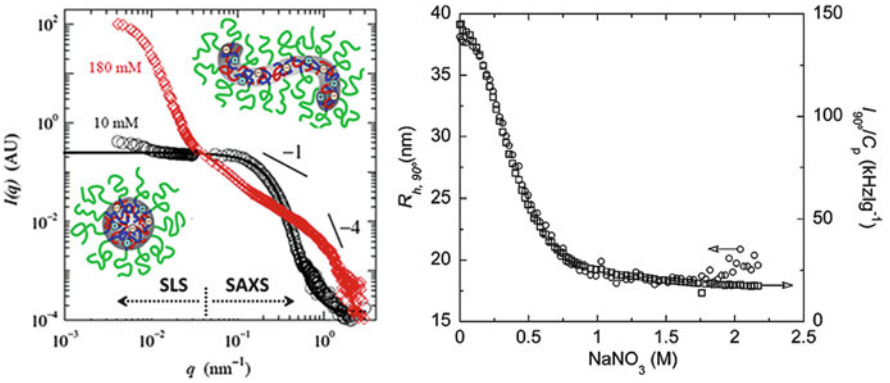

Fig. 3 (**a**) Light and X-ray scattering experiments on H-C3Ms of poly(*N*-methyl-2-vinylpyridinium)-*b*-poly(ethylene oxide) ($PM2VP_{41}$-*b*-PEO_{204}) and poly(acrylic acid) (PAA_{13}) reveal a salt-induced sphere-to-cylinder transition (SCT) for short PAA chains, as evidenced by a power-law slope of approximately −1 in a log-log plot of excess scattering vs. the scattering wave vector *q*. Adapted with permission from Ref. [30] (**b**) Light scattering salt titration of C3Ms of poly(4-(2-amino hydrochloride-ethylthio)butylene)-*block*-poly(ethylene oxide) $PAETB_{49}$-*b*-PEO_{212} and poly(4-(2-sodium carboxylate-ethylthio)butylene)-*block*-poly(ethylene oxide) ($PCETB_{47}$-*b*-PEO_{212}) at p*H* = 7.2, C_p = 0.90–0.64 g L^{-1}, f_+ = 0.490, *T* = 25.0 °C demonstrating an unusually high critical ionic strength far exceeding physiological salt concentrations (~150 mM NaCl). From Ref. [40]

for polymeric amphiphiles [27, 89]. For example, the micellar aggregation number P_{agg} and hydrodynamic radius R_h decrease with increasing copolymer block length ratio N_{corona}/N_{core} [27, 48, 64, 90–94]. Interestingly, the size of H-C3Ms is entirely independent of N_{hp} up to a critical molecular weight beyond which micellar size increases with increasing N_{hp} [27, 30].

Co-assembly under stoichiometric conditions at low salt concentrations mostly generates spherical micelles, but it is possible to access other morphologies. A variety of cylindrical micelles has been observed, [30, 43, 69, 70, 95–97] as well as rod-like and pearl-necklace complexes comprising a single, high molecular weight (co)polymer chain onto which many low molecular weight surfactants or copolymer chains attach [98, 99]. Transitions from spheres to cylinders have been induced by an increase in ionic strength (Fig. 3a) [30], an increase in the overall concentration of polymer/surfactant complex [95] and mixing fraction away from stoichiometric compositions [43, 70]. The salt-induced sphere-to-cylinder transition (SCT) can be rationalized using simple geometrical arguments much alike the SCT of micelles of polymeric amphiphiles in selective solvents. An increase in ionic strength may concomitantly swell the coacervate core and compactify polymeric chains in the micellar corona, increasing hereby the critical packing parameter, P_c, favouring a sphere-to-cylinder transition [30, 100]. Rubinstein and Zhulina predict that this morphological transition only occurs in micellar solutions of polymeric amphiphiles when the micelles are of the so-called crew-cut morphology [101], that

is, the core radius, R_c, exceeds the shell radius, R_s. Scattering studies on C3Ms confirm that they are indeed within or close to the crew-cut regime [48, 50].

Ellipsoidal C3Ms were obtained upon co-assembly of two dissimilar block copolymers with the relatively immiscible corona blocks poly(ethylene oxide) and poly(acryl amide) [102–104]. Needlelike hybrid C3Ms containing lanthanum hydroxide nanoparticles form upon mineralization within C3Ms of poly(acrylic acid)-based copolymers and multivalent precursors for the nanoparticles [73, 105, 106]. Several other unusual morphologies have been observed, such as stringlike complexes [107], ringlike complexes [107], buckle-like structures [108], stiff nanorods [75, 109] and irregularly shaped large particles [110].

Complex coacervate core vesicles (C3Vs) have been reported by various groups upon incorporation of miktoarm star polymers, (fluorinated) surfactants and neutral-ionic copolymers with short ionic blocks [57, 59, 78, 111–119]. Plamper and co-workers successfully imaged relatively large adsorbed C3Vs with in situ liquid cell TEM, which may pave the way for future imaging studies on morphology transitions [59]. As in C3Ms [53, 81–83, 120–126], proteins can be effectively encapsulated and protected from enzymatic degradation in C3Vs [111]. Fluorescence microscopy is often used to demonstrate entrapment of molecules and polymers within the vesicles [111, 114–116].

2.5 Stability

Since the electrostatic driving force for micellization weakens with increasing ionic strength, the critical polymer concentration above which micelles form (known as the CMC) is salt-dependent [31, 51, 127]. Based on the mean-field model for complex coacervation by Voorn and Overbeek [10], Wang et al. argued that the CMC increases exponentially with the square root of the salt concentration, $\mathrm{CMC} \propto \exp(\sqrt{c_{salt}})$, and found good agreement with their light scattering experiments [31]. As a consequence of the I_c-dependent CMC, addition of salt at a fixed polymer concentration c_p may increase the CMC so much that it exceeds c_p. The ionic strength above which micelles disintegrate is called the critical ionic strength I_{cr} where $c_p \sim \mathrm{CMC}$. This dissociation is typically reversible [82, 127]. Spruijt et al. demonstrated that I_{cr} is predictably dependent on the degree of polymerization N of the polyelectrolyte blocks [30]. Other important factors besides c_p and N are the type of oppositely charged species, solution pH, mixing fraction, as well as the type and valency of the added salt [127, 128]. The I_{cr} of C3M solutions at charge stoichiometry in the presence of monovalent salts typically ranges from tens to hundreds of mM (see Ref. [49] for an overview). A facile route to increase the I_{cr} of C3Ms by a factor 10–100 is to exploit additional driving forces for micellization, such as hydrophobic interactions and metal-ligand coordination [40, 73, 74, 129]. For example, Voets et al. have shown that additional hydrophobic interactions can be utilized to increase the stability of C3Ms to prevent dissociation at physiological salt concentrations (Fig. 3b) [40], which is vital for biomedical application

as carriers of therapeutics. Moreover, (reversible) cross-linking of segments in the micellar core and corona was shown to be effective in vitro and in vivo [130–134].

Various methods can be used to probe micellar disintegration below the CMC and above the I_{cr}; light scattering and fluorescence spectroscopy are most common [31, 49, 57, 135, 136]. Pyrene is suitable if the C3Ms contain sufficiently hydrophobic compartments, such as surfactant micelles or collapsed chains like poly(*N*-isopropylacrylamide) above their lower critical solution temperature [57, 79, 136]. Otherwise, more polar dyes like eosin B and auramine O can be utilized [56, 135].

2.6 Exchange Dynamics and Formation/Dissolution Kinetics

While static properties of C3Ms are widely investigated, little is known about the kinetics of C3M formation and dissolution [82, 84]. This may seem surprising given the relevance of these aspects for mundane yet vital aspects like sample equilibration as well as properties of applied interest such as controlled release and pharmacokinetic profiles [39, 80, 137, 138]. Studies on polyelectrolyte multilayers (PEM) and macroscopic coacervates demonstrate that ionic strength has a dramatic impact on the strength of individual ionic bonds, relaxation dynamics, PEM structure and dissolution [139–143]. A similarly large impact of ionic strength on the kinetics of C3M formation and disruption is anticipated. Force measurements on polyelectrolyte complexes have shown that the energetic cost of breaking up such a complex strongly depends on how it is broken up. Separation of individual polyelectrolytes requires much higher forces than redistribution of ion pairs [29, 144], which implies that C3M formation, C3M dissociation and exchange dynamics may strongly depend on molecular weight (differences) and involve ion pairs rather than individual polyelectrolytes whenever possible. This may also (partially) explain the chain length recognition observed by Harada and Kataoka, who reported selective complexation of oppositely charged diblock copolymers of matched length from mixtures of both matched and unmatched lengths [145]. Complexes of unmatched pairs carry excess charge which may make them more soluble and less prone to micellization. Furthermore, based on ITC and rheological data, Laugel et al. proposed that the mechanics and thermodynamics of macroscopic coacervates are linked: the authors found that coacervates behave solid-like when their formation is exothermic and liquid-like when their formation is endothermic [33]. In micelles this will likely be accompanied by a large change in the exchange dynamics.

So what is known about the kinetics of C3M association and dissociation? In 1998, Cohen Stuart and co-workers first studied the formation kinetics of H-C3Ms for poly((dimethylamino)ethyl methacrylate)-*co*-poly-(glyceryl methacrylate) (PDMAEMA-*co*-PGMA) and poly(acrylic acid) (PAA) [17]. A strong excess

scattering was observed in stopped-flow experiments which relaxed to a long-time baseline in a salt-dependent manner: the higher the salt concentration, the faster the decay. Interestingly, the timescale of the intensity decay decreases a factor 10^4 upon an increase in ionic strength from pure water to 0.3M NaCl. These findings were attributed to macroscopic phase separation at short timescales after which the dense phase rearranges into micelles. The results are in line with salt-dependent timescales reported in various other studies of exchange and structural reorganization processes within polyelectrolyte complexes [146–149]. In a more recent study on H-C3Ms of poly(acrylic acid) and poly([4-(2-aminoethylthio)butylene] hydrochloride)$_{49}$-*block*-poly(ethylene oxide)$_{212}$, Hofs et al. attribute a similar large excess scattering to the formation of a transient network of C3Ms which disintegrates into individual C3Ms within a timeframe of several milliseconds to several (tens of) hours [150]. Holappa et al. observed two processes in the kinetics of micellization of H-C3Ms of PEO-*b*-PMAA and PMOTAC probed by fluorescence spectroscopy. By analogy with micellization of amphiphilic polymers, these were attributed to 'merging and splitting' of C3Ms and 'insertion and expulsion' of single chains, the latter supposedly being the faster process [151]. Liu and co-workers observed two distinct processes during stopped-flow light scattering experiments on the formation and dissociation of D-C3Ms of poly(ethylene oxide)-*b*-poly(sodium 4-styrene sulfonate) and poly(ethylene oxide)-*b*-poly(quaternized 2-(dimethylamino)ethyl methacrylate) [47]. Stopped-flow small-angle X-ray scattering experiments of Uchman et al. showed that ordered structures form very fast (<50 ms) within the core of C3Ms composed of block copolymers and surfactant micelles [36].

Polymer exchange (rates) between DNA-containing C3Ms has (have) been studied by several groups aiming to tune drug delivery, release and efficacy [41, 152–155]. Premature DNA release in the blood stream by exchange reactions with BSA should be prevented. Katayose et al. demonstrated that the nuclease resistance of DNA in the blood stream is inversely proportional to the rate of exchange [153]. By contrast, exchange reactions with intracellular polyions such as mRNA, chromatin and sulphonated sugars should be promoted to release the DNA at the target location. Thus, it is important to identify C3Ms which promote intracellular exchange on-site and block extracellular exchange during trafficking as much as possible. Key parameters are core block affinity, solubility and p*H* (charge density) [40]. In addition, various chemical routes have been explored to tune (or prevent) unimer exchange, such as covalent or reversible (e.g. with disulphide bonds) cross-linking of core or corona segments [132].

3 Applications of Electrostatically Driven Assembly

Applications particularly in the field of drug delivery, controlled release and biomaterials have been a major research interest since the earliest reports on C3Ms from about 20 years ago. A wide selection of reviews is available on this topic [68, 86, 137, 138, 156–158]. Here, we briefly highlight recent work dedicated to

usage of C3Ms as responsive, nanostructured building blocks for functional soft materials.

3.1 Responsive Materials

The inherently responsive character of C3Ms makes them interesting building blocks for a wide range of technologies. In solution, C3Ms have been used as nanoreactor for mineralization and gelation [73, 105, 106, 159, 160]. C3Ms loaded with catalytically active nanoparticles and/or fluorescent dyes may find use as thermoswitchable and recyclable catalysts, sensors or diffusional nanoprobes [134, 161–165]. Co-assemblies with magnetic particles may find use in micro-rheology and as micro-actuators in microfluidics and in therapeutics [75, 109, 166–168]. Furthermore, C3Ms are powerful nanocontainers for fragile compounds, such as enzymes, antibodies and DNA, which require protection to prevent enzymatic degradation, aggregation and denaturation [82, 86]. The incorporation of inorganic nanoparticles may enhance stability and reduce drug release rates considerably [45, 74].

Transient networks may form at elevated micellar volume fractions, due to non-covalent cross-linking of the cores of multiple micelles. Both disordered [42, 52, 65, 71] and ordered hydrogels [19, 66, 169] have been engineered with interesting properties, such as shear-thinning, self-healing and shape-memory behaviour [170]. Incorporation of inorganic particles such as clay may further improve the mechanical properties [71, 170]. Oscillatory rheology studies of Lemmers et al. demonstrated that the zero-shear plateau modulus of transient homopolymer/terpolymer networks is virtually salt-independent despite a strong salt dependence of the characteristic relaxation times. Small-angle X-ray scattering experiments revealed that this is because the number of elastically active chains (bridges) spanning the micellar cores is virtually salt-independent as is the bridging distance, since micellar size decreases while the number of micelles increases with increasing salt concentration [52]. Another particularly insightful study is the work of Ortony et al., who observed that the nanometre-sized coacervate domains in their triblock copolymer gels contain less water and more polymer than the micron-sized coacervate domains of the corresponding homopolymers. The authors attributed this difference to the elevated osmotic pressure in the hydrogel caused by the dense PEO microenvironment surrounding the spherical coacervate nodes in the transient network [19]. In future, (drug) loading and controlled release will likely gain increasing attention as well as the structure and mechanics of composite networks.

C3Ms are also responsive to the presence of surfaces; generally, they partially wet solids to which they are exposed, which makes C3M solutions a readily applicable formulation for coating of surfaces irrespective of surface chemistry, shape, dimensions and surface roughness. Adhesion is strongly dependent on a multitude of factors including coacervate cohesive energy, surface affinity and ionic strength, which may be exploited for regeneration. Surfaces coated with

C3Ms suppress adsorption of various proteins to an extent which is dependent on surface chemistry, protein type, etc. [62, 171–174]. A promising strategy towards denser brushes with improved antifouling characteristics has been introduced by de Vos et al. [175]. Herein, ionic-neutral copolymers are adsorbed onto a surface grafted with polymers of opposite charge.

3.2 Multicompartment Micelles

The internal organization of C3Ms can be directed beyond segregation into two distinguishable domains: the core and the corona. A combination of techniques is typically used to demonstrate such compartmentalization experimentally, including scattering methods, electron microscopy, 2D ^{1}H NMR spectroscopy and fluorescence spectroscopy [36, 102, 104, 176]. Micelles with heterogeneous coronas have been realized (Fig. 1) by co-assembly of oppositely charged block copolymers with two different neutral, water-soluble blocks that are relatively immiscible and/or vary greatly in hydrophilicity (i.e. segment-solvent interaction parameter). Lateral segregation generates so-called Janus micelles [102–104], radial segregation gives core-shell-corona structures [177] and simultaneous lateral and radial segregation results in patchy or raspberry-like micelles [178]. By contrast, sufficiently miscible coronal segments give rise to core-shell C3Ms with a homogeneous core and corona [176, 177].

Micelles displaying a precise spatial arrangement of components within their core have also been reported. For example, Yan and co-workers prepared wormlike C3Ms from a conventional and a supramolecular polyelectrolyte that co-assemble into long tapes (‘nanoladders’) with a ‘grid-like’ internal structure due to precise arrangement of metal ions [69]. Voets and co-workers reported that spherical silver nanoparticles could be positioned either in the core of C3Ms or shell of core-shell-corona micelles due to their selective interaction with the 2MVP monomers of P2MVP-*b*-PEO copolymers [72].

Combining electrostatic and hydrophobic driving forces of assembly is an attractive strategy towards multicompartment micelles [4–6, 12–14, 46, 95, 179–183] and may find use as a handle towards control over secondary aggregation into superstructures [184]. The core of C3Ms assembled from surfactant micelles and copolymers is disordered at low to intermediate and may be ordered at high surfactant packing fractions. Disordered phases within the micellar core exhibit a single structure peak in small-angle scattering experiments [77, 185–187], while ordered core structures such as locally hexagonal and fcc/*Pm3n* cubic phases are evidenced by the appearance of multiple Bragg peaks [41, 95].

References

1. Biesheuvel PM, Cohen Stuart MA (2004) Electrostatic free energy of weakly charged macromolecules in solution and intermacromolecular complexes consisting of oppositely charged polymers. Langmuir 20:2785–2791. doi:10.1021/la0362041
2. Borue VY, Erukhimovich IY (1990) A statistical theory of globular polyelectrolyte complexes. Macromolecules 23:3625–3632. doi:10.1021/ma00217a015
3. Castelnovo M, Joanny JF (2000) Formation of polyelectrolyte multilayers. Langmuir 16:7524–7532. doi:10.1021/la000211h
4. Castelnovo M, Joanny JF (2001) Complexation between oppositely charged polyelectrolytes: beyond the random phase approximation. Eur Phys J E 6:377–386. doi:10.1007/s10189-001-8051-7
5. Kramarenko EY, Khokhlov AR (2007) Effect of formation of ion pairs on the stability of stoichiometric block ionomer complexes. Polym Sci Ser A 49:1053–1063. doi:10.1134/s0965545x07090131
6. Kramarenko EY, Khokhlov AR, Reineker P (2006) Stoichiometric polyelectrolyte complexes of ionic block copolymers and oppositely charged polyions. J Chem Phys 125(19), 194902. doi:10.1063/1.2387173
7. Kudlay A, de la Cruz MO (2004) Precipitation of oppositely charged polyelectrolytes in salt solutions. J Chem Phys 120:404–412. doi:10.1063/1.1629271
8. Kudlay A, Ermoshkin AV, de la Cruz MO (2004) Complexation of oppositely charged polyelectrolytes: effect of ion pair formation. Macromolecules 37:9231–9241. doi:10.1021/ma048519t
9. Oskolkov NN, Potemkin II (2007) Complexation in asymmetric solutions of oppositely charged polyelectrolytes: phase diagram. Macromolecules 40:8423–8429. doi:10.1021/ma0709304CCC:$37.00
10. Overbeek GJT, Voorn MJ (1957) Phase separation in polyelectrolyte solutions. Theory of complex coacervation. J Cell Comp Physiol 49:7–26. doi:10.1002/jcp.1030490404
11. Sindelka K, Limpouchova Z, Lisal M, Prochazka K (2014) Dissipative particle dynamics study of electrostatic self-assembly in aqueous mixtures of copolymers containing one neutral water-soluble block and one either positively or negatively charged polyelectrolyte block. Macromolecules 47:6121–6134. doi:10.1021/ma501018x
12. van der Gucht J, Spruijt E, Lemmers M, Cohen Stuart MA (2011) Polyelectrolyte complexes: bulk phases and colloidal systems. J Colloid Interface Sci 361:407–422. doi:10.1016/j.jcis.2011.05.080
13. Veis A (2011) A review of the early development of the thermodynamics of the complex coacervation phase separation. Adv Colloid Interface Sci 167:2–11. doi:10.1016/j.cis.2011.01.007
14. Voets IK, Leermakers FAM (2008) Self-consistent field theory for obligatory coassembly. Phys Rev E 78(6 Pt 1). doi:10.1103/PhysRevE.78.061801
15. Harada A, Kataoka K (1995) Formation of polyion complex micelles in an aqueous milieu from a pair of oppositely-charged block-copolymers with poly(ethylene glycol) segments. Macromolecules 28:5294–5299
16. Kabanov AV, Bronich TK, Kabanov VA, Yu K, Eisenberg A (1996) Soluble stoichiometric complexes from poly(N-ethyl-4-vinylpyridinium) cations and poly(ethylene oxide)-block-polymethacrylate anions. Macromolecules 29:6797–6802. doi:10.1021/ma960120k
17. Cohen Stuart MA, Besseling NAM, Fokkink RG (1998) Formation of micelles with complex coacervate cores. Langmuir 14:6846–6849
18. Bungenberg de Jong HG, Kruyt HR (1929) Coacervation (Partial miscibility in colloid systems). In: Proceedings of the Koninklijke Nederlandse Akademie van Wetenschappen 32, 849–856
19. Ortony JH et al (2014) Fluidity and water in nanoscale domains define coacervate hydrogels. Chem Sci 5:58–67. doi:10.1039/c3sc52368c

20. Pergushov DV, Muller AHE, Schacher FH (2012) Micellar interpolyelectrolyte complexes. Chem Soc Rev 41:6888–6901. doi:10.1039/c2cs35135h
21. Synatschke CV et al (2013) Micellar interpolyelectrolyte complexes with a compartmentalized shell. Macromolecules 46:6466–6474. doi:10.1021/ma400934n
22. Synatschke CV, Schacher FH, Fortsch M, Drechsler M, Muller AHE (2011) Double-layered micellar interpolyelectrolyte complexes-how many shells to a core? Soft Matter 7:1714–1725. doi:10.1039/c0sm01195a
23. Lysenko EA et al (2004) Formation of multilayer polyelectrolyte complexes by using block ionomer micelles as nucleating particles. J Phys Chem B 108:12352–12359
24. Pergushov DV et al (2004) Micelles of polyisobutylene-block-poly(methacrylic acid) diblock copolymers and their water-soluble interpolyelectrolyte complexes formed with quaternized poly(4-vinylpyridine). Polymer 45:367–378. doi:10.1016/j.polymer.2003.10.086
25. Cai YL, Armes SP (2004) A zwitterionic ABC triblock copolymer that forms a "Trinity" of micellar aggregates in aqueous solution. Macromolecules 37:7116–7122. doi:10.1021/ma048789b
26. Jin GW et al (2012) Formation of polyion complex micelles with tunable isoelectric points based on zwitterionic block copolymers. Macromol Res 20:1249–1256. doi:10.1007/s13233-012-0177-0
27. van der Burgh S, de Keizer A, Cohen Stuart MA (2004) Complex coacervation core micelles. Colloidal stability and aggregation mechanism. Langmuir 20:1073–1084. doi:10.1021/la035012n
28. Zhulina EB, Borisov OV (2012) Theory of block polymer micelles: recent advances and current challenges. Macromolecules 45:4429–4440. doi:10.1021/ma300195n
29. Spruijt E, Sprakel J, Cohen Stuart MA, van der Gucht J (2010) Interfacial tension between a complex coacervate phase and its coexisting aqueous phase. Soft Matter 6:172–178. doi:10.1039/b911541b
30. van der Kooij HM et al (2012) On the stability and morphology of complex coacervate core micelles: from spherical to wormlike micelles. Langmuir 28:14180–14191. doi:10.1021/la303211b
31. Wang J et al (2010) Complex coacervate core micelles from iron-based coordination polymers. J Phys Chem B 114:8313–8319. doi:10.1021/jp1003209
32. Ou Z, Muthukumar M (2006) Entropy and enthalpy of polyelectrolyte complexation: Langevin dynamics simulations. J Chem Phys 124:154902
33. Laugel N et al (2006) Relationship between the growth regime of polyelectrolyte multilayers and the polyanion/polycation complexation enthalpy. J Phys Chem B 110:19443–19449. doi:10.1021/jp062264z
34. Hofs B, Voets IK, de Keizer A, Cohen Stuart MA (2006) Comparison of complex coacervate core micelles from two diblock copolymers or a single diblock copolymer with a polyelectrolyte. Phys Chem Chem Phys 8:4242–4251. doi:10.1039/b605695d
35. Courtois J, Berret J-F (2010) Probing oppositely charged surfactant and copolymer interactions by isothermal titration microcalorimetry. Langmuir 26:11750–11758. doi:10.1021/la101475x
36. Uchman M et al (2013) Thermodynamic and kinetic aspects of coassembly of PEO-PMAA block copolymer and DPCl surfactants into ordered nanoparticles in aqueous solutions studied by ITC, NMR, and time-resolved SAXS techniques. Macromolecules 46:2172–2181. doi:10.1021/ma302503w
37. Pozar J, Kovacevic D (2014) Complexation between polyallylammonium cations and polystyrenesulfonate anions: the effect of ionic strength and the electrolyte type. Soft Matter 10:6530–6545. doi:10.1039/c4sm00651h
38. Nisha CK, Manorama SV, Ganguli M, Maiti S, Kizhakkedathu JN (2004) Complexes of poly (ethylene glycol)-based cationic random copolymer and calf thymus DNA: a complete biophysical characterization. Langmuir 20:2386–2396. doi:10.1021/la035737r

39. Lindhoud S, Norde W, Cohen Stuart MA (2009) Reversibility and relaxation behavior of polyelectrolyte complex micelle formation. J Phys Chem B 113:5431–5439. doi:10.1021/jp809489f
40. Voets IK, de Keizer A, Cohen Stuart MA, Justynska J, Schlaad H (2007) Irreversible structural transitions in mixed micelles of oppositely charged diblock copolymers in aqueous solution. Macromolecules 40:2158–2164. doi:10.1021/ma0614444
41. Vitorazi L, Berret JF, Loh W (2013) Self-assembly of complex salts of cationic surfactants and anionic-neutral block copolymers. Dispersions with liquid-crystalline internal structure. Langmuir 29:14024–14033. doi:10.1021/la402624u
42. Lemmers M et al (2012) The influence of charge ratio on transient networks of polyelectrolyte complex micelles. Soft Matter 8:104–117. doi:10.1039/c1sm06281f
43. Yan Y et al (2008) Spherocylindrical coacervate core micelles formed by a supramolecular coordination polymer and a diblock copolymer. Soft Matter 4:2207–2212. doi:10.1039/b808151d
44. Kabanov VA, Zezin AB (1984) Soluble interpolymeric complexes as a new class of synthetic poly-electrolytes. Pure Appl Chem 56:343–354. doi:10.1351/pac198456030343
45. Pothayee N et al (2012) Magnetic block ionomer complexes for potential dual imaging and therapeutic agents. Chem Mater 24:2056–2063. doi:10.1021/cm3004062
46. Uchman M et al (2012) Coassembly of poly(ethylene oxide)-block-poly(methacrylic acid) and n-dodecylpyridinium chloride in aqueous solutions leading to ordered micellar assemblies within copolymer aggregates. Macromolecules 45:6471–6480. doi:10.1021/ma301510j
47. Zhang JY, Chen SG, Zhu ZY, Liu SY (2014) Stopped-flow kinetic studies of the formation and disintegration of polyion complex micelles in aqueous solution. Phys Chem Chem Phys 16:117–127. doi:10.1039/c3cp53608d
48. Voets IK et al (2009) Towards a structural characterization of charge-driven polymer micelles. Eur Phys J E 30:351–359
49. Voets IK, de Keizer A, Cohen Stuart MA (2009) Complex coacervate core micelles. Adv Colloid Interface Sci 147–148:300–318
50. Wang J, Voets IK, Fokkink R, van der Gucht J, Velders A (2014) Controlling the number of dendrimers in dendrimicelle nanoconjugates from 1 to more than 100. Soft Matter 10 (37):7337–4. doi:10.1039/c4sm01143k
51. Yan Y, de Keizer A, Cohen Stuart MA, Drechsler M, Besseling NAM (2008) Stability of complex coacervate core micelles containing metal coordination polymer. J Phys Chem B 112:10908–10914. doi:10.1021/jp8044059
52. Lemmers M, Voets IK, Cohen Stuart MA, van der Gucht J (2011) Transient network topology of interconnected polyelectrolyte complex micelles. Soft Matter 7:1378–1389
53. Lindhoud S et al (2009) Salt-induced disintegration of lysozyme-containing polyelectrolyte complex micelles. Langmuir 25:11425–11430. doi:10.1021/la901591p
54. Spruijt E, Westphal AH, Borst JW, Cohen Stuart MA, van der Gucht J (2010) Binodal compositions of polyelectrolyte complexes. Macromolecules 43:6476–6484
55. Annaka M, Morishita K, Okabe S (2007) Electrostatic self-assembly of neutral and polyelectrolyte block copolymers and oppositely charged surfactant. J Phys Chem B 111:11700–11707. doi:10.1021/jp074404q
56. Warnant J et al (2012) Physicochemical properties of pH-controlled polyion complex (PIC) micelles of poly(acrylic acid)-based double hydrophilic block copolymers and various polyamines. Anal Bioanal Chem 403:1395–1404. doi:10.1007/s00216-012-5947-1
57. Pispas S (2011) Self-assembled nanostructures in mixed anionic-neutral double hydrophilic block copolymer/cationic vesicle-forming surfactant solutions. Soft Matter 7:474–482. doi:10.1039/c0sm00499e
58. Voorn MJ (1956) Complex coacervation. Ph.D thesis, University of Utrecht
59. Plamper FA et al (2013) Spontaneous assembly of miktoarm stars into vesicular interpolyelectrolyte complexes. Macromol Rapid Commun 34:855–860. doi:10.1002/marc.201300053

60. Sousa-Herves A, Fernandez-Megia E, Riguera R (2008) Synthesis and supramolecular assembly of clicked anionic dendritic polymers into polyion complex micelles. Chem Commun (27):3136–3138. doi:10.1039/b805208e
61. Wang J et al (2012) Stable polymer micelles formed by metal coordination. Macromolecules 45:7179–7185
62. Brzozowska AM, de Keizer A, Norde W, Detrembleur C, Cohen Stuart MA (2010) Grafted block complex coacervate core micelles and their effect on protein adsorption on silica and polystyrene. Colloid Polym Sci 288:1081–1095. doi:10.1007/s00396-010-2228-4
63. Serefoglou E, Oberdisse J, Staikos G (2007) Characterization of the soluble nanoparticles formed through coulombic interaction of bovine serum albumin with anionic graft copolymers at low pH. Biomacromolecules 8:1195–1199. doi:10.1021/bm061094t
64. Chen W, Chen HR, Hu JH, Yang WL, Wang CC (2006) Synthesis and characterization of polyion complex micelles between poly(ethylene glycol)-grafted poly(aspartic acid) and cetyltrimethyl ammonium bromide. Colloids Surf A Physicochem Eng Asp 278:60–66
65. Lemmers M, Sprakel J, Voets IK, van der Gucht J, Cohen Stuart MA (2010) Multiresponsive reversible gels based on charge-driven assembly. Angew Chem Int Ed 49:708–711. doi:10.1002/anie.200905515
66. Krogstad DV et al (2013) Effects of polymer and salt concentration on the structure and properties of triblock copolymer coacervate hydrogels. Macromolecules 46:1512–1518. doi:10.1021/ma302299r
67. Stapert HR, Nishiyama N, Jiang DL, Aida T, Kataoka K (2000) Polyion complex micelles encapsulating light-harvesting ionic dendrimer zinc porphyrins. Langmuir 16:8182–8188. doi:10.1021/la000423e
68. Nishiyama N, Jang WD, Kataoka K (2007) Supramolecular nanocarriers integrated with dendrimers encapsulating photosensitizers for effective photodynamic therapy and photochemical gene delivery. New J Chem 31:1074–1082. doi:10.1039/b616050f
69. Xu L et al (2014) Self-assembly of ultralong polyion nano-ladders facilitated by ionic recognition and molecular stiffness. J Am Chem Soc. doi:10.1021/ja410443n
70. Yan Y et al (2007) Wormlike aggregates from a supramolecular coordination polymer and a diblock copolymer. J Phys Chem B 111:11662–11669. doi:10.1021/jp0718146
71. Lemmers M et al (2012) Physical gels based on charge-driven bridging of nanoparticles by triblock copolymers. Langmuir 28:12311–12318. doi:10.1021/la301917e
72. Voets IK, de Keizer A, Frederik PM, Jellema R, Cohen Stuart MA (2009) Environment-sensitive stabilization of silver nanoparticles in aqueous solutions. J Colloid Interface Sci 339:317–324
73. Gerardin C et al (2003) Highly stable metal hydrous oxide colloids by inorganic polycondensation in suspension. Angew Chem Int Ed 42:3681–3685. doi:10.1002/anie.200350917
74. Sanson N, Bouyer F, Destarac M, In M, Gerardin C (2012) Hybrid polyion complex micelles formed from double hydrophilic block copolymers and multivalent metal ions: size control and nanostructure. Langmuir 28:3773–3782. doi:10.1021/la204562t
75. Berret JF (2011) Controlling electrostatic co-assembly using ion-containing copolymers: from surfactants to nanoparticles. Adv Colloid Interface Sci 167:38–48. doi:10.1016/j.cis.2011.01.008
76. Shiraishi K, Kawano K, Maitani Y, Yokoyama M (2010) Polyion complex micelle MRI contrast agents from poly(ethylene glycol)-b-poly(L-lysine) block copolymers having Gd-DOTA; preparations and their control of T-1-relaxivities and blood circulation characteristics. J Control Release 148:160–167. doi:10.1016/j.jconrel.2010.08.018
77. Berret JF, Cristobal G, Herve P, Oberdisse J, Grillo I (2002) Structure of colloidal complexes obtained from neutral/polyelectrolyte copolymers and oppositely charged surfactants. Eur Phys J E 9:301–311. doi:10.1140/epje/i2002-10063-7
78. Gohy JF, Mores S, Varshney SK, Jerome R (2003) Self-organization of water-soluble complexes of a poly(2-vinylpyridinium)-block-poly(ethylene oxide) diblock with fluorinated anionic surfactants. Macromolecules 36:2579–2581. doi:10.1021/ma025665v

79. Oikonomou EK, Bokias G, Iliopoulos I, Kallitsis JK (2013) Sequential association of anionic/thermosensitive diblock copolymers with cationic surfactants. Macromolecules 46:1082–1092. doi:10.1021/ma302535k
80. Miyata K, Nishiyama N, Kataoka K (2012) Rational design of smart supramolecular assemblies for gene delivery: chemical challenges in the creation of artificial viruses. Chem Soc Rev 41:2562–2574. doi:10.1039/c1cs15258k
81. Lee Y et al (2010) Efficient delivery of bioactive antibodies into the cytoplasm of living cells by charge-conversional polyion complex micelles. Angew Chem Int Ed 49:2552–2555. doi:10.1002/anie.200905264
82. Harada A, Kataoka K (1999) On-off control of enzymatic activity synchronizing with reversible formation of supramolecular assembly from enzyme and charged block copolymers. J Am Chem Soc 121:9241–9242. doi:10.1021/ja9919175
83. Lindhoud S, de Vries R, Schweins R, Cohen Stuart MA, Norde W (2009) Salt-induced release of lipase from polyelectrolyte complex micelles. Soft Matter 5:242–250. doi:10.1039/b811640g
84. Harada A, Kataoka K (2003) Switching by pulse electric field of the elevated enzymatic reaction in the core of polyion complex micelles. J Am Chem Soc 125:15306–15307. doi:10.1021/ja038572h
85. Li YM, Zhou Y, De B, Li LB (2014) Folate-modified pluronic-polyethylenimine and cholic acid polyion complex micelles as targeted drug delivery system for paclitaxel. J Microencapsul 31:805–814. doi:10.3109/02652048.2014.940010
86. Yoon H, Dell EJ, Freyer JL, Campos LM, Jang WD (2014) Polymeric supramolecular assemblies based on multivalent ionic interactions for biomedical applications. Polymer 55:453–464. doi:10.1016/j.polymer.2013.12.038
87. Oe Y et al (2014) Actively-targeted polyion complex micelles stabilized by cholesterol and disulfide cross-linking for systemic delivery of siRNA to solid tumors. Biomaterials 35:7887–7895. doi:10.1016/j.biomaterials.2014.05.041
88. Bayo-Puxan N, Dufresne MH, Felber AE, Castagner B, Leroux JC (2011) Preparation of polyion complex micelles from poly(ethylene glycol)-block-polyions. J Control Release 156:118–127. doi:10.1016/j.jconrel.2011.07.027
89. Voets IK et al (2007) Electrostatically driven coassembly of a diblock copolymer and an oppositely charged homopolymer in aqueous solutions. Macromolecules 40:8476–8482. doi:10.1021/ma071356zCCC:$37.00
90. Balomenou I, Bokias G (2005) Water-soluble complexes between cationic surfactants and comb-type copolymers consisting of an anionic backbone and hydrophilic nonionic poly(N,N-dimethylacrylamide) side chains. Langmuir 21:9038–9043. doi:10.1021/la0503505
91. Matralis A, Sotiropoulou M, Bokias G, Staikos G (2006) Water-soluble stoichiometric polyelectrolyte complexes based on cationic comb-type copolymers. Macromol Chem Phys 207:1018–1025. doi:10.1002/macp.200600803
92. Harada A, Kataoka K (2003) Effect of charged segment length on physicochemical properties of core-shell type polyion complex micelles from block ionomers. Macromolecules 36:4995–5001. doi:10.1021/ma025737i
93. Dubruel P et al (2002) Synthetic polyamines as vectors for gene delivery. Polym Int 51:948–957. doi:10.1002/pi.866
94. Pispas S (2006) Soluble complexes of sodium poly(isoprene-b-methacrylate) micelles with cationic surfactants in aqueous media. J Phys Chem B 110:2649–2655. doi:10.1021/jp056008i
95. Berret JF (2009) Sphere-to-cylinder transition in hierarchical electrostatic complexes. Colloid Polym Sci 287:801–810. doi:10.1007/s00396-009-2032-1
96. Liu NJ, Wang BY, Liu WS, Bu WF (2011) Luminescent polymeric hybrids formed by platinum(II) complexes and block copolymers. Chem Commun 47:9336–9338. doi:10.1039/c1cc12192h

97. Osada K et al (2010) Quantized folding of plasmid DNA condensed with block catiomer into characteristic rod structures promoting transgene efficacy. J Am Chem Soc 132:12343–12348. doi:10.1021/ja102739b
98. Bastardo LA et al (2007) Soluble complexes in aqueous mixtures of low charge density comb polyelectrolyte and oppositely charged surfactant probed by scattering and NMR. J Colloid Interface Sci 312:21–33. doi:10.1016/j.jcis.2006.09.004
99. Golinska MD, de Wolf F, Cohen Stuart MA, Hernandez-Garcia A, de Vries R (2013) Pearl-necklace complexes of flexible polyanions with neutral-cationic diblock copolymers. Soft Matter 9:6406–6411. doi:10.1039/c3sm50536g
100. Israelachvili JN, Mitchell DJ, Ninham BW (1976) Theory of self-assembly of hydrocarbon amphiphiles into micelles and bilayers. J Chem Soc Faraday Trans Ii 72:1525–1568. doi:10.1039/f29767201525
101. Zhulina EB, Adam M, LaRue I, Sheiko SS, Rubinstein M (2005) Diblock copolymer micelles in a dilute solution. Macromolecules 38:5330–5351. doi:10.1021/ma048102n
102. Voets IK et al (2006) Double-faced micelles from water-soluble polymers. Angew Chem Int Ed 45:6673–6676. doi:10.1002/anie.200601000
103. Voets IK et al (2008) On the transition between a heterogeneous and homogeneous corona in mixed polymeric micelles. Langmuir 24:12221–12227. doi:10.1021/la801816p
104. Voets IK et al (2009) Spontaneous symmetry breaking: formation of Janus micelles. Soft Matter 5:999–1005
105. Bouyer F, Gerardin C, Fajula F, Putaux JL, Chopin T (2003) Role of double-hydrophilic block copolymers in the synthesis of lanthanum-based nanoparticles. Colloids Surf A 217:179–184. doi:10.1016/s0927-7757(02)00574-5
106. Bouyer F, Sanson N, Destarac M, Gerardin C (2006) Hydrophilic block copolymer-directed growth of lanthanum hydroxide nanoparticles. New J Chem 30:399–408. doi:10.1039/b516368d
107. Jiang X et al (2011) String-like micellar nanoparticles formed by complexation of PEG-b-PPA and plasmid DNA and their transfection efficiency. Pharm Res 28:1317–1327. doi:10.1007/s11095-011-0436-3
108. Gohy JF, Varshney SK, Jerome R (2001) Morphology of water-soluble interpolyelectrolyte complexes formed by poly(2-vinylpyridinium)-block-poly(ethylene oxide) diblocks and poly(4-styrenesulfonate) polyanions. Macromolecules 34:2745–2747. doi:10.1021/ma002131q
109. Fresnais J, Berret JF, Frka Petesic B, Sandre O, Perzynski R (2008) Electrostatic co assembly of iron oxide nanoparticles and polymers: towards the generation of highly persistent superparamagnetic nanorods. Adv Mater 20:3877–3881
110. Solomatin SV, Bronich TK, Eisenberg A, Kabanov VA, Kabanov AV (2007) Nanomaterials from ionic block copolymers and single-, double-, and triple-tail surfactants. Langmuir 23:2838–2842. doi:10.1021/la062693o
111. Kishimura A, Koide A, Osada K, Yamasaki Y, Kataoka K (2007) Encapsulation of myoglobin in PEGylated polyion complex vesicles made from a pair of oppositely charged block lonomers: a physiologically available oxygen carrier. Angew Chem Int Ed 46:6085–6088. doi:10.1002/anie.200701776
112. Anraku Y, Kishimura A, Oba M, Yamasaki Y, Kataoka K (2010) Spontaneous formation of nanosized unilamellar polyion complex vesicles with tunable size and properties. J Am Chem Soc 132:1631–1636. doi:10.1021/ja908350e
113. Anraku Y, Kishimura A, Yamasaki Y, Kataoka K (2013) Living unimodal growth of polyion complex vesicles via two-dimensional supramolecular polymerization. J Am Chem Soc 135:1423–1429. doi:10.1021/ja3096587
114. Hu ZJ, Jonas AM, Varshney SK, Gohy JF (2005) Dilution-induced spheres-to-vesicles morphological transition in micelles from block copolymer/surfactant complexes. J Am Chem Soc 127:6526–6527. doi:10.1021/ja050053m
115. Bronich TK et al (2002) Synthesis of vesicles on polymer template. J Am Chem Soc 124:11872–11873. doi:10.1021/ja020509p

116. Kabanov AV, Bronich TK, Kabanov VA, Yu K, Eisenberg A (1998) Spontaneous formation of vesicles from complexes of block ionomers and surfactants. J Am Chem Soc 120:9941–9942. doi:10.1021/ja981922t
117. Koide A et al (2006) Semipermeable polymer vesicle (PICsome) self-assembled in aqueous medium from a pair of oppositely charged block copolymers: physiologically stable micro-/nanocontainers of water-soluble macromolecules. J Am Chem Soc 128:5988–5989. doi:10.1021/ja057993r
118. Korobko AV, Backendorf C, van der Maarel JRC (2006) Plasmid DNA encapsulation within cationic diblock copolymer vesicles for gene delivery. J Phys Chem B 110:14550–14556. doi:10.1021/jp057363b
119. Korobko AV, Jesse W, van der Maarel JRC (2005) Encapsulation of DNA by cationic diblock copolymer vesicles. Langmuir 21:34–42. doi:10.1021/la047967r
120. Lindhoud S, de Vries R, Norde W, Cohen Stuart MA (2007) Structure and stability of complex coacervate core micelles with lysozyme. Biomacromolecules 8:2219–2227. doi:10.1021/bm0700688
121. Lindhoud S, Norde W, Cohen Stuart MA (2010) Effects of polyelectrolyte complex micelles and their components on the enzymatic activity of lipase. Langmuir 26:9802–9808
122. Harada A, Kataoka K (1998) Novel polyion complex micelles entrapping enzyme molecules in the core: preparation of narrowly-distributed micelles from lysozyme and poly(ethylene glycol)-poly(aspartic acid) block copolymer in aqueous medium. Macromolecules 31:288–294
123. Yuan XF, Yamasaki Y, Harada A, Kataoka K (2005) Characterization of stable lysozyme-entrapped polyion complex (PIC) micelles with crosslinked core by glutaraldehyde. Polymer 46:7749–7758. doi:10.1016/j.polymer.2005.02.121
124. Harada A, Kataoka K (1999) Novel polyion complex micelles entrapping enzyme molecules in the core. 2. Characterization of the micelles prepared at nonstoichiometric mixing ratios. Langmuir 15:4208–4212. doi:10.1021/la981087t
125. Kawamura A, Harada A, Kono K, Kataoka K (2007) Self-assembled nano-bioreactor from block ionomers with elevated and stabilized enzymatic function. Bioconjug Chem 18:1555–1559. doi:10.1021/bc070029t
126. Balasubramanian V, Onaca O, Enea R, Hughes DW, Palivan CG (2010) Protein delivery: from conventional drug delivery carriers to polymeric nanoreactors. Expert Opin Drug Deliv 7:63–78. doi:10.1517/17425240903394520
127. Solomatin SV et al (2003) Environmentally responsive nanoparticles from block ionomer complexes: effects of pH and ionic strength. Langmuir 19:8069–8076. doi:10.1021/la0300151
128. Solomatin SV, Bronich TK, Eisenberg A, Kabanov VA, Kabanov AV (2004) Colloidal stability of aqueous dispersions of block ionomer complexes: effects of temperature and salt. Langmuir 20:2066–2068. doi:10.1021/la034895f
129. Sanson N, Bouyer F, Gérardin C, In M (2004) Nanoassemblies formed from hydrophilic block copolymers and multivalent ions. Phys Chem Chem Phys 6:1463–1466
130. Herlambang S et al (2011) Disulfide crosslinked polyion complex micelles encapsulating dendrimer phthalocyanine directed to improved efficiency of photodynamic therapy. J Control Release 155:449–457. doi:10.1016/j.jconrel.2011.06.019
131. Jaturanpinyo M, Harada A, Yuan XF, Kataoka K (2004) Preparation of bionanoreactor based on core-shell structured polyion complex micelles entrapping trypsin in the core cross-linked with glutaraldehyde. Bioconjug Chem 15:344–348. doi:10.1021/bc034149m
132. Kim JO et al (2013) Cross-linked polymeric micelles based on block ionomer complexes. Mendeleev Commun 23:179–186. doi:10.1016/j.mencom.2013.07.001
133. Kakizawa Y, Harada A, Kataoka K (1999) Environment-sensitive stabilization of core-shell structured polyion complex micelle by reversible cross-linking of the core through disulfide bond. J Am Chem Soc 121:11247–11248. doi:10.1021/ja993057y

134. Bourouina N, Cohen Stuart MA, Kleijn JM (2014) Complex coacervate core micelles as diffusional nanoprobes. Soft Matter 10:320–331. doi:10.1039/c3sm52245h
135. Zhao L, Yan Y, Huang JB (2012) Redox-gated potential micellar carriers based on electrostatic assembly of soft coordination suprapolymers. Langmuir 28:5548–5554. doi:10.1021/la300590t
136. Atanase LI, Riess G (2013) Micellization of pH-stimulable poly(2-vinylpyridine)-b-poly (ethylene oxide) copolymers and their complexation with anionic surfactants. J Colloid Interface Sci 395:190–197. doi:10.1016/j.jcis.2012.12.058
137. Kataoka K, Harada A, Nagasaki Y (2012) Block copolymer micelles for drug delivery: design, characterization and biological significance. Adv Drug Deliv Rev 64:37–48. doi:10.1016/j.addr.2012.09.013
138. Lee Y, Kataoka K (2009) Biosignal-sensitive polyion complex micelles for the delivery of biopharmaceuticals. Soft Matter 5:3810–3817. doi:10.1039/b909934d
139. Kovacevic D, van der Burgh S, de Keizer A, Cohen Stuart MA (2002) Kinetics of formation and dissolution of weak polyelectrolyte multilayers: role of salt and free polyions. Langmuir 18:5607–5612
140. Spruijt E, Sprakel J, Lemmers M, Cohen Stuart MA, van der Gucht J (2010) Relaxation dynamics at different time scales in electrostatic complexes: time-salt superposition. Phys Rev Lett 105(20). doi:10.1103/PhysRevLett.105.208301
141. Spruijt E, Cohen Stuart MA, van der Gucht J (2013) Linear viscoelasticity of polyelectrolyte complex coacervates. Macromolecules 46:1633–1641. doi:10.1021/ma301730n
142. Spruijt E, van den Berg SA, Cohen Stuart MA, van der Gucht J (2012) Direct measurement of the strength of single ionic bonds between hydrated charges. ACS Nano 6:5297–5303. doi:10.1021/nn301097y
143. Weinbreck F, de Vries R, Schrooyen P, de Kruif CG (2003) Complex coacervation of whey proteins and gum arabic. Biomacromolecules 4:293–303. doi:10.1021/bm025667n
144. Spruijt E, Cohen Stuart MA, van der Gucht J (2010) Dynamic force spectroscopy of oppositely charged polyelectrolyte brushes. Macromolecules 43:1543–1550
145. Harada A, Kataoka K (1999) Chain length recognition: core-shell supramolecular assembly from oppositely charged block copolymers. Science 283:65–67. doi:10.1126/science.283.5398.65
146. Bakeev KN, Izumrudov VA, Kuchanov SI, Zezin AB, Kabanov VA (1992) Kinetics and mechanism of interpolyelectrolyte exchange and addition-reactions. Macromolecules 25:4249–4254. doi:10.1021/ma00043a003
147. Dautzenberg H, Rother G (2004) Response of polyelectrolyte complexes to subsequent addition of sodium chloride: time-dependent static light scattering studies. Macromol Chem Phys 205:114–121. doi:10.1002/macp.200350083
148. Kabanov AV, Kabanov VA (1998) Interpolyelectrolyte and block ionomer complexes for gene delivery: physicochemical aspects. Adv Drug Deliv Rev 30:49–60. doi:10.1016/s0169-409x(97)00106-3
149. Chelushkin PS et al (2008) Polyion complex nanomaterials from block polyelectrolyte micelles and linear polyelectrolytes of opposite charge. 2. Dynamic properties. J Phys Chem B 112:7732–7738. doi:10.1021/jp8012877
150. Hofs B, de Keizer A, Cohen Stuart MA (2007) On the stability of (highly aggregated) polyelectrolyte complexes containing a charged-block-neutral diblock copolymer. J Phys Chem B 111:5621–5627. doi:10.1021/jp0714318
151. Holappa S, Kantonen L, Andersson T, Winnik F, Tenhu H (2005) Overcharging of polyelectrolyte complexes by the guest polyelectrolyte studied by fluorescence spectroscopy. Langmuir 21:11431–11438. doi:10.1021/la051866r
152. Kakizawa Y, Kataoka K (2002) Block copolymer micelles for delivery of gene and related compounds. Adv Drug Deliv Rev 54:203–222

153. Katayose S, Kataoka K (1998) Remarkable increase in nuclease resistance of plasmid DNA through supramolecular assembly with poly(ethylene glycol) poly(L-lysine) block copolymer. J Pharm Sci 87:160–163. doi:10.1021/js970304s
154. Katayose S, Kataoka K (1997) Water-soluble polyion complex associates of DNA and poly (ethylene glycol)-poly(L-lysine) block copolymer. Bioconjug Chem 8:702–707. doi:10.1021/bc9701306
155. Dautzenberg H, Konak C, Reschel T, Zintchenko A, Ulbrich K (2003) Cationic graft copolymers as carriers for delivery of antisense-oligonucleotides. Macromol Biosci 3:425–435
156. Kataoka K, Harada A, Nagasaki Y (2001) Block copolymer micelles for drug delivery: design, characterization and biological significance. Adv Drug Deliv Rev 47:113–131. doi:10.1016/s0169-409x(00)00124-1
157. Attia ABE et al (2011) Mixed micelles self-assembled from block copolymers for drug delivery. Curr Opin Colloid Interface Sci 16:182–194. doi:10.1016/j.cocis.2010.10.003
158. Osada K, Christie RJ, Kataoka K (2009) Polymeric micelles from poly(ethylene glycol)-poly (amino acid) block copolymer for drug and gene delivery. J R Soc Interface 6:S325–S339. doi:10.1098/rsif.2008.0547.focus
159. De Santis S, Diociaiuti M, Cametti C, Masci G (2014) Hyaluronic acid and alginate covalent nanogels by template cross-linking in polyion complex micelle nanoreactors. Carbohydr Polym 101:96–103. doi:10.1016/j.carbpol.2013.09.033
160. Colfen H (2001) Double-hydrophilic block copolymers: synthesis and application as novel surfactants and crystal growth modifiers. Macromol Rapid Commun 22:219–252. doi:10.1002/1521-3927(20010201)22:4<219::aid-marc219>3.0.co;2-g
161. Motornov M, Roiter Y, Tokarev I, Minko S (2010) Stimuli-responsive nanoparticles, nanogels and capsules for integrated multifunctional intelligent systems. Prog Polym Sci 35:174–211. doi:10.1016/j.progpolymsci.2009.10.004
162. Zhang J, Liu Y, Li Y, Zhao HX, Wan XH (2012) Hybrid assemblies of Eu-containing polyoxometalates and hydrophilic block copolymers with enhanced emission in aqueous solution. Angew Chem Int Ed 51:4598–4602. doi:10.1002/anie.201107481
163. Liu B, Bazan GC (2004) Homogeneous fluorescence-based DNA detection with water-soluble conjugated polymers. Chem Mater 16:4467–4476. doi:10.1021/cm049587x
164. Liu B, Bazan GC (2004) Interpolyelectrolyte complexes of conjugated copolymers and DNA: platforms for multicolor biosensors. J Am Chem Soc 126:1942–1943. doi:10.1021/ja038667j
165. Yang C-C, Tian Y, Jen AKY, Chen W-C (2006) New environmentally responsive fluorescent N-isopropylacrylamide copolymer and its application to DNA sensing. J Polym Sci Part A Polym Chem 44:5495–5504. doi:10.1002/pola.21629
166. Fresnais J, Ishow E, Sandre O, Berret JF (2009) Electrostatic co-assembly of magnetic nanoparticles and fluorescent nanospheres: a versatile approach towards bimodal nanorods. Small 5:2533–2536. doi:10.1002/smll.200900703
167. Chevry L, Sampathkumar NK, Cebers A, Berret JF (2013) Magnetic wire-based sensors for the microrheology of complex fluids. Phys Rev E 88(6), 062306. doi:10.1103/PhysRevE.88.062306
168. Chevry L, Colin R, Abou B, Berret JF (2013) Intracellular micro-rheology probed by micron-sized wires. Biomaterials 34:6299–6305. doi:10.1016/j.biomaterials.2013.05.002
169. Hunt JN et al (2011) Tunable, high modulus hydrogels driven by ionic coacervation. Adv Mater 23:2327. doi:10.1002/adma.201004230
170. Tamesue S et al (2013) Linear versus dendritic molecular binders for hydrogel network formation with clay nanosheets: studies with ABA triblock copolyethers carrying guanidinium ion pendants. J Am Chem Soc 135:15650–15655. doi:10.1021/ja408547g
171. Brzozowska AM et al (2009) Reduction of protein adsorption on silica and polystyrene surfaces due to coating with complex coacervate core micelles. Colloids Surf A 347:146–155. doi:10.1016/j.colsurfa.2009.03.036

172. Brzozowska AM, Zhang Q, de Keizer A, Norde W, Cohen Stuart MA (2010) Reduction of protein adsorption on silica and polysulfone surfaces coated with complex coacervate core micelles with poly(vinyl alcohol) as a neutral brush forming block. Colloids Surf A 368:96–104. doi:10.1016/j.colsurfa.2010.07.023
173. Hofs B, Brzozowska A, de Keizer A, Norde W, Cohen Stuart MA (2008) Reduction of protein adsorption to a solid surface by a coating composed of polymeric micelles with a glass-like core. J Colloid Interface Sci 325:309–315. doi:10.1016/j.jcis.2008.06.006
174. van der Burgh S, Fokkink R, de Keizer A, Cohen Stuart MA (2004) Complex coacervation core micelles as anti-fouling agents on silica and polystyrene surfaces. Colloids Surf A 242:167–174. doi:10.1016/j.colsurfa.2004.04.068
175. de Vos WM, Meijer G, de Keizer A, Cohen Stuart MA, Kleijn JM (2010) Charge-driven and reversible assembly of ultra-dense polymer brushes: formation and antifouling properties of a zipper brush. Soft Matter 6:2499–2507. doi:10.1039/b926017j
176. Voets IK, de Keizer A, Cohen Stuart MA, de Waard P (2006) Core and corona structure of mixed polymeric micelles. Macromolecules 39:5952–5955. doi:10.1021/ma060965o
177. Voets IK et al (2008) Temperature responsive complex coacervate core micelles with a PEO and PNIPAAm corona. J Phys Chem B 112:10833–10840. doi:10.1021/jp8014832
178. Voets IK et al (2009) Electrostatic hierarchical co-assembly in aqueous solutions of two oppositely charged double hydrophilic diblock copolymers. Eur Polym J 45:2913–2925. doi:10.1016/j.eurpolymj.2009.06.020
179. Feng J, Ruckenstein E (2006) Self-recognition and aggregation between diblock (charged/neutral) polyelectrolytes by Monte Carlo simulations. J Chem Phys 124(12), 124913. doi:10.1063/1.2177248
180. Gus'kova OA, Pavlov AS, Khalatur PG, Khokhlov AR (2007) Molecular bottle brushes in a solution of semiflexible polyelectrolytes and block copolymers with an oppositely charged block: a molecular dynamics simulation. J Phys Chem B 111:8360–8368. doi:10.1021/jp067222p
181. Kriz J, Dybal J, Dautzenberg H (2001) Cooperative interactions of unlike macromolecules: 3. NMR and theoretical study of the electrostatic coupling of sodium polyphosphates with diallyl(dimethyl)ammonium chloride-acrylamide copolymers. J Phys Chem A 105:7486–7493. doi:10.1021/jp010185b
182. Krotova MK, Vasilevskaya VV, Khokhlov AR (2009) The effect of a low-molecular-mass salt on stoichiometric polyelectrolyte complexes composed of oppositely charged macromolecules with different solvent affinities. Polym Sci Ser A 51:1075–1082. doi:10.1134/s0965545x09100046
183. Ziebarth J, Wang YM (2010) Coarse-grained molecular dynamics simulations of DNA condensation by block copolymer and formation of core-corona structures. J Phys Chem B 114:6225–6232. doi:10.1021/jp908327q
184. Brzozowska AM, Keesman KJ, de Keizer A, Leermakers FAM (2011) Formation and structure of ionomer complexes from grafted polyelectrolytes. Colloid Polym Sci 289:889–902. doi:10.1007/s00396-010-2368-6
185. Wang W et al (2012) Complex coacervate micelles formed by a C18-capped cationic triblock thermoresponsive copolymer interacting with SDS. Soft Matter 8:11514–11525. doi:10.1039/c2sm26567b
186. Stepanek M et al (2012) Wormlike core-shell nanoparticles formed by co-assembly of double hydrophilic block polyelectrolyte with oppositely charged fluorosurfactant. Soft Matter 8:9412–9417. doi:10.1039/c2sm25588j
187. Berret JF et al (2004) Electrostatic self-assembly of oppositely charged copolymers and surfactants: a light, neutron, and X-ray scattering study. Macromolecules 37:4922–4930
188. Voets IK, Leermakers FA, de Keizer A, Charlaganov M, Cohen Stuart MA (2011) In: Muller AHE, Borisov O (eds) Self organized nanostructures of amphiphilic block copolymers I vol. 241. Advances in polymer science. pp 163–185

Theoretical Principles of Fluorescence Spectroscopy

Zuzana Limpouchová and Karel Procházka

Contents

Abstract The chapter outlines general principles of fluorescence spectroscopy. Basic principles of radiative and nonradiative transitions (including the Jablonski diagram and Franck–Condon principle) are described and explained. The fundamentals of important fluorescence techniques, such as the steady-state and time-resolved measurements, fluorescence anisotropy, solvent relaxation method, fluorescence quenching, and nonradiative energy transfer, are discussed in detail. Special attention is devoted to the fast dynamics of individual transitions and processes influencing them at the molecular level. The end of the chapter focuses on excimers and exciplexes and mainly on the weakly bound complexes (so-called J and H aggregates), because the literature describing their behavior is relatively rare and pertinent pieces of information are not easy to find.

Z. Limpouchová (✉) • K. Procházka (✉)
Department of Physical and Macromolecular Chemistry, Faculty of Science, Charles University in Prague, Hlavova 2030, 128 40 Prague 2, Czech Republic
e-mail: zl@natur.cuni.cz; karel.prochazka@natur.cuni.cz

K. Procházka (ed.), *Fluorescence Studies of Polymer Containing Systems*, Springer Series on Fluorescence 16, DOI 10.1007/978-3-319-26788-3_4

Keywords Steady-state fluorescence spectra • Time-resolved fluorescence decays • Fluorescence anisotropy • Fluorescence quenching • Nonradiative excitation energy transfer • Solvent relaxation • Excimer • J and H aggregates

1 Introduction

Fluorescence spectroscopy is a technique that is frequently used for studying the conformation and dynamics of natural and synthetic macromolecules. This is a very versatile experimental method, which has been used in both macromolecular and colloid science and in biomedical research and also in a number of studies of low-molar-mass compounds. At present, various sophisticated fluorometers can be found among the equipment of a number of laboratories that perform polymer, biopolymer, and biomedical research (not only standard high-resolution steady-state and time-resolved apparatuses, but also fluorescent microscopes equipped with detectors and software packages that enable monitoring and analysis of multicolor time-resolved emissions from tiny polymeric nanodomains or individual organelles in living cells, etc.). The widespread use of hi-tech and simultaneously user-friendly fluorescence techniques offers new possibilities for research in various fields, but simultaneously leads to the danger of misinterpretation of the results of advanced fluorescence techniques in routine studies. Fluorescence spectroscopy is an indirect technique. The emission characteristics are influenced by an intricate interplay of different factors and should be interpreted with care and precaution. Plausible and unambiguous conclusions not only depend on profound knowledge of fluorescence principles, but almost always require additional information on the studied system provided by independent methods.

In addition to the complicated response of the fluorophore to various stimuli, one more aspect should be borne in mind. Only a small number of systems contain intrinsic fluorophores and are inherently fluorescent. Such systems (e.g., tryptophan-containing proteins) can be studied directly and reliable information on the positions, mobility, and accessibility of tryptophan residues for different molecules can be relatively easily obtained. In a majority of cases, a successful fluorescence study requires the addition of a low content of an extrinsic fluorescent probe, which modifies not only optical but also other properties of the studied system. An extrinsic probe "feels" only the effect of its immediate microenvironment, which has undoubtedly been altered by its insertion. Even though the change in the system is negligible at a macroscopic level, most fluorescence methods report the behavior of the tiny perturbed part of the system. Therefore, the extent and nature of possible perturbation of the system must also be investigated to enable description of the behavior of the unperturbed system.

The broad applicability of various fluorescence methods for investigation of both the static and the dynamic properties of different systems is based on two pillars:

1. Fluorescence is a spontaneous spin-allowed emission of a photon from the excited state, accompanied by the transition of the fluorophore to the ground state. It is a phenomenon that concerns energetically rich species (excited fluorophores) that strongly interact with the surrounding molecules and their properties (including the fluorescence characteristics) are influenced by interactions with the microenvironment. Therefore, fluorescence measurements provide useful (even though indirect) information on the host system. Because only the immediately neighboring molecules interact with the fluorophore, fluorescence techniques can be used for probing micro- and nanodomains, in which the fluorescent probe is embedded, over very short distances.
2. The excitation (absorption of a photon) and the red-shifted emission are two distinct events that are separated by a time window ranging from units to hundreds of nanoseconds depending on the fluorophore and the host system. This enables monitoring fast kinetics, because a number of molecular processes proceed on this timescale in small volumes delimited by distances comparable with the range of intermolecular interactions and affect the time-dependent emission characteristics. They include translational and rotational diffusion of the fluorophore, reorientation of molecules in the solvation shell, segmental dynamics of flexible macromolecules, and nonradiative excitation energy transfer, etc.

2 The Jablonski Diagram and Characteristics of Time-Dependent Fluorescence

It is common and convenient to discuss radiative and nonradiative transitions, as well as other processes that either lead to photochemical reactions or influence emission on the basis of the Jablonski diagram (Fig. 1), which provides a scheme of the energy levels of the electronic and vibrational states of a molecule and outlines possible routes between the states [1]. The vertical axis corresponds to increasing energy of different stable states with optimum geometry (i.e., with a minima on the energy hypersurfaces). The horizontal axis does not have any physical meaning. It is used to provide sufficient space for inclusion and description of the relevant processes. When discussing the spectroscopic characteristics of single molecules, the lines usually represent energies that can be obtained by quantum chemistry calculations in vacuum, while in condensed systems, e.g., in solutions, they represent the Gibbs free energies (i.e., potentials of the mean force) of the solvated fluorophores. The arrows (straight and curved) indicate possible transitions between different states. Typical values of the rate constants of the relevant processes are given next to the arrows.

The observation and investigation of a spontaneous emission of photons from a macroscopic sample assumes the excitation of a certain fraction of molecules to higher electronic energy states. Excitation can be achieved by different means (absorption of light, excitation energy transfer, chemical reaction, etc.). This part

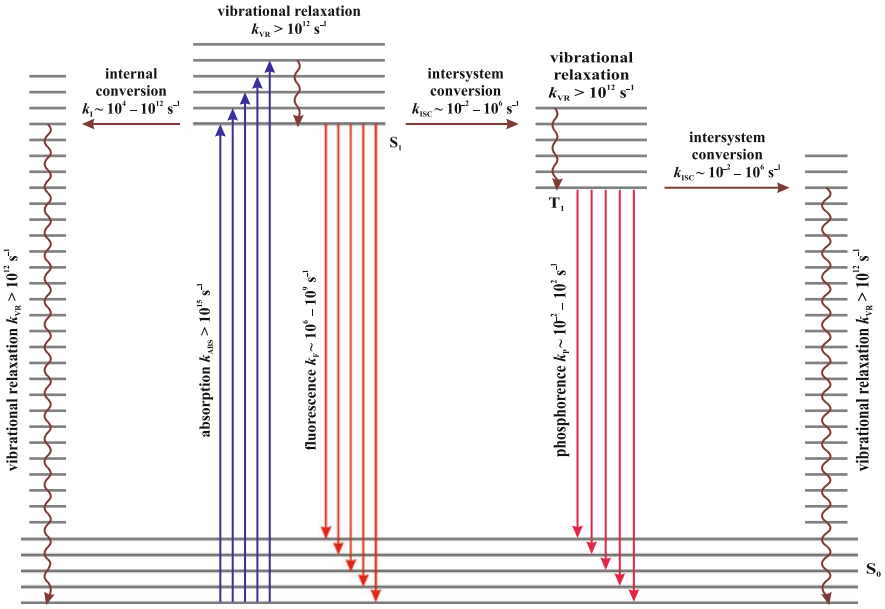

Fig. 1 Jablonski diagram: the energies of the ground electronic singlet state S_0, excited singlet S_1, and triplet T_1 (together with relevant vibrational states) are depicted by *horizontal lines*; the most important optical and nonradiative transitions are depicted by *arrows* and *wavy lines*, respectively; the typical values (in orders of magnitudes) of rate constants of the processes have been also included. Adapted from Springer, Self Organized Nanostructures of Amphiphilic Block Copolymers I, 241, 2011, 187–249, figure 1, [2]. Copyright 2011. With kind permission from Springer Science and Business Media

of the review focuses on the spectroscopic process (absorption of photons), which assumes irradiation of the sample by incident light of an appropriate wavelength. Under the current conditions of spectroscopic measurements, which employ fairly weak excitation light intensity, only a low fraction of the molecules of the fluorophore (less that 10^{-6}) interact (collide) with passing photons, absorb them, and become excited. Before discussing emission from a macroscopic sample, we will analyze all the processes that can occur at the level of a single molecule.

We will concentrate on the behavior of common fluorophores at ambient temperatures, i.e., on molecules with fully paired spin only of the valence electrons, i.e., we will not discuss the photophysical behavior of radicals, biradicals, etc. Under ambient conditions, the fluorophore occurs in the lowest vibrational state of the lowest electronic state (ground state, S_0). The probability of absorption of a photon is proportional to the square of the transition dipole moment (which, to a first approximation, represents the difference between the dipole moments in the excited and ground states). It is convenient to formulate the optical selection rules which summarize the roles of several important factors [3–5]. The most severe restriction concerns the spin. Within the Born–Oppenheimer approximation, which postulates that the slow motion of nuclei can be (from a mechanistic point of view) separated

from the fast motion of electrons, the spin must be conserved. In the opposite case, the transition is strictly forbidden. In reality, the spin–orbit interaction in molecules containing atoms with several valence electrons (carbon, nitrogen, oxygen, etc.) relaxes this selection rule and, in addition to spin-allowed transitions (fluorescence), also singlet–triplet and triplet–singlet transitions (intersystem crossing) can be observed in some systems. In the latter case, the radiative transition is called phosphorescence. However, the probability of intersystem crossing is very low. It is weakened by a factor of ca. 10^{-5}–10^{-7} in comparison with a fully allowed transition. The second restriction concerns the symmetry of the wave functions of states involved in the transition. As the transition dipole moment operator is antisymmetric and its product with the wave functions of both states must be symmetric to yield a nonzero value after 3D integration over the space, a strictly symmetry-allowed transition can occur only between two states described by symmetric and antisymmetric wave functions (or vice versa). Nevertheless, antisymmetric vibrations can relax the symmetry selection rule and various "forbidden" transitions (weakened only by a factor of 10^{-1} to 10^{-3}) can be observed in a number of systems (e.g., some strong bands in the fluorescence spectra of condensed aromatic molecules, such as naphthalene, anthracene, etc., are, strictly speaking, symmetry-forbidden transitions and occur only thanks to antisymmetric vibrations). The last condition concerns the overlap of wave functions: a large value of the transition dipole moment (difference between the dipole moments in the two states) requires the redistribution of the cloud of electrons during the transition, but the electronic wave functions of both states should acquire nonzero (preferentially large) values in the same places, i.e., the wave functions must overlap reasonably in space to yield a nonzero value after the integration of their product with the transition dipole moment operator. The overlap of the ground and exited wave functions differs from one fluorophore to another and the weakening factor ranges from 10^{-1} to 10^{-5}; e.g., the $n \rightarrow \pi^*$ transition (absorption) in compounds containing an aliphatic carbonyl group involves a transition from the non-bonding orbital localized on the oxygen atom to the antibonding orbital localized mainly on the carbon atom—in this particular case, the overlap is small and the absorption is weak in spite of considerable redistribution of electrons.

The transition of a molecule to a higher excited state due to the absorption of a photon is one of the fastest processes on Earth. It is accomplished in times shorter than 10^{-15} s. No chemical process can proceed with a comparable speed and only a few nuclear processes, which occur over extremely short length scales of 10^{-15} m, are faster. This means that the transition proceeds adiabatically without interaction of the fluorophore with the microenvironment and there is no change in either the positions of the nuclei of atoms forming the fluorophore or in the arrangement of the surrounding molecules. It follows that the molecule retains the ground-state geometry immediately upon excitation. The consequences of the high transition speed can be easily illustrated for a diatomic molecule (see Fig. 2). In this case, the energy of the states depends only on the distance between the two nuclei and can be expressed by the Morse function. A detailed energy scheme can be appropriately depicted in 2D representation and individual photophysical processes can be

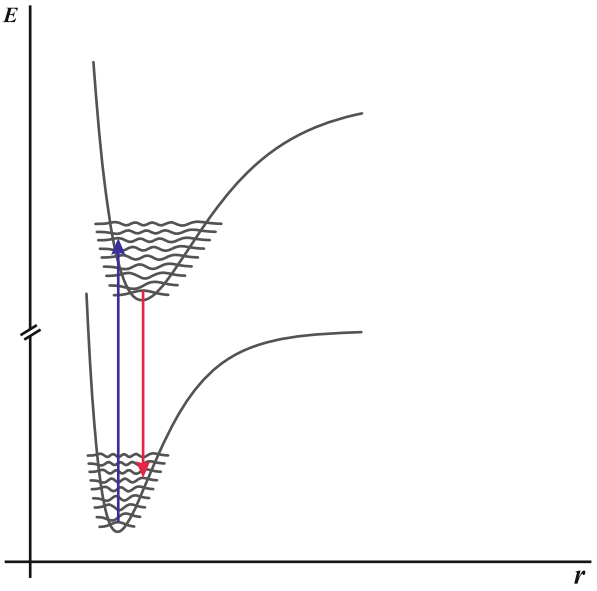

Fig. 2 The Franck–Condon principle: the energies of the ground and the first excited singlet states, S_0 (*lower curve*) and S_1 (*upper curve*), respectively, of a diatomic molecule are presented as functions of the distance between atoms, *r*. Several vibration wave functions (*note*: the probabilities of interatomic distances are proportional to the square of the corresponding wave functions) are also depicted. The *vertical arrows* stand for the most probable absorption and emission.

comprehensively discussed and simply explained. The lowest curve shows the energy of the ground state (vertical axis) as a function of the separation of the two nuclei (horizontal axis). The horizontal wave lines depict several selected vibrational states. The grey curves show the corresponding wave functions (note that the geometry of the molecule with a given separation of nuclei is proportional to the square of the corresponding wave function value for this distance). The curve corresponding to the bonding excited state is shifted to the right because the excited (energetically richer) bimolecular molecule is generally larger.

At ambient temperatures, the ground-state molecule occurs in the lowest vibrational state and the most probable distance between the nuclei r_E lies close to the position of the minimum of the lowest Morse curve. As the distance of the nuclei does not change during excitation, it is evident that the absorption of a photon generates not only electronically, but also vibrationally excited states (to satisfy the condition of sufficient overlap of the vibrational wave functions of the two states—the Franck–Condon principle [6, 7]—see Fig. 2).

The most probable transitions are depicted by the upward pointing vertical arrows. Upon excitation, the molecule tries to get rid of the excess energy as fast as possible. The fastest process possible in condensed media (although slower by several orders of magnitude than the absorption) is vibrational relaxation. This is a nonradiative process and it proceeds in most nonviscous solutions on timescales of 10^{-14} to 10^{-12} s. The excess energy (of excited vibrations) is rapidly and efficiently transferred to the surrounding medium during collisions with neighboring molecules, because the masses of the colliding particles are comparable and the frequency coincides with the frequency of intermolecular collisions. After the

vibrational relaxation, the excited molecule ends up in the lowest vibrational state of the electronic excited state and then the emission of a photon, i.e., radiative transition to the ground state (fluorescence) can occur. However, a number of fast nonradiative processes compete with fluorescence. They will be discussed later.

The probability of the spin-allowed $S_1 \rightarrow S_0$ emission of a photon (fluorescence) depends, similarly to the absorption probability, on a change in the dipole moment during the transition and on the energy difference between the states. For a fully (spin, symmetry, and overlap) allowed transition, the quantum mechanics calculation yields a rate constant of about 10^9 s^{-1}. This means that the natural mean lifetimes of the excited state of common fluorophores are nanoseconds. The real lifetimes of a number of important fluorophores can be longer (tens to hundreds of nanoseconds) if the transition is not fully allowed, but it can be much shorter (in the picosecond range) if nonradiative processes efficiently deplete the excited state. In both cases, the normalized fluorescence intensity (number of photons emitted per second from a unit volume of a macroscopic ensemble of fluorophores normalized by a number of incident photons passing this volume) is weaker than expected. In an overwhelming majority of cases (flexible molecules strongly interacting with the surrounding medium), the nonradiative depletion of the excited state quenches the fluorescence completely and only a small number of rigid molecules (e.g., condensed aromatic rings) are fluorophores of practical use. It is necessary to realize that, regardless of the actual lifetime of the excited state, the single act of emission of a photon and the $S_1 \rightarrow S_0$ transition proceed in times of ca. 10^{-15} ns and the ground-state fluorophore ends up in a vibrationally excited state (see Fig. 2, where the emission is depicted by the downward pointing arrows). Then a fast vibrational relaxation takes place on a ps timescale and the fluorophore returns to its lowest possible energetic state, which (together with vibrational relaxation after the excitation) explains the intrinsic Stokes shift of the emission towards the red part of the spectral region with respect to the absorption wavelength [8].

Because both the absorption and emission proceed between states S_0 and S_1 and their probabilities depend on the same dipole moments, it is not surprising that there is (in most cases) a linear relationship between the molar absorption coefficient and the rate constant of the spontaneous emission (the higher the absorption probability, the higher the emission intensity). However, because the competing processes often deplete the excited state faster than fluorescence, the observed emission intensity is usually considerably weaker than expected. The relationship between the absorption coefficients of $S_0 \rightarrow S_i$ excitations ($i \geq 2$) and the rate of $S_1 \rightarrow S_0$ emission is not straightforward. If the molecule is excited to higher electronic states S_2, S_3, etc., in an overwhelming majority of cases, the excited molecule reaches the lowest vibrational level of the lowest excited S_1 state by a cascade of vibrational relaxation processes on a ps timescale before the emission of a photon occurs. There are only a few exceptions from the rule postulating that the emission always proceeds from S_1, e.g., azulene [9] exhibits fluorescence from S_2.

So far we have considered various processes at the level of only one molecule. However, fluorescence spectroscopy is used for studying macroscopic samples. Thus, the emission of photons from a large number of excited fluorophores is

monitored and analyzed (except for single-molecule fluorescence spectroscopy and fluorescence-correlation spectroscopy). Under current spectroscopic conditions, the concentration of fluorophores is usually low (typically 10^{-6}–10^{-5} mol L^{-1}) and the intensity of the irradiation is fairly weak. Hence, only a small fraction of the fluorophore molecules are excited, typically less than 10^{-6}, but this still represents a large ensemble of 10^9 excited molecules per milliliter. Therefore, it is necessary to discuss the kinetics of depletion of excited states in a large (macroscopic) ensemble of fluorophores. The depletion of excited states is a stochastic process that involves a number of independent competing contributions (internal conversion, intersystem crossing, etc.). The probabilities of the individual processes depend on the chemical nature of the fluorophore and on its interaction with its microenvironment [10]. Individual processes will be discussed later.

First, we will describe the fluorescence kinetics after excitation with an ultrafast excitation pulse that can be approximated by a δ-pulse in the absence of nonradiative processes that could deplete the excited state (idealized case of time-resolved fluorescence decay measurements) [11, 12]. In a system of equivalent fluorophores (embedded in a homogeneous medium and interacting equally with the microenvironment), all the excited molecules have the same probability of emission of a photon but, due to the stochastic nature of the spontaneous emission, only the relationships concerning large numbers of fluorophores can be formulated. It is obvious that the number of photons released per unit time (rate of emission, or fluorescence intensity, $F \propto dN_F/dt$) in the system without competing nonradiative processes equals the total rate of de-excitation (depletion of the excited state), $-dN/dt$, which is proportional to the number of fluorophores excited at a given time, $N(t)$. Hence, we can write: $-dN/dt = k_R N(t)$, where k_R is the rate constant of the radiative transition (in this case, it is the rate constant of fluorescence, k_F). Integration yields kinetics that obeys the single exponential decay (first-order kinetics), i.e.,

$$N(t) = N_0 \exp(-k_R\ t), \quad \text{or} \quad F(t) = F_0 \exp(-k_R\ t), \tag{1}$$

where N_0 or F_0 is the number of excited molecules or fluorescence intensity, respectively, immediately upon excitation. In a great majority of practically important cases, the experimental decay is not single exponential because either the underlying photophysics is more complicated or the fluorophores embedded in a nonhomogeneous medium are not equivalent (individual fluorophores interact differently with their microenvironment). In almost all cases, some nonradiative processes compete to a certain extent with fluorescence. They contribute to the depletion of the excited state upon excitation and the fluorescence is weaker and decays faster. In this case, the experimental rate constant k_{exp} is the sum of the rate constants k_i of all the processes depleting the excited state (including the radiative process), $k_{exp} = \Sigma k_i$. The fluorescence quantum yield (the ratio of the number of emitted photons N_F to the number of absorbed photons N_{abs}), $\Phi_F = N_F/N_{abs}$, is lower than one (given by the relationship $\Phi_F = k_R/\Sigma k_i$) and the fluorescence intensity is weaker; it is attenuated (with respect to the ideal value) by the same factor $k_R/\Sigma k_i$.

The fluorescence lifetime is defined as the time at which the intensity of emission decays to $1/e$ of its initial value, i.e., $\tau_F = 1/k_{exp}$.

As was explained above, a number of nonradiative processes can deplete the excited state and quench the fluorescence. The first common process is internal conversion, IC. Its probability depends on the structure and properties of the molecule and on interaction with the surrounding molecules, and its rate varies over a wide range of orders of magnitude. For flexible and strongly interacting molecules, IC can proceed on a picosecond timescale and can efficiently deplete the excited state before considerably slower emission takes place. This process actually means that most molecules are nonfluorescent and only a relatively small number of rigid molecules are strong fluorophores. This also explains why the fluorescence intensity decreases with increasing temperature, with increasing polarity of the solvent and with its decreasing viscosity.

The second important nonradiative process is $S_1 \rightarrow T_1$ intersystem crossing, ISC, which is strictly forbidden by the spin selection rule at the level of the Born–Oppenheimer approximation, but the selection rule is relaxed in real systems by spin–orbital interaction for almost all the molecules that contain atoms with more electrons. The easiness of ISC depends on the energy difference between states S_1 and T_1 and, for molecules with energetically close S_1 and T_1 states, this process can be very fast and efficient (k_{ICS} ca. 10^{12} s^{-1}) due to the resonance effect and intermixing of the S_1 and T_1 states, while it practically does not come into account for molecules with a large energy difference. If the $S_1 \rightarrow T_1$ transition takes place, the molecule occurs in an unenviable situation. The probability of the radiative $T_1 \rightarrow S_0$ transition (phosphorescence) is low because the process is spin forbidden and the energy difference between the states is large. The molecule contains a considerable amount of excess energy and therefore is very reactive and on average remains in the reactive state for quite a long time and undergoes a number of collisions with the surrounding molecules. Therefore, the probability of photochemical reaction (i.e., the transformation of the original molecule in another one) is high and most photochemical reactions involve molecules (reactants or photosensitizers) in the excited T_1 state. Because the energy of the T_1 state is lower than that of the S_1 state, the phosphorescence is red shifted with respect to the fluorescence. Its intensity is very low due, in part, to its low natural rate (rate constant k_P ca. 10^{-3} to 10^3 s^{-1}) and to competitive depletion of the excited state by vibrational relaxation, collision energy transfer, etc.

If states S_1 and T_1 are energetically close, the molecule can "escape" from the T_1 state and return to the S_1 state. It is obvious that the T_1 molecule must gain some energy to reach the level where the energies of states T_1 and S_1 overlap. The required excess energy can be generated by intermolecular collisions with the surrounded molecules or by triplet–triplet annihilation, which requires interaction of two excited species. In both cases, delayed emission from S_1 occurs. The first mechanism is called delayed fluorescence of type E (because eosin is an important molecule which exhibits this type of delayed fluorescence) and the second mechanism is referred as type P (according to pyrene). In both cases, it is a slow radiative

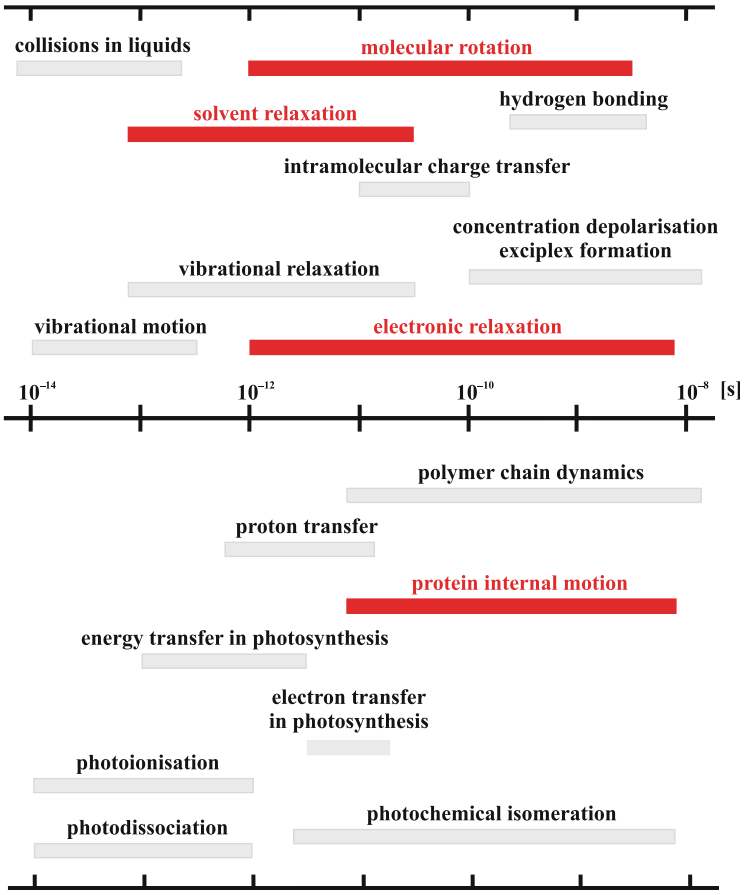

Fig. 3 The outline of fast dynamic processes that proceed at rates comparable with that of the radiative depletion of the excited state and can be studied by time-resolved fluorescence techniques (TRF): the rate of the polymer chain dynamics (vibrational motion and relaxation) strongly overlaps that of electronic relaxation and can be studied by TRF. Adapted from Springer, Self Organized Nanostructures of Amphiphilic Block Copolymers I, 241, 2011, 187–249, figure 3, [2]. Copyright 2011. With kind permission from Springer Science and Business Media

process with low intensity. In the first case, the rate constant equals that of phosphorescence, i.e., k_P; in the second case it equals $½k_P$.

The advantage of fluorescence measurement for studying the dynamic behavior of various systems follows from the fact that a number of processes can occur in the time window between absorption and emission. Either the fluorophore itself can undergo some changes (transition between electronic states, conformational changes, changes in position due to rotational or translational diffusion) or the surrounding molecules can reorganize (solvent relaxation, close approach of quenchers, etc.). Figure 3 gives a survey of practically important dynamic processes that proceed at rates comparable with fluorescence, affect the fluorescence

characteristics (position, width and shape of the fluorescence spectra, quantum yield, decay time, etc.), and can be studied by time-resolved fluorescence spectroscopy (TRFS). Some of them, which play an important role in fluorescence studies of polymer dynamics, conformations, and assembly, will be discussed in detail in the following text.

3 Fluorescence Quenching

All nonradiative processes that contribute to the depletion of the excited state shorten the fluorescence lifetime and weaken the emission intensity. Some of them arise as inherent features of the fluorophore (e.g., internal conversion) and their effect depends on its interaction with solvent and on temperature. They predetermine the natural fluorescence lifetime, τ_{F0}, which is defined as the lifetime in the absence of additional components that can quench the fluorescence.

Compounds that strongly interact with an excited fluorophore and quench its fluorescence are called "quenchers." Efficient quenching requires close approach of the quencher to the fluorophore, which means that a fluorescence quenching study yields information on a tiny volume element in which the fluorophore is embedded and on the processes that proceed in its vicinity. Hence, it can be used for probing tiny nanodomains of the system. Fluorescence quenching experiments are usually not difficult from the experimental point of view and they have often been used in biochemistry and polymer science since the early 1950s [13]. In homogeneous bulk solutions, the time-resolved data provide information on the rate of diffusion; in nanoheterogeneous systems with specifically embedded probes (e.g., covalently attached to the polymer chain), they can answer the question of whether a particular domain is accessible to the particular (polar or nonpolar) quencher, i.e., if the domain itself is polar or nonpolar.

Fluorescence quenching processes can be divided into two main categories: (1) dynamic (collision) and (2) static quenching. In the first case, the quencher (usually a transition or heavy metal ion or its complex, a molecule containing a heavy atom, or just oxygen dissolved in the solution) collides with the fluorophore and the excitation energy is transferred to the quencher and later dissipated in the surrounding medium. This quenching mechanism contributes to the depletion of the excited state, shortens the fluorescence lifetime, and weakens the fluorescence intensity. Both the fluorescence intensity F and lifetime τ_F obey the well-known Stern–Volmer relation [14].

$$\frac{F_0}{F} = \frac{\tau_{F,0}}{\tau_F} = 1 + K_{SV} c_Q \tag{2}$$

where the symbols without and with subscript $_0$ apply to the system with and without quencher, respectively, K_{SV} is the Stern–Volmer quenching constant which can be expressed as a product of the dynamic quenching rate constant k_q

and the fluorescence lifetime in the absence of the quencher, $\tau_{F,0}$, and c_Q is the concentration of the quencher. Detailed mechanism is relatively complicated and involves several steps. If we assume only free diffusion of both the fluorophore and quencher in the bulk solution and neglect the transient terms, k_q is a product of the quenching efficiency, which depends on the fluorophore–quencher pair, and the diffusion-limited bimolecular collision rate constant, k (defined by the Smoluchowski equation, $k = 4\pi D_s R_s N_A$, where D_s and R_s are the sum of the effective diffusion constants and the molecular radii of the components, respectively, and N_A is the Avogadro number).

Static quenching does not assume diffusion of components. It is a result of the reversible formation of a nonfluorescent fluorophore–quencher complex in the ground state. A fraction of the fluorophore is bound in a complex and makes no contribution to the emission, but the remaining fraction is not affected and exhibits fluorescence with the natural lifetime, $\tau_{F,0}$. The emission intensity is weaker and obeys the Stern–Volmer plot

$$\frac{F_0}{F} = 1 + K_A c_Q \tag{3}$$

where K_A is the association constant describing the reversible formation of the complex and where the fluorescence lifetime is not affected by the presence of the quencher. A combination of steady-state and time-resolved measurements allows unambiguous discrimination between the different types of quenching. Moreover, the static and dynamic quenching mechanisms differ significantly in the temperature dependence of their efficiency. Increasing temperature accelerates diffusion and amplifies dynamic quenching but promotes the dissociation of the complex and restricts static quenching. Hence K_{SV} (and the slope of Stern–Volmer plot) increases and K_A (and the slope) decreases with temperature.

In some real systems, it is possible to encounter a combination of both types of quenching. The Stern–Volmer plots are frequently not linear because various transient effects may cause the upward curvature of the plot. On the other hand, downward curvature and leveling-off of the plots can be a result of uneven (hindered) accessibility of a fraction of fluorophores in micro-heterogeneous media. A number of specific models for analyzing fluorescence decays affected by quenching have been proposed in the literature [8, 15].

4 Resonance Energy Transfer

The fluorescence resonance energy transfer (FRET), also called nonradiative excitation energy transfer (NRET) or direct energy transfer (DET), is one of the processes that quench the fluorescence of an excited fluorophore. In contrast to collision quenching, the excitation energy of the donor is transferred to another molecule (acceptor) over nanometer distances and the underlying mechanism does

not require the close contact of interacting species. When the energy is transferred, the originally excited donor returns nonradiatively to the ground state and the acceptor becomes excited. The acceptor can be a practically important fluorophore, which then exhibits its characteristic fluorescence, or a molecule that is efficiently deactivated by a nonradiative internal conversion. Analogously to collision quenching, NRET is a widely used fluorescence variant that has been employed in polymer and colloid science since the middle of the twentieth century. The FRET mechanism was first elucidated by Förster more than 60 years ago. It assumes a "long-range" interaction of the dipole moment of the excited donor with the dipole moment of the ground-state acceptor (in the nanometer range). The orbitals of the two species do not overlap and the resonance mechanism of weakly coupled dipoles controls the rate of the transfer. Efficient energy transfer requires approximately the same or slightly lower energy of the excited acceptor than that of the donor, because some excess energy can be dissipated in vibrational energy. From the spectroscopic point of view, the condition of total energy conservation means that the absorption spectrum of the acceptor has to overlap with the emission spectrum of the donor. The greater the overlap, the more efficient and faster is the energy transfer. The theory [16–18] predicts a steep dependence of the transfer rate constant, k_T, on the distance between the donor and the acceptor

$$k_T = \frac{1}{\tau_D}\left(\frac{r_0}{r}\right)^6 \tag{4}$$

where τ_D is the fluorescence lifetime of the donor in the absence of the acceptor and r_0 is the Förster radius, defined as the critical donor–acceptor distance for which the rate of fluorescence emission of photons (in a macroscopic sample) and energy transfer are the same. At the level of a single donor–acceptor pair, this means that, if the molecules are separated by r_0, the probability of emission of a photon from an excited donor is the same as that of resonant energy transfer. As already indicated, r_0 depends on the overlap of the emission and absorption spectra of the donor and acceptor, respectively. The normalized overlap integral J is defined by the following formula

$$J = \frac{\int F_D(\lambda)\varepsilon_A(\lambda)\lambda^4 d\lambda}{\int F_D(\lambda)d\lambda} \tag{5}$$

where $F_D(\lambda)$ and $\varepsilon_A(\lambda)$ are the emission spectrum of the donor and molar absorption coefficient of the acceptor as functions of the wavelength λ, respectively. However, the Förster radius also depends on the mutual orientation of the dipoles (expressed by the orientation factor, κ) and on the fluorescence quantum yield of the donor in the absence of the acceptor, Q_D. The complete formula reads

$$(r_0)^6 = \frac{9(\ln 10)\kappa^2 Q_D J}{128\pi^5 n^4 N_A} \tag{6}$$

where n is the refractive index and N_A is the Avogadro number. This formula shows that the larger the overlap, the larger is the region of efficient interaction and longer is r_0. If the current chemical units are used, i.e., $(\text{mol/L})^{-1}\,\text{cm}^3$ for the absorption coefficient, and cm for the wavelength, then the value of $(r_0)^6$ can be enumerated (in Å) using the following mathematical prescription: $r_0 = 9.78 \times 10^3 (n^{-4} Q_D \kappa^2 J)^{1/6}$.

The transfer efficiency, E, is defined as the ratio of the transfer rate constant, k_T, to the sum of rate constants, k_i, of all the processes that deplete the excited state (radiative and nonradiative, i.e., including the rate of unaffected fluorescence and that of FRET, k_T and k_F, respectively), $E = k_T/\sum k_i$. Experimentally, E can be determined by measurement of the quantum yields (or fluorescence intensities of the donor in the presence and absence of the acceptor, F_{DA} and F_D, respectively, or by time-resolved measurement of the corresponding fluorescence lifetimes, τ_{DA} and τ_D). If the acceptor is fluorescent (which is not a necessary condition), its emission can also be used for evaluation of E. However, the latter approach is not often used and its precision is usually lower (because the acceptor intensity can be affected by a number of complicating factors and also direct acceptor excitation contributes to its emission):

$$E = 1 - \frac{F_{DA}}{F_D} = 1 - \frac{\tau_{DA}}{\tau_D} = \frac{\varepsilon_{AD}(\lambda_1)}{\varepsilon_{DA}(\lambda_1)} \left(\frac{F_{AD}(\lambda_2)}{F_A(\lambda_2)} - 1 \right) \tag{7}$$

where $\varepsilon_{AD}(\lambda_1)$ and $\varepsilon_{DA}(\lambda_1)$ are the absorption coefficients of the donor and acceptor, respectively, at the wavelength of the absorption, λ_1, in the sample containing both donor and acceptor and $F_A(\lambda_2)$ and $F_{AD}(\lambda_2)$ are the fluorescence intensities of the same concentrations of acceptor at λ_2 in the absence and presence of the donor, respectively, both excited at λ_1 and monitored at λ_2.

The orientation factor between fixed dipoles is given by

$$\kappa^2 = (\cos\vartheta_T - 3\cos\vartheta_D \cos\vartheta_A) \tag{8}$$

where ϑ_T is the angle between the donor emission dipole and the acceptor absorption dipole, and ϑ_D and ϑ_A are the angle between the vector joining the donor and the acceptor and the corresponding dipoles, respectively. The factor κ^2 ranges from 0 for perpendicular orientation to 4 for parallel orientation of the dipoles. However, in solutions, the fluorophores are randomly oriented and undergo fairly rapid rotational diffusion. For very fast rotation in an isotropic, low viscosity solvent, when the molecules assume all mutual orientations with equal probability, time and ensemble averaging yields the "fast dynamic random limit" $\kappa^2 = 2/3$.

Nonradiative excitation energy transfer affects the time-resolved fluorescence decay and shortens the experimental values of the average fluorescence lifetime of the donor. In a macroscopic system, the shape of the decay curve depends on the

spatial distribution of the quenchers with respect to the donors and the time-resolved measurements can be used for studying the distribution and motion of the quenchers in complex systems. Early theoretical works [16, 19] were focused on isotropic systems with randomly distributed fluorophores and quenchers. In such systems, all fluorophores are influenced evenly by surrounding quenchers and the average number of quenchers in a thin spherical layer with radius r around each donor is proportional to r^2. The decay rate in a macroscopic system of fluorophores and quenchers can be generally obtained as the solution of the stochastic master equation which describes the time derivative of the average probability $\langle \rho(t) \rangle$ that the excitation at time t is still localized at the same fluorophore which was excited at time $t = 0$. The derivative gives the rate of deactivation of the excited fluorophores and (similarly to other common stochastic processes) is proportional to the number of excited fluorophores at a given time, i.e., $d\langle \rho(t) \rangle / dt = - k_{\text{exp}} \langle \rho(t) \rangle$. The effective rate constant depends on the spatial distribution of the quenchers with respect to the fluorophores

$$k_{\text{exp}} = \frac{1}{\tau_{\text{D}}} + \frac{1}{\tau_{\text{D}}} \sum_{k=1}^{N} \left(\frac{r_0}{r_k} \right)^6 = \frac{1}{\tau_{\text{D}}} + \frac{1}{\tau_{\text{D}}} \int W(r) \left(\frac{r_0}{r} \right)^6 dr \tag{9}$$

where r_k are the distances of the quenchers from a randomly chosen fluorophore and $W(r)$ is the distribution function of the numbers of quenchers at a distance r (in a random mixture proportional to r^2). Solution of the differential equation $-dN/dt = k_{\text{exp}} \cdot N(t)$, or $-dF_{\text{DA}}/dt = k_{\text{exp}} \cdot F_{\text{DA}}(t)$, with k_{exp} given by Eq. (9) and $W(r)$ proportional to r^2 yields the following time-resolved decay of the fluorescence intensity, $F_{\text{DA}}(t)$:

$$F_{\text{DA}}(t) = F_0 \exp\left[-\left(\frac{t}{\tau_{\text{D}}} \right) - 2\left(\frac{c}{c_0} \right) \sqrt{\frac{t}{\tau_{\text{D}}}} \right] \tag{10}$$

where c_0 is the critical concentration, $c_0 = 3000/(2\pi^{3/2} N_{\text{A}} r_0^3)$. The derived equation has been checked experimentally and was found to describe the experimental decays reasonably well. When the fluorophores and quenchers are embedded in small volumes, the decays must be described by more complicated relationships. The complication derives from the fact that individual fluorophores, which are located at different places with respect to the center of the closed volume element or in volumes differing in size, are surrounded by different numbers of quenchers and cannot be considered to be equivalent probes, e.g., those located close to the walls are affected only from one side, while those in the middle are affected on average by a spherically symmetrical set of quenchers (see Fig. 4). The NRET effect in small volumes was studied by Fayer and independently also by Winnik and appropriate formulas have been proposed and tested [20–25] and they will be discussed in the next chapters.

Fluorescence quenching and FRET belong among very popular and frequently employed fluorescence variants. They have been widely used in various fields

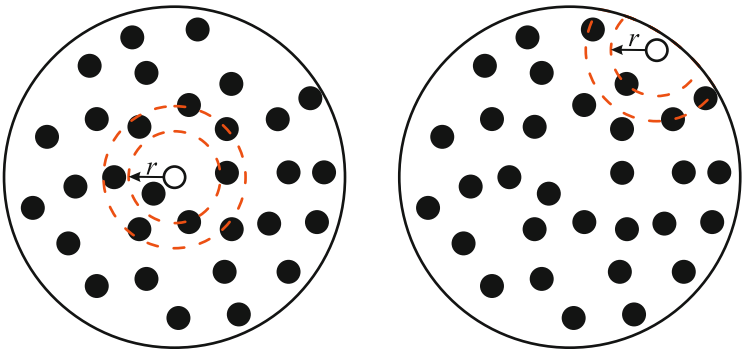

Fig. 4 Distribution of acceptors around a donor in small restricted volumes; the figure shows the importance of the location of the donor in confined and spatially restricted systems

including polymer and biopolymer research. FRET has been used in studies of polymer miscibility [26, 27] and polymer chain conformations [28–30]. Collision quenching, which provides information on the accessibility of fluorophores embedded in heterogeneous materials for different quenchers, has been used to study the properties of nanodomains, etc. [2, 31–34]. Both methods represent classical "benchmark" fluorescence techniques in polymer science. Their specific use for studies of polymer conformations, dynamics, and self-assembly will be discussed in detail in the following chapters.

5 The Solvent Relaxation Method

The solvent relaxation method (SRM) belongs to specific, fairly advanced variants of time-resolved fluorescence measurements. It has been used less in polymer science than fluorescence depolarization, quenching, or FRET, but it provides unique information on the polarity and microviscosity of the solvate shell of the probe (or more precisely on the mobility of molecules in the solvate shell) and interesting papers on the systems of low-molar-mass compound and also on self-assembled colloid and polymer systems have appeared in recognized journals in recent years [35–43]. Before discussing the use of SRM for the investigation of polymer systems, we will outline the principle of the method for a dilute solution of fluorophores in an isotropic polar solvent. We would like to point out that the probes used in SMR should be polarity dependent, i.e., they should exhibit a large shift in the emission band with polarity, but their photophysics should be simple (see the later discussion); otherwise interpretation of the data becomes complicated and specific for a given system—without the possibility of formulating general conclusions.

The principle of the solvent relaxation method is depicted in Fig. 5 for a fluorophore immersed in a polar solvent (with equilibrium ground-state relative

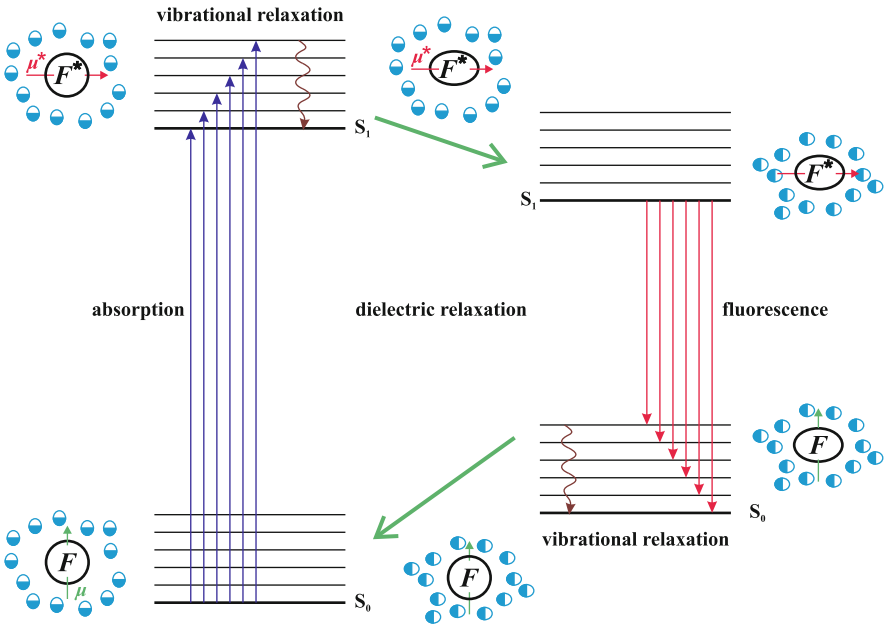

Fig. 5 Solvent relaxation: energies of the electronic states of a solvated fluorophore are depicted by *bold lines*, vibrational states by *thin lines*; the *long arrows* and *wavy lines* show individual processes; the changes of the dipole moment and geometry of the fluorophore upon excitation and emission are depicted by different orientations of the *short arrow* and the ellipsoidal prolongation. The changes in the arrangement and orientation of polar solvent molecules are indicated by *bicolor circles*. Adapted from Springer, Self Organized Nanostructures of Amphiphilic Block Copolymers I, 241, 2011, 187–249, figure 4, [2]. Copyright 2011. With kind permission from Springer Science and Business Media

permittivity, ε) and a higher dipole moment $\boldsymbol{\mu}_1$ in its excited state than that in the ground state $\boldsymbol{\mu}_0$. The vertical axis corresponds to the Gibbs free energy of the solvated fluorophore. As already mentioned, a necessary condition for the absorption, as well as for the emission of a photon, is a change in the dipole moment. Prior to excitation, the orientation of the polar solvent molecules in the solvation shell minimizes the Gibbs free energy, G, of the ground-state system. In this case, it is related mainly to the electrostatic interaction of the dipole moment of the fluorophore with the dipole moments of close solvent molecules. The fluorophore undergoes fairly rapid translational and rotational diffusion, but the solvent molecules are smaller than the fluorophore and the optimum structure of the solvate shell catches up with the random motion of the fluorophore and the time fluctuations in G are small.

As the absorption of a photon and a consequent redistribution of the "electron cloud" occur in less than 10^{-15} s, the change in the dipole moment, $\Delta\boldsymbol{\mu} = \boldsymbol{\mu}_1 - \boldsymbol{\mu}_0$, of the fluorophore (to be exact, the part corresponding to the redistribution of electrons) is almost instantaneous compared with the rate of motion of the nuclei and

the surrounding molecules. Therefore, immediately upon excitation, the geometry of the fluorophore (bond lengths and angles) and the arrangement of molecules in the solvate shell still correspond to the ground state. The solvation is not optimum and the Gibbs free energy soon after the excitation is higher than that of the properly equilibrated excited system. Two processes contribute to the minimization of G in the excited state: vibrational relaxation (which recovers the equilibrium geometry of the excited probe on a timescale of ca. 10^{-12} s) and slightly slower reorganization of the solvate shell (the rate of which depends on the solvent viscosity and temperature), which proceeds on a sub-nanosecond scale at ambient temperatures in nonviscous solvents). While the first process occurs in all the systems and causes the inherent Stokes red shift of the fluorescence with respect to the absorption regardless of the polarity of the probe and of the solvent, the second one takes place only in polar solvents and adds a polarity-dependent contribution to the Stokes shift. The extent of solvent relaxation depends on the strength of the dipole–dipole interactions between the fluorophore and molecules in the solvate shell (i.e., on the change in the dipole moment and on the local polarity of the microenvironment) and its rate depends on the mobility of the solvated molecules (i.e., on the local viscosity of the microenvironment). In nonviscous solvents, it proceeds quite rapidly and it can partially overlap with the vibrational relaxation. In this case, complete dielectric relaxation is usually complete before the emission of a photon (i.e., before the emission of an overwhelming majority of the photons in macroscopic samples), which means that most photons are emitted from the fully relaxed state S_1 on a nanosecond timescale. However, the emission is a stochastic process and its rate decays exponentially. Hence, at short times, some "hot photons" are emitted from non-relaxed states with higher energy than that of the fully relaxed state S_1 and ultrafast time-resolved measurements enable their detection.

Even though fluorescence decay in macroscopic systems proceeds in the nanosecond time region, the act of single emission (and transition from S_1 to S_0) occurs in times shorter than 10^{-15} s. Hence, immediately after the emission of a photon from the fully relaxed S_1 state, the geometry of the fluorophore and the structure of the solvate shell do not correspond to the ground state S_0, but still correspond to the excited state. This is followed by a cascade of processes that resemble the mirror image of the above-described relaxations after the excitation. However, it is necessary to bear in mind that the reorganization of the solvent shell at short times (after the "hot emission") requires less solvent reorganization because it proceeds from a non-equilibrated (high energy) S_1 state back to S_0 and the solvation shells of both states roughly correspond to the relaxed S_0 state.

A simple quantitative treatment of the solvent relaxation-induced Stokes shift is based on a model that assumes that the fluorophore is located in a cavity with radius a in a dipolar medium characterized by the bulk dielectric permittivity ε and refractive index n (we should recall that the high-frequency limit of the dielectric permittivity ε_∞ equals the square of the refractive index n^2). Classical treatment yields the Lippert equation [44] describing the difference, $\Delta\tilde{\nu} = \tilde{\nu}_A - \tilde{\nu}_F$, between the wavenumbers of the emission and absorption maxima of the fully relaxed system:

$$\Delta\tilde{\nu} \sim \frac{2(\mu_1 - \mu_0)^2}{hca^3}\left(\frac{\varepsilon - 1}{2\varepsilon + 1} - \frac{n^2 - 1}{2n^2 + 1}\right) \tag{11}$$

where h is the Planck constant and c is the speed of light in a vacuum, and $\mu_1 - \mu_0$ is the difference between magnitudes of corresponding dipole moments. This equation makes it possible to examine the local polarities of nano- to microdomains in heterogeneous systems (provided that the partitioning of the fluorophore between different domains can be estimated independently).

In this chapter, we generally avoid discussion of the technical details of time-resolved measurements, such as the principle of the time-correlated single photon counting technique, extraction of the net decay curve by the deconvolution method, etc. However, in this case, it is necessary to outline the principle of the solvent relaxation measurement and data evaluation (called "spectral reconstruction"). Application of the solvent relaxation method requires the measurement of a number of decay curves at different emission wavelengths, λ_{Em} (excited at the same excitation wavelength, λ_{Ex}). All the decay curves are measured with approximately the same statistics and are normalized. Emission from states populated immediately upon excitation yields decays in the blue part of the emission spectrum. The red-shifted decays correspond to emission from states which are not present at the very beginning and are created relatively slowly by the relaxation of the solvate shell on nanosecond and sub-nanosecond timescales. Therefore, the decay curves for longer wavelengths contain the rising (built-up) part at short times and later they achieve a maximum and finally decrease. The next step is reconstruction of the time-resolved spectra. It also requires measurement of the steady-state emission spectrum (excitation at the same wavelength as the time-resolved decays), because the intensity of the emission at λ_{Em} and t is proportional to the product of the steady-state intensity for a given wavelength, $F_{SS}(\lambda_{Em})$, and the fraction of the time-dependent intensities, $f(\lambda_{Em},t) = F_{TR}(\lambda_{Em},t)/F_{TR}(\lambda_{Em},t=0)$. The properly normalized intensities of the time-resolved spectra, $F_{TRS}(\lambda_{Em},t)$, are given by the relation

$$F_{TRS}(\lambda_{Em}, t) = \frac{F_{SS}(\lambda_{Em})F_{TR}(\lambda_{Em}, t)}{\int_0^\infty F_{TR}(\lambda_{Em}, t)dt} \tag{12}$$

and the final output is the normalized time dependence of the frequency of the emission, $\nu_{Em}(t)$ in the form of the correlation function (wavelengths of intensity maxima of emission bands are usually converted to the frequency scale):

$$\frac{[\nu_{Em}(t) - \nu_{Em}(t=\infty)]}{[\nu_{Em}(t=0) - \nu_{Em}(t=\infty)]} = C(t) \tag{13}$$

While the estimation of $\nu_{Em}(t=\infty)$ in the fully relaxed systems is not a problem, the value immediately upon excitation is often subject to ambiguities, especially in nonviscous highly polar solvents. In a number of cases, the relaxation is simply too

fast for the time resolution of the detection used and $v_{Em}(t=0)$ cannot be detected with sufficient accuracy. One more complication has to be taken into account in heterogeneous systems. Some amphiphilic or strongly nonpolar fluorophores, which bind to nanoparticles and are used in studies of nanoparticle solutions, are not sufficiently soluble in pure polar solvents and form self-quenched aggregates. Heterogeneous systems will be treated in the next part, but the estimation of $v_{Em}(t=0)$ is a general problem and therefore will be briefly discussed here. Maroncelli et al. [45] proposed an approximate method that can be used in all cases. It assumes knowledge of the frequencies of the absorption band of the probe in the polar solvent employed, $v_{A,p}$, and in a reference nonpolar solvent, $v_{A,np}$, which do not change with time and can be easily measured by UV–vis absorption spectroscopy providing that the probe is soluble in both solvents. Further, it requires knowledge of the emission frequency in a nonpolar solvent, $v_{Em,np}$, which again does not change with time, because the solvent relaxation proceeds only in polar solvents. Hence, it corresponds to the frequency of the maximum of the steady-state emission spectrum and can be estimated without problems. The value of the frequency in the polar solvent immediately upon excitation, $v_{Em,p}(t=0)$, can be evaluated from the simple formula

$$\nu_{Em,p}(t=0) = \nu_{Em,np} + (\nu_{A,p} - \nu_{A,np}). \tag{14}$$

6 Solvent Relaxation in Heterogeneous Systems

So far, a large number of low-molar-mass systems have been studied by ultrafast fluorescence techniques in sub-nanosecond time regions [35–39]. Recently, a relatively slow (nanosecond) relaxation process proceeding in mixed low-molar-mass solvents, consisting in redistribution of components of the solvent mixture in the solvate shell of the fluorophore upon the excitation, has also been reported [40–43, 46, 47]. However, an important part of experimental studies is still concerned with "relatively slowly relaxing" biological systems, such as lipid membranes [48–50], proteins [51, 52], nucleic acids [53], and also colloidal [54] and polymer systems [55–57].

In the next part, we will focus our attention on nanosecond processes that occur in shells of self-assembled polymer micelle-like nanoparticles in aqueous media [56, 57]. Fluorescent probes that strongly bind to the nanoparticles have usually been employed to obtain information on the shell or on the immediate vicinity of nanoparticles. Suitable probes include amphiphilic fluorophores, i.e., fluorescent surfactants, such as prodan, laurdan, or patman (see chapter "Fluorescence Studies of Polymer Containing Systems", Fig. 2). They contain a fairly polar fluorescent head-group and a nonpolar aliphatic tail, which secures the favorable "hydrophobic interaction" and sorption on polymer nanoparticles. They bind to micelles [55, 56] and their localization depends on the polarity of the head-group and on the length of the tail. In the case of patman, the strongly polar head is usually located in the peripheric part of the solvated shell and the nonpolar tail is oriented towards the

core/shell interface, i.e., buried in the inner shell. Probes with less polar heads (laurdan) can be buried quite deep in the nanoparticle (close to the core/shell interface). The micellar shell represents a fairly concentrated polymer system, which does not contain enough water in its innermost part (close to the core-shell interface) and the solvation of some components can be incomplete. The buried probe competes with polymer segments for water molecules and the complex solvent redistribution is significantly slowed down and differs in many aspects from the simple dielectric relaxation in isotropic low-molar-mass solutions.

The complexity of the dielectric response derives from the fact that micellar systems are "micro-heterogeneous" and contain components that differ significantly in size and in mobility: small and mobile solvent molecules, slightly larger fluorescent probes, and fairly large nanoparticles (with characteristic dimensions ranging from several nm up to 10^2 nm and molar masses 10^6–10^7 g/mol). The properties of nanoparticles that influence the fluorescence of probes, e.g., the density and effective polarity of the water-soluble shell, the degree of ionization in weak polyelectrolyte shells, solvation of shell-forming units, and water structure, vary in the direction from the central part of the nanoparticle to the periphery [58, 59]. Appreciable changes occur at distances comparable with the size of the fluorophore. Therefore, not only the redistribution of water molecules upon excitation but also the motion of the fluorophore with respect to the nanoparticle can occur during the lifetime of the excited state. In some systems, partial redistribution of amphiphilic probes between the core and shell has also been observed [55].

In micro-heterogeneous systems, the time dependence of the half-width of the time-resolved emission band should be measured and plotted as a function of time because it provides important information on the extent of the monitored process. It has been shown [60] that the half-width should be more or less constant in homogeneous systems (in fact, it should decrease slightly). The process proceeds differently in spatially inhomogeneous systems. Because the properties of the system vary in space, individual fluorophores distributed in different parts of the system are not equivalent and their solvent shells respond at different rates to the changing local electric field. This inhomogeneity gives rise to a new phenomenon that reflects the time distribution of the relaxation phases of different solvent shells. The observed transient inhomogeneity increases significantly at intermediate times and attenuates at long times [60].

Monitoring of the half-width of the emission band provides information about whether the entire process, or just a part of it, was included within the time window of the experiment. If only a decrease is observed, the early part of the relaxation process is beyond the time resolution of the relevant apparatus. In contrast, if only the rising part is observed, the process is slow and the fluorescence lifetime is too short and does not allow monitoring of the entire relaxation process. The following chapters give some examples of studies of self-assembling polymer systems by the solvent relaxation method.

7 Time-Resolved Fluorescence Anisotropy

As already explained, the probability of photon absorption by a given molecule depends on a number of factors (see the optical selection rules). If polarized light is employed [61], it also depends on the orientation of the absorption transition dipole moment, $\boldsymbol{\mu}_{\mathrm{A}}$, with respect to the polarization plane of the excitation light (described by the angle ϕ). Molecules with their absorption dipole moment parallel to the polarization plane of the excitation light are excited preferentially, while those oriented perpendicularly are not excited at all. For a general orientation with angle ϕ, the dipole moment can be decomposed into parallel and perpendicular components, $\boldsymbol{\mu}_{\mathrm{A}}\cos\phi$, and $\boldsymbol{\mu}_{\mathrm{A}}\sin\phi$, respectively, and the excitation probability is proportional to $(\cos\phi)^2$.

Fluorophores in solutions (i.e., their dipole moments) are oriented randomly prior to excitation and undergo rotational diffusion. Nevertheless, immediately upon excitation by a sufficiently intense ultrafast polarized light pulse, the population of excited molecules with absorption dipole moment parallel to the plane of the polarized excitation light predominates. Several processes contribute to the relaxation of the anisotropic population of excited molecules; in addition to processes that deplete the excited state (both radiative and nonradiative): (1) the rotational Brownian motion of fluorophores and (2) the excitation energy migration among fluorophores also play an important role. The probability of nonradiative energy migration depends strongly on the distance between the fluorophores (see the part describing energy transfer). Consequently, the rate of the latter depolarizing process in macroscopic solutions can be significantly suppressed at high dilutions. The absorption and emission transition dipole moments, $\boldsymbol{\mu}_{\mathrm{A}}$ and $\boldsymbol{\mu}_{\mathrm{E}}$, can form any angle ω , but they are usually parallel in fluorophores that contain symmetry planes, which means that the emission at early times following polarized excitation is also strongly polarized in the same plane and the time-dependent fluorescence anisotropy provides information on the depolarization processes; in dilute systems, it corresponds predominantly to the rotational diffusion of the probe. Relaxation of the system can be followed by measuring the time-resolved anisotropy,

$$r(t) = \frac{\left[I_{\parallel}(t) - I_{\perp}(t)\right]}{\left[I_{\parallel}(t) + 2I_{\perp}(t)\right]} \tag{15}$$

where $I_{\parallel}(t)$ and $I_{\perp}(t)$ are the parallelly and perpendicularly polarized emission intensities at time t after the excitation, respectively. The sum $S(t) = \left[I_{\parallel}(t) + 2I_{\perp}(t)\right]$ in the denominator is proportional to the population of molecules in the excited state, i.e., it represents the total fluorescence intensity and does not depend on the orientation of the molecule. The polarized fluorescence decay $I(t,\phi)$ measured at arbitrary angle ϕ can be expressed in the following form:

$$I(t,\phi) = \frac{1}{3}\left[1 + \left(3\cos^2\phi - 1\right)r(t)\right]S(t) \tag{16}$$

In measurements at the so-called "magic angle," i.e., with the detector of polarized light oriented at $\phi_M = 54.7^\circ$ with respect to the polarization plane of the excitation beam, the experiment directly yields the decay $I(t,\phi_M) = S(t)$ unaffected by anisotropy, because in this case: $(3\cos^2\phi_M - 1 = 0)$.

From a theoretical point of view, the experimentally accessible time-resolved anisotropy, $r(t)$, represents the autocorrelation function of orientations of the emission transition dipole moment $\boldsymbol{\mu}_E(t)$ at time t and the absorption transition dipole moment $\boldsymbol{\mu}_A(t=0)$ at the instant of excitation, $t = 0$, and can be expressed as

$$r(t) = 2/5\langle P_2(\boldsymbol{\mu}_A(t=0)\boldsymbol{\mu}_E(t))\rangle \tag{17}$$

where P_2 is the second-order Legendre polynomial and the brackets denote the ensemble averaging. The initial anisotropy is given by $r(t=0) = (0.6\cos^2\omega - 0.2)$ and depends on the mutual orientation of $\boldsymbol{\mu}_A(t=0)$ and $\boldsymbol{\mu}_E(t=0)$. The two following limiting values are acquired for parallel (the highest positive value 0.4) and perpendicular (the lowest negative value -0.2) orientation. Even though perpendicular orientation of both dipole moments is not very common, such situation can occur if the fluorophore is excited to a higher state than the emitting state and the molecule (e.g., perylene, [12]) undergoes one or more nonradiative transitions between different excited states with mutually perpendicular orientation of dipole moments before emission. For completeness, it should be pointed out that the emission is totally depolarized from the very beginning in molecules in which the angle between dipole moments corresponds to the magic angle. On the other hand, in perfectly ordered systems of fluorophores with mutually parallel absorption and emission dipole moments, e.g., in a fluorophore crystal with corresponding dipole moments that are mutually parallel, the anisotropy defined by Eq. (15) would theoretically be $r(t) = 1$ and would not depend on time. In real crystals, $r(t)$ can be slightly lower due to defects in lattice structure and vibrations.

In a number of fluid systems, rotational diffusion proceeds on timescales comparable with the fluorescence decay and can be employed to study the viscosity of the microenvironment, segmental motion of the polymer chains, local geometrical constraints, and changes in the above characteristics caused by external stimuli, etc. In nonviscous systems of small molecules, fluorescence anisotropy due to rotational diffusion usually decays faster than fluorescence, but in viscous solutions and also in various polymer and biopolymer systems, full angular randomization is often achieved at times much longer than that corresponding to the depletion of the excited state and it is not possible to monitor the whole fluorescence anisotropy decay experimentally. However, careful data fitting (based on an appropriate model) provides reasonably accurate time characteristics together with the so-called "residual anisotropy" value (see the later discussion for its physical meaning).

8 Models of Rotational Diffusion (RD) and Their Advanced Variants

In dilute systems of small molecules (where energy migration can be neglected), the anisotropy decays are commonly fitted to curves derived on the basis of the rotational diffusion model. There exist several variants of this model. The oldest and simplest approach, which has mostly been used for interpretation of the data obtained from systems of small molecules, is known as the Debye hydrodynamic model [62–69]. The fluorophore is modeled by a solid (generally asymmetrical) ellipsoid immersed in a viscous liquid. Its rotational diffusion coefficient is given by the Stokes–Einstein equation [70] and its orientation with respect to the fixed laboratory system of coordinates can be characterized by three Euler angles $\boldsymbol{\Omega}$. It is assumed that the molecule rotates through a very small angle between individual collisions and its reorientation can be described by the rotational diffusion equation:

$$\frac{\partial}{\partial t} f(\boldsymbol{\Omega}, t) = -f(\boldsymbol{\Omega}, t), \tag{18}$$

which yields the probability density $f(\boldsymbol{\Omega}, t)$ describing the orientation of the molecule at time t (expressed by Euler angles $\boldsymbol{\Omega}$) regardless of the electronic state. $\mathbf{H}$ is the Hamiltonian operator, $\mathbf{H} = \sum_{i=1}^{3} \sum_{j=1}^{3} \mathbf{L}_i D_{ij} \mathbf{L}_j$, $\mathbf{L}_i$ is the quantum mechanical operator of the angular momentum defined according to Rose [71], and D_{ij} are the components of the diffusion tensor. Knowledge of $f(\boldsymbol{\Omega}, t)$ allows calculation of the polarized intensities $I_{\parallel}(t)$ and $I_{\perp}(t)$ and consequently the time-resolved anisotropy, $r(t)$, as the sum of several terms, each of them decaying exponentially with time [72]:

$$r(t) = \sum_{i=1}^{5} A_i \exp\left(\frac{-t}{\tau_{ri}}\right) \tag{19}$$

where the individual correlation times τ_{ri} are functions of the principal components of the diffusion tensor, i.e., $\tau_{ri} = f(D_1, D_2, D_3)$ and the pre-exponential factors depend both on the components of the diffusion tensor and on the orientation of the absorption and emission transition dipole moments, $\boldsymbol{\mu}_A$ and $\boldsymbol{\mu}_E$, respectively (angles α_j and β_j), with respect to the principal axes of diffusion, i.e., $A_i = f(D_1, D_2, D_3, \alpha_j, \beta_j)$. In the general case of a low symmetry molecule, there are five exponential terms, but only three correlation times τ_{ri} are independent. If the symmetry of the fluorophore increases, the number of exponentials decreases. As it is difficult to discern more than two exponential terms experimentally (the nominator in Eq. (15) is a fairly small difference between two large numbers, while the denominator is their sum), only the cases when the number of exponentials reduces to one or two are important in practice. This can happen [73], e.g., if the fluorophore can be approximated by a rotationally symmetric ellipsoid $D_1 = D_{\parallel} \neq D_2 = D_3 = D_{\perp}$ (symmetric-top) and $\boldsymbol{\mu}_A$ or $\boldsymbol{\mu}_E$ are simultaneously perpendicular to the axis of

rotational symmetry, the anisotropy decay is described by two exponential terms (two correlation times). Other possibility for two rotational correlation times is that $\boldsymbol{\mu}_A$ or $\boldsymbol{\mu}_E$ is parallel with one of diffusion axes. If $\boldsymbol{\mu}_A$ and $\boldsymbol{\mu}_E$ are parallel for symmetric top, single exponential decay occurs (one correlation time). Single exponential decay is also obtained for a spherical top, i.e., if all the main components of the diffusion tensor are equal, $D_1 = D_2 = D_3$.

Because the fluorophore interacts with solvent molecules and binds them, creating the solvate shell, the D_i values cannot be predicted on the basis of a simple atomistic model of the rotating molecule. The solvation depends both on the fluorophore and on the solvent and varies considerably from one system to another [74]. Two limiting situations have been considered in the literature: (1) the stick condition—when the first solvent shell moves together with the fluorophore, and (2) the slip condition, i.e., the opposite extreme situation, when the solvent molecules do not bind to the fluorophore. However, the rotation of the fluorophore is still not free in the latter case. It is hindered by the necessity of redistributing the molecules of the solvent to create the free space necessary for a change of the fluorophore position, which generates the hydrodynamic friction. Redistribution of the solvent molecules depends strongly on the shape of the rotating object. This is quite small for spherical particles. The rotation of a prolate ellipsoid around its long axis does not require almost any solvent redistribution, but that around the short axes (perpendicular to the long one) does require redistribution and the corresponding D_i value obtained by fluorescence measurement is significantly larger than the net value based on the atomistic model. The stick condition assumes that, in addition to the motion of the firmly bound solvent shell, a non-negligible displacement of solvent molecules occurs at longer distances from the fluorophore for the same reasons as discussed above.

Very interesting special anisotropy decay has been predicted for a symmetric molecule approximated by disc with perpendicular orientation of $\boldsymbol{\mu}_A$ and $\boldsymbol{\mu}_E$, both lying in the plane of the disc, which we designate, for a clear and unambiguous discussion, as the *yz* plane and assume that the light beam comes in the *x* direction and polarization plane is *xz* (see Fig. 6a). The net principal D_i components of the molecule in the direction of the main symmetry axes C_∞ (axis *x*) and in the directions of the two perpendicular axes C_2 in the disc plane (the *z* and *y* directions coinciding with the orientations of $\boldsymbol{\mu}_A$ or $\boldsymbol{\mu}_E$, respectively) do not differ much. However, the rotation of the disc around the *x* axes does not require almost any redistribution of the solvent molecules, while the rotations around *y* or *z* require the continuous displacement of a number of solvent molecules and the corresponding correlation time τ_{r2} is ca. 10 times longer than τ_{r1}. Because $\boldsymbol{\mu}_A$ and $\boldsymbol{\mu}_E$ are perpendicular to each other, $r_0(t = 0) = -0.2$. The anisotropy increases rapidly at short times after excitation (with τ_{r1}) as a result of rapid 1D rotational diffusion around the *x* axis, which randomizes the orientations of the excited molecules in the *yz* plane (in which both dipole moments lie) and eliminates the excess of excited molecules emitting perpendicularly polarized light with respect to the excitation polarization. Note that full randomization of the orientations of the excited fluorophores in 3D is not achieved at short times because the rotations around the second and third axis are slow. This is why $r(t)$ does not converge to

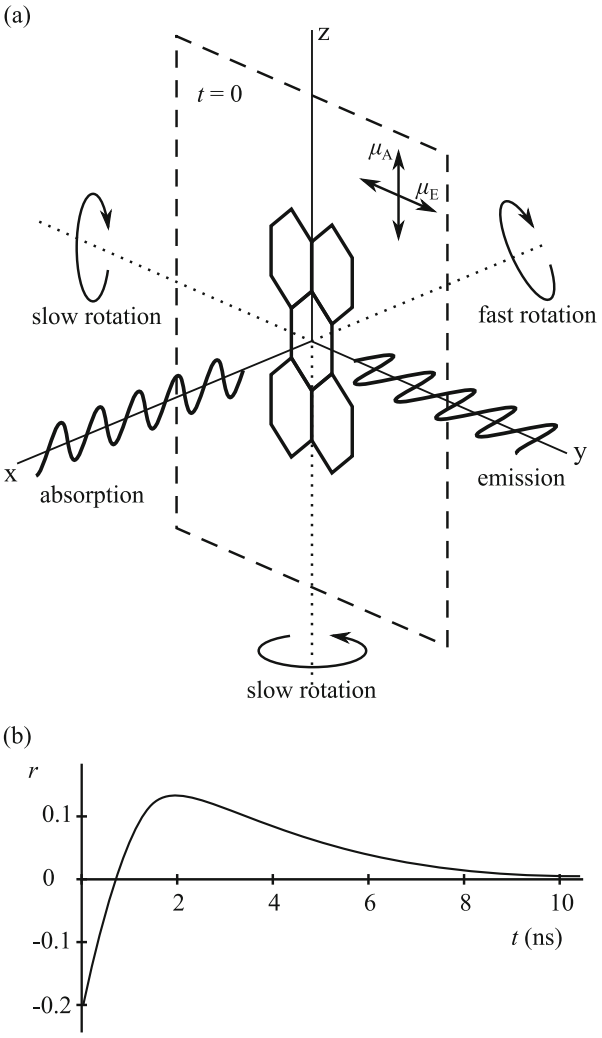

Fig. 6 Unusual shape of the fluorescence anisotropy decay curve, obtained, e.g., for perylene excited to the S_2 state, i.e., in the UV region far from the "zero–zero" transition. (**a**) Schematics explaining physical reasons of the non-monotonous time dependence, which is due to a combination of two facts: (1) the absorption and emission dipole moments are perpendicular to each other, and (2) hydrodynamic friction affects the rotation of the molecule with respect to different axes of symmetry. (**b**) Schematic shape of experimental curve, $r(t)$. Timescale depends on the viscosity of the solvent used

zero, but increases to slightly positive values 0.1–0.2 (depending on the difference between the effective D_i values) and then slowly decays to zero (with τ_{r2}) as the 3D randomization continues. The example described above is not only interesting from the theoretical point of view, but it is also important in practice, because it has been experimentally observed for commonly used fluorophores, such as perylene. If perylene is excited in the short wavelength part of its absorption spectrum to the S_2 state, which is polarized perpendicularly to the S_1 state, the nonradiative transition $S_2 \rightarrow S_1$ takes place first and then the perpendicularly polarized emission (with respect to the absorption) occurs [75, 76]. Schematic shape of the anisotropy curve corresponding to the above-described behavior of perylene and analogously behaving planar fluorophores is shown in Fig. 6b. In experiments, only two

(maximally three) rotational correlation times can be evaluated with reasonable accuracy. The experimental accuracy depends mainly on the difference between the individual correlation times and on the ratio of the rate of the orientation relaxation to the fluorescence decay. This means that both the experimental pre-exponential factors A_i and correlations times τ_{ri} frequently represent the effective weighted averages of parameters corresponding to several different rotations. The best resolution is usually obtained for systems where the anisotropy decays are slightly faster than the fluorescence intensity decays. Moreover, the fact that mutual orientation of $\boldsymbol{\mu}_A$ and $\boldsymbol{\mu}_E$ is not known for a number of fluorophores hinders interpretation of the anisotropy data. Theoretical analysis predicts that experimental coefficients A_i may depend on the excitation and emission wavelength, but should not depend on the viscosity of the medium and on the temperature: as has already been explained, the initial anisotropy $r_0(t=0)$ for perylene excited to S_2 is -0.2, while $r_0(t=0)$ is close to 0.4 for S_1 excitation. In isotropic systems of small mobile molecules, the anisotropy should decay to zero at long times and therefore the residual anisotropy should also be zero, $r_\infty = 0$. A nonzero value r_∞ means that the rotational movement in 3D is restricted due (1) to bonding (or incorporation) of the probe (in)to a very large and heavy rigid object or (2) to strong anisotropy of the medium. In the first case, some correlation times are extremely long compared with the fluorescence lifetime and the true r_∞ value cannot be obtained experimentally; in the second case, the rotation does not proceed freely in all 3 dimensions.

The rotational diffusion model has been revised and improved by several authors and a few advanced models that remove the most severe simplifications have been proposed. The extended diffusion model (ED) eliminates the condition of small angular changes between individual collisions [77–81], i.e., it assumes that reorientation of the molecules proceeds in a sequence of mutually independent (both short and long) diffusion steps. Molecules rotate freely and the angular momentum does not change between the collisions. The probability of steps of different length is given by the Poisson distribution. Collisions between molecules are considered to be fast events compared to the average time of the diffusion steps between them. Two variants of the ED model, differing in the character of the angular momentum changes, have been proposed. The so-called J-diffusion assumes that changes in the orientation of the angular momentum are completely random (i.e., all changes in the direction of rotation are equally probable), but changes in its magnitude obey the Boltzmann distribution. The M-diffusion variant assumes that the angular momentum magnitude does not change after the collision; only its orientation changes randomly.

In both cases, the time-resolved anisotropy decay acquires a complex form of an infinite series. Gordon [77] has shown that the decay may, in special cases, exhibit damped oscillations, which has been observed experimentally, but the original RD model was unable to offer an explanation of this rather exotic behavior. Numerical calculations by McClung [79] validated the ED prediction for spherical molecules. For asymmetric molecules, the calculations confirmed the formulae based on the J-diffusion model and indicated that the assumptions used in the M-diffusion model are less realistic [81].

Another attempt to improve the RD model was made by Fixman and Rider for linear molecules in 1969 [82] and later by McClung for spherical and asymmetric top in the early 1980s [83, 84]. In accordance with the theoretical background employed (already existing in other fields of physics), the model is called the Fokker–Planck–Langevin (FPL) model. Theoretical treatment assumes that the rotational movement of a rigid molecule (e.g., ellipsoid) immersed in a viscous liquid is affected (1) by the slowly changing frictional force (depending on the viscosity of the solvent and fluorophore–solvent interactions) and (2) by fairly rapidly changing Brownian forces, which mimics collisions with solvent molecules. The model allows formulation and solution of the rotational Fokker–Planck equation for the conditional probability density that the molecule rotates at time t in a given direction with a particular angular velocity. The anisotropy decay is then expressed as a rapidly converging infinite series of exponentials. From the practical point of view, it is important that a strongly truncated series with only a few terms provides quite accurate values of the rotation correlation times of test systems. The FPL and ED models represent two very different approaches for treatment of the interaction of the fluorophore with the solvent molecules and for explaining the influence of the microenvironment on the rotation of the fluorophore. Both models eliminate the assumption of small diffusion steps, but the physical assumptions are quite different from each other. In the ED model, the molecules may undergo large changes in their orientation and in the magnitude of their angular momenta during collisions, which are considered to be almost instantaneous events compared with the length of the unaffected rotation between them. The FPL model employs the slowly changing friction force and more rapidly changing Brownian force. Its main difference with respect to ED is as follows: Because the two forces are balanced (to maintain a constant temperature of the system), a relatively large number of emulated collisions are required to cause a large change in the rotation of the fluorophore. Lévi et al. published a comparison of anisotropy decays based on ED and FPL with experimental data for linear and spherical molecules [85]. Both models offer an almost indistinguishable macroscopic description of the rotational motion of molecules in liquid media and it was not possible to decide which description is physically more relevant. The authors recommend great care and precaution when drawing conclusions from model fitting of experimental data.

Other interesting extensions of the RD model (similar to ED) include the partially relaxed rotation model (PRR) [86] for a symmetric-top rotor and its generalization, the 2τ model. The basic assumptions are based on the experimentally verified fact that the rotation of an oblong ellipsoid around its long symmetry axis C_∞ does not require almost any displacement of the surrounding molecules and is effectively free, but the tumbling motion accompanied by changes in the spatial orientation of this axis is a complex relaxation process controlled by collisions with solvent molecules. Hence the uncorrelated binary collisions affect only the motion in directions perpendicular to C_∞. Distribution of the angular velocities around C_∞ is given by the Maxwell–Boltzmann distribution and the relaxation of the tumbling motion is described by the characteristic time, τ_1. In a more general 2τ model, the relaxation of the rotation around C_∞ (described by τ_2) is

also considered. At the limit of long relaxation times, this model converges into (a) PRR, if $\tau_2 \to \infty$, (b) ED-J, if $\tau_1 \to \infty$, or (c) a free rotor (symmetric-top RD with slippery condition), if both $\tau_1 \to \infty$ and $\tau_2 \to \infty$.

9 Fluorescence Anisotropy in a System of Flexible Fluorescent Molecules

The time-resolved fluorescence anisotropy is a suitable tool for studying complex motion of polymer chains. However, the data must be interpreted with care and precaution. Fluorescence spectroscopy in general (and anisotropy in particular) provides indirect information on the studied host system. The more advanced is the experimental technique and the model used for fitting the data, the greater is the risk of misinterpretation. In fact, the basic assumption that the motion of the probe is a good indicator of that of the host system is the most problematic aspect. The rotation of dispersed probes is undoubtedly affected by the host system, but interpretation of the anisotropy results is difficult and often ambiguous. Moreover, only a few polymer and biopolymer systems (e.g., tryptophan-containing proteins, polyvinylcarbazole) are intrinsically fluorescent. In most other cases, the fluorophore has to be added to the host system. It can be simply dispersed in the solution and, in this case, it is usually called a "probe," or it can be chemically attached to the system of interest and then it is usually called a "label." Hydrophobic probes interact with hydrophobic domains formed within the polymer chain in aqueous or highly polar media and bind to them and therefore can be used for monitoring the behavior of specific parts of the chain, but the chemical attachment of a label (as a co-monomer within the chain or as a pendant group) provides a much better opportunity for detailed studies. However, one should bear in mind that the presence of the fluorophore in the chain (generally in the studied host system) always influences the properties of a tiny part of the chain/system. In spite of the fact that chemical modification is negligible and has almost no impact on the macroscopic behavior of the system, the fluorescence monitors the behavior of the small domain of the host system that has been affected. For safe interpretation of the fluorescence data for a polymer system, the fluorescence study should be combined with other methods that provide independent data, or it should be corroborated by already existing knowledge of the system. Only in these cases can the high potential of fluorescence methods be fully exploited.

An ideal fluorescence probe or label for anisotropy measurements should meet the following requirements:

1. It should specifically monitor the behavior of a known part of the molecule,
2. It should perturb the behavior of the host system as little as possible,
3. It should have simple spectroscopic properties (single exponential decay and a lifetime somewhat longer than the monitored anisotropy decay, etc.),

4. Its simple rigid shape and orientation of dipole moments should enable unambiguous interpretation of the anisotropy decay of the free probe in isotropic media,
5. Chemical attachment of the label to the polymer should enable simple interpretation of the fast components of anisotropy relaxation.

Because of the variability of fluorescent or fluorescently labeled polymers and the complexity of the relaxation processes that come into account, no general model for anisotropy decay in polymer systems has been proposed so far; however, a number of papers analyzing decays in different systems have been published [2, 87–96] and will be outlined in the next part.

If the fluorophore is part of a large flexible molecule, e.g., it is a co-monomer incorporated in a flexible polymer chain or a pendant group covalently attached to a polymer chain or to a large polymeric nanoparticle, its reorientation relaxation is a complex process, which includes (1) fairly slow rotation of the whole nano-object, (2) reorientation motion of the probe with respect to some specific parts of the chain or of the nanoparticle (e.g., with respect to nano-structured domains differing in flexibility or in other important properties), and (3) fairly fast motion of the polymer structural units and rotation of the fluorophore around one or more single bonds, if it is attached to the chain or to the nano-object by a linker. From the practical point of view, it is convenient to classify the molecules according to the ratio of the fast correlation time to the longest time, which describes the motion of the whole particle.

If the relaxation times are fairly fast and comparable, all of them can, in principle, be measured. Moreover, if such a particle is immersed in an isotropic medium, the fluorescence anisotropy decays to zero. For a number of high-molar-mass macromolecules and self-assembled polymer nanoparticles, the longest relaxation time is significantly longer than the fluorescence lifetime and exceeds the capabilities of fluorescence measurements because the excited state is depleted long before full 3D relaxation occurs, which means that, at times when the fluorescence intensity is low and converges to zero, the anisotropy is still high and poor statistics of the emitted photons does not allow reliable extrapolation and evaluation of the long relaxation time. In a relatively narrow nanosecond time window, the slow relaxation (often several order of magnitudes slower than the fast one) does not show any appreciable decrease in $r(t)$ and it seems that the anisotropy has already leveled-off in spite of the fact that the fluorescent macromolecule or nanoparticle is immersed in an isotropic medium. Therefore, the formulas used for fitting the data for a polymer system usually contain a constant term—the residual anisotropy, r_∞ (pre-exponential factor of the term corresponding to $\tau_{\text{slow}} \to \infty$).

The motion of fluorophores incorporated in the form of co-monomers in flexible chains has been studied by Monnerie, Valeur et al. in a number of papers [97–99] from the 1970s. Since the flexible chains usually contain atoms in the sp^3 hybridization of bond-forming orbitals, the authors assumed that the internal rotation of small parts of the chains mimics the rotation of the crankshaft, i.e., it represents a

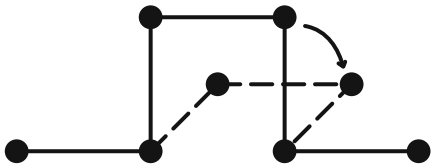

Fig. 7 Schematic representation of the crankshaft motion of the part of the polymer chain

simultaneous rotation of the part of the chain containing three segments connected by two external bonds to the rest of the chain (see Fig. 7).

Because the configurations of the chains which predominantly contain the "trans" and "gauche" conformations of short parts formed by four C atoms (in sp^3 hybridization) fit fairly well to the tetrahedral lattice (see chapter "Conformational and Dynamic Behavior of Polymer and Polyelectrolyte Chains in Dilute Solutions," Fig. 3), to a first approximation they assumed that the basic motion of the fluorophore can be described as a "jump-like rotation" on the tetrahedral lattice with one characteristic time, ρ (which depends on the characteristic "jump" frequency and the conformation structure of the chain), in the form [100, 101]:

$$r(t) = r_0 \exp\left(\frac{t}{\varrho}\right) \operatorname{erfc}\left(\sqrt{\frac{t}{\varrho}}\right) \tag{20}$$

In a more realistic model, which takes into account the fact that the chain conformation can deviate from the strict tetrahedral geometry, the anisotropy $r(t)$ acquires a more complex form (it contains two characteristic correlation times) [98]

$$r(t) = r_0 \exp\left(-\frac{t}{\theta}\right) \exp\left(\frac{t}{\varrho}\right) \operatorname{erfc}\left(\sqrt{\frac{t}{\varrho}}\right) \tag{21}$$

where θ is an additional correction relaxation time, which accounts for the perturbation relaxation of segments from orientations determined by the lattice. The derived equation has been used for the interpretation of experimental data on a solution of anthracene-labeled polystyrene in a good solvent (emission transition dipole moment parallel to the local part of the chain) and for 9,10-diphenylanthracene-labeled polystyrene (dipole moment perpendicular) [102–104]. The agreement was found to be satisfactory except for the short time region. Later, the crankshaft motion model was revised and the simultaneous rotation of several bonds was considered (not only two, but also three and nine simultaneously rotating bonds). Note that the original concept assumes the rotation of a part of the chain that contains three segments, but true rotation occurs only around two external bonds. The most important conclusion drawn from this model is the fact that the effective potential of hindered rotation is much lower if several bonds are involved compared with that for simple crankshaft motion.

Two models have been developed independently by Hall and Helfand [105] and by Monnerie at al. [106]. For the Hall–Helfand model (HH), the anisotropy decays according to the equation

$$r(t) = r(t=0)\exp\left(-\frac{t}{\tau_1}\right)\exp\left(-\frac{t}{\tau_2}\right)I_0\left(\frac{t}{\tau_1}\right) \tag{22}$$

and, in the second case known as the generalized diffusion and loss model (GDL), according to the equation

$$r(t) = r(t=0)\exp\left(-\frac{t}{\tau_1}\right)\exp\left(-\frac{t}{\tau_2}\right)\left[I_0\left(\frac{t}{\tau_1}\right) + I_1\left(\frac{t}{\tau_1}\right)\right] \tag{23}$$

where τ_1 and τ_2 are two correlation times and $I_i(t/\tau_1)$ are the modified Bessel functions. The mean correlation time τ_C can be calculated in the former case as

$$\tau_C = \left(\frac{1}{\tau_1\tau_2} + \frac{1}{\tau_2^2}\right)^{-1/2} \tag{24}$$

and in the latter case as

$$\tau_C = \left(\frac{2}{\tau_1\tau_2} + \frac{1}{\tau_2^2}\right)^{-1/2}\left[\frac{1}{\tau_1}\left\{\frac{1}{\tau_1} + \frac{1}{\tau_2} + \left(\frac{2}{\tau_1\tau_2} + \frac{1}{\tau_2^2}\right)^{1/2}\right\}^{-1} + 1\right] \tag{25}$$

Ediger et al. synthesized anthracene-labeled polystyrene and very carefully measured the anisotropy decays in a number of solvents of differing viscosity. They obtained very good data and used both models for analyzing anisotropy decays. Nevertheless, the experimental papers published by Ediger et al. are somewhat confusing. In their first paper [103], they concluded that the GDL model provides slightly better fits than the HH model, but 1 year later, in their second paper [104], they announced that the HH model is actually better than the EDL model. In fact, the differences were negligible and the two models provided fits of comparable quality. The Hall–Helfand model suffices with simpler mathematical treatment, which is more attractive for experimentalists, but both models involve two fitting parameters and, at the present time with advanced computers (in contrast to the epoch 20 years ago), complicated mathematical formulas for data treatment do not cause any problems.

Because the fluorophores are often attached by a single bond or by a short linker to a fairly large (roughly spherical) rigid macromolecule or nano-object, a model of a fluorophore rotating around one axis attached to a large spherical object was described by Gottlieb and Wahl [107]. The axis of rotation is assumed to be fixed in a radial position with respect to the bulky rigid macromolecular object (e.g., globular protein) and the fluorophore can either (1) freely rotate without any

hindrance (free internal rotation) or (2) perform a temperature-activated jump diffusion among discrete positions (T-JD). The following expression for $r(t)$ has been obtained for the free internal rotation:

$$r(t) = \exp\left(\frac{-t}{\tau_{cM}}\right)\left[\alpha_1 + \alpha_2 \exp\left(\frac{-t}{\tau_{cF}}\right) + \alpha_3 \exp\left(\frac{-2t}{\tau_{cF}}\right)\right] \tag{26}$$

where τ_{cM} and τ_{cF} are the depolarization correlation times of the particle and the fluorophore, respectively, which can be interpreted in both cases as the neat rotation correlation times, and α_i are constants depending on the orientation of transition dipole moments with respect to the axis of rotation of the fluorophore. The time-resolved anisotropy $r(t)$ has a similar form for the T-JD model:

$$r(t) = \exp\left(\frac{-t}{\tau_{cM}}\right)[\alpha_1 + \alpha_2 \exp(-Kwt)], \tag{27}$$

but the parameters have different physical meanings; K is the normalization constant, w is the jump frequency, and α_i depends on the angles between the transition dipole moments and the axis connecting the fluorophore with the bulk globule. A more general model for a freely rotating fluorophore attached to a more slowly rotating nonfluorescent symmetrical carrier was described by Burghardt [108] and a similar system with more complex relaxation processes was studied by Tanaka et al. [109] (internal rotation under the potential barrier). Numerical simulations based on this model were able to fit experimental decays from tryptophan in cytochrome C very well [110]. A discontinuous jump model for large carriers with fluorophores that can acquire a finite number of positions has also been published by Weber [111].

Szabo proposed an interesting model-free formula for the time-resolved anisotropy in a macroscopically isotropic system [112]. He expressed $r(t)$ as the autocorrelation function of orientations of the emission dipole moment at time t and absorption dipole moment at time $t = 0$ in a form suitable for general treatment of various systems, and particularly those with possible internal rotation:

$$r(t) = \frac{2}{5} \frac{\left\langle\left\langle k_F(t)\rho(v,t)P_2\left(\boldsymbol{\mu}_E(t)\cdot\boldsymbol{\mu}_A(t=0)\right)\right\rangle\right\rangle}{\left\langle\left\langle k_F(t)\rho(v,t)\right\rangle\right\rangle} \tag{28}$$

The physical meaning of the individual symbols is as follows: $k_F(t)$ is the time-dependent rate constant of the radiative depletion of the excited state, $\rho(v,t)$ is the normalized time-dependent emission spectrum, i.e., the denominator $\langle\langle k_F(t)\rho(v,t)\rangle\rangle$ describes the total fluorescence, $S(t)$, P_2 is the Legendre polynomial of the second order which correlates with the mutual angular orientations of $\boldsymbol{\mu}_E(t)$ and $\boldsymbol{\mu}_A(t=0)$, and denotes averaging with respect to possible orientations and energy states. He also employed the master equation, which describes the time change of the conditional probability $p\left(i,\boldsymbol{\Omega};t/(j,\boldsymbol{\Omega_0};t=0\right)$ that the fluorophore is in energy state i and

its orientation is described by three Euler angles $\boldsymbol{\Omega}$ at time t, if it was in electronic state j and its orientation was $\boldsymbol{\Omega_0}$ at $t = 0$. This equation has the form

$$\frac{\partial}{\partial t}\left[p\left(i, \boldsymbol{\Omega}; t/(j, \boldsymbol{\Omega}_0; t = 0)\right]\right. = \{\boldsymbol{L}(i, \boldsymbol{\Omega}) - \boldsymbol{k}(i, \boldsymbol{\Omega})\} p\left(i, \boldsymbol{\Omega}; t/(j, \boldsymbol{\Omega}_0; t = 0), \quad (29)\right.$$

where $\boldsymbol{L}$ is the operator, which, in addition to the changes in the angular momentum, also comprises the electronic transitions and $\boldsymbol{k}(i,\boldsymbol{\Omega})$ is the complex rate constant of irreversible transitions. The explicit form of the operator $\{\boldsymbol{L}(i, \boldsymbol{\Omega}) - \boldsymbol{k}(i, \boldsymbol{\Omega})\}$ results from the particular model used for describing the system of interest. The set of integro-differential Eq. (29) makes it possible to consider and include a number of phenomena in a unified fashion. It can account for energy migration and transfer, because the rate constants $\boldsymbol{k}(i,\boldsymbol{\Omega})$ depend on the distance and mutual orientation of the fluorophores (and quenchers). Very general formulation of the problem permits treatment of the effect of heterogeneity of the medium and its effect on the emission characteristics. The analytical solution is possible only for a small number of particular forms of the $\boldsymbol{L}(i, \boldsymbol{\Omega})$ operator. Solution of the equation is generally feasible if the energy and orientation relaxations are uncoupled and also if the overall and internal relaxations are uncoupled.

Realistic description of the relaxation behavior of systems with possible internal rotation is very complex and almost all the models had to introduce simplifying (sometimes even oversimplifying) assumptions. In spite of a number of theoretical studies, interpretation of the experimental data is mostly highly intuitive and is based on semiempirical formulas.

10 Rigid Molecules in Anisotropic Medium

Fluorescence anisotropy studies are very common in biochemical and biological research. They have been widely used in the past two decades to study the structures of various biological membranes formed by lipid bilayers [113–117]. Hence, a number of appropriate models have been proposed for interpretation of the experimental data for membranes and other organized biopolymer systems. In spite of the fact that this review is aimed at synthetic polymers and does not concern biopolymers and biologically important systems, the motion of probes embedded in dense 2D polymer brushes and in dense inner parts of coronas of self-organized polymeric nanoparticles is similar to that studied in biological membranes and therefore it will be mentioned.

The movement of a fluorophore embedded in a bilayer (generally in an anisotropic medium) is controlled by the 3D potential preferring certain (nonequivalent) orientations of the fluorophore in all three dimensions. At long times upon excitation, the system does not relax completely in all 3D and the residual anisotropy is not zero. To date no general theory has been formulated; however, particular models for the most frequently studied systems have been published by a number

of researchers. In the following text, we will briefly outline the most important models developed for analyzing fluorescence anisotropy decays in membranes.

In most cases, the theories focus on symmetric-top fluorophores. Kinosita et al. [115] published one of the oldest suitable models. Its analysis is applicable for a macroscopically isotropic suspension of planar lipid bilayers, which are assumed to be large and immobile during the anisotropy decay measurement. Individual bilayer planes are oriented randomly with respect to the polarization plane of the excitation light (i.e., the fluorophores are also oriented randomly and uniformly in 3D), which means that the probability of excitation of probes in different bilayer planes mutually differs and the emission polarization is also strongly polarized at early times following excitation. Note that the angularly random orientation of small mobile fluorophores in an isotropic medium prior to excitation also yields polarized emission at early times following a short excitation pulse. It is important to realize that random orientations of individual bilayer planes, which yield the static isotropic properties of the suspension, do not average the time-resolved fluorescence response in all three dimensions. The motion of probes in bilayers is locally anisotropic and does not completely relax in 3D, because the positions of the bilayers are kinetically frozen during the lifetime of the excited state. The basic assumptions of the model can be summarized as follows: (1) the bilayer does not move at times relevant for the decay measurement, (2) the probe rotates around one axis, which can move, and its orientation undergoes the diffusion motion in the potential field, which is symmetrical with respect to the direction perpendicular to the bilayer plane and depends on the angle φ between the instantaneous orientation of the axis of rotation and its time-averaged (perpendicular) orientation. Due to the orientation constraint, the anisotropy does not decay to zero and the ratio r_∞/r_0 characterizes the effective anisotropy of the medium (often called the degree of orientation constraint) and the initial slope of r(t) gives the average velocity with which the fluorophore wobbles within a confined angle. There are several variants of this model. (1) The diffusion-in-a-cone model assumes the simplest form of the angular potential: $W(\varphi) = 0$, for $\varphi \leq \varphi_{\max}$, and $W(\varphi) = \infty$, for $\varphi > \varphi_{\max}$. This model has been applied to three types of fluorophores: (a) rod-shaped rotors with emission transition dipole moment parallel to the symmetry axis (wobbling-in-a-cone model), (b) rod-shaped rotors with emission transition dipole moment perpendicular to the symmetry axis (spinning-in-an-equatorial-band model), and (c) disk-shaped molecules with absorption and emission transition dipole moments in the plane of the disk, which undergo free in-plane rotation and restricted out-of-plane rotation.

In his later work, Kinoshita et al. extended the model by assuming Gaussian distribution of the probe orientations before the excitation with respect to the bilayer [116]. The authors compared the theoretical predictions of the Gaussian model with the original model and concluded that, if only two parameters are used, the details of the microscopic description do not have a decisive impact on the quality of the predicted fits. Lipari et al. [117] generalized the approach proposed by Kinosita by taking into account segmental motion of the lipid molecules and

assuming that the individual internal modes of motion are independent. The authors presented a model-independent equation for the residual anisotropy, r_∞

$$r_\infty = \frac{2}{5} P_2(\cos\varphi_A)\, P_2(\cos\varphi_E) S^2 \tag{30}$$

where $S = \langle P_2(\cos\varphi)\rangle$ is the order parameter, φ is the variable angle between the symmetry axis of the fluorophore and the perpendicular line to the bilayer plane, φ_A and φ_E are the angles between the absorption and emission dipole moments, respectively, and the fluorophore symmetry axis, P_2 is the second-order Legendre polynomial, and the brackets denote ensemble averaging.

At present, there are a number of models differing in the detailed description of various flexible fluorescent molecules and systems with complex relaxations or fluorophores embedded in heterogeneous media. We will not go into greater detail and will give only one example of generic complications that can occur if the polarity-dependent fluorophore is embedded in a micro-heterogeneous environment. A typical example is an amphiphilic polarity-dependent fluorophore, partially bound to polymeric micelles and partially dissolved in an aqueous medium [118]. Free probes (component 1) dissolved in an aqueous solvent (molar fraction x_1) experience high rotational mobility (their rotational correlation time is short) and their fluorescence, $F_1(t)$, is partly quenched by interaction with the polar environment (i.e., the fluorescence lifetime is short). The probes (2) bound to polymeric nanoparticles (molar fraction $x_2 = 1–x_1$, fluorescence intensity $F_2(t)$) "feel" a more hydrophobic environment (their lifetime is long) and their rotation is slow and hindered. The average fluorescence anisotropy, $r(t)$, is weighted by the fractional fluorescence intensities:

$$r(t) = \frac{x_1 r_1(t)\, F_1(t) + x_2\, r_2(t)\, F_2(t)}{x_1 F_1(t) + x_2 F_2(t)} \tag{31}$$

At short times, the fluorescence contribution of fast-emitting probes (proportional to the number of photons emitted per unit time) is important and generates a considerable weighting factor for the fast anisotropy decay, $r_1(t)$. Therefore, the overall anisotropy $r(t)$ decays quite rapidly to relatively low values at early times. At later times, the fluorescence $F_1(t)$ (not anisotropy) drops almost to zero, but $F_2(t)$ is still important. The average anisotropy starts to increase at intermediate times when $F_1(t)$ and $F_2(t)$ are comparable and passes through a local maximum when $F_1(t)$ is weaker than $F_2(t)$. At long times, only a slow anisotropy decay $r_2(t)$ is observed because $F_2(t)$ decays slowly and is still measurable, while $F_1(t)$ is practically zero. An example of complex anisotropy decay caused by the time-dependent variable weighting of the anisotropy contributions is depicted in Fig. 8. The figure shows results of fluorescence anisotropy measurements for high-molar-mass diblock copolymer polystyrene-*block*-poly(methacrylic acid) tagged by a low fraction of 2-vinylnaphthalene (on average less than one fluorophore per chain).

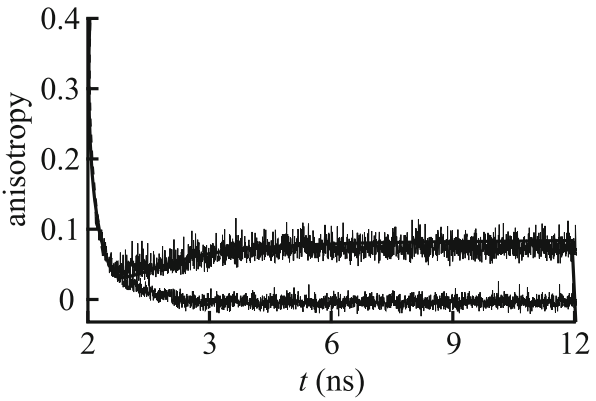

Fig. 8 Complex anisotropy decay (the *upper curve*) in a system containing two types of chemically identical probes differing in fluorescence lifetime and in mobility (as a result of different interaction with the microenvironment) compared with a simple one for a system with equivalent probes (the *bottom curve* decaying fast to zero). Adapted from Springer, Journal of Fluorescence 4, 1994, 353–356, figure 1, [118]. Copyright 1994. With kind permission from Springer Science and Business Media

The copolymer was dissolved (1) in a good common solvent of both blocks (1,4-dioxane)—monotonous curve decaying fast to zero, and (2) in a 1,4-dioxane-methanol (73 vol.%), which is a selective solvent for poly(methacrylic acid). In the selective solvent, the multimolecular micelles are formed and pendant naphthalenes are trapped in their compact and nonpolar polystyrene cores. However, the micelles coexist in mobile equilibrium with a low fraction of non-micellized unimer chains. Therefore, some pendant fluorophores are exposed to a fairly polar solvent mixture and undergo fairly fast motion. The curve measured for micellar systems has a complex shape, because it reflects the presence of two types of probes that differ both in fluorescence lifetime and in mobility. Comment: in the studied micellar system, the tagged chains were co-micellized with virtually identical non-tagged chains to lower the content of naphthalene and suppress potential complicating effects due to excitation energy migration in micelle cores. Because the rotation of micelles is much slower than the fluorescence decay, the anisotropy curve does not drop to zero on the timescale of the measurement.

11 Excimers and Exciplexes

Excimers are short-lived (transient) excited dimers formed by the bimolecular reaction of one excited fluorescent monomer (M^*) and one ground-state monomer (M) upon excitation of a low fraction of monomers. They exhibit strong fluorescence, which is red shifted with respect to that of the monomer. The main difference between excimers and excited dimers formed in the ground state prior to the

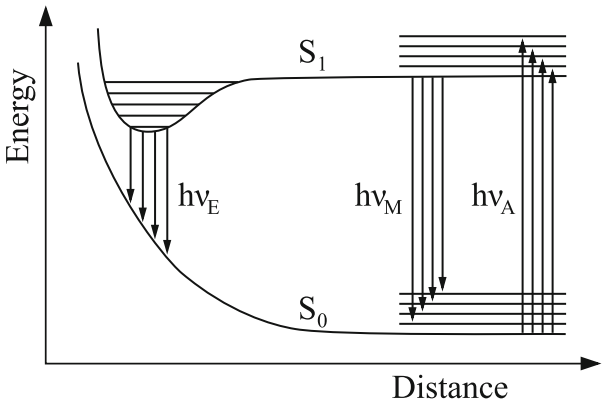

Fig. 9 The scheme of energy levels of the excited monomer and excimer as functions of the distance between the excited and ground-state monomers

excitation consists in the fact that the monomers involved in excimers do not form dimers in the ground state. Excimer formation assumes that one of the ground-state monomers, which are present in excess in the system and undergo random self-diffusion, comes close enough to the excited monomer (fluorophore) before the excited species becomes de-excited. Typical distances between molecules needed for the excimer formation are ca. 0.3 nm. It is obvious that excimers form easily in relatively concentrated solutions of fluorophores with long lifetimes of the excited state. Because the concentration of excited species is very low and there is no energy barrier on the excited energy landscape which could hinder (slow down) the formation of excimers, the reaction rate is controlled by the random self-diffusion of ground-state fluorophores. The formation of excimers can be described by the stoichiometric equation

$$M^* + M^\circ \rightleftharpoons D^* \tag{32}$$

The scheme of energy levels as functions of the distance between the monomers is shown in Fig. 9. The ground state is a purely repulsive state, i.e., at short distances, the interaction energy of two monomers decreases monotonously and steeply with their distance. The excited state exhibits a fairly deep minimum with a distinct vibrational structure. The stabilization energy is usually quite large and the red shift in the emission wavelength of the excimer with respect to the monomer fluorescence can be as large as 100 nm (e.g., for naphthalene or pyrene). The potential well of the exited dimer is smooth and relatively broad—it spans several tenths of nm and the repulsive ground-state energy changes considerably in this region. Therefore, the red-shifted excimer emission spectrum is broad. In spite of the fact that the excimer has distinct vibrational structure, its emission band is featureless without any structure, because the dimer dissociates instantaneously after the emission of a photon.

Figure 10 depicts the steady-state emission spectra of pyrene dissolved in 1,4-dioxane (normalized to the allowed third vibrational band in the monomer spectrum) for increasing concentrations. The formation of excimers belongs to

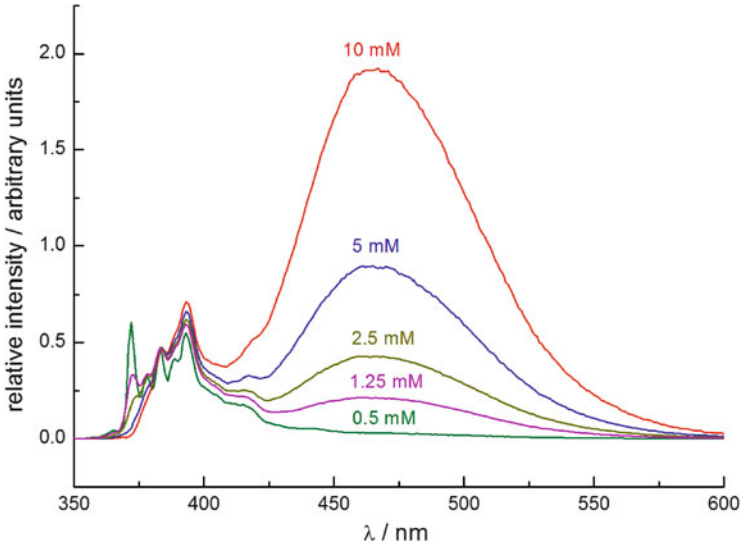

Fig. 10 Steady-state spectra depicting the pyrene excimer formation in 1,4-dioxane as a function of pyrene concentration. In case of pyrene dissolved in a fairly polar 1,4-dioxane, the I_1/I_3 ratio in pyrene monomer spectrum is higher than 1, but the excimer formation affects its value, which decreases in excimer containing solutions

the category of quenching processes (in this case self-quenching): the intensity of the monomer emission decreases and that of the excimer increases with increasing concentration of the fluorophore. Note that we present the normalized spectra (normalized to the monomer emission) and hence the monomer intensity decrease does not appear. As already mentioned, the long excited state (i.e., fluorescence) lifetime of the monomer facilitates the formation of excimers, and therefore pyrene, which has one of the longest excited state lifetimes among practically important fluorophores (more than three hundreds ns), exhibits strong excimer emission at relatively low concentrations compared with other fluorophores with shorter excited state lifetimes.

The effect of excimer kinetics on fluorescence decays of monomers and excimers upon excitation with a short pulse was studied first by Birks et al. [119]. They took into account all the relevant processes that proceed after the excitation of a low fraction of monomers by an ultrashort pulse and derived the rate equations describing the monomer and excimer decays. Most processes involved in the "Birks scheme" are monomolecular and depend only on the concentration of the excited species and on the first-order rate constant; one of them is a bimolecular process and depends on the concentrations of both the excited and ground-state molecules. They include (1) monomer fluorescence, $M^* \rightarrow M + h\nu_M$, (rate constant k_{fM}), (2) internal monomer quenching, $M^* \rightarrow M$, (k_{iM}), (3) excimer formation, $M^* + M \rightarrow D^*$ (bimolecular reaction, i.e., the rate depends on the product of the rate constant and concentration of the ground-state

monomer, c, i.e., on $k_{DM} \cdot c$), (4) excimer dissociation, $D^* \rightarrow M^* + M$, (k_{MD}), (5) excimer fluorescence, $D^* \rightarrow D + h\nu_D$, ($k_{fD}$), and (6) nonradiative excimer quenching, $D^* \rightarrow D$, (k_{iD}). To simplify the notation, they used combined parameters, $k_M = k_{fM} + k_{iM}$, $X = k_M + k_{DM} \cdot c$, $k_D = k_{fD} + k_{iD}$, and $Y = k_D + k_{MD}$. The set of differential equations that describe the reaction kinetics can be written as

$$\frac{d[M^*]}{dt} = -X[M^*] + k_{MD}[D^*] \tag{33}$$

$$\frac{d[D^*]}{dt} = -Y[D^*] + k_{DM}c[M^*] \tag{34}$$

and their solution is

$$[M^*] = \frac{[M^*]_0}{(\lambda_2 - \lambda_1)}\{(\lambda_2 - X)\exp(-\lambda_1 t) + (X - \lambda_1)\exp(-\lambda_2 t)\} \tag{35}$$

$$[D^*] = \frac{[M^*]_0 k_{DM} c}{(\lambda_2 - \lambda_1)}\{\exp(-\lambda_1 t) - \exp(-\lambda_2 t)\} \tag{36}$$

$$\lambda_{1,2} = \frac{1}{2}\left[X + Y \mp \sqrt{\left\{(X - Y)^2 + 4k_{DM}k_{MD}c\right\}}\right] \tag{37}$$

The time-resolved fluorescence intensities, $F_M(t)$ and $F_D(t)$, are proportional to the instantaneous concentrations of the excited monomers and excimers, respectively. The monomer decay is a sum of two exponentials, which means that it decreases faster than the unquenched monomer decay. The excimer is not present immediately after excitation and is formed by a diffusion-controlled process, i.e., the emission increases at early times, passes maximum, and at later times decays more slowly than the monomer fluorescence. The realistic (experimental) decays, $F_i(t)_{exp}$, are schematically shown in Fig. 11.

They are convolutions of theoretical decays, $F_i(t)_{theor}$, with the narrow pulse profile, $P(t)$, i.e.,

$$F_i(t)_{exp} = \int_0^t F_i(t^*)_{theor} P(t - t^*)dt^* \tag{38}$$

Note that, in the time-resolved measurements, the experimental monomer fluorescence decays always "copy" the excitation profile at early times and show an apparent build-up part, which is corrected and removed iteratively by the deconvolution procedure during their analysis. The relative excimer-to-monomer quantum yield, F_D/F_M, where $F_M = \int_0^\infty F_M(t)dt$ and $F_D = \int_0^\infty F_D(t)dt$, can be evaluated from the equation

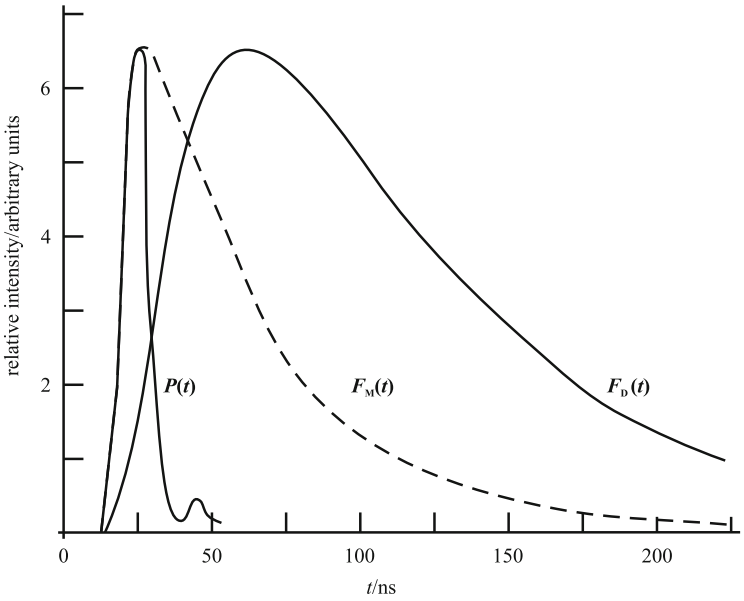

Fig. 11 The time-resolved monomer, $F_M(t)$, and excimer, $F_D(t)$, fluorescence decays calculated according to Birks scheme, taking into account the convolution of decay curves with the excitation profile, $P(t)$. Reproduced from Proceedings of the Royal Society of London Series A, Mathematical and Physical Sciences 275, 1963, 575–588, figure 1, [119]. Copyright 1963. With kind permission from The Royal Society

$$\frac{F_D}{F_M} = \frac{k_{fD}\, k_{DM}}{k_{fM}\, Y} c \tag{39}$$

Measurements of excimer kinetics are widely used fluorescence methods for studying the dynamics of multiply labeled polymer chains. For probes attached to the chain, the kinetic scheme is more complex and the resulting decays are also substantially more complicated. Because the chapter on hydrophobically modified polymers treats this topic very thoroughly, we will not go into more detail here.

Exciplexes are transient charge-transfer (CT) species formed in bimolecular quenching reactions of excited states. The chemistry and kinetics of exciplexes have been intensely studied and their role in photo-induced electron-transfer reactions has been well documented and recognized [120, 121]. One of the best studied systems is the excited complex of anthracene (acceptor) and *N*,*N*-dimethylaniline (donor). Exciplexes do not form in the ground state, but their behavior is often similar to that of excited charge-transfer complexes formed in the ground state. The properties of exciplexes are complex, because they usually reflect both the locally excited acceptor–donor state, A^*D, and the charge-transfer radical-ion state, A^-B^+. If the charge-transfer rate is predominant, the exciplex is reminiscent of the contact radical-ion pair or the solvent-separated radical-ion pair. Exciplexes play an

important role in a number of important electron-transfer processes, including processes in polymer systems [122], but this topic will not be discussed in detail here and the reader is referred to the above references and to a number of existing textbooks and excellent reviews on charge-transfer processes and on the chemistry and physics of exciplexes.

12 The Effect of Ground-State Aggregation on Fluorescence Spectra

The last part of this chapter is devoted to the general impact of weak ground-state complexation (both reversible association and irreversible aggregation) on fluorescence spectra, i.e., we will outline the spectroscopic characteristics of "J" and "H" aggregates, which are usually formed in systems of rigid planar aromatic molecules with highly delocalized π electrons, such as xanthine dyes (e.g., fluorescein) or porphyrins (see Fig. 12). As the formation of "J" and "H" aggregates occurs in a number of polymer systems (e.g., in solutions of polymeric micelles) [123] and textbook-like explanation of the principles of their formation is rare (in comparison with the literature on excimers), we will devote more space to discussion of the spectroscopic consequences of this type of aggregation. As multimolecular aggregates have been studied most frequently, we will use the term aggregation through the following text, even though the general discussion and explanation also apply to both reversible associates and dimers.

To begin with, we would like to stress once more that we will discuss the spectroscopic processes in systems of weakly bound complexes. In a number of cases, the aggregation is induced (or mediated) by interaction with the surrounding medium or with other components of the mixture. Let us give one typical example: planar fluorescent molecules are often adsorbed on surfaces (or on nanoparticles). The driving force for this process is the enthalpy of adsorption. As the concentration of adsorbed molecules increases and reaches a certain critical value, the adsorbed molecules start to repel each other. However, the repulsion between relatively large planar molecules depends sensitively on their mutual orientation and therefore the adsorbed molecules self-organize in stacks. Partially overlapping coplanar arrangement of aromatic rings relatively far from each other (ca. 1 nm) minimizes the mutual repulsion. The above example demonstrates that adsorption is a prerequisite for aggregation and that the aggregates would not form spontaneously in solutions.

Fig. 12 Porphyrins

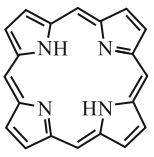

porphyrin

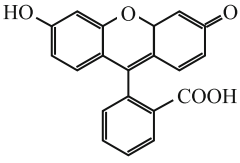

fluorescein

In contrast to excimers, the organized interacting structures are formed in the ground state and survive in the form of undissociated excited species upon excitation and the interaction of excited π^* electrons with π electrons of neighbor molecules leads to changes in their optical spectra. In 1964, Kasha [124–126] explained the changes in nondegenerate absorption bands by the exciton theory, which was originally developed by Frenkel in 1931 [127]; this theory accounts for the mutual correlation between the surplus and deficiency of negative charges in solid materials. The term "exciton" describes the bound state of an electron and an "electron hole" in supramolecular structures. It is currently used for interpretation of the optoelectronic properties of solid state materials (mainly semiconductors) and can be used to explain the spectroscopic characteristics of fluorophore crystals [128]. Kasha has shown that this concept is also applicable for small associates of two or more molecules. He mostly studied the dimers of planar aromatic molecules with transition dipole moments of both monomers lying in the same plane. In this case, the interaction strength can be characterized by the distance between the centers of gravity of the two molecules and by one angle, which describes the orientation of the dipoles with respect to the line connecting the two centers of gravity (see Fig. 13) [129].

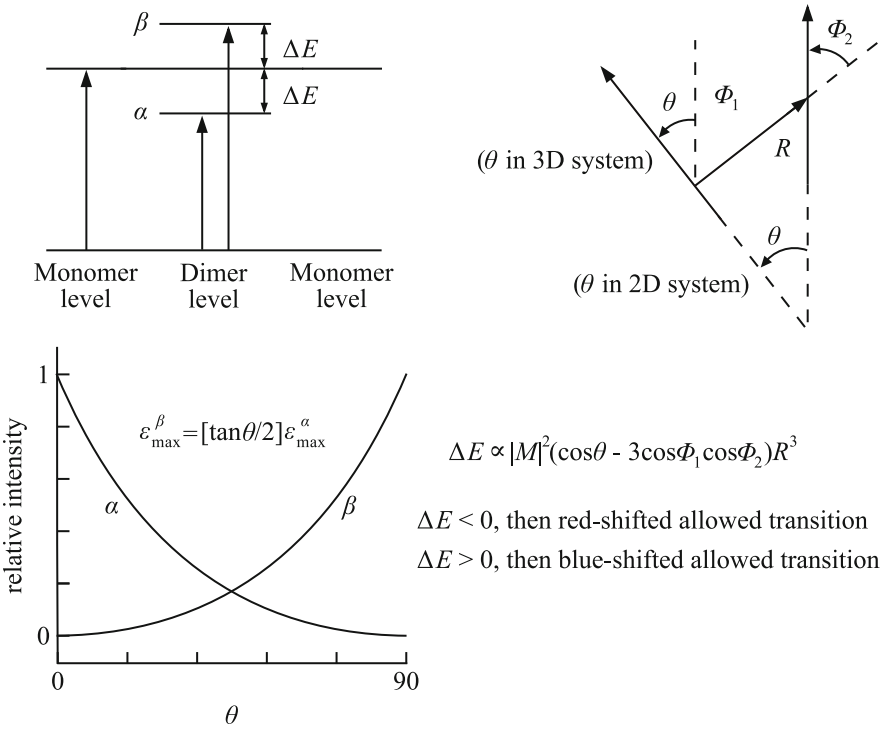

Fig. 13 Geometric and energetic scheme of formation of "J" and "H" dimers. Adapted with permission from Chemistry—a European Journal 7, 2001, 2733–273, figure 1, [129]. Copyright 2001 WILEY-VCH Verlag GmbH, Weinheim, Fed. Rep. of Germany

Efficient interaction assumes optimum approach of the two molecules and the spectral change is controlled only by one angle, θ. For a skew arrangement of the two dipole moments, the situation is more complicated and three angles, θ, ϕ_1, and ϕ_2, have to be used.

In 2D (coplanar orientation), the splitting of the excited energy levels and the spectroscopic behavior of the dimer are controlled by angle θ between the transition dipole moment and the line joining the centers of gravity of the two molecules and by their distance r. Bottom part of the figure depicts the relative intensity of transitions to the α and β states as a function of θ. In 3D (i.e., the skew arrangement), the behavior depends on three angles, θ, ϕ_1, and ϕ_2.

The interaction leads to symmetric splitting of the energy level of the π* orbitals into two different states α and β. The energy difference describing the increase (and decrease) in the states with respect to the excited monomer $|\Delta E|$is given by the following [131]:

$$|\Delta E| = \frac{\nu_2 - \nu_1}{2} \sim \frac{\left((\mu_{tr})_M\right)^2}{R^3} |\cos(\theta) + 3\sin^2(\theta/2)| \tag{40}$$

where $(\mu_{tr})_M$ is the magnitude of the transition moment of the monomer, v_2 and v_1 are the frequency maxima of the two bands α and β, and the energy difference between them is $2|\Delta E|$. The value of $(\mu_{tr})_M$ can be obtained by measuring the intensity of the monomer band, because it holds that

$$\left((\mu_{tr})_M\right)^2 = \frac{9.19 \times 10^{-39}}{\langle \nu_M \rangle} \int \varepsilon(\nu)\ d\nu \tag{41}$$

where $\varepsilon(v)$ is the absorption coefficient at frequency v and $\langle v_M \rangle$ is the average frequency of the monomer absorption band. If $\theta < 54.7°$ (lower than the magic angle), dimers or aggregates of the "J" type are formed. If $\theta > 54.7°$, dimers or aggregates of the "H" type are formed. The spectral characteristics of the two types of aggregates differ considerably [130, 131].

The extreme (limiting) arrangement of the "J" dimer is the linear "head-to-tail" arrangement with $\theta = 0°$. In this case, the transition dipole moment is parallel to the line joining the centers of gravity of the two molecules and equals $(\mu_{tr})_{DJ} = \sqrt{2} \cdot (\mu_{tr})_M$. Only the transition (excitation) to the lower state α is allowed (red shift of the absorption band), from which a strong emission (also significantly red shifted) can proceed. For the "H" dimer, the extreme (limiting) arrangement is the coplanar "face-to-face" arrangement with $\theta = 90°$ (aromatic cycles usually form this type of associates). The resulting dipole moment has the same magnitude as in the previous case, i.e., $(\mu_{tr})_{DH} = \sqrt{2} \cdot (\mu_{tr})_M$, but it is perpendicular to the line connecting the two centers of gravity. In this case, only excitation to the higher state β is allowed, i.e., we see only one blue-shifted band in the absorption spectrum. The splitting of the energy levels is usually higher because the parallel arrangement allows closer approach of the fluorophores and stronger interaction. The theory predicts

that the absorption band of the "H" dimer is broader than that of the monomer and depends on the number of aggregated monomers *n,* i.e., its half-width is $\Delta\lambda_{1/2} = (\sqrt{n})(\Delta\lambda_{1/2})_{\mathrm{M}}$. Radiative transition to the ground state is theoretically allowed but, after the absorption of a photon, very rapid nonradiative transition to the lower α state proceeds on an approx. three orders of magnitude faster timescale (than the emission), from which the radiative transition is forbidden. This actually means that the excess energy is dissipated by a cascade of nonradiative processes and "H" dimers are effectively nonfluorescent species.

However, not all fluorophores form the above-described extreme (limiting) associates. Aromatic molecules with lower symmetry (which do not have a symmetry plane perpendicular to the aromatic ring) usually form both types of associates, but the transition moments form a general angle θ with the joint line of the centers of gravity. In this case, the resulting transition moment can be decomposed into two components—parallel and perpendicular to the joining line. Both transitions (excitations from the ground state to the α and β states) are partly allowed, but the blue-shifted absorption bands is more intense than the red-shifted one in "H" aggregates and the opposite is true in "J" aggregates. In general, a relatively weak fluorescence from "H" aggregates can also occur. If the absorption bands are sufficiently separated and allow reasonable spectral decomposition, then angle θ can be estimated from spectra, because it holds that [132, 133]:

$$\tan^2\left(\frac{\theta}{2}\right) = \left(\frac{(\mu_{\mathrm{tr}})_2}{(\mu_{\mathrm{tr}})_1}\right)^2 = \frac{B_2/B_1}{\langle\nu_2\rangle/\langle\nu_1\rangle} \tag{42}$$

where $(\mu_{\mathrm{tr}})_2$ a $(\mu_{\mathrm{tr}})_1$ are the magnitudes of moments of transitions to the higher and lower energy states, respectively, which can be estimated from areas of bands B_2 and B_1, and the average frequencies of the absorption bands, $\langle\nu_i\rangle$ (which can be approximated by the corresponding maxima).

Because the bands are close to each other, $(\langle\nu_2\rangle/\langle\nu_1\rangle) \cong 1$, the last term (denominator) is often omitted. A number of practically important fluorophores of both the "H" and "J" types are formed, depending on the conditions. Rhodamine B forms "H" aggregates in aqueous media and "J" aggregates in solutions in aliphatic alcohols [134, 135]. Other compounds (e.g., some derivatives of porphyrins) form both types simultaneously under certain conditions, but the rates of their formation may differ considerably [136].

The impact of aggregation on porphyrin spectra in the region of the Soret band is substantially more complicated than the above-outlined scheme, because it involves double degenerate transition. Gouterman [137, 138] proposed a model which takes into account four orbitals. Two mutually perpendicular transition dipole moments are oriented in lines that connect two opposite NH groups. Ribó, Rubires et al. [129, 139] analyzed the possibilities for the formation of "H" and "J" aggregates for various porphyrin and metallo-porphyrin derivatives. They also reinvestigated and reanalyzed the published data on polymeric 10,20-poly(5,15-diaryl-Zn-porphyrines), synthesized and studied by Osuka et al. [140–142], Fig. 14. They showed that the arrangement of dipole moments depicted in upper part

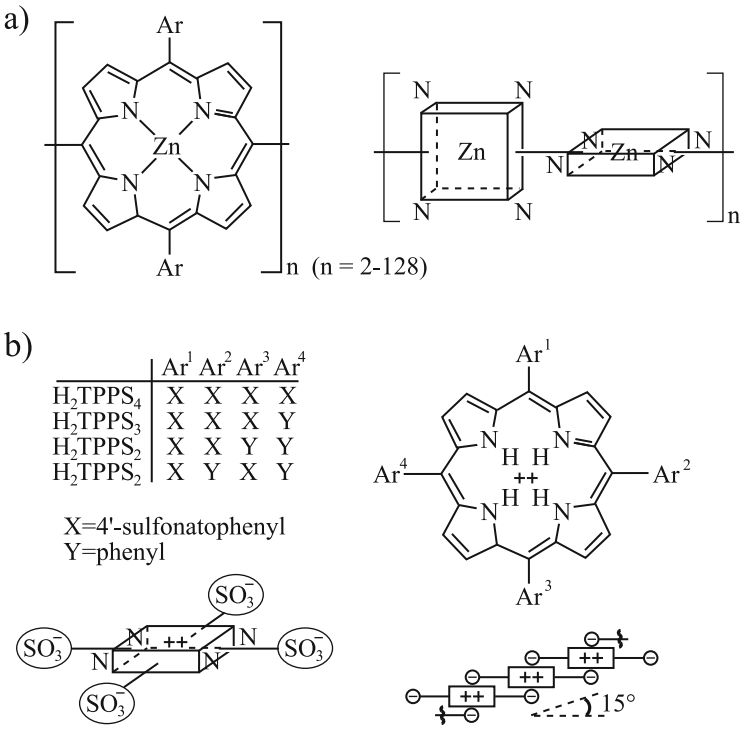

Fig. 14 (**a**) The most probable orientation of cycles in polymeric 10,20-poly(5,15-diaryl-Zn-porphyrins. (**b**) Self-assembly of anionic SO_3^- substituted porphyrins. The substituents are listed in a table which is a part of the scheme. The angle between the plane of the porphyrin skeletons and the line connecting their centers of gravity is 15°—see the *right bottom part* of the scheme. Adapted with permission from Chemistry—a European Journal 7, 2001, 2733–273, scheme 1, [129]. Copyright 2001 WILEY-VCH Verlag GmbH, Weinheim, Fed. Rep. of Germany

of Fig. 15a (symmetry group C_2) is compatible with one degenerate intense red-shifted band and one weak blue-shifted band with an intensity ratio of 3:1. The arrangement of dipole moments shown in the bottom part of Fig. 15a (symmetry group D_{2d}) yields one non-displaced absorption band (i.e., in the same position as that of the monomer) and one red-shifted nondegenerate band. The intensities of the two bands should be the same and the frequency difference between the bands depends on the degree of polymerization. The experimental spectrum agrees with the latter model, which suggests that the arrangement of dipole moments corresponds to symmetry D_{2d}. The authors also studied the spontaneous assembly of two protonated porphyrins containing four symmetrically attached negatively charged 4′-sulfonatophenyl groups [129, 139]. Taking into account strong electrostatic interactions, the most probable arrangement is that shown in Fig. 14b. The experimental value of angle α, which reflects the overlap of two coplanar planes of porphyrin skeletons, i.e., the angle between the plane defined by the porphyrin rings and the line connecting their centers of gravity, is $\alpha = 15°$.

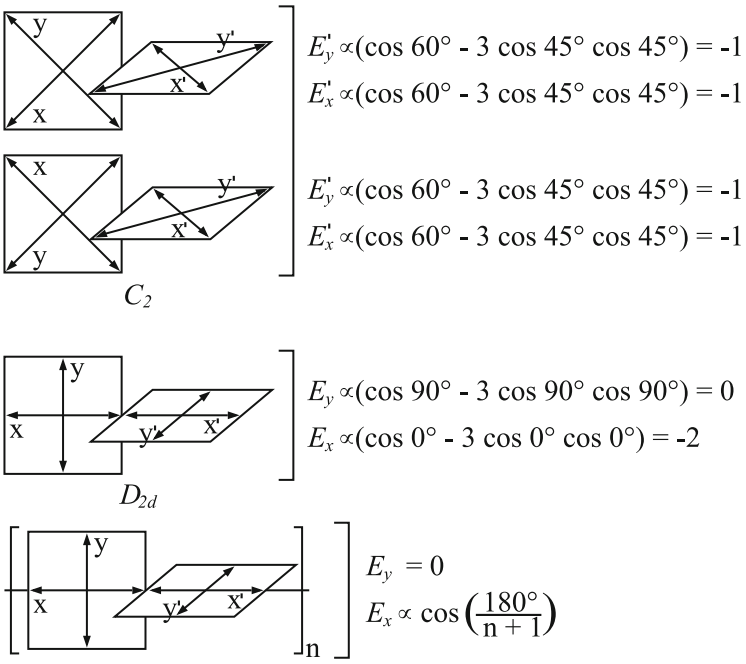

Fig. 15 (continued)

Figure 15a shows the arrangements of two porphyrin derivatives corresponding to C_2 and D_{2d} arrangements and enumerates relative changes of energy levels with respect to monomer level. The correlation diagrams in Fig. 15b depict changes in the energy levels of the excited states during gradual "insertion" of two coplanar porphyrin aromatic rings above each other as a function of angle α between the line joining the centers of gravity and the plane in which the aromatic rings lie (see the bottom right-hand side part of Fig. 14b).

Individual cases in Fig. 15b differ in the arrangement of the dipole moments with respect to each other and with respect to the direction of the "insertion." The left-hand side corresponds to "J" dimers (side-to-side π stacking) for $\alpha = 0°$ and the right-hand side corresponds to "H" dimers (face-to-face π stacking) for $\alpha = 90°$. The symmetries of all the limiting (extreme) arrangements are listed in the figure. The energies of states to which the transition is more allowed are depicted by full curves. We see that, in the first case (symmetry C_{2v} or C_{2h}), the spectrum should consist of two double degenerate red- and blue-shifted states.

In the second and third case, the spectrum should contain four nondegenerate bands. In the second case, the energy of two states should not depend on α and, in

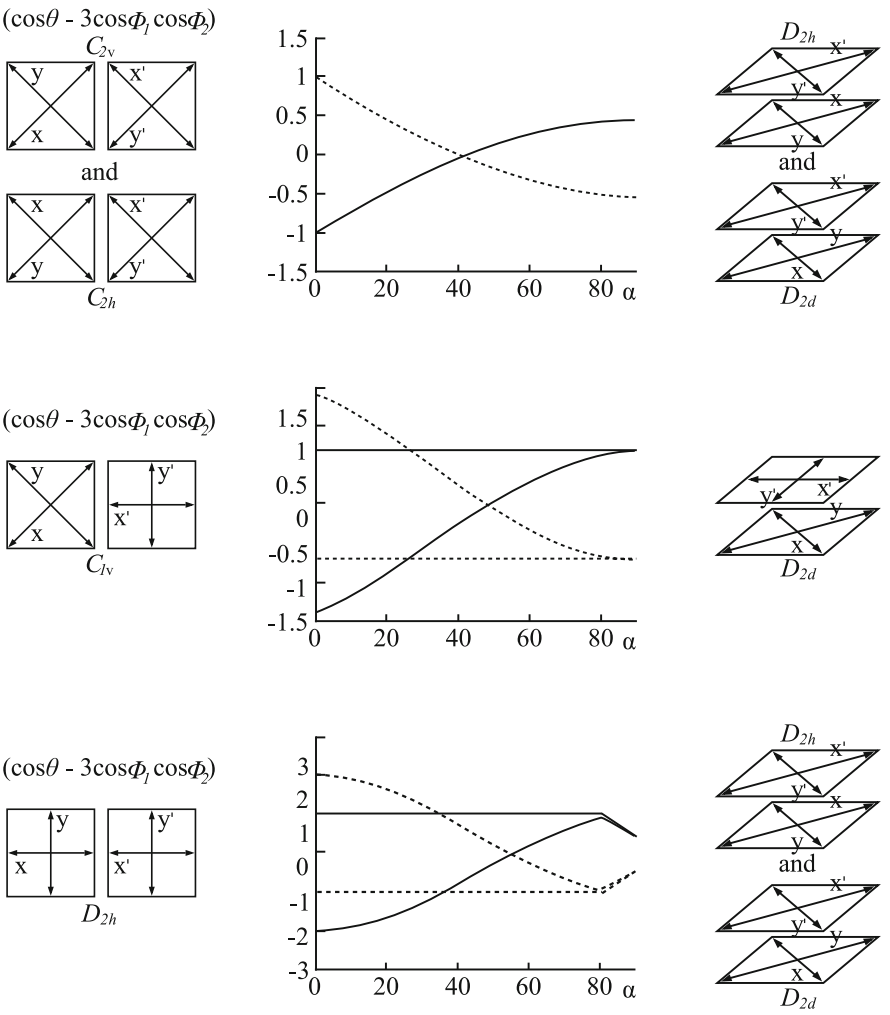

Fig. 15 (**a**) Possible arrangements of dipole moments and energy states of polymeric porphyrin derivatives (*left column*) in side-to-side arrangements (dihedral angle 90°). Relative changes of energies of possible dimer states with respect to the degenerate monomer (*right column*). The dimer yields four possible states, whose polarizations are shown in the scheme. Symmetry C_2 yields an intense degenerate red-shifted and a weak degenerate blue-shifted absorption band. Symmetry D_{2d} yields one intact (unshifted) and one red-shifted band with the same intensities. Adapted with permission from Chemistry—a European Journal 7, 2001, 2733–273, figure 3, [129]. Copyright 2001 WILEY-VCH Verlag GmbH, Weinheim, Fed. Rep. of Germany. (**b**). Correlation diagram depicting the changes in the energy of the states during the "insertion" of two coplanar aromatic porphyrin rings above each other (*middle column*), side-to-side J-arrangement, α=0° (*left column*) and face-to-face H-arrangement, α=90° (*right column*). Angle α is the angle defined by the plane of the rings and the line joining the centers of gravity of the two molecules (see the *bottom part* of the figure 14). *Full curves* depict the energy of states to which transition is allowed and the *broken curves* depict the energy of states corresponding to forbidden transitions. Adapted with permission from Chemistry—a European Journal 7, 2001, 2733–273, figure 5 [129]. Copyright 2001 WILEY-VCH Verlag GmbH, Weinheim, Fed. Rep. of Germany

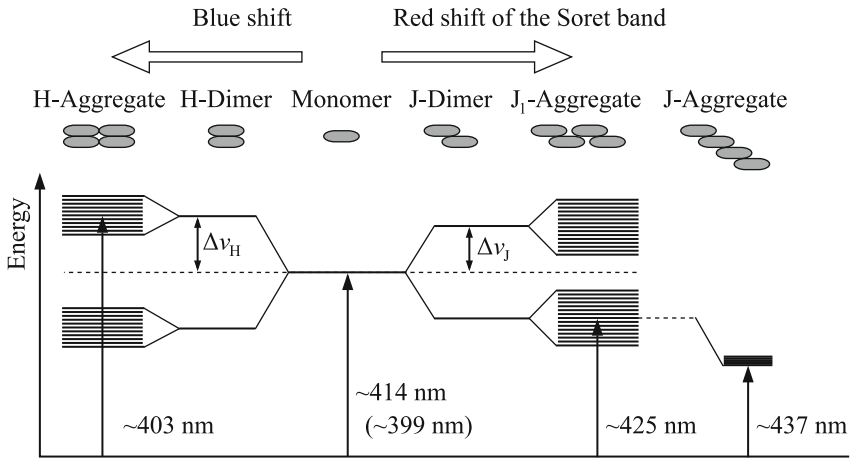

Fig. 16 Graphical summary of possible arrangements of "J" and "H" aggregates and of the corresponding energy levels. Adapted with permission from J. Phys. Org. Chem. 17, 2004, 890–897, figure 5, [143]. Copyright 2004. Wiley InterScience

the third case, it depends only in a narrow range of $\alpha \in (80–90°)$. For $\alpha = 90°$, i.e., for the face-to-face arrangement, two pairs of states become degenerate. The experimental spectrum contains only two bands, one shifted to the red and the other to the blue part of the spectrum, i.e., two degenerate bands which are compatible only with C_{2v} or C_{2h} symmetry. Evaluation of the energy split yields a fairly low angle $\alpha = 15°$, which means that the experimentally observed aggregates can be classified as "J" aggregates.

To complete the part on porphyrins, possible structures and energies of "J" and "H" associates are schematically summarized in Fig. 16.

The spectra of both "J" and "H" dimers and aggregates and the principles of their formation are now fairly well understood. Spectral decomposition enables estimation of the concentrations of the individual forms of the fluorophore in the studied system under the given conditions. However, the spectral shifts depend on the number of aggregated molecules and various spectral characteristics are often affected by slow kinetics of aggregation, which hinders the analysis.

Acknowledgment This work was supported by the Czech Science Foundation (Grants P106-13-02938S and P106-12-0143). The authors would like to thank to Lucie Suchá and Karel Šindelka for help with graphics.

Appendix: Simple Quantum Mechanics Explanation of Nondegenerate Transitions Between Energy Levels in "J" and "H" Dimers

The ground-state wave function of a dimer composed of molecules A and B, $\Psi_G = \Phi = \psi_A \psi_B$, is a totally symmetrical product with respect to all the symmetry operations of the dimer AB. The first excited state can be described by two equivalent wave functions, $\Phi_1 = \psi_A \psi_B^* \cdot \text{and} \cdot \Phi_2 = \psi_A^* \psi_B$. Their energies are degenerate. The delocalized stationary states corresponding to the "exciton," i.e., to the state in which the excited electron is not localized in any of them, are described by a symmetrical and antisymmetrical combination of the two above functions:

$$\Psi_+ = \left(1/\sqrt{2}\right)\ \left(\Phi_1 + \Phi_2\right) = \left(1/\sqrt{2}\right)\ \left(\psi_A \psi_B^* + \psi_A^* \psi_B\right) \tag{43}$$

$$\Psi_- = \left(1/\sqrt{2}\right)\ \left(\Phi_1 - \Phi_2\right) = \left(1/\sqrt{2}\right)\ \left(\psi_A \psi_B^* - \psi_A^* \psi_B\right) \tag{44}$$

The node of the wave function does not correspond to a change in the sign of the wave function, but to a change in the orientation of the dipole moment. The energies of states Ψ_+ and Ψ_- are $E \pm = \Delta E \pm E'$, where ΔE is the energy difference between the excited and ground states of the monomer and E' is the perturbation (energy splitting) due to interaction of the excited and ground-state dipoles. The value $+E'$ corresponds to Ψ_+ and similarly for –E′. This value can be calculated using the perturbation Hamiltonian and the wave functions of the unperturbed degenerate states Φ_1 and Φ_2. The perturbation Hamiltonian can be expressed as the classic expression for the energy of interacting dipoles. If we take into account only the changes in the dipoles in one dimension (which is the case for most fluorophore dimers), we can write

$$H_{\text{pert}} = \frac{e^2}{4\pi\varepsilon_0 r^3} \sum_{ij} x_A^i x_B^j \tag{45}$$

where e is the elementary charge, ε_0 is the dielectric permittivity of vacuum, and x^i describes the positions of the electrons in molecule A (x^j in molecule B).

After insertion in (45), we get

$$E' = \iint \Phi_1 \hat{H}_{\text{pert}} \Phi_2 d\tau_A d\tau_B = \frac{e^2}{4\pi\varepsilon_0 r_{AB}^3} \iint \psi_A \psi_B^* \sum_{ij} x_A^i x_B^j \psi_A^* \psi_B d\tau_A d\tau_B \tag{46}$$

Because x^i describes the positions in A only and x^j in B only, expression (44) can be rewritten

$$E' = \frac{1}{4\pi\varepsilon_0 r_{AB}^3}\left[\int \psi_A \sum ex_A^i \psi_A^* d\tau_A\right]\left[\int \psi_B \sum ex_B^j \psi_B^* d\tau_B\right] = \frac{1}{4\pi\varepsilon_0 r_{AB}^3}\vec{\mu}_A \ \vec{\mu}_B \tag{47}$$

where $\vec{\mu}_A$ and $\vec{\mu}_B$ are the transition moments of the individual molecules. The transition moments of the dimer are

$$\vec{\mu}_+ = \iint \Psi_G(\vec{\mu}_A + \vec{\mu}_B)\Psi_+ d\tau_A d\tau_B \tag{48}$$

$$\vec{\mu}_- = \iint \Psi_G(\vec{\mu}_A + \vec{\mu}_B)\Psi_- d\tau_A d\tau_B \tag{49}$$

After the insertion of the expressions for the wave functions and application of the orthogonality properties of the wave functions of different states of the same molecule, we get

$$\vec{\mu}_+ = \left(\tfrac{1}{\sqrt{2}}\right)(\vec{\mu}_A + \vec{\mu}_B) \tag{50}$$

$$\vec{\mu}_- = \left(\tfrac{1}{\sqrt{2}}\right)(\vec{\mu}_A - \vec{\mu}_B) \tag{51}$$

The above-outlined simple theoretical description provides a clue to deciding which transition is allowed and which is forbidden. For a coplanar arrangement of two aromatic rings with both dipole moments oriented in the same direction, energy contribution E' is positive, Eq. (47). State Ψ_+ has higher energy than Ψ_- and also than the excited state of the monomer. The transition moment for transition $\Psi_G \rightarrow \Psi_+$ is $\vec{\mu}_+ = \left(\tfrac{1}{\sqrt{2}}\right)(2\vec{\mu}_A) \neq 0$ and this transition is allowed. Transition $\Psi_G \rightarrow \Psi_-$ is forbidden because $\vec{\mu}_- = 0$. If the dipole moments are antiparallel, E' is negative. This means that Ψ_+ has lower energy and that transition $\Psi_G \rightarrow \Psi_+$ is forbidden because the two contributions to the final dipole moment cancel each other. It follows that the absorption spectra are identical in the two cases. Using analogous qualitative analysis for the orientation of aromatic rings in one plane, we can find that, for the "head-to-tail" as well as the "head-to-head" orientation of the dipole moments, the allowed transition will be the excitation to the lower excited state. The energy of the lower state will be the same in both cases and the dimers will be strongly fluorescent species.

References

1. Jablonski A (1935) Über den Mechanismus der Photolumineszenz von Farbstoffphosphoren. Zeitschrift für Physik 94:9
2. Prochazka K, Limpouchova Z, Uhlik F, Kosovan P, Matejicek P, Stepanek M, Uchman M, Kuldova J, Sachl R, Humpolickova J, Hof M, Muller A, Borisov O (2011) Fluorescence spectroscopy as a tool for investigating the self-organized polyelectrolyte systems. Self Organ Nanostruct Amphiphilic Block Copolym I 241:187–249. doi:10.1007/12_2010_56
3. Turro NJ, Ramamurthy V, Scaiano JC (2009) Principles of molecular photochemistry: an introduction. University Science, Sausalito
4. Guillet J (1987) Polymer photophysics and photochemistry: an introduction to the study of photoprocesses in macromolecules. CUP, Cambridge
5. Fleming G (1986) Chemical applications of ultrafast spectroscopy. Oxford University Press, Oxford
6. Franck J, Dymond EG (1926) Elementary processes of photochemical reactions. Trans Faraday Soc 21:536–542. doi:10.1039/TF9262100536
7. Condon E (1926) A theory of intensity distribution in band systems. Phys Rev 28 (6):1182–1201
8. Lakowicz JR, Masters BR (2008) Principles of fluorescence spectroscopy. J Biomed Opt 13 (2):9901
9. Beer M, Longuethiggins HC (1955) Anomalous light emission of azulene. J Chem Phys 23 (8):1390–1391. doi:10.1063/1.1742314
10. Winnik MA (1986) Photophysical and photochemical tools in polymer science. Springer, New York
11. Doi M, See H (1996) Introduction to polymer physics. Clarendon Press Oxford
12. Michl J, Bonačić-Koutecký V (1990) Electronic aspects of organic photochemistry. Wiley, New York
13. Kasha M (1952) Collisional perturbation of spin-orbital coupling and the mechanism of fluorescence quenching—a visual demonstration of the perturbation. J Chem Phys 20 (1):71–74. doi:10.1063/1.1700199
14. Stern O, Volmer M (1919) The extinction period of fluorescence. Phys Z 20:183–188
15. Lakowicz, J. (1983) Principles of Fluoresence Spectroscopy, Plenum Press, New York, NY
16. Forster T (1949) Experimentelle und theoretische untersuchung des zwischenmolekularen ubergangs von elektronenanregungsenergie. Z Naturforsch Sect A A J Phys Sci 4(5):321–327
17. Forster T (1959) 10th spiers memorial lecture—transfer mechanisms of electronic excitation. Discuss Faraday Soc 27:7–17
18. Van Der Meer W, Coker G, Chen S-YS (1994) Resonance energy transfer: theory and data. VCH, New York
19. Haan SW, Zwanzig R (1978) Forster migration of electronic excitation between randomly distributed molecules. J Chem Phys 68(4):1879–1883. doi:10.1063/1.435913
20. Ediger MD, Domingue RP, Fayer MD (1984) Picosecond studies of excitation transport in a finite volume—the clustered transport-system octadecyl rhodamine-b in triton x-100 micelles. J Chem Phys 80(3):1246–1253. doi:10.1063/1.446802
21. Ediger MD, Fayer MD (1984) Electronic excitation transport in disordered finite volume systems. J Phys Chem 88(25):6108–6116. doi:10.1021/j150669a012
22. Ediger MD, Fayer MD (1983) Electronic excited-state transport among molecules distributed randomly in a finite volume. J Chem Phys 78(5):2518–2524. doi:10.1063/1.445003
23. Farinha JPS, Spiro JG, Winnik MA (2004) Dipole–dipole electronic energy transfer: fluorescence decay functions for arbitrary distributions of donors and acceptors in systems with cylindrical symmetry. J Phys Chem B 108(42):16392–16400. doi:10.1021/jp048807
24. Yekta A, Winnik MA, Farinha JPS, Martinho JMG (1997) Dipole–dipole electronic energy transfer. Fluorescence decay functions for arbitrary distributions of donors and acceptors.

2. Systems with spherical symmetry. J Phys Chem A 101(10):1787–1792. doi:10.1021/jp9633963
25. Tcherkasskaya O, Spiro JG, Ni SR, Winnik MA (1996) Energy transfer in restricted geometry: polyisoprene-poly(methyl methacrylate) block copolymer interfaces. J Phys Chem 100 (17):7114–7121. doi:10.1021/jp9522021
26. Morawetz H (1999) On the versatility of fluorescence techniques in polymer research. J Polym Sci Part A Polym Chem 37(12):1725–1735. doi:10.1002/(sici)1099-0518(19990615)37:12<1725::aid-pola1>3.0.co;2-d
27. Chen CT, Morawetz H (1989) Characterization of polymer miscibility by fluorescence techniques—blends of styrene copolymers carrying hydrogen-bond donors with polymethacrylates. Macromolecules 22(1):159–164. doi:10.1021/ma00191a031
28. Matejicek P, Uhlik F, Limpouchova Z, Prochazka K, Tuzar Z, Webber S (2002) Experimental study of hydrophobically modified amphiphilic block copolymer micelles using light scattering and nonradiative excitation energy transfer. Macromolecules 35(25):9487–9496. doi:10.1021/ma012074g
29. Uhlik F, Limpouchova Z, Jelinek K, Prochazka K (2003) A Monte Carlo study of shells of hydrophobically modified amphiphilic copolymer micelles in polar solvents. J Chem Phys 118(24):11258–11264. doi:10.1063/1.1575732
30. Matejicek P, Podhajecka K, Humpolickova J, Uhlik F, Jelinek K, Limpouchova Z, Prochazka K, Spirkova M (2004) Polyelectrolyte behavior of polystyrene-block-poly (methacrylic acid) micelles in aqueous solutions at low ionic strength. Macromolecules 37 (26):10141–10154. doi:10.1021/ma049258q
31. Soleimani M, Haley JC, Majonis D, Guerin G, Lau W, Winnik MA (2011) Smart polymer nanoparticles designed for environmentally compliant coatings. J Am Chem Soc 133 (29):11299–11307. doi:10.1021/ja203080p
32. Uhlik F, Limpouchova Z, Matejicek P, Prochazka K, Tuzar Z, Webber SE (2002) Nonradiative excitation energy transfer in hydrophobically modified amphiphilic block copolymer micelles: theoretical model and Monte Carlo simulations. Macromolecules 35 (25):9497–9505. doi:10.1021/ma012073o
33. Limpouchova Z, Prochazka K (1994) A Monte-Carlo study of insoluble block orientations in swollen cores of multimolecular block-copolymer micelles. Collect Czech Chem Commun 59(4):803–819. doi:10.1135/cccc19940803
34. Viduna D, Limpouchova Z, Prochazka K (1997) Conformations of self-avoiding tethered chains and nonradiative energy transfer and migration in dense and constrained systems. A model for cores of polymeric micelles. Macromolecules 30(23):7263–7272. doi:10.1021/ma970002c
35. Chakrabarty D, Chakraborty A, Seth D, Sarkar N (2005) Effect of water, methanol, and acetonitrile on solvent relaxation and rotational relaxation of coumarin 153 in neat 1-hexyl-3-methylimidazolium hexafluorophosphate. J Phys Chem A 109(9):1764–1769. doi:10.1021/jp0460339
36. Brown R, Middelhoek R, Glasbeek M (1999) Solvation dynamics of fluoroprobe in diethylether. J Chem Phys 111(8):3616–3622. doi:10.1063/1.479641
37. Middelhoek ER, Vandermeulen P, Verhoeven JW, Glasbeek M (1995) Picosecond time-dependent stokes shift studies of fluoroprobe in liquid solution. Chem Phys 198(3):373–380. doi:10.1016/0301-0104(95)00219-e
38. Rosenthal SJ, Jimenez R, Fleming GR, Kumar PV, Maroncelli M (1994) Solvation dynamics in methanol—experimental and molecular-dynamics simulation studies. J Mol Liq 60 (1–3):25–56. doi:10.1016/0167-7322(94)00738-1
39. Jimenez R, Fleming GR, Kumar PV, Maroncelli M (1994) Femtosecond solvation dynamics of water. Nature 369(6480):471–473. doi:10.1038/369471a0
40. Cichos F, Willert A, Rempel U, vonBorczyskowski C (1997) Solvation dynamics in mixtures of polar and nonpolar solvents. J Phys Chem A 101(44):8179–8185. doi:10.1021/jp9716694

41. Molotsky T, Huppert D (2003) Solvation statics and dynamics of coumarin 153 in dioxane-water solvent mixtures. J Phys Chem A 107(41):8449–8457. doi:10.1021/jp034760i
42. Das SK, Sahu PK, Sarkar M (2013) Probing the microscopic aspects of 1-butyl-3-methylimidazolium trifluoroacetate ionic liquid and its mixture with water and methanol: a photophysical and theoretical (DFT) study. J Fluoresc 23(6):1217–1227. doi:10.1007/s10895-013-1252-4
43. Das SK, Sarkar M (2012) Steady-state and time-resolved fluorescence behavior of coumarin-153 in a hydrophobic ionic liquid and ionic liquid-toluene mixture. J Mol Liq 165:38–43. doi:10.1016/j.molliq.2011.10.004
44. Lippert E (1957) Spektroskopische Bestimmung des Dipolmomentes aromatischer Verbindungen im ersten angeregten Singulettzustand. Z Elektrochem 61(8):962–975. doi:10.1002/bbpc.19570610819
45. Fee RS, Maroncelli M (1994) Estimating the time-zero spectrum in time-resolved emission measurements of solvation dynamics. Chem Phys 183(2–3):235–247. doi:10.1016/0301-0104(94)00019-0
46. Mukherjee S, Sahu K, Roy D, Mondal SK, Bhattacharyya K (2004) Solvation dynamics of 4-aminophthalimide in dioxane-water mixture. Chem Phys Lett 384(1–3):128–133. doi:10.1016/j.cplett.2003.11.098
47. Chee CK, Hunt BJ, Rimmer S, Soutar I, Swanson L (2011) Time-resolved fluorescence anisotropy studies of the cononsolvency of poly(N-isopropyl acrylamide) in mixtures of methanol and water. Soft Matter 7(3):1176–1184. doi:10.1039/c0sm00836b
48. Badea MG, Detoma RP, Brand L (1978) Nanosecond relaxation processes in liposomes. Biophys J 24(1):197–212
49. Chattopadhyay A, Mukherjee S (1993) Fluorophore environments in membrane-bound probes—a red edge excitation shift study. Biochemistry 32(14):3804–3811. doi:10.1021/bi00065a037
50. Hutterer R, Schneider FW, Lanig H, Hof M (1997) Solvent relaxation behaviour of n-anthroyloxy fatty acids in PC-vesicles and paraffin oil: a time-resolved emission spectra study. Biochim Biophys Acta Biomembr 1323(2):195–207. doi:10.1016/s0005-2736(96)00186-1
51. Gafni A, Detoma RP, Manrow RE, Brand L (1977) Nanosecond decay studies of a fluorescence probe bound to apomyoglobin. Biophys J 17(2):155–168
52. Toptygin D, Gronenborn AM, Brand L (2006) Nanosecond relaxation dynamics of protein GB1 identified by the time-dependent red shift in the fluorescence of tryptophan and 5-fluorotryptophan. J Phys Chem B 110(51):26292–26302. doi:10.1021/jp064528n
53. Brauns EB, Madaras ML, Coleman RS, Murphy CJ, Berg MA (1999) Measurement of local DNA reorganization on the picosecond and nanosecond time scales. J Am Chem Soc 121(50):11644–11649. doi:10.1021/ja992456q
54. Bagchi B, Jana B (2010) Solvation dynamics in dipolar liquids. Chem Soc Rev 39(6):1936–1954. doi:10.1039/b902048a
55. Sachl R, Stepanek M, Prochazka K, Humpolickova J, Hof M (2008) Fluorescence study of the solvation of fluorescent probes prodan and laurdan in poly(epsilon-caprolactone)-block-poly(ethylene oxide) vesicles in aqueous solutions with tetrahydrofurane. Langmuir 24(1):288–295. doi:10.1021/la702277t
56. Humpolickova J, Stepanek M, Prochazka K, Hof M (2005) Solvent relaxation study of pH-dependent hydration of poly(oxyethylene) shells in polystyrene-block-poly(2-vinylpyridine)-block-poly(oxyethylene) micelles in aqueous solutions. J Phys Chem A 109(48):10803–10812. doi:10.1021/jp053348v
57. Matejicek P, Humpolickova J, Prochazka K, Tuzar Z, Spirkova M, Hof M, Webber SE (2003) Hybrid block copolymer micelles with partly hydrophobically modified polyelectrolyte shells in polar and aqueous media: experimental study using fluorescence correlation spectroscopy, time-resolved fluorescence, light scattering, and atomic force microscopy. J Phys Chem B 107(32):8232–8240. doi:10.1021/jp022221s

58. Forster S, Wenz E, Lindner P (1996) Density profile of spherical polymer brushes. Phys Rev Lett 77(1):95–98. doi:10.1103/PhysRevLett.77.95
59. Forster S, Zisenis M, Wenz E, Antonietti M (1996) Micellization of strongly segregated block copolymers. J Chem Phys 104(24):9956–9970
60. Jurkiewicz P, Sykora J, Olzynska A, Humpolickova J, Hof M (2005) Solvent relaxation in phospholipid bilayers: principles and recent applications. J Fluoresc 15(6):883–894. doi:10.1007/s10895-005-0013-4
61. Michl J, Thulstrup EW (1986) Spectroscopy with polarized light: solute alignment by photoselection, in liquid crystals, polymers, and membranes. VCH-Wiley, Deerfield Beach
62. Debye PJW (1945) Polar molecules. Dover, New York
63. Cross AJ, Fleming GR (1984) Analysis of time-resolved fluorescence anisotropy decays. Biophys J 46(1):45–56
64. Favro LD (1960) Theory of the rotational Brownian motion of a free rigid body. Phys Rev 119(1):53–62. doi:10.1103/PhysRev.119.53
65. Tao T (1969) Time-dependent fluorescence depolarization and Brownian rotational diffusion coefficients of macromolecules. Biopolymers 8(5):609–632. doi:10.1002/bip.1969.360080505
66. Ehrenber M, Rigler R (1972) Polarized fluorescence and rotational Brownian motion. Chem Phys Lett 14(5):539–544. doi:10.1016/0009-2614(72)87202-6
67. Kawski A (1993) Fluorescence anisotropy—theory and applications of rotational depolarization. Crit Rev Anal Chem 23(6):459–529. doi:10.1080/10408349308051654
68. Boens N, Novikov E, Ameloot M (2006) Compartmental modeling of the fluorescence anisotropy decay of a cylindrically symmetric Brownian rotor: identifiability analysis. Chemphyschem 7(12):2559–2566. doi:10.1002/cphc.200600309
69. Chuang TJ, Eisenthal KB (1972) Theory of fluorescence depolarization by anisotropic rotational diffusion. J Chem Phys 57(12):5094–5097. doi:10.1063/1.1678194
70. Teraoka I (2002) Polymer solutions: an introduction to physical properties. Wiley, New York
71. Rose ME (1995) Elementary theory of angular momentum. Courier Dover, New York
72. Belford GG, Belford RL, Weber G (1972) Dynamics of fluorescence polarization in macromolecules. Proc Natl Acad Sci USA 69(6):1392–1393. doi:10.1073/pnas.69.6.1392
73. Limpouchova Z, Prochazka K, Fidler V, Dvorak J, Bednar B (1993) Molecular-movements and dynamics in solutions studied by fluorescence depolarization measurement. Collect Czech Chem Commun 58(2):213–233. doi:10.1135/cccc19930213
74. Polimeno A, Saielli G, Nordio PL (1998) A diffusive model for interpreting solvation dynamics in isotropic and ordered liquid phases. Chem Phys 235(1–3):313–331. doi:10.1016/s0301-0104(98)00076-7
75. Barkley MD, Kowalczyk AA, Brand L (1981) Fluorescence decay studies of anisotropic rotations of small molecules. J Chem Phys 75(7):3581–3593. doi:10.1063/1.442468
76. Christensen RL, Drake RC, Phillips D (1986) Time-resolved fluorescence anisotropy of perylene. J Phys Chem 90(22):5960–5967. doi:10.1021/j100280a100
77. Gordon RG (1966) On rotational diffusion of molecules. J Chem Phys 44(5):1830–1836. doi:10.1063/1.1726949
78. McClung RED (1969) Rotational diffusion of spherical-top molecules in liquids. J Chem Phys 51(9):3842–3852. doi:10.1063/1.1672600
79. McClung RED (1972) Rotational diffusion of symmetric top molecules in liquids. J Chem Phys 57(12):5478–5491. doi:10.1063/1.1678249
80. St. Pierre AG, Steele WA (1972) Collisional effects upon rotational correlations of symmetric top molecules. J Chem Phys 57(11):4638–4648
81. Leicknam JC, Guissani Y (1981) On extended diffusion-models for asymmetric-top molecules in liquids. Mol Phys 42(5):1105–1120. doi:10.1080/00268978100100841
82. Fixman M, Rider K (1969) Angular relaxation of symmetrical top. J Chem Phys 51 (6):2425–2438. doi:10.1063/1.1672362

83. McClung RED (1980) The Fokker-Planck-Langevin model for rotational Brownian-motion. 1. General-theory. J Chem Phys 73(5):2435–2442. doi:10.1063/1.440394
84. McClung RED (1981) The Fokker-Planck-Langevin model for rotational Brownian-motion. 3. Symmetric top molecules. J Chem Phys 75(11):5503–5513. doi:10.1063/1.441954
85. Levi G, Marsault JP, Marsaultherail F, McClung RED (1980) The Fokker-Planck-Langevin model for rotational Brownian-motion. 2. Comparison with the extended rotational diffusion-model and with observed infrared and Raman band shapes of linear and spherical molecules in fluids. J Chem Phys 73(5):2443–2453
86. Lascombe J, Besnard M, Maraval P (1982) A new extended diffusion-model for rotational motion of symmetric-top molecules in the liquid-phase. Chem Phys 72(1–2):177–184. doi:10.1016/0301-0104(82)87078-x
87. Ghiggino K, Tan K, Phillips D (1985) Polymer photophysics. Chapman and Hall, London
88. Yip J, Duhamel J, Qiu XP, Winnik FM (2011) Long-range polymer chain dynamics of pyrene-labeled poly(N-isopropylacrylamide)s studied by fluorescence. Macromolecules 44 (13):5363–5372. doi:10.1021/ma2007865
89. Monnerie L (1991) Segmental dynamics of polymer melts. J Non Cryst Solids 131:755–765. doi:10.1016/0022-3093(91)90678-y
90. Uhlik F, Kosovan P, Limpouchova Z, Prochazka K, Borisov OV, Leermakers FAM (2014) Modeling of ionization and conformations of starlike weak polyelectrolytes. Macromolecules 47(12):4004–4016. doi:10.1021/ma500377y
91. Kosovan P, Limpouchova Z, Prochazka K (2006) Molecular dynamics simulation of time-resolved fluorescence anisotropy decays from labeled polyelectrolyte chains. Macromolecules 39(9):3458–3465. doi:10.1021/ma052557a
92. Kiserow D, Prochazka K, Ramireddy C, Tuzar Z, Munk P, Webber SE (1992) Fluorometric and quasi-elastic light-scattering study of the solubilization of nonpolar low-molar mass compounds into water-soluble block-copolymer micelles. Macromolecules 25(1):461–469. doi:10.1021/ma00027a072
93. Nagl S, Schaeferling M, Wolfbeis OS (2005) Fluorescence analysis in microarray technology. Microchim Acta 151(1–2):1–21. doi:10.1007/s00604-005-0393-9
94. Duhamel J (2014) Global analysis of fluorescence decays to probe the internal dynamics of fluorescently labeled macromolecules. Langmuir 30(9):2307–2324. doi:10.1021/la403714u
95. Duhamel J (2012) New insights in the study of pyrene excimer fluorescence to characterize macromolecules and their supramolecular assemblies in solution. Langmuir 28 (16):6527–6538. doi:10.1021/la2047646
96. Ercole F, Davis TP, Evans RA (2010) Photo-responsive systems and biomaterials: photochromic polymers, light-triggered self-assembly, surface modification, fluorescence modulation and beyond. Polym Chem 1(1):37–54. doi:10.1039/b9py00300b
97. Valeur B, Rempp P, Monnerie L (1974) Insertion of anthracene fluorophore in polystyrene chain—study of local movements via inhibition and fluorescence polarization. C R Hebd Seances Acad Sci Ser C 279(25):1009–1012
98. Valeur B, Monnerie L (1976) Dynamics of macromolecular chains. 3. Time-dependent fluorescence polarization studies of local motions of polystyrene in solution. J Polym Sci Part B Polym Phys 14(1):11–27. doi:10.1002/pol.1976.180140102
99. Viovy JL, Frank CW, Monnerie L (1985) Fluorescence anisotropy decay studies of local polymer dynamics in the melt. 2. Labeled model compounds of variable chain-length. Macromolecules 18(12):2606–2613. doi:10.1021/ma00154a042
100. Valeur B, Jarry JP, Geny F (1975) Dynamics of macromolecular chains. 1. Theory of motions on a tetrahedral lattice. J Polym Sci Part B Polym Phys 13(4):667–674. doi:10.1002/pol.1975.180130401
101. Valeur B, Monnerie L, Jarry JP (1975) Dynamics of macromolecular chains. 2. Orientation relaxation generated by elementary 3-bond motions and notion of an independent kinetic segment. J Polym Sci Part B Polym Phys 13(4):675–682. doi:10.1002/pol.1975.180130402

102. Ediger MD (1991) Time-resolved optical studies of local polymer dynamics. Annu Rev Phys Chem 42:225–250. doi:10.1146/annurev.physchem.42.1.225
103. Waldow DA, Ediger MD, Yamaguchi Y, Matsushita Y, Noda I (1991) Viscosity dependence of the local segmental dynamics of anthracene-labeled polystyrene in dilute-solution. Macromolecules 24(11):3147–3153. doi:10.1021/ma00011a018
104. Adolf DB, Ediger MD, Kitano T, Ito K (1992) Viscosity dependence of the local segmental dynamics of anthracene-labeled polyisoprene in dilute-solution. Macromolecules 25 (2):867–872. doi:10.1021/ma00028a055
105. Hall CK, Helfand E (1982) Conformational state relaxation in polymers—time-correlation functions. J Chem Phys 77(6):3275–3282. doi:10.1063/1.444204
106. Viovy JL, Monnerie L, Brochon JC (1983) Fluorescence polarization decay study of polymer dynamics—a critical discussion of models using synchrotron data. Macromolecules 16 (12):1845–1852. doi:10.1021/ma00246a009
107. Gottlieb YY, Wahl P (1963) Etude theorique de la polarisation de fluorescence des macromolecules portant un groupe emetteur mobile autour dun axe de rotation. J Chim Phys Phys Chim Biol 60(7–8):849–856
108. Burghardt TP (1983) Fluorescence depolarization by anisotropic rotational diffusion of a luminophore and its carrier molecule. J Chem Phys 78(10):5913–5919. doi:10.1063/1.444596
109. Tanaka F, Mataga N (1987) Fluorescence quenching dynamics of tryptophan in proteins—effect of internal-rotation under potential barrier. Biophys J 51(3):487–495
110. Takano T, Dickerson RE (1981) Conformation change of cytochrome-C. 1. - Ferrocytochrome-C structure refined at 1.5 A resolution. J Mol Biol 153(1):79–94. doi:10.1016/0022-2836(81)90528-3
111. Weber G (1989) Perrin revisited—parametric theory of the motional depolarization of fluorescence. J Phys Chem 93(16):6069–6073. doi:10.1021/j100353a026
112. Szabo A (1984) Theory of fluorescence depolarization in macromolecules and membranes. J Chem Phys 81(1):150–167. doi:10.1063/1.447378
113. Munishkina LA, Fink AL (2007) Fluorescence as a method to reveal structures and membrane-interactions of amyloidogenic proteins. Biochim Biophys Acta Biomembr 1768 (8):1862–1885. doi:10.1016/j.bbamem.2007.03.015
114. Lentz BR (1993) Use of fluorescent-probes to monitor molecular order and motions within liposome bilayers. Chem Phys Lipids 64(1–3):99–116. doi:10.1016/0009-3084(93)90060-g
115. Kinosita K, Kawato S, Ikegami A (1977) Theory of fluorescence polarization decay in membranes. Biophys J 20(3):289–305
116. Kinosita K, Ikegami A, Kawato S (1982) On the wobbling-in-cone analysis of fluorescence anisotropy decay. Biophys J 37(2):461–464
117. Lipari G, Szabo A (1980) Effect of librational motion on fluorescence depolarization and nuclear magnetic-resonance relaxation in macromolecules and membranes. Biophys J 30 (3):489–506
118. Procházka K, Limpouchová Z, Webber SE, Munk P (1994) Time-resolved fluorescence anisotropy measurements on fluorescently tagged amphiphilic micelles. J Fluoresc 4 (4):353–356. doi:10.1007/BF01881455
119. Birks JB, Munro IH, Dyson DJ (1963) Excimer fluorescence. 2. Lifetime studies of pyrene solutions. Proc R Soc Lond Ser A Math Phys Sci 275(1360):575–588. doi:10.1098/rspa.1963.0187
120. Gould IR, Young RH, Mueller LJ, Farid S (1994) Mechanisms of exciplex formation—roles of superexchange, solvent polarity, and driving-force for electron-transfer. J Am Chem Soc 116(18):8176–8187. doi:10.1021/ja00097a027
121. Beens H, Weller A (1975) Excited molecular π-complexes in solution. In: Birks JB (ed) Organic molecular photophysics, vol 2. Wiley, New York, pp 159–215

122. Gould IR, Young RH, Farid S (1991) Dynamics of photoinduced electron transfer in solution. In: Honda K (ed) Photochemical processes in organized molecular systems. Elsevier, New York
123. Stepanek M, Podhajecka K, Prochazka K, Teng Y, Webber SE (1999) Fluorometric and ultraviolet–visible absorption study of poly(methacrylic acid) shells of high-molar-mass block copolymer micelles. Langmuir 15(12):4185–4193. doi:10.1021/la981129d
124. Kasha M, Rawls HR, El-Bayoumi MA (1965) The exciton model in molecular spectroscopy. Pure Appl Chem 11(3–4):371–392
125. Kasha M (1976) Multiple excitation in composite molecules. In: Di Bartolo B, Pacheco D, Goldberg V (eds) Spectroscopy of the excited state, vol 12. NATO advanced study institutes series. Springer, Berlin, pp 368–368. doi:10.1007/978-1-4684-2793-6_16
126. McRae EG, Kasha M (1964) The molecular exciton model. In: Augenstein L, Mason R, Rosenberg B (eds) Physical processes in radiation biology. Academic, New York, pp 23–42
127. Frenkel JA (1931) On the transformation of light into heat in solids. II. Phys Rev 37(10):1276
128. Jelley EE (1936) Spectral absorption and fluorescence of dyes in the molecular state. Nature 138(3502):1009–1010
129. Ribo JM, Bofill JM, Crusats J, Rubires R (2001) Point-dipole approximation of the exciton coupling model versus type of bonding and of excitons in porphyrin supramolecular structures. Chemistry 7(13):2733–2737. doi:10.1002/1521-3765(20010702)7:13<2733::aid-chem2733>3.0.co;2-q
130. del Monte F, Mackenzie JD, Levy D (2000) Rhodamine fluorescent dimers adsorbed on the porous surface of silica gels. Langmuir 16(19):7377–7382. doi:10.1021/la000540+
131. Chaudhuri R, Arbeloa FL, Arbeloa IL (2000) Spectroscopic characterization of the adsorption of rhodamine 3B in hectorite. Langmuir 16(3):1285–1291. doi:10.1021/la990772c
132. Parr RG (1964) Quantum theory of molecular electronic structure. Benjamin, New York
133. Murrell JN (1971) The theory of the electronic spectra of organic molecules. Chapman and Hall, London
134. Chambers RW, Kajiwara T, Kearns DR (1974) Effect of dimer formation of electronic absorption and emission-spectra of ionic dyes—rhodamines and other common dyes. J Phys Chem 78(4):380–387. doi:10.1021/j100597a012
135. Fujii T, Nishikiori H, Tamura T (1995) Absorption-spectra of rhodamine-b dimers in dip-coated thin-films prepared by the sol-gel method. Chem Phys Lett 233(4):424–429. doi:10.1016/0009-2614(94)01477-d
136. Vergeldt FJ, Koehorst RBM, Vanhoek A, Schaafsma TJ (1995) Intramolecular interactions in the ground and excited-state of tetrakis(n-methylpyridyl)porphyrins. J Phys Chem 99 (13):4397–4405. doi:10.1021/j100013a007
137. Gouterman M (1961) Spectra of porphyrins. J Mol Spectrosc 6(1):138–163. doi:10.1016/0022-2852(61)90236-3
138. Gouterman M, Snyder LC, Wagniere GH (1963) Spectra of porphyrins. 2. 4 orbital model. J Mol Spectrosc 11(2):108–127. doi:10.1016/0022-2852(63)90011-0
139. Ribo JM, Rubires R, El-Hachemi Z, Farrera JA, Campos L, Pakhomov GL, Vendrell M (2000) Self-assembly to ordered films of the homoassociate solutions of the tetrasodium salt of 5,10,15,20-tetrakis(4-sulfonatophenyl) porphyrin dihydrochloride. Mater Sci Eng C Biomim Supramol Syst 11(2):107–115. doi:10.1016/s0928-4931(00)00147-8
140. Aratani N, Osuka A, Kim YH, Jeong DH, Kim D (2000) Extremely long, discrete meso–meso-coupled porphyrin arrays. Angew Chem Int Ed 39(8):1458–1462. doi:10.1002/(sici)1521-3773(20000417)39:8<1458::aid-anie1458>3.0.co;2-e
141. Kim YH, Jeong DH, Kim D, Jeoung SC, Cho HS, Kim SK, Aratani N, Osuka A (2001) Photophysical properties of long rod like meso–meso-linked zinc(II) porphyrins investigated by time-resolved laser spectroscopic methods. J Am Chem Soc 123(1):76–86. doi:10.1021/ja0009976

142. Osuka A, Maruyama K (1988) Synthesis of naphthalene-bridged porphyrin dimers and their orientation-dependent exciton coupling. J Am Chem Soc 110(13):4454–4456. doi:10.1021/ja00221a079
143. Prochazkova K, Zelinger Z, Lang K, Kubat P (2004) meso-Tetratolylporphyrins substituted by pyridinium groups: aggregation, photophysical properties and complexation with DNA. J Phys Org Chem 17(10):890–897. doi:10.1002/poc.783

Historical Perspective of Advances in Fluorescence Research on Polymer Systems

Karel Procházka

Contents

Abstract The chapter describes the most important fluorescence studies of polymer systems. It maps the progress in the study of polymer conformations, dynamics, self-assembly, and other properties of polymer systems by different fluorescence methods from the historical perspective. It offers the selection of seminal studies by pioneers of "polymer fluorescence" (as representative as possible), papers that significantly contributed to the solution of important problems, and also the up-to-date studies that follow the world trends of polymer research. Great attention is given to studies of dynamic processes. The end of the chapter addresses the opto-electroactive π-conjugated polymers. This topic exceeds the scope of the chapter and only some aspects of the fluorescence of π-conjugated polymers are reviewed. Special attention is devoted to the application of single-molecule fluorescence spectroscopy in the research of opto-electroactive polymers.

Keywords Nonradiative excitation energy transfer • Time-resolved fluorescence anisotropy • Dynamics of polymer chains • π-Conjugated polymers • Single-molecule spectroscopy

K. Procházka (✉)
Department of Physical and Macromolecular Chemistry, Faculty of Science, Charles University in Prague, Hlavova 2030, 128 40 Prague 2, Czech Republic
e-mail: karel.prochazka@natur.cuni.cz

K. Procházka (ed.), *Fluorescence Studies of Polymer Containing Systems*, Springer Series on Fluorescence 16, DOI 10.1007/978-3-319-26788-3_5

1 Introduction

This chapter describes the most important fluorescence studies of the behavior of polymer chains in solutions, gels, and melts and in the bulk amorphous state. Because the book contains several chapters devoted to specific systems and methods, we try to avoid duplicities concerning, e.g., self-assembled core-shell nanoparticles, the behavior of hydrophobically modified chains, and FCS studies of polymers in solutions, and turn our attention to other aspects. Nevertheless, it was sometimes necessary to mention some topics treated in the other chapters.

Based on an historical perspective, we begin our discussion with classical studies aimed at the compatibility and miscibility of polymer chains with different chemical natures, because fluorescent studies have contributed significantly to understanding of the behavior of polymer blends. The middle part of the chapter is concerned with dilute polymer solutions whose properties reflect the behavior of isolated chains. Then the discussion is extended to concentrated solutions and polymer melts. The next part is related to the topic of associating polymers from a different viewpoint than that adopted in the other chapters of this book. Finally, we have added some comments on fluorescence studies of photo(electro)active polymers, because this field is a "hot topic" in contemporary polymer research.

The following text outlines experimental approaches and papers investigating the behavior of "unmodified" chains. As was already explained, fluorescence studies of almost all interesting polymers require the incorporation of a fluorophore (often a fairly hydrophobic one) in the chain or its attachment as a pendant group, which represents a certain modification of the original system. Because the fluorophore interacts only with its immediate microenvironment, strictly speaking it always provides information on the modified part of the chain (it very often accentuates some hydrophobic features caused by the chemical modification). To avoid any confusion, we will explain what we mean by the term "unmodified chain." The macroscopic behavior of the system is virtually unaffected if the number of fluorophores bound to the chain is low (one or only a few *per* chain). In this case, measurements on a series of samples with decreasing fluorophore content enable us to draw quite reliable conclusions concerning the dynamic and conformational characteristics of the unmodified system. The term "hydrophobically modified polymers" describes systems containing large numbers of hydrophobic units—sometimes blocks or grafts (intentionally attached to or incorporated in the chains) that are significantly more hydrophobic than the parent chain and substantially modify the macroscopic behavior of the system. The hydrophobic units can be both fluorescent and non-fluorescent. Massively hydrophobically modified systems will not be discussed here because a chapter "Pyrene-Labeled Water-Soluble Macromolecules as Fluorescent Mimics of Associative Thickeners" is devoted to this topic.

The discussion of the results of fluorescence studies of single chains (the middle part of the chapter) also deserves a short explanatory comment. The conformational changes and segmental dynamics are interpreted at the level of typical

conformations which may give a false impression that single chains have been studied. It should be borne in mind that macroscopic ensembles of chains, e.g., their dilute solutions, are currently being investigated by fluorescence methods. Consequently, the discussed characteristics reflect the distributions of various chain conformations and mostly represent the ensemble-average values. However, in addition to common spectroscopic methods aimed at ensemble-based data, a specific spectroscopic method also exists that really investigates single molecules—namely single-molecule fluorescence spectroscopy. Its principle and application will be briefly outlined at the end of this chapter in connection with conjugated (opto)electronically active polymers.

2 Fluorescence Resonance Energy Transfer Studies of Polymer Systems

The general overview begin with studies of fluorescence resonant energy transfer (FRET), known also under alternative names, such as nonradiative energy transfer (NRET) or direct energy transfer (DET). The physical basis for this phenomenon and principles of its experimental measurement were already explained in chapter "Theoretical Principles of Fluorescence Spectroscopy." Nevertheless, we will repeat the most important facts and extend the description beyond the well-known Förster limit [1, 2]. If a system containing n_D energy donors and n_T energy acceptors (traps) is illuminated by a light beam of appropriate wavelength, a low fraction of the donor molecules become excited. The excited donors are far apart and are surrounded by non-excited donors and by ground-state acceptors (traps). The excitation can either generate the emission of a photon from the donor, or the excess energy can be transferred to a trap by resonance energy transfer. In many cases, the traps lose the excess energy via nonradiative routes and only the quenching of the donor is observed, but sometimes the traps emit red-shifted fluorescence. As the FRET efficiency depends sensitively on the distance between the excited donor and the ground-state trap, only a limited number of traps in the vicinity of the excited donor affect its emission and FRET serves as a gauge for distance measurements. In some systems of fluorophores with relatively small Stokes shifts, the absorption and emission bands of the donor overlap non-negligibly and excitation energy can also migrate among the donors. If the excitation energy migrates only among the donors (in systems without traps), the time-resolved fluorescence characteristics of non-polarized emission are not affected, but the rate of fluorescence depolarization changes in measurements with polarized light [3]. If diffusive excitation energy migration occurs in systems containing both donors and traps, the excitation energy migration among donors affects the energy transfer route to traps [2, 4]. Fluorescence decay of the donor in the presence of traps, $F_D(t)$, can be described by the following master equation:

$$-\frac{dF_{\mathrm{D}}(t)}{dt}=\frac{F_{\mathrm{D}}(t)}{\tau_0}+\frac{F_{\mathrm{D}}(t)}{\tau_0}\sum_{k=1}^{n_{\mathrm{T}}}\left(\frac{r_0^{\mathrm{DT}}}{r_k}\right)^6 \tag{1}$$

where τ_0 is the donor decay time in the absence of traps, r_0^{DT} is the Förster radius of the donor–trap pair, and r_k are the distances of the individual traps from the excited donor. The time-dependent fluorescence intensity $F_{\mathrm{D}}(t)$ is proportional to the probability density $\rho_{\mathrm{D}}(t)$ that, at time t, the excitation is still located on the originally excited donor. The integration of the differential Eq. (1) yields the fluorescence intensity $\langle F_{\mathrm{D}}(t)\rangle$ averaged over all the possible arrangements of traps around the excited donor. Provided that a physically reasonable approximation for the distribution of the donor–trap distances $P(r)$ is available, the following formula can be written for the normalized fluorescence decay $\langle F_{\mathrm{D}}(t)\rangle$:

$$\langle F_{\mathrm{D}}(t)\rangle=\exp\left(-\frac{t}{\tau_0}\right)\left[\int_0^{r_{\mathrm{C}}}\exp\left(-\frac{1}{\tau_0}\left(\frac{r_0^{\mathrm{DT}}}{r}\right)^6 t\right)P(r)dr\right]^{n_{\mathrm{T}}} \tag{2}$$

where r_{C} is the cutoff distance, for which NRET is negligible. In a system with random distribution of trap positions around the donor, $P(r)$ is proportional to r^2 and the solution for $r_{\mathrm{C}}\to\infty$ and $n_{\mathrm{T}}\to\infty$ yields the Förster result [see Eq. (10) in chapter "Theoretical Principles of Fluorescence Spectroscopy"]. In real systems and particularly in concentrated polymer solutions or melts, the distribution of donors and traps (attached to polymer chains) is not random because strong correlation effects caused by the excluded volume and long-range interactions play a non-negligible role. Note that the correlations between the fluorophore positions are mediated by mutual interactions between polymer segments. Several authors have investigated the role of inter-chain correlations. Frederickson used the statistical thermodynamic approach when studying the melt of end-labeled chains [5]. He employed the total pair correlation function $h(r)=g(r)-1$, which is related to the radial distribution function, $g(r)$. The radial distribution function $g(r)$ describes the "structure" of the system. Term $4\pi r^2 g(r)$ gives the probability density that another molecule will be found within distance r from a randomly chosen molecule. The treatment based on the assumption that the correlations are important yields the general equation

$$\langle F_{\mathrm{D}}(t)\rangle=\exp\left(-\frac{t}{\tau_0}\right)\exp\left\{-\int_0^{\infty}\rho\left(1-\frac{1}{\tau_0}\left\{\frac{r_0^{\mathrm{DT}}}{r}\right\}^6 t\right)(1+h(r))d\boldsymbol{r}\right\} \tag{3}$$

where ρ is the average density of the traps, $\boldsymbol{r}=(x,y,z)$ is the vector describing the position of traps with respect to the donor, and r is its length. Using the end-to-end correlation function proposed by de Gennes [6], Frederickson derived a relatively complicated expression which can be used (in a retrospective way) to gain information about the correlations. The authors who followed the original Frederickson approach realized that, in relatively concentrated polymer systems containing both

donors and traps, the energy migration among donors complicates and affects the final energy transfer to traps. Therefore, Torkelson et al. [4] included also the donor–donor total correlation function in their model and obtained an equation containing more terms than that derived by Frederickson, which they used for comparing experimental data from semi-dilute solutions of polyisoprene chains end labeled by phenanthrene and anthracene with the theoretically derived decay. The authors found good agreement between the experimental and theoretically predicted data based on the de Gennes model. Several theoretical models for various strongly correlated systems were subsequently developed by other authors and will be discussed later.

As already mentioned, the classical experimental NRET papers published by the pioneers of fluorescence studies in polymer science in 1970s–1990s, e.g., by Morawetz, Winnik, Fayer [7–15], and others, were concerned mainly with the aspect of polymer miscibility and preparation of functional polymer blends. The design and development of functional polymer blends is a very important topic from the technological and application points of view. However, it is difficult to fabricate suitable blends. High-molar-mass polymers (even those that do not differ much in polarity and dissolve in the same solvent) are usually incompatible and do not mix in melts and in concentrated solutions in common solvents due, in part, to unfavorable energetic interactions between chemically different nonpolar compounds (this effect is amplified in polymer systems by multiple repetition of the same structural unit in polymer chain) and to low entropy of polymer–polymer mixing. As already explained in chapter "Conformational and Dynamic Behavior of Polymer and Polyelectrolyte Chains in Dilute Solutions," the mixing of nonpolar compounds is generally unfavorable from the enthalpy point of view. Even in the case of very similar compounds like benzene and toluene, the enthalpy of mixing is positive (the process is endothermic). The high miscibility of low-molar-mass compounds is a result of the large entropy of mixing. The Flory–Huggins theory of concentrated polymer solutions (see Eq. (1) in chapter "Conformational and Dynamic Behavior of Polymer and Polyelectrolyte Chains in Dilute Solutions") predicts that the entropy of mixing a polymer with a solvent is very low compared to that for small molecules, and if two amorphous polymers are mixed above their glass transition temperatures, the increase in entropy is even smaller. As was already outlined in chapter "Conformational and Dynamic Behavior of Polymer and Polyelectrolyte Chains in Dilute Solutions," the main difference between the mixing of small molecules and long polymer chains is easily understandable: Imagine a solution of n_M small monomers dissolved in a low-molar-mass solvent. In this solution, every monomer can move independently in the whole volume, which increases the disorder of the system enormously. In the language of statistical thermodynamics, small molecules have high translational entropy and therefore the total entropy of the intermixed system is high. If we perform a hypothetical polymerization, we connect large numbers (N) of monomers in linear chains. The solution will contain n_P polymer chains, each composed of an average of N monomers, i.e., $n_M = N \cdot n_P$. In the polymer solution, all the N monomers interconnected in one chain move together, which results in a substantial loss of

the translational entropy. The chains are usually flexible and can adopt a number of different conformations, which slightly increases the entropy of the mixture, but does not compensate for the large decrease due to chain connectivity. This general feature of polymer systems is very inconvenient from the practical point of view because it hinders the fabrication of polymer blends and composite materials. Because the design, development, and study of polymer blends is a very important topic and many papers focused on this field constitute seminal fluorescence studies in macromolecular science, we will provide a brief overview of the most important papers and achievements despite the fact that they do not fall conceptually in the main stream of interest of this book.

Efforts to blend chemically different polymers often result in a spatially inhomogeneous distribution of fluorophores in the polymer matrix. In a number of cases, this leads to nano-heterogeneous materials containing small domains separated by sharp interfaces. In these cases, the dispersed or end-attached donors and acceptors (which differ in polarity with respect to the polymer chains) may concentrate (1) both in the same domain, (2) each of them in the different domains, or (3) in the interfacial region. In all cases, severe geometrical restrictions and significant edge effects influence the fluorescence behavior of the embedded probes and affect FRET. Energy transfer and migration in restricted geometries have been studied by a number of research groups, namely by Blumen and Klafter [16–19], Winnik et al. [15, 20–24], and Fayer et al. [9–14] both experimentally and theoretically and various models have been proposed for NRET in restricted geometries. The basic difficulty with the interpretation of FRET data from small volume elements follows from the fact that, while FRET in infinite systems depends only on the spatial distribution of acceptors, in confined geometries it also depends on the spatial distribution of donors—see Fig. 4 in chapter "Theoretical Principles of Fluorescence Spectroscopy" which compares the numbers of randomly distributed traps located a distance $\langle r, r + dr \rangle$ around two different donors located either in the center of a small spherical volume or close to the wall. It shows that the former donor is affected by a larger number of traps than the latter located close to the wall. Hence, the main goal is to derive an appropriate distribution function of donor–trap distances which takes into account both the geometrical confinements and physical interactions and ensures correct ensemble averaging.

In the early 1980s, Klafter and Blumen [19, 25, 26] derived a relatively simple expression for the donor fluorescence decay in an infinite system of fluorophores embedded in the fractal lattice:

$$F_{\mathrm{D}}(t) = F_{\mathrm{D}}^{0} \exp\left[-\left(\frac{t}{\tau_{\mathrm{D}}}\right) - P\left(\frac{t}{\tau_{\mathrm{D}}}\right)^{\beta} \right] \tag{4}$$

where F_{D}^{0} represents the fluorescence intensity at zero time, τ_{D} is the unquenched donor lifetime, and P is a parameter proportional to the probability that the trap resides within a sphere of the Förster donor-to-trap radius r_0^{DT}, which depends on the bulk concentration of the traps. Exponent β is a concentration-independent

parameter equal to $d/6$, where d is the fractal dimension. In confined geometries, d loses its original physical meaning and is referred to as the "apparent dimension." The value of $d < 3$, i.e., $\beta < 0.5$, is a signature of the influence of restricted geometry on FRET. Computer simulations confirm that, in small spheres of the radius approaching r_0^{DT} (with uniform distribution of both probes), the magnitude of β decreases because the edge effects become more and more important. Winnik et al. experimentally studied the FRET from sharp polymer interfaces in polyisoprene–poly(methacrylate) block copolymer films and used the modified Eq. (4) with one additional term accounting for ca. 3 % of probes distributed outside interfaces; they found fairly good agreement between the experimental and theoretically predicted donor decays [15].

Aspects of energy migration among identical fluorophores and their impact on fluorescence anisotropy decay were amply studied by Fayer and his coworkers in the 1980s–1990s. Following the original works by Haan and Zwanzig [3], they developed a unified model for the excitation energy migration based on the generalized ensemble-average probability $G^S(t)$ that the excitation is localized at time t at the originally excited fluorophore [10, 11, 14, 27]. Their mathematical treatment proved to be suitable for the description of FRET in a number of systems, e.g., in anisotropic, constrained, and heterogeneous systems (nanostructured blends), among clusters of fluorophores (in hydrophobically modified polymers—see chapter "Pyrene-Labeled Water-Soluble Macromolecules as Fluorescent Mimics of Associative Thickeners"), etc. Later they used the derived formulas to interpret their own experimental data [12]. They studied, e.g., the dynamic process of phase separation in binary blends composed of poly(vinyl acetate), PVA, and a minority component: statistical copolymer poly(methyl methacrylate-*co*-2-vinylnaphthalene), PMMA2VN, which served also as a marker of the behavior, and ternary blends containing a small amount of PMMA2VN and larger amount of PMMA immersed in excess PVA. First, the polymers were dissolved and molecularly mixed in benzene, freeze-dried, and pressed into pellets at room temperature. Then the pellets were heated above the glass transition temperature for a specific annealing time, fast cooled, and studied by FRET. Fast cooling preserved the structures formed spontaneously at high temperatures. Series of measurements for different annealing times allowed estimation of the onset of phase separation and yielded interesting information on the expansion of the marker chains.

One of very important practical aspects that require analysis of the data based on FRET in restricted volumes is interpolymer diffusion. In experimental measurements, two thin films of the chemically identical polymer (or two compatible polymers), one labeled by the donor and second by the acceptor, are pressed together and heated above the glass transition temperature and the one-dimensional diffusion along the z axes (let's assume the horizontal axis) is monitored by FTER measurement as a function of the annealing time, t_{an}. A number of these measurements have been performed, but many of them have not been analyzed properly and it was shown by Winnik [15, 28–30] that improper analysis may yield very erroneous values of the diffusion coefficients. Correct analysis is

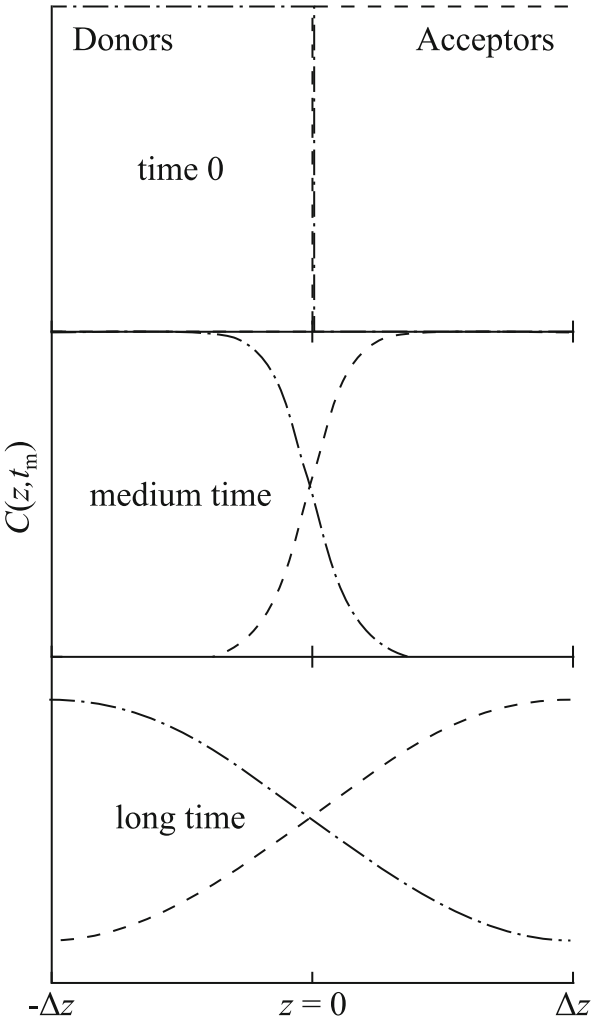

Fig. 1 Concentration profiles of donor- and acceptor-labeled polymer chains at different annealing times. Adapted with permission from Macromolecules 28, 1995, 6084–6088, figure 1, [15]. Copyright 1995. American Chemical Society

difficult because the distributions of the donors and acceptors are inhomogeneous and change with time. Hence, the donors located in different positions with respect to the axis of the 1D diffusion are surrounded and affected by different numbers of non-randomly distributed acceptors. The concentration profiles of both probes are schematically depicted in Fig. 1 for zero, medium, and long annealing times, t_{an}.

Several models differing in the accuracy of description of the process have been developed. A primitive step-function model assumes three distinct regions separated by sharp interfaces: a homogeneously intermixed region containing both the donor- and acceptor-labeled chains and two unmixed regions, each containing only one type of labeled chains. In the non-intermixed domains, the fluorescence decays

are single exponential while the Förster equation has been used in the intermixed domain. The total decay is then described as

$$F_D(t, t_{an}) = B_1(t_{an})\exp\left[-\frac{t}{\tau_D} - 2\gamma\left(\frac{t}{\tau_D}\right)^{1/2}\right] + B_2(t_{an})\exp\left[-\frac{t}{\tau_D}\right] \quad (5)$$

where t_{an} is the time of annealing, $B_1(t_{an})$ and $B_2(t_{an})$ are proportional to the number of excited donors in the mixed or unmixed domains, respectively, and $\gamma = c_A/c_{A0}$; c_A is the concentration of acceptors in the intermixed domain and c_{A0} is the critical concentration of acceptors for which the probability of donor emission equals to that of energy transfer to acceptors.

This model is unrealistic for several reasons: (1) it oversimplifies the concentration profile and in the middle region it uses the decay rate for an infinitely large homogeneous system thus ignoring both (2) the inhomogeneous surrounding of excited donors and (3) their nonequivalent positions with respect to the concentration profile. This model has been improved independently by Dhinojwala and Torkelson [31, 32] and by Liu and Winnik [29] by dividing the concentration profile into thin slices and assuming that the donor "feels" a uniform local concentration of acceptors in each slice. This "mean-local-concentration" model is still unrealistic because it ignores the effect of geometrical constraints, which play an important role in confined geometries. As has already been mentioned, the main difference between FRET in infinite systems and in a small volume is as follows: While the donor decay in infinite systems depends only on the distribution of the acceptors and not on the distribution of the donors, in confined geometries the decay from individual donors also depends on their localization in the system. While the "mean-local-concentration" model was able to describe the interpolymer diffusion at long annealing times, t_{an}, quite well, it failed at short annealing times. Trying to remove these limitations Winnik, Martinho et al. [30, 33, 34] developed a more realistic model, which assumes that donors in a certain slice can transfer their excitation energy to any slice with a different concentration of acceptors. This approach yields the decay of the donor fluorescence as a function of the short decay time, t (ns), and the long annealing time, t_{an} (minutes and hours):

$$F_D(t, t_{an}) \propto \exp\left[-\frac{t}{\tau_D}\right] \int_0^{(z_1+z_2)} c_D(z, t_{an})\exp[-g(t, z, t_{an})]dz \quad (6)$$

where $c_D(z, t_{an})$ is the concentration profile of the donors, which depends on the position on the axis of diffusion z (z_1 and z_2 are the thicknesses of the original films pressed together) and function $g(t, z, t_{an})$ describes the appropriate decay rate under the existing constraints (i.e., in thin slices). The exponential term inside the integral is the survival probability that the donors in the slice of the film positioned at coordinate z are still excited at time t upon excitation when the film has been annealed for t_{an}. The shape of $g(t, z, t_{an})$ was derived using the general formalism developed by Blumen and Klafter [16–18, 25, 26, 29]. As the energy transfer is

significant only for small donor–acceptor distances, the integrand can be expressed as an expansion series around z. The first term obtained after the appropriate mathematical treatment is identical with that used in the "mean-local-concentration" model and the analysis of the second term shows that it is important only in systems with large Förster donor–trap radii, r_0^{DT} compared to the width of the slices, which suggests that both simpler models of Dhinojwala and Torkelson [31, 32] and of Liu and Winnik [29] mostly provide reasonable means for analyzing the FRET results of interpolymer diffusion experiments, except for very short times and very large Förster radii.

3 Excimer Studies of Polymer Miscibility

The compatibility and intermixing of polymers in concentrated solutions and in bulk has also been studied by excimer fluorescence. Frank et al. [35–46] developed a suitable technique and published a number of papers mostly in the 1990s. The basic principle is relatively simple—a fluorescent polymer A, namely poly (2-vinylnaphthalene), P2VN, is "mixed" with a non-fluorescent polymer B. The "mixing" can be achieved, e.g., by the spin casting of dilute solutions in a common solvent. The pendant naphthalene groups in the poly(2-vinylnaphthalene) chain are separated by distances suitable for the formation of coplanar excimers. If P2VN were dissolved in a solvent, its chain is fairly flexible and mobile pendant groups could rotate and form excimers on a nanosecond timescale [47, 48]. However, the situation is different in the bulk polymer formed by fairly long P2NV chains below the glass transition temperature. The fast segmental motion is kinetically frozen, but a number of naphthalene groups are close to each other in the dense polymer matrix and their non-negligible fraction occurs in positions corresponding (or closely similar) to the excimer arrangement. Because the lifetime of the P2VN monomer fluorescence is long (ca. 50 ns) and the overlap of the monomer excitation and emission spectra is non-negligible, both intra- and inter-chain excitation energy migrations occur in bulk P2VN. As the randomly formed excimer-forming sites act as low-energy traps, the excitation is efficiently and fastly transported to these traps. The spatial distribution of excimer-forming sites (EFS) and the excitation energy transport (EET) depend on the chain conformations. Frank et al. have shown that the excimer fluorescence in polymer blends containing P2NV strongly depends on the compatibility of the chains and on their intermixing. If the chains of two types mix well, the average distances between the suitably arranged pendant fluorophores increase and steric effects hinder both the formation of EFS during the preparation of the film and the excess energy migration upon excitation, which means that the excimer fluorescence is weakened [46, 49, 50]. Quantitative interpretation of the experimental data is relatively complicated, because two decisive photophysical effects, (1) the population of EFS and (2) complex EET via various routes, are difficult to separate. In intermixed polymer coils, several types of excimer-forming

sites exist and the degree of chain coiling and intermixing influence both the population of EFS (their spatial distribution) and the EET mode by which the EFS are sampled. Frank et al. [38] carefully studied a number of systems (homologous series of alkyl methacrylates, polymers differing in molar mass, different blending conditions, and preparation procedures, etc.) and found that the ratio of excimer-to-monomer intensities F_E/F_M passes through a minimum if the solubility parameters of both the polymer components are equal. This finding was later confirmed by other authors [51, 52] who studied different polymer systems.

The excimer fluorescence studies of hydrophobically modified polymers, developed by Winnik, Yekta, Duhamel, and others, which have been widely used also by other groups for solution of various problems, are treated in a chapter "Pyrene-Labeled Water-Soluble Macromolecules as Fluorescent Mimics of Associative Thickeners."

4 Fluorescence Depolarization Studies of the Dynamics of Dilute Polymer Solutions

Time-resolved anisotropy measurements belong to popular fluorescence techniques used to study the local motions of polymer chains. For a coherent discussion of the important findings obtained by depolarization measurements, it is instructive to analyze the possible motions of flexible polymer chains. A typical example of a flexible chain is polystyrene in toluene (good solvent) or in cyclohexane at 35 °C (theta-solvent). Such a chain containing 10^4 structural units (molar mass ca. 10^6) has a contour length of ca. 1.2×10^3 nm. In dilute solutions, it forms a random coil and the average (root-mean-square) distance of its ends in the ϑ-solvent is ca. 70 nm; its average radius of gyration is almost 30 nm. The longest relaxation time of this chain in cyclohexane (low viscosity solvent), which describes the reorientation of the end-to-end vector, is ca. 10 μs. However, in this relatively long time, large numbers of very fast conformational changes of shorter parts of the chain occur; the chain can change its shape considerably and therefore the end-to-end vector changes both its size and orientation. It is generally recognized that the rate of the large-scale motion of flexible polymers is a universal phenomenon, i.e., it depends on the length of the chain and on the solvent viscosity, but does not depend on the chemical structure of the polymer [53].

Two general classical bead-spring models have been developed for the description and analysis of the motions of flexible chains (see chapter "Conformational and Dynamic Behavior of Polymer and Polyelectrolyte Chains in Dilute Solutions"). The Rouse model [54] is simpler (it does not take into account hydrodynamic correlations). The more advanced Zimm model accounts for hydrodynamic correlations and provides better description of the behavior [55]. In both cases, solution of the derived equations provides the so-called normal modes (relaxation times of different types of motions). The first mode describes the slowest motion of the

whole chain and higher modes describe faster motions of smaller parts. While the abovementioned models describe slow motions quite well, the fast dynamics of small parts of the chain (often called segmental dynamics) do not correspond to their predictions. Fast relaxations are not universal and depend on the chemical and structural details of the individual chains. In some cases, they also depend on specific interactions with the solvent. The apparent dilemma of universal vs. specific behavior can be better understood when the energy barriers which hinder the reorientation motion are analyzed. Even though the large-scale motion comprises a number of local motions, the most energetically demanding process that opposes the motion of the chain is massive reorganization of the solvent molecules. This is the rate-determining process involving the highest energetic barrier and all the barriers corresponding to the individual contributing local motions are significantly lower. Another important observation is that the specific polymer–solvent interactions do not affect large-scale motions. This means that the solvent behaves as a continuous viscous medium and the correlation times corresponding to large-scale motions of a polymer chain of a given length at constant temperature and constant solvent quality are proportional only to the bulk solvent viscosity.

Fast internal (segmental) motion proceeds on sub-nanosecond to nanosecond timescales and can be studied by NMR [56] or EPR [57, 58] and relatively comfortably also by time-resolved fluorescence anisotropy. All the internal motions exhibit a complex dependence on the external conditions. As already mentioned, they are influenced (1) by the solvent and (2) by the chemical nature and structural details of the chain architecture, i.e., their rates depend on the barriers of hindered internal rotation, etc. Moreover, the chain connectivity plays an important role and all fast motions of inner parts of the chain proceed in a highly cooperative fashion. It is obvious that an isolated conformational transition, e.g., rotation around a single bond, cannot occur in the middle of the chain without simultaneous cooperative motions of other parts. If other degrees of freedom were frozen at this instant, this type of motion would be physically impossible because it would require fast relocation of large and rigid parts of the chain. The simplest model for cooperative motion is cooperative three-bond motion (see Fig. 7 in chapter "Theoretical Principles of Fluorescence Spectroscopy"), which is reminiscent of the motion of a crankshaft and is therefore called "crankshaft-like" motion [59–61]. This type of motion was considered by Monnerie and Valeur [62–64] in their model for time-resolved anisotropy decay, $r(t)$. However, soon afterwards Monnerie [65] with coworkers and independently Hall and Helfand [66] realized that the energy barrier for the three-bond "crankshaft-like" motion is too high and would be much lower if several bonds moved simultaneously in a concerted manner. Both research groups proposed their models of simultaneous several-bond motion—the Hall and Helfand model and the so-called generalized diffusion and loss model of Monnerie. For more details concerning these models and for the definition and physical meaning of $r(t) = \left[I_{\parallel}(t) - I_{\perp}(t)\right] / \left[I_{\parallel}(t) + 2I_{\perp}(t)\right]$, see chapter "Theoretical Principles of Fluorescence Spectroscopy," Eq. (15).

In the early 1990s, Ediger et al. [67] experimentally studied the local dynamics of long and relatively monodisperse polyisoprene (PI) chains labeled in the middle by one anthracene unit (see Fig. 2), which also shows the orientation of the transition dipole moment incorporated as a co-monomer in the middle of the chain in dilute solutions in a series of solvents differing substantially in their viscosity (the viscosity coefficients covered two decades). From the orientation of the dipole moment, it is evident that the hindered rotation of the rigid anthracene unit around the bonds connecting it to the PI chain does not affect the fluorescence depolarization, which guarantees that the pure segmental motion is monitored by measuring $r(t)$. They fitted and analyzed the anisotropy decays using the Hall–Helfand model and studied the dependence of the mean reorientation correlation time, in this case given by $\tau_c = \left(\frac{1}{\tau_1\tau_2} + \frac{1}{\tau_2^2}\right)^{-1/2}$, on the bulk solvent viscosity and compared the results with the predictions from the classical Kramers' theory [68].

Kramers theoretically investigated the passage of a particle over an energetic barrier in the presence of friction caused by collisions with the other molecules. He obtained an Arrhenius-type expression for the rate constant of this process, i.e., an exponential dependence on the height of the barrier E_A. The pre-exponential term contains the mass of the particle, the friction coefficient, and parameters describing the shape of the barrier. At the high friction limit, the equation simplifies and acquires the form

$$\tau_c \propto \eta^1 \exp\left(\frac{E_A}{RT}\right) \tag{7}$$

(where η stands for the viscosity), which means that the reorientation correlation time τ_c should depend linearly on the bulk viscosity. Ediger with his colleagues [67] studied the effect of viscosity both by ^{13}C NMR and by time-resolved fluorescence anisotropy and found that $\tau_c \propto \eta^\alpha$ where exponent α is less than 1; for NMR he obtained $\alpha = 0.41$, while the fluorescent study provided $\alpha = 0.76$. They explained the difference as being a consequence of the chain modification: anthracene is significantly heavier and more hydrophobic than the isoprene unit and its presence affects the local dynamics. However, the power dependence of τ_c on the viscosity is intriguing and shows that the solvent molecules play important role, even though they do not specifically interact with the polymer segments (the dependences were the same for

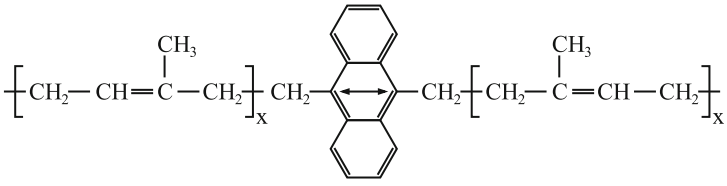

Fig. 2 Polyisoprene chain labeled by one anthracene unit in the middle of the chain. The orientation of transition dipole moments is indicated by the *arrow*

a whole series of solvents differing in their chemical structure and by two orders of magnitude in their viscosities). The results suggest that, in addition to the inherent barriers to the coordinated hindered rotation of several bonds, the presence of the solvent molecules increases the experimental barrier, i.e., $E_{exp} = E_A + \alpha E_\eta$, where E_η is an additional energy barrier due to interaction of the polymer segments with the solvent molecules. A similar nonlinear dependence of the rate of the isomerization on the solvent viscosity was observed by Fleming [69, 70], who explained the role of the solvent in an analogous way. However, the effect of the viscosity on the chain dynamics is more complex. For the assumed dependence of τ_c on η, parameter A, defined as $A = [(\tau_c/\eta)\ \exp(-E_A/RT)]$, or its logarithm should not depend on η and hence the A vs. log η plot should yield a constant value for all solvents. Careful analysis of experimental data shows that A decreases with increasing solvent viscosity, which indicates that the behavior is more complicated. Because the frequency of fast motions is high, the authors considered the theory of frequency-dependent friction, which was originally proposed by Grote and Hynes [71] for elucidation of an apparently peculiar dependence of the rates of some chemical reactions on the viscosity. This theory assumes that two different timescales have to be taken into account to describe the reaction properly. One timescale is based on the average residence time of the particle in the potential energy well. The other is a faster timescale necessary for passage of the particle across the top of the barrier. If the latter time is much shorter than the former, the low-frequency motions, which contribute to the zero-sheer viscosity, are simply too slow and do not affect the motion of the particle over the top of the barrier. In this case, the high-frequency viscosity is effectively much lower than the low-frequency (or zero-sheer) viscosity and the process proceeds very rapidly compared with the predictions based on the simple Kramers' theory and the zero-shear viscosity. Analysis and interpretation of the experimental results by Ediger et al. suggest that the very same mechanism is operative in the fast internal motions of flexible polymer chains.

We have chosen this particular (relatively old, but very important and highly didactic) study intentionally because we wanted to demonstrate how complex a thorough fluorescence study of polymer systems has to be (or should be).

The segmental dynamics is usually slower than the rotational motion of the solvent molecules and the presence of a polymer in the solvent results in slower dynamics of the solvent molecules. However, in some systems, e.g., in solutions of highly mobile polyisoprene (PI) chains in viscous solutions, the segmental dynamics is faster than the random motion of the solvent molecules. This happens if PI samples are dissolved, e.g., in "Arocolor 1248" (which is a viscous mixture of randomly chlorinated biphenyls), which presumably self-organize around the polymer chains and strongly affect the friction. The surprising finding that the addition of polymer chains to the solvent accelerates its dynamics was actually obtained by fast mechanical dynamic analysis, dielectric relaxation, and NMR studies [72–75]. Gisser and Ediger [76] carefully analyzed the NMR data and proposed a plausible explanation. Later this concept was extended by Ngai et al. [77, 78] for mixtures of low fractions of fluorescently labeled polymer A with an excess of polymer B taking into account that the B matrix is a solvent for the minority

polymer. Inspired by the influence of the faster chain dynamics on the slower dynamics, the authors developed a useful and successful fluorescence method for investigating polymer blends.

5 Dynamics of Concentrated Solutions and Polymer Melts

Fluorescence anisotropy studies of concentrated solutions are important for two reasons. Firstly, they bridge the gap between the results for dilute solutions, which can be interpreted relatively easily on the basis of the existing models, and the practically important dynamic behavior of bulk polymers, which is very complicated and its theoretical description and appropriate analysis are difficult. Secondly, they elucidate the contribution of the local friction to the macroscopic viscosity $\eta(c,T,M)$ of concentrated polymer solutions. The viscosity coefficient $\eta(c,T,M)$, where c is the polymer concentration, M is its molar mass, and T is temperature, can be expressed as

$$\eta(c,T,M) = A\zeta_0(c,T)g(c,M) \tag{8}$$

where A is a constant for the given polymer–solvent system, $\zeta_0(c,T)$ is the friction coefficient of one repeating unit, and $g(c,M)$ is the known dependence of η on c and M. This expression enables separation of the topological and frictional contributions to the viscosity and simultaneously it shows that η, which is proportional to the longest relaxation time (describing the reorientation of the end-to-end vector), is simultaneously proportional to ζ_0, which reflects the reorientation of the smallest parts of the chain. It suggests that the large-scale motion is a relatively straightforward result of a number of local motions. However, no theory based on the molecular structure and interacting potentials is available for the prediction of $\zeta_0(c,T)$ dependence. Therefore, fluorescence measurements, which study the fastest reorientation motions, are a suitable tool for testing the validity of Eq. (8).

Fujita and coworkers [79] studied fluorescently labeled polyoxyethylene chains and found a good correlation between the concentration dependence of the friction coefficient evaluated from the anisotropy measurements and from the macroscopic viscosity. Fujita developed the "free-volume theory" which describes reasonably well the concentration dependence of ζ_0 in the whole concentration region, [80] but it does not enable prediction of the parameters at a molecular level. Hyde et al. [81] used the Fujita theory for fairly successful interpretation of the experimental data. An interesting paper has been published by Viovy and Monnerie [82]. The authors studied concentrated solutions of anthracene-labeled polystyrene in toluene. They found good correlation of the local dynamics with the viscosity in the range of high concentrations and made one very important observation: the local dynamics are unaffected by the overlap of the polymer chains that occurs at concentrations higher than c^* (concentration of the first overlap—see chapter "Conformational and Dynamic Behavior of Polymer and Polyelectrolyte Chains in Dilute Solutions").

This observation is in a striking contrast to the concentration dependence of the viscosity in the transition region between dilute and concentrated solutions.

Equation (8) also describes the dependence of the bulk viscosity $\eta(T,M)$ of polymer melts on T and M. However, the bulk viscosity does not depend on the concentration in this case. The relation shows the correlation between the slow large-scale motion and the fast segmental motions of the chains in bulk polymer melts at elevated temperatures. From the point of view of the temperature-dependent dynamic behavior, a fundamental question concerns the shortest length scale of the fast motions that control the glass transition temperature. The incertitude follows from the fact that it is not intuitively clear whether the fast motion proceeds on the scale of one or several tens of repeating units. Viovy et al. studied the dynamics of labeled polybutadiene chains in melts by fluorescence anisotropy measurements and published several papers on this subject [83–85]. They confirmed that there is good correlation between the viscosity and the friction coefficients and found that the functional shape of the correlation function was temperature independent, which means that the mechanism of the monitored dynamic process does not change with temperature. Later they used 9,10-dialkylanthracenes with increasing oligomer alkyl chain lengths and found that the correlation times for chains with more than 14 carbons on each side do not change and correspond to those in "infinitely" long chains. Therefore, they decided that the length scale of the fastest chain motions corresponds to the part of the chain containing ca. 30 carbons. Because of the short timescale of the lifetimes of excited singlet states, fluorescence measurements can be employed only at fairly high temperatures (more than 100 K above the glass transition temperature) when the chain dynamics is fast and the correlation times are comparable with the fluorescence lifetimes (10^1 ns). However, Rutherford and Soutar used phosphorescence depolarization, which allowed them to probe the behavior at relatively low temperatures [86].

The dynamics of polymer melts can also be studied indirectly via the rotational reorientation of rigid probes dispersed in the polymer matrix. Several other authors employed this approach and, in addition to the temperature dependence, they also studied the effect of the probe size and shape [87–92]. They compared the depolarization correlation times of probes dispersed in the polymer matrix with those covalently attached to the polymer chains. They found the same type of temperature dependence of the depolarization characteristics of free (dispersed) and chemically attached probes (correlated with the temperature dependence of the viscosity), but the correlation times of the free probes were shorter, probably for two reasons: first, the probe is not directly attached to the chain and provides information on the chain indirectly, and second, the size of the employed probes was smaller than the 30-carbon part of the chain, which was identified by Viovy as the shortest rate-determining unit.

6 Fluorescence Depolarization Studies of Chain Conformations in Dilute Solutions

The conformational behavior of polymer and polyelectrolyte chains in dilute solutions is an interesting and practically important aspect and has been a subject of numerous studies since early 1950s. While the dynamics of polymers can be studied more or less directly by time-resolved depolarization measurements, the conformations and conformational transitions are studied indirectly via changes in the reorientation correlation times. However, because the correlation times depend sensitively on the chain conformations and the changes accompanying the structural transitions are usually quite pronounced, the conclusions concerning the conformational behavior are reliable in the overwhelming majority of cases.

Poly(methacrylic acid), PMAA, is an archetype of interestingly behaving and practically important polyelectrolyte and its behavior has been long studied by various techniques, e.g., by viscometry, calorimetry, and other methods [93–96]. PMAA is also one of the first polyelectrolytes, the conformational behavior of which has been systematically studied by fluorescence methods, particularly by time-resolved fluorescence, since the 1980s. Early fluorescence studies on PMAA were published by Morawetz et al. [97–100] and by Ghiggino et al. [101]. At that time, the currently generally accepted "pearl necklace" model of polyelectrolyte conformations in thermodynamically bad solvents [102] had not yet been published, but it was already well known that the little ionized PMAA chain forms very compact globular structures at low pH values, while at high pH values when the degree of ionization is high, the chain uncoils and expands, forming stretched rodlike conformations. In the 1980s, the term "hypercoiling" or "supercoiling" was commonly used for compact PMMA conformations at low pH values and the term "polysoap-reminiscent polyelectrolyte" can be found in the older literature on PMAA. About 10 years before the famous "pearl necklace" model was published by Dobrynin et al., Ghiggino actually offered an acceptable tentative explanation of the conformational behavior of PMAA (which is an annealed PE) using a very similar model to that presented later by Dobrynin for quenched PEs. Unfortunately, he did not publish the data and his model in a regular (periodical) journal, but in Polymer Photophysics edited by D. Phillips [101], which is probably the main reason why his discovery remained largely unknown to the broader scientific community. In the early 1990s (i.e., still before the Dobrynin paper), the pH-dependent conformational behavior of PMAA was studied by Bednář et al. [103, 104] The authors studied the behavior of chains of different lengths randomly labeled by pendant dansyl groups (see Fig. 3) attached to the chain by a short spacer and compared it with that of analogously labeled poly (acrylic acid). The content of fluorescent groups was low and varied from 1 to 5 per chain. The authors measured the fluorescence decays and the fluorescence anisotropy decays in a broad pH range from 2 to 9.

Dansyl is a suitable group for this type of studies, because its fluorescence is polarity dependent. Its quantum yield is high and the fluorescence lifetime is long in

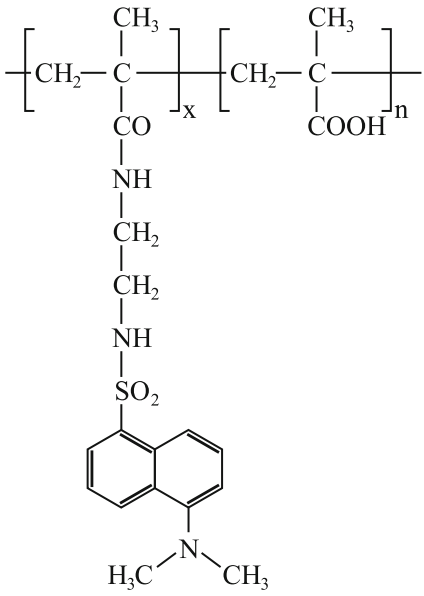

Fig. 3 Poly(methacrylic acid) labeled by pendant dansyl fluorophore

nonpolar media and both characteristics are appreciably diminished in polar media. Nevertheless, the photophysics of dansyl are relatively simple and the interpretation of $r(t)$ decays is straightforward. In practice this means that, at low pH values, when the probes are entrapped inside compact "supercoiled" globules and experience low polarity of their immediate microenvironment, both the fluorescence lifetime and the reorientation correlation time are long. At high pHs, when the chain forms a stretched rodlike conformation, the probes are exposed to the polar aqueous medium and can rapidly rotate around the bonds connecting them to the chain so that both measured times are short. The total fluorescence intensity (measured at the magic angle) decays non-exponentially in all cases and can be fitted, to a first approximation, by a double-exponential curve (with τ_{F1} and τ_{F2}). Because the double-exponential fits did not provide a fully random distribution of the experimental errors and some non-negligible "humps" were noticeable mainly in the region of short times (but also at long times), the authors assumed that the probes in the individual polymer globules do not experience the same polarity and used two relatively narrow Gaussian distributions of lifetimes with fixed maxima corresponding to τ_{F1} and τ_{F2}. At that time, computer power was fairly low compared to present-day standards and the parameters of the Gaussian functions were obtained by a laborious iterative method aimed at the best possible fit (low κ^2 and random distribution of residuals) with fixed contributions of the fast and slow lifetimes—the same as those defined by the pre-exponentials in the original double-exponential fit. The main conclusions drawn from the advanced analysis were the following: For all the studied dansyl-labeled PMAA samples (differing in molar masses and in the degree of labeling), the distributions of both lifetime components, τ_{F1} and τ_{F2}, depend on the pH. They shift to shorter values with

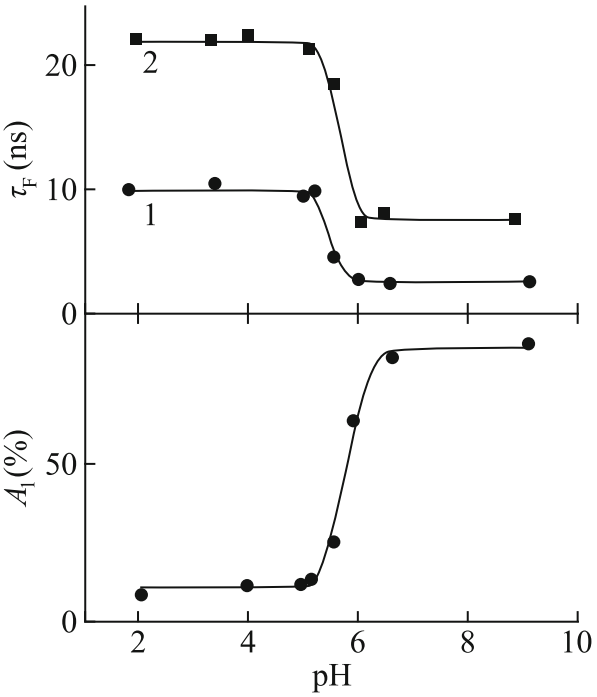

Fig. 4 *Upper part*: The fast fluorescence lifetime component, τ_{F1} (*curve 1*), and slow fluorescence lifetime component, τ_{F2} (*curve 2*), as functions of pH obtained by double-exponential fit. *Bottom part*: The relative amplitude of the fast fluorescence decay, A_1 (in %). Adapted with permission from Macromolecules 24, 1991, 2054–2059, figure 1, [104]. Copyright (1991) American Chemical Society

increasing pH values. The dependences of average values $\langle\tau_{F1}\rangle$ and $\langle\tau_{F2}\rangle$, as well as those obtained from double-exponential fits, τ_{F1} and τ_{F2}, follow sigmoidal curves with pronounced drops and inflexion points at ca. pH 6, depending slightly on the ionic strength of the solution. The relative contribution of the fast lifetime, A_1 (in %), increases with pH and its dependence on pH can also be described by a sigmoidal curve with an inflexion point at ca. pH 6. Dependences of τ_{F1}, τ_{F2}, and A_1 on pH for one of the studied samples are depicted in Fig. 4. The distributions of the lifetimes for the same sample and three selected pH values are shown in Fig. 5. The experimental anisotropy decays, $r(t)$, were mostly fitted by double-exponential curves with the residual anisotropy term, r_∞. Because the dansyl fluorescence quantum yield is fairly low at high pH values and the statistical quality of the depolarization data in alkaline buffers is poor, the authors decided to fit the data at high pH values by single-exponential decays and based the discussion of the results of depolarization measurements in the whole pH range on the mean rotation correlation time τ_r alone. The dependences of mean rotation correlation times from different samples in solutions with the same ionic strength collapse on one "master curve," which is shown in Fig. 6 together with the dependence of the mean fluorescence lifetime τ_F for the sample, the components τ_{F1} and τ_{F2} of which are depicted in the Fig. 5. The authors explained this behavior, including the fact that all the mean rotation correlation times τ_r of samples differing substantially in their molar mass collapse in one "master curve," by the Ghiggino model which, similarly

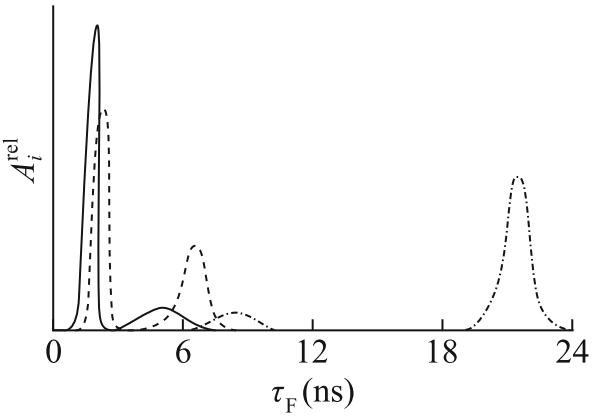

Fig. 5 The distribution of fluorescence lifetimes (amplitudes A_i^{rel}) for three selected pH values: pH 8.7 (*solid*), pH 6.0 (*dashed*), and pH 3.88 (*dash-dotted*). Adapted with permission from Macromolecules 24, 1991, 2054–2059, figure 5, [104]. Copyright (1991) American Chemical Society

to the Dobrynin model, assumes the formation of several compact globules within one chain. According to Ghiggino, the size of globules depends mainly on pH and ionic strength of the solution, but does not almost depend on the length of the annealed polyelectrolyte chain. Let's analyze and discuss the results in more detail: the fact that the decays are essentially double exponential in the entire studied pH region indicates that, in all cases, two classes of pendant dansyl probes exist on polymer chains and "feel" different hydrophobicity of the environment: the probes (1) entrapped in compact globules and (2) the water-exposed probes attached to the stretched parts of the chain. The distributions of τ_{F1} are narrow, indicating that the water-exposed probes experience almost the same polarity of the environment. The distributions of the "entrapped" probes are appreciably broader because the dansyls entrapped in different positions within the collapsed domains "feel" different polarity of the microenvironment. The probes located in the center of the globule are protected well against interactions with the water molecules, while those close to the polymer–water interface are screened less well. The data in Figs. 4, 5, and 6 show that, at low pH, the water-exposed dansyl probes "feel" lower effective hydrophobicity than the probes "hidden" in the coiled parts of the chain at high pH values. This slightly surprising finding cannot be explained solely by the polarity of the medium but is a result of strong interactions in the ionized system (containing not only the ionized polymer chains, but also small ions) at basic pH values. At high pHs, the loose and only slightly coiled chain domains of the highly ionized annealed PE chain (which are somewhat less ionized than the average degree of ionization) do neither preclude nor hinder close approach of small ions to the probes and efficient quenching of their fluorescence.

The fact that the rotation correlation times of probes attached to PMAA chains with substantially different molar masses (starting at ca. 20×10^4 g/mol) obey the same dependence on pH confirms the assumption that all the chains form different numbers of globules of the same size, each of them formed by parts of the chain roughly corresponding to 20×10^4 g/mol. The formation of the pearl necklace structure is further supported by high residual anisotropy at low pH: the globules

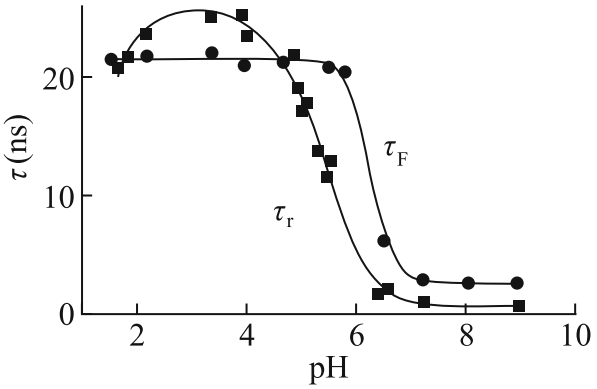

Fig. 6 The comparison of the pH dependence of mean rotation correlation times τ_r from different samples in solutions with the same ionic strength (collapsed on one "master curve") with the pH dependence of the mean fluorescence lifetime τ_F for the sample, the components τ_{F1} and τ_{F2} of which are depicted in the Fig. 5. Springer, Self Organized Nanostructures of Amphiphilic Block Copolymers I, 241, 2011, 187–249, figure 7, [105]. Copyright 2011. With kind permission from Springer Science and Business Media

connected to each other by elongated parts of the chain can relatively easily rotate in 1D, but the two remaining rotational directions would require slow rotation of the whole interconnected object, which is outside the time window of fluorescence measurements. It is worth noting that the fast anisotropy decays at high pH also exhibit quite high residual anisotropy. This observation can be easily explained: the chain is stretched and the probe can rapidly rotate around the axis defined by the linker. Analogously to the previous case, the rotation proceeds in 1D and full randomization of the emission components assumes slow reorientation of the whole stretched and electrostatically stiffened PMAA chain (see chapter "Conformational and Dynamic Behavior of Polymer and Polyelectrolyte Chains in Dilute Solutions").

Comparison of the dependences of mean times τ_F and τ_r on the pH (Fig. 6) is also interesting. The onsets of increasing parts of the two curves (when pH decreases) roughly coincide. However, the lifetimes increase more steeply with decreasing pH than the rotation correlation times, which pass through maximum value at pH 4. The sudden steep change in τ_F is caused by the fact that the fluorophore "feels" only the interactions with its immediate microenvironment, which changes rapidly from the very beginning of the conformational transition. The rotation correlation time τ_r reflects the size of the forming globules. The data suggest that the process does not proceed as a fully cooperative sudden transition, but that the globules grow progressively with decreasing pH. However, the size of the globules is strongly affected by their compactness, which increases with decreasing pH and causes a decrease of rotation correlation times in the pH region below pH 4. In the early 2000s, some authors of this experimental paper performed the molecular dynamics

simulation of the pH-dependent behavior of PMAA and found good semiquantitative agreement of the experimental and simulation data [106].

Shortly after the work published by Bednář, Soutar and coworkers also studied the behavior of several annealed PEs (including PMAA) in water by fluorescence methods [107]. He and his coworkers also observed profound transitional changes accompanied by pronounced changes in the fluorescence characteristics. Later they focused on the thermoresponsive behavior of *N*-isopropylacrylamide, NIPAM, and other polymers [108–110]. The solution behavior of NIPAM in water is very interesting. It dissolves in water at low temperatures, but its lower critical solution temperature (LCST—see chapter "Conformational and Dynamic Behavior of Polymer and Polyelectrolyte Chains in Dilute Solutions") is reached at ca. 32 °C and two phases separate at higher temperatures forming turbid cloudy solutions which fully reversibly clarify upon cooling. The existence of LCST in the temperature region below the normal boiling point of the pure solvent is rather rare and in this case it is due to a specific hydrophobic-to-hydrophilic balance (appropriate amphiphilicity) which induces pronounced changes in the solvation shell of the NIPAM units upon heating. This theoretically interesting and practically important behavior attracted the interest of a number of research groups [111–114]. In spite of substantial information obtained by various researchers, the debate concerning the major determinant of the coil-to-globule transition is still continuing. Some authors accentuate the breakdown of hydrogen bonds between the polymer and water [115, 116], while others attribute the chain collapse to the "hydrophobic effect," which should affect the water structure surrounding the hydrophobic substituents of the polymer [113, 114, 117, 118]. It is likely that both effects contribute to this interesting behavior [119, 120]. Poly(*N*-isopropylacrylamide) and its copolymers are attractive "smart" stimuli-responsive polymers from a practical point of view, because their aqueous solutions respond very quickly to changing temperatures. The rapidity of the response has been attributed to a two-stage mechanism: individual chains collapse in globules prior to aggregation of the resultant globules [117, 121–124]. Soutar and coworkers investigated a large series of PNIPAM copolymers with various polymers differing in their hydrophobicity and confirmed the prediction that LCST can be manipulated and tailored by the copolymer composition.

At the end of the section devoted to studies of the collapse of polymer chains in dilute solutions, we will consider an interesting paper published relatively recently by Soutar et al. [125] This paper is devoted to the aspects of "cosolvency" and "cononsolvency," which are intriguing phenomena observed in dispersions of certain solutes in mixed solvents. While "cosolvency" is a relatively common phenomenon consisting in the fact that a mixture of two (or more) poor solvents becomes a good solvent for the same solute, e.g., certain compositions of water/methanol mixtures act as a good solvent for poly(methyl methacrylate) which is insoluble in both of them [126], "cononsolvency" is a rarer occurrence: in this case a solute (soluble in all the components of the solvent mixture) is insoluble in the mixture at the same temperature. An example of such a system is PNIPAM in methanol–water mixtures [127, 128]. So far, there is no consensus concerning the

main reason for the peculiar behavior of the ternary water–methanol–PNIPAM system. Based on simple solution theory, it is obvious that the effective water–methanol interactions are preferred over the interactions of PNIPAM segments with the solvent components. However, this phenomenological description does not tell us which molecular mechanism is responsible for the observed behavior. Recently, the "string of pearls" model was proposed for PNIPAM on the basis of light scattering and computer simulation data [128]. It focuses on polymer–solvent interactions and assumes that, below LCST, the polymer consists of highly solvated stretched parts and more coiled dehydrated parts. The structure is reminiscent of the "pearl necklace" structure of PEs, but the reason for its formation in PNIPAM systems is different. In stretched parts, water and methanol molecules compete for NIPAM units (competitive binding). Upon heating, the bound solvent molecules are released in a cooperative manner and "cooperative dehydration" occurs, followed by the formation of relatively compact polymer coils. An alternative explanation ascribes the coil collapse to the deterioration of the average bulk solvent quality rather than to polymer–solvent interactions [129]. The non-monotonously changing solvent quality of the mixture derives from the appreciably changing strength of the water–methanol interactions in a broad range of solvent compositions. To rationalize this hypothesis, it was argued that some transient "water–methanol complexes" of different stoichiometry form in the bulk solvent.

Soutar et al. [125] measured the time-resolved anisotropy, $r(t)$, for dilute solutions of PNIPAM, randomly labeled by ca. 5 mol.% acenaphthylene in water, methanol, and in the whole region of their mixtures at temperatures covering the LCST dependence (see Fig. 7) on the composition of the solvent mixture. They found that the anisotropy decays are double exponential in all cases. They used the "string of pearls" model for the system in pure water and in water–methanol mixtures, where they ascribed the short time to the rotation of probes in the highly solvated parts of the PNIPAM chain and the long time to the rotation of probes in coiled dehydrated parts. Because they also observed the double-exponential

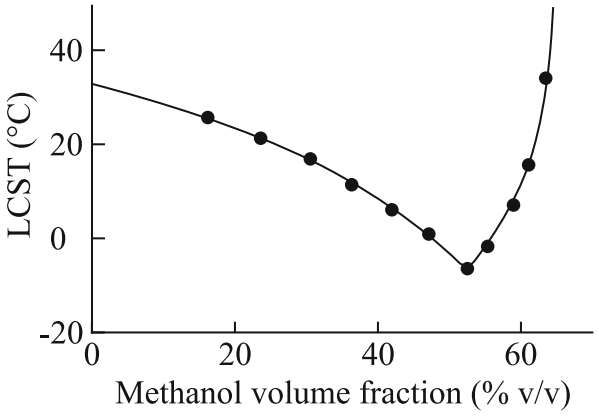

Fig. 7 Schematic LCST phase diagram of PNIPAM [0.1 wt%] as a function of the composition of the methanol–water solvent mixture. Adapted from Soft Matter 7, 2010, 1176–1184, figure 1, [125] with permission of The Royal Society of Chemistry

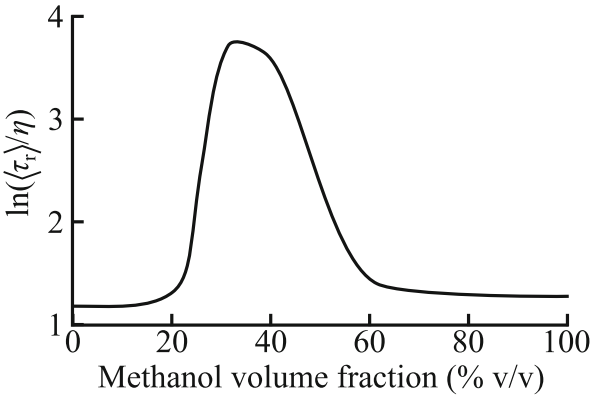

Fig. 8 The logarithm of the mean rotation correlation times normalized by the viscosity coefficients on methanol volume fraction at 20 °C. Adapted from Soft Matter 7, 2010, 1176–1184, figure 4, [125] with permission of The Royal Society of Chemistry

fluorescence anisotropy decay in pure methanol (good solvent) regardless of the temperature, they tentatively suggested that there exist the parts of chains differing in rigidity on nm length scales: loose H-bonding between NIPAM segments is responsible for the faster motion of more flexible parts of the chain and the strong H-bonding between the segments and methanol molecules actually slows down the segmental dynamics.

The authors used the mean rotation correlation time, $\langle \tau_r \rangle$, for comprehensive discussion of the behavior of the ternary mixture. Figure 8 shows the logarithm of the mean rotation correlation times normalized by the viscosity coefficients on the mixed solvent, i.e., $\ln(\langle \tau_r \rangle / \eta)$ vs. methanol volume fraction. The curve indicates that, in the region of compositions between 20 and 60 % methanol, the solvent quality and dynamic behavior of labeled chains differ significantly from both the methanol-rich and the water-rich regions.

Soutar and coworkers analyzed the cooperative character of the conformational transition (cooperative dehydration or more precisely de-solvation) in mixtures differing in composition using the method that they developed earlier [130, 131] and plotted $\ln(\langle \tau_r \rangle / \eta)$ vs. reciprocal temperature, $1/T$ (see Fig. 9, where the experimental dependence is schematically depicted). The curves in water-rich media show a very sharp decrease at LCST, which is a signature of cooperative dehydration. Increasing content of methanol reduces the magnitude of the changes in the plotted values (i.e., the magnitude of the conformational transition) and also "smears" the sharpness of the transitions. The methanol-rich mixtures behave effectively as good solvents for PNIPAM at ambient temperatures and no sharp change of plotted curves (suggesting no transition) was observed. This study did not answer all the questions concerning the molecular mechanism of the "cononsolvency," but has greatly contributed to understanding the PNIPAM behavior in mixed aqueous solvents.

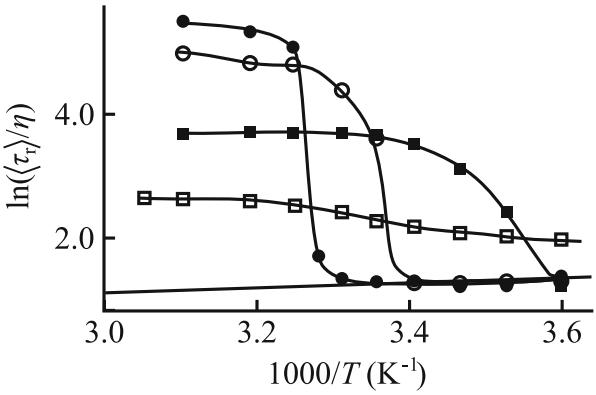

Fig. 9 The logarithm of the rotation correlation times normalized by the viscosity coefficients on methanol volume fraction as function of 1/*T*. Adapted from Soft Matter 7, 2010, 1176–1184, figure 6, [125] with permission of The Royal Society of Chemistry

7 Comments on Self-Assembly Studies

The self-assembly of amphiphilic block copolymers and polyelectrolytes is amply treated in other chapters of this book. The individual studies will not be discussed in detail in this part. We will pursue a different line of thought. We will compare the enormous research potential of fluorescence spectroscopy with other currently used experimental methods to show its specific features and advantages for self-assembly studies.

For this purpose, we have chosen the most typical and relatively simple example of the self-assembled polymer systems, i.e., the solution of copolymer micelles formed by high-molar-mass diblock copolymers with one hydrophobic and one hydrophilic block of comparable lengths in aqueous media [132–135]. The micelles formed in such a system contain several tens to a few hundreds of associated polymer chains (depending on the lengths of the blocks and segment–solvent interactions, etc.) and consist of compact spherical cores with a radius of ca. 10 nm formed by the insoluble blocks and diffuse shells formed by the soluble blocks (neutral or polyelectrolyte). The hydrodynamic radius ranges from several tens to usually less than two hundred nm and, for the PE block (especially in the case of annealed PEs), it depends on the pH and ionic strength of the bulk solvent [136]. Nanoparticles of this size strongly scatter UV–vis light, X-rays, and also neutrons. Therefore, the most frequently used experimental approaches for their characterization and study employ different variants of the scattering methods [137–139]. Fluorescence spectroscopy has been employed less than scattering methods, but is a frequently used technique in studying polymeric nanoparticles [47, 48, 140–143]. It has been used more often than other spectroscopic techniques, such as NMR [144–146], EPR [147], microscopy imaging [148, 149], ultracentrifugation [150, 151], and other separation techniques [152–154].

Let us compare the advantages and weak points of scattering and fluorescence methods for studying polymeric nanoparticles. The great advantage of scattering methods for self-assembly studies is the high scattering power of polymeric

nanoparticles. The intensity of the light scattered by a particle with radius R is proportional to R^6, which ensures a strong signal and high sensitivity of scattering methods, providing that the "optical contrast" between the polymer and solvent is sufficient. The "contrast" depends on the difference between the scattering power of the monomer unit and of the solvent molecule; e.g., in case of the visible light, the scattering contrast is the refractive index increment, (dn/dc), where n is the refractive index of the solution and c is the weight concentration of the polymer. Scattering methods very sensitively detect the onset of the association process with changing concentration, temperature, or solvent composition and enable the evaluation of the sizes of scattering particles. A steep dependence of the intensity of the scattered light, I_{sc}, on the size of the particles, i.e., $I_{sc} \propto R^6 \propto V^2$, where V is their effective volume, translates into a quadratic dependence on the molar mass M, i.e., $I_{sc} \propto M^2$. In the macroscopic ensemble, this means that the experimental molar mass is the weight average molar mass and the size characteristics measured by the light scattering are the z-averages, e.g., the radius of gyration, which can be evaluated by the static (or elastic) light scattering, is defined as $\langle R_g \rangle_z = \left(\sum R_{gi} N_i M_i^2 / \sum N_i M_i^2 \right)$; similarly the experimental hydrodynamic radius obtained by the dynamic light scattering is based on the z-average of diffusion coefficients D_i, i.e., $\langle R_H \rangle \propto \langle D_i \rangle_z^{-1}$. In strongly polydisperse systems, the contribution of large particles to the scattering is strong, which may sometimes be a significant disadvantage. For example, in a system of relatively uniform nanoparticles with radius of ca. 10 nm containing an admixture of a few percent of large particles (with R of the order 10^2 nm), the scattering is dominated by the low fraction of large particles and information on almost 100 % of the small particles is lost.

In contrast to the scattering techniques, the use of fluorescence methods requires the presence of fluorescent probes and provides indirect information on the system, which is a disadvantage. However, a great advantage lies in the fact that a low fraction of fluorescently tagged nanoparticles can be studied in a system containing a large excess of different non-fluorescent but highly scattering particles. Other advantage is that the studies can be targeted at different features of the system structure and behavior, e.g., the solvent relaxation studies can elucidate the role of the solvation of micellar shells [142, 143].

Because chapter "Fluorescence Correlation Spectroscopy Studies of Polymer Systems" is devoted to the application of fluorescence correlation spectroscopy (FCS) to polymer systems, we will not discuss its application in detail here, but would like to mention that FCS provides analogical data to dynamic light scattering (DLS), i.e., the diffusion coefficients of fluorescent chains or nanoparticles, but, in contrast to DLS results, which are the z-weighted averages, the FCS results are weighted differently. In a system of dissolved single-tagged polydisperse chains, the contributions of chains of different lengths to the diffusion coefficient are weighted by the number fractions. An indisputable advantage of FCS is the ability to study fluorescently labeled nanoparticles in mixtures with the unlabeled particles and the simultaneous DLS and FCS measurements of labeled particles provide complex information on their properties and polydispersity [155].

Nonpolar micellar cores can solubilize various hydrophobic fluorophores. Therefore, a number of papers describe the fluorescence studies of untagged self-assembled nanoparticles with added probes. The best-known example is the use of pyrene for estimation of the onset of the association process and studies of the micellar properties. A number of steady-state and time-resolved measurements of pyrene fluorescence have been performed in both polymer and colloid systems [156–162]. The simplest and commonest measurement of c.m.c. is based on the fact that the excitation and emission spectra of pyrene are polarity dependent. When the micelles start to form at c.m.c. in aqueous media, the strongly hydrophobic pyrene is solubilized in the cores and its spectra change substantially. The low-energy band of L_a ($S_2 \rightarrow S_0$) in the excitation spectrum shifts from 338 to 332.5 nm and the vibrational structure of the emission spectrum in the 360 to 400 nm region also changes significantly. The third vibrational band corresponds to the allowed transition and its intensity is not affected by the polarity. The first band, which corresponds to the symmetry forbidden transition, is weak in nonpolar media, but is intense in polar media due to strong dipolar interactions with the surrounding molecules [163]. Hence, analogously to numerous studies on colloids, the concentration-dependent onset of the micellization of amphiphilic block copolymers in aqueous media can be monitored by pyrene fluorescence, i.e., by plotting the ratio of intensities of the first-to-the-third band, I_1/I_3 vs. ($-\log c$). However, the critical micelle concentration (c.m.c.) of high-molar-mass copolymers is usually very low (some polymeric micelles are kinetically frozen and c.m.c. does not exist at all). In this case, the sigmoidal curve of I_1/I_3 vs.($-\log c$) is also obtained, but it is a result of the dilution, which cannot be taken as a signature of c.m.c. [164]. During the progressive dilution, the ratio of the total volume of micellar cores to the volume of the bulk solvent decreases and the partitioning of pyrene between the micelles and the bulk aqueous medium changes. The dilution provokes the release of pyrene in the aqueous phase. Pyrene is only poorly soluble in water, but its fluorescence in saturated aqueous solutions is readily measurable by sensitive spectrometers. The partition coefficient of pyrene between the polystyrene cores and water is high, ca. 10^6 [164, 165], but, at high dilutions around c.m.c., the ratio of the total volume of all the micellar cores in the solution to the bulk solvent is lower than 10^{-6}, which means that more pyrene molecules (exhibiting a high ratio I_1/I_3 of ca. 1.9) are present in the aqueous phase than in micellar cores (where the emission of solubilized pyrene has a low ratio I_1/I_3 of ca. 1.1). Therefore, the measured I_1/I_3 values increase with dilution. In the early 1990s, Winnik at al. [140] actually solved the problem and proposed a method for unambiguous estimation of low c.m.c. of polymer systems. The authors carefully studied a series of polystyrene-*block*-polyoxyethylene copolymers differing substantially in their total length and also in the block length by steady-state and time-resolved fluorescence methods. They found that the ratio of the molar extinction coefficients of pyrene in micelles and in water is $\varepsilon_m/\varepsilon_w = 3.9$ and the analogous ratio of the fluorescence quantum yields (which can be expressed as the ratio of mean fluorescence lifetimes) is $\phi_m/\phi_w = \tau_m/\tau_w = 1.8$. Using the Lambert–Beer law, they expressed the ratio of the intensities in the excitation spectrum, $F = I_{338}/I_{332.5}$ at 333 and 332.5 nm,

respectively, as a function of the polymer concentration and showed that the plot in the form

$$\xi(c) = \frac{(F - F_{\min})}{(F_{\max} - F)} \text{ vs. } c \tag{9}$$

(where $F_{\min}$ and $F_{\max}$ correspond to the bulk water and to the micelles, respectively) yields a straight line, which is directed toward the beginning of the system of coordinates ($c = 0$, $R = 0$) in the kinetically frozen systems without c.m.c. The presence of c.m.c. in reversible systems is manifested by a plot consisting of two linear parts. The less steep part (at low concentrations) goes to ($c = 0$, $\xi = 0$) when extrapolated to infinite dilution and the more steeply growing part (observed at high concentrations) yields c.m.c. as an intercept with the horizontal c-axis. This method should be used for the c.m.c. measurement and for discrimination between reversible and kinetically frozen systems. At high dilutions, when the measured ratio F approaches $F_{\max}$, the experimental errors increase, but their acceptable scatter is a good test of the experimental accuracy. Unfortunately, a high percentage of published data (including recent data) suggests that only a few researchers among polymer scientists who used pyrene fluorescence are aware of the Winnik method and this is the main reason why we mention this apparently trivial application here.

The versatility of solubilization studies is based on the fact that a great variety of fluorophores can be solubilized in different domains of nanostructured nanoparticles, e.g., either in micellar shells [166, 167] or in cores (see the next part for more details), which facilitates targeted studies of various properties (compactness, rigidity polarity, etc.). However, non-fluorescent species can also be solubilized to alter the properties of micelles and fluorescence characteristics of already present fluorophores. To demonstrate the broad applicability of measurements with the solubilized probes, we give a few examples of studies aimed at different aspects. Procházka, Kiserow et al. studied the micellization of polystyrene-*block*-poly(methacrylic acid) labeled by 2-vinylnaphthalene monomer and dimer attached to the free end of the polystyrene block in 1,4-dioxane–methanol and in 1,4-dioxane–water mixtures and in purely aqueous media and investigated the effect of solubilization of the nonpolar compounds in the micellar cores [47, 48, 141]. In 1,4-dioxane media (good common solvent), the chains are molecularly dissolved and are fairly flexible. Therefore, the time-resolved anisotropy, $r(t)$, measured in a 1,4-dioxane-rich solution of the copolymer containing only one pendant naphthalene rapidly decayed to zero. The measured depolarization was due, in part, to the fast rotation around the bond connecting it to the chain and to fairly fast segmental motion of the chain end. The onset of micellization on the 1,4-dioxane–methanol and on the 1,4-dioxane–water composition scale was demonstrated by a sudden slowing of the anisotropy decay and by the appearance of appreciably high residual anisotropy. The fluorescence behavior of the sample labeled with the 2-vinylnaphthalene dimer was also interesting. The sample exhibited strong excimer fluorescence in good common solvents. The time-resolved measurements revealed that the excimers are formed by fast rotational motion of

two vicinal pendant naphthalenes with respect to each other. The rapid increase in the excimer emission in short times after the excitation (characteristic time ca. 1 ns) indicated that the pendant aromatic naphthalene rings easily acquire the necessary coplanar position within the lifetime of the excited state of the monomer. In compact micellar cores (in methanol-rich or water-rich media), the naphthalene fluorophores are trapped and strongly immobilized in random positions inside compact cores and the excimer emission was very weak. The time-resolved measurements showed that weak excimer emission occurs from a low fraction of appropriately pre-organized pairs. The excimer fluorescence decay curves did not show the rising part. The onset of the micellization vs. solvent composition monitored by both fluorescence methods coincided nicely with that measured by light scattering, which confirmed the applicability of the above fluorescence methods for self-assembly studies. The authors further studied the effect of the solubilization of toluene in micellar cores on the fluorescence of pendant tags. From the point of view of fluorescence measurements, toluene is an indifferent compound—it does not quench the naphthalene fluorescence and, as its low polarity is similar to that of polystyrene, it does also not affect the effective polarity of the micellar cores. However, it swells the cores and partially liberates the segmental dynamics. The study has shown that the slow step-by-step addition of toluene to the aqueous solution of micelles and its consequent solubilization in the polystyrene cores accelerated the anisotropy decays and promoted the excimer fluorescence (including the recovery of the rising build-up part).

Because the copolymer micelles serve as well-defined and well-characterized models of (usually worse-defined, i.e., considerably polydisperse) biopolymer nanocontainers for targeted drug delivery purposes, a number of studies were aimed at the controlled uptake and release of nonpolar compounds from micelles. Munk, Procházka, Webber et al. [164, 165, 168, 169] studied the release of aromatic fluorophores from the polystyrene-*block*-poly(methacrylic acid) micelles in aqueous media. The cores of the micelles were loaded by the probe during preparation of the micelles, when the samples were dissolved in a solvent mixture rich in 1,4-dioxan, where reversible micelles with swollen cores are formed spontaneously. Relatively concentrated aqueous solutions of micelles with probes in their cores were prepared by dialysis against solvents with increasing water content and finally against the aqueous buffers. They contained the micelles highly loaded by the fluorophore. To be precise, the fluorophore partitioned between micelles and the bulk solvent (the saturated solution of the probe). The individual aromatic fluorophores used (naphthalene, anthracene, phenanthrene, pyrene, perylene) were strongly hydrophobic and the concentrations of their saturated solutions were in the range 10^{-5} to 10^{-7} mol/L. Their release from micelles was triggered by a sudden several-hundred-fold dilution by pure water. The fluorescence of probes released in the bulk solvent was quenched by a water-soluble quencher (Tl^{+}) and the time-dependent decrease in the steady-state fluorescence, which is proportional to the total number of fluorophore molecules in all the micellar cores, was monitored on a timescale of minutes to hours. The results were interpreted using the numerical solution of the differential equation describing the diffusion of

probes from spherical cores under the constraint of a constant amount of probes in the system. Note that the slow diffusion inside the cores toward the core-shell interface is the slowest rate-determining process. The decrease in the emission intensity nicely followed the theoretically predicted curve and this relatively simple measurement allowed the evaluation of the extremely low diffusion coefficient of pyrene in glassy polystyrene, $D = 9.4 \times 10^{-19}$ cm^{2}s^{-1}. This small value, which is actually one of the smallest experimental diffusion coefficient values ever reported, shows that the diffusion motion of the bulky pyrene molecule is strongly hindered in compact polystyrene cores, which are presumably glassy at ambient temperatures. The glass transition temperature of high-molar-mass polystyrene is ca. 100 °C, but it depends on the chain length and also on the size of the polystyrene domains and therefore it decreases with decreasing size of the micellar cores. AFM studies of polymeric micelles deposited on the mica surface suggest that the mobility of the chains in the micellar cores is higher than that in the bulk polystyrene and therefore the rigidity of the cores is lower than that of the bulk PS. The studies by Matejíček et al. [148, 149, 170, 171] suggest that the cores with a radius ca. 10 nm should still be in the glassy state.

A prerequisite of the self-assembly studies with specifically tagged block copolymers is their successful targeted synthesis. A series of tailored monodisperse and specifically tagged samples, e.g., tagged at the end of one block, at the ends of both blocks, in between the blocks, etc. (together with their untagged analogues), was prepared by Ramireddy and Munk [172] in the early 1990s and the samples were studied for several years by Webber, Kiserow, Procházka et al.. Some studies have already been cited [47, 48, 141, 143, 171] and others will be described in a later part. The micelles formed by samples tagged by the excitation energy donor at the beginning of the insoluble block and by the energy acceptor in between the blocks contained the donor tags in the cores and acceptors at the core-shell interface. A number of experimental and also Monte Carlo simulation studies were aimed at the distribution of chain ends in the cores [173–176]. Other samples with tags in between the blocks and at the end of the soluble block were used for studying the distribution of the ends of the shell-forming PMAA chains [177–180]. In this case, the attachment of the strongly hydrophobic fluorophore (anthracene) at the free end of the PMMA block represents a considerable modification of the shell. The study was actually aimed at the behavior of the modified micelles, which is also a very relevant issue, because the functional nanocontainers for drug delivery purposes contain various targeting groups, which are intentionally attached to the stabilizing water-soluble shell. If the targeting groups differ in polarity from the shell-forming chains, e.g., if they are less polar, they can be buried in the shell similarly to the hydrophobic fluorescent probes [148]. The study showed that the hydrophobically end-modified shell-forming blocks form two types of conformations: A major part of the chains are quite stretched and their ends are relatively far from the core-shell interface, which is reminiscent of the behavior of untagged chains. However, a minor fraction of the chains form fairly collapsed recoiled conformations and the tagged ends come very close to the core-shell interface, i.e., the distribution of distances of the tags from the core-shell interface is bimodal (see Fig. 10).

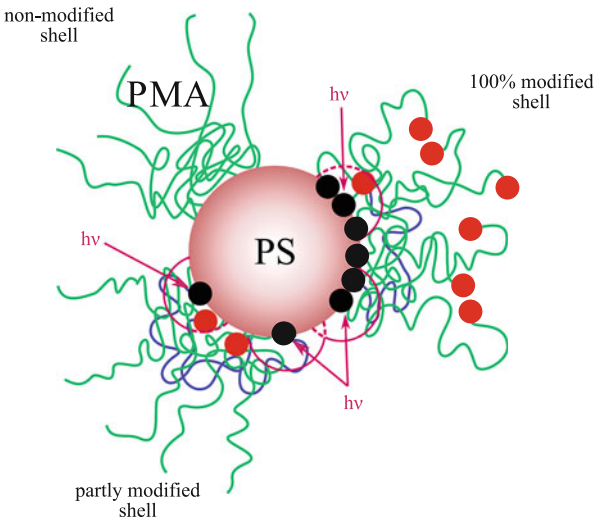

Fig. 10 Schematic structure of the hydrophobically modified polystyrene-block-poly(methacrylic acid), PS-PMAA, micelles in aqueous media. *Right*-hand part: 100 % modified shell, *upper left*-hand part: non-modified shell, *bottom left*-hand part: partially modified shell (mixed micelles containing both the modified and non-modified PMMA blocks), *black circles*: excitation energy donor (naphthalene), *red circles*: excitation energy trap (anthracene), *green curves*: stretched PMMA blocks, *blue curves*: collapsed (recoiled) PMMA blocks, and *dashed red semicircles*: the volume around the excited energy donor delimited by the Förster radius. Note that the PMAA shell is in all cases strongly inhomogeneous. It contains a compact inner layer formed by relatively collapsed non-dissociated parts of PMAA chains, and a diffuse peripheric layer formed by fairly stretched ionized parts of chains

In the double-tagged system with energy donors in between the blocks, this special bimodal radial distribution of traps means that a certain fraction of the excited donors are not quenched by NRET, but another fraction is affected very strongly. Experimentally, this is manifested by a very broken plot of the ratio $F_{DA}(t)/F_D(t)$ vs. time t, where $F_{DA}(t)$ is the fluorescence from the double-tagged micelles and $F_D(t)$ is the decay measured in a virtually identical micellar system formed by chains of almost the same length of both blocks tagged only by naphthalene in between the blocks (see Fig 11). Simulations have shown that the strongly "broken-like" curves cannot be obtained for systems with continuous distributions of donor-to-trap distances [177, 178]. In systems formed by an excess of pure PE (i.e., untagged) chains with a small admixture of end-tagged ones, all the tagged chains collapse and the fluorophores (anthracene) come close to the energy donors (naphthalene) embedded in the core-shell interface. This is manifested by very strong naphthalene quenching and strong anthracene emission (if naphthalene is excited). The pure PE chains are stretched and compensate the entropy decrease due to the collapse of the tagged chains. This finding suggests that, if some functional groups that are attached to the real medically applicable drug delivery systems were less polar than the stabilizing chains, they could hide in the shell and thus lose their biological activity.

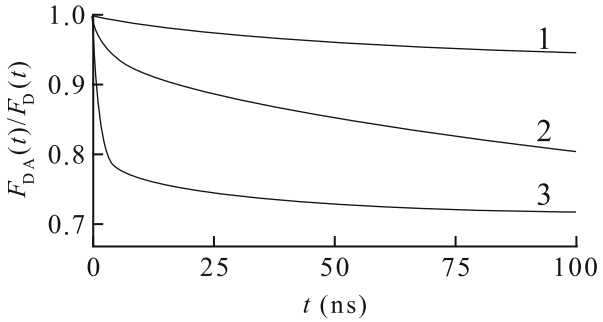

Fig. 11 Relative fluorescence decays of naphthalene tags. $F_{DA}(t)/F_D(t)$ vs. time t. $F_{DA}(t)$ is the fluorescence from the double-tagged micelles and $F_D(t)$ is the decay measured in a virtually identical micellar system formed by chains of almost the same length of both blocks tagged only by naphthalene in between the blocks in a 1,4-dioxane–water mixtures with 5, 20, and 100 vol % water, respectively (*curves 1*, *2*, and *3*). Adapted with permission from Macromolecules 35, 2002, 9497–9505, figure 7, [178]. Copyright 2002. American Chemical Society

A number of experimental fluorescence studies of specific self-assembling copolymer systems will be described in the next chapter.

8 Comments of Fluorescence Studies of π-Conjugated Polymers

Conjugated polymers (CPs) have attracted the interest of scientists for several decades, because they are promising materials for manufacturing (opto)electronic devices, such as light-emitting diodes [181], chemical sensors [182], solar cells [183], and field-effect transistors [184]. Even though silicon-based materials still predominate in the mass production of electronic devices, recent advances in research on organic polymer (opto)electroactive materials revealed a number of promising properties which promote the gradual replacement of traditional materials by CPs. Moreover, CPs are flexible materials with low specific density and are easy to process compared to the silicon compounds used so far. Last but not least, a number of chemically different CPs can be synthesized and their properties can be tuned by targeted modification of their covalent and configurational structures. The performance of CP-based devices, which are usually produced in the form of thin active layers, depends on a number of factors, i.e., not only on the energy band gap, but also on chain conformations, on mutual arrangement of neighboring chains in the film, and on chain mobility, which influence the charge transport and fluorescence properties, etc. While measurement of the functional properties of thin films (thermomechanical properties, electric conductivity, spectra, etc.) is easy and straightforward, the relationship between the functional properties and the structures of these materials is complex, its investigation is difficult, and its understanding is still limited. The complex behavior of CPs is caused by several inherent

features related to delocalization of the π electrons. Efficient π-conjugation, which is the prerequisite for successful applications of CPs, assumes the parallel alignment of p_z orbitals in neighboring sp^2-hybridized C atoms within the polymer chain. Extensive delocalization of π electrons can be achieved only for specific chain conformations, which implies that the conformational variability of well-conjugated sequences in the CP chains is restricted. In summary, the configuration rigidity of double bonds together with a fairly restricted rotation around single bonds (which partly adopt double bond character due to delocalization of the π electrons) and energetic stabilization of the conformations with delocalized electrons results in the formation of rigid conjugated segments which are responsible for the fluorescence of CP materials because they behave as individual fluorophores. They are connected by structurally distorted short units that can be regarded as structural defects. Hence, the conjugated polymers are structurally diverse in their very nature, but their chains are relatively stiff, which results in (1) limited solubility and (2) a high tendency toward aggregation, which strongly hinders the study of the structure–property relationship at the level of single molecules. Conventional spectroscopic methods applied to bulk polymer materials or to their dilute solutions provide information on the ensemble-average properties, i.e., on the properties of systems containing different arrangements of single chains and their aggregates, and the analysis and interpretation of spectroscopic characteristics are difficult. The fluorescence data are furthermore affected by the very efficient intra- and intermolecular nonradiative resonance energy transfer from the high-energy states to the low-energy states. An unambiguous interpretation of the relationship between the fluorescence and structural characteristics at the molecular level is almost impossible because, in condensed systems of chains differing in conformations and in interactions with the microenvironment, there are different energy transfer routes from the high- to low-energy states which funnel the excitation energy efficiently and very rapidly to low-energy states before the emission occurs.

In the case of polyacetylene (PA), which is an archetype of CPs, there are four stable (low-energy) stereoconformations of parts of PA chains: trans-transoid, trans-cisoid, cis-transoid, and cis-cisoid; see Fig. 12 (the first and second parts of the stereo-descriptor refer to the configuration/conformation of the double and single bonds, respectively). As already explained, only very short parts of the chains acquire regular conformations, and the effective conjugation length (the number of conjugated double bonds in stretched conformations), which affects the electric and luminescence properties, is quite short (for PA it is a part of the chain containing ca. 10 double bonds). The structural defects are usually created randomly during the synthesis, and the distribution of conjugation lengths is broad. The structure of the CP chains can be also affected by the post-synthetic processing. While the isomerization of the double bond requires high energy (i.e., photonic [185, 186] or ultrasonic irradiation [187] is needed to provoke the change), the conformations of single bonds can be manipulated quite easily by various external stimuli, such as the pH, temperature, additives, etc. [188], which enables tuning of the properties and optimizing the performance of developed devices.

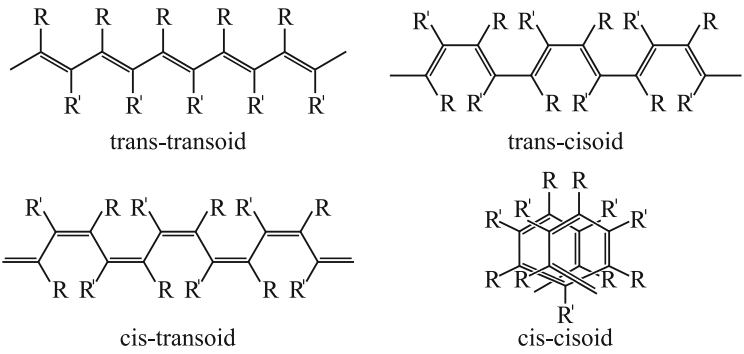

Fig. 12 Possible stereoconformations of polyacetylene chains

Even though the PA-based polymers are classical model CP polymers, very little work has been done on the development of light-emitting PAs because of the low emission quantum yield of the unsubstituted PA, its low conductivity, and its low solubility. Nevertheless, Tang et al., Masuda et al., and others [188–193] extensively studied the potential for improving the functional properties by attaching various pendant groups with different electronic and steric effects to the PA chain (both fully organic and hybrid organic–inorganic, e.g., containing Si atoms) and proposed a number of reasonable light-emitting systems, particularly of the poly (di-substituted acetylene) type [188, 194–204]. It was shown that, e.g., the bi-substitution of hydrogen atoms in PA by bulky aromatic substituents (by phenyl and simultaneously by biphenylyl bearing other groups) causes significant twisting and stabilization of twisted chain conformations, which shortens the conjugation length, increases the band gap, and shifts the infrared emission of the unsubstituted PA to the visible region. The energy transfer from the absorbing pendant groups to the π-conjugated skeleton increases the emission yield of the skeleton and the di-substituted PAs exhibit strong green or blue fluorescence (as seen in Fig. 13).

Systematic studies have shown that very efficient fluorescence-emitting materials can be prepared by the attachment of pendant silole rings to the PA skeleton [205]. If, e.g., pentaphenyl-silole, PPS, which itself strongly emits green light, is attached directly to an unsubstituted PA which, as already mentioned, is a weak red emitter, the efficient fluorescence resonant energy transfer (FRET) from excited pendant groups to the skeleton induces fairly strong red emission from the conjugated part of the skeleton (Fig. 13). However, if PPS is attached via oxygen to the aliphatic substituent of poly(1-phenyl-2-nonylacetylene), which is itself a strong blue emitter, the FRET from the skeleton to the pendant groups produces strong green emission (Fig. 13). This is a nice example showing that different types of substitution of PA chains not only shift the emission wavelength and emission yield but can also reverse the direction of energy transfer.

As the ultimate use of CPs in (opto)electronic devices requires detailed knowledge of their UV–vis absorption and emission characteristics, it is not surprising

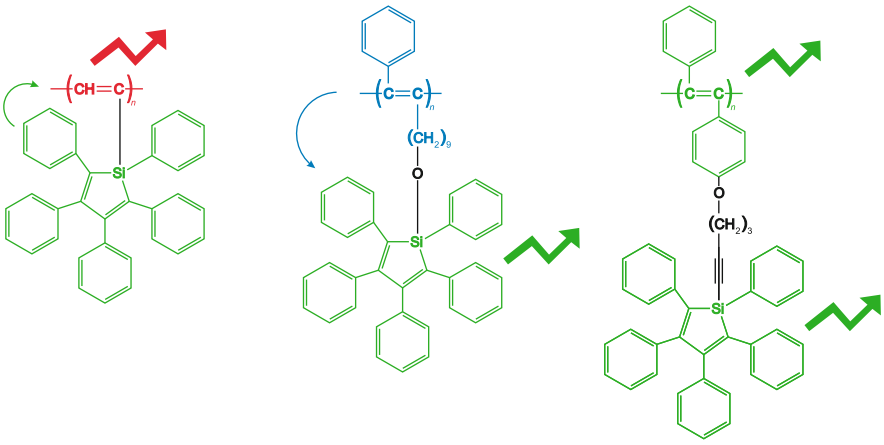

Fig. 13 Excitation energy transfer and luminescence from substituted polyacetylenes. In the first case, the silole ring absorption followed by the energy transfer (*thin curved arrow*) to PA chain results in a fairly strong red emission (*bold broken arrow*), while the PA absorption and consequent energy transfer from PA to the pendant silole ring results in a strong green emission. Reprinted with permission from Chem. Rev. 109, 2009, 5799–5867, chart 9, [193]. Copyright 2009. American Chemical Society

that large numbers of spectroscopic studies have been devoted to various π-conjugated polymers. It is not our ambition to present an exhaustive list here or to give a detailed discussion of all the studies that have been performed. A number of excellent original and review articles have been published on this subject [206–213]. We would like to highlight modern trends in research on the relationship between the structure and functional properties of CPs. We will concentrate on the role of chain conformations and on the intricate interplay of intra- versus interchain energy transfer and will give a few examples of studies of CP materials suitable for the design of organic emitting diodes (OLEDs), e.g., polythiophene, poly(phenylene-vinylene), or polyfluorene derivatives. In particular, we would like to outline recent advances in single-molecule spectroscopy (SMS), which were made possible by the development of sensitive fluorescence techniques.

Single-molecule spectroscopy monitors and analyses the spectroscopic signal from single molecules. It was successfully developed in several spectroscopic areas and concerns methods whose inherent sensitivity enables the study of very dilute systems—these include especially surface-enhanced Raman scattering (SERS) and fluorescence spectroscopy. Two basic variants exist for fluorescence SMS: (1) SMS of static systems, which will be described in more detail later, and (2) SMS of flowing systems, which comprises several approaches also including fluorescence correlation spectroscopy (FCS). The general prerequisite of SMS measurements is the ability to monitor and analyze fairly low fluorescence signals from very small and well-focused volumes with sufficient accuracy. As a matter of fact, sensitivity is not the main problem. At first, single photon counting is a sensitive detection method. Then, the fluorescent molecule with a lifetime of several ns, passing the

laser beam in times of about 1 ms in flowing systems, will be excited many times (theoretically up to 10^6 times). As the most photostable compounds decompose before the absorption of 10^5 photons [210], usually only 10^1–10^3 photons can be detected in various systems, but these numbers of photons are sufficient for sensitive detection. However, the background noise due to traces of fluorescent impurities in the solvent and to other disturbing effects, such as possible reflections and Rayleigh and Raman scattering, is the main problem. Several ways of reducing the noise have been developed for flow systems, e.g., solvent photobleaching before mixing with the studied sample [214]. Because the noise mostly comes from excess solvent, the most important condition is to ensure detection of the signal from the smallest possible volume. Four different approaches to small detection volumes in flow systems are listed below: (1) a hydrodynamically focused stream of the sample solution crossing the narrowly focused laser beams (volumes of ca.10 μm x 10 μm x 10 μm, i.e., ca. 1 pL) [215, 216], (2) levitated or slowly falling microdroplets crossing the excitation laser beam (volumes of ca. 1 fL to 1 pL) [217, 218], (3) microcapillaries and microchannels crossed by the laser beam (volumes ca. 1 fL to 1 pL) [219], and (4) confocal (one or two photon) excitation and detection (volumes of ca. 1 fL) [220]. FCS is a special variant of the latter technique, but it will not be treated in this part because another chapter is devoted to the application of FCS for polymers. When referring to SMS in the following parts of this chapter, we will always be referring to the static SMS variant. The principles and all the details of the above SMS variants were recently nicely described in an interesting review by Keller et al. [210].

Successful static SMS measurement assumes wide field illumination of a thin polymer film combined with sensitive single photon counting detection from highly spatially resolved areas of ca. 0.1 μm^2. Solutions of the studied polymers are usually diluted to the nanomolar region and spin cast on a solid support. The measurements are performed either at ultralow temperatures (to suppress the noise) or at ambient temperatures. The active polymers can be mixed with an excess of an inert polymer or covered by a thin layer of transparent inert polymer to suppress undesirable effects [207]. In all SMS studies, it is first necessary to answer the important question of whether or not the analyzed signal comes from single molecules. The criterion for answering this key question can be based on several observations. From a practical point of view, the following physical features of the system should be fulfilled: (1) the brightness of all the individual (randomly distributed) emitting spots in the microscope image of the studied surface area with deposited molecules should be approximately the same, (2) the polarized excitation and emission images should indicate that the individual emitting spots are characterized by fixed transition absorption and emission dipole moments, and (iii) all the individual spots should exhibit discrete and mutually independent photochemistry. The third criterion is obvious for small single molecules, but for CPs the spectroscopic behavior depends on how efficiently the fluorophores are coupled—not only in individual chains, but also in the bulk material. The above criterion provides a useful practical guide, but ultimate proof requires a more sophisticated measurement based on the fact that (iv) a single molecule emits only one photon which can be registered by

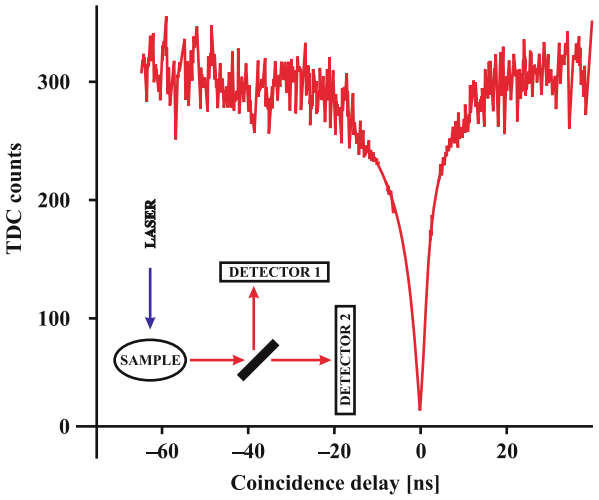

Fig. 14 Single-molecule spectroscopy detection. The proof that the measured signal comes from one molecule is based on the fact that the time-correlated simultaneous detection of two photons by two mutually delayed detectors drops to zero when the time delay vanishes. Adapted from Adv. Mater. 22, 2010, 1689–1721, figure 3, [207]. Copyright 2010. Wiley-VCH Verlag Gmbh

only one detector at any given time. Therefore, the most frequently used method employs two time-correlated detectors. The measured signal is divided by a 50–50 % beam splitter and the coincidence rate of the simultaneous detection of two photons is measured as a function of the delay time between the two detectors. When the delay time is zero, the probability of double detection drops to zero and the coincidence rate should also be zero, to prove that the signal is monitored from a single molecule (see Fig. 14).

The first applications of SMS for CPs were reported by Barbara et al. in 1996–1997. The group of researchers from the University of Minnesota and MIT (originally also from the Ohio State University) studied high-molar-mass poly (p-pyridyl vinylene) [221] and later also derivatized poly(p-phenylene vinylene)-poly(pyridyl vinylene) CP samples [222] by fluorometry using near-field optical microscopy (NFOM) for resolving the single emitting spots in a film spin cast from very dilute solutions. They observed that the spectra, quantum yields, and time-resolved characteristics of the individual emitting spots (which they persuasively identified as individual chains) significantly differ from the ensemble-averaged characteristics measured in solutions. Later they found considerable dynamic (time-dependent) fluctuations in the fluorescence intensity at the single-molecule level manifested by sudden reversible photobleaching steps. When analyzing the origin and mechanism of these fluctuations, Barbara and coworkers realized that the fluorescence intensity at the single-molecule level should be theoretically proportional to the product of the probabilities of the absorption and emission. Therefore, they investigated the role of factors that can decisively affect these two probabilities. They focused on (1) the excitation power, (2) the relative orientation of the absorption transition dipole moment to the polarization plane of the excitation beam, (3) the absorption cross section, and (4) the fluorescence quantum yield and concluded that none of them causes the observed fluctuations. In this seminal study, they revealed the true source of the fluctuations and actually explained the

inherently low photoluminescence efficiency of CPs. At that time, the fluctuating intensity of fluorescent molecules was usually attributed to spectral diffusion [223], which is a common phenomenon in SMS and the probable reason for this behavior in many systems. It originates from the fact that the single-molecule spectrum is not the ensemble-average spectrum from a large system of fluorophores. Each individual molecule is submitted to different instantaneous interactions with its temporally changing microenvironment and the position of the SMS spectral bands (which are usually quite narrow compared with the ensemble-average spectra) fluctuates non-negligibly on the wavelength scale. The fluctuations are rapid and proceed on a sub-nanosecond timescale. If the fluorophore is excited at a fixed wavelength, the fluctuations of the absorption band position on the wavelength scale (due to spectral diffusion) affect the probability of the absorption at different times and cause fast fluctuations in the emission intensity. Barbara and coworkers designed an ingenious experiment and showed that the discrete jump-like fluctuations in the emission intensity are not due to spectral diffusion. Realizing that, for spectral diffusion, the time fluctuations in the blue-edge- and red-edge-excited spectra should be complementary because spectral shifts to shorter wavelengths increase the emission intensity of the blue-edge excited spectra and shifts to longer wavelengths increase intensity of the red-edge excited spectra, they performed simultaneous time-dependent measurements and analyzed the corresponding emission signals. They found that the blue-edge- and red-edge-excited signals were not complementary, but virtually identical, which completely rules out spectral diffusion and shows that the fluctuations have some other cause. Carefully analyzing other potential sources of intensity fluctuations, they came to the conclusion that the discrete jumps in the fluorescence intensity are caused by the reversible photochemical generation of defects along the polymer chain, such as pairs of separated charges, i.e., cation radicals and anion radicals. The pronounced discrete jumps in the intensity suggest that the exciton is very mobile and the subset of individual fluorophores within the chain behaves as one communicating species; in other words: the migration of the excitation energy is rapid and efficient and the excitons can collide with the quenching defects on a timescale much shorter than the fluorescence lifetime. The jumps from the "dark regime" to the emitting one indicate that the defects can spontaneously "self-heal" and disappear.

The discovery that the excitation is very mobile and fluctuates within the macromolecular chain and that it can be sensitively and reversibly influenced by tiny changes in the structure represented a breakthrough in the research on and understanding of the function of PCs at the molecular level, but its impact was practically not noticed by the scientific community; in fact, it took several years before other researchers appreciated its value in its entirety and employed its conclusions in their further research.

Since the beginning of this century, Barbara and his coworkers [224, 225] and later also his younger colleagues and successors [226–229] have been developing and optimizing SMS and have published a number of articles on CPs. Paul F. Barbara unfortunately died at a relatively young age in 2010, but, in tribute to his contribution, his younger colleagues, who continue in his research, consider him

to be the inventor and founder of the research route they pursue and still include his name in the list of authors. Recent papers focus on different problems: they study the effect of the structure of the polymer chain, its regioregularity, effect of pendant groups, and the role of the solvent from which the thin film has been spin cast [209] on the rate and efficiency of the excitation energy transfer from high- to low-energy regions. The studies show that very efficient 3D exciton funneling from high- to low-energy regions proceeds in collapsed disordered chains [213], which effectively behave as single fluorophore systems, while the extended (either regioregular or intentionally stiffened ladder-type polymers) [208] behave as multichromophore systems. Excitation energy transfer is significantly slower in latter systems, but occurs over fairly long distances. Studies of the relationship between single chain structures (including the bending of fluorophores [230] and their mutual orientation [231]) and the optoelectronic properties of CPs are very relevant topics with respect to the contents of this issue, but we will confine ourselves to mentioning the excellent reviews by Lupton in Advanced Materials in 2010 and by others [206, 207, 210, 222].

Acknowledgment This work was supported by the Czech Science Foundation (Grants P106-12-0143). The authors would like to thank Lucie Suchá and Karel Šindelka for their help with graphics.

References

1. Forster T (1959) 10th spiers memorial lecture—transfer mechanisms of electronic excitation. Discuss Faraday Soc 27:7–17
2. Van Der Meer W, Coker G, Chen S-YS (1994) Resonance energy transfer: theory and data. VCH, New York
3. Haan SW, Zwanzig R (1978) Forster migration of electronic excitation between randomly distributed molecules. J Chem Phys 68(4):1879–1883. doi:10.1063/1.435913
4. Mendelsohn AS, Delacruz MO, Torkelson JM (1993) Correlations in polymer melts and solutions as investigated by fluorescence nonradiative energy-transfer—a novel comparison of theory to experiment by fluorescence intensity decay measurements. Macromolecules 26 (25):6789–6799. doi:10.1021/ma00077a015
5. Fredrickson GH (1986) Intermolecular correlation-functions from Forster energy-transfer experiments. Macromolecules 19(2):441–447. doi:10.1021/ma00156a035
6. de Gennes PG, Pincus PA (1970) Pair correlations in a ferromagnetic colloid. Physik Der Kondensiterten Materie 11(3):189–198
7. Chen CT, Morawetz H (1989) Characterization of polymer miscibility by fluorescence techniques—blends of styrene copolymers carrying hydrogen-bond donors with polymethacrylates. Macromolecules 22(1):159–164. doi:10.1021/ma00191a031
8. Morawetz H (1999) On the versatility of fluorescence techniques in polymer research. J Polym Sci Part A Polym Chem 37(12):1725–1735. doi:10.1002/(sici)1099-0518(19990615)37:12<1725::aid-pola1>3.0.co;2-d
9. Baumann J, Fayer MD (1986) Excitation transfer in disordered two-dimensional and anisotropic 3-dimensional systems—effects of spatial geometry on time-resolved observables. J Chem Phys 85(7):4087–4107. doi:10.1063/1.450880
10. Ediger MD, Fayer MD (1983) Electronic excited-state transport among molecules distributed randomly in a finite volume. J Chem Phys 78(5):2518–2524. doi:10.1063/1.445003

11. Ediger MD, Fayer MD (1983) New approach to probing polymer and polymer blend structure using electronic excitation transport. Macromolecules 16(12):1839–1844. doi:10.1021/ma00246a008
12. Hussey DM, Fayer MD (1999) Phase separation in binary and ternary polymer composites studied with electronic excitation transport. Macromolecules 32(20):6638–6645. doi:10.1021/ma9904114
13. Keller L, Hussey DM, Fayer MD (1996) Calculations of electronic excitation transfer: applications to ordered phases in polymeric materials. J Phys Chem 100(24):10257–10264. doi:10.1021/jp953710d
14. Marcus AH, Fayer MD (1991) Electronic excitation transfer in clustered chromophore systems—calculation of time-resolved observables for intercluster transfer. J Chem Phys 94(8):5622–5630. doi:10.1063/1.460498
15. Farinha JPS, Martinho JMG, Yekta A, Winnik MA (1995) Direct nonradiative energy-transfer in polymer interphases—fluorescence decay functions from concentration profiles generated by Fickian diffusion. Macromolecules 28(18):6084–6088. doi:10.1021/ma00122a013
16. Blumen A, Manz J (1979) Concentration and time-dependence of the energy-transfer to randomly distributed acceptors. J Chem Phys 71(11):4694–4702. doi:10.1063/1.438253
17. Blumen A, Klafter J, Zumofen G (1986) Influence of restricted geometries on the direct energy-transfer. J Chem Phys 84(3):1397–1401. doi:10.1063/1.450481
18. Blumen A (1980) Direct energy-transfer via exchange to randomly distributed acceptors. J Chem Phys 72(4):2632–2640. doi:10.1063/1.439408
19. Klafter J, Silbey R (1980) Electronic-energy transfer in disordered-systems. J Chem Phys 72(2):843–848. doi:10.1063/1.439236
20. Tomba JP, Ye X, Li F, Winnik MA, Lau W (2008) Polymer blend latex films: miscibility and polymer diffusion studied by energy transfer. Polymer 49(8):2055–2064. doi:10.1016/j.polymer.2008.02.024
21. Spiro JG, Farinha JPS, Winnik MA (2003) Thermodynamics and morphology of latex blend films. Macromolecules 36(20):7791–7802. doi:10.1021/ma021579j
22. Pham HH, Farinha JPS, Winnik MA (2000) Cross-linking, miscibility, and interface structure in blends of poly(2-ethylhexyl methacrylate) copolymers. An energy transfer study. Macromolecules 33(16):5850–5862. doi:10.1021/ma991832o
23. Feng JR, Yekta A, Winnik MA (1996) Direct non-radiative energy transfer across a sharp polymer interface. Chem Phys Lett 260(1–2):296–301. doi:10.1016/0009-2614(96)00853-6
24. Anghel DF, Toca-Herrera JL, Winnik FM, Rettig W, von Klitzing R (2002) Steady-state fluorescence investigation of pyrene-labeled poly(acrylic acid)s in aqueous solution and in the presence of sodium dodecyl sulfate. Langmuir 18(14):5600–5606. doi:10.1021/la011827p
25. Klafter J, Blumen A (1984) Fractal behavior in trapping and reaction. J Chem Phys 80(2):875–877. doi:10.1063/1.446743
26. Blumen A, Klafter J, Silbey R (1980) Theoretical-studies of energy-transfer in disordered condensed media. J Chem Phys 72(10):5320–5332. doi:10.1063/1.439023
27. Gochanour CR, Fayer MD (1981) Electronic excited-state transport in random-systems—time-resolved fluorescence depolarization measurements. J Phys Chem 85(14):1989–1994. doi:10.1021/j150614a008
28. Ni SR, Zhang P, Wang YC, Winnik MA (1994) Energy-transfer studies of the boundary-layer interphase in polystyrene poly(methyl methacrylate) block-copolymer films. Macromolecules 27(20):5742–5750. doi:10.1021/ma00098a031
29. Liu YS, Li L, Ni SR, Winnik MA (1993) Recovery of acceptor concentration distribution in a direct energy-transfer experiment. Chem Phys 177(3):579–589
30. Yekta A, Winnik MA, Farinha JPS, Martinho JMG (1997) Dipole–dipole electronic energy transfer. Fluorescence decay functions for arbitrary distributions of donors and acceptors.

2. Systems with spherical symmetry. J Phys Chem A 101(10):1787–1792. doi:10.1021/jp9633963
31. Dhinojwala A, Wong GK, Torkelson JM (1992) Quantitative-analysis of rotational-dynamics in doped polymers above and below the glass-transition temperature—a novel application of 2nd-order nonlinear optics. Macromolecules 25(26):7395–7397. doi:10.1021/ma00052a050
32. Dhinojwala A, Torkelson JM (1994) A reconsideration of the measurement of polymer interdiffusion by fluorescence nonradiative energy-transfer. Macromolecules 27 (17):4817–4824. doi:10.1021/ma00095a024
33. Bodunov EN, Berberan-Santos MN, Martinho JMG (2002) Electronic energy transfer in polymers labeled at both ends with fluorescent groups. J Lumin 96(2–4):269–278. doi:10.1016/s0022-2313(01)00227-7
34. Bodunov EN, Berberan-Santos MN, Martinho JMG (2001) Electronic energy transfer in linear polymers randomly labelled with chromophores. Chem Phys 274(2–3):243–253. doi:10.1016/s0301-0104(01)00545-6
35. Frank CW, Harrah LA (1974) Excimer formation in vinyl-polymers. 2. Rigid solutions of poly(2-vinylnaphthalene) and polystyrene. J Chem Phys 61(4):1526–1541. doi:10.1063/1.1682097
36. Frank CW (1974) Excimer formation in vinyl-polymers. 3. Fluid and rigid solutions of poly (4-vinylbiphenyl). J Chem Phys 61(5):2015–2022. doi:10.1063/1.1682204
37. Frank CW (1975) Observation of relaxation processes near glass-transition by means of excimer fluorescence. Macromolecules 8(3):305–310. doi:10.1021/ma60045a012
38. Frank CW, Gashgari MA (1979) Excimer fluorescence as a molecular probe of polymer blend compatibility. 1. Blends of poly(2-vinylnaphthalene) with poly(alkyl methacrylates). Macromolecules 12(1):163–165. doi:10.1021/ma60067a038
39. Frank CW, Gashgari M-A, Chutikamontham P, Haverly VJ (1980) Excimer fluorescence as a molecular probe of polymer blend compatibility II. The effect of concentration on blends of aromatic vinyl polymers with poly (alkylmethacrylates). In: Structure and properties of amorphous polymers: proceedings of the second Cleveland symposium on macromolecules, Elsevier, Cleveland, OH, 31 October–2 November 1978, p 187
40. Semerak SN, Frank CW (1981) Excimer fluorescence as a molecular probe of blend miscibility. 3. Effect of molecular-weight of the host matrix. Macromolecules 14(2):443–449. doi:10.1021/ma50003a039
41. Gashgari MA, Frank CW (1981) Excimer fluorescence as a molecular probe of blend miscibility. 4. Effect of temperature in solvent casting. Macromolecules 14(5):1558–1567. doi:10.1021/ma50006a081
42. Gelles R, Frank CW (1982) Energy migration in the aromatic vinyl-polymers. 2. Miscible blends of polystyrene with polyvinyl methyl-ether). Macromolecules 15(3):741–747. doi:10.1021/ma00231a012
43. Gelles R, Frank CW (1982) Energy migration in the aromatic vinyl-polymers. 3. - 3-dimensional migration in polystyrene polyvinyl methyl-ether). Macromolecules 15 (3):747–752. doi:10.1021/ma00231a013
44. Semerak SN, Frank CW (1983) Excimer fluorescence as a molecular probe of blend miscibility—comparison with differential scanning calorimetry. Adv Chem Ser 203:757–771
45. Semerak SN, Frank CW (1984) Excimer fluorescence as a molecular probe of polymer blend miscibility. 6. Effect of molecular-weight in blends of poly(2-vinylnaphthalene) with poly (methyl methacrylate). Macromolecules 17(6):1148–1157. doi:10.1021/ma00136a008
46. Thomas JW, Frank CW (1985) Energy migration in the aromatic vinyl-polymers. 4. Blends of poly(2-vinylnaphthalene) with poly(cyclohexyl methacrylate). Macromolecules 18 (5):1034–1039. doi:10.1021/ma00147a039
47. Kiserow D, Prochazka K, Ramireddy C, Tuzar Z, Munk P, Webber SE (1992) Fluorometric and quasi-elastic light-scattering study of the solubilization of nonpolar low-molar mass compounds into water-soluble block-copolymer micelles. Macromolecules 25(1):461–469. doi:10.1021/ma00027a072

48. Prochazka K, Kiserow D, Ramireddy C, Tuzar Z, Munk P, Webber SE (1992) Time-resolved fluorescence studies of the chain dynamics of naphthalene-labeled polystyrene-block-poly (methacrylic acid) micelles in aqueous-media. Macromolecules 25(1):454–460. doi:10.1021/ma00027a071
49. Gashgari MA, Frank CW (1988) Excimer fluorescence as a molecular probe of polymer blend miscibility. 7. Nonequilibrium solvent casting effects in blends of poly(2-vinylnaphthalene) with poly(normal-butyl methacrylate) and poly(methyl methacrylate). Macromolecules 21 (9):2782–2790. doi:10.1021/ma00187a024
50. Tao WC, Frank CW (1990) Excimer fluorescence as a molecular probe of polymer blend miscibility. 9. Effects of guest concentration and annealing in blends of poly (2-vinylnaphthalene) with poly(cyclohexyl methacrylate). Macromolecules 23 (13):3275–3283. doi:10.1021/ma00215a013
51. Soutar I (1981) Studies of intramolecular excimer formation in synthetic polymers. Ann NY Acad Sci 366(1):24–34. doi:10.1111/j.1749-6632.1981.tb20743.x
52. Li XB, Winnik MA, Guillet JE (1983) A fluorescence method to determine the solubility parameters delta-h of soluble polymers at infinite dilution—cyclization dynamics of polymers. Macromolecules 16(6):992–995. doi:10.1021/ma00240a032
53. Ediger MD (1991) Time-resolved optical studies of local polymer dynamics. Annu Rev Phys Chem 42:225–250. doi:10.1146/annurev.physchem.42.1.225
54. Rouse PE (1953) A theory of the linear viscoelastic properties of dilute solutions of coiling polymers. J Chem Phys 21(7):1272–1280. doi:10.1063/1.1699180
55. Zimm BH (1956) Dynamics of polymer molecules in dilute solution—viscoelasticity, flow birefringence and dielectric loss. J Chem Phys 24(2):269–278. doi:10.1063/1.1742462
56. Glowinkowski S, Gisser DJ, Ediger MD (1990) C-13 nuclear-magnetic-resonance measurements of local segmental dynamics of polyisoprene in dilute-solution—nonlinear viscosity dependence. Macromolecules 23(14):3520–3530. doi:10.1021/ma00216a021
57. Pilar J, Labsky J, Marek A, Budil DE, Earle KA, Freed JH (2000) Segmental rotational diffusion of spin-labeled polystyrene in dilute toluene solution by 9 and 250 GHz ESR. Macromolecules 33(12):4438–4444. doi:10.1021/ma0002242
58. Pilar J, Labsky J (1991) EPR study of chain rotational-dynamics in dilute aqueous-solutions of spin-labeled poly(methacrylic acid) at different degrees of neutralization. Macromolecules 24(14):4188–4194. doi:10.1021/ma00014a036
59. Jones AA, Stockmayer WH (1977) Models for spin relaxation in dilute-solutions of randomly coiled polymers. J Polym Sci Part B Polym Phys 15(5):847–861. doi:10.1002/pol.1977.180150508
60. Verdier PH, Stockmayer WH (1962) Monte Carlo calculations on dynamics of polymers in dilute solution. J Chem Phys 36(1):227–235. doi:10.1063/1.1732301
61. Schatzki TF (1962) Statistical computation of distribution functions of dimensions of macromolecules. J Polym Sci 57(165):337–356. doi:10.1002/pol.1962.1205716526
62. Monnerie L, Geny F (1969) Monte-Carlo simulation of Brownian movement in a macromolecular chain. I. Description of model and simulation. J Chim Phys Phys Chim Biol 66 (10):1691
63. Valeur B, Jarry JP, Geny F (1975) Dynamics of macromolecular chains. 1. Theory of motions on a tetrahedral lattice. J Polym Sci Part B Poly Phys 13(4):667–674. doi:10.1002/pol.1975.180130401
64. Valeur B, Monnerie L, Jarry JP (1975) Dynamics of macromolecular chains. 2. Orientation relaxation generated by elementary 3-bond motions and notion of an independent kinetic segment. J Polym Sci Part B Polym Phys 13(4):675–682. doi:10.1002/pol.1975.180130402
65. Viovy JL, Monnerie L, Brochon JC (1983) Fluorescence polarization decay study of polymer dynamics—a critical discussion of models using synchrotron data. Macromolecules 16 (12):1845–1852. doi:10.1021/ma00246a009
66. Hall CK, Helfand E (1982) Conformational state relaxation in polymers—time-correlation functions. J Chem Phys 77(6):3275–3282. doi:10.1063/1.444204

67. Adolf DB, Ediger MD, Kitano T, Ito K (1992) Viscosity dependence of the local segmental dynamics of anthracene-labeled polyisoprene in dilute-solution. Macromolecules 25 (2):867–872. doi:10.1021/ma00028a055
68. Kramers HA (1940) Brownian motion in a field of force and the diffusion model of chemical reactions. Physica 7(4):8
69. Courtney SH, Fleming GR (1985) Photoisomerization of stilbene in low viscosity solvents—comparison of isolated and solvated molecules. J Chem Phys 83(1):215–222. doi:10.1063/1.449811
70. Velsko SP, Fleming GR (1982) Photochemical isomerization in solution—photophysics of diphenyl butadiene. J Chem Phys 76(7):3553–3562. doi:10.1063/1.443393
71. Grote RF, Hynes JT (1980) The stable states picture of chemical-reactions. 2. Rate constants for condensed and gas-phase reaction models. J Chem Phys 73(6):2715–2732. doi:10.1063/1.440485
72. Morris RL, Amelar S, Lodge TP (1988) Solvent friction in polymer-solutions and its relation to the high-frequency limiting viscosity. J Chem Phys 89(10):6523–6537. doi:10.1063/1.455372
73. von Meerwall ED, Amelar S, Smeltzly MA, Lodge TP (1989) Solvent and probe diffusion in Aroclor solutions of polystyrene, polybutadiene, and polyisoprene. Macromolecules 22 (1):295–304. doi:10.1021/ma00191a054
74. Fytas G, Rizos A, Floudas G, Lodge TP (1990) Solvent mobility in polystyrene Aroclor solutions by depolarized Rayleigh-scattering. J Chem Phys 93(7):5096–5104. doi:10.1063/1.459670
75. Rizos A, Fytas G, Lodge TP, Ngai KL (1991) Solvent rotational mobility in polystyrene Aroclor and polybutadiene Aroclor solutions. 2. A photon-correlation spectroscopic study. J Chem Phys 95(4):2980–2987. doi:10.1063/1.461800
76. Gisser DJ, Ediger MD (1992) Local polymer and solvent dynamics in Aroclor solutions—implications for solvent modification. Macromolecules 25(4):1284–1293. doi:10.1021/ma00030a013
77. Ngai KL, Rizos AK (1994) A connection between the modification of solvent dynamics by polymer in polymer-solutions and component dynamics in miscible polymer blends. Macromolecules 27(16):4493–4497. doi:10.1021/ma00094a010
78. Roland CM, Ngai KL (1991) Dynamic heterogeneity in a miscible polymer blend. Macromolecules 24(9):2261–2265. doi:10.1021/ma00009a021
79. Tanaka H, Yanagida T, Teramoto A, Fujita H (1967) Studies of concentrated polymer solutions by fluorescence polarization method. I. Polyethylene oxide in water. J Phys Chem 71(8):2416. doi:10.1021/j100867a005
80. Fujita H (1961) Free-volume model of diffusion in polymer solutions. Adv Polym Sci 3:1–47
81. Hyde PD, Ediger MD, Kitano T, Ito K (1989) Local segmental dynamics of polyisoprene in concentrated-solutions and in the bulk. Macromolecules 22(5):2253–2259. doi:10.1021/ma00195a044
82. Viovy JL, Monnerie L (1986) A study of local chain dynamics in concentrated polystyrene solutions using fluorescence anisotropy decay. Polymer 27(2):181–184. doi:10.1016/0032-3861(86)90323-x
83. Viovy JL, Frank CW, Monnerie L (1985) Fluorescence anisotropy decay studies of local polymer dynamics in the melt. 2. Labeled model compounds of variable chain-length. Macromolecules 18(12):2606–2613. doi:10.1021/ma00154a042
84. Viovy JL, Monnerie L, Merola F (1985) Fluorescence anisotropy decay studies of local polymer dynamics in the melt. 1. Labeled polybutadiene. Macromolecules 18(6):1130–1137. doi:10.1021/ma00148a014
85. Veissier V, Viovy JL, Monnerie L (1989) Local dynamics of cis-polyisoprene in dilute-solution and in the melt—a fluorescence anisotropy decay study. Polymer 30(7):1262–1268. doi:10.1016/0032-3861(89)90046-3

86. Rutherford H, Soutar I (1980) Phosphorescence studies of relaxation effects in bulk polymers. 2. Emission depolarization study of relaxation mechanisms in poly(methyl methacrylate). J Polym Sci Part B Polym Phys 18(5):1021–1034. doi:10.1002/pol.1980.180180509
87. Jarry JP, Monnerie L (1979) Fluorescence depolarization study of the glass-rubber relaxation in a polyisoprene. Macromolecules 12(5):927–932. doi:10.1021/ma60071a028
88. Queslel JP, Jarry JP, Monnerie L (1986) Stationary fluorescence depolarization study of mobility of rigid probes in bulk elastomers—motion of dimethylanthracene and 3 trans-diphenylpolyenes inserted in polyisoprene, polybutadiene and random butadiene-styrene copolymers. Polymer 27(8):1228–1234. doi:10.1016/0032-3861(86)90011-x
89. Fofana M, Veissier V, Viovy JL, Monnerie L (1989) Investigation of the mobility of poly-butadienes. 2. Fluorescence anisotropy decay of rod-like rigid probes. Polymer 30(1):51–57. doi:10.1016/0032-3861(89)90382-0
90. Fofana M, Veissier V, Viovy JL, Monnerie L, Johari GP (1988) Studies of the mobility of probes in poly(propylene oxide). 1. Fluorescence anisotropy decay. Polymer 29(2):245–250. doi:10.1016/0032-3861(88)90329-1
91. Hyde PD, Ediger MD (1989) Time-resolved optical study of the rotational mobility of small probe molecules in bulk polyisoprene. Macromolecules 22(3):1510–1512. doi:10.1021/ma00193a093
92. Hyde PD, Ediger MD (1990) Rotational-dynamics of anthracene and 9,10-dimethylanthracene in polyisoprene. J Chem Phys 92(2):1036–1044. doi:10.1063/1.458166
93. Katchalsky A (1951) Solutions of polyelectrolytes and mechanochemical systems. J Polym Sci 7(4):393–412. doi:10.1002/pol.1951.120070403
94. Crescenz V, Delben F, Quadrifo F (1972) Calorimetric investigation of poly(methacrylic acid) and poly(acrylic acid) in aqueous-solution. J Polym Sci Part A 2 Polym Phys 10 (2):357–368. doi:10.1002/pol.1972.160100215
95. Delben F, Quadrifo F, Crescenz V (1972) Enthalpy of dissociation of poly(methacrylic acid) in aqueous-solution. Eur Polym J 8(7):933–935. doi:10.1016/0014-3057(72)90054-7
96. Arnold R, Overbeek JTG (1950) The dissociation and specific viscosity of polymethacrylic acid. Recueil Des Travaux Chimiques Des Pays-Bas J R Neth Chem Soc 69(2):192–206
97. Bednar B, Morawetz H, Shafer JA (1984) Kinetics of the cooperative complex-formation and dissociation of poly(acrylic acid) and poly(oxyethylene). Macromolecules 17(8):1634–1636. doi:10.1021/ma00138a037
98. Bednar B, Li ZM, Huang YH, Chang LCP, Morawetz H (1985) Fluorescence study of factors affecting the complexation of poly(acrylic acid) with poly(oxyethylene). Macromolecules 18 (10):1829–1833. doi:10.1021/ma00152a007
99. Wang YC, Morawetz H (1986) Study of the equilibrium and the kinetics of the fluorescence enhancement on mixing solutions of auramine-o and poly(methacrylic acid). Macromolecules 19(7):1925–1930. doi:10.1021/ma00161a024
100. Horsky J, Morawetz H (1988) Kinetics of the conformational transition of poly(methacrylic acid) after a ph jump. 2. Studies of nonradiative energy-transfer. Makromol Chem-Macromol Chem Phys 189(10):2475–2483
101. Ghiggino K, Tan K, Phillips D (1985) Polymer photophysics. Chapman and Hall, London
102. Dobrynin AV, Rubinstein M, Obukhov SP (1996) Cascade of transitions of polyelectrolytes in poor solvents. Macromolecules 29(8):2974–2979. doi:10.1021/ma9507958
103. Limpouchova Z, Prochazka K, Fidler V, Dvorak J, Bednar B (1993) Molecular-movements and dynamics in solutions studied by fluorescence depolarization measurement. Collect Czech Chem Commun 58(2):213–233. doi:10.1135/cccc19930213
104. Bednar B, Trnena J, Svoboda P, Vajda S, Fidler V, Prochazka K (1991) Time-resolved fluorescence study of chain dynamics. 1. Poly(methacrylic acid) in dilute water solutions. Macromolecules 24(8):2054–2059. doi:10.1021/ma00008a053
105. Prochazka K, Limpouchova Z, Uhlik F, Kosovan P, Matejicek P, Stepanek M, Uchman M, Kuldova J, Sachl R, Humpolickova J, Hof M, Muller A, Borisov O (2011) Fluorescence spectroscopy as a tool for investigating the self-organized polyelectrolyte systems. Self

organized nanostructures of amphiphilic block copolymers I. 241:187–249. doi:10.1007/12_2010_5
106. Kosovan P, Limpouchova Z, Prochazka K (2006) Molecular dynamics simulation of time-resolved fluorescence anisotropy decays from labeled polyelectrolyte chains. Macromolecules 39(9):3458–3465. doi:10.1021/ma052557a
107. Soutar I, Swanson L (1994) Luminescence studies of polyelectrolyte behavior in solution. 3. Time-resolved fluorescence anisotropy measurements of the conformational behavior of poly(methacrylic acid) in dilute aqueous-solutions. Macromolecules 27(15):4304–4311. doi:10.1021/ma00093a035
108. Chee CK, Rimmer S, Shaw DA, Soutar I, Swanson L (2001) Manipulating the thermoresponsive behavior of poly(N-isopropylacrylamide). 1. On the conformational behavior of a series of N-isopropylacrylamide—styrene statistical copolymers. Macromolecules 34 (21):7544–7549. doi:10.1021/ma010360m
109. Barker IC, Cowie JMG, Huckerby TN, Shaw DA, Soutar I, Swanson L (2003) Studies of the "smart" thermoresponsive behavior of copolymers of N-isopropylacrylamide and N, N-dimethylacrylamide in dilute aqueous solution. Macromolecules 36(20):7765–7770. doi:10.1021/ma034250m
110. Chee CK, Rimmer S, Soutar I, Swanson L (2006) Fluorescence investigations of the conformational behaviour of poly(N-vinylcaprolactam). React Funct Polym 66(1):1–11. doi:10.1016/j.reactfunctpoplym.2005.07.007
111. Taylor LD, Cerankowski LD (1975) Preparation of films exhibiting a balanced temperature-dependence to permeation by aqueous-solutions—study of lower consolute behavior. J Polym Sci Part A Polym Chem 13(11):2551–2570. doi:10.1002/pol.1975.170131113
112. Schild HG (1992) Poly (n-isopropylacrylamide)—experiment, theory and application. Prog Polym Sci 17(2):163–249. doi:10.1016/0079-6700(92)90023-r
113. Feil H, Bae YH, Feijen J, Kim SW (1993) Effect of comonomer hydrophilicity and ionization on the lower critical solution temperature of n-isopropylacrylamide copolymers. Macromolecules 26(10):2496–2500. doi:10.1021/ma00062a016
114. Shibayama M, Mizutani S, Nomura S (1996) Thermal properties of copolymer gels containing N-isopropylacrylamide. Macromolecules 29(6):2019–2024. doi:10.1021/ma951390q
115. Prange MM, Hooper HH, Prausnitz JM (1989) Thermodynamics of aqueous systems containing hydrophilic polymers or gels. AlChE J 35(5):803–813. doi:10.1002/aic.690350511
116. Otake K, Inomata H, Konno M, Saito S (1990) Thermal-analysis of the volume phase-transition with n-isopropylacrylamide gels. Macromolecules 23(1):283–289. doi:10.1021/ma00203a049
117. Kubota K, Fujishige S, Ando I (1990) Single-chain transition of poly(n-isopropylacrylamide) in water. J Phys Chem 94(12):5154–5158. doi:10.1021/j100375a070
118. Inomata H, Goto S, Saito S (1990) Phase-transition of n-substituted acrylamide gels. Macromolecules 23(22):4887–4888. doi:10.1021/ma00224a023
119. Lin SY, Chen KS, Liang RC (1999) Thermal micro ATR/FT-IR spectroscopic system for quantitative study of the molecular structure of poly(N-isopropylacrylamide) in water. Polymer 40(10):2619–2624. doi:10.1016/s0032-3861(98)00512-6
120. Lin SY, Chen KS, Run-Chu L (1999) Drying methods affecting the particle sizes, phase transition, deswelling/reswelling processes and morphology of poly(N-isopropylacrylamide) microgel beads. Polymer 40(23):6307–6312. doi:10.1016/s0032-3861(98)00872-6
121. Yamamoto I, Iwasaki K, Hirotsu S (1989) Light-scattering study of condensation of poly (n-isopropylacrylamide) chain. J Phys Soc Jpn 58(1):210–215. doi:10.1143/jpsj.58.210
122. Wu C, Zhou SQ (1995) Thermodynamically stable globule state of a single poly (n-isopropylacrylamide) chain in water. Macromolecules 28(15):5388–5390. doi:10.1021/ma00119a036

123. Winnik FM (1990) Phase-transition of aqueous poly-(n-isopropylacrylamide) solutions—a study by nonradiative energy-transfer. Polymer 31(11):2125–2134. doi:10.1016/0032-3861(90)90085-d
124. Chee CK, Rimmer S, Soutar I, Swanson L (1997) Time-resolved fluorescence anisotropy studies of the temperature-induced intramolecular conformational transition of poly (N-isopropylacrylamide) in dilute aqueous solution. Polymer 38(2):483–486. doi:10.1016/s0032-3861(96)00636-2
125. Chee CK, Hunt BJ, Rimmer S, Soutar I, Swanson L (2011) Time-resolved fluorescence anisotropy studies of the cononsolvency of poly(N-isopropyl acrylamide) in mixtures of methanol and water. Soft Matter 7(3):1176–1184. doi:10.1039/c0sm00836b
126. Cowie JMG, Mohsin MA, McEwen IJ (1987) Alcohol water cosolvent systems for poly (methyl methacrylate). Polymer 28(9):1569–1572. doi:10.1016/0032-3861(87)90360-0
127. Winnik FM, Ringsdorf H, Venzmer J (1990) Methanol water as a co-nonsolvent system for poly(n-isopropylacrylamide). Macromolecules 23(8):2415–2416. doi:10.1021/ma00210a048
128. Tanaka F, Koga T, Kojima H, Winnik FA (2009) Temperature- and tension-induced coil-globule transition of poly(N-isopropylacrylamide) chains in water and mixed solvent of water/methanol. Macromolecules 42(4):1321–1330. doi:10.1021/ma801982e
129. Zhang GZ, Wu C (2001) The water/methanol complexation induced reentrant coil-to-globule-to-coil transition of individual homopolymer chains in extremely dilute solution. J Am Chem Soc 123(7):1376–1380. doi:10.1021/ja003889s
130. Chee CK, Rimmer S, Soutar I, Swanson L (2001) Fluorescence investigations of the thermally induced conformational transition of poly(N-isopropylacrylamide). Polymer 42 (12):5079–5087. doi:10.1016/s0032-3861(00)00821-1
131. Chee C-K, Hunt BJ, Rimmer S, Rutkaite R, Soutar I, Swanson L (2009) Manipulating the thermoresponsive behaviour of poly(N-isopropylacrylamide) 3. On the conformational behaviour of N-isopropylacrylamide graft copolymers. Soft Matter 5(19):3701–3712. doi:10.1039/b903356d
132. Riess G (2003) Micellization of block copolymers. Prog Polym Sci 28(7):1107–1170. doi:10.1016/s0079-6700(03)00015-7
133. Kabanov AV, Batrakova EV, Alakhov VY (2002) Pluronic (R) block copolymers as novel polymer therapeutics for drug and gene delivery. J Control Release 82(2–3):189–212. doi:10.1016/s0168-3659(02)00009-3
134. Hamley IW (2003) Nanotechnology with soft materials. Angew Chem Int Ed 42 (15):1692–1712. doi:10.1002/ange.200200546
135. Kwon GS, Kataoka K (2012) Block copolymer micelles as long-circulating drug vehicles. Adv Drug Deliv Rev 64:237–245. doi:10.1016/j.addr.2012.09.016
136. Matejicek P, Podhajecka K, Humpolickova J, Uhlik F, Jelinek K, Limpouchova Z, Prochazka K, Spirkova M (2004) Polyelectrolyte behavior of polystyrene-block-poly (methacrylic acid) micelles in aqueous solutions at low ionic strength. Macromolecules 37 (26):10141–10154. doi:10.1021/ma049258q
137. Plestil J, Kriz J, Tuzar Z, Prochazka K, Melnichenko YB, Wignall GD, Talingting MR, Munk P, Webber SE (2001) Small-angle neutron scattering study of onion-type micelles. Macromol Chem Phys 202(4):553–563. doi:10.1002/1521-3935(20010201)202:4<553::aid-macp553>3.0.co;2-6
138. Prochazka K, Glockner G, Hoff M, Tuzar Z (1984) Micellization of a radial copolymer with 4 polystyrene-block-polybutadiene branches. Makromol Chem-Macromol Chem Phys 185 (6):1187–1197
139. Uchman M, Stepanek M, Prochazka K, Mountrichas G, Pispas S, Voets IK, Walther A (2009) Multicompartment nanoparticles formed by a heparin-mimicking block terpolymer in aqueous solutions. Macromolecules 42(15):5605–5613. doi:10.1021/ma9008115
140. Wilhelm M, Zhao CL, Wang YC, Xu RL, Winnik MA, Mura JL, Riess G, Croucher MD (1991) Polymer micelle formation. 3. Poly(styrene-ethylene oxide) block copolymer micelle

formation in water—a fluorescence probe study. Macromolecules 24(5):1033–1040. doi:10.1021/ma00005a010
141. Prochazka K, Kiserow DJ, Webber SE (1995) Fluorescence polarization study of polymer micelles. Acta Polym 46(4):277–290. doi:10.1002/actp.1995.010460401
142. Stepanek M, Matejicek P, Humpolickova J, Prochazka K (2005) Reversible aggregation of polystyrene-block-poly(2-vinylpyridine)-block-poly(ethylene oxide) block copolymer micelles in acidic aqueous solutions. Langmuir 21(23):10783–10790. doi:10.1021/la0516680
143. Sachl R, Stepanek M, Prochazka K, Humpolickova J, Hof M (2008) Fluorescence study of the solvation of fluorescent probes prodan and laurdan in poly(epsilon-caprolactone)-block-poly (ethylene oxide) vesicles in aqueous solutions with tetrahydrofurane. Langmuir 24 (1):288–295. doi:10.1021/la702277t
144. Uchman M, Gradzielski M, Angelov B, Tosner Z, Oh J, Chang T, Stepanek M, Prochazka K (2013) Thermodynamic and kinetic aspects of coassembly of PEO-PMAA block copolymer and DPCl surfactants into ordered nanoparticles in aqueous solutions studied by ITC, NMR, and time-resolved SAXS techniques. Macromolecules 46(6):2172–2181. doi:10.1021/ma302503w
145. Kriz J (2012) Interaction of premicellar states of a PEO-PPO-PEO triblock copolymer with partially hydrophobic substances: NMR study. J Phys Chem B 116(14):4386–4393. doi:10.1021/jp3003323
146. Tuzar Z, Kadlec P, Stepanek P, Kriz J, Nallet F, Noirez L (2008) Micelles of a diblock copolymer of styrene and ethylene oxide in mixtures of 2,6-lutidine and water. Langmuir 24 (24):13863–13865. doi:10.1021/la803397g
147. Szajdzinska-Pietek E, Schlick S (2005) Self-assembling of ion-containing polymers and surfactants in aqueous solutions studied by ESR and fluorescence probes. J Mol Liq 117 (1–3):153–164. doi:10.1016/j.molliq.2004.08.007
148. Matejicek P, Humpolickova J, Prochazka K, Tuzar Z, Spirkova M, Hof M, Webber SE (2003) Hybrid block copolymer micelles with partly hydrophobically modified polyelectrolyte shells in polar and aqueous media: experimental study using fluorescence correlation spectroscopy, time-resolved fluorescence, light scattering, and atomic force microscopy. J Phys Chem B 107(32):8232–8240. doi:10.1021/jp022221s
149. Matejicek P, Stepanek M, Uchman M, Prochazka K, Spirkova M (2006) Atomic force microscopy and light scattering study of onion-type micelles formed by polystyrene-block-poly(2-vinylpyridine) and poly(2-vinylpyridine)-block-poly(ethylene oxide) copolymers in aqueous solutions. Collect Czech Chem Commun 71(5):723–738. doi:10.1135/cccc20060723
150. Tian MM, Qin AW, Ramireddy C, Webber SE, Munk P, Tuzar Z, Prochazka K (1993) Hybridization of block-copolymer micelles. Langmuir 9(7):1741–1748. doi:10.1021/la00031a022
151. Pacovska M, Prochazka K, Tuzar Z, Munk P (1993) Formation of block-copolymer micelles—a sedimentation study. Polymer 34(21):4585–4588. doi:10.1016/0032-3861(93)90171-6
152. Stepanek M, Podhajecka K, Tesarova E, Prochazka K, Tuzar Z, Brown W (2001) Hybrid polymeric micelles with hydrophobic cores and mixed polyelectrolyte/nonelectrolyte shells in aqueous media. 1. Preparation and basic characterization. Langmuir 17(14):4240–4244. doi:10.1021/la010246x
153. Podhajecka K, Stepanek M, Prochazka K, Brown W (2001) Hybrid polymeric micelles with hydrophobic cores and mixed polyelectrolyte/nonelectrolyte shells in aqueous media. 2. Studies of the shell behavior. Langmuir 17(14):4245–4250. doi:10.1021/la010247p
154. Matejicek P, Zednik J, Uselova K, Plestil J, Fanfrlik J, Nykanen A, Ruokolainen J, Hobza P, Prochazka K (2009) Stimuli-responsive nanoparticles based on interaction of metallacarborane with poly(ethylene oxide). Macromolecules 42(13):4829–4837. doi:10.1021/ma900484y

155. Humpolickova J, Prochazka K, Hof M, Tuzar Z, Spirkova M (2003) Fluorescence correlation spectroscopy using octadecylrhodamine B as a specific micelle-binding fluorescent tag; light scattering and tapping mode atomic force microscopy studies of amphiphilic water-soluble block copolymer micelles. Langmuir 19(10):4111–4119. doi:10.1021/la0209334
156. Gehlen MH, Deschryver FC (1993) Time-resolved fluorescence quenching in micellar assemblies. Chem Rev 93(1):199–221. doi:10.1021/cr00017a010
157. Van der Auweraer M, Roelants E, Verbeeck A, De Schryver F (1989) Fluorescence quenching in micellar solutions by charged and neutral quenchers. In: Mittal K (ed) Surfactants in solution. Springer, New York, pp 141–157
158. Winnik FM (1993) Photophysics of preassociated pyrenes in aqueous polymer-solutions and in other organized media. Chem Rev 93(2):587–614. doi:10.1021/cr00018a001
159. Yip J, Duhamel J, Qiu XP, Winnik FM (2011) Long-range polymer chain dynamics of pyrene-labeled poly(N-isopropylacrylamide)s studied by fluorescence. Macromolecules 44 (13):5363–5372. doi:10.1021/ma2007865
160. Duhamel J (2012) New insights in the study of pyrene excimer fluorescence to characterize macromolecules and their supramolecular assemblies in solution. Langmuir 28 (16):6527–6538. doi:10.1021/la2047646
161. Almgren M, Alsins J, Mukhtar E, Vanstam J (1988) Fluorescence quenching dynamics in rod like micelles. J Phys Chem 92(15):4479–4483. doi:10.1021/j100326a046
162. Bales BL, Almgren M (1995) Fluorescence quenching of pyrene by copper(ii) in sodium dodecyl-sulfate micelles—effect of micelle size as controlled by surfactant concentration. J Phys Chem 99(41):15153–15162. doi:10.1021/j100041a035
163. Ham JS (1953) A new electronic state in benzene. J Chem Phys 21(4):756–758. doi:10.1063/1.1699014
164. Prochazka K, Martin TJ, Munk P, Webber SE (1996) Polyelectrolyte poly(tert-butyl acrylate)-block-poly(2-vinylpyridine) micelles in aqueous media. Macromolecules 29 (20):6518–6525. doi:10.1021/ma960630e
165. Teng Y, Morrison ME, Munk P, Webber SE, Prochazka K (1998) Release kinetics studies of aromatic molecules into water from block polymer micelles. Macromolecules 31 (11):3578–3587. doi:10.1021/ma971721u
166. Stepanek M, Prochazka K (1999) Fluorometric studies of the polyelectrolyte shell of block copolymer micelles in aqueous media. Langmuir 15(26):8800–8806. doi:10.1021/la9903651
167. Stepanek M, Krijtova K, Prochazka K, Teng Y, Webber SE (1999) Interaction of fluorescent surfactant 5-(N-octadecanoyl)aminofluorescein with polystyrene-block-poly(methacrylic acid) micelles. Colloids Surf A Physicochem Eng Asp 147(1–2):79–87. doi:10.1016/s0927-7757(98)00742-0
168. Stepanek M, Krijtova K, Prochazka K, Teng Y, Webber SE, Munk P (1998) Solubilization and release of hydrophobic compounds from block copolymer micelles. I. Partitioning of pyrene between polyelectrolyte micelles and the aqueous phase. Acta Polym 49(2–3):96–102
169. Stepanek M, Krijtova K, Limpouchova Z, Prochazka K, Teng Y, Munk P, Webber S (1998) Solubilization and release of hydrophobic compounds from block copolymer micelles. II. Release of pyrene from polyelectrolyte micelles under equilibrium conditions. Acta Polym 49(2–3):103–107
170. Stepanek M, Humpolickova J, Prochazka K, Hof M, Tuzar Z, Spirkova M, Wolff T (2003) Light scattering, atomic force microscopy and fluorescence correlation spectroscopy studies of polystyrene-block-poly(2-vinylpyridine)-block-poly(ethylene oxide) micelles. Collect Czech Chem Commun 68(11):2120–2138. doi:10.1135/cccc20032120
171. Stepanek M, Matejicek P, Humpolickova J, Havrankova J, Podhajecka K, Spirkova M, Tuzar Z, Tsitsilianis C, Prochazka K (2005) New insights on the solution behavior and self-assembly of polystyrene/poly(2-vinylpyridine) 'hairy' heteroarm star copolymers with highly asymmetric arms in polar organic and aqueous media. Polymer 46(23):10493–10505. doi:10.1016/j.polymer.2005.08.031

172. Ramireddy C, Tuzar Z, Prochazka K, Webber SE, Munk P (1992) Styrene tert-butyl methacrylate and styrene methacrylic-acid block copolymers—synthesis and characterization. Macromolecules 25(9):2541–2545. doi:10.1021/ma00035a037
173. Prochazka K, Limpouchova Z (1994) Conformations of insoluble blocks in swollen micellar cores of multimolecular block-copolymer micelles studied by Monte-Carlo simulation technique. Collect Czech Chem Commun 59(4):782–802. doi:10.1135/cccc19940782
174. Viduna D, Limpouchova Z, Prochazka K (1997) Conformations of self-avoiding tethered chains and nonradiative energy transfer and migration in dense and constrained systems. A model for cores of polymeric micelles. Macromolecules 30(23):7263–7272. doi:10.1021/ma970002c
175. Limpouchova Z, Viduna D, Prochazka K (1997) Mixed systems of tethered chains in spherical volumes. A model for cores of mixed copolymer micelles. Macromolecules 30 (25):8027–8035. doi:10.1021/ma970001k
176. Prochazka K (1995) Monte-Carlo study of tethered chains in spherical volumes. J Phys Chem 99(38):14108–14116. doi:10.1021/j100038a050
177. Matejicek P, Uhlik F, Limpouchova Z, Prochazka K, Tuzar Z, Webber S (2002) Experimental study of hydrophobically modified amphiphilic block copolymer micelles using light scattering and nonradiative excitation energy transfer. Macromolecules 35(25):9487–9496. doi:10.1021/ma012074g
178. Uhlik F, Limpouchova Z, Matejicek P, Prochazka K, Tuzar Z, Webber SE (2002) Nonradiative excitation energy transfer in hydrophobically modified amphiphilic block copolymer micelles. Theoretical model and Monte Carlo simulations. Macromolecules 35 (25):9497–9505. doi:10.1021/ma012073o
179. Uhlik F, Limpouchova Z, Jelinek K, Prochazka K (2003) A Monte Carlo study of shells of hydrophobically modified amphiphilic copolymer micelles in polar solvents. J Chem Phys 118(24):11258–11264. doi:10.1063/1.1575732
180. Uhlik F, Limpouchova Z, Jelinek K, Prochazka K (2004) Polyelectrolyte shells of copolymer micelles in aqueous solutions: a Monte Carlo study. J Chem Phys 121(5):2367–2375. doi:10.1063/1.1763571
181. Friend RH, Gymer RW, Holmes AB, Burroughes JH, Marks RN, Taliani C, Bradley DDC, Dos Santos DA, Bredas JL, Logdlund M, Salaneck WR (1999) Electroluminescence in conjugated polymers. Nature 397(6715):121–128. doi:10.1038/16393
182. McQuade DT, Pullen AE, Swager TM (2000) Conjugated polymer-based chemical sensors. Chem Rev 100(7):2537–2574. doi:10.1021/cr9801014
183. Coakley KM, McGehee MD (2004) Conjugated polymer photovoltaic cells. Chem Mater 16 (23):4533–4542. doi:10.1021/cm049654n
184. Facchetti A (2011) pi-Conjugated polymers for organic electronics and photovoltaic cell applications. Chem Mater 23(3):733–758. doi:10.1021/cm102419z
185. Nakamura M, Tabata M, Sone T, Mawatari Y, Miyasaka A (2002) Photoinduced cis-to-trans isomerization of poly(2-ethynylthiophene) prepared with a Rh(norbornadiene)Cl (2) catalyst. H-1 NMR, UV, and ESR studies. Macromolecules 35(6):2000–2004. doi:10.1021/ma0101198
186. Sun JZ, Chen HZ, Xu RS, Wang M, Lam JWY, Tang BZ (2002) Electric field induced cis-to-trans isomerization of polyphenylacetylene in solid state. Chem Commun 11:1222–1223. doi:10.1039/b200830k
187. Lee PPS, Lam JWY, Li BS, Poon TWH, Tang BZ (1999) Ultrasound-induced isomerization of stereoregular poly(phenylacetylene). Abstr Pap Am Chem Soc 218:U425–U425
188. Lam JWY, Tang BZ (2005) Functional polyacetylenes. Acc Chem Res 38(9):745–754. doi:10.1021/ar040012f
189. Tang BZ, Chen HZ, Xu RS, Lam JWY, Cheuk KKL, Wong HNC, Wang M (2000) Structure-property relationships for photoconduction in substituted polyacetylenes. Chem Mater 12 (1):213–221. doi:10.1021/cm990552k

190. Wang X, Wu JC, Xu HY, Wang P, Tang BZ (2008) Preparation and property of two soluble oxadiazole-containing functional polyacetylenes. J Polym Sci Part A Polym Chem 46 (6):2072–2083. doi:10.1002/pola.22542
191. Qu J, Shiotsuki M, Sanda F, Masuda T (2007) Synthesis and properties of helical polyacetylenes carrying cholesteryl moieties. Macromol Chem Phys 208(8):823–832. doi:10.1002/macp.200600601
192. Zhang XA, Chen MR, Zhao H, Gao Y, Wei Q, Zhang S, Qin AJ, Sun JZ, Tang BZ (2011) A facile synthetic route to functional poly(phenylacetylene)s with tunable structures and properties. Macromolecules 44(17):6724–6737. doi:10.1021/ma2014657
193. Liu JZ, Lam JWY, Tang BZ (2009) Acetylenic polymers: syntheses, structures, and functions. Chem Rev 109(11):5799–5867. doi:10.1021/cr900149d
194. Hu R, Leung NLC, Tang BZ (2014) AIE macromolecules: syntheses, structures and functionalities. Chem Soc Rev 43(13):4494–4562. doi:10.1039/c4cs00044g
195. Masuda T (2007) Substituted polyacetylenes. J Polym Sci Part A Polym Chem 45 (2):165–180. doi:10.1002/pola.21782
196. Lam JWY, Dong YP, Kwok HS, Tang BZ (2006) Light-emitting polyacetylenes: synthesis and electrooptical properties of poly(1-phenyl-1-alkyne)s bearing naphthyl pendants. Macromolecules 39(20):6997–7003. doi:10.1021/ma0612576
197. Hu RR, Lam JWY, Tang BZ (2013) Recent progress in the development of new acetylenic polymers. Macromol Chem Phys 214(2):175–187. doi:10.1002/macp.201200389
198. Ou DX, Qin JG, Li Z (2012) A new disubstituted polyacetylene bearing DDTC moieties: postfunctional synthetic strategy, selective and sensitive chemosensor towards mercury ions. Polymer 53(25):5691–5698. doi:10.1016/j.polymer.2012.10.006
199. Muroga T, Sakaguchi T, Hashimoto T (2012) Synthesis and photoluminescence properties of heterocycle-containing poly(disubstituted acetylene)s. Polymer 53(20):4380–4387. doi:10.1016/j.polymer.2012.08.009
200. Sivkova R, Vohlidal J, Blaha M, Svoboda J, Sedlacek J, Zednik J (2012) Poly(disubstituted acetylene)s with pendant naphthalimide-based fluorophore groups. Macromol Chem Phys 213(4):411–424. doi:10.1002/macp.201100509
201. Duchoslavova Z, Sivkova R, Hankova V, Sedlacek J, Svoboda J, Vohlidal J, Zednik J (2011) Synthesis and spectral properties of novel poly(disubstituted acetylene)s. Macromol Chem Phys 212(16):1802–1814. doi:10.1002/macp.201100160
202. Park H, Jeong H, Lee WE, Yoon KB, Oh CJ, Kwak G (2011) Positive-/negative-, erasable-/immobilized-, mono-/multi-color fluorescence image patterning of molecular-scale porous polymer film via a microcontact printing method using various chemical inks. Macromol Rapid Commun 32(4):360–365. doi:10.1002/marc.201000623
203. Zeng Q, Jim CKW, Lam JWY, Dong YQ, Li Z, Qin JU, Tang BZ (2009) A new disubstituted polyacetylene for the detection of alpha-amino acids. Macromol Rapid Commun 30 (3):170–175. doi:10.1002/marc.200800616
204. Lou XD, Zeng Q, Zhang Y, Wan ZM, Qin JG, Li Z (2012) Functionalized polyacetylenes with strong luminescence: "turn-on" fluorescent detection of cyanide based on the dissolution of gold nanoparticles and its application in real samples. J Mater Chem 22(12):5581–5586. doi:10.1039/c2jm15516h
205. Lam JWY, Tang BZ (2003) Liquid-crystal line and light-emitting polyacetylenes. J Polym Sci Part A Polym Chem 41(17):2607–2629. doi:10.1002/pola.10802
206. Bolinger JC, Traub MC, Brazard J, Adachi T, Barbara PF, Vanden Bout DA (2012) Conformation and energy transfer in single conjugated polymers. Acc Chem Res 45(11):1992–2001. doi:10.1021/ar300012k
207. Lupton JM (2010) Single-molecule spectroscopy for plastic electronics: materials analysis from the bottom-up. Adv Mater 22(15):1689–1721. doi:10.1002/adma.200902306
208. Pina J, de Melo JS, Burrows HD, Buennagel TW, Dolfen D, Kudla CJ, Scherf U (2009) Photophysical and spectroscopic investigations on (oligo)thiophene-arylene step-ladder

copolymers. The interplay of conformational relaxation and on-chain energy transfer. J Phys Chem B 113(49):15928–15936. doi:10.1021/jp9054022
209. Chen P-Y, Rassamesard A, Chen H-L, Chen S-A (2013) Conformation and fluorescence property of poly(3-hexylthiophene) isolated chains studied by single molecule spectroscopy: effects of solvent quality and regioregularity. Macromolecules 46(14):5657–5663. doi:10.1021/ma400852q
210. Ambrose WP, Goodwin PM, Jett JH, Van Orden A, Werner JH, Keller RA (1999) Single molecule fluorescence spectroscopy at ambient temperature. Chem Rev 99(10):2929–2956. doi:10.1021/cr980132z
211. Wang D, Yuan Y, Mardiyati Y, Bubeck C, Koynov K (2013) From single chains to aggregates, how conjugated polymers behave in dilute solutions. Macromolecules 46 (15):6217–6224. doi:10.1021/ma4011523
212. Watanabe K, Suda K, Akagi K (2013) Hierarchically self-assembled helical aromatic conjugated polymers. J Mater Chem C 1(16):2797–2805. doi:10.1039/c3tc00045a
213. Huser T, Yan M, Rothberg LJ (2000) Single chain spectroscopy of conformational dependence of conjugated polymer photophysics. Proc Natl Acad Sci USA 97(21):11187–11191. doi:10.1073/pnas.97.21.11187
214. Affleck RL, Ambrose WP, Demas JN, Goodwin PM, Schecker JA, Wu JM, Keller RA (1996) Reduction of luminescent background in ultrasensitive fluorescence detection by photobleaching. Anal Chem 68(13):2270–2276. doi:10.1021/ac9512517
215. Li LQ, Davis LM (1995) Rapid and efficient detection of single chromophore molecules in aqueous-solution. Appl Opt 34(18):3208–3217
216. Keller RA, Ambrose WP, Goodwin PM, Jett JH, Martin JC, Wu M (1996) Single molecule fluorescence analysis in solution. Appl Spectrosc 50(7):A12–A32
217. Barnes MD, Ng KC, Whitten WB, Ramsey JM (1993) Detection of single rhodamine-6g molecules in levitated microdroplets. Anal Chem 65(17):2360–2365. doi:10.1021/ac00065a032
218. Mahoney PP, Hieftje GM (1994) Fluorometric analysis on individual nanoliter sample droplets. Appl Spectrosc 48(8):956–958. doi:10.1366/0003702944029785
219. Lee YH, Maus RG, Smith BW, Winefordner JD (1994) Laser-induced fluorescence detection of a single-molecule in a capillary. Anal Chem 66(23):4142–4149. doi:10.1021/ac00095a005
220. Eigen M, Rigler R (1994) Sorting single molecules—application to diagnostics and evolutionary biotechnology. Proc Natl Acad Sci USA 91(13):5740–5747. doi:10.1073/pnas.91.13.5740
221. Blatchford JW, Gustafson TL, Epstein AJ, VandenBout DA, Kerimo J, Higgins DA, Barbara PF, Fu DK, Swager TM, MacDiarmid AG (1996) Spatially and temporally resolved emission from aggregates in conjugated polymers. Phys Rev B 54(6):R3683–R3686
222. Van den Bout DA, Yip WT, Hu DH, Fu DK, Swager TM, Barbara PF (1997) Discrete intensity jumps and intramolecular electronic energy transfer in the spectroscopy of single conjugated polymer molecules. Science 277(5329):1074–1077
223. Stein AD, Fayer MD (1992) Spectral diffusion in liquids. J Chem Phys 97(5):2948–2962. doi:10.1063/1.463036
224. Yip WT, Hu DH, Yu J, Vanden Bout DA, Barbara PF (1998) Classifying the photophysical dynamics of single- and multiple-chromophoric molecules by single molecule spectroscopy. J Phys Chem A 102(39):7564–7575. doi:10.1021/jp981808x
225. Hu DH, Yu J, Barbara PF (1999) Single-molecule spectroscopy of the conjugated polymer MEH-PPV. J Am Chem Soc 121(29):6936–6937. doi:10.1021/ja990139d
226. Barbara PF, Gesquiere AJ, Park SJ, Lee YJ (2005) Single-molecule spectroscopy of conjugated polymers. Acc Chem Res 38(7):602–610. doi:10.1021/ar040141w
227. English DS, Harbron EJ, Barbara PF (2000) Probing photoinduced intersystem crossing by two-color, double resonance single molecule spectroscopy. J Phys Chem A 104 (40):9057–9061. doi:10.1021/jp001992y

228. Grey JK, Kim DY, Norris BC, Miller WL, Barbara PF (2006) Size-dependent spectroscopic properties of conjugated polymer nanoparticles. J Phys Chem B 110(51):25568–25572. doi:10.1021/jp065990a
229. Yu ZH, Barbara PF (2004) Low-temperature single-molecule spectroscopy of MEH-PPV conjugated polymer molecules. J Phys Chem B 108(31):11321–11326. doi:10.1021/jp038005g
230. Adachi T, Vogelsang J, Lupton JM (2014) Chromophore bending controls fluorescence lifetime in single conjugated polymer chains. J Phys Chem Lett 5(12):2165–2170. doi:10.1021/jz500810k
231. Stangl T, Bange S, Schmitz D, Wuersch D, Hoeger S, Vogelsang J, Lupton JM (2013) Temporal switching of homo-FRET pathways in single-chromophore dimer models of pi-conjugated polymers. J Am Chem Soc 135(1):78–81. doi:10.1021/ja3108643

Fluorescence Spectroscopy Studies of Amphiphilic Block Copolymer Micelles in Aqueous Solutions

Miroslav Štěpánek

Contents

Abstract We discuss applications of selected fluorescence spectroscopy techniques for the studies of block copolymer micelles in aqueous solution, focusing on solvent relaxation measurements using polarity-sensitive fluorescent probes, on fluorescence quenching studies, and on using fluorescent pH indicators for studies of micelles with polyelectrolyte coronas.

Keywords Block copolymer micelles • Fluorescent probes • Fluorescence spectroscopy

1 Introduction

Fluorescence emission in the condensed state is influenced by interactions of the emitting molecule with its surroundings. The emission spectrum of the fluorophore as well as the lifetime of its excited state can generally be sensitive to the polarity and viscosity of the solvent or to the presence of specific molecules or ions in the

M. Štěpánek (✉)
Department of Physical and Macromolecular Chemistry, Faculty of Science, Charles University in Prague, Prague, Czech Republic
e-mail: miroslav.stepanek@natur.cuni.cz

K. Procházka (ed.), *Fluorescence Studies of Polymer Containing Systems*, Springer Series on Fluorescence 16, DOI 10.1007/978-3-319-26788-3_6

vicinity of the fluorophore on the distances up to several nm. The nanometer range of the fluorophore sensitivity to the properties of their microenvironment makes fluorescence spectroscopy a suitable tool for studying local properties (polarity and viscosity of the binding site of the probe, its accessibility to small molecules or ions) of nanosized objects like macromolecules, micelles, vesicles, or various colloidal particles.

While studies of biological macromolecules (proteins and nucleic acids) [1, 2] and phospholipid vesicles [3–5] using fluorescence spectroscopy techniques are numerous and many reviews have already been published, much less attention has been paid to surfactant micelles [6–9], and fluorescence studies of block copolymer micelles are even scarcer [10–12] so far despite the fast growing number of publications on block copolymer self-assembly in the literature.

Block copolymer self-assembled nanoparticles [13–15] form in selective solvents, that is, solvents for only some of the blocks and precipitant for the others. In the simplest case of a diblock copolymer, core/shell nanoparticles such as micelles or vesicles are formed, the core of which consists of collapsed or weakly swollen solvophobic blocks and the shell (also referred to as the corona) of strongly swollen solvophilic blocks. In the case of amphiphilic micelles in aqueous solutions, water is too strong a precipitant for core blocks, and such polymers are not directly soluble in water (unless the hydrophobic block is very short), and the aqueous solutions have to be prepared indirectly using a cosolvent (a solvent for the core block miscible with water) which can be removed from the solution by dialysis or distillation after the dissolution of the copolymer [16].

Amphiphilic block copolymer micelles prepared by the latter procedure are in a kinetically frozen, nonequilibrium state as the exchange of copolymer chains (so-called unimers) among the micelles is prevented by high activation energies for the release of the unimers and for the insertion of the unimers to the micelle. The shell of a block copolymer micelle can be treated as a dense polymer brush tethered to a curved interface. Physical properties gradually change with the distance from the core/shell interface in the radial direction, r. Most importantly, the segment density decreases, and (in the case of a weak polyelectrolyte corona) the degree of ionization or protonation increases with the increasing distance r [17]. As a result, block copolymer micelles exhibit much higher internal heterogeneity as compared with surfactant micelles.

Since synthetic copolymers seldom exhibit intrinsic fluorescence, either covalently bound fluorescent labels or non-covalently bound fluorescent probes are necessary for the vast majority of fluorescence studies of block copolymer micelles. The former are mostly attached during the synthesis of the copolymer [18]. This could be done conveniently by using a fluorescent initiator and/or fluorescent terminating agent. In such cases, the labels are located at the ends of the blocks or in between of them. Fluorescent probes can be used for studies of amphiphilic block copolymer micelles in aqueous solutions where strong hydrophobic effect allows for binding of the probe either in the micellar core (hydrophobic probes) [19] or in the inner part of the shell close to the core/shell interface (amphiphilic probes) [20]. The latter, developed mainly for membrane studies, are derivatives of

hydrophilic fluorophores with long aliphatic chains giving them amphiphilic character [21].

This chapter brings a short review of fluorescence studies on block copolymer micelles. From the variety of fluorescence spectroscopy applications, we focus rather on those which are based on general principles of the technique than on those that require specifically designed fluorophores and also omit those that have been extensively reviewed before like fluorescence resonance energy transfer [1].

2 Polarity-Sensitive Fluorescent Probes

In this section, we will not discuss polarity-sensitive probes, the mechanism of which is based on the specific electronic structure (even though one of them, pyrene [19], belongs to the most widely used) and focuses on fluorophores used for monitoring the solvent relaxation after the transition of the probe to the electronically excited state [22]. Let us first briefly explain the mechanism of these fluorescent probes (Fig. 1).

The change of the electronic state of the fluorophore upon absorption of a photon is accompanied by an instantaneous change of the fluorophore's dipole moment which is followed by the reorientation motion of the surrounding solvent molecules until their permanent dipole moments are again oriented parallel with the changed dipole moment of the fluorophore. The latter process, called solvent relaxation, leads to the decrease of the energy of the system (the fluorophore + the solvent cage) which could manifest itself as the red shift of the emitted radiation, depending on how fast the solvent relaxation is as compared with the lifetime of the fluorophore's excited state, τ.

Let us first consider that the characteristic time of the solvent relaxation, τ_R, is much larger than τ. In such a case, no spectral change due to the interaction with the solvent can be observed in the emission spectrum because the de-excitation of the fluorophore occurs prior to the solvent relaxation. In the opposite case when $\tau_R >> \tau$, the emission occurs from the fully relaxed state. The observed red shift of the emission spectrum is independent on the time after excitation and reflects only the strength of the dipole–dipole interaction between the fluorophore and the surrounding solvent molecules. The most interesting situation occurs when the characteristic time of the solvent relaxation is comparable to τ. In such a case, the red shift of the spectrum will increase with the time after excitation as it will correspond to the emission from more relaxed states. Hence, the dynamics of the solvent molecules around the fluorophore is translated into the time dependence of the maximum and the half-width of the emission band which can be followed by the time-resolved emission spectroscopy measurements.

The time-resolved emission spectrum (TRES) is usually not measured directly. Instead, it is obtained by the so-called spectral reconstruction method from a series of emission decays $D(\omega,t)$ measured by various wave numbers ω. TRES is then

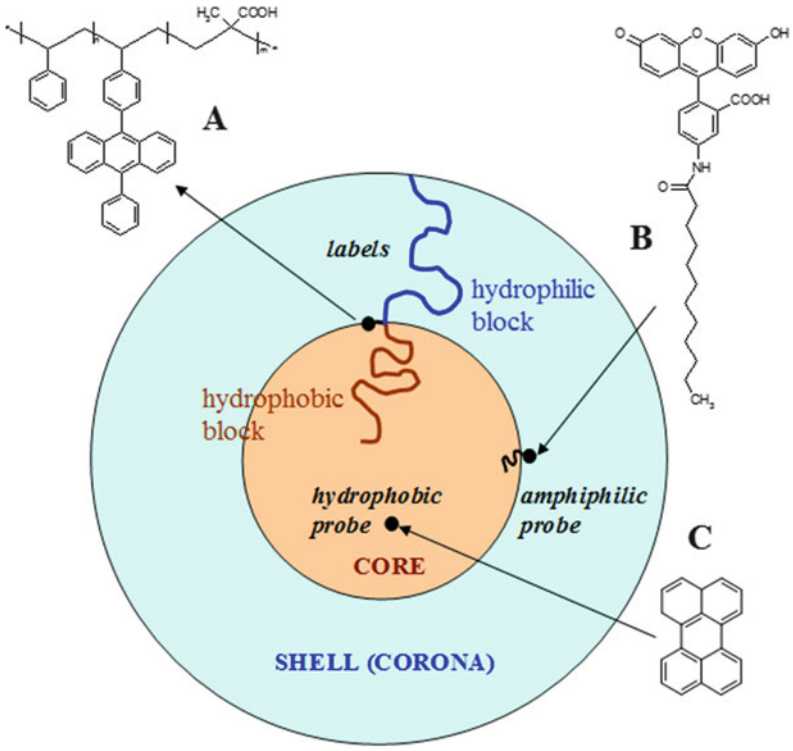

Fig. 1 Examples of localization of fluorophores in an amphiphilic block copolymer micelle (polystyrene-*block*-poly(acrylic acid)): (**a**) fluorescent label (9,10-diphenylanthracene covalently bound between hydrophilic and amphiphilic block), (**b**) amphiphilic probe (*N*-(dodecanoyl) aminofluorescein) solubilized at the core/shell interface, and (**c**) hydrophobic probe (pyrene) solubilized in the core

calculated by the simple normalization using the steady-state spectrum of the fluorophore, $S(\omega)$, as [23, 24]

$$F(\omega,t)=\frac{D(\omega,t)S(\omega)}{\int_0^{\infty}D\left(\omega,t^{'}\right)\mathrm{d}t^{'}} \tag{1}$$

In the simplest case, the shape of the emission band can be approximated by the lognormal function:

$$S(\omega,t)=h(t)\exp\left\{-\ln(2)\ln^2\left[\frac{\Delta(t)+2\gamma(t)[\omega-\varpi(t)]}{\Delta(t)\gamma(t)}\right]\right\} \tag{2}$$

where $h(t)$ is the height of the emission band, $\varpi(t)$ is the emission maximum wave number, and the $\Delta(t)$ and $\gamma(t)$ are the asymmetry parameters. The emission

maximum wave number is further treated in the normalized form as the correlation function $C(t)$:

$$C(t) = \frac{\varpi(t) - \varpi_\infty}{\varpi_0 - \varpi_\infty} \tag{3}$$

where ϖ_0 and ϖ_∞ are the maximum wave numbers at $t = 0$ and at $t \to \infty$, respectively. The decay rate of the $C(t)$ function can be described by the relaxation time τ_R:

$$\tau_R = \int_0^\infty C(t)\mathrm{d}t \tag{4}$$

In the case when the probe exhibits multiple relaxation times as a result of heterogeneity of the binding sites, Eq. 4 provides the mean relaxation time. Even though some characteristics of the τ_R distribution can in principle be obtained by fitting the $C(t)$ function by a multiple-exponential decay function, a more reliable way to follow the heterogeneity of the system in terms of solvent relaxation is to plot the full width at half maximum (FWHM) of the emission band, $\sigma(t)$, as a function of time. The $\sigma(t)$ function can be calculated from the asymmetry parameters of the lognormal function, $\Delta(t)$ and $\gamma(t)$, as

$$\sigma(t) = \Delta(t)\frac{\sinh\gamma(t)}{\gamma(t)} \tag{5}$$

In a homogeneous system, only the maximum moves toward lower wave numbers, but the FWHM does not change with time. In a heterogeneous system, however, we often observe an increase in FWHM with the time because of the simultaneous emission of slow-relaxing higher energy states and fast-relaxing lower energy states which leads to the broadening of the emission band. In the later stages of the relaxation process, energy levels of the slow-relaxing states approach those of the fast-relaxing ones which are already fully relaxed, and the FWHM decreases again. The $\sigma(t)$ function thus exhibits a maximum for solvent relaxation in the heterogeneous system.

Even though the emission behavior of all fluorophores in solution is influenced by solvent relaxation, solvent relaxation studies typically use fluorophores, the dipole moment of which increases strongly upon excitation, causing a very pronounced effect on the emission spectra. Many of them are derivatives of aminonaphthalene (Fig. 2).

While in water at room temperature (and other low-molar-mass solvents of similar viscosity), the reorientation of the solvent molecules typically occurs in several tens of picoseconds, the rotational motion of the solvent trapped in nanostructured polymer systems such as in micellar shells is substantially slowed down, and its relaxation can be followed on the subnanosecond or nanosecond time scale [23].

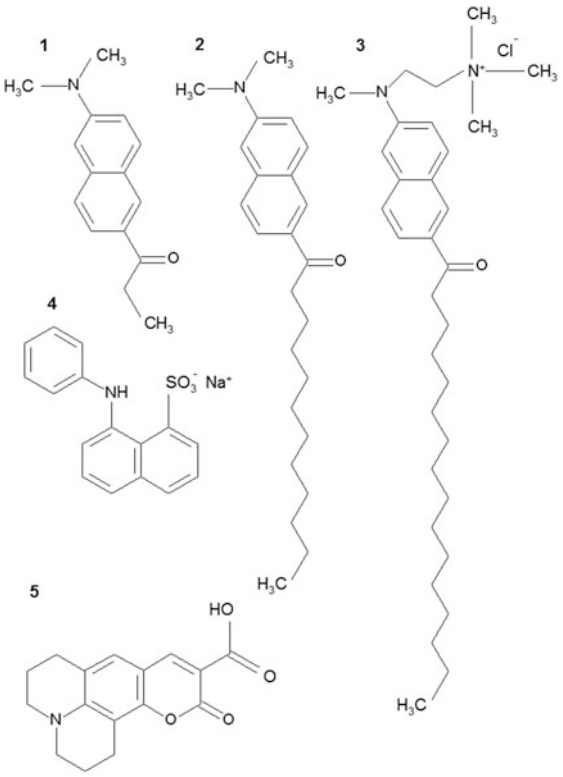

Fig. 2 Fluorescent probes for solvent relaxation measurements: (**1**) Prodan, (**2**) Laurdan, (**3**) Patman, (**4**) 8-anilino-1-naphthalenesulfonic acid (1,8-ANS), (**5**) Coumarin 343

While there are many papers in the literature on the solvent relaxation in solutions of proteins, surfactant micelles, and phospholipid vesicles studied by time-resolved emission spectroscopy [25–27], similar studies focused on block copolymer micelles are scarce. In most cases, amphiphilic fluorescent probes localized in the inner part of the shells of amphiphilic block copolymer micelles in aqueous solutions were used for the studies. The studies reveal the heterogeneity of the binding sites of the probe that manifest itself by multiple-exponential fluorescence decays. In the case of block copolymer micelles, interpretation of the relaxation behavior can be complicated by redistribution of the probe molecules in the micelles during its excited-state lifetime of the probe [28]. The redistribution occurs as a result of the increased polarity of the excited probe as compared with its ground electronic state.

Block copolymer micelle studies carried out with poly(ethylene oxide)-*block*-poly(propylene oxide)-*block*-poly(ethylene oxide) triblock copolymers (Pluronics) and Coumarin 343 [29, 30] as a fluorescent probe demonstrated that both the fluorescence lifetime and the emission maximum strongly depend on the probe localization in the Pluronic micelle. Water molecules in the interior of the micelles close to the core/shell interface relaxed much more slowly than those in the outer part of the shell which had almost the same mobility as bulk water.

Procházka et al. [31] studied solvent relaxation in the shells of polystyrene-*block*-poly(ethylene oxide) (PS–PEO), polystyrene-*block*-poly(2-vinylpyridine) (PS–PVP), and polystyrene-*block*-poly(2-vinylpyridine)-*block*-poly(ethylene oxide) (PS–PVP–PEO) in aqueous solutions, using Patman as a fluorescent probe. While in the case of the PEO shell of the PS–PEO micelle, a slow relaxation was observed because the mobility of water molecules in the shell was hindered by the strong hydrogen bonding to PEO chains, the solvent cage of the probe in the shell of PS–PVP micelles appeared to relax much faster. Interestingly, water in PS–PVP–PEO terpolymer micelles exhibited a slow relaxation as in the case of the PS–PEO diblock, but the relaxation time became pH responsive due to the presence of the weak polyelectrolyte PVP block.

3 Fluorescence Quenching

Fluorescence quenching [32] is a phenomenon that consists in the decrease of fluorescence intensity caused by an external stimulus, such as a change in temperature, pressure, solvent composition, and other factors. Here we will further deal with fluorescence quenching caused by the addition of specific substances, called quenchers, to the fluorescent system. Let us neglect the trivial case of the internal filter effect which decreases the fluorescence intensity either by absorption of the excitation radiation or by reabsorption of the emitted fluorescence by the quencher and focus on processes that consist in interactions between the fluorophore and quencher molecules.

Let us first consider the case of the dynamic quenching, which means that the interaction between the fluorophore and the quencher occurs in the excited state of the fluorophore, F*, either as a collision or a long-range resonance energy transfer between F* and Q, both leading to nonradiative deactivation of F*. The excited-state lifetime τ can be expressed by the sum of the rate constants of individual deactivation processes:

$$\tau = \frac{1}{k_f + k_i + k_q[Q]} \tag{6}$$

where k_f, k_i, and k_q, respectively, are the rate constants of fluorescence, internal conversion, and pseudo-bimolecular quenching and are the quencher concentration in the system. The ratio between the lifetime in the absence of the quencher ($[Q] = 0$), τ_0, and that in the presence of the quencher is given by the equation

$$\frac{\tau_0}{\tau} = \frac{k_f + k_i + k_q[Q]}{k_f + k_i} = 1 + \frac{k_q}{k_f + k_i}[Q] = 1 + k_q\tau_0[Q] = 1 + K_{SV}[Q] \tag{7}$$

The Eq. (7) is known as the Stern–Volmer equation [33] and $K_{SV} = k_q\tau_0$ as the Stern–Volmer quenching constant. Plotting the τ_0/τ ratio as a function of [Q] thus

produces the linear dependence, the slope of which has a meaning of the ratio between the rate constant for the bimolecular quenching and the rate constant for the intramolecular deactivation processes.

In the steady state, the rate of the activation of the excited state by absorption of exciting radiation, v_{abs}, is equal to the rate of its deactivation by fluorescence, by internal conversion, and by quenching, so that

$$v_{abs} = [F^*]\left(k_f + k_i + k_q[Q]\right) \tag{8}$$

where [F*] is the steady-state concentration of the fluorophore in the excited state. Since $I = k_f[F^*]$, the ratio between the fluorescence intensity in the presence of the quencher, I, and that in the absence of the quencher (at $[Q] = 0$) is expressed by the equation

$$\frac{I_0}{I} = \frac{k_f + k_i + k_q[Q]}{k_f + k_i} = 1 + K_{SV}[Q] \tag{9}$$

In other words, the Stern–Volmer equation holds also for the I_0/I ratio which can be easily obtained from steady-state fluorescence measurements. However, the acquisition of I_0/I instead of τ_0/τ does not allow for distinguishing dynamic quenching occurring in the excited state of the fluorophore from the so-called static quenching. The latter mechanism consists in the formation of a nonfluorescent complex of the quencher Q with the fluorophore F in the ground state:

$$Q + F \rightleftharpoons QF \tag{10}$$

The concentrations of the free fluorophore, [F], the fluorophore–quencher complex [QF], and the quencher [Q] then fulfill the equation

$$[F]_0 = [QF] + [F] = [F] + K_S[Q][F] \tag{11}$$

where $[F]_0$ is the overall concentration of the fluorophore in the system and $K_S = [QF]/[Q][F]$ is the stability constant of the complex QF. Assuming that the steady-state fluorescence intensity is proportional to the concentration of the free fluorophore, the I_0/I ratio is given by the formula

$$\frac{I_0}{I} = \frac{[F]_0}{[F]} = 1 + K_S[Q] \tag{12}$$

which is formally identical to the Stern–Volmer Eq. (9), but the meaning of the constant K_S is entirely different. Fluorescence emission decay measurements allow for distinguishing between static and dynamic quenching. While in the case of dynamic quenching the emission lifetimes follow the Stern–Volmer equation, the static quenching mechanism consists in the removal of a fraction of the fluorophore

by its binding in a nonfluorescent complex and thus does not affect the emission lifetime.

In the case that both static and dynamic quenching occurs, the I_0/I ratio is (unlike the τ_0/τ ratio) affected by both processes, and the plot of I_0/I vs. [Q] produces an upward curved dependence:

$$\frac{I_0}{I} = (1 + K_{SV}[Q])(1 + K_S[Q]) \tag{13}$$

In a microheterogeneous system with multiple types of the binding sites of the probe, the sites can have different accessibilities for the quencher, which are expressed by multiple quenching constants. The overall intensity of the quenched fluorescence is then given by a formula

$$\frac{I}{I_0} = \sum_{i=1}^{n} \frac{f_i}{1 + K_i[Q]} \tag{14}$$

where $f_1, \ldots, f_n$ are the fractions of fluorescence intensity corresponding to fluorophores bound to the individual types of the binding sites ($f_1 + f_2 + \cdots + f_n = 1$) with the quenching constants $K_1, \ldots, K_n$. In the simplest case of a system containing only two types of binding sites of which one with the intensity fraction f has the quenching constant K and the other with the fraction $1 - f$ is inaccessible to the quencher (the quenching constant, $K' = 0$), Eq. (11) can be rearranged as

$$\frac{I}{I_0 - I} = \frac{1}{f}\left(1 + \frac{1}{K[Q]}\right) \tag{15}$$

Plotting $I/(I_0 - I)$ as a function of $[Q]^{-1}$ provides a linear dependence, the intercept of which is equal to f^{-1}. Equation (12) has often been used in studies of the protein structure to determine the amount of tryptophan residues located on the surface of the protein and those buried inside the tertiary structure of the protein [34].

As the fluorescence quenching technique allows for distinguishing fluorescent probes in the bulk solution from those solubilized in the micellar core or in the interior part of the shell, it has been used for studying solubilization of hydrophobic or amphiphilic low-molar-mass compounds in amphiphilic block copolymer micelles [35–37]. If a hydrophobic fluorophore is used as a model compound, the method can be used both for measurements of equilibrium partitioning of the hydrophobe between the micellar pseudophase and the aqueous phase, as well as for following the release of the hydrophobic compounds from the micelles. The latter studies are of great importance in pharmacology for characterization of containers for controlled drug release based on block copolymer micelles [38].

4 Fluorescent pH Indicators

Fluorescent electrolytes, the emission quantum yield of which strongly depends on whether they are in a neutral or ionic form, have often been used as pH indicators. The best known example of such a fluorescent probe is fluorescein, which fluoresces only in its dianionic form, while the monoanionic form and the neutral form are basically nonfluorescent.

In nanostructured systems, the pK of the indicator may differ from that in water because of a different dielectric permittivity of its microenvironment. In charged systems, an additional shift of the pK value may appear as a result of the interaction of the probe with the local electric field.

The latter phenomenon was well described already in the 1970s by Fernández and Fromherz [39] who studied the pK shift of hydroxycoumarin (fluorescent in the anionic form) and aminocoumarin (fluorescent in the neutral form) amphiphilic derivatives, solubilized in ionic surfactant micelles. The study demonstrated that the attraction of the proton to the negatively charged surface of anionic micelles hinders dissociation of acids (which thus behave as weaker ones as compared to water) and promotes protonation of bases (which thus behave as stronger ones as compared to water). The positively charged surface acts oppositely. The authors showed that the potential of the electric double layer, Ψ, is related to the shifted pK of the indicator as

$$\mathrm{p}K = \mathrm{p}K_{\mathrm{int}} + \frac{\Psi}{2.303RT} \tag{16}$$

where $\mathrm{p}K_{\mathrm{int}}$ is the intrinsic pK of the indicator at the local dielectric permittivity of the probe microenvironment. The $\mathrm{p}K_{\mathrm{int}}$ values can be assessed by measurements with nonionic surfactant micelles, assuming that the local ε at the interface between the aqueous solution and the interior of the micelle formed by long aliphatic chains is very similar to that of ionic surfactant micelles. The obtained Ψ values, however, were much larger for amphiphilic coumarins indicating that the response is very sensitive to the exact localization of the probe with respect to the electric double layer of the micelle.

In the case of block copolymer micelles with weak polyelectrolyte shells, the situation is much more complex. Firstly, the amphiphilic pH indicators do not bind only at the core/shell interfacial layer, but they can be solubilized also in the inner part of the shell. Secondly, the electric field surrounding the indicator probe cannot be described by the simple electric double layer as in the case of ionic surfactant micelles, because the shell thickness is typically several tens of nm with the degree of dissociation (or protonation) of the polyelectrolyte block and consequently the charge density gradually increasing with the increasing radial distance from the core–shell micelles.

Fluorescence measurements with *N*-(dodecanoyl)aminofluorescein (DAF) [40] bound in polystyrene-*block*-poly(methacrylic acid) (PS–PMAA) micelles in

alkaline aqueous solution (pH 9.2) provided pK values of DAF that corresponded to the electric potential of ca. −50 mV according to Eq. (16) using neutral micelles of polystyrene-*block*-poly(ethylene oxide) as the reference system for the estimation of pK_{int}. The obtained value of Ψ was very similar to ζ potential obtained from electrophoretic light scattering measurements for the same system. On the other hand, the obtained fluorescence titration curves were not only shifted with respect to the aqueous solution as predicted from the Fernández–Fromherz theory, but they were also less steep. This behavior was caused by the heterogeneity of DAF binding sites in the micelles which resulted in a distribution of apparent pK values.

5 Conclusions

In this chapter, we overviewed several fluorescence techniques suitable for studies of colloidal particles in aqueous solutions and discussed their application in the research of amphiphilic block copolymer micelles. Unlike surfactant micelles or phospholipid vesicles, amphiphilic block copolymer micelles have no sharp interface between the hydrophobic interior of the particles and the bulk solution, which results in greater heterogeneity of localization sites of fluorescent probes in the polymeric micelles and consequently in more difficult interpretation of data in comparison with surfactant micelles and phospholipid vesicles.

References

1. Klostermeier D, Millar DP (2001) Time-resolved fluorescence resonance energy transfer: a versatile tool for the analysis of nucleic acids. Biopolymers 61:159–179
2. Lukinavicius G, Johnsson K (2011) Switchable fluorophores for protein labeling in living cells. Curr Opin Chem Biol 15:768–774
3. Jurkiewicz P, Sýkora J, Olzynska A, Humpolíčková J, Hof M (2005) Solvent relaxation in phospholipid bilayers: principles and recent applications. J Fluoresc 15:883–894
4. Lentz BR (1993) Use of fluorescent-probes to monitor molecular order and motions within liposome bilayers. Chem Phys Lipids 64:99–116
5. Silvius JR, Nabi IR (2006) Fluorescence-quenching and resonance energy transfer studies of lipid microdomains in model and biological membranes (review). Mol Membr Biol 23:5–16
6. Grieser F, Dummond CJ (1988) The physicochemical properties of self-assembled surfactant aggregates as determined by some molecular spectroscopic probe techniques. J Phys Chem 92:5580–5593
7. Almgren M (1992) Diffusion-influenced deactivation processes in the study of surfactant aggregates. Adv Colloid Interface Sci 41:9–32
8. Winnik FM, Regismond STA (1996) Fluorescence methods in the study of the interactions of surfactants with polymers. Colloids Surf A Physicochem Eng Asp 118:1–39
9. Behera GB, Mishra BK, Behera PK, Panda M (1999) Fluorescent probes for structural and distance effect studies in micelles, reversed micelles and microemulsions. Adv Colloid Interface Sci 82:1–42

10. Szajdzinska-Pietek E, Schlick S (2005) Self-assembling of ion-containing polymers and surfactants in aqueous solutions studied by ESR and fluorescence probes. J Mol Liq 117:153–164
11. Nakashima K, Bahadur P (2006) Aggregation of water-soluble block copolymers in aqueous solutions: recent trends. Adv Colloids Interface Sci 123:75–96
12. Duhamel J (2012) New insights in the study of pyrene excimer fluorescence to characterize macromolecules and their supramolecular assemblies in solution. Langmuir 28:6527–6538
13. Hamley IW (1998) Physics of block copolymers. Oxford University Press, New York
14. Riess G (2003) Micellization of block copolymers. Prog Polym Sci 28:1107–1170
15. Hadjichristidis N, Pispas S, Floudas GA (2003) Block copolymers. Synthetic strategies, physical properties and applications. Wiley, Hoboken, NJ
16. Tian MM, Qin AW, Ramireddy C, Webber SE, Munk P, Tuzar Z, Prochazka K (1993) Hybridization of block-copolymer micelles. Langmuir 9:1741–1748
17. Uhlík F, Limpouchová Z, Jelínek K, Procházka K (2004) Polyelectrolyte shells of copolymer micelles in aqueous solutions: a Monte Carlo study. J Chem Phys 121:2367–2375
18. Robin MP, O'Reilly RK (2015) Strategies for preparing fluorescently labelled polymer nanoparticles. Polym Int 64:174–182
19. Wilhelm M, Zhao CL, Wang YC, Xu RL, Winnik MA, Mura JL, Riess G, Croucher MD (1991) Polymer micelle formation. 3. Poly(styrene-ethylene oxide) block copolymer micelles formation in water—a fluorescence probe study. Macromolecules 24:1033–1040
20. Štěpánek M, Podhájecká K, Procházka K, Teng Y, Webber SE (1999) Fluorometric and ultraviolet-visible absorption study of poly(methacrylic acid) shells of high-molar-mass block copolymer micelles. Langmuir 15:4185–4193
21. Saldanha C, Santos NC, Martins-Silva J (2002) Fluorescent probes DPH, TMA-DPH and C-17-HC induce erythrocyte exovesiculation. J Membr Biol 190:75–82
22. Maroncelli M (1993) The dynamics of solvation in polar liquids. J Mol Liq 57:1–37
23. Horng ML, Gardecki JA, Papazyan A, Maroncelli M (1995) Subpicosecond measurements of polar solvation dynamics—Coumarin-153 revisited. J Phys Chem 99:17311–17337
24. Fee RS, Maroncelli M (1994) Estimating the time-zero spectrum in time-resolved emission measurements of solvation dynamics. Chem Phys 183:235–247
25. Parasassi T, Krasnowska EK, Bagatolli L, Gratton E (1998) LAURDAN and PRODAN as polarity-sensitive fluorescent membrane probes. J Fluoresc 8:365–373
26. Hawe A, Sutter M, Jiskoot W (2008) Extrinsic fluorescent dyes as tools for protein characterization. Pharm Res 25:1487–1499
27. Hutterer R, Schneider FW, Sprinz H, Hof M (1996) Binding and relaxation behaviour of prodan and patman in phospholipid vesicles: a fluorescence and H-1 NMR study. Biophys Chem 61:151–160
28. Šachl R, Štěpánek M, Procházka K, Humpolíčková J, Hof M (2008) Fluorescence study of the solvation of fluorescent probes prodan and laurdan in poly(epsilon-caprolactone)-block-poly (ethylene oxide) vesicles in aqueous solutions with tetrahydrofurane. Langmuir 24:288–295
29. Singh PK, Kumbhakar M, Pal H, Nath S (2008) Effect of electrostatic interaction on the location of molecular probe in polymer-surfactant supramolecular assembly: a solvent relaxation study. J Phys Chem B 112:7771–7777
30. Sen P, Ghosh S, Sahu K, Mondal SK, Roy D, Bhattacharyya K (2006) A femtosecond study of excitation wavelength dependence of solvation dynamics in a PEO-PPO-PEO triblock copolymer micelle. J Chem Phys 124:204905
31. Humpolíčková J, Štěpánek M, Procházka K, Hof M (2005) Solvent relaxation study of pH-dependent hydration of poly(oxyethylene) shells in polystyrene-block-poly (2-vinylpyridine)-block-poly(oxyethylene) micelles in aqueous solutions. J Phys Chem A 109:10803–10812
32. Matyus L, Szöllosi J, Jenei A (2006) Steady-state fluorescence quenching applications for studying protein structure and dynamics. J Photochem Photobiol B Biol 83:223–236
33. Stern O, Volmer M (1919) Über die Abklingzeit der Fluoreszenz. Phys Z 20:183–188

34. Lehrer SS (1971) Solute perturbation of protein fluorescence—quenching of tryptophyl fluorescence of model compounds and of lysozyme by iodide ion. Biochemistry 10:3254–3263
35. Webber SE (1998) Polymer micelles: an example of self-assembling polymers. J Phys Chem B 1998(102):2618–2626
36. Luo LB, Eisenberg A (2001) Thermodynamic size control of block copolymer vesicles in solution. Langmuir 17:6804–6811
37. Štěpánek M, Procházka K (1999) Fluorometric studies of the polyelectrolyte shell of block copolymer micelles in aqueous media. Langmuir 15:8800–8806
38. Kwon GS, Naito M, Yokoyama M, Okano T, Sakurai Y, Kakaoka K (1995) Physical entrapment of adriamycin in AB block-copolymer micelles. Pharm Res 12:192–195
39. Fernández MS, Fromherz P (1977) Lipoid pH indicators as probes of electrical potential and polarity of micelles. J Phys Chem 81:1755–1761
40. Štěpánek M, Procházka K, Brown W (2000) Time-dependent behavior of block polyelectrolyte micelles in aqueous media studied by potentiometric titrations, QELS and fluorometry. Langmuir 16:2502–2507

Pyrene-Labeled Water-Soluble Macromolecules as Fluorescent Mimics of Associative Thickeners

Jean Duhamel

Contents

Abstract The strong hydrophobicity of the chromophore pyrene combined with its ability to form an excimer has led to its use as a fluorescent replacement of the hydrophobes typically used in associative thickeners to prepare water-soluble polymers (WSPs) labeled with a small number of pyrene pendants to yield pyrene-labeled WSPs (Py-WSPs). Since the kinetics of excimer formation by diffusion are coupled, the fluorescence decays of the pyrene monomer and excimer can be analyzed globally to assess the fraction of pyrene labels that are isolated in solution and form excimer by diffusion and the fraction (f_{agg}) of pyrenes that are pre-associated and form excimer instantaneously upon direct absorption of a photon. This review describes how new developments in the global analysis of the fluorescence decays of the pyrene monomer and excimer of Py-WSP aqueous solutions yield quantitative information about the associative strength f_{agg} of Py-WSP. Most importantly for fluorescent mimics of associative thickeners, the review describes the viscoelastic behavior of a series of pyrene-labeled hydrophobically modified alkali swellable emulsion copolymers. Based on the viscoelasticity results, Py-WSPs appear to be excellent fluorescent mimics of non-fluorescent commercial associative thickeners, displaying similar behavior in terms of massive shear thinning and increase in zero-shear viscosity with polymer concentration. Consequently, the experiments described in this review provide a

J. Duhamel (✉)
Department of Chemistry, Institute for Polymer Research, Waterloo Institute for Nanotechnology, University of Waterloo, Waterloo, ON, Canada, N2L 3G1
e-mail: jduhamel@uwaterloo.ca

K. Procházka (ed.), *Fluorescence Studies of Polymer Containing Systems*,
Springer Series on Fluorescence 16, DOI 10.1007/978-3-319-26788-3_7

solid foundation for the characterization of the behavior of Py-WSP in aqueous solution by both fluorescence and rheology measurements.

Keywords Pyrene aggregates and excimer • Associative thickeners • Fluorescence Blob Model • Model free analysis • Fluorescence • Surfactants

1 Introduction

Over the past decades, amphiphilic macromolecules have found numerous industrial applications as polymeric surfactants in personal care products, associative thickeners and colloidal stabilizers in paints, or shear-thinning agents for enhanced oil recovery [1–9]. These amphiphilic macromolecules are typically water-soluble polymers (WSPs) which have been hydrophobically modified with a small amount of covalently attached hydrophobes to yield a hydrophobically modified WSP or HMWSP. In aqueous solution, the hydrophobes of HMWSPs minimize their exposure to water by self-assembling into hydrophobic aggregates which are stabilized by the solvated WSP segments. The hydrophobic content, the nature of the WSP whether it is neutral, ionic, pH-, or temperature-responsive, and the overall molecular architecture of a HMWSP are all parameters whose balance determines whether a HMWSP will undergo an open or close association mechanism. Among these parameters, the hydrophobic content is critical in the design of a HMWSP since a HMWSP with too large a hydrophobic content will precipitate in water before a sufficiently large polymer concentration can be reached to induce interpolymeric association while too low a hydrophobic content will fail to induce association.

There are three main families of commercially relevant associative thickeners (AT) [10]. One main family of ATs comprises the hydrophobically modified hydroxyethyl cellulose [11]. Hydrophobically modified ethoxylated urethanes or HEURs are obtained by condensation polymerization of short poly(ethylene glycol)s (PEGs) and diisocyanates in the presence of long chain aliphatic alcohols (C_{12} or greater) [12]. Consequently, HEURs are linear chains of PEG stitched together with rigid diurethane segments terminated with aliphatic groups. Hydrophobically modified alkali swellable emulsion (HASE) copolymers are produced as a latex suspension by copolymerizing under acidic pH methacrylic acid, ethyl acrylate, and a macromonomer constituted of a PEG chain terminated at one end with a hydrophobe and connected at the other end to a methylstyrene monomer via a urethane bond [2]. Under the form of a latex, the HASE suspension has a very low viscosity comparable to that of water. Under basic conditions however, the methacrylate anions generated along the HASE backbone favor the solubilization of the polymer which is associated with the breakup of the latex and the formation of a polymeric network which thickens the solution dramatically.

Not only do HMWSPs self-assemble in water but their amphiphilic nature enables them to also interact with small amphiphilic molecules such as surfactants

and lipids and these associations induce particularly interesting solution properties [13–16]. In the presence of the proper quantities of HMWSPs and surfactants, the viscosity of the solution can increase by several orders of magnitude as the surfactant enhances the ability of the HMWSPs to associate intermolecularly and create an extended network in solution [13].

Because of their important industrial applications, the solution properties of HMWSPs have been intensively studied. Numerous techniques have been used to probe different aspects of the associative behavior of HMWSPs in water. Since aqueous solutions of HMWSPs have remarkable viscoelastic properties, rheology has been instrumental in characterizing these properties such as the distribution of relaxation times of HMWSP solutions or the concentration of elastically active junctions from G_o, the plateau value of the storage modulus at high frequency [9, 10, 15, 17]. Surprisingly considering the complex behavior of AT solutions, HEUR aqueous solutions are characterized by a single relaxation time [9]. Surface tension, conductivity measurements with surfactant-selective electrodes, and isothermal calorimetry can detect the onset concentration (CAC) where associations between surfactants and HMWSPs take place and the concentration C_m where the HMWSPs are saturated with surfactants and binding of surfactant onto HMWSPS can no longer be detected upon further addition of surfactant [8, 18]. Dynamic Light Scattering (DLS) yields the distribution of the hydrodynamic diameters (D_h) of the species present in solution, the small species with a D_h of less than 10 nm representing isolated HMWSPs with the larger species being aggregates of HMWSPs. Since the LS signal is dominated by larger objects, isolated HMWSPs are no longer detected by DLS at HMWSP concentrations sufficiently large to generate a large population of aggregated HMWSPs [19]. The aggregation number and diameter of the hydrophobic domains generated by the associations of HMWSPs into polymeric micelles have been determined by time-resolved fluorescence experiments on free molecular pyrene physically bound to the micelles [20] and small angle neutron scattering (SANS) [21], respectively. Together, these techniques provide a means to characterize the fascinating properties of HMWSPs in aqueous solutions in terms of their rheological behavior, dimension of the hydrophobic microdomains generated by the hydrophobes, and concentration regime where HMWSPs self-assemble into extended networks.

While the information retrieved from these techniques is highly relevant to the study of HMWSPs, it is noticeable that the behavior of the hydrophobes, which are themselves critical for the self-assembly of the HMWSPs in the first place, cannot be probed easily by any of these techniques. Yet the level of clustering of hydrophobes along a WSP chain [22–24], the molecular volume occupied by the hydrophobe [25], or the spacer length separating the hydrophobes from the main chain [26] have been shown to be important parameters that control the associative behavior of HMWSPs in aqueous solution. There is much to learn on how interactions between hydrophobes are affected at the molecular level by these parameters, and in turn, how these hydrophobic interactions affect the associative behavior of HMWSPs in solution. The primary requirement for a technique capable of retrieving such information would be that it distinguishes whether the hydrophobes are in one of two states, namely isolated or aggregated.

The ability of pyrene, a hydrophobic fluorophore, to form an excimer upon encounter between an excited and a ground-state pyrene monomer has made pyrene the ideal candidate to probe the hydrophobic interactions taking place in aqueous solutions of HMWSPs by replacing the hydrophobic pendants of HMWSPs by pyrene derivatives and monitoring the extent of pyrene excimer formation by fluorescence [27]. 1-Pyrenemethanol, 1-pyrenemethylamine, 1-pyreneacetic acid, 1-pyrenebutanol, 1-pyrenebutyric acid, and 1-pyrenebutylamine are examples of commercially available derivatives of pyrene that can be used to label a WSP with small amounts of pyrene to generate a pyrene-labeled WSP (Py-WSP) where pyrene acts as the hydrophobic moiety of an equivalent non-fluorescent HMWSP. The astounding photophysical properties of pyrene allow one to probe the local environment surrounding a pyrene monomer by inferring its micropolarity from the I_1/I_3 ratio (the ratio of the fluorescence intensity of the first over the third peak in the fluorescence spectrum of the pyrene monomer) of a 1-pyrenemethoxy or 1-pyrenemethylamine derivative or its microviscosity from the magnitude of the pyrene lifetime (τ_M). Indeed, τ_M for a WSP randomly labeled with 1-pyrenemethylamine typically ranges between ~120 and 150 ns in aerated water but can be larger than 200 ns in a highly viscous hydrophobic environment that shields pyrene from contact with oxygen dissolved in water [28]. Furthermore, hydrophobically driven pyrene–pyrene interactions can be assessed from the I_E/I_M ratio (the ratio of the fluorescence intensity of the pyrene excimer over that of the monomer), the P_A ratio (the peak to trough ratio of the pyrene absorption spectrum), comparison of the P_E and P_M ratios (the peak to trough ratio of the fluorescence excitation spectra of the pyrene monomer and excimer, respectively), and the magnitude of the A_{E-}/A_{E+} ratio (the ratio of the sum of the negative pre-exponential factors over that of the positive pre-exponential factors obtained from the multiexponential fit of the excimer decays). The relationship that exists between these photophysical properties of pyrene and the associative behavior of Py-WSPs in aqueous solutions is now well established and has been thoroughly reviewed numerous times [27–30].

Despite the abundance of information retrieved about the behavior of the hydrophobic pyrene labels of Py-WSPs by monitoring the parameters I_1/I_3, τ_M, I_E/I_M, P_A, P_E, P_M, and A_{E-}/A_{E+} presented above, it is remarkable that all these parameters provide only qualitative information about the behavior of the pyrene labels. Considering the wealth of knowledge about the photophysical properties of pyrene harnessed over the past five decades since the kinetics of pyrene excimer formation were first handled by Birks [31], it might look somewhat surprising that so little effort might have been devoted toward developing procedures aiming to retrieve the molar fraction of aggregated pyrene, f_{agg}. Yet in terms of the characterization of the hydrophobic interactions taking place between the pyrene labels of a Py-WSP in water, f_{agg} appears to represent a much more accurate description of the extent of hydrophobic association compared to the ratios I_E/I_M, P_A, P_E, P_M, and A_{E-}/A_{E+} discussed earlier which only offer qualitative information about what f_{agg} is likely to be. The main reason for the dearth of scientific reports on f_{agg} comes from the complexity associated with the multiexponential analysis of the pyrene

monomer and excimer fluorescence decays acquired with aqueous solutions of Py-WSPs [32–34]. This complexity together with the knowledge that sums of exponentials yield unreliable kinetic parameters in the analysis of fluorescence decays [35] provided a grim outlook to the scientific community for tackling the issue.

Over the past 15 years, the Fluorescence Blob Model (FBM) in 1999 [36] and the Model Free Analysis (MFA) in 2005 [37] were introduced to, first, deal with the distribution of excimer rate constants that led to the multiexponential character of the fluorescence decays acquired with Py-WSPs and, second, provide a robust analytical framework to analyze the monomer and excimer fluorescence decays globally to yield reliable f_{agg} values. The aim of this chapter is to describe the mathematic rationale underlying the application of the FBM and MFA to retrieve f_{agg} from the decay analysis and present experimental examples describing the implementation of these robust analytical tools.

2 Fluorescence Decay Analysis

In the vast majority of instances, the pyrene monomer fluorescence decays acquired with aqueous solutions of Py-WSPs, particularly when the pyrene labels are randomly incorporated into a WSP, are always multiexponential in nature. This experimental observation is a consequence of the distribution of distances between an excited pyrene and a ground-state pyrene or pyrene aggregate formed in water that leads to a distribution of rate constants for excimer formation by diffusion [30–32, 34]. Unfortunately, the analysis of multiexponential decays is notoriously difficult to handle and unless the decay times resulting from the photophysical processes are well resolved (i.e., separated by a factor of at least 2) as is the case for pyrene end-labeled short alkyl oligomers, the parameters retrieved from a triexponential fit should be considered with utmost caution [32]. Indeed early reports [38, 39] on the analysis of the fluorescence decays of Py-WSP based on the DMD model [40] or one of its variants introduced originally by Zachariasse to deal with the multiexponential decays of pyrene end-labeled oligomers yielded sets of parameters whose validity has been questioned [41].

The kinetic analysis of these multiexponential decays required a radical departure from the classic photophysical approach that attempted to assign a rate constant representing a specific photophysical process to each decay time. Instead, it was proposed that an excited pyrene label covalently attached onto a WSP would probe a restricted volume in the solution [34]. This proposal came from the consideration that the motion of an excited pyrene label is strongly hindered as it must drag the polymer segment it is attached to in order to move through the crowded polymer coil and that its ability to form an excimer is limited by the time it remains excited since no excimer formation can take place upon encounter between two ground-state pyrenes. The volume probed by the excited pyrene label was referred to as a *blob* which could then be used to compartmentalize the polymeric ensemble of

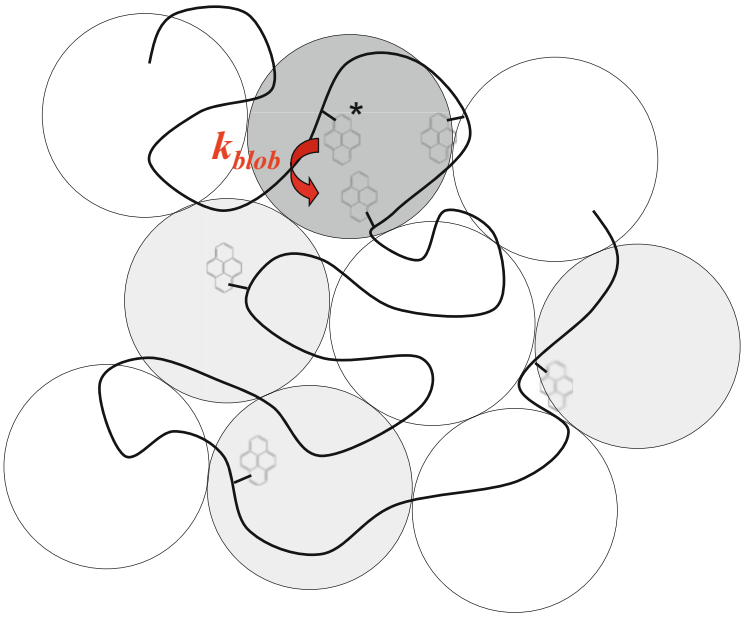

Scheme 1 Compartmentalization of a polymer coil into *blobs* among which the pyrene labels distribute themselves randomly

associated Py-WSPs into a cluster of *blobs* among which ground-state (GS) pyrene monomers and pyrene aggregates would distribute themselves randomly according to a Poisson distribution as depicted in Scheme 1. Based on this proposal, the kinetics of pyrene excimer formation could be handled in the following manner. Inside a *blob*, diffusive backbone motions would bring a GS pyrene within striking distance of an excited pyrene with a rate constant k_{blob}. The presence of two pyrene labels within a short distance of each other, a distance also referred to as a capture radius (R_{C}) [42–44], allows hydrophobic forces to drive the encounter between an excited and a GS pyrene with a rate constant k_2 which has been found to be much larger than k_{blob} [31, 32]. Any multiple i of GS pyrenes present in a *blob* results in a rate constant for diffusive motions given by the product $i \times k_{\text{blob}}$. GS pyrenes or pyrene aggregates can diffuse in and out of a *blob* according to the product of the exchange rate constant and the local concentration of *blobs* inside the polymeric assembly, namely the product $k_{\text{e}} \times [blob]$. The kinetic analysis of the fluorescence decays of the pyrene monomer and excimer yields k_{blob}, $k_{\text{e}} \times [blob]$, the average number of GS pyrene monomers and pyrene aggregates per *blob* $\langle n \rangle$, k_2, and the molar fractions f_{diff}, f_{free}, f_{k2}, and f_{E0} of the pyrene species Py^*_{diff}, Py^*_{free}, Py^*_{k2}, and $E0^*$ that diffuse in solution with a rate constant k_{blob} do not form excimer, form excimer with a rate constant k_2, and form an excimer instantaneously upon direct excitation, respectively. In many cases, a small contribution (f_{EL}) of long-lived dimers (EL^*) has been found as a result of poorly stacked pyrene monomers [45]. The parameter f_{E0}, or the sum ($f_{\text{E0}}+f_{\text{EL}}$) if the EL^* species is also present,

could be taken as a measure of f_{agg}, the molar fraction of aggregated hydrophobes for a HMWSP in aqueous solution. The *blob* analogy applied to handle the complex kinetics of pyrene excimer formation in polymers randomly labeled with pyrene, including Py-WSPs in aqueous solution, has led this mathematical treatment to be referred to as the Fluorescence Blob Model (FBM).

The first application of the FBM to determine f_{agg} for a series of poly(*N*,*N*-dimethyl-acrylamide)s randomly labeled with different amounts of pyrene (Py-PDMA) was conducted in the following manner [43]. First the fluorescence decays of the pyrene monomer were fitted according to the FBM to yield k_{blob}, $\langle n \rangle$, the product $k_e \times [blob]$, and the fractions f_{Mdiff} and f_{Mfree} of the pyrene species Py^*_{diff} and Py^*_{free} detected in the monomer decay. These early experiments were carried out with a Photon Research Associate time-resolved fluorometer originally purchased in the 1970s whose poor temporal resolution did not detect the too short-lived pyrene species Py^*_{k2}. The parameters retrieved from the FBM of the pyrene monomer decays were then fixed for the analysis of the excimer fluorescence decays which yielded the excimer lifetimes τ_{E0} and τ_{EL} and the molar fractions f_{Ediff}, f_{EE0}, and f_{EEL} of the pyrene species Py^*_{diff}, $E0^*$, and EL^* found in the excimer decays. The fractions f_{Mdiff}, f_{Mfree}, f_{Ediff}, f_{EE0}, and f_{EEL} could then be combined to yield the molar fractions f_{diff}, f_{free}, f_{E0}, and f_{EL} representing all the pyrene species in the solution. This first study constituted a proof of principle that the complex fluorescence decays of pyrene monomer and excimer acquired with aqueous solutions of Py-PDMA could be analyzed in a quantitative manner to yield physically relevant kinetic and structural parameters. It was found that $f_{E0}+f_{EL}=f_{agg}$ increased with increasing pyrene content and that f_{agg} decreased when increasing volumes of acetone were added to the aqueous solutions of Py-PDMA. These results were reasonable since higher pyrene contents would induce stronger pyrene aggregation in water while increasing amounts of acetone mixed in water would reduce pyrene association as acetone is a good solvent for pyrene. This protocol was applied to probe the hydrophobic interactions of a series of pyrene-labeled hydrophobically modified alkali swellable emulsion copolymers (Py-HASE) [46, 47].

This early success in the sequential analysis of complex fluorescence decays led to the implementation of a program that would analyze globally the fluorescence decays of the pyrene monomer and excimer of any Py-WSP according to the FBM to yield k_{blob}, $k_e \times [blob]$, $\langle n \rangle$, k_2, and the molar fractions f_{diff}, f_{free}, f_{k2}, f_{E0}, and f_{EL} [48]. In so doing, a complete description of a broad range of Py-WSP aggregates in water could be obtained in terms of kinetic behavior with the rate constant k_{blob}, k_2, and $k_e \times [blob]$ and structural composition with the molar fractions f_{diff}, f_{free}, f_{k2}, f_{E0}, and f_{EL}. This global analysis was applied to monitor the interactions of Py-HASEs with surfactants [49–51].

At about the same time, this laboratory got involved in the characterization of other pyrene-labeled macromolecules such as pyrene-labeled lipids associating in a membrane bilayer [52] or a 2K semi-telechelic poly(ethylene oxide) (Py_1-PEO) forming polymeric micelles in water [53] for which the notion of an excited pyrene diffusing inside a *blob* might be more challenging to apply. While the FBM analysis

of fluorescence decays acquired with such pyrene-labeled macromolecules might be difficult to justify from a physical standpoint as the concept of *blobs* could not be easily introduced to model pyrene excimer formation in these systems, the actual parameters retrieved from the analyses based on the FBM were yielding quite sensible trends. A smaller k_{blob} value would reflect slower diffusive motions within a pyrene-labeled macromolecule, whereas an increase in $f_{E0}+f_{EL}=f_{agg}$ would indicate an increased level of association between the pyrene labels. These observations led to the realization that it should be possible to describe the diffusion-controlled pyrene excimer formation without making any physical assumption on this process while still retaining the ability to determine the molar fractions f_{diff}, f_{free}, f_{E0}, and f_{EL} quantitatively. The implementation of the MFA was a result of these considerations [35].

In the MFA, the monomer fluorescence decay is fitted with a sum of exponentials whose pre-exponential factors a_i and decay times τ_i describe pyrene excimer formation by diffusion. These same a_i and τ_i parameters obtained from the monomer decay analysis were also fixed to the same values in the excimer decay analysis and the monomer and excimer decays were fitted globally with this set of constraints. It is important to stress at this stage the importance of these constraints as they are the key for retrieving reliable parameters that accurately describe the kinetics of pyrene excimer formation in pyrene-labeled macromolecules. While these constraints were readily built in the programs that used a FBM-based global analysis of the monomer and excimer fluorescence decays so that the parameters k_{blob}, $\langle n \rangle$, and $k_e \times [blob]$ could be retrieved from the global fit of both monomer and excimer fluorescence decays, it was not so obvious from our earlier papers that these constraints were also incorporated in the programs that used the MFA. Indeed, global analysis of the pyrene monomer and excimer fluorescence decays had been carried out earlier by many other research groups [36, 37, 54–56], and the equations used for these fits shared many similarities with those used in the MFA. The crucial distinction was that all previous analyses focused on the decay times used in the exponentials that were kept the same in the monomer and excimer decay analysis while omitting to consider the pre-exponential factors which were left free to float. Imposing that the pre-exponential factors in the excimer decays be a function of the monomer pre-exponential factors a_i and decay times τ_i reduced the number of degrees of freedom and brought to the fore an unprecedented level of accuracy in their recovery. In turn, this improved accuracy in the recovery of the pre-exponential factors and decay times led to an accurate description of the expected behavior of the Py-WSP aqueous solutions. Since this analysis did not make any assumption on the process of pyrene excimer formation, it was referred to as the Model Free Analysis or MFA. The MFA yielded the average rate constant of pyrene excimer formation $\langle k \rangle$ found to equal $\sum a_i / \sum a_i \tau_i - 1/\tau_M$ as well as the molar fractions $f_{diff}, f_{free}, f_{E0}$, and f_{EL}. In any study where the monomer and excimer fluorescence decays were fitted globally according to the FBM or MFA, identical parameters were retrieved confirming that both analyses are internally consistent and provide a robust analytical tool to describe pyrene excimer formation

quantitatively [35, 39, 48, 49]. A number of selected examples of application of the FBM and MFA to the characterization of pyrene-labeled water-soluble macromolecules are presented hereafter.

3 Applications of the FBM and MFA

Molar Fractions of the Pyrene Species in Solution One of the main claims made by this laboratory about fitting the monomer and excimer decays globally according to the FBM and MFA is that these analyses yield a set of parameters that are representative of the pyrene-labeled macromolecules being investigated. One important experiment conducted toward validating this claim probed the self-assembly of a pyrene-labeled Gemini surfactant in water [57]. The chemical structure of the Gemini surfactant referred to as Py-3-12 considered is given in Fig. 1a. Py-3-12 is constituted of two hydrophobic tails, namely a 1-pyrenehexyl and a dodecyl hydrophobes connected by a propyl linker via two dimethylammonium cations. The self-assembly of Py-3-12 in water was monitored by UV-Vis absorption and steady-state and time-resolved fluorescence as a function of surfactant concentration. As the Py-3-12 concentration was increased from the critical micellar concentration (CMC) of 0.22 mM to 0.6 mM, the P_A value of Py-3-12 solutions was found to decrease from 1.8 to 1.6 suggesting strong hydrophobic aggregation of the pyrene labels. Yet this conclusion based on the P_A values was contradicted by the A_{E-}/A_{E+} ratio of -0.70 ± 0.04 found from the excimer decay analysis whose value suggested a low level of aggregation between the pyrene pendants. In the end, the A_{E-}/A_{E+} ratios were found to properly describe the state of the pyrene labels. The apparent broadening of the absorption spectra of Py-3-12 in

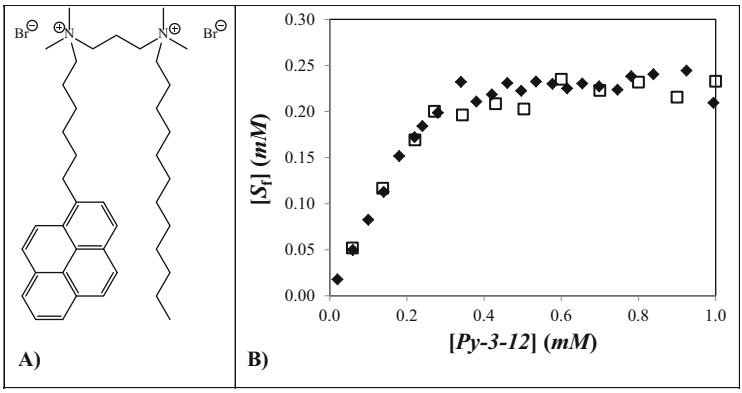

Fig. 1 (**a**) Chemical structure of Py-3-12. (**b**) Plot of the concentration of unmicellized Py-3-12 surfactant [S_f] as a function of total Py-3-12 concentration. Fluorescence decays were acquired with the front-face (*filled diamond*) and right-angle (*open square*) geometry [55]. "Reprinted with permission from *Langmuir* **2011**, *27*, 3361–3371. Copyright 2014 American Chemical Society"

water as a function of surfactant concentration was a consequence of a 2 nm shift in the absorption spectrum of 1-pyrenehexyl from 343 nm in water to 345 nm when isolated in SDS micelles. As the Py-3-12 surfactant partitioned itself between water and the micelles, the two absorption bands were observed in the Py-3-12 solution resulting in an artificially broader absorption spectrum. Interestingly, the dodecyl chains of the Py-3-12 surfactant provided sufficient oil content in the micelles to solubilize the pyrene labels and minimize pyrene aggregation.

The monomer and excimer decays of the Py-3-12 solutions were acquired and fitted globally according to the MFA. The restricted geometry experienced by the pyrene labels in the Py-3-12 micelles led to the formation of two types of excimer, the shorter- and longer-lived excimers *E*0* and *EL** having a lifetime τ_{E0} and τ_{EL} above the CMC of 31 ± 2 and 59 ± 4 ns, respectively. MFA of the decays yielded the molar fractions f_{diff}, f_{free}, f_{E0}, and f_{EL}. The fraction f_{free} decreased from 0.9 to 0.2 as the Py-3-12 concentration was increased from 0.06 to 1.00 mM. These surfactant concentrations were chosen to bracket the 0.22 mM CMC of Py-3-12. The level of pyrene aggregation, $f_{E0} + f_{EL} = f_{agg}$, remained low and equal to 0.14 ± 0.03 over the entire range of Py-3-12 concentration studied, as expected from the A_{E-}/A_{E+} ratios. Most interestingly, multiplying f_{free} by the concentration of Py-3-12 surfactant yielded the concentration of free Py-3-12 surfactant in solution [S_f]. [S_f] increased with increasing surfactant concentration up to 0.22 mM above which [S_f] remained constant. This trend shown in Fig. 1 agrees perfectly with what would be expected of a surfactant whose CMC was found to equal 0.22 mM by surface tension measurements. This result strongly supports the notion that the global MFA of the monomer and excimer fluorescence decays acquired with Py-3-12 in water provides an accurate representation of the state of the pyrene labels. It was also the first time that this well-known effect about surfactants was probed by using pyrene excimer fluorescence. The average rate constant of pyrene excimer formation $\langle k \rangle$ was found to equal $7.8\ (\pm 0.8) \times 10^8\ s^{-1}$. As it turns out, this rate constant is comparable to that found in a fourth-generation pyrene end-labeled dendrimer where the local pyrene concentration generated by 16 pyrene labels in the dendrimers is very large [58], as large as that found in the Py-3-12 micelles.

While application of the MFA to the fluorescence decays of the Py-3-12 solutions in water has provided the strongest evidence so far that this type of fluorescence decay analysis can accurately retrieve the molar fractions of the pyrene species present in solution, other studies have provided further support that this is indeed the case. The study with the poly(*N*,*N*-dimethylacrylamide) randomly labeled with pyrene (Py-PDMA) has already been mentioned [43]. The pyrene labels of Py-PDMA were strongly aggregated in water, with f_{agg} increasing with increasing pyrene content. As acetone, an organic solvent that is miscible with water and can dissolve pyrene, was added to the aqueous solution, f_{agg} decreased continuously with increasing amount of acetone added to the solution. A similar study where f_{agg} was monitored as a function of the addition of an agent aiming to reduce the hydrophobically driven aggregation of the pyrene labels of a Py-WSP consisted in adding the surfactant sodium dodecyl sulfate (SDS) to a pH 9 aqueous

solution of Py-HASE [35]. The pyrene content of the Py-HASE equaled 36 μmol g^{-1}. At pH 9, the methacrylate monomers were negatively charged allowing complete dissolution of the polymer. At SDS concentration lower than 1.25 mM, most pyrene labels were aggregated and the global fit of the fluorescence decays according to the FBM and MFA yielded an f_{agg} value of 0.70 ± 0.05. Higher SDS concentrations resulted in a marked decrease in f_{agg} as the surfactant interacted with the pyrene aggregates by forming mixed micelles of SDS and pyrene in a process that isolated the pyrene labels.

In another example, known amounts of pyrene derivatives were purposely added to two solutions containing two different pyrene-labeled macromolecules [59]. In the first experiment, known amounts of a 2K semi-telechelic PEO chain labeled at one end with pyrene (Py_1-PEO(2K)) were introduced to a solution of a telechelic 2K PEO chain doubly end labeled with pyrene (Py_2-PEO(2K)). In a second experiment, 1-pyrenebutanol was added to solutions of a fourth-generation dendrimer end labeled with 16 pyrenyl units (Py_{16}-G4). The pyrene derivatives Py_1-PEO(2K) and 1-pyrenebutanol were selected as they represent typical fluorescent impurities encountered in the study by fluorescence of a doubly end-labeled PEO chain (Py_2-PEO) or a pyrene end-labeled dendrimer (Py_{16}-G4). The overall pyrene concentration was kept at 2.5×10^{-6} M, low enough to ensure that excimer formation would occur intramolecularly and that the pyrene derivatives that were added to the pyrene-labeled macromolecules would not induce intermolecular pyrene excimer formation. In each experiment, global MFA of the monomer and excimer fluorescence decays yielded the fraction f_{free} of pyrene labels that would not form excimer. The recovered f_{free} matched the value that was expected based on the composition of the mixtures. As f_{free} increased from 0.0 to 0.9 with increasing amounts of pyrene derivative added to the solution of excimer-forming pyrene-labeled macromolecules Py_2-PEO(2K) and Py_{16}-G4, the parameters describing pyrene excimer formation remained unchanged since excimer formation within the macromolecule was unaffected by the presence of the pyrene derivative.

Taken together, the experiments that were described above justified the claim that global fits of the monomer and excimer fluorescence decays according to the FBM and MFA provide a reliable means to determine the molar fractions of the different pyrene species present in solution. Considering the variety of pyrene-labeled macromolecules that have been synthesized to date, be they synthetic in nature [27, 29–31] or from a biological origin like DNA [60, 61] or proteins [62], the ability to characterize the nature of the pyrene labels, whether they form excimer by diffusion (Py^*_{diff} and Py^*_{k2}), are isolated in the macromolecule and cannot form excimer (Py^*_{free}), or are aggregated and form excimer instantaneously upon absorption of a photon ($E0^*$ and EL^*), offers a new and reliable means to probe these macromolecules at the molecular level. Examples of applications of these new analytical tools to the characterization of Py-WSPs are presented hereafter.

Associative Behavior of Py-HASE In 1997, the then Union Carbide company provided this laboratory with about 1 L of three samples of Py-HASE latex with

solid contents of about 30 wt% and having pyrene contents (λ_{Py}) determined in our first publication as 11, 42, and 65 μmol g^{-1} [44]. These samples will be referred to as Py(12)-HASE, Py(42)-HASE, and Py(65)-HASE65, respectively. Due to the repeated precipitations conducted to recover the Py-HASE samples from the emulsions, some variation in λ_{Py} values was observed from batch to batch. Nevertheless, by providing such large quantities of Py-HASE samples, Union Carbide enabled the implementation of an experiment rarely attempted with pyrene-labeled macromolecules, namely the characterization of the viscoelastic properties of associative thickeners whose hydrophobes had been replaced by pyrene labels. The dearth of examples for such investigations in the scientific literature is rooted in the large quantities of pyrene-labeled polymers that are required to conduct rheology experiments. Low viscosity samples for which the bob and cup geometry is necessary require gram quantities of Py-WSPs for each run. Compared to the ~50 mg quantities of pyrene-labeled sample typically prepared for fluorescence measurements, the difference in the amount of polymer needed to be synthesized for a rheology experiment is striking.

Supplied as a slightly acidic latex solution, the Py-HASE samples could be dissolved in tetrahydrofuran (THF), an organic solvent that dissolves both polymer and the pyrene labels [44]. The Py-HASE samples were also soluble in basic aqueous solution at pH 9. In both THF and basic aqueous solutions, the Py-HASE samples formed excimer with an I_E/I_M ratio that increased with λ_{Py}. But whereas the pyrene excimer fluorescence decays exhibited a pronounced rise time in THF, this rise time was practically absent from the Py-HASE samples in aqueous solutions indicating that pyrene excimer formation was induced by direct excitation of pyrene aggregates. Accordingly the A_{E-}/A_{E+} ratios observed for the excimer fluorescence decays of the Py-HASE samples in THF took values that were always more negative than −0.80, while their value was always more positive than −0.15 in aqueous solutions. These observations were corroborated by the global FBM analysis of the pyrene monomer and excimer fluorescence decays that yielded similar fractions of aggregated pyrenyl pendants for Py(42)-HASE and Py(65)-HASE found to equal 0.05 ± 0.01 and 0.58 ± 0.09 in THF and aqueous solution, respectively. In the organic solvent, the pyrene labels are soluble and very little aggregation is observed whereas water promotes hydrophobic associations of the labels. Certainly the most intriguing result from this analysis was not the exact value of f_{agg} but rather that f_{agg} was not equal to unity implying that a substantial amount of hydrophobes in the Py-HASE samples were not aggregated, even at Py-HASE concentrations as high as 10 g L^{-1}. This conclusion was confirmed later on using Py-HASE concentrations of up to 50 g L^{-1} [45]. This observation matters as the determination of many parameters used to predict the behavior of HMWSPs in solution, such as their aggregation number or junction density in a viscoelastic gel, often assumes that all hydrophobes are involved in hydrophobic associations. As our results demonstrated, this was certainly not the case for the Py-HASE samples and f_{agg} values substantially different from unity have also been found for other Py-WSPs such as a series of pyrene end-labeled poly(ethylene oxide)s

used as fluorescent mimics of HEURs [42]. Of course the discrepancy from unity observed for f_{agg} obtained with the Py-HASEs could have been due to the poor hydrophobicity of pyrene which might be insufficient to induce proper rheological properties. To address this concern, the viscoelastic properties of the Py-HASE aqueous solutions at pH 9 with 0.05 M KCl were characterized by static and dynamic rheology [45].

At the time where the rheology experiments with the Py-HASE samples were conducted, the ability of pyrene to act as a decent hydrophobe for the synthesis of associative thickeners had been demonstrated in a single example. In 1991, Richey et al. had prepared a HEUR sample where the hydrophobes had been replaced with 1-pyrenebutanol [63]. The Py-HEUR sample exhibited the typical fluorescence expected for a Py-WSP and its aqueous solution was found to have a large zero-shear viscosity and undergo shear thinning, both typical properties of associative thickeners in aqueous solution. These results suggested that pyrene induces hydrophobic associations strong enough to trigger the peculiar viscoelastic properties expected from aqueous solutions of HEURs. As for typical associative thickeners, the dissolution of the Py-HASE samples in basic aqueous solution, particularly those with a higher pyrene content, led to a rapid increase in solution viscosity with increasing Py-HASE concentration. Furthermore, the more concentrated Py-HASE solutions shear thinned, the solution viscosity decreasing by more than 4 orders of magnitude in some cases. The rapid increase of the zero-shear viscosity (η_o) with Py (35)-HASE concentration was illustrated in Fig. 2, where η_o was plotted as a function of Py(35)-HASE concentration. After a transitory concentration regime above the overlap concentration of the Py-HASEs, η_o was found to scale as [Py-HASE]^a where the exponent a took values of 3.5 ± 0.0, 8.0 ± 0.3, and 12.8 ± 0.4 for Py-HASE samples with λ_{Py} values of 12, 35, and 48 μmol g^{-1}. At a concentration of 45 g L^{-1}, the Py-HASE solutions had a viscosity of 61, 2730, and 6240 Pa s that increased with increasing pyrene content of 12, 35, and 48 μmol g^{-1}, respectively.

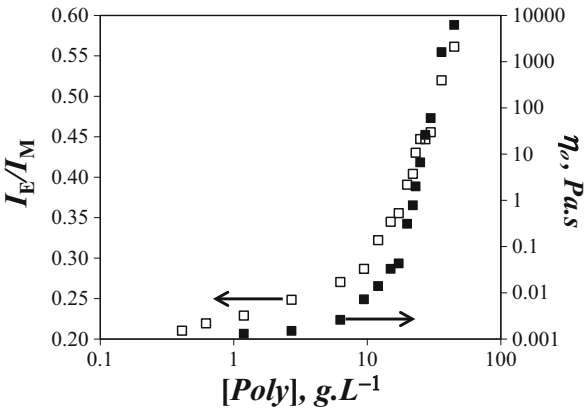

Fig. 2 Zero-shear viscosity and I_E/I_M ratios as a function of polymer concentration for Py(35)-HASE in basic aqueous solutions (pH 9, 0.05 M KCl, 0.01 M Na_2CO_3) [45]. "Reprinted with permission from *J. Phys. Chem. B* **2005**, *109*, 17406–17416. Copyright 2014 American Chemical Society"

Compared with the massive increase in η_o observed with increasing polymer concentration, the ratio I_E/I_M was found to increase to a much lesser extent. While η_o increased by seven orders of magnitude when the Py(35)-HASE concentration was increased from 1 to 45 g L^{-1}, the I_E/I_M ratio increased by less than threefold. Nevertheless, the increase in I_E/I_M was noticeable and indicated that intermolecular interactions occurred. Furthermore, it took place in the same concentration range where η_o increased suggesting that the increase in intermolecular hydrophobic association between the pyrene labels coincided with the increase in η_o, an expected result if it was due to the formation of an extended polymeric network between Py-HASE molecules.

The increase of the I_E/I_M ratio shown with Py(35)-HASE concentration in Fig. 2 was also observed with the other Py-HASE sample and it could be used as a measure of the ability of a given Py-HASE sample to generate intermolecular interactions, and thus its ability to form a viscoelastic polymeric network. Interestingly the increase in I_E/I_M with Py-HASE concentration, and thus the ability of a Py-HASE sample to form a network, differed with the pyrene content of the Py-HASE sample. The Py-HASE sample having a low pyrene content showed a much more pronounced increase in I_E/I_M with polymer concentration than the Py-HASE sample having a larger pyrene content. This result reflected the less compact structure of the coil of a Py-HASE polymer sample with a low pyrene content where the pyrene labels are more accessible to induce intermolecular associations. A Py-HASE sample with a large pyrene content would be more collapsed due to stronger intramolecular hydrophobic interactions resulting in a weaker ability to form intermolecular interactions. The increasing collapsed nature of the polymer coils observed for Py-HASE samples having increasing pyrene contents was corroborated by intrinsic viscosity measurements whereby the $[\eta]$ value of the Py-HASE samples was found to decrease with increasing pyrene content. This result was also confirmed by FBM analysis of the fluorescence decays which indicated that f_{agg} increased with increasing pyrene content of Py-HASE [44, 45].

The storage and loss moduli of the Py-HASE solutions were determined as a function of frequency to estimate the terminal relaxation time of the network (T_d) and the high-frequency plateau modulus (G_o). In general, G_o was found to decrease with increasing pyrene content, reflecting the lesser ability of the Py-HASE with a high pyrene content to form intermolecular elastically active chains. This result was somewhat contradictory to the much larger zero-shear viscosity (η_o) observed for the Py-HASE solutions prepared with polymers having a high pyrene content. This apparent contradiction was resolved by noting that the increase in the terminal relaxation time T_d with pyrene content was much more pronounced than the decrease in G_o with increasing pyrene content. Since η_o was found to equal the product $T_d \times G_o$, the overall result was that $T_d \times G_o$, and thus η_o, increased with increasing pyrene content.

Together, the results obtained from the fluorescence and rheology experiments led to the proposal that the peculiar viscoelastic behavior of Py-HASE could be rationalized with the following interpretation depicted in Fig. 3. A Py-HASE

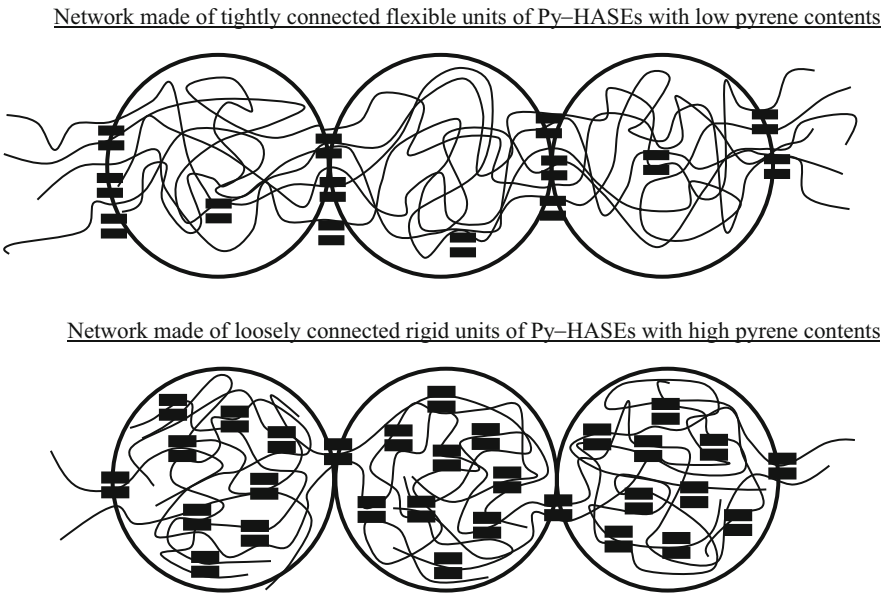

Fig. 3 Schematic representation of a network made of Py – HASE circular units held by hydrophobic aggregates (*double horizontal bands*). The *top* and *bottom* panels represent Py – HASEs having a low and high pyrene content, respectively [45]. "Reprinted with permission from *J. Phys. Chem. B* **2005**, *109*, 17406–17416. Copyright 2014 American Chemical Society"

sample with a high pyrene content would generate closed clusters of several Py-HASE chains that would be tightly connected into a rigid network held together by numerous hydrophobic associations. These clusters would then be connected with each other via a few elastically active hydrophobic aggregates, resulting in low G_o values. Under shear, the disruption of the few elastically active crosslinks leading to the observed shear-thinning behavior would occur on a timescale dictated by the slow relaxation time T_d of the rigid clusters. In the case of the Py-HASE sample having a low pyrene content, this sample was found to generate fewer hydrophobic associations suggesting the formation of less rigid clusters that would be connected to each other by a larger number of elastically active crosslinks, thus yielding larger G_o values. In turn, the clusters being less rigid would result in smaller T_d values.

In summary, the combination of rheology and pyrene fluorescence provided detailed insights into the complex viscoelastic behavior of aqueous solutions of Py-HASE. Most importantly, it demonstrated that the hydrophobicity of pyrene is sufficient to endow a Py-WSP with a rheological behavior that closely mimics that of the equivalent non-fluorescent HMWSP.

Interactions of Py-HASE with Surfactants When aqueous solutions are prepared with a constant concentration of a HMWSP and increasing amounts of surfactant are added to the HMWSP solution, the solution viscosity is found to undergo

dramatic changes over a narrow range of surfactant concentration, the viscosity typically passing through a maximum several orders of magnitude greater compared to the viscosity of the HMWSP solution without surfactant [13, 15, 16]. Over the years, two explanations have been proposed to rationalize this behavior. Both revolve around the notion that since η_o equals the product $T_d \times G_o$, an increase in η_o with increasing surfactant concentration is due to either an increase of T_d and/or G_o. The first explanation proposed that the addition of surfactant enhanced the networking ability of the HMWSP by creating mixed micelles composed of surfactant molecules and hydrophobic pendants from the HMWSP [13]. The process increases the solution viscosity until the optimum network is obtained and the viscosity passes through a maximum before decreasing again as more surfactants encapsulate the hydrophobes, isolating the HMWSPs and resulting in a breakdown of the polymeric network. Following this line of thoughts, changes in viscosity would then result from changes in the concentration of mixed micelles that incorporate the hydrophobes of different chains of HMWSPs and constitute elastically active junctions. These changes would be associated with changes in G_o that would be reflected in changes in η_o as experimentally observed. While this proposal was intuitively logical, it was contradicted by a later study where the parameters T_d and G_o were measured for a HMWSP as a function of the concentration of surfactant added [16]. It was found that with increasing surfactant concentration, G_o remained constant while T_d increased. This study led to a second proposal whereby addition of a surfactant to a HMWSP solution did not change the concentration of elastically active junctions, thus the constant G_o value observed as a function of surfactant concentration, but rather changed the terminal relaxation time of the polymeric network, namely T_d. The discrepancy between the two proposed rationals led to the idea that experiments conducted with the Py-HASE samples and sodium dodecyl sulfate (SDS) might shed some light onto the interactions that take place between the hydrophobic pyrenes and SDS and how the pyrenes distribute themselves among mixed micelles.

The interactions between Py-HASE and SDS could be easily recognized from the changes observed in the fluorescence spectra as SDS was added to the Py-HASE solution [35, 46–49]. For each aqueous solution prepared with a set Py-HASE concentration, two regimes in SDS concentration could be identified. At low SDS concentration, pyrene aggregates led to weak excimer emission resulting in low I_E/I_M ratios. As the SDS concentration increased, SDS surfactants interacted with the pyrene aggregates, releasing some pyrene monomers into the water phase, and enabling some diffusion between the pyrene hydrophobes leading to more efficient excimer formation and emission. As a result, the I_E/I_M ratio began to increase. As more SDS was added, excimer formation occurred principally by diffusive encounters between two pyrenes inside a mixed micelle and the I_E/I_M ratio passed through a maximum corresponding to the highest concentration of pyrene pendants per mixed micelles. Past this SDS concentration, further SDS addition reduced the pyrene occupancy of the mixed micelles resulting in isolated pyrene monomers along the HASE backbone that were encapsulated in SDS micelles and could no

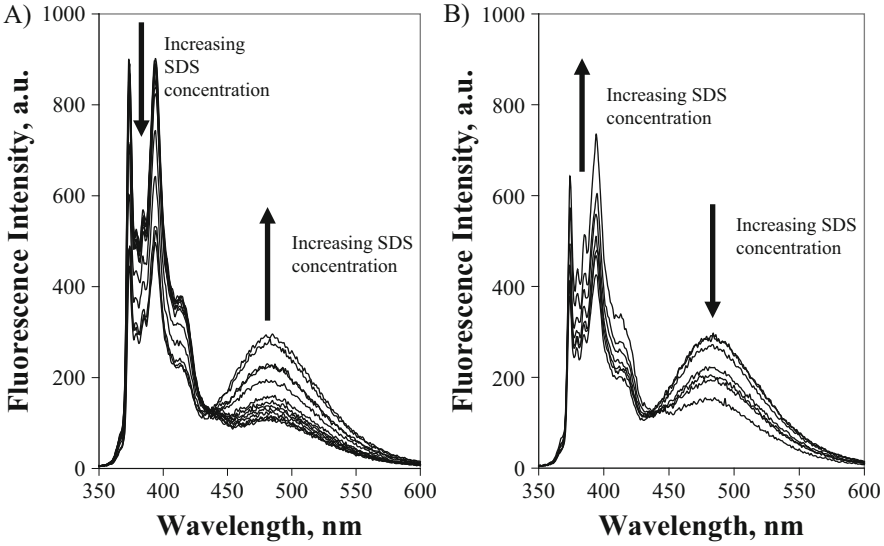

Fig. 4 Fluorescence emission spectra of a 10 g L^{-1} Py(38)–HASE in 0.01 M Na_2CO_3, pH 9 solution with SDS concentrations ranging from 0 to 8 mM (**a**), and from 9 to 50 mM (**b**). All samples were excited at 344 nm [48]. "Reprinted with permission from *Macromolecules* **2006**, *39*, 1144–1155. Copyright 2014 American Chemical Society"

longer form excimer. Consequently, a plot of I_E/I_M as a function of SDS concentration showed an increase in I_E/I_M with increasing SDS concentration followed by a decrease in I_E/I_M as further SDS was added to the solution. This behavior is illustrated in Figs. 4 and 5 for the 10 g L^{-1} Py(38)-HASE solution. Similar results were obtained with the solutions acquired with five other Py(38)-HASE concentrations of 0.01, 0.1, 1.0, 2.5, and 6.0 g L^{-1}.

Information about the polarity of the environment experienced by the pyrene labels of the 10 g L^{-1} Py(38)-HASE solution was determined from the I_1/I_3 ratios. The ratios I_1/I_3 of the fluorescence spectra shown in Fig. 4 were determined and they were plotted in Fig. 5 as a function of SDS concentration. The I_1/I_3 ratio remained constant at 1.59 ± 0.01 with SDS concentration up to an SDS concentration of 2.3 mM before reaching a constant value of 1.27 ± 0.04 for SDS concentrations greater than 10.7 mM. These I_1/I_3 ratios agreed closely with those of a model compound, namely a 2K PEO chain terminated at one end with a 1-pyrenemethoxy unit (Py_1-PEO(2K)), that yielded an I_1/I_3 ratio of 1.69 ± 0.03 and 1.38 ± 0.02 at low and high SDS concentration, respectively. The I_1/I_3 ratios obtained for Py(38)-HASE were slightly lower than those obtained with Py_1-PEO (2K) because the interior of the Py(38)-HASE coil contains some hydrophobic stretches of ethyl acrylate which create a less polar environment for the 1-pyrenemethoxy pendants than that encountered with Py_1-PEO(2K).

Besides the polarity of the environment experienced by the pyrene monomer, the level of pyrene aggregation could be inferred from the A_{E-}/A_{E+} ratios obtained from

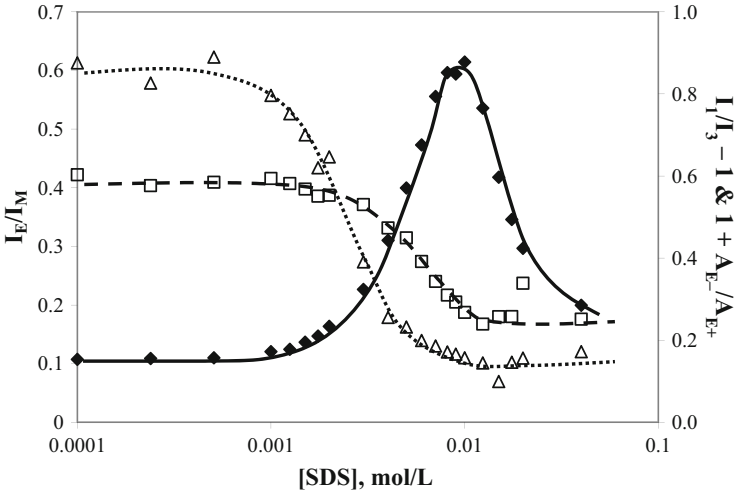

Fig. 5 Plot of I_E/I_M (*solid line*), $I_1/I_3 - 1$ (*dashed lines*), $1 + A_{E-}/A_{E+}$ (*dotted lines*) vs. SDS concentration for a 10 g L^{-1} Py(38)–HASE solution with 0.01 M Na_2CO_3 at pH 9 [48]. "Reprinted with permission from *Macromolecules* **2006**, *39*, 1144–1155. Copyright 2014 American Chemical Society"

the multiexponential analysis of the excimer fluorescence decays. The A_{E-}/A_{E+} ratios were also plotted in Fig. 5. The A_{E-}/A_{E+} ratios took a small and constant value equal to -0.16 ± 0.05 at low SDS concentration below 1.1 mM before becoming much more negative and equal to -0.86 ± 0.03 at high SDS concentrations above 5.5 mM. These values obtained for the A_{E-}/A_{E+} ratios were clear indication that the pyrene labels are aggregated at low SDS concentration but form excimer via diffusive encounter between two unassociated pyrene monomers at high SDS concentration. This behavior corresponds to what would be expected from the associations between a surfactant and a HMWSP in aqueous solution.

While informative, the ratios I_1/I_3 and A_{E-}/A_{E+} only provide a qualitative description of how the pyrene hydrophobic labels of Py(38)-HASE behave in aqueous solution. A much more accurate description is obtained by fitting globally the monomer and excimer decays according to the FBM or the MFA. Such analysis yields the molar fractions corresponding to the different states of the pyrene labels, namely the fractions f_{diff}, f_{free}, and f_{agg} which have been described earlier. These fractions were plotted as a function of SDS concentration in Fig. 6 for the 10 g L^{-1} Py(38)-HASE solution. At low SDS concentration, f_{agg} is the largest fraction and equals 0.61 ± 0.05 reflecting the high level of aggregation of the hydrophobic pyrene labels. SDS begins to interact with the pyrene aggregates at concentrations lower than 1 mM which reduces f_{agg}. These interactions between SDS and the pyrene aggregates result in the release of pyrene monomers into the water phase as indicated by the increase in f_{free}. Past an SDS concentration of 1 mM, sufficient SDS molecules are interacting with the pyrene hydrophobes to induce an increase in pyrene excimer formation by diffusion and f_{diff} increases. The creation of mixed

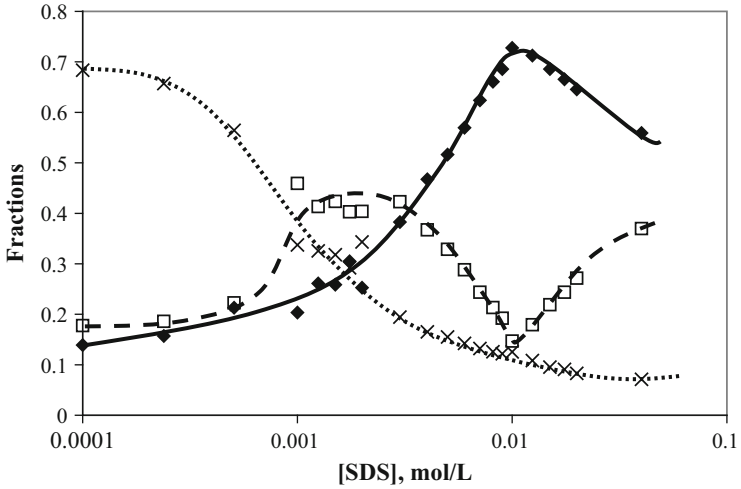

Fig. 6 f_{agg} (*dotted lines*), f_{diff} (*solid lines*), and f_{free} (*dashed lines*) as a function of SDS concentration for a 10 g L^{-1} Py(38)–HASE in 0.01 M Na_2CO_3 solution at pH 9 [48]. "Reprinted with permission from *Macromolecules* **2006**, *39*, 1144–1155. Copyright 2014 American Chemical Society."

micelles composed of pyrene labels and SDS molecules generates hydrophobic microdomains inside the Py(38)-HASE coil which results in the incorporation of the pyrene monomer that had been expelled earlier into the water phase back into the mixed micelles as indicated by the decrease in f_{free} for SDS concentrations greater than 2 mM. The concomitant increase in f_{diff} and decrease in f_{free} that occurred with increasing SDS concentration above 2 mM continued up to an SDS concentration of 10 mM above which the trends inverted with f_{diff} decreasing and f_{free} increasing with increasing SDS concentration. In this high SDS concentration regime, the pyrene labels are isolated inside mixed micelles that are mostly composed of one pyrene label and several SDS molecules. The trends shown in Fig. 6 for the molar fractions f_{diff}, f_{free}, and f_{agg} are reasonable and, to this day, they provide the most quantitative description currently available on the interactions taking place between the hydrophobes of a HMWSP and a surfactant.

In Fig. 6, f_{diff} peaks at an SDS concentration of 10 mM, close to the SDS concentration of 8.5 mM where the I_E/I_M ratio passes through its maximum in Fig. 5. Furthermore, FBM analysis of the fluorescence decays indicates that the pyrene labels of Py(38)-HASE are aggregated at low SDS concentration (high f_{agg} value in Fig. 6) which is also the concentration regime where the I_E/I_M ratio takes its lowest value. These trends suggested that the formation of excimer by diffusive encounters between two pyrene monomers led to stronger excimer emission and, thus, a larger I_E/I_M ratio than the emission resulting from an excimer formed by the direct excitation of a pyrene aggregate. This observation agreed with earlier reports that suggested that pyrene aggregates formed by Py-WSPs in aqueous solution lead to weaker excimer emission upon direct excitation than pyrene monomers forming

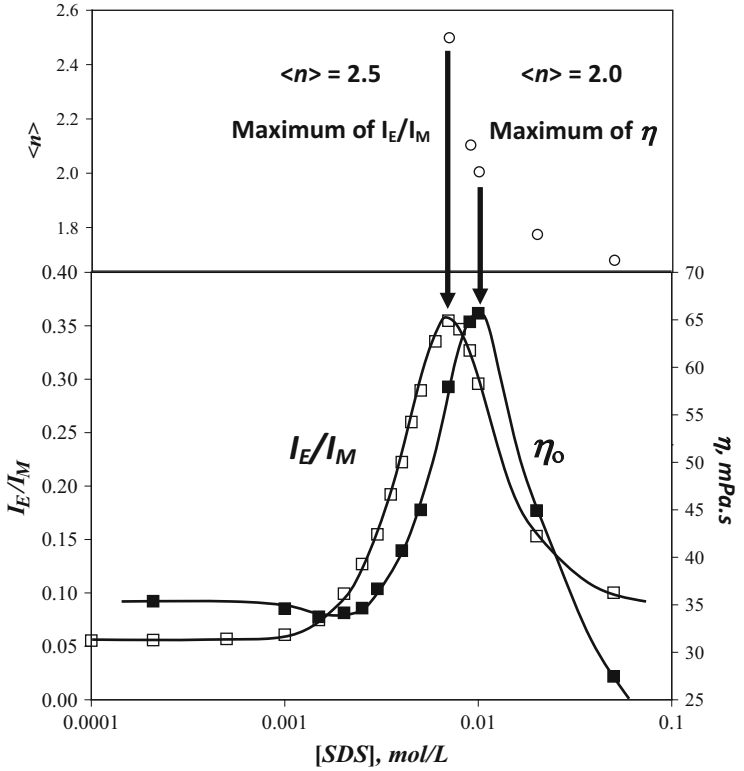

Fig. 7 Values of $\langle n \rangle$ (*top*) and I_E/I_M and η (*bottom*) plotted as a function of [SDS] for a Py(38)–HASE concentration of 6.0 g L^{-1} in 0.01 M Na_2CO_3 solution at pH 9. "Reprinted with permission from *Macromolecules* **2006**, *39*, 1144–1155. Copyright 2014 American Chemical Society"

excimer by diffusive encounters. In the case of Py(38)-HASE, the ability of the FBM analysis to recover the molar fractions of pyrene species that emit as isolated monomers or pyrene aggregates led to the conclusion that the fluorescence quantum yield of the excimer formed by diffusive encounters between the pyrene labels of Py(38)-HASE is 4.5 times larger than that of the pyrene aggregates [47]. This result rationalizes why the Py(38)-HASE aqueous solutions yield low I_E/I_M values at low SDS concentration where excimer is formed principally through direct excitation of weakly emitting pyrene aggregates but high when enough SDS is added to the solution to ensure pyrene excimer formation by diffusion inside the mixed micelles.

Having characterized at the molecular level the associative strength f_{agg} of a Py-HASE sample as SDS was added to the solution, the zero-shear viscosity (η_o) of a 6 g L^{-1} Py(38)-HASE solution was measured with an Ubbelohde viscometer as increasing amounts of SDS were added to the solution. Figure 7 shows a plot of η_o and I_E/I_M as a function of SDS concentration. The trends obtained for η_o and I_E/I_M were quite similar, both passing through a pronounced maximum in the same range of SDS concentrations, at an SDS concentration of 7.1 mM for the I_E/I_M ratio and

10 mM for η_o. However, it was noticeable that both trends were shifted relative to each other.

The origin of this shift could be traced back to the pyrene occupancy in the mixed micelles. An optimal network would be theoretically expected to have on average two hydrophobes of a HMWSP per elastically active junction. As it turns out, the average number of pyrenes per junction could be determined experimentally from the global fit of the monomer and excimer fluorescence decays according to the FBM. Indeed, the nature of the *blob* was expected to change as a function of SDS concentration. At low SDS concentration, a *blob* corresponds to the volume probed by an excited pyrene within the Py(38)-HASE coil, but as more SDS is added and mixed micelles form, the motion of an excited pyrene is now restricted to the volume of a mixed micelle. Consequently, the undefined *blobs* used by the FBM at low SDS concentration are being replaced by the more concrete mixed micelles at high SDS concentration. At high SDS concentration, the pyrene labels distributed themselves among the mixed micelles according to a Poisson distribution so that the average number of pyrenes per mixed micelle $\langle n \rangle$ retrieved from the FBM analysis was equivalent to the average number of hydrophobes per hydrophobic junction. For this equivalence to fully apply however, excimer formation needed to occur by diffusive encounters between pyrene labels which corresponded to SDS concentrations greater than 7.1 mM where the 6 g L^{-1} Py(38)-HASE solution yielded its maximum I_E/I_M ratio. A plot of $\langle n \rangle$ as a function of SDS concentration is shown in Fig. 7. As more SDS was added to the solution, $\langle n \rangle$ decreased continuously reflecting the dilution of the pyrene labels among an increasing number of mixed micelles. At the SDS concentration of 7.1 mM where I_E/I_M peaked, $\langle n \rangle$ took a value of 2.5 which decreased to 2.0 at the SDS concentration of 10 mM where η_o took its maximum value. Thus, the SDS concentration at the maximum in I_E/I_M corresponds to a situation where excimer formation by diffusion is enhanced by a high local pyrene concentration inside the mixed micelles resulting in a large pyrene occupancy $\langle n \rangle$ of 2.5. As more SDS was added to the solution, the pyrene labels distributed themselves into the increased population of mixed micelles until the pyrene occupancy equaled 2.0. As expected, an average number of two hydrophobes per elastically active junction should yield an optimal polymeric network resulting in a large η_o value. As experimentally observed in Fig. 7, η_o followed closely the behavior of $\langle n \rangle$, passing through a maximum for an $\langle n \rangle$ value of 2.0 corresponding to an optimally arranged polymeric network.

The close correlation found for Py(38)-HASE between the value of $\langle n \rangle$ and η_o [48], η_o passing through a maximum for an $\langle n \rangle$ value of 2, was recently confirmed in another study that monitored the interactions between SDS and a Py-HASE sample having a pyrene content of 12 μmol g^{-1} [49]. Due to its lower pyrene content, Py(12)-HASE had been found to generate more intermolecular associations compared to the Py(38)-HASE sample [45]. The molar fractions of the pyrene species in solution determined by fitting the monomer and excimer decays globally according to both the FBM and MFA resulted in trends as a function of SDS concentration that were similar to those obtained for Py(38)-HASE in Fig. 6. More interestingly, the fluorescence experiments with Py(12)-HASE were repeated at polymer

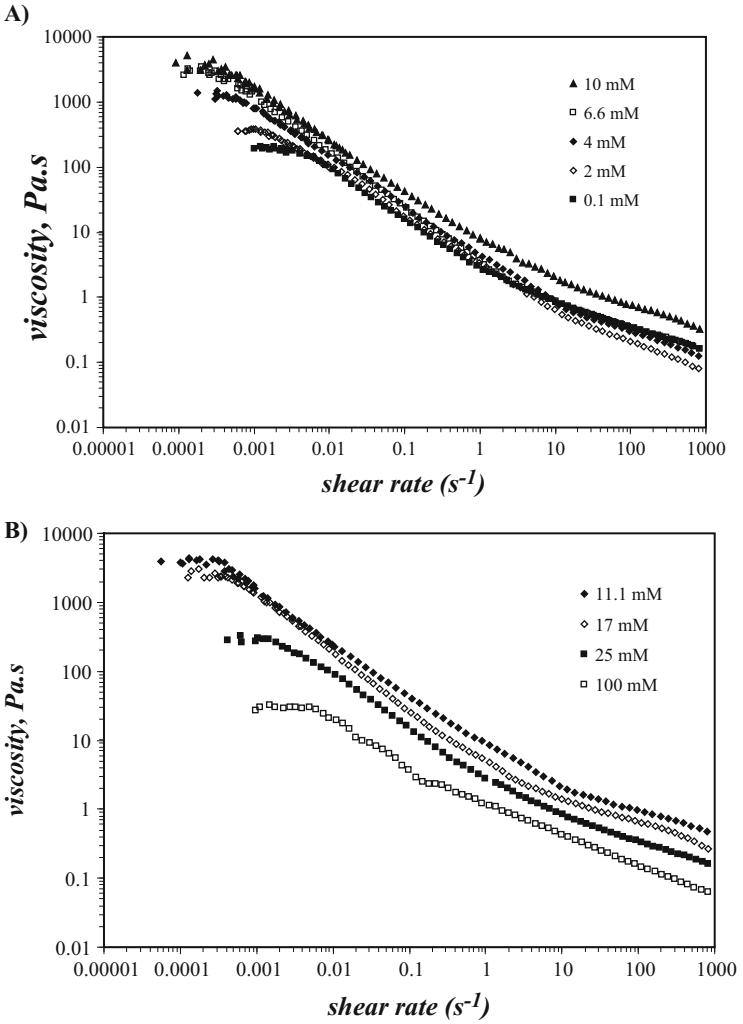

Fig. 8 Steady-shear viscosity as a function of shear rate for Py(12)-HASE at 57 g L^{-1} with SDS concentrations ranging from (**a**) 0.1–10 mM and (**b**) 11.1–100 mM [49]. "Reprinted with permission from *J. Phys. Chem. B* **2014**, *118*, 351–361. Copyright 2014 American Chemical Society"

concentration of 57 g L^{-1} where the zero-shear solution viscosity increased 20 folds from 200 Pa s with no SDS to 4000 Pa s with an SDS concentration of 11.1 mM. Larger SDS concentrations led to a precipitous decrease in η_o [49]. The large viscosities obtained with the 57 g L^{-1} Py(12)-HASE solution could be monitored as a function of shear rate with a rheometer. Figure 8 indicates that all Py(12)-HASE solutions showed a small Newtonian regime at low shear rate before undergoing clear shear-thinning behavior at high shear rate. As observed in Fig. 7, global fluorescence decay analysis based on the FBM showed that at the

SDS concentration of 11.1 mM where η_o passed through a maximum, $\langle n \rangle$ took a value of 2.0 suggesting again that the maximum η_o value was obtained when the hydrophobes of a HMWSP would distribute themselves among the mixed micelles to generate an optimal polymeric network.

The correlation found between η_o and $\langle n \rangle$ suggests that since $\langle n \rangle$ represents the average number of hydrophobes per mixed micelle, it might be related to the density (ν) of elastically active junctions provided by $G_o = \nu k_B T$. The fluorescence data indicated that the pyrene hydrophobes were not much aggregated for Py(12)-HASE at SDS concentrations greater than 8.5 mM. In this SDS concentration range, the concentration of elastically active junctions can be expected to equal the concentration of mixed micelles that result in interpolymeric elastic bridges. This concentration of mixed micelles is referred to as [Mic](inter) and it acknowledges the fact that the mixed micelles can host hydrophobes from a same or different Py (12)-HASE molecules. Only those mixed micelles hosting hydrophobes from different Py(12)-HASE molecules yield elastically active junctions. An expression of the concentration [Mic](inter) is given in Eq. (1).

$$[\text{Mic}](\text{inter}) = \nu = [1 - \exp(-\langle n \rangle) - \langle n \rangle \exp(-\langle n \rangle)] \times \frac{[Py]}{\langle n \rangle} \times f_{\text{diff}}(\text{inter}) \qquad (1)$$

The first term in Eq. (1) represents the probability of having two or more pyrenes per mixed micelle having an average occupancy of $\langle n \rangle$, $[Py]$ is the pyrene concentration in the Py(12)-HASE solution, and f_{diff}(inter) is the fraction of pyrene labels that form excimer intermolecularly. The fraction f_{diff}(inter) is obtained by subtracting f_{diff}(intra) obtained at high SDS concentration from the value of f_{diff} obtained experimentally from the FBM analysis of the fluorescence decays. A plot of ν as a function of SDS concentration is shown in Fig. 9 for the solutions of Py (12)-HASE and SDS. For SDS concentrations greater than 10 mM where the pyrene labels are no longer aggregated due to the presence of SDS, the decrease in η_o with

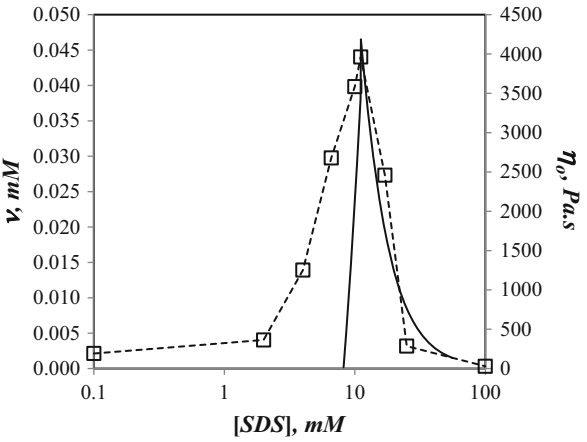

Fig. 9 Plot of the density of elastically active junctions (*solid line*) estimated from Eq. (1) and the zero-shear viscosity (*square with dashed lines*) as a function of SDS concentration for a 57 g L^{-1} Py(12)-HASE solution

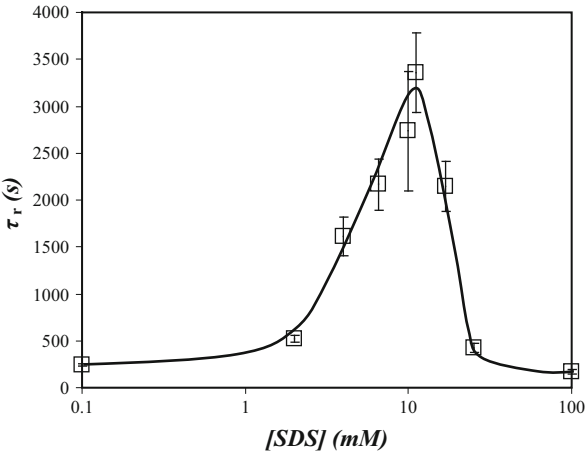

Fig. 10 Plot of τ_r as a function of SDS concentration for the 57 g L^{-1} Py(12)-HASE solution [49]. "Reprinted with permission from *J. Phys. Chem. B* **2014**, *118*, 351–361. Copyright 2014 American Chemical Society"

increasing SDS concentration is nicely correlated with the decrease in the density of elastically active junctions. The agreement between ν and η_o is poorer for SDS concentrations smaller than 10 mM due to the presence of a larger number of pyrene aggregates that are not accounted for by Eq. (1).

The viscosity profiles shown as a function of shear rate in Fig. 8 were used to estimate the relaxation time of the polymeric network (τ_r) by taking the inverse of the shear rate corresponding to the intercept between the Newtonian regime at low shear rates and the shear-thinning behavior at higher shear rates. A plot of τ_r as a function of SDS concentration is shown in Fig. 10. The same behavior as that of η_o shown in Fig. 9 was observed where τ_r passes through a maximum at an SDS concentration of 11.1 mM. These results suggest that both G_o ($=\nu k_B T$) and τ_r pass through a maximum with increasing SDS concentration and that at SDS concentrations lower than 11.1 mM, the addition of SDS contributes to enhancing the number of elastically active junctions and slowing down the relaxation of the network, while at SDS concentrations larger than 11.1 mM, an increase in SDS concentration leads to the isolation of pyrene hydrophobes inside mixed micelles containing one pyrene and several SDS molecules resulting in the precipitous decrease of ν.

The obvious disruption in the polymeric network illustrated by the massive shear-thinning behavior of the Py(12)-HASE solutions observed in Fig. 8 suggested that fluorescence should be able to probe the rearrangement of the hydrophobes between inter- and intramolecular associations at low and high shear rates, respectively. To this end, an optical interface using optical fibers was installed between the rheometer and the spectrofluorometer allowing the acquisition of fluorescence spectra of the solutions prepared with 57 g L^{-1} Py(12)-HASE and different SDS concentrations while being sheared at different shear rates. Figure 11 shows the fluorescence spectra of a 57 g L^{-1} Py(12)-HASE solution containing 11.1 mM SDS acquired at shear rates of 0, 0.005, 0.05, 1, 10, and 500 s^{-1} corresponding to

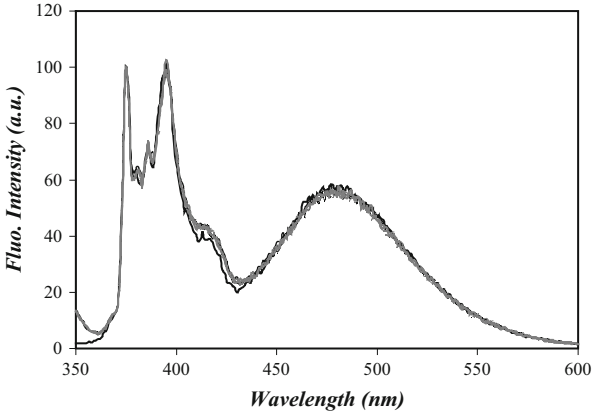

Fig. 11 Fluorescence emission spectra normalized at 375 nm of 57 g L^{-1} Py(12)-HASE solution with an SDS concentration of 11.1 mM acquired in a triangular fluorescence cell (*thick black line*) and with shear rates of 0 (*thin black line*), 0.005 (*black dashed lines*), 0.05 (*black dotted lines*), 1 (*gray thick line*), 10 (*gray thick dashed lines*), and 500 (*gray thick dotted lines*) s^{-1} [49]. "Reprinted with permission from *J. Phys. Chem. B* **2014**, *118*, 351–361. Copyright 2014 American Chemical Society"

solution viscosity equal to 4000, 411, 69, 7.5, 2.0, and 0.6 Pa s (see Fig. 8b). Although the solution viscosity decreased by close to 4 orders of magnitude over this range of shear rates, the fluorescence spectra of the Py(12)-HASE solutions overlapped perfectly regardless of shear rate. The same observation was made at SDS concentrations of 0.1, 6, 11.1, and 17 mM which flanked both sides of the zero-shear viscosity maximum in Fig. 9.

These clear-cut results led to the conclusion that the equilibrium that exists between isolated and aggregated hydrophobes is not affected by shear so that the same fractions of isolated and aggregated pyrenes are found in solution regardless of the massive decrease in viscosity induced by shear. Shear thinning of a polymeric network of associative thickeners is believed to reflect a rearrangement of the hydrophobes whose association into hydrophobic aggregates undergoes a switch from an open to a close association mechanism. The open association mechanism yields more intermolecular interactions that increase the concentration v of elastically active junctions and results in a high solution viscosity, but as shear is applied to the solution, the polymeric network is disrupted which results in the formation of hydrophobic aggregates within a same polymer molecule, reduces v, and thus the solution viscosity. However, this rearrangement of the hydrophobes with its dramatic effect on the ability of an AT solution to shear thin does not affect the equilibrium between isolated and aggregated hydrophobes as demonstrated by the perfect overlap of the fluorescence spectra in Fig. 11 acquired with a 57 g L^{-1} Py(12)-HASE solution containing 11.1 mM SDS.

Together, these studies conducted on a series of Py-HASE samples that used a combination of fluorescence and rheology to probe the behavior of aqueous solutions of Py-HASE at, respectively, the molecular and macroscopic levels provide to

date the most detailed description of the behavior of the hydrophobes of a commercially available AT and how they affect the balance between intra- and intermolecular hydrophobic associations.

Associative Behavior of Pyrene Singly (Py_1-PEO) and Doubly (Py_2-PEO) End-Labeled PEOs Due to their similarity to HEURs, namely a stretch of linear PEO terminated at both ends with a hydrophobe, the hydrophobic associations induced by pyrene doubly labeled PEOs have been under scientific scrutiny for more than three decades. In 1982, Winnik reported that an aqueous solution of a 9.6K PEO chain end capped with 1-pyrenebutyric acid yielded an unexpectedly high I_E/I_M ratio compared to the value obtained in 10 organic solvents [64]. This result represented a solid evidence that hydrophobic associations were taking place in water between the hydrophobic pyrene labels of Py_2-PEO(9.6K). The demonstration that pyrene excimer fluorescence reflected the level of hydrophobic associations between the pyrene labels of Py_2-PEO led to further and more detailed investigations.

Shortly after this early study by Winnik, the hydrophobic interactions between the pyrene labels of Py_2-PEO in water were investigated by Frank and Gast as a function of PEO molecular weight and the capture radius (R_C) describing the distance over which hydrophobic interactions extend their reach was determined to equal 20 Å [40]. A 20 Å R_C value implies that two pyrene molecules separated by less than $2 \times R_C = 40$ Å will diffuse rapidly toward each other to form a pyrene aggregate. The R_C value was determined from careful analysis of the fluorescence spectra acquired with a series of Py_2-PEO samples with an M_n value of 4.8, 9.2, and 11.2K. The interactions of Py_2-PEO with the hydrophilic and hydrophobic surface of, respectively, silica [65] and polystyrene latex [66] particles were also investigated by taking advantage of the changes in the I_E/I_M ratio that were observed as the Py_2-PEO samples interacted with the particles. The changes in the I_E/I_M ratio of Py_1-PEO [67] and Py_2-PEO(8K) [68] were also monitored in the presence of surfactant. As micelles formed in solution, they generated hydrophobic microdomains that were targeted by the hydrophobic pyrene labels and where they formed excimer effectively. In the case of the Py_2-PEO(8K) sample which was labeled with 1-pyrenemethanol, the location of the 1-pyrenemethoxy probe, whether in water or inside a micelle, could be inferred from its I_1/I_3 ratio [66].

While all these studies recognized the existence of pyrene aggregates in water, none actually determined the fraction of aggregated pyrene (f_{agg}). Only in 1992 was a first protocol introduced that used the difference in fluorescence quenching experienced by a pyrene monomer and a pyrene aggregate to determine f_{agg} for a Py_2-PEO(9.6K) sample [69]. This study established that only 7 % of the Py_2-PEO (9.6K) chains were forming pyrene aggregates, which translated into an f_{agg} value of 0.07 since each chain of Py_2-PEO(9.6K) bore two pyrene labels. Considering the many rheological studies conducted on Py-WSPs that showed that the hydrophobicity of pyrene is sufficient to confer a strong associative character to a Py-WSP in aqueous solution [45, 49, 61], the fact that only 7 % of all pyrene labels were

forming pyrene aggregates for Py_2-PEO(9.6K) was a bit surprising. Certainly, the long PEO segments of Py_2-PEO(9.6K) helped solubilize isolated pyrene monomers in water.

The first global analysis of the monomer and excimer fluorescence decays of a series of Py_2-PEO samples was conducted in 1998 [43]. The Py_2-PEO samples were constituted of a Py_2-PEO(3.8K) core flanked with two PEO overhangs of different sizes on both sides and were graciously supplied by M.A. Winnik. Only the polymer constructs with overhangs of 12, 17, and 47 ethylene oxide units were considered as they formed excimer intramolecularly at the polymer concentration used in the fluorescence experiments. The constructs having 2 or no ethylene oxide overhang were too hydrophobic and they aggregated intermolecularly even at polymer concentration as low as 3.8 mg L^{-1}. 1-Pyrenebutanol was used to label the Py_2-PEO(3.8K) constructs. The kinetic analysis of the decays followed closely the notion of capture radius (R_C) first introduced by Frank and Gast [40]. At the low polymer concentrations used in this study where pyrene excimer formation occurred solely intramolecularly, the kinetic analysis assumed that excimer formation occurred in a sequential manner, the pyrene labels being brought within a distance $2 \times R_C$ by diffusion with a rate constant k_{11} before undergoing a rapid rearrangement subject to hydrophobic forces with a rate constant k_2. This kinetic analysis referred to as the sequential model (SM) represented a simplification of the FBM as the diffusion of the pyrene labels could be handled with a single rate constant compared to the distribution of rate constants required by the FBM. As the size of the overhang decreased, k_{11} increased as diffusion was made easier with the smaller overhang. The fraction f_{agg} increased from 0.4 to 0.6 as the size of the overhang decreased.

The kinetics of excimer formation were also investigated for a Py_2-PEO(9.6K) sample in water, different organic solvents, and their mixture with water [54]. The pyrene monomer and excimer decays could be fitted globally with three exponentials using free-floating pre-exponential factors. Unfortunately, the natural lifetime of the unquenched pyrene monomer was estimated from that of 1-methylpyrene which is not an ideal model compound due to its ~30 ns shorter lifetime compared to that of the 1-pyrenemethoxy labels used for the Py_2-PEO(9.6K) construct [70]. Thus, the kinetic parameters retrieved from this analysis were expected to be somewhat off. Also no final results were provided from the analysis of the fluorescence decays acquired with Py_2-PEO(9.6K) solutions in water suggesting that the analysis did not yield reasonable parameters.

The SM was also applied to analyze globally the monomer and excimer fluorescence decays acquired with a series of Py_2-PEO(M_n) constructs with M_n values equal to 2, 5, 10, and 16.5K and prepared with 1-pyrenemethanol [42]. Solutions of Py_2-PEO(2K) and Py_2-PEO(5K) were insoluble in water at polymer concentrations greater than 2×10^{-5} and 2×10^{-4} M, respectively, due to the greater hydrophobicity of these two samples. Regardless of the Py_2-PEO construct having an M_n greater than 2K, excimer formation occurred solely intramolecularly at concentrations lower than $C_P = 4 \times 10^{-5}$ M, but it took place intra- and intermolecularly at larger concentrations. In other words, the boundary between the regimes where

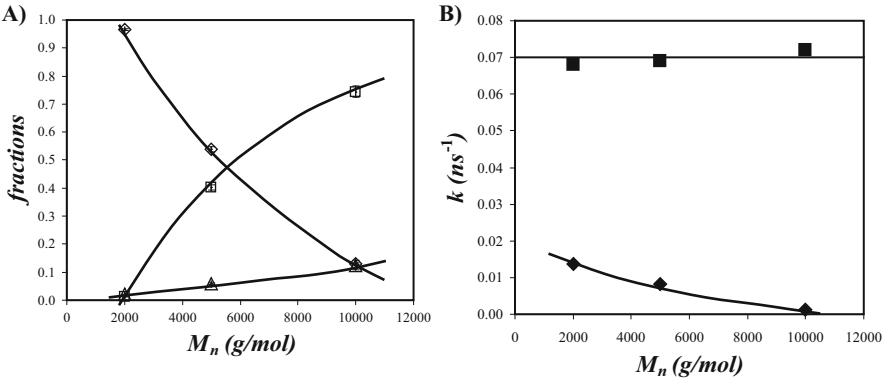

Fig. 12 (**a**) molar fractions of f_{agg}^{SM} (*open diamond*), f_{diff}^{SM} (*open square*), and f_{free}^{SM} (*open triangle*) and (**b**) rate constants of k_{11} (*filled diamond*) and k_2 (*filled square*) as a function of PEO molecular weight for the Py_2-PEO(M_n) constructs in water [42]. "Reprinted with permission from *Langmuir* **2013**, *29*, 2821–2834. Copyright 2014 American Chemical Society"

excimer was formed intra- and intermolecularly was dictated by the pyrene concentration and not the length of the PEO segment of the Py_2-PEO constructs investigated.

The SM model was expanded to include the possibility of having intermolecular excimer formation so that the kinetics of excimer formation could be analyzed above and below the critical concentration of 4×10^{-5} M. The SM global analysis of the fluorescence decays showed that below $C_P = 4 \times 10^{-5}$ M, f_{diff} increased and f_{agg} decreased with increasing PEO length as the longer PEO chain was capable of better solvating the hydrophobic pyrene label in water. For Py_2-PEO(2K), f_{agg} equaled 0.96 and most pyrene labels were aggregated. Above $C_P = 4 \times 10^{-5}$ M, f_{diff} decreased and f_{agg} increased with increasing polymer concentration indicating stronger hydrophobic association between the pyrene labels. The rate constant k_{12} for intermolecular diffusive encounters increased also with increasing polymer concentration in this concentration regime, a consequence of intermolecular excimer formation. The rate constant k_{11} for intramolecular diffusive encounters decreased steeply with increasing PEO chain length and was always much smaller than k_2 found to equal 7.3 ($\pm$0.5) $\times 10^7$ s^{-1} at all polymer concentrations and for all Py_2-PEO constructs. These trends have been summarized in Fig. 12a, b that plot, respectively, the fractions of the pyrene species and the rate constants as a function of M_n for the different polymer constructs.

Finally, f_{agg} which was determined in a direct manner via the SM analysis could be used to determine R_C which had been found to equal 2.0 nm by Frank and Gast [40]. Using a similar analysis based on the renormalization of the Gaussian distribution of the end-to-end distances of the Py_2-PEO constructs to account for the hydrophobic interactions taking place over a distance $2 \times R_C$ between the two pyrene hydrophobes, an R_C value of 2.1 $\pm$ 0.2 nm was recovered in perfect agreement with the value obtained by Frank and Gast.

In summary, the SM model which is a simplification of the FBM formalism was successfully applied to globally fit the monomer and excimer decays of different types of Py_2-PEO constructs [42, 68]. The analysis provided the fractions of all the pyrene species present in solution and the rate constants for the processes leading to pyrene excimer formation. The information retrieved from this kinetic analysis could then be used to describe in a quantitative manner the behavior of these HMWSPs in water.

Molar Extinction Coefficient of Pyrene Aggregates The presence of pyrene aggregates is known to induce a broadening of the pyrene absorption spectrum [27, 29, 31]. While amply documented in the literature, this effect which suggests that the absorption spectrum of a pyrene aggregate differs substantially from that of a pyrene monomer had never led to the determination of the spectrum of the molar absorbance coefficient of pyrene aggregates in water. The reason for this state of affair is that the vast majority of Py-WSPs are prepared with more than one pyrene label per chain so that pyrene aggregates are always present in solution, even at extremely low Py-WSP concentration since pyrene aggregates will still form intramolecularly. Consequently, it becomes impossible to isolate the absorption spectrum of a pyrene monomer covalently attached to the polymer from that of the pyrene aggregates by diluting the Py-WSP solution since a Py-WSP always contains a mixture of isolated pyrene monomers and pyrene aggregates. As a result, the typical procedure that consists in monitoring the absorption spectrum of a mixture of two compounds A and B capable of forming a complex AB as a function of the concentration of A to drive the equilibrium to the complex is ineffective in the case of Py-WSPs where the absorption spectrum does not change much with Py-WSP concentration. This observation is illustrated in Fig. 13 that shows the absorption spectrum of a poly(*N*,*N*-dimethylacrylamide) randomly labeled with 645 μmol of 1-pyrenemethylamine per gram of polymer (Py(645)-PDMA) which showed hardly any change in its spectral features over a range of polymer concentrations spanning three orders of magnitude [71].

As it turns out, time-resolved fluorescence can be used to circumvent this complication. Fluorescence decays of the pyrene monomer and excimer of aqueous solutions of Py-PDMA samples were acquired with a 1 nm slit width on the excitation monochromator of the time-resolved fluorometer as a function of the excitation wavelength which was changed by 1 nm increments. Global FBM analysis of the monomer and excimer decays yielded the fractions $f_{\mathrm{diff}}(\lambda)$, $f_{\mathrm{free}}(\lambda)$, $f_{k2}(\lambda)$, $f_{\mathrm{E0}}(\lambda)$, and $f_{\mathrm{EL}}(\lambda)$ as a function of wavelength. Since the pyrene aggregates absorb light more effectively at higher wavelengths compared to the pyrene monomer, the fractions $f_{\mathrm{diff}}(\lambda)$, $f_{\mathrm{free}}(\lambda)$, $f_{k2}(\lambda)$, $f_{\mathrm{E0}}(\lambda)$, and $f_{\mathrm{EL}}(\lambda)$ were found to fluctuate as a function of wavelength, which they ought not to do if they were absolute molar fractions. This was illustrated by plotting $f_{\mathrm{M}}(\lambda) = f_{\mathrm{diff}}(\lambda) + f_{\mathrm{free}}(\lambda) + f_{k2}(\lambda)$ which represents the contribution of the different pyrene monomer species to the fluorescence decays as a function of excitation wavelength in Fig. 14.

In fact, the fractions $f_{\mathrm{diff}}(\lambda)$, $f_{\mathrm{free}}(\lambda)$, $f_{k2}(\lambda)$, $f_{\mathrm{E0}}(\lambda)$, and $f_{\mathrm{EL}}(\lambda)$ obtained from the analysis of the fluorescence decays are a function of the real molar fractions

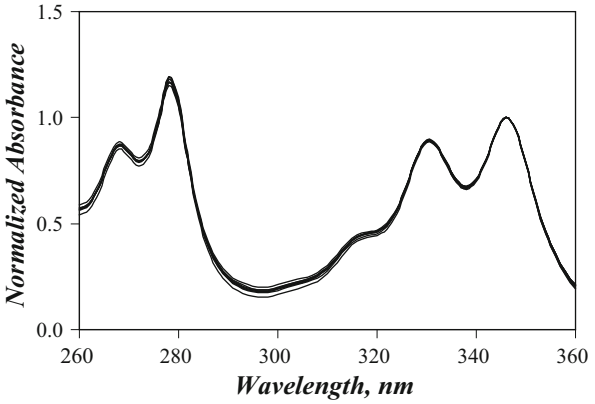

Fig. 13 Spectra of the normalized absorbance of Py(645)-PDMA with optical densities of 0.05, 0.13, 0.39, 0.86, 1.7, 4.8, 9.5, 15, 33, and 57. The spectra were normalized at 346 nm [69]. "Reprinted with permission from *J. Phys. Chem. B* **2008**, *112*, 15301–15312. Copyright 2014 American Chemical Society"

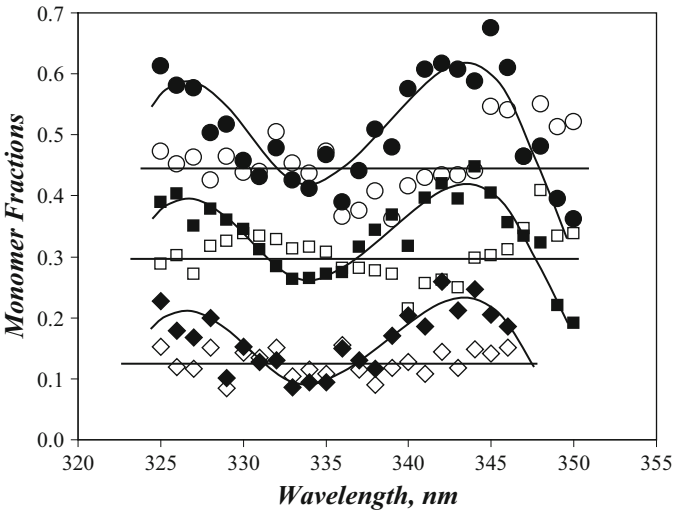

Fig. 14 Fluorescence fractions $f_M(\lambda)$ (*filled circle*, *filled square*, *filled diamond*) and molar fraction $f_M^M(\lambda)$ (*open circle*, *open square*, *open diamond*) obtained for 4.8 g L^{-1} Py(263)-PDMA (*circles*), 15 g L^{-1} Py(479)-PDMA in water (*squares*), and 0.09 g L^{-1} Py(645)-PDMA in water (*diamonds*) [69]. "Reprinted with permission from *J. Phys. Chem. B* **2008**, *112*, 15301–15312. Copyright 2014 American Chemical Society"

$f_{diff}^M, f_{free}^M, f_{k2}^M, f_{E0}^M$, and f_{EL}^M that are independent of the excitation wavelength (λ_{ex}) as well as the molar absorbance coefficients of the pyrene monomer ($\varepsilon_M(\lambda)$) and pyrene aggregates ($\varepsilon_{E0}(\lambda)$). If the molar absorbance coefficients $\varepsilon_M(\lambda)$ and $\varepsilon_{E0}(\lambda)$

were equal, the fractions $f_{diff}(\lambda)$, $f_{free}(\lambda)$, $f_{k2}(\lambda)$, $f_{E0}(\lambda)$, and $f_{EL}(\lambda)$ would remain constant with λ_{ex} and equal $f^{M}_{diff}, f^{M}_{free}, f^{M}_{k2}, f^{M}_{E0}$, and f^{M}_{EL}. The fact that $f_{diff}(\lambda), f_{free}(\lambda)$, $f_{k2}(\lambda), f_{E0}(\lambda)$, and $f_{EL}(\lambda)$ did not remain constant with λ_{ex} was a clear indication that $\varepsilon_M(\lambda)$ and $\varepsilon_{E0}(\lambda)$ are not equal, as suggested by a solid body of experimental evidence [27, 29, 30], and that a detailed analysis of the fractions $f_{diff}(\lambda), f_{free}(\lambda)$, $f_{k2}(\lambda), f_{E0}(\lambda)$, and $f_{EL}(\lambda)$ might yield a quantitative measure of $\varepsilon_{E0}(\lambda)$.

To this end, relationships were established between the four fractions $f_{diff}(\lambda)$, $f_{free}(\lambda), f_{k2}(\lambda)$, and $f_{E0}(\lambda)$ ($f_{EL}(\lambda)$ is redundant since it equals $1 - f_{diff}(\lambda) - f_{free}(\lambda) - f_{k2}(\lambda) - f_{E0}(\lambda)$) obtained at each excitation wavelength and the parameters $f^{M}_{diff}, f^{M}_{free}$, f^{M}_{k2}, f^{M}_{E0}, $\varepsilon_M(\lambda)$, and $\varepsilon_{E0}(\lambda)$. Thus, these relationships yielded four independent equations that depended on six variables. The molar absorbance coefficient of the pyrene monomer in water $\varepsilon_M(\lambda)$ was determined by preparing a Py-PDMA sample with a very low pyrene content of 6 μmol g^{-1} (Py(6)-PDMA). Py(6)-PDMA generated a minimum level of pyrene aggregation which allowed the determination of $\varepsilon_M(\lambda)$ from the absorption spectrum. Equating the absorbance of an aqueous solution of a Py-PDMA sample determined experimentally to the concentrations of pyrene species present in solution provided a fifth equation that enabled the determination of the molar fractions f^{M}_{diff}, f^{M}_{free}, f^{M}_{k2}, f^{M}_{E0}, and most importantly, $\varepsilon_{E0}(\lambda)$, the molar absorbance coefficient of a pyrene aggregate.

Figure 14 shows how strongly the fraction $f_M(\lambda) = f_{diff}(\lambda) + f_{free}(\lambda) + f_{k2}(\lambda)$ undulates as a function of λ_{ex} and how these undulations were reduced for the molar fraction $f^{M}_{M} = f^{M}_{diff} + f^{M}_{free} + f^{M}_{k2}$ retrieved from the analysis. These experiments were carried out for Py-PDMA samples having a pyrene content of 263, 479, and 645 μmol g^{-1} and at polymer concentrations of 30 g L^{-1} for Py(263)-PDMA, 0.1, 0.7, and 30 g L^{-1} for Py(479)-PDMA, and 1 and 30 g L^{-1} for Py(645)-PDMA representing a total of 6 different polymer solutions.

Together 150 monomer fluorescence decays and 150 excimer fluorescence decays were acquired and fitted globally according to the FBM to yield six sets of fractions $f_{diff}(\lambda)$, $f_{free}(\lambda)$, $f_{k2}(\lambda)$, $f_{E0}(\lambda)$, and $f_{EL}(\lambda)$ for each polymer solution. The procedure described above was applied to these six sets of $f_{diff}(\lambda)$, $f_{free}(\lambda)$, $f_{k2}(\lambda)$, $f_{E0}(\lambda)$, and $f_{EL}(\lambda)$ values which varied with the pyrene content and polymer concentration of the Py-PDMA samples. However, the procedure accounted successfully for these variations yielding a tight set of $\varepsilon_{E0}(\lambda)$ values for a range of λ_{ex} between 325 and 350 nm with 1 nm increments (Fig. 15). This study provided the first spectrum of the molar absorbance coefficient $\varepsilon_{E0}(\lambda)$ of pyrene aggregates in water. The P_A value obtained from the $\varepsilon_{E0}(\lambda)$ spectrum equaled 1.5 ± 0.1, much lower than the P_A value of 2.5 found for the isolated pyrene monomers of Py(6)-PDMA.

This success led us to determine the $\varepsilon_{E0}(\lambda)$ spectrum of pyrene aggregates formed by another Py-WSP, namely Py_1-PEO(2.5K) in water [72]. Since Py_1-PEO(2.5K) is known to form micelles in water, excimer formation took place through diffusive encounters between solvated Py_1-PEO(2.5K) chains and Py_1PEO(2.5K) micelles, rapid rearrangement of the pyrene moieties inside a micelle, or direct excitation of pyrene aggregates. In other words, the pyrene labels

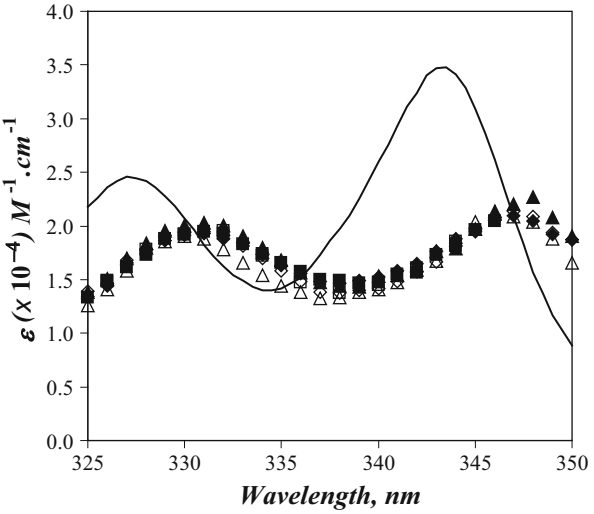

Fig. 15 Molar absorption coefficient of the pyrene monomer ($\varepsilon_M(\lambda)$, *solid line*) and pyrene aggregates ($\varepsilon_{E0}(\lambda)$) for Py(263)-PDMA with a concentration of 4.8 g L^{-1} (*open triangle*), Py (479)-PDMA with a concentration of 0.01 g L^{-1} (*open square*), 0.08 g L^{-1} (*open diamond*), and 1.8 g L^{-1} (*filled triangle*), and Py(645)-PDMA with a concentration of 0.09 g L^{-1} (*filled square*) and 2.2 g L^{-1} (*filled diamond*) [69]. "Reprinted with permission from *J. Phys. Chem. B* **2008**, *112*, 15301–15312. Copyright 2014 American Chemical Society"

did not distribute themselves according to a Poisson distribution in the solution as they did with the randomly labeled Py-PDMA samples. Consequently, the FBM which had been instrumental in the determination of the $\varepsilon_{E0}(\lambda)$ spectrum for Py-PDMA solutions could not be applied to study pyrene excimer formation in Py_1-PEO(2.5K) aqueous solutions. Instead the MFA was employed to fit globally the monomer and excimer fluorescence decays acquired as a function of λ_{ex} for three aqueous solutions of Py_1-PEO(2.5K) with polymer concentrations of 5, 10, and 13 mM. In this study, 75 monomer decays and 75 excimer decays were acquired and fitted globally according to the MFA.

The fluorescence decays analysis yielded three sets of $f_{diff}(\lambda)$, $f_{free}(\lambda)$, $f_{k2}(\lambda)$, $f_{E0}(\lambda)$, and $f_{EL}(\lambda)$ values that were processed according to the protocol outlined earlier to yield three tight sets of $\varepsilon_{E0}(\lambda)$ values demonstrating that the analysis accounted satisfyingly for the variations in the fraction due to changes in the Py_1-PEO(2.5K) concentration. These three sets of $\varepsilon_{E0}(\lambda)$ values were averaged to yield the molar absorbance coefficient $\varepsilon_{E0}(\lambda)$ of the pyrene aggregates generated by Py_1-PEO(2.5K) in water over the wavelength range between 325 and 347 nm with 1 nm increments.

The $\varepsilon_{E0}(\lambda)$ spectra obtained for the pyrene aggregates of Py-PDMA [69] and Py_1-PEO(2.5K) [43] are compared in Fig. 16. As for the Py-PDMA aqueous solutions, the $\varepsilon_{E0}(\lambda)$ spectrum of pyrene aggregates generated by concentrated solutions of Py_1-PEO(2.5K) was substantially broader than that of Py_1-PEO

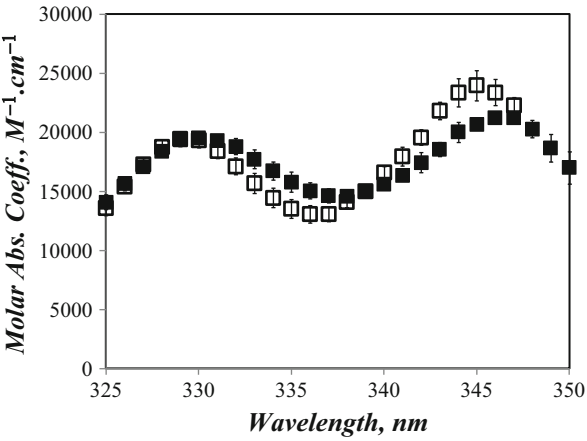

Fig. 16 Averaged molar absorbance coefficients of pyrenes that are aggregated, $\langle \varepsilon_{E0} \rangle$, determined for Py_1-n2.5K) (*open square*) and Py-PDMA (*filled square*) in water [43]. "Reprinted with permission from *J. Phys. Chem. B* **2012**, *116*, 1226–1233. Copyright 2014 American Chemical Society"

(2.5K) at low concentration yielding P_A values of 1.8 ± 0.1 and 2.6 at high and low Py_1-PEO(2.5K) concentrations, respectively. The slight differences in P_A values obtained for aqueous solutions of Py_1-PEO(2.5K) (1.8 ± 0.1) and Py-PDMA (1.5 ± 0.1) might reflect differences in the nature of the pyrene aggregates. In any case, the $\varepsilon_{E0}(\lambda)$ spectra shown in Fig. 16 display similar spectral features being much broader and red shifted by 3–4 nm compared to that of isolated pyrene monomers and with a maximum value that is reduced by ~40 % compared to the maximum $\varepsilon_M(\lambda)$ value obtained in the monomer absorption spectrum. These observations are reasonable and agree satisfyingly with the bulk of qualitative information available in the scientific literature pertaining to the expected spectral features of pyrene aggregates. But whereas all this information is qualitative in nature, the experiments that were conducted with Py-PDMA and Py_1-PEO(2.5K) provided the first set of values for the molar absorbance coefficient of pyrene aggregates in water.

4 Conclusions

This chapter has highlighted some of the recent analytical developments that have been implemented by this laboratory to retrieve quantitative information on the level of pyrene aggregation from the global analysis of the fluorescence decays of the pyrene monomer and excimer acquired with aqueous solutions of Py-WSPs. Rheology experiments with a series of Py-HASEs clearly illustrated that the hydrophobicity of a pyrene molecule is sufficient to induce the viscoelastic behavior typically expected from associative thickeners. Consequently, associative thickeners where the hydrophobe was replaced by pyrene constitute excellent model compounds to study their level of association quantitatively by fitting the fluorescence decays of the pyrene monomer and excimer globally according to the FBM,

MFA, or SM. This review has illustrated how fluorescence decay analyses based on the FBM, MFA, and SM have led to the determination of f_{agg} for several Py-WSPs, namely Py-HASE, Py-PDMA, Py_2-PEO, and Py_1-PEO, and how variations in f_{agg} could be monitored as a function of the concentration of surfactant added to a Py-HASE solution. The good agreement between the results obtained by fluorescence on Py-WSPs and the general understanding reported in the literature about the non-fluorescent equivalent of these HMWSPs suggests that the FBM, MFA, and SM provide a robust methodology to analyze the complex fluorescence decays of Py-WSPs in aqueous solutions.

Acknowledgements Although all former and present graduate students from the Duhamel laboratory contributed to some extent in the work described in this review, I would like to extend a special thanks to Drs. Sabesh Kanagalingam, Telmo Prazeres, Howard Siu, Christine Keyes, and Shaohua Chen on whose contributions this review was mostly based. Also, none of this work could have been carried out without the generous funding of the Natural Science and Engineering Research Council of Canada.

References

1. Glass JE (ed) (1989) Polymers in aqueous media: performance through Association Advances in chemistry series 226. American Chemical Society, Washington, DC
2. Schulze DN, Glass JE (eds) (1991) Polymers as rheology modifiers; ACS symposium series 462. American Chemical Society, Washington, DC
3. Kwak JCT (ed) (1998) Polymer-surfactant systems; Surfactant science series 77. Dekker, New York
4. Goddard EO, Ananthapadamanabham KP (eds) (1993) Interactions of surfactants with polymers and proteins. CRC Press, Boca Raton, FL
5. Winnik MA, Yekta A (1997) Associative polymers in aqueous solution. Curr Opin Colloid Interface Sci 2:424–436
6. Glass JE (2001) A perspective on the history of and current research in surfactant-modified, water-soluble polymers. J Coat Technol 73:79–98
7. Da GM,M, Burrows HD, Lindman B (2002) Polymer-surfactant association as seen by fluorescence. Progr Colloid Polym Sci 120:13–22
8. Tam KC, Wyn-Jones E (2006) Insights on polymer surfactant complex structures during the binding of surfactants to polymers as measured by equilibrium and structural techniques. Chem Soc Rev 35:693–709
9. Annabale T, Buscall R, Ettelaie R, Whittlestone D (1993) The rheology of solutions of associating polymers: comparison of experimental behavior with transient network theory. J Rheol 37:695–726
10. Lundberg DJ, Glass JE, Eley RR (1991) Viscoelastic behaviour among HEUR thickeners. J Rheol 35:1255–1274
11. Zhao G, Khin CC, Chen SB (2005) Nonionic surfactant and temperature effects on the viscosity of hydrophobically modified hydroxyethyl cellulose solutions. J Phys Chem B 109:14198–14204
12. Glass JE (1999) Adsorption of hydrophobically modified, ethoxylated urethane thickeners on latex and titanium dioxide disperse phases. Adv Colloid Interface Sci 79:123–148
13. Magny B, Iliopoulos I, Zana R, Audebert R (1994) Mixed micelles formed by cationic surfactants and anionic hydrophobically modified polyelectrolytes. Langmuir 10:3180–3187

14. Ringsdorf H, Venzmer J, Winnik FM (1991) Fluorescence studies of hydrophobically modified poly(*N*-isopropylacrylamide) or how to play accordion on a liposome. Makromol Chem Macromol Symp 46:427–431
15. Annabale T, Buscall R, Ettelaie R, Shepherd P, Whittlestone D (1994) Influence of surfactants on the rheology of associating polymers in solution. Langmuir 10:1060–1070
16. Jiménez-Regalado E, Selb J, Candau F (2000) Effect of surfactant on the viscoelastic behavior of semidilute solutions of multisticker associating polyacrylamides. Langmuir 16:8611–8621
17. Tripathi A, Tam KC, McKinley GH (2006) Rheology and dynamics of associative polymers in shear and extension: theory and experiments. Macromolecules 39:1981–1999
18. Dai S, Tam KC, Wyn-Jones E, Jenkins RD (2004) Isothermal titration calorimetry and electromotive forces studies on binding interactions of hydrophobic ethoxylated urethane and sodium dodecyl sulfate of different molecular masses. J Phys Chem B 108:4979–4988
19. Chassenieux C, Nicolai T, Durand D (1997) Association of hydrophobically end-capped poly (ethylene oxide). Macromolecules 30:4952–4958
20. Yekta A, Xu B, Duhamel J, Adiwidjaja H, Winnik MA (1995) Fluorescence studies of associating polymers in water. Determination of the chain-end aggregation number and a model for the association process. Macromolecules 28:956–966
21. Beaudoin E, Borisov O, Lapp A, Billon L, Hiorns RC, François J (2002) Neutron scattering of hydrophobically modified poly(ethylene oxide) in aqueous solutions. Macromolecules 35:7436–7447
22. Volpert E, Selb J, Candau F (1996) Influence of the hydrophobe structure on composition, microstructure, and rheology in associating polyacrylamides prepared by micellar copolymerization. Macromolecules 29:1452–1463
23. Candau F, Regalado EJ, Selb J (1998) Scaling behaviour of the zero-shear viscosity of hydrophobically modified polyacrylamides. Macromolecules 31:5550–5552
24. Regalado EJ, Selb J, Candau F (1999) Viscoelastic behavior of semidilute solutions of multisticker polymer chains. Macromolecules 32:8580–8588
25. Morishima Y, Nomura S, Ikeda T, Seki M, Kamachi M (1995) Characterization of unimolecular micelles of random copolymers of sodium 2-(Acrylamido)-2-methylpropanesulfonate and methacrylamides bearing bulky hydrophobic substituents. Macromolecules 28:2874–2881
26. Sheng WP, Tam KC, Jenkins RD, Bassett DR (2000) Calorimetric studies of model hydrophobically modified alkali-soluble emulsion polymers with varying spacer chain length in ionic surfactant solutions. Macromolecules 33:1727–1733
27. Winnik FM (1993) Photophysics of preassociated pyrenes in aqueous polymer solutions and in other organized media. Chem Rev 93:587–614
28. Siddique B, Duhamel J (2011) Effect of polypeptide sequence on polypeptide self-assembly. Langmuir 27:6639–6650
29. Winnik FM, Regismond STA (1996) Fluorescence methods in the study of the interactions of surfactants with polymers. Colloids Surf A: Physicochem Eng Aspects 118:1–39
30. Duhamel J (2012) Internal dynamics of dendritic molecules probed by pyrene excimer formation. Polymers 4:211–239
31. Birks JB, Dyson DJ, Munro IH (1963) 'Excimer' fluorescence. II. Lifetime studies of pyrene solutions. Proc R Soc A 275:575–588
32. Duhamel J (2006) Polymer chain dynamics in solution probed with a fluorescence Blob model. Acc Chem Res 39:953–960
33. Duhamel J (2012) New insights in the study of pyrene excimer fluorescence to characterize macromolecules and their supramolecular assemblies in solution. Langmuir 28:6527–6538
34. Duhamel J (2014) Global analysis of fluorescence decays to probe the internal dynamics of fluorescently labeled macromolecules. Langmuir 30:2307–2324
35. James DR, Ware WR (1985) A Fallacy in the interpretation of fluorescence decay parameters. Chem Phys Lett 120:455–459

36. Mathew A, Siu H, Duhamel J (1999) A *Blob* model to study chain folding by fluorescence. Macromolecules 32:7100–7108
37. Siu H, Duhamel J (2005) Comparison of the association level of a hydrophobically modified associative polymer obtained from an analysis based on two different models. J Phys Chem B 109:1770–1780
38. Seixas de Melo J, Costa T, Francisco A, Maçanita AL, Gago S, Gonçalves IS (2007) Phys Chem Chem Phys 9:1370–1385
39. Seixas de Melo J, Costa T, Miguel MG, Lindman B, Schillén KJ (2003) Phys Chem 107:12605–12621
40. Zachariasse KA, Busse R, Duveneck G, Kühnle W (1985) Intramolecular monomer and excimer fluorescence with dipyrenylpropanes: double-exponential versus triple-exponential decays. J Photochem 28:237–253
41. Fowler MA, Duhamel J, Bahun GJ, Adronov A, Zaragoza-Galán G, Rivera E (2012) Studying pyrene-labeled macromolecules with the model free analysis. J Phys Chem B 116:14689–14699
42. Char K, Frank CW, Gast AP (1989) Consideration of hydrophobic attractions in end-to-end cyclization. Macromolecules 22:3177–3180
43. Lee S, Duhamel J (1998) Monitoring the hydrophobic interactions of internally pyrene-labeled poly(ethylene oxide)s in water by fluorescence spectroscopy. Macromolecules 31:9193–9200
44. Chen S, Duhamel J (2013) Probing the hydrophobic interactions of a series of pyrene end-labeled poly(ethylene oxide)s in aqueous solution using time-resolved fluorescence. Langmuir 29:2821–2834
45. Kanagalingam S, Ngan CF, Duhamel J (2002) Effect of solvent quality on the level of association and encounter kinetics of hydrophobic pendants covalently attached onto a water-soluble polymer. Macromolecules 35:8560–8570
46. Prazeres TJV, Beingessner R, Duhamel J, Olesen K, Shay G, Bassett DR (2001) Characterisation of the association level of pyrene-labelled HASEs by fluorescence. Macromolecules 34:7876–7884
47. Prazeres TJV, Duhamel J, Olesen K, Shay G (2005) Correlations between the viscoelastic behavior of pyrene-labeled associative polymers and the associations of their fluorescent hydrophobes. J Phys Chem B 109:17406–17416
48. Siu H, Duhamel J (2004) Global analysis of the fluorescence decays of a pyrene-labelled polymer using a *blob* model. Macromolecules 37:9287–9289
49. Siu H, Duhamel J (2005) The importance of considering non-fluorescent pyrene aggregates for the study of pyrene-labeled associative thickeners by fluorescence. Macromolecules 38:7184–7186
50. Siu H, Duhamel J (2006) Associations between a pyrene-labeled hydrophobically modified alkali swellable emulsion copolymer and sodium dodecyl sulfate probed by fluorescence, surface tension, and rheology. Macromolecules 39:1144–1155
51. Chen S, Siu H, Duhamel J (2014) Interactions between hydrophobically modified alkali-swellable emulsion polymers and sodium dodecyl sulfate probed by fluorescence and rheology. J Phys Chem B 118:351–361
52. Siu H, Duhamel J, Sasaki D, Pincus JL (2010) Nanodomain formation in lipid membranes probed by time-resolved fluorescence. Langmuir 26:10985–10994
53. Siu H, Prazeres TJV, Duhamel J, Olesen K, Shay G (2005) Characterization of the aggregates made by short poly(ethylene oxide) chains labelled at one end with the dye pyrene. Macromolecules 38:2865–2875
54. Costa T, Seixas de Melo J, Burrows HD (2009) Fluorescence behavior of a pyrene-end-capped poly(ethylene oxide) in organic solvents and in dioxane-water mixtures. J Phys Chem B 113:618–626
55. Costa T, Seixas de Melo J, Migeul MD, Lindman B, Schillén K (2009) Complex formation between a fluorescently-labeled polyelectrolyte and a triblock copolymer. J Phys Chem B 113:6205–6214

56. Costa T, Seixas de Melo JS, Castro CS, Gago S, Pillinger M, Gonçalves IS (2010) Picosecond dynamics of dimer formation in a pyrene labeled polymer. J Phys Chem B 114:12439–12447
57. Keyes-Baig C, Duhamel J, Wettig S (2011) Characterization of the behavior of a pyrene substituted Gemini surfactant in water by fluorescence. Langmuir 27:3361–3371
58. Yip J, Duhamel J, Bahun G, Adronov A (2010) A study of the branch ends of a series of pyrene-labeled dendrimers based on pyrene excimer formation. J Phys Chem B 114:10254–10265
59. Chen S, Duhamel J, Bahun G, Adronov A (2011) Effect of fluorescent impurities in the study of pyrene-labeled macromolecules by fluorescence. J Phys Chem B 115:9921–9929
60. Malinovskii VL, Wenger D, Häner R (2010) Nucleic acid-guided assembly of aromatic chromophores. Chem Soc Rev 39:410–422
61. Østergaard ME, Hrdlicka PJ (2011) Pyrene-functionalized oligonucleotides and locked nucleic acids (LNAs): tools for fundamental research, diagnostics, and nanotechnology. Chem Soc Rev 40:5771–5788
62. Bains G, Patel AB, Narayanaswami V (2011) Pyrene: a probe to study protein conformation and conformational changes. Molecules 16:7909–7935
63. Richey B, Kirk AB, Eisenhart EK, Fitzwater S, Hook J (1991) Interactions of associative thickeners with paint components as studied by the use of a fluorescently labeled model thickener. J Coat Technol 63:31–40
64. Cheung S-T, Winnik MA, Redpath AEC (1982) The effects of solvent on end-to-end cyclization of poly(ethylene oxide) probed by intramolecular pyrene excimer formation. Makromol Chem 183:1815–1824
65. Char K, Gast AP, Frank CW (1988) Fluorescence studies of polymer adsorption. I. Rearrangement and displacement of pyrene-terminated poly(ethylene glycol) on colloidal silica particles. Langmuir 4:989–998
66. Char K, Frank CW, Gast AP (1989) Fluorescence studies of polymer adsorption. 3. Adsorption of pyrene-end-labeled poly(ethylene glycol) on colloidal polystyrene particles. Langmuir 5:1335–1340
67. Quina F, Abuin E, Lissi E (1990) Effect of pyrene chain end labeling on the interaction of poly (ethylene oxide) with sodium dodecyl sulfate in aqueous solution. Macromolecules 23:5173–5175
68. Hu Y-Z, Zhao C-L, Winnik MA, Sundararajan PR (1990) Fluorescence studies of the interaction of sodium dodecyl sulfate with hydrophobically modified poly(ethylene oxide). Langmuir 6:880–883
69. Duhamel J, Yekta A, Hu Y, Winnik MA (1992) Evidence for intramolecular hydrophobic association in aqueous solutions of pyrene end-capped poly(ethylene oxide). Macromolecules 25:7024–7030
70. Chen S, Duhamel J, Winnik MA (2011) Probing end-to-end cyclization beyond Willemski and Fixmann. J Phys Chem B 115:3289–3302
71. Siu H, Duhamel J (2008) Molar extinction coefficient of pyrene aggregates in water. J Phys Chem B 112:15301–15312
72. Siu H, Duhamel J (2012) Molar absorption coefficient of pyrene aggregates in water generated by a poly(ethylene oxide) capped at a single end with pyrene. J Phys Chem B 116:1226–1233

Fluorescence Correlation Spectroscopy Studies of Polymer Systems

Dominik Wöll

Contents

D. Wöll (✉)
Institute for Physical Chemistry, RWTH Aachen University, Landoltweg 2, 52074 Aachen, Germany
e-mail: woell@pc.rwth-aachen.de

K. Procházka (ed.), *Fluorescence Studies of Polymer Containing Systems*,
Springer Series on Fluorescence 16, DOI 10.1007/978-3-319-26788-3_8

Abstract This chapter discusses the potential of fluorescence correlation spectroscopy (FCS) to study polymer systems. It introduces the technique and its variations, describes analysis methods, points out advantages and limitations, and summarizes FCS studies of molecular and macromolecular probes in polymer solutions, polymer gels, polymer nanoparticles, and polymeric micellar systems. In addition, a comparison with other experimental methods is presented and the potential of a combination with simulations discussed.

Keywords Fluorescence correlation spectroscopy • Fluorescence microscopy • Fluorescent probes • Polymer solutions • Polymer gels • Polymer nanoparticles • Polymeric micellar systems • Translational diffusion

1 Introduction

Fluorescence correlation spectroscopy (FCS) is a powerful method to measure the timescales of dynamics within different environments and allows for a determination of some photophysical properties of the fluorescent probes. Even though most studies have so far addressed biological questions, FCS could also give valuable insights into polymer systems [1]. Its particular advantages are that it allows for measurements with only minor sample amounts. Since the labeling concentrations are very low, a significant disturbance of the systems can be excluded. Thus, structures and their dynamics can be resolved in situ with a good spatial resolution at the diffraction limit of optical light, i.e., on a sub-μm length scale. The elucidation of diffusional processes on this scale is essential for a deeper understanding of the relationship between polymer structure and dynamics and its manifestation on the macroscopic properties of the polymer. The complexity of this relationship challenges all experimental and theoretical methods, and only combining their strengths will allow us to gain a consistent picture of polymers from the nanoscopic to the microscopic scale. Unraveling these secrets is still amongst the very dreams of polymer scientists and probably can foster the development of novel sophisticated functional materials with tunable properties.

This book chapter is intended to review the current state of the art of FCS and to emphasis the advantages, but also the limits of this technique for the measurement in polymer systems. It will discuss analysis methods for FCS data and point out the potential of FCS for future studies on polymers and their applications.

2 FCS Measurements and Analysis

2.1 FCS Setup

Already in 1972, Magde, Webb, and Elson published the first paper on fluorescence correlation spectroscopy yielding chemical rate constants and diffusion coefficients [2], followed by a series of further reports on these novel techniques [3–5]. However, several further developments were necessary for FCS to reach its current power which has been reviewed several times as for example in [6–10]. One key step in the evolution of FCS was its combination with confocal microscopy to enhance spatial resolution basically down to the diffraction limit of the fluorescence light and the concomitant increase in sensitivity [11]. Further important technical improvements concern the quality of optical components and the sensitivity and time resolution of detectors. Additionally, better labels and labeling strategies have become available, a point which should not be underestimated.

In a typical FCS experiment, as shown in Fig. 1, a collimated laser beam is focused by an objective lens into a diffraction-limited confocal volume within the sample placed on a glass cover slide. Part of the light emitted from this confocal volume is collected by the same objective and separated from excitation light using a dichroic mirror and an emission filter. The emission light is focused onto a pinhole blocking most of the light not originating from the confocal volume, thereby, as shown in Fig. 2, improving mainly the axial z-resolution. However, to a minor extent, also the lateral x- and y-resolution are improved. This way, the overall size of the confocal volume typically can be reduced to ca. 0.1 femtoliter. The photons passing through the pinhole are detected with a photo detector, typically an avalanche photo diode (APD). Such APDs possess good quantum efficiencies and, with appropriate electronics, allow for the determination of the arrival times of single photons with an accuracy in the picosecond range.

2.2 Autocorrelation Analysis

The number of detected photons within a certain time interval is typically binned and determines the measured fluorescence intensity. This intensity fluctuates on different timescales caused by different diffusional, photochemical, or photophysical processes. The timescales of these processes can be most straightforward analyzed using the autocorrelation function

$$G(\tau) = \frac{\langle \delta I(t) \cdot \delta I(t+\tau) \rangle}{\langle I(t) \rangle^2} = \frac{\langle I(t) \cdot I(t+\tau) \rangle}{\langle I(t) \rangle^2} - 1 \tag{1}$$

of the fluorescence intensity $I(t)$ or its deviations $\delta I(t) = I(t) - \langle I(t) \rangle$ from the mean intensity. This function describes the (average) correlation between the

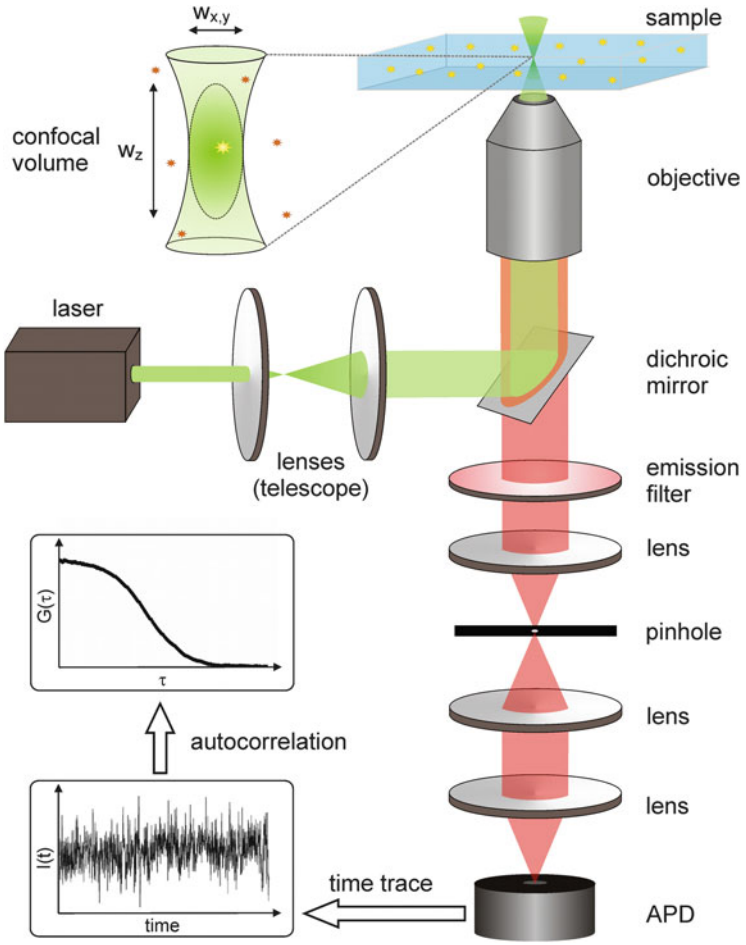

Fig. 1 Typical FCS setup (figure reproduced and adapted from Wöll [1] with permission of The Royal Society of Chemistry)

intensity at a time t with the intensity at a time shifted by the time interval τ. It can be interpreted as the conditional probability density of detecting photons, provided one photon is detected at zero time. The autocorrelation function contains information about the timescale of all processes that cause fluctuations in the fluorescence intensity.

Translational diffusion can be typically observed on timescales longer than 0.1 millisecond. In the μs range, the autocorrelation function often drops due to triplet blinking [12]. After excitation, the fluorophore undergoes intersystem crossing from a singlet (typically S_1) to a triplet state (typically T_1) and remains dark during the lifetime of this triplet state before it relaxes back to the singlet system, where it can fluoresce again by cycling between the S_0 and the S_1 states.

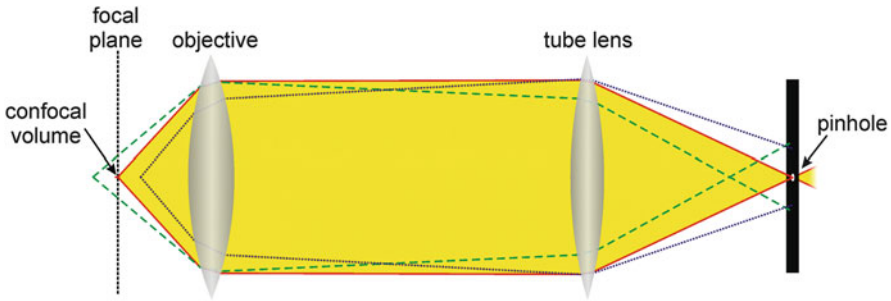

Fig. 2 Effect of the pinhole on the axial resolution of a confocal microscope. Only light originating from the confocal volume (*red solid line*, *yellow area*) can pass the pinhole without loss. Light from planes further away from the objective (*green dotted line*) focuses already in front of the pinhole (*green dotted line* and *blue dotted line*) and, thus, is mainly blocked, whereas light from planes closer to the objective is not yet focused at the plane of the pinhole and, therefore, most of this light also cannot pass (figure reproduced from Wöll [1] with permission of The Royal Society of Chemistry)

Photoisomerizations between two states with different fluorescence intensities can also be observed in the μs range [13]. The fast photophysics within different singlet states, i.e., the excitation from the singlet ground state and the emission of a fluorescence photon from an excited singlet state, are determined by the absorption cross section, the light intensity, and the fluorescence lifetime. This causes an intensity increase within nanoseconds which is called antibunching [14]. For concentrations with statistically less than one fluorescence molecule in the confocal volume, it is impossible to observe two fluorescence photons instantaneously because after one photon has been emitted, the fluorophore is in the electronic ground state. It requires time to be excited again and to emit a second photon. Thus, the autocorrelation functions approach a value of zero for very short (sub-ns) time intervals. Finally, rotational motion of single molecules with a well-defined transition dipole moment also causes intensity fluctuations. They can span a rather large timescale between sub-nanoseconds and milliseconds depending on the viscosity of the medium and even stronger on the probe size, since, according to the Stokes–Einstein–Debye equation, the rotational diffusion coefficient of a probe is indirectly proportional to the third power of its radius. However, care has to be taken when the fluorophore is part of a larger probe molecule and can reorient independently within this molecule. In this case, the fluorophore does not reflect the rotational motion of the probe but a complex combination of probe rotation and its own reorientation within the probe molecule.

The autocorrelation curve can then be fitted to autocorrelation functions calculated using reasonable models for the respective processes which are in detail explained in Chapter 5 of the "Handbook of Fluorescence Spectroscopy and Imaging" [15]. Here, we rather concentrate on providing the formulas typically used for fitting.

2.3 Analysis of Translational Diffusion

Translational diffusion can be described by a model with a 3D Gaussian intensity profile of the confocal volume which possesses the same width w_{xy} in the lateral x- and y-direction but a different width w_z in the axial z-direction. This can be related to the autocorrelation [see Eq. (1)] using the following equation:

$$G_{\mathrm{tr}}(\tau) = \frac{1}{N}\left(1 + \frac{\tau}{\tau_{\mathrm{D}}}\right)^{-1}\left(1 + \left(\frac{w_{xy}}{w_z}\right)^2 \frac{\tau}{\tau_{\mathrm{D}}}\right)^{-\frac{1}{2}} \tag{2}$$

wherein N is the average number of fluorescent probes in the confocal volume and τ_{D} is the diffusional correlation time. The square root term corrects for the difference of the axial and lateral size of the elliptical confocal volume. Typical values are ca. 300 nm for w_{xy} and ca. 1.5 μm for w_z.

The highest sensitivity for the determination of τ_{D} is realized when the confocal volume contains in average approximately one independently diffusing probe, which is the case for sub-nanomolar concentrations. If the probe concentration is too low, the events of a probe diffusing through the confocal volume become rather seldom and (random) background noise will dominate the signal resulting in no correlation to be detectable. For much higher concentrations, the relative intensity of the fluctuations of the fluorescence signal becomes less, and thus the sensitivity of FCS decreases. However, it has been recently shown that with a high count rate detector system and applying laser fluctuation corrections, FCS diffusion measurements were possible even with fluorescent probe concentrations in the μM range [16].

The correlation time τ_{D} depends on the exact dimensions of the confocal volume and is therefore not a quantity to compare translational motion in different systems with each other. Therefore, in most cases, the diffusion coefficient D is calculated using Einstein's mean square displacement

$$\tau_{\mathrm{D}} = \frac{4D}{w_{xy}^2} \tag{3}$$

which results in

$$G_{\mathrm{tr}}(\tau) = \frac{1}{N}\left(1 + \frac{4D\tau}{w_{xy}^2}\right)^{-1}\left(1 + \frac{4D\tau}{w_z^2}\right)^{-\frac{1}{2}} \tag{4}$$

The dimensions w_{xy}^2 and w_z^2 have to be determined by a reference measurement. For aqueous systems, a common and reliable reference is rhodamine 6G (Rh6G) in water with a diffusion coefficient of 4.14×10^{-10} m^2 s^{-1} [17]. The ratio w_z^2/w_{xy}^2 is typically in the range between 5 and 8. The diffusion coefficient D can be used to

determine the hydrodynamic radii of diffusing molecules, nanoparticles, or aggregates using the Stokes–Einstein equation

$$r_{\mathrm{h}} = \frac{k_{\mathrm{B}}T}{6\pi\eta D} \tag{5}$$

with the Boltzmann constant k_{B}, the sample temperature T, and the viscosity η.

It should however be kept in mind that Eqs. (2) and (4) only describe translational diffusion, if the shape of the focal spot convoluted with the detection efficiency profile is Gaussian, and if the emitters are point like. Micelles or other aggregates with multiple labels distributed over the whole nanoparticle require an analysis using the form factor of the distribution of labels on the particle [18]. Furthermore, in order to obtain reliable diffusion coefficients for complex systems, it has been reported that the minimum lag time, the maximum lag time, and the averaging time are critical parameters which have to be chosen appropriately [19].

If several independent diffusants with different diffusion coefficients are present in the sample, the autocorrelation function can be approximated by the summation of the terms of Eq. (4):

$$G_{\mathrm{tr}}(\tau) = \frac{1}{N}\sum_{i=1}^{n} f_i \cdot Q_i^2 \cdot \left(1 + \frac{4D_i\tau}{w_{xy}^2}\right)^{-1} \left(1 + \frac{4D_i\tau}{w_z^2}\right)^{-\frac{1}{2}} \tag{6}$$

where D_i are the individual diffusion coefficients of the species i with a number fraction of f_i and a fluorescence quantum yield of Q_i. If the individual diffusion coefficients differ by more than an order of magnitude, they can be unambiguously identified as distinct shoulders in $G(\tau)$. A smaller difference makes it difficult to distinguish individual contributions. In principle, if it spans several orders of magnitude, the distribution of D_i's can be yielded using a maximum entropy method [20] or a multicomponent analysis using the CONTIN algorithm [21]. Yet, the statistical quality of the measured $G(\tau)$ is the limiting factor of such types of analysis.

2.4 Analysis of Anomalous Diffusion

Another challenge is the analysis of anomalous diffusion from FCS measurements. Deviations from normal diffusion can be caused by internal chain motions [22–24] of (bio-)polymers, by molecular crowding [24–30], or by the restriction of diffusion to a certain "corral" region [31]. Different approaches have been suggested to deal with anomalous diffusion. One of the possibilities to describe anomalous diffusion uses a power law scaling of time τ^{α} [23, 26, 29, 30, 32, 33]. The scaling parameter α can depend on the timescale investigated and thus allows for a distinction between

translational and chain diffusion [22]. The ensemble average mean square displacement (MSD) $\langle \Delta r^2(\tau) \rangle$ with time τ can thus be expressed as follows:

$$\left\langle \Delta r^2(\tau) \right\rangle = 6D\tau^{\alpha} \tag{7}$$

If the probability distribution of displacements is Gaussian, the exponent α can be obtained by a combination of Eqs. (7) and (4) yielding [34]

$$G_{\mathrm{tr}}(\tau) = \frac{1}{N}\left(1 + \frac{2\left\langle \Delta r^2(\tau) \right\rangle}{3w_{xy}^2}\right)^{-1}\left(1 + \frac{2\left\langle \Delta r^2(\tau) \right\rangle}{3w_z^2}\right)^{-\frac{1}{2}} \tag{8}$$

Using this approach, the internal dynamics of long DNA molecules was studied and discussed in the framework of theories for polymer dynamics [35–37]. Different scaling regimes with exponents α of 2/3 and 1 were found for the internal dynamics at intermediate timescales and the crossover to the diffusion of the whole chain at long timescales, respectively. It has however been carefully checked whether the assumptions for using Eq. (8) are justified by the underlying microscopic model of diffusion. Without the verification by such a specific microscopic model, false conclusions might be drawn about subdiffusive behavior [38]. In general, single particle or single molecule tracking are more suitable to distinguish between different types of diffusion [39]. For a non-Gaussian distribution of displacements, Höfling et al. [40] derived a relation between the particle trajectory and autocorrelation function $G(t)$. This, however, requires information about entire trajectories and the averaged information from FCS experiments is not sufficient for its application.

Apart from the abovementioned analytical tools, a technical approach to detect anomalous diffusion has been reported. Sample-volume-controlled-(SVC-) FCS can directly detect anomalous diffusion by changing the diameter of the collimated excitation laser beam [41, 42]. One of the challenges of this approach is however the control over the optical parameters such as distortions of the confocal volume [43].

At constant focus size, it was shown that FCS cannot distinguish between diffusion constrained by elastic force, walking confined diffusion, and hop diffusion averaged over many measurements [44]. The simulations indicate that the mean square displacements of all these types of restricted diffusion can reliably be interpreted using one archetypal model presented by the following equation:

$$\left\langle \Delta r^2(\tau) \right\rangle = 6D_{\mathrm{L}}\tau + \frac{6}{5}a^2\left(1 - \exp\frac{-\gamma(5D_{\mathrm{S}}\tau)}{a^2}\right) \tag{9}$$

wherein D_{L} and D_{S} present the (macroscopic) diffusion coefficient measured for long time intervals and the (microscopic) diffusion coefficient measured for short time intervals, respectively. Equation (9) is only valid if the D_{L} and D_{S} are sufficiently well separated. Furthermore, a is an effective confinement radius and γ an exponential decay constant which depends on the model used ($\gamma = 1$ for diffusion constrained by elastic force, $\gamma \approx 0.866$ for walking confined diffusion, and $\gamma \approx 0.822$ for hop diffusion).

It should be emphasized at this point that FCS correlation curves can be often fitted equally well by an anomalous diffusion model and using two diffusion time constants. However, it has to be carefully analyzed which of the two models is more appropriate. Combining FCS results with simulations [45], Vagias et al. [46] for example showed that for the case of attractive tracer–polymer interactions, only a two-component diffusion process is a physically meaningful model.

2.5 *Full Correlation FCS to Detect Triplet Kinetics, Rotational Diffusion, and Fluorescence Antibunching*

In addition to translational diffusion, FCS is in principle also capable of determining the timescale of any process which causes fluctuations of the fluorescence signal. These processes are in particular triplet kinetics, isomerization, rotational diffusion, and fluorescence antibunching. Their timescales are typically shorter than the one of translational diffusion. One technical problem for measuring correlations on such short timescales is that measurements with one APD possess a dead time in the µs range, i.e., the detector is "blind" for this time interval after the detection of one photon. Therefore, any information about correlation of photons on a shorter timescale is lost. Additionally, depending on the detectors used, afterpulsing might cause artifacts. In order to obtain correlation values at shorter timescales, a Hanbury Brown and Twiss setup [47] can be used which splits the emission light and detects the photons on two independent detectors [48, 49]. Cross-correlation of the photon arrival times on the two detectors enables full correlation fluorescence correlation spectroscopy (fcFCS) measurements from the time range of picoseconds to the several minutes which can result in cross-correlation curves as presented in Fig. 3.

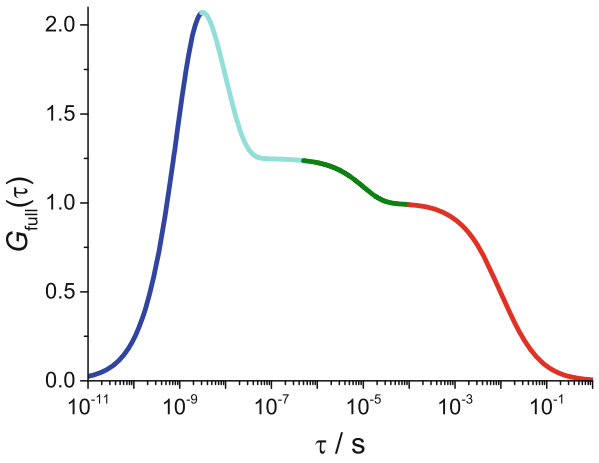

Fig. 3 Example of a full correlation FCS curve. The following parameters [see Eq. (10)] were used to simulate antibunching (*blue*), and correlation drops due to rotational diffusion (*cyan*), triplet blinking (*green*), and translational motion (*red*): $\tau_{AB} = 10^{-9}$ s; $\tau_R = 10^{-8}$ s; $R = 1$; $\tau_T = 10^{-5}$ s; $f_T = 0.2$; $\tau_D = 10^{-2}$ s; $\omega = 7$; $N = 1$

It was shown that for processes well separated in time, the correlation function can be simplified by factorization [50]. Therefore, the curve in Fig. 3 was constructed using the following combined equation with terms for translational diffusion, triplet blinking, rotational diffusion, and antibunching (each process in the corresponding line):

$$\begin{aligned} G_{\text{full}}(\tau) = & \frac{1}{N}\left(1+\frac{\tau}{\tau_{\text{D}}}\right)^{-1}\left(1+\frac{\tau}{\omega^2\tau_{\text{D}}}\right)^{-\frac{1}{2}} \\ & \cdot\left(1+\frac{f_{\text{T}}}{1-f_{\text{T}}}\cdot\exp\left(-\frac{\tau}{\tau_{\text{T}}}\right)\right) \\ & \cdot\left(1+R\cdot\exp\left(-\frac{\tau}{\tau_{\text{R}}}\right)\right) \\ & \cdot\left(1-\exp\left(-\frac{\tau}{\tau_{\text{AB}}}\right)\right) \end{aligned} \tag{10}$$

wherein N is the average number of independent emitters in the confocal volume, τ_{D} the translational diffusion time, ω a geometric factor (the ratio between axial and lateral diameter of the ellipsoid confocal volume), f_{T} the triplet fraction, τ_{T} the triplet lifetime, τ_{R} the rotational diffusion time, R the rotational amplitude, and τ_{AB} the antibunching time.

In the following we want to comment on the contribution of rotational diffusion. The theory to analyze rotational diffusion from FCS measurements was developed by Ehrenberg and Rigler [51] and Aragon and Pecora [52, 53]. Strictly spoken, the third term of Eq. (10) is only valid for the rotation of a spherical rotor with parallel transition dipole moments for absorption and emission and also with the same hydrodynamic properties in the ground and in the excited state. Furthermore, only the term with quantum number $l = 2$ of the angular momentum operator $\mathbf{L}^2$ has been considered [52, 54]. The sensitivity to measure rotational diffusion coefficients depends also on the polarization settings of the FCS setup, as nicely documented by Enderlein and coworkers [55, 56].

3 Technical Variations of FCS

As in most other experimental techniques, there is also a constant development and improvement involved in FCS which broadens its range, applicability, and accuracy. These developments resulted in advances such as dual-focus FCS, total internal reflection FCS, and STED-FCS which will be discussed in this section. Apart from this progress, a multitude of other variations have been reported which cannot be covered within this book chapter. These include FCS with two-photon excitation [57–61], spatial fluorescence cross-correlation spectroscopy (FCCS) which can be used to investigate microflows [62], dual-color FCCS to correlate

the fluctuations from two spectrally distinct fluorophores in order to analyze kinetics or association [63], pulsed interleaved excitation (PIE) FCS [56, 64], fluorescence triple correlation spectroscopy (F3CS) [65], and filtered FCS [66].

One of the main tasks in FCS is to obtain the maximum amount of (useful) information from the fluorescence light with reasonable effort and costs. Therefore, as many photons as possible should be detected including their parameters such as polarization, color, detection time, etc. [67]. Improvements have, however, not only been restricted to an improved detection of photons and their parameters, but also implemented new excitation and detection geometries.

3.1 Dual-Focus FCS

Enderlein and coworkers introduced dual-focus FCS (2fFCS) [68] in which two laser foci are alternately excited and detected. The distance between both laser foci serves as an internal distance reference, i.e., an intrinsic ruler. This avoids reference measurements which are otherwise necessary to relate diffusion time and diffusion coefficient. The accuracy of the obtained diffusion coefficients is sufficiently high to allow for sensitive measurements of temperature on a micrometer scale [69]. In addition, 2fFCS greatly reduces the dependency of FCS results on the size and shape of the excitation volume which due to optical saturation effects can vary significantly with excitation intensity. It is also less sensitive to slight changes in the refractive index [70], coverslip thickness, laser beam geometry, or optical saturation which can cause severe distortions of the confocal volume [43, 71] and, thus, can result in significant errors and misinterpretations in single focus FCS. The robustness of 2fFCS against optical and photophysical artifacts has been demonstrated for the investigation of systems with inherently large optical aberrations as they are often found in heterogeneous polymer systems [72]. However, when rather large colloids or macromolecules are used as probes for 2fFCS, their size with respect to the excitation laser focus has to be taken into account [73].

3.2 Total Internal Reflection FCS: Investigation of Interfaces

One of the challenges to investigate interfaces by FCS is the selective collection of the fluorescence emitted in the vicinity of the surface. The axial resolution of a confocal microscope results in averaging of the fluorescence emission within approx. 1 μm. As a consequence, surface effects are in most cases obscured in "normal" FCS measurements. With the evanescent wave of a laser beam totally reflected at the solid–liquid interface, however, the excitation can be restricted to a ca. 100 nm thin layer at the interface. This so-called total internal reflection FCS

(TIR-FCS) allows for an investigation of dynamic processes at liquid−solid interfaces [74–78]. Koynov and coworkers could for example measure diffusion coefficients of molecules and quantum dots at water−glass interfaces [77].

3.3 Superresolution in FCS

Superresolution microscopy methods have revolutionized optical microscopy within approx. the last two decades [79]. These methods can be separated in localization-based methods [80], which exploit the possibility to localize the isolated emission patterns of single molecules with high accuracy, and in methods which restrict the volume of excitation by stimulated emission. The latter can be combined with FCS resulting in STED-FCS (stimulated-emission-depletion FCS) [81, 82], where the excitation volume is minimized by an intensive donut-shaped STED laser pulse which depopulates basically all excited states except for a central volume of sub-diffraction size. This way, the spatial resolution Δd in lateral direction can be reduced to

$$\Delta d = \frac{\lambda}{2n \cdot \sin\alpha \sqrt{1 + \frac{I_{\max}}{I_S}}} \tag{11}$$

where n is the refractive index, α the half of the opening angle of the collected light, λ and $I_{\max}$ are the wavelength and maximum intensity of the STED beam, and I_S represents the STED laser intensity at which the probability of fluorescence emission is reduced by half. STED-FCS has been used to study membrane dynamics [81, 83], but also found its way into polymer science. King et al. studied the mobility of end-labeled polystyrene chains in solutions of polystyrene in toluene near the polymer overlap concentration c^*. At concentrations higher than c^*, they found two modes of motion: self-diffusion and correlated segment fluctuations [84]. Leutenegger et al. went even one step further and combined STED-FCS with TIRF (see previous section) in order to achieve both high axial and lateral confinement reaching measurement volumes beyond 1 attoliter [85] (Fig. 4).

3.4 Temperature Control in FCS

Temperature is an important parameter which can significantly influence the properties and applicability of polymer systems. In order to capture all the interesting transitions in polymers, it is of considerable interest to be able to perform FCS measurements in polymers in an extended temperature range from cryogenic temperatures up to several hundred degrees centigrade with accurate temperature control and without artifacts from temperature gradients or convection. A setup

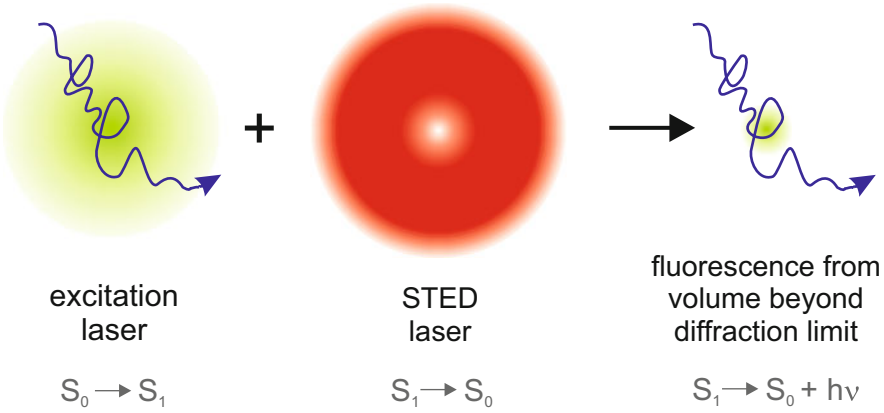

Fig. 4 STED-FCS: The principle of STED-FCS

with high-temperature accuracy and stability has been reported by Müller et al. [86] Elevated temperatures above ca. 80 °C can cause severe damages of the optical components of the microscope due to heat transfer from the heating table. Flier et al. [87] developed a heating device which allows for measurements at higher temperatures of up to 150 °C using indium tin oxide (ITO) covered glass slides, resistively heated by the application of a controlled voltage. This restricts the heated mass to a minimum and therefore protects the optics from being overheated.

4 Limitations of FCS

4.1 Refractive Index Changes

FCS measurements possess some intrinsic limitations which should always be kept in mind. One of the most severe pitfalls are refractive index changes which can cause severe distortions of the confocal volume [43, 71, 88]. Such refractive index changes can in particular appear in heterogeneous polymer systems where the different compartments are composed of different polymers or solvents. The distorted confocal volume causes failure of the equations typically used for the FCS analysis which assume an ellipsoid shape of the confocal volume [see Eq. (2)]. Creating different models with the distorted volume is a hard or even impossible task. Also the determination of diffusion coefficients using reference measurements with the typical aqueous systems, i.e., Rh6G in water, will result in errors [89]. Therefore, alternative calibration methods had to be found. Zettl et al. used the known molecular weight dependence of the diffusion of rhodamine B (RhB)-labeled polymer chains of different lengths in very dilute solution to determine the size of the confocal volume and thus to calibrate the diffusion coefficient obtained

by FCS [90, 91]. The observation volume can also be calibrated using fluorescently labeled silica nanoparticles [92, 93] or dye-labeled polystyrene (PS) of known molecular mass [94], with the diffusion coefficient in dilute solution known from DLS measurements. One way to reduce the problems with distortions of the confocal volume is to measure at relatively small penetration depths of ca. 10 μm which is still reasonably far in the solution to avoid biased results due to influences of the interface. Another possibility to measure in systems with significant refractive index changes is dual-focus FCS as described in one of the previous sections [68]. Apart from the refractive index, slight changes in coverslip thickness, laser beam geometry, pinhole adjustment, or optical saturation can also lead to misinterpretations [43].

4.2 Spatial Resolution

The spatial resolution of FCS has been discussed in some papers [95, 96]. It has been stated that FCS is capable of resolving dynamics at the nanoscale, i.e., far beyond the limits of optical resolution [96]. On the other hand, it was mentioned that, as for all optical techniques, the diffraction limit has to be considered [95]. In general, it is possible to observe dynamics with a spatial accuracy beyond the diffraction limit of light. However, one has to be aware that, even though photon arrival times can be determined with picosecond accuracy, the obtained information about dynamics is averaged over time. This means dynamic heterogeneities which can be caused by mesh size fluctuations or fast structural changes cannot be observed directly and at the most could be estimated with an appropriate model explicitly implemented into the autocorrelation fit function. In addition, for the determination of spatially resolved diffusion coefficients from FCS measurements by changing the position of the focus, the diffraction limit determines the resolution. This can be only improved by superresolution techniques such as STED-FCS as states above.

4.3 Choice of the Fluorescent Probes

Just as for any other fluorescence microscopy technique, the choice of the fluorescent probe is of significant importance for FCS. Drops in the autocorrelations curves can occur as a result of photophysical and photochemical processes. In particular, the contribution of saturation effects and triplet blinking has been investigated [97, 98] and the rates of intersystem crossing and triplet decay as well as the excitation cross section of fluorophores could be determined [12]. In addition, antibunching is determined by the photophysics of the fluorophore. Therefore, the choice of appropriate dyes is essential to obtain meaningful results. Apart from that, the fluorescent probe should also serve as a selective label to

observe the diffusing species of interest. However, the interaction between dyes and polymer chains can also result in misinterpretations and should be carefully checked.

5 FCS in Polymer Solutions

FCS is a suitable technique to study polymer dynamics in solution, and the diffusional processes investigated by FCS provide important information about the local mechanical and viscoelastic properties of polymer solutions. Typically, a tiny amount of fluorescently labeled polymer chains or free dyes is added to the polymer solutions to be investigated or vice versa. This has not only the advantage of requiring minor amounts of fluorescent dyes or labeled polymers, but also minimizes the disturbance of the system by the introduced fluorophores.

One very interesting question concerning polymer solutions is how the diffusion of dye-labeled polymer chains and molecular probes changes with varying concentration and molecular weight of the probe and the surrounding. Principally, three different polymer concentration regimes can be distinguished: (i) dilute solutions in which diffusion is fully governed by the hydrodynamic radius of the diffusing species, (ii) semidilute solutions in which the polymer coils start to overlap, and (iii) concentrated solutions in which the chains strongly interact with each other. The border between the dilute and the semidilute regime is often called c^*, whereas the border between semidilute and concentrated regime is typically referred to as c^{**}. The semidilute and the concentrated solutions can be further divided into an unentangled and an entangled regime, the border of which is normally referred to as the entanglement concentration c_E. In the latter regime, topological constraints caused by entanglement dominate the dynamics. The transition between the regimes depends primarily on concentration and molecular weight of the polymer. In the following, the contributions of FCS to elucidate molecular dynamics in the various regimes will be discussed.

In this context, it is essential to discuss how the diffusion of single molecules or particles can be connected to the viscosity, if viscosity is a concept which still holds for length scales in the nanometer range. In fact, viscosity is a strong function of the length scale at which it is probed [99, 100], and already almost 30 years ago, the concept of length scale-dependent viscosity has been developed [101, 102]. Brochard and de Gennes suggested that the motion of a particle with a radius $R_0 \gg R_g$ (radius of gyration) is governed by the bulk viscosity [103]. As its size, however, becomes close to the tube diameter or smaller, the diffusion coefficient can increase dramatically by up to a few orders of magnitude. For entangled polymer solutions, this behavior is additionally governed by the entanglement spacing d_t (tube diameter) [104]. This was verified by diffusion measurements of particles with different diameter $2R_0$ which was comparable to the entanglement tube diameter using fluctuation correlation spectroscopy, i.e., correlation of the luminescence of gold nanoparticles after multiphoton excitation [105].

A similar approach was presented by Hołyst et al. who studied the diffusion of differently sized probes ranging from RhB molecules (1.7 nm) up to silica spheres (114 nm) in polyethylene glycol (PEG) solutions with a combination of FCS, capillary electrophoresis, and macroviscosity measurements (see Fig. 5) [106]. They found that the large probes diffused as expected from the macroviscosity of the solutions, whereas the diffusion of the small probes was clearly faster. As a consequence of this behavior, they distinguish between a macroviscosity experienced by larger probes and a nanoviscosity felt by small probes where the latter was observed to be up to a factor of 100 times smaller than the macroviscosity. A comparable result was also obtained for the diffusion of 2–44 nm sized probes in PVA solutions by Michelman-Ribeiro et al. [107]. The crossover from probing nanoviscosity to probing macroviscosity was found at a length scale at which the probe reached a size of approximately the radius of gyration of the polyethylene glycol (PEG) polymer under investigation [106]. It could be shown that the dependency of viscosity η on the ratio between an effective probe size and the correlation length ξ of the polymer follows a stretched exponential function. Probes smaller than the radius of gyration R_g of the polymer experience the nanoviscosity and the effective probe size is the probe radius R, whereas it equals the radius of gyration R_g for probe molecules of larger size which feel the macroviscosity of the polymer solution [106]. Thus,

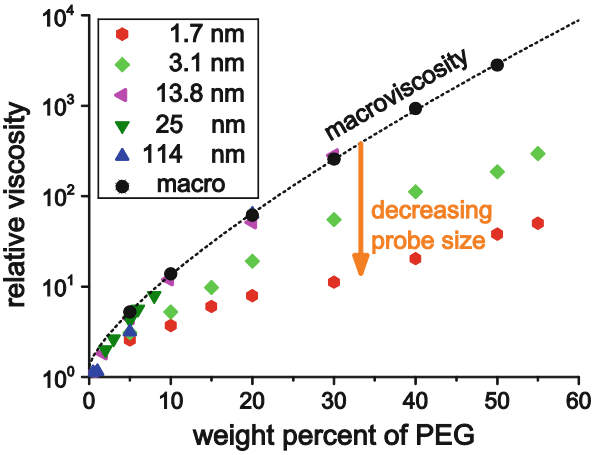

Fig. 5 Viscosity determined using diffusion measurements of differently sized probes in PEG 20000 solution. Small probes experience nanoviscosity, whereas large probes follow the macroviscosity which is shown as the *dashed black line* as a guide to the eye. The crossover length scale between nano- and macroviscosity in PEG20000 is larger than 3.1 nm and smaller than 13 nm (reproduced and adapted from Hołyst et al. [106] with permission of the PCCP Owner Societies)

$$\frac{\eta}{\eta_0} = \begin{cases} \frac{\eta_{\text{nano}}}{\eta_0} = \exp\left(b\left(\frac{R}{\xi}\right)^a\right) & \text{for} \quad R < R_g \\ \frac{\eta_{\text{macro}}}{\eta_0} = \exp\left(b\left(\frac{R_g}{\xi}\right)^a\right) & \text{for} \quad R > R_g \end{cases} \tag{12}$$

where the ratio between radius of gyration and correlation length ξ depends on the polymer concentration and the overlap concentration according to

$$\frac{R_g}{\xi} = \left(\frac{c}{c^*}\right)^{\beta} \tag{13}$$

where β depends on the Flory parameter v according to

$$\beta = -\frac{\nu}{(1 - 3 \cdot \nu)} \tag{14}$$

and for a three-dimensional polymer coil in a good solvent equals to ¾. Using the relationship shown in Eq. (12), all measured data of viscosity versus probe size could be plotted on one master curve. Furthermore, the parameter b in Equation (12) could be related to an excess activation energy for viscous flow compared to the one observed for pure solvent. The intrinsic viscosity was found to be directly proportional to this activation energy [108].

6 Diffusion of Small Molecular Probes

Small molecular probes sense the local viscosity and, therefore, no significant difference for their mobility in solutions of polymers of different (high) molecular weight is found. FCS measurements of the diffusion coefficients of a perylene monoimide dye for various concentrations of solutions of different molecular weight polystyrenes in acetophenone verified that all points fall onto the same master curve which could be fitted with a stretched exponential [109]. That means that from the perspective of the probes, the change in molecular weight of the polymer between 110 and 450 kg/mol does not seem to make a difference. At low polymer concentrations, the diffusion of the small probes is even not significantly influenced by the presence of polymer chains at all since it can diffuse basically unhindered through the polymer meshes. In a concentration range between ~6c^* and 20c^*, small molecules in polymer solutions were found to exhibit normal diffusion,[110] in contrast to larger nanoparticles for which a subdiffusive behavior was found (see below). The effect of the probe size on translational and rotational motion of perylene diimide derivatives of different size was monitored during the free radical bulk polymerization of styrene [54]. The increasing viscosity during bulk polymerization causes a drop in diffusion coefficient. The relative drop in rotational diffusion coefficient, i.e., the current diffusion coefficient D divided by

the diffusion coefficient D_0 in pure monomer solution (conversion = 0), was found to be similar for all probe sizes. All plots of D/D_0 versus the conversion showed the same behavior whereas significant differences were observed for the relative changes in the translational diffusion coefficient. The decrease in translational diffusion of the smallest dye resembles the rotational diffusion data. With respect to this scaling, the translational diffusion of the larger probes is significantly lowered, pointing to a change from probing nanoviscosity, apparently the property determining rotational diffusion, toward macroviscosity. A similar behavior was observed for the diffusion of the enzyme aldolase in aqueous solutions of polyethylene oxide. It was argued that the viscosity experienced for rotational motion is significantly reduced in comparison to the one experienced for translational motion due to entropic reasons [108].

Diffusion of small molecular probes was also studied in polymer melts. Herein, the diffusion of molecular tracers senses the glass transition temperature-dependent local segmental dynamics of the polymer matrix, rather than its macroscopic viscosity [111, 112]. The dependence of the diffusion coefficient on temperature could be fitted using a Vogel–Fulcher–Tammann function with an activation energy increasing with the tracer size and depending on the polymer. A combination of FCS and laser scanning confocal microscopy allowed for monitoring the dynamics of phase separation in a PS/poly(methyl phenyl siloxane) blend, two polymer components with a difference in glass transition temperature of more than 113 K and an upper critical solution temperature [113]. In polymer blends, the topology of the matrix polymer plays a pivotal role. Cherdhirankorn et al. observed significant differences in the diffusion of terrylene diimide probes in a polymer melt of linear and star-shaped 1,4-polyisoprenes, respectively [26]. FCS measurements are however not limited to small probes as will be shown in the following section.

7 Diffusion of Macromolecular Probes

Fluorescence-labeled polymer chains have been investigated by FCS to determine macromolecular diffusion in different polymer concentration regimes. Most studies were performed on labeled PS chains in toluene solutions of non-labeled PS of similar length.

For highly dilute and non-interacting solutions, this allows for the determination of self-diffusion coefficients D_0. Proceeding to the dilute regime where the polymer chains can interact with each other but still do not overlap, the dynamics is dominated by the hydrodynamic radius of the diffusing probe. According to the Kirkwood–Riseman theory [114], the diffusion coefficient can be calculated as follows:

$$D = D_0 - k_f \cdot c \tag{15}$$

where D_0 is the diffusion coefficient at infinite dilution (see above) and k_f is a

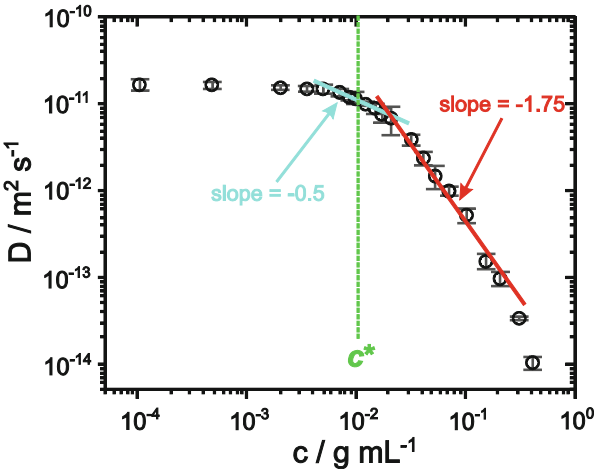

Fig. 6 Diffusion coefficient of labeled PS in toluene solutions as a function of polymer concentration and its prediction according to reptation and scaling theory (adapted with permission from Liu et al. [94]. Copyright 2005 American Chemical Society)

proportionality factor. This linear dependence of the diffusion coefficient on polymer concentration could be confirmed by the FCS measurements of Zettl et al. [90].

Further increase of the concentration above the overlap concentration c^* [115] causes a transition from the dilute to the semidilute regime. FCS measurements have verified that the concept of an overlap concentration is very useful as the plot of the diffusional correlation time versus the polymer concentration changes the slope at c^* [91]. In such a graph, linear fits of both regimes interact at the overlap concentration which depends on the molecular weight of the dissolved polymer chains. For increasing molecular mass, c^* shifts to lower concentrations. Fitting the dependency of c^* on molecular mass resulted in a Flory exponent of 0.59 in excellent agreement with the value of 0.588 predicted by theory for a polymer in a good solvent [116].

A very detailed study over a broad range of concentrations between 10^{-4} and 0.4 g/mL of high molecular weight PS chains ($M_W = 390$ kg/mol) in toluene was performed by Liu et al. [94]. In the dilute regime ($c < c^* \approx 0.01$ g/mL), they obtained basically a constant diffusion coefficient, i.e., $D \sim c^0$. Proceeding to the unentangled semidilute regime ($c^* \approx 0.01$ g/mL $< c < c_E \approx 0.02$ g/mL), where the polymer coils overlap but do not entangle effectively, a scaling of $D \sim c^{-1/2}$ in agreement with theory was determined [117]. When entanglements start to dominate the diffusional behavior at $c > c_E \approx 0.02$ g/mL, the scaling changes to $D \sim c^{-7/4}$ as predicted by basic scaling and reptation theory [115, 118]. The different regimes and their scaling behavior with polymer concentration are illustrated in the double-logarithmic plot in Fig. 6. FCS diffusion measurements of perylene-monoimide-labeled PS chains in unentangled and entangled semidilute solutions gave comparable results [109]. Additionally, in both of these studies, it was shown that the transition between the different regimes is rather smooth. In unentangled semidilute solutions of low molecular weight, the diffusion measurements of fluorescence-labeled polymer chains elucidate a linear dependency between viscosity and

temperature [58]. The activation energies obtained from Arrhenius fitting of these data for different polymer concentrations can be related to free volume theory [119].

Apart from the scaling of the diffusion coefficient of polymer chains with concentration, the dependency on their molecular weight is of high interest. For PS in the good solvent toluene, a scaling of $D \sim M^{-3/5}$ and $D \sim M^{-2}$ for dilute and semidilute entangled solutions was determined, respectively [24]. The question how the molecular weight of the surrounding chains depends on the diffusion coefficient of a small fraction of labeled PS chains in toluene has also been addressed [109]. It was found that higher molecular weights of the matrix polymer result in slower diffusion of the macromolecular probes as long as the molecular weight of the matrix does not exceed five times the molecular weight of the probe. For large matrix molecular weight, a master curve was obtained when plotting D normalized to the diffusion coefficient in infinite dilute solution versus the polymer concentration normalized to the overlap concentration of the diffusing fluorescently labeled polymer species. The obtained scaling parameters were -0.5 and -1.75 for the unentangled and entangled semidilute regime, respectively, in agreement with the previously mentioned study by Liu et al. [94]. In entangled polymer solutions, the motion of polymer chains is not independent from other chains anymore since the chains are coupled to each other through the entanglements. Therefore, in addition to self-diffusion, a collective diffusion mode could be observed in a semidilute solution of PS chains with a molecular weight of 515 kg/mol PS chains and a concentration of 13 wt [24]. This collective mode has a significant impact, for example, on the production of nanofibers [24].

For highly concentrated polymer solutions, FCS measurements revealed subdiffusive motion as an additional mode on an intermediate timescale between the fast collective diffusion and the slow self-diffusion [24]. In such slow systems, however, FCS reaches its limits when probe motion becomes so slow that the number of molecules moving into or out of the confocal volume within the measurement time is too small to allow for reliable statistics. Increasing the measurement time is often not straightforward since all fluorescence dyes have only a limited photostability. If a dye bleaches within the confocal volume, it will fake a faster diffusional motion than its real value. Therefore, for the study of such concentrated systems, wide-field fluorescence microscopy and subsequent single molecule tracking is a much better method [120] and has been utilized to study the glass transition [87, 121].

8 Diffusion of Nanoparticles in Polymers

As already discussed for molecular probes, the probe size plays a pivotal role for the analysis of polymer systems. Its size with respect to characteristic length scales of the investigated system determines the dynamics to be measured. For sufficiently large nanoparticles with diameters in the 100 nm range microviscosity can be

accessed. This technique is often referred to as passive microrheology [122–124]. In addition to its spatial resolution, the big advantage of microrheology is that only tiny sample volumes are required, a challenge for other rheometers.

Mukhopadhyay and coworkers observed the diffusion of differently sized gold nanoparticles (NPs) within an entangled liquid of poly(*n*-butyl methacrylate) (PBMA) above the glass transition temperature [105]. Instead of using a fluorescence signal for detection, they used the multiphoton absorption-induced luminescence of gold nanoparticles to perform fluctuation correlation spectroscopy measurement. One key parameter for the diffusion behavior is the ratio of particle size and tube diameter within the entangled polymer. Small nanoparticles can use this path to "sneak" through the polymer meshes whereas for larger particles Stokes–Einstein behavior is recovered. The size of the probes with respect to the mesh size also determines the diffusional mode of the nanoparticles. Small molecules or nanoparticles exhibit normal diffusion whereas anomalous diffusion was found for larger particles [110].

Slight anomalous diffusion is also observed for the motion of nanoparticles in agarose, i.e., polysaccharide, gels when its size amounts to approx. half of the critical size for which particles become trapped in the gel [32]. This behavior indicates that the diffusion through the gel of slightly larger mesh size than the particle diameter is hindered by the interactions of the saccharide which act as obstacles, but the particles can still jump from pore to pore. For nanoparticles of larger size, the connectivity of the pores decreases rapidly, and the particles get trapped because percolating paths for them become very rare.

9 FCS in Polymer Gels

This section will concentrate on FCS measurements in covalently (chemically) cross-linked polymer gels. The diffusion inside gels is affected by several parameters, in particular by the mesh size of the gel, its microstructure, the degree of swelling, the size of the diffusing species, and interactions between diffusing species and gel. At low polymer concentration, there is no significant difference between solutions of linear or cross-linked chains. Above a certain threshold concentration, the diffusion of stronger cross-linked gels decreases more rapidly when increasing the polymer concentration [125, 126]. This threshold concentration is, for example, approx. 3% w/v for PVA gels as shown by Michelman-Ribeiro et al. [127]. The cross-links act as obstacles for the diffusing species and affect their motion. This hindrance becomes more pronounced the higher the cross-link density and depends strongly on the size of the probe compared to the mesh size of the cross-linked polymer. Modesti et al. report that the most reasonable description for the diffusion in polymer networks is obtained by assuming that the cross-link effect is additive to the effective friction coefficient of the probes, i.e., the friction coefficient in the network equals the effective friction coefficient for the probe in the pure solvent plus a friction coefficient caused by the permanent cross-links

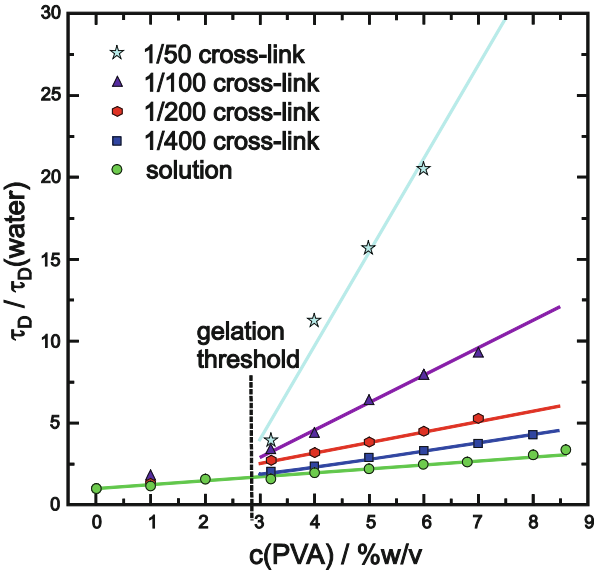

Fig. 7 Scaled characteristic diffusion time of fluorescent TAMRA molecules in PVA solutions and gels at several cross-link densities as a function of polymer concentration with linear fits. The times are scaled by the diffusion time of the probe in water. The *vertical dashed line* indicates the approximate gelation threshold (adapted from Michelman-Ribeiro et al. [127])

[125]. The description of polymers bearing very high cross-link densities with this model however fails, presumably due to pronounced swelling heterogeneities, i.e., the solvent preferably swells the more weakly cross-linked matrix and, thus, even at rather low degrees of swelling, opens up percolating regions of lower polymer density in which the dye can diffuse rather easily. Such an explanation is also underlined by our own observations on heterogeneous diffusion in polymer solutions during their cross-linking free radical bulk polymerization [128]. Interestingly, such a behavior is also observed for the linear bulk polymerization of MMA and is probably one of the main reasons for a pronounced Trommsdorff effect [129]. The change of diffusion behavior of three different proteins with hydrodynamic radii between 1 and 5 nm during swelling of cross-linked polyethyleneglycol networks hydrogel matrices with mesh sizes of ca. 14–19 nm can be explained by free volume theory [130]. A theory which explicitly considers the confinement a particle experiences from polymer chemical cross-links and which describes nanoparticle diffusion as subsequent activated hopping processes due to polymer network fluctuations has been recently published [131]. As already mentioned before, FCS is not only capable of studying the effect of cross-links in readily synthesized gels, but allows also for an investigation of the polymerization or cross-linking process itself. This way, the photo-crosslinking of PS microbeads with UV light was followed using FCS [132] (Fig. 7).

10 FCS in Charged Polymer Systems

Charges often play an important role for the properties of polymer systems. Therefore, it is not surprising that this topic was also addressed using FCS. Pristinski et al. investigated the translational diffusion of Alexa-labeled polymethacrylic acid in aqueous solution as a function of polymer concentration, solution pH, and ionic strength [133]. Below the overlap concentration c^* only minor changes were observed when varying the concentration. Beyond c^*, the diffusion coefficients dropped significantly with increasing polymer concentration. A change from pH 5 to pH 8 resulted in an increased charge on the PMAA chains resulting in their twofold expansion. Enhanced ion concentrations of alkaline metal ions caused a chain contraction. Both dependencies could be detected using FCS diffusion measurements. Also the electrostatic interaction of oppositely charged polymers, in particular the complexation between negatively charged rhodamine-labeled oligonucleotides and cationic polymers, was studied [134]. The interaction of small (cationic) Rh6G dye molecules with (anionic) polystyrene sulfonate (PSS) polymers resulted in a fraction of free and a fraction of polymer-bound dye molecules [135]. The fraction of bound probes could be decreased by elevated salt levels indicating a dynamic exchange process between the free and bound cationic dyes. In another study, determination of the hydrodynamic radius of fluorescently labeled dextran could explain their solvent-dependent uptake into polyelectrolyte multilayer microcapsules [136]. FCS was also used to confirm the layer-by-layer assembly of PNIPAM microgel particles with (three) alternating layers of oppositely charged polymers as shown in Fig. 8 [137]. In general, a combination of simulations and theoretical studies with FCS measurements has a high potential to elucidate the effect of interaction in more detail. This is not only limited to charged species but can also take into account different interactions between polymer chains and probes [46].

11 FCS in Responsive Polymers

Responsive polymers have attracted considerable interest. Thermoresponsive systems which change their polarity and, thus, their shape and behavior within a physiological range between ca. 30 to 40 °C (see Fig. 9) have for example potential as drug delivery systems. Exploiting the potential of these polymers requires a detailed knowledge of their structure and dynamics at the nanoscopic and mesoscopic scale. The most studied responsive polymer, so far, has been poly(*N*-isopropylacrylamide) (PNIPAM) which exhibits a lower critical solution temperature (LCST) at around 32 °C. Below this temperature, PNIPAM chains in water are in a swollen state. At the LCST a volume phase transition occurs and the gel collapses and expels water. FCS allows for the investigation of the diffusion of small molecules and labeled PNIPAM chains in PNIPAM hydrogels. It was shown

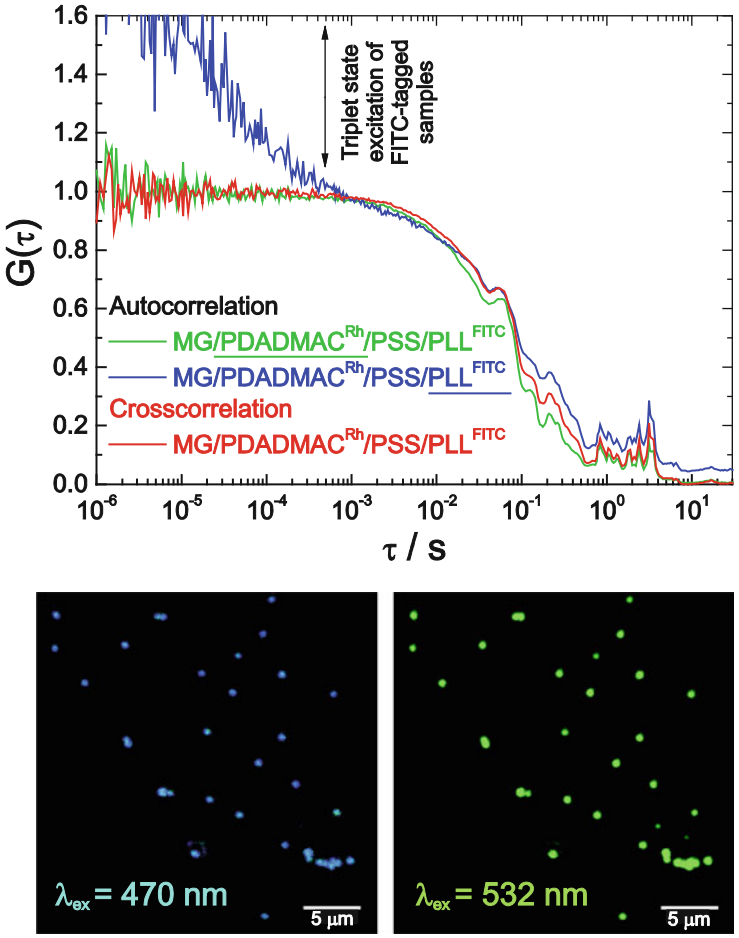

Fig. 8 FCS proves that the two differently labeled polyelectrolytes are anchored to the same PNIPAM microgel and, thus, that the layer-by-layer assembly has been successful. *Top*: Auto- and cross-correlation function of the coated PNIPAM nanoparticles. *Bottom*: Confocal fluorescence images of dried particles when excited at 470 nm (*left*) and 532 nm (*right*), respectively (adapted with permission from the Journal of Physical Chemistry [137]. Copyright (2007) American Chemical Society)

that the dependency of the diffusion coefficient on polymer concentration follows a stretched exponential [138]. Conventional hydrogels cross-linked with organic cross-linkers, however, suffer from severe disadvantages for technical and medical usage due to their low mechanical toughness, limited swelling ratio at equilibrium, and poor transparency. Clearly improved properties were reported for PNIPAM hydrogels cross-linked with clay nanoparticles [139]. These systems have also been studied by FCS using free probes [140] and covalent labeling of the clay nanoparticles [141]. In the latter case, FCS was used to verify the covalent labeling

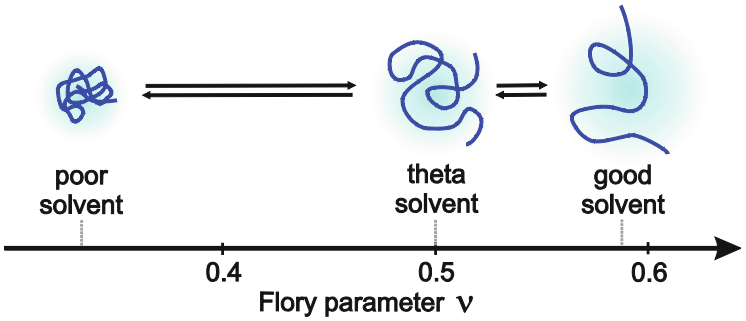

Fig. 9 Shapes and Flory parameters v of polymer chains in different solvent quality. The *three dotted lines* denote the theoretical values of v for different solvent qualities

and wide-field fluorescence microscopy studies revealed an anomalous diffusion of the clay nanoparticles in the hydrogels which significantly changed during the volume phase transition.

The temperature-induced change of mobility of differently sized probes through PNIPAM gels anchored to a solid substrate and, thus, with swelling restricted to one dimension was investigated by the Koynov group [126, 138]. In the swollen gel at low temperature, the small Alexa 647 probe exhibited a diffusion behavior which could be described with one diffusion coefficient, whereas the larger probe, green fluorescent protein (cylindrical shape with approx. $4.2 \times 2.4 \times 2.4$ nm^3[142]), significantly deviated from this single Fickian diffusion. Thus, the length scale of hindrance of probe motion due to the hydrogel structure is in a range between the sizes of both probes. In the transition regime from the swollen to the collapsed state around the volume phase transition temperature, two fractions of molecules with different diffusion coefficients were found for both dyes. This reflects the decreasing length scale of heterogeneous behavior of the probes caused by the denser polymer network which now also affects the diffusion of the small dye. After the collapse transition occurred at a swelling ratio of about 1.5, all dye molecules were expelled from the collapsed hydrogel films and thus moved freely outside of the polymer layer on the surface.

The diffusion of labeled dextranes in nanocomposites consisting of thermoresponsive PNIPAM microgels in a poly(acrylamide) hydrogel matrix could be measured with spatially resolved 2fFCS inside the microgel nanoparticles and in the surrounding hydrogel matrix [143]. The diffusion behavior of the probes in these nanocomposites depends on the cross-linking density of the microgels. For weakly cross-linked microgels, the nanocomposite forms an interpenetrating polymer network. As a consequence, swelling and deswelling of the microgel are obstructed and the mobility of embedded fluorescently labeled dextran probes is reduced. For highly cross-linked microgels, they collapse upon increasing the temperature above the volume phase transition temperature. This results in a heterogeneous swelling of the hydrogel matrix and the formation of pores near

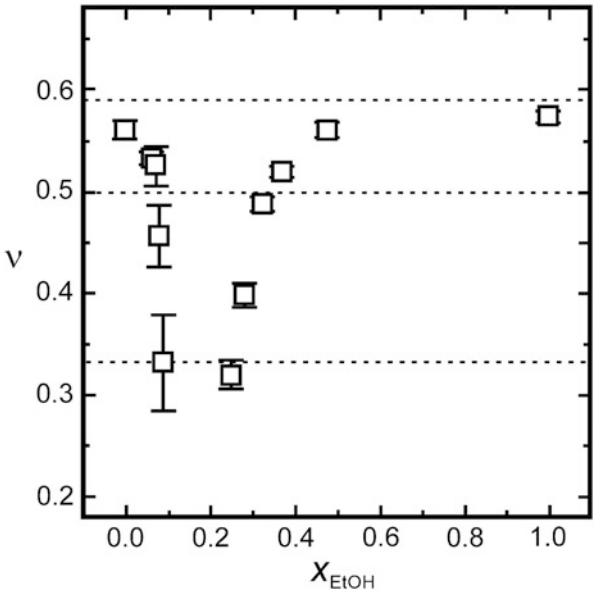

Fig. 10 Flory exponents ν as a function of the mol fraction x_{EtOH} of ethanol. The *three dotted lines* denote the theoretical values for the different solvent qualities as given in Fig. 9 (adapted with permission from Macromolecules [149]. Copyright (2012) American Chemical Society)

the surface of the microgels. Such behavior allows for tailoring of pore structures, thus enabling a control of the motion through these systems.

Amongst other polymers, PNIPAM exhibits a peculiar behavior in solvent mixtures. This polymer is, e.g., well soluble in water and in ethanol, but not in certain mixing ratios of these solvents. The reasons for this phenomenon called cononsolvency are still under discussion [144–147]. Cooperative hydration and competitive hydrogen bonding are current concepts to explain cononsolvency [148] Wang et al. applied FCS on fluorescently labeled PNIPAM of different degrees of polymerization and different water–ethanol compositions.[149] One technical challenge in these measurements was the change in refractive index upon addition of the cononsolvent ethanol to the aqueous polymer solution and the concomitant change in the confocal volume size and shape [43]. The change in refractive index was investigated using reference measurements of fluorescent nanoparticle diffusion in glycerol–water mixtures of known refractive indices by DLS. It was concluded that the effect of the refractive index mismatch and the consequential distortion of the confocal volume can be neglected for small distance of the focal point from the coverslip (ca. 10 µm is also in our view an appropriate distance for such measurements). From the diffusion times accessed by FCS, the hydrodynamic radii of the PNIPAM coils were determined for different polymer chain lengths and solvent mixtures. From the dependency of the hydrodynamic radius r_h on the polymer chain length N, the Flory scaling exponent [115] ν was determined as $r_h \propto N^{\nu}$. As shown in Fig. 10, the values in pure ethanol and pure water are close to the predicted values for good solvents. In water–ethanol mixtures, the solvent quality for PNIPAM becomes significantly lower. Between a mole fraction x_{EtOH} of 0.09 and 0.25, no

uniform fluorescent signal could be detected in solution due to the (reversible) formation of suspended aggregates.

FCS studies were not only performed in PNIPAM, but also in thermoresponsive poly(2-oxazolines) [150] and to investigate the diffusion of nanoparticles in methylcellulose [151]. At low temperature, the latter exhibits a transient polymer mesh networks in the fluid state which at higher temperatures switches to a gelled state due to a formation of fibrillar structures.

Apart from using temperature for the switching, also other triggers such as pH, salt concentration, and solvent composition have been reported. Changes in pH value and ionic strength result in different interactions between polymer chains and between the probes and the polymers and are especially pronounced for charged species [133]. FCS studies at different humidity are sparse,[152] but may give a lot of interesting information about the changes of the polymer dynamics during swelling and deswelling.

12 FCS in Polymeric Systems Near Interfaces

The way that polymer chains diffuse at an interface is of high practical importance for example for coating applications. This question, however, turned out to be rather complex and measurements as well as theoretical considerations are challenging. The reason for this complexity are the numerous interactions and conformations that have to be considered at interfaces. A variation of FCS that is quite suitable to investigate surfaces is TIR-FCS where the sensitivity of FCS measurements at solid–liquid interfaces is significantly enhanced [76–78]. However, so far most FCS studies at interfaces have been performed in the "classical way."

It was, for example, found that end-labeled polyethylene glycol (PEG) chains adsorbed onto a hydrophobic self-assembled monolayer of octadecyltriethoxysilane coated onto a fused silica coverslip exhibit a flat "pancake" conformation due to significant adsorption of the polymer chains on the surface [60, 153]. This interaction causes that the diffusion coefficient scales with the number of chain segments according to a strong power law scaling with an exponent of $-3/2$, in contrast to the scaling of $-1/2$ in solution (see also Fig. 11). Not surprisingly, surface diffusion depends on surface coverage [154, 155]. At low surface coverages, an increase of the translational diffusion coefficient with increasing surface concentration was observed and attributed to a decrease of adsorption sites per molecule as chains switch from pancake to loop–train–tail conformation. When polymer chains start to overlap at the surface, the diffusion slows down significantly, due to crowding and entanglement with neighboring chains.

Translational diffusion within polymer brushes can be also accessed by FCS studies. It depends on the local viscosity within the brush and on probe size, thus causing different results for small and macromolecular probes [156]. For charged polymers, pH and ionic strength plays an additional role. If the dyes and the brushes are oppositely charged a dynamic association of dye molecules with the polymer

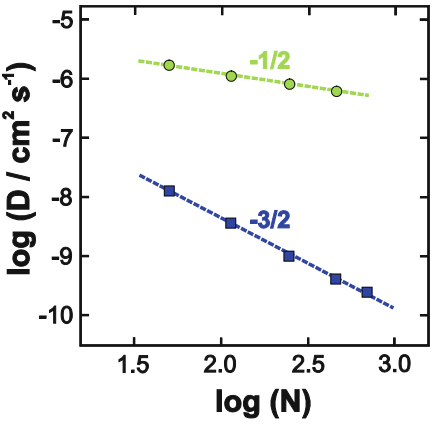

Fig. 11 Center-of-mass diffusion coefficients D in solution (*green circles*) and at the surface (*blue squares*) plotted against the degree of polymerization N in double-logarithmic scale. The solution data can be well fitted by a linear function with a slope of $-1/2$. For surface diffusion a slope of $-3/2$ was obtained (reproduced and adapted with permission from [60]. Copyright 2002 American Chemical Society)

brush can be observed. The association and dissociation kinetics can be adjusted by the pH or the addition of ions [157].

When the polymer brushes or surface coating are thermoresponsive, surfaces can be also sensitive to temperature. Wang et al. studied lateral diffusion of fluorescently labeled polyelectrolyte poly(2-vinylpyridine) (P2VP) on the surface of thermoresponsive poly(*N*-isopropylacrylamide) (PNIPAM) brushes [93]. At the low pH used for the measurements, the P2VP chains were fully charged and thus exhibited an extended coil conformation. Gradually increasing the temperature resulted in an increase in the diffusion coefficient of the P2VP probes as expected from the concomitant decrease of viscosity. However, at the volume phase transition temperature the diffusion coefficient started to decrease again. This behavior was attributed to the collapse of the PNIPAM chain conformation changing the hairy to a closely packed layer.

Apart from solid–liquid interfaces, also liquid–liquid interfaces can be investigated using FCS. As an example, the adsorption dynamics of proteins at the oil–water interface was measured [21]. However, changes in refractive index at the interfaces should be carefully considered in order to avoid misinterpretations. A thoughtful analysis of such effects has been performed by Donsmark et al. who determined the molecular detection function of their system using numerical wave-optical calculations [21].

13 FCS in Polymeric Micellar Systems

Polymeric amphiphiles can form different architectures such as spheres, disks, rods, vesicles, or flocs [158]. For applications, it is of paramount importance to understand how the shape and size of these assemblies varies with polymer concentration, quality of the solvent, and the lengths of the building blocks. FCS can

significantly contribute to solve these questions due to its capability to follow micellization and aggregation of polymers and detect their motion even at very low concentrations. Nörenberg et al. investigated the interaction of polymer and surfactant in solutions which can form mixed polymer–surfactant micelles. One of the main advantages using FCS was the very low concentration at which these measurement could be performed so that viscosity effects arising from interacting polymer tails and chains or Coulomb interactions could be neglected [159]. The majority of FCS studies in polymeric micellar systems, however, focus on the micellization and aggregation behavior of amphiphilic block copolymers which is expected to differ from common surfactants as the solvophobic and solvophilic parts of the molecule are much larger and also can be varied to a much greater extent.

Compared to other methods, the advantage of FCS is the ability to detect a very low critical micelle concentration [158, 160–163] (CMC) and a very low critical aggregation concentration [158, 160, 161] (CAC) as they often appear in block copolymer solutions. This could for example be demonstrated by Colombani et al. who could access the CMC of a diblock copolymers by FCS, but only obtained an upper estimate analyzing the absorption band of pyrene which is very sensitive to local polarity of its surrounding [162].

The principle of CMC or CAC measurements, respectively, by FCS is as follows. At concentrations below the CMC/CAC, the probes diffuse freely in solution and, therefore, FCS curves can be fitted with one correlation time. Once micelles or aggregates form, a fraction of the fluorescence probes will be implemented into the assemblies, whereas the remaining probes remain in solution. The fraction of probes in the assemblies diffuses significantly slower than the free probes in solution and will result in a longer diffusion time. Thus, the unimer concentration at which a fraction with a longer diffusion time appears in the autocorrelation curve can be defined as the CMC or CAC, respectively. Experimentally, this could be demonstrated by Bonné et al. [161]. Using rhodamine 6G as a fluorescence probe, they found that with increasing concentration of an amphiphilic poly(2-alkyl-2-oxazoline) diblock copolymer in water a second correlation time appeared at the CMC. The fraction of this correlation time reflecting the incorporated probe gradually increased with increasing polymer concentration. The two correlation times, however, remained constant, indicating that only the number of micelles but not their size increased.

For a correct determination of CMC or CAC, it is essential to know the interactions of the probe with the micelles or aggregates, respectively. Binding of the dye to the micelles/aggregates is always a dynamic equilibrium process. If the time constants of the binding and unbinding process, however, are in a time range similar to the duration that a dye on average requires to diffuse through the confocal volume, a mixture of both diffusion times will be measured. For higher micelle concentrations, the periods of free diffusion become shorter. Thus, even though the size of the micelles stays constant, the average time it takes a fluorescent probe to diffuse through the confocal volume becomes longer and the (time-averaged) diffusion coefficient smaller. Thus, as shown in Fig. 12, the hydrodynamic radius

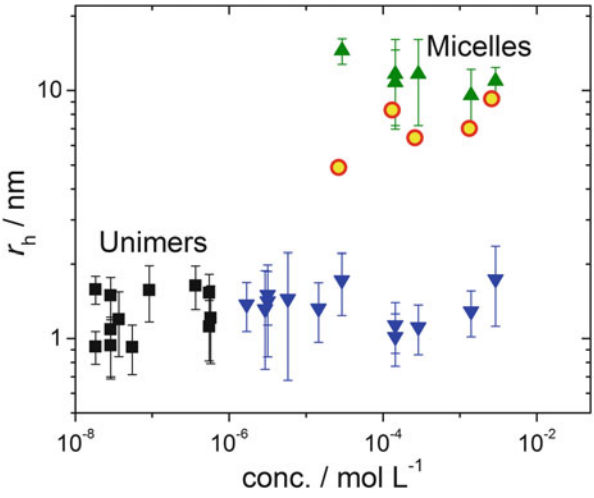

Fig. 12 (Apparent) hydrodynamic radii r_h as determined by FCS on P [(NOx)10(MOx)32] with different tracers. *Squares*: solutions containing only labeled copolymers. *Triangles*: solutions containing both fluorescence-labeled and non-labeled copolymers. *Circles*: solutions containing non-labeled polymers and Rh6G (adapted from Colloid and Polymer Sci. [161]. Copyright (2007) Springer)

seems to grow with increasing polymer concentration, and the magnitude of this effect will depend on the equilibrium constant of binding of the dye to the micelle. As a consequence, despite the fact that the addition of a small amount of a low molar mass dye to the polymer solutions is a straightforward way of studying the aggregation of amphiphilic copolymers by FCS, great care has to be taken that the dyes show significant binding to the micelles. Otherwise, a wrong dependence of the hydrodynamic radii on polymer concentration will be observed, i.e., a too small radius will be obtained at low polymer concentration [161]. A good example for a suitable dye–polymer combination is octadecyl rhodamine B (ORB) which was found to be a suitable dye for probing the micellization of PS-poly(methyl acrylate) (PMA) block copolymers [164]. In this block copolymer, the ORB binds strongly to the core-shell interface of the PS-PMA micelles with its nonpolar aliphatic tail buried in and partially adsorbed to the PS core. The triplet quantum yield of ORB is basically negligible and, therefore, the corresponding parameters do not have to be implemented in the model for fitting the correlation curve. Another advantageous property of ORB is its self-quenching in water, in which the probe molecules are only weakly soluble and, thus, form aggregates. These ORB molecules show only weak fluorescence and do not significantly contribute to the monitored FCS fluctuations, thus lowering the background. As a consequence, the FCS fluctuations originate mainly from the ORB molecules bound to the core-shell interface of the PS-PMA micelles, increasing the sensitivity of this method.

Circumvention of the abovementioned problem of a dynamic binding equilibrium is possible using probes covalently attached to the copolymers. Even though this requires an often elaborate covalent labeling of the polymeric amphiphile, the results are nonambiguous [161]. Figure 12 shows that only two hydrodynamic radii are obtained, one corresponding to the unimers and the other representing the micelles. The fraction of the unimers gradually decreases whereas the one of the

micelles increases due to the increase of the number of micelles and therefore the probability of finding a labeled unimer in the micelle.

Apart from the determination of the CMC, the average size of micelles and aggregates [158, 160–162] can be studied using FCS. Combining Eq. (3) and the Stokes–Einstein equation (5), the hydrodynamic radius can be calculated from the diffusion time, if the size w_{xy} of the confocal volume is known. This size can be obtained by a reference measurement of a dye with known diffusion coefficient. A common and reliable reference is Rh6G in water with a diffusion coefficient 4.14×10^{-10} m^2 s^{-1} [71]. However, as already mentioned above, it should be checked that the binding behavior of the probing dye does not bias the results. Otherwise the hydrodynamic radius of the micelles might be misinterpreted to increase, i.e., micelles seem to grow with increasing monomer concentrations.

FCS studies on micellization and aggregation of polyoxazolines, an interesting polymer class due to their biocompatibility, non-toxicity, and immuno-response [165], have also been reported. The polarity of these polyoxazolines can be well adjusted by appropriate substitution with different alkyl groups, also allowing to tune their micellization and aggregation properties. In addition, polyoxazolines exhibit a lower critical solution temperature (LCST) which can also be tuned by appropriate substitution of the polymer backbone. Bonné et al. performed FCS using polyoxazolines covalently labeled at the end of the hydrophobic poly(2-*n*-nonyl-2-oxazoline) block or the hydrophilic poly(2-methyl-2-oxazoline) block, respectively, and found that the position of the label did not significantly influence micellization [161].

Polyoxazolines also exhibit a thermoresponsive aggregation behavior around the cloud point which could be investigated using a combination of FCS with varying temperature from r.t. up to ca. 50 °C, turbidimetry, and small-angle neutron scattering [150]. Different combinations of iso-propyl-(^{i}PrOx), *n*-propyl-(^{n}PrOx) and *n*-nonyl-(NOx) substituted polyoxazolines were investigated. Thermoresponsive P(^{i}PrOx) and P(^{n}PrOx) homopolymers show a behavior similar to the one encountered with other thermoresponsive homopolymers, such as PNIPAM [166], with the cloud point significantly depending on concentration and on the degree of polymerization, decreasing with increasing concentration and increasing degree of polymerization. At room temperature, both homopolymers were dissolved as unimers. At the cloud point (above 40 °C for P(^{i}PrOx) and 24–38 °C for P(^{n}PrOx)) the polymer chains collapsed and formed large aggregates (Fig. 13a). This aggregation process was fully reversible for P(^{i}PrOx) whereas the aggregates of P(^{n}PrOx) could not be fully dissolved upon cooling, presumably due to crystallization of the *n*-propyl side chains. The aggregation of the copolymers with a P^{i}PrOx and a P^{n}PrOx block was dominated by the behavior of P^{n}PrOx, the block with the lower cloud point. In this mixture, aggregates formed directly (Fig. 13b) at the cloud point of P^{n}PrOx. In gradient copolymers with, on average, 2 or 4 out of 50 iso-propyl side groups replaced by the very hydrophobic *n*-nonyl side group, a complex aggregation behavior was obtained due to the interplay between intra- and intermolecular association mediated by the hydrophobic ^{n}PrOx side chains. Already below the cloud point, aggregates formed due to the strong interaction of

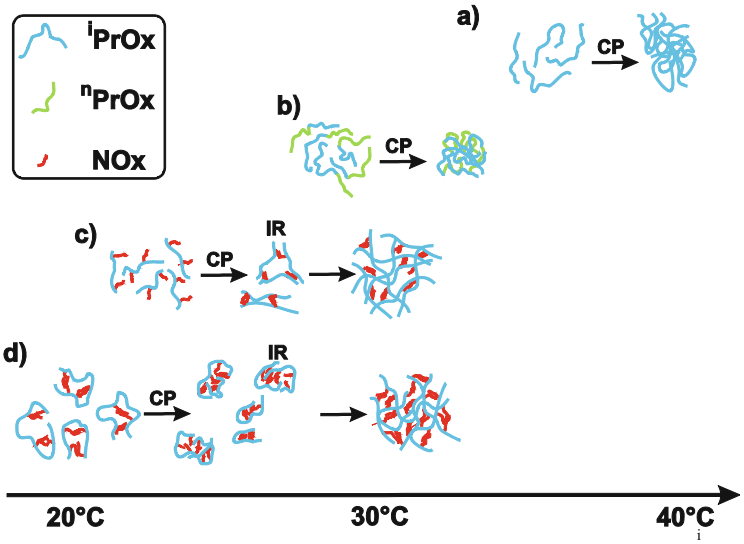

Fig. 13 Temperature-dependent aggregation behavior of (**a**) P(^{i}PrOx) homopolymers, (**b**) P(^{i}PrOx$_{25}$-b-^{n}PrOx$_{25}$) diblock copolymers, (**c**) P[^{i}PrOx$_{48}$NOx$_{2}$]$_{grad}$, and (**d**) P[^{i}PrOx$_{46}$NOx$_{4}$]$_{grad}$ gradient copolymers. The *different colors* indicate the different monomer types. CP stands for cloud point and IR for the intermediate regime (adapted from Colloid and Polymer Sci [150] Copyright (2012) Springer)

the strongly hydrophobic *n*-nonyl side groups (Fig. 13c, d). This effect was more pronounced for the gradient copolymers with a higher number of *n*-nonyl side groups. The hydrophobic interaction of these groups also shifts the collapse resulting in large aggregates to a few Kelvin above the cloud point. These aggregates, however, could not be detected with FCS, because sedimentation occurred due to their large size.

FCS is not only restricted to assembly studies of block copolymers and homopolymers, but also more complex aggregation systems can be analyzed. As an example, Štěpánek et al. investigated the solution behavior and self-assembly of a heteroarm star copolymer consisting of ca. 20 short PS and 20 long P2VP arms [167].

14 Comparison of FCS with Other Methods

Some observables that can be measured with FCS are in principle also accessible by other techniques. Thus, it is important to know the strengths and weaknesses of these methods with respect to FCS.

Dynamic light scattering (DLS, also known as photon correlation spectroscopy), for example, is an often used method to investigate the dynamics of particles,

micelles, and aggregates. The advantage of FCS, however, is the tiny amount of fluorescence probes required, which is approx. 3 orders of magnitude lower than the particle concentration in DLS [168]. Such small concentrations are of particular advantage for probing low micelle and aggregate concentrations. FCS also allows for the simultaneous detection of free dye, micelles, and large aggregates which is more difficult in DLS due to the fact that the scattered intensity is proportional to the particle mass and concentration [167]. Therefore, also small aggregates can be detected in the presence of large aggregates [160]. This advantage, however, disappears if the fluorescence signal is proportional to the particle or aggregate size, i.e., if a non-negligible amount of monomers or unimers are labeled. For polydisperse particles, micelles, or aggregates, it is important to keep in mind that FCS measures number-averaged molar masses (M_n) whereas weight-averaged molar masses (M_w) are obtained during DLS measurements [164].

Quasielastic neutron scattering (QENS) can detect diffusional processes at sub-nanometer length scales and with temporal resolution in picosecond time range [169]. In contrast to optical techniques, clearly higher spatial accuracy, however, comes along with a high technical demand, i.e., the necessity of a neutron source together with all its costs and security requirements. In addition, neutron scattering cross sections are ca. 10^9 times smaller than the absorption cross section of good fluorophores, resulting in long measuring times of hours. These long measuring times prohibit the scanning of many different sample areas and, thus, limit the imaging possibilities of QENS.

Combinations of FCS with DLS [158, 160, 163, 164], neutron scattering [150], or the application of all three techniques [170] to maximize the information about polymer systems have been successful.

15 FCS and Simulations

The combination of FCS with simulations in order to support the conclusions drawn from measurements bears a huge potential to gain a deeper understanding of dynamics in polymer systems. So far, only few such combined studies have been performed as discussed in a recent perspective article [171]. In contrast to measurements, different parameters can be well controlled and varied in simulations and interactions can be switched on and off. The comparison of the autocorrelation functions obtained from simulations under different assumptions with the measured FCS autocorrelation curves can subsequently point out the most appropriate model to describe polymer dynamics in different systems. One of the big challenges for FCS simulations is the large range of timescales which has to be accessed, typically from microseconds to seconds. The continuing development of computer technology helps to increase the time span and the number of particles which can be simulated with reasonable computational resources (CPU or GPU time, respectively). Yet, in order to cover the most interesting time range, even with the most powerful computational units the detailed level of the simulations has to be

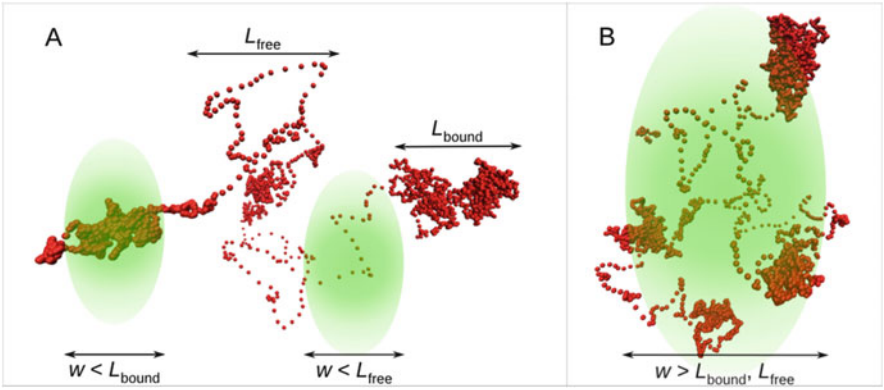

Fig. 14 Simulation of the trajectory of a tracer which can reversibly bind to polymer in a dilute polymer solution. When bound, the diffusion is strongly hindered whereas free diffusion is assumed in the non-bound periods. Panel (**a**) shows the case when the two length scales of the volumes with bound and unbound tracer are greater than the focal spot dimension, *w*, while panel (**b**) shows the opposite situation. In case (**a**), two distinct diffusion processes are resolved by FCS. In case (**b**), a single average process is observed. (adapted from Physical Review Letters [46] Copyright (2013) American Physical Society)

considerably reduced (coarse-graining) [172]. Such a simplification, however, can also bias the results calculated from the simulated data, and it is essential to carefully cross-check that the interpretations do not go beyond the approximations of the underlying model.

Concerning FCS, the most interesting observables from the simulations are the trajectories of single diffusion molecules or particles, respectively. From these trajectories, the mean square displacements and the autocorrelation functions can be calculated. This way, it can be analyzed how heterogeneity expresses itself in the FCS results, i.e., how anomalous diffusion is averaged over the relevant FCS time and length scales. Also, the question how interactions between dye and polymer chains influence FCS results has been recently addressed using a combination of FCS experiments with simulations [46] (Fig. 14).

16 Conclusion and Outlook

FCS has proven to be a suitable method for the investigation of dynamics in polymer systems. One of the main advantages consists in the high sensitivity of fluorescence detection, the potential to probe dynamics on a broad range of time-scales, and the possibility to measure in situ. Further development might focus on variation of local detection and, therefore, some kind of FCS imaging which allows to probe dynamics in different sample areas, e.g., inside and outside of gel and in the vicinity of gel surface. Also, improved labeling strategies and novel functional dyes are needed for example for a distinction of probes in areas of different polarity

or different local mobility. The limits of FCS are often set by the investigated systems which apart from bearing fluorescence impurities might scatter or refract light in an uncontrolled way at refractive index changes and therefore distort the confocal volume. The time resolution of scanning FCS approaches is limited by the period of time required to get sufficient photon counts in order to obtain reliable correlation functions. Despite these challenges, FCS has already contributed significantly to gain a deeper understanding of polymer physics. As shown in this book chapter, the studies so far focused mainly on diffusion of differently sized molecular and macromolecular probes in polymer solutions, classical and responsive polymer gels, polymer melts, glasses, and micellization, and aggregation systems. Combination of FCS with other experimental techniques or with simulations and theory will in future contribute to the establishment of FCS as a standard method to study polymer systems.

Acknowledgments The author acknowledges the support from the RWTH Aachen University and from the Zukunftskolleg, the Center of Applied Photonics, and the Graduate School of Chemical Biology at the University of Konstanz.

References

1. Wöll D (2014) Fluorescence correlation spectroscopy in polymer science. RSC Adv 4:2447–2465
2. Magde D, Webb WW, Elson E (1972) Thermodynamic fluctuations in a reacting system—Measurement by fluorescence correlation spectroscopy. Phys Rev Lett 29(11):705–708
3. Elson EL, Magde D (1974) Fluorescence correlation spectroscopy. 1. Conceptual basis and theory. Biopolymers 13(1):1–27
4. Magde D, Elson EL, Webb WW (1974) Fluorescence correlation spectroscopy. 2. Experimental realization. Biopolymers 13(1):29–61
5. Magde D, Webb WW, Elson EL (1978) Fluorescence correlation spectroscopy. 3. Uniform translation and laminar-flow. Biopolymers 17(2):361–376
6. Elson EL (2011) Fluorescence correlation spectroscopy: past, present, future. Biophys J 101 (12):2855–2870
7. Haustein E, Schwille P (2007) Fluorescence correlation spectroscopy: novel variations of an established technique. Annu Rev Biophys Biomol Struct 36:151–169
8. Krichevsky O, Bonnet G (2002) Fluorescence correlation spectroscopy: the technique and its applications. Rep Prog Phys 65:251–297
9. Rigler R, Elson EL (eds) (2001) Fluorescence correlation spectroscopy. Theory and applications. Springer, Berlin, Heidelberg, New York
10. Schwille P (2001) Fluorescence correlation spectroscopy and its potential for intracellular applications. Cell Biochem Biophys 34:383–408
11. Rigler R, Mets Ü, Widengren J, Kask P (1993) Fluorescence correlation spectroscopy with high count rate and low-background—analysis of translational diffusion. Eur Biophys J 22 (3):169–175
12. Widengren J, Mets Ü, Rigler R (1995) Fluorescence correlation spectroscopy of triplet-states in solution—a theoretical and experimental-study. J Phys Chem 99(36):13368–13379
13. Widengren J, Schwille P (2000) Characterization of photoinduced isomerization and back-isomerization of the cyanine dye Cy5 by fluorescence correlation spectroscopy. J Phys Chem A 104(27):6416–6428

14. Kask P, Piksarv P, Mets Ü (1985) Fluorescence correlation spectroscopy in the nanosecond time range: photon antibunching in dye fluorescence. Eur Biophys J 12:163–166
15. Sauer M, Hofkens J, Enderlein J (2011) Handbook of fluorescence spectroscopy and imaging—from single molecules to ensembles. Wiley-VCH, Weinheim
16. Laurence TA, Ly S, Bourguet F, Fischer NO, Coleman MA (2014) Fluorescence correlation spectroscopy at micromolar concentrations without optical nanoconfinement. J Phys Chem B 118(32):9662–9667
17. Müller CB, Loman A, Pacheco V, Koberling F, Willbold D, Richtering W, Enderlein J (2008) Precise measurement of diffusion by multi-color dual-focus fluorescence correlation spectroscopy. EPL 83(4):46001
18. Starchev K, Zhang J, Buffle J (1998) Applications of fluorescence correlation spectroscopy—particle size effect. J Colloid Interface Sci 203(1):189–196
19. Tcherniak A, Reznik C, Link S, Landes CF (2009) Fluorescence correlation spectroscopy: criteria for analysis in complex systems. Anal Chem 81:746–754
20. Sengupta P, Garai K, Balaji J, Periasamy N, Maiti S (2003) Measuring size distribution in highly heterogeneous systems with fluorescence correlation spectroscopy. Biophys J 84 (3):1977–1984
21. Donsmark J, Rischel C (2007) Fluorescence correlation spectroscopy at the oil – water interface: hard disk diffusion behavior in dilute β-lactoglobulin layers precedes monolayer formation. Langmuir 23(12):6614–6623
22. Shusterman R, Gavrinyov T, Krichevsky O (2008) Internal dynamics of superhelical DNA. Phys Rev Lett 100(9):098102
23. Winkler RG, Keller S, Rädler JO (2006) Intramolecular dynamics of linear macromolecules by fluorescence correlation spectroscopy. Phys Rev E 73(4):041919
24. Zettl U, Hoffmann ST, Koberling F, Krausch G, Enderlein J, Harnau L, Ballauff M (2009) Self-diffusion and cooperative diffusion in semidilute polymer solutions as measured by fluorescence correlation spectroscopy. Macromolecules 42(24):9537–9547
25. Banks DS, Fradin C (2005) Anomalous diffusion of proteins due to molecular crowding. Biophys J 89(5):2960–2971
26. Cherdhirankorn T, Floudas G, Butt H-J, Koynov K (2009) Effects of chain topology on the tracer diffusion in star polyisoprenes. Macromolecules 42:9183–9189
27. Masuda A, Ushida K, Okamoto T (2005) Direct observation of spatiotemporal dependence of anomalous diffusion in inhomogeneous fluid by sampling-volume-controlled fluorescence correlation spectroscopy. Phys Rev E 72(6):060101
28. Reitan NK, Juthajan A, Lindmo T, de Lange Davies C (2008) Macromolecular diffusion in the extracellular matrix measured by fluorescence correlation spectroscopy. J Biomed Opt 13 (5):054040–054040
29. Wachsmuth M, Waldeck W, Langowski J (2000) Anomalous diffusion of fluorescent probes inside living cell nuclei investigated by spatially-resolved fluorescence correlation spectroscopy. J Mol Biol 298(4):677–689
30. Weiss M, Elsner M, Kartberg F, Nilsson T (2004) Anomalous subdiffusion is a measure for cytoplasmic crowding in living cells. Biophys J 87(5):3518–3524
31. Saxton MJ (1995) Single-particle tracking: effects of corrals. Biophys J 69(2):389–398
32. Fatin-Rouge N, Starchev K, Buffle J (2004) Size effects on diffusion processes within agarose gels. Biophys J 86(5):2710–2719
33. Weiss M, Hashimoto H, Nilsson T (2003) Anomalous protein diffusion in living cells as seen by fluorescence correlation spectroscopy. Biophys J 84(6):4043–4052
34. Bernheim-Groswasser A, Shusterman R, Krichevsky O (2006) Fluorescence correlation spectroscopy analysis of segmental dynamics in actin filaments. J Chem Phys 125(8):084903
35. Kalkbrenner T, Arnold A, Tans SJ (2009) Internal dynamics of supercoiled DNA molecules. Biophys J 96(12):4951–4955
36. Petrov EP, Ohrt T, Winkler RG, Schwille P (2006) Diffusion and segmental dynamics of double-stranded DNA. Phys Rev Lett 97(25):258101

37. Shusterman R, Alon S, Gavrinyov T, Krichevsky O (2004) Monomer dynamics in double- and single-stranded DNA polymers. Phys Rev Lett 92(4):048303
38. Sokolov IM (2012) Models of anomalous diffusion in crowded environments. Soft Matter 8 (35):9043–9052
39. Ernst D, Köhler J, Weiss M (2014) Probing the type of anomalous diffusion with single-particle tracking. Phys Chem Chem Phys 16:7686–7691
40. Höfling F, Bamberg KU, Franosch T (2011) Anomalous transport resolved in space and time by fluorescence correlation spectroscopy. Soft Matter 7(4):1358–1363
41. Masuda A, Ushida K, Okamoto T (2005) New fluorescence correlation spectroscopy enabling direct observation of spatiotemporal dependence of diffusion constants as an evidence of anomalous transport in extracellular matrices. Biophys J 88(5):3584–3591
42. Masuda A, Ushida K, Okamoto T (2006) New fluorescence correlation spectroscopy (FCS) suitable for the observation of anomalous diffusion in polymer solution: time and space dependences of diffusion coefficients. J Photochem Photobiol A 183(3):304–308
43. Enderlein J, Gregor I, Patra D, Dertinger T, Kaupp UB (2005) Performance of fluorescence correlation spectroscopy for measuring diffusion and concentration. ChemPhysChem 6:2324–2336
44. Piskorz TK, Ochab-Marcinek A (2014) A universal model of restricted diffusion for fluorescence correlation spectroscopy. J Phys Chem B 118(18):4906–4912
45. Košovan P, Uhlík F, Kuldová J, Štěpánek M, Limpouchová Z, Procházka K, Benda A, Humpolíčková J, Hof M (2011) Monte Carlo simulation of fluorescence correlation spectroscopy data. Collect Czechoslov Chem Commun 76(3):207–222
46. Vagias A, Raccis R, Koynov K, Jonas U, Butt H-J, Fytas G, Košovan P, Lenz O, Holm C (2013) Complex tracer diffusion dynamics in polymer solutions. Phys Rev Lett 111 (8):088301
47. Hanbury Brown R, Twiss RQ (1956) Correlation between photons in 2 coherent beams of light. Nature 177(4497):27–29
48. Felekyan S, Kühnemuth R, Kudryavtsev V, Sandhagen C, Becker W, Seidel CAM (2005) Full correlation from picoseconds to seconds by time-resolved and time-correlated single photon detection. Rev Sci Instrum 76(8):083104
49. Wahl M, Rahn H-J, Gregor I, Erdmann R, Enderlein J (2007) Dead-time optimized time-correlated photon counting instrument with synchronized, independent timing channels. Rev Sci Instrum 78:033106
50. Widengren J, Mets Ü, Rigler R (1999) Photodynamic properties of green fluorescent proteins investigated by fluorescence correlation spectroscopy. Chem Phys 250(2):171–186
51. Ehrenberg M, Rigler R (1974) Rotational Brownian-motion and fluorescence intensity fluctuations. Chem Phys 4(3):390–401
52. Aragón SR, Pecora R (1975) Fluorescence correlation spectroscopy and Brownian rotational diffusion. Biopolymers 14(1):119–137
53. Aragón SR, Pecora R (1976) Fluorescence correlation spectroscopy as a probe of molecular-dynamics. J Chem Phys 64(4):1791–1803
54. Dorfschmid M, Müllen K, Zumbusch A, Wöll D (2010) Translational and rotational diffusion during radical bulk polymerization: a comparative investigation by full correlation fluorescence correlation spectroscopy (fcFCS). Macromolecules 43:6174–6179
55. Loman A, Gregor I, Stutz C, Mund M, Enderlein J (2010) Measuring rotational diffusion of macromolecules by fluorescence correlation spectroscopy. Photochem Photobiol Sci 2010 (9):627–636
56. Pieper CM, Enderlein J (2011) Fluorescence correlation spectroscopy as a tool for measuring the rotational diffusion of macromolecules. Chem Phys Lett 516(1-3):1–11
57. Berland KM, So PT, Gratton E (1995) Two-photon fluorescence correlation spectroscopy: method and application to the intracellular environment. Biophys J 68(2):694–701
58. Grabowski C, Mukhopadhyay A (2008) Diffusion of polystyrene chains and fluorescent dye molecules in semidilute and concentrated polymer solutions. Macromolecules 41:6191–6194

59. Schwille P, Haupts U, Maiti S, Webb WW (1999) Molecular dynamics in living cells observed by fluorescence correlation spectroscopy with one- and two-photon excitation. Biophys J 77(4):2251–2265
60. Sukhishvili SA, Chen Y, Müller JD, Gratton E, Schweizer KS, Granick S (2002) Surface diffusion of poly(ethylene glycol). Macromolecules 35(5):1776–1784
61. Zhao JJ, Bae SC, Xie F, Granick S (2001) Diffusion of polymer-coated nanoparticles studied by fluorescence correlation spectroscopy. Macromolecules 34(10):3123–3126
62. Dittrich PS, Schwille P (2002) Spatial two-photon fluorescence cross-correlation spectroscopy for controlling molecular transport in microfluidic structures. Anal Chem 74 (17):4472–4479
63. Schwille P, Meyer-Almes FJ, Rigler R (1997) Dual-color fluorescence cross-correlation spectroscopy for multicomponent diffusional analysis in solution. Biophys J 72 (4):1878–1886
64. Kügel W, Muschielok A, Michaelis J (2012) Bayesian-inference-based fluorescence correlation spectroscopy and single-molecule burst analysis reveal the influence of dye selection on DNA hairpin dynamics. ChemPhysChem 13(4):1013–1022
65. Ridgeway WK, Millar DP, Williamson JR (2012) The spectroscopic basis of fluorescence triple correlation spectroscopy. J Phys Chem B 116(6):1908–1919
66. Felekyan S, Kalinin S, Sanabria H, Valeri A, Seidel CA (2012) Filtered FCS: species auto- and cross-correlation functions highlight binding and dynamics in biomolecules. ChemPhysChem 13(4):1036–1053
67. Kühnemuth R, Seidel CAM (2001) Principles of single molecule multiparameter fluorescence spectroscopy. Single Mol 2(4):251–254
68. Dertinger T, Pacheco V, von der Hocht I, Hartmann R, Gregor I, Enderlein J (2007) Two-focus fluorescence correlation spectroscopy: a new tool for accurate and absolute diffusion measurements. ChemPhysChem 8(3):433–443
69. Müller CB, Weiss K, Loman A, Enderlein J, Richtering W (2009) Remote temperature measurements in femto-liter volumes using dual-focus-fluorescence correlation spectroscopy. Lab Chip 9(9):1248–1253
70. Pal N, Verma SD, Singh MK, Sen S (2011) Fluorescence correlation spectroscopy: an efficient tool for measuring size, size-distribution and polydispersity of microemulsion droplets in solution. Anal Chem 83(20):7736–7744
71. Dertinger T, Loman A, Ewers B, Müller CB, Kramer B, Enderlein J (2008) The optics and performance of dual-focus fluorescence correlation spectroscopy. Opt Express 16 (19):14353–14368
72. Müller CB, Eckert T, Loman A, Enderlein J, Richtering W (2009) Dual-focus fluorescence correlation spectroscopy: a robust tool for studying molecular crowding. Soft Matter 5 (7):1358–1366
73. Müller CB, Loman A, Richtering W, Enderlein J (2008) Dual-focus fluorescence correlation spectroscopy of colloidal solutions: Influence of particle size. J Phys Chem B 112 (28):8236–8240
74. Ivanov D, Shcheslavskiy V, Marki I, Leutenegger M, Lasser T (2009) High volume confinement in two-photon total-internal-reflection fluorescence correlation spectroscopy. Appl Phys Lett 94(8):083902–083903
75. Thompson NL, Burghardt TP, Axelrod D (1981) Measuring surface dynamics of biomolecules by total internal reflection fluorescence with photobleaching recovery or correlation spectroscopy. Biophys J 33(3):435–454
76. Thompson NL, Wang X, Navaratnarajah P (2009) Total internal reflection with fluorescence correlation spectroscopy: Applications to substrate-supported planar membranes. J Struct Biol 168(1):95–106
77. Yordanov S, Best A, Butt H-J, Koynov K (2009) Direct studies of liquid flows near solid surfaces by total internal reflection fluorescence cross-correlation spectroscopy. Opt Express 17(23):21149–21158

78. Yordanov S, Best A, Weisshart K, Koynov K (2011) An easy way to enable total internal reflection-fluorescence correlation spectroscopy (TIR-FCS) by combining commercial devices for FCS and TIR microscopy. Rev Sci Instrum 82:036105
79. Hell SW (2007) Far-field optical nanoscopy. Science 316(5828):1153–1158
80. Fürstenberg A, Heilemann M (2013) Single-molecule localization microscopy—near-molecular spatial resolution in light microscopy with photoswitchable fluorophores. Phys Chem Chem Phys 15(36):14919–14930
81. Eggeling C, Ringemann C, Medda R, Schwarzmann G, Sandhoff K, Polyakova S, Belov VN, Hein B, von Middendorff C, Schönle A, Hell SW (2009) Direct observation of the nanoscale dynamics of membrane lipids in a living cell. Nature 457(7233):1159–1162
82. Kastrup L, Blom H, Eggeling C, Hell SW (2005) Fluorescence fluctuation spectroscopy in subdiffraction focal volumes. Phys Rev Lett 94(17):178104
83. Mueller V, Honigmann A, Ringemann C, Medda R, Schwarzmann G, Eggeling C (2013) Chapter One - FCS in STED microscopy: studying the nanoscale of lipid membrane dynamics. In: Sergey YT (ed) Methods in enzymology, vol 519. Academic Press, New York, pp 1–38
84. King JT, Yu C, Wilson WL, Granick S (2014) Super-resolution study of polymer mobility fluctuations near c*. ACS Nano 8(9):8802–8809
85. Leutenegger M, Ringemann C, Lasser T, Hell SW, Eggeling C (2012) Fluorescence correlation spectroscopy with a total internal reflection fluorescence STED microscope (TIRF-STED-FCS). Opt Express 20(5):5243–5263
86. Müller CB, Richtering W (2008) Sealed and temperature-controlled sample cell for inverted and confocal microscopes and fluorescence correlation spectroscopy. Colloid Polym Sci 286 (11):1215–1222
87. Flier BMI, Baier MC, Huber J, Müllen K, Mecking S, Zumbusch A, Wöll D (2012) Heterogeneous diffusion in thin polymer films as observed by high-temperature single-molecule fluorescence microscopy. J Am Chem Soc 134(1):480–488
88. Hess ST, Webb WW (2002) Focal volume optics and experimental artifacts in confocal fluorescence correlation spectroscopy. Biophys J 83(4):2300–2317
89. Enderlein J, Gregor I, Patra D, Fitter J (2004) Art and artefacts of fluorescence correlation spectroscopy. Curr Pharm Biotechnol 5(2):155–161
90. Zettl H, Häfner W, Böker A, Schmalz H, Lanzendorfer M, Müller AHE, Krausch G (2004) Fluorescence correlation spectroscopy of single dye-labeled polymers in organic solvents. Macromolecules 37(5):1917–1920
91. Zettl H, Zettl U, Krausch G, Enderlein J, Ballauff M (2007) Direct observation of single molecule mobility in semidilute polymer solutions. Phys Rev E 75(6):061804
92. Koynov K, Mihov G, Mondeshki M, Moon C, Spiess HW, Müllen K, Butt HJ, Floudas G (2007) Diffusion and conformation of peptide-functionalized polyphenylene dendrimers studied by fluorescence correlation and 13C NMR spectroscopy. Biomacromolecules 8 (5):1745–1750
93. Wang W, Zhang C, Wang S, Zhao J (2007) Diffusion of single polyelectrolytes on the surface of poly(N-isopropylacrylamide) brushes. Macromolecules 40(26):9564–9569
94. Liu RG, Gao X, Adams J, Oppermann W (2005) A fluorescence correlation spectroscopy study on the self-diffusion of polystyrene chains in dilute and semidilute solution. Macromolecules 38(21):8845–8849
95. Enderlein J (2012) Polymer dynamics, fluorescence correlation spectroscopy, and the limits of optical resolution. Phys Rev Lett 108(10):108101
96. Krichevsky O (2013) Comment on "Polymer dynamics, fluorescence correlation spectroscopy, and the limits of optical resolution". Phys Rev Lett 110(15):159801
97. Davis LM, Shen G (2006) Accounting for triplet and saturation effects in FCS measurements. Curr Pharm Biotechnol 7(4):287–301
98. Widengren J, Rigler R, Mets Ü (1994) Triplet-state monitoring by fluorescence correlation spectroscopy. J Fluoresc 4(3):255–258

99. Won J, Onyenemezu C, Miller WG, Lodge TP (1994) Diffusion of spheres in entangled polymer solutions: a return to stokes-einstein behavior. Macromolecules 27(25):7389–7396
100. Ye X, Tong P, Fetters LJ (1998) Transport of probe particles in semidilute polymer solutions. Macromolecules 31(17):5785–5793
101. Dixon PK, Nagel SR, Weitz DA (1991) The length scale dependence of viscosity approaching the glass transition in glycerol. J Chem Phys 94(10):6924–6925
102. Kiyachenko YF, Litvinov YI (1985) Increase in scale length in a liquid as the glass transition temperature is approached. JETP Lett 42(5):266–269
103. Brochard Wyart F, De Gennes PG (2000) Viscosity at small scales in polymer melts. Eur Phys J E 1:93–97
104. Yamamoto U, Schweizer KS (2011) Theory of nanoparticle diffusion in unentangled and entangled polymer melts. J Chem Phys 135(22). doi:10.1063/1.3664863
105. Grabowski CA, Mukhopadhyay A (2014) Size effect of nanoparticle diffusion in a polymer melt. Macromolecules 47(20):7238–7242
106. Hołyst R, Bielejewska A, Szymanski J, Wilk A, Patkowski A, Gapinski J, Zywocinski A, Kalwarczyk T, Kalwarczyk E, Tabaka M, Ziebacz N, Wieczorek SA (2009) Scaling form of viscosity at all length-scales in poly(ethylene glycol) solutions studied by fluorescence correlation spectroscopy and capillary electrophoresis. Phys Chem Chem Phys 11 (40):9025–9032
107. Michelman-Ribeiro A, Horkay F, Nossal R, Boukari H (2007) Probe diffusion in aqueous poly(vinyl alcohol) solutions studied by fluorescence correlation spectroscopy. Biomacromolecules 8(5):1595–1600
108. Wiśniewska A, Sozański K, Kalwarczyk T, Kędra-Królik K, Pieper C, Wieczorek SA, Jakieła S, Enderlein J, Hołyst R (2014) Scaling of activation energy for macroscopic flow in poly(ethylene glycol) solutions: entangled—non-entangled crossover. Polymer 55 (18):4651–4657
109. Cherdhirankorn T, Best A, Koynov K, Peneva K, Müllen K, Fytas G (2009) Diffusion in polymer solutions studied by fluorescence correlation spectroscopy. J Phys Chem B 113:3355–3359
110. Omari RA, Aneese AM, Grabowski CA, Mukhopadhyay A (2009) Diffusion of nanoparticles in semidilute and entangled polymer solutions. J Phys Chem B 113(25):8449–8452
111. Best A, Pakula T, Fytas G (2005) Segmental dynamics of bulk polymers studied by fluorescence correlation spectroscopy. Macromolecules 38(10):4539–4541
112. Cherdhirankorn T, Harmandaris V, Juhari A, Voudouris P, Fytas G, Kremer K, Koynov K (2009) Fluorescence correlation spectroscopy study of molecular probe diffusion in polymer melts. Macromolecules 42(13):4858–4866
113. Doroshenko M, Gonzales M, Best A, Butt H-J, Koynov K, Floudas G (2012) Monitoring the dynamics of phase separation in a polymer blend by confocal imaging and fluorescence correlation spectroscopy. Macromol Rapid Commun 33(18):1568–1573
114. Kirkwood JG, Riseman J (1948) The intrinsic viscosities and diffusion constants of flexible macromolecules in solution. J Chem Phys 16(6):565–573
115. de Gennes P-G (1979) Scaling concepts in polymer physics. Cornell University Press, London
116. Rubinstein M, Colby RH (2003) Polymer physics. Oxford University Press, Oxford
117. Hess W (1986) Self-diffusion and reptation in semidilute polymer solutions. Macromolecules 19(5):1395–1404
118. Doi M, Edwards DA (1986) The theory of polymer dynamics. Oxford University Press, New York
119. Vrentas JS, Duda JL (1977) Diffusion in polymer-solvent systems. 2. Predictive theory for dependence of diffusion-coefficients on temperature, concentration, and molecular-weight. J Polym Sci B 15(3):417–439

120. Wöll D, Kölbl C, Stempfle B, Karrenbauer A (2013) Novel method for automatic single molecule tracking of blinking molecules at low intensities. Phys Chem Chem Phys 15:6196–6205
121. Orrit M (2013) Towards a molecular view of glass heterogeneity. Angew Chem Int Ed 52 (1):163–166
122. Joly L, Ybert C, Bocquet L (2006) Probing the nanohydrodynamics at liquid-solid interfaces using thermal motion. Phys Rev Lett 96(4):046101
123. Rathgeber S, Beauvisage HJ, Chevreau H, Willenbacher N, Oelschlaeger C (2009) Microrheology with fluorescence correlation spectroscopy. Langmuir 25(11):6368–6376
124. Solomon MJ, Lu Q (2001) Rheology and dynamics of particles in viscoelastic media. Curr Opin Colloid Interface Sci 6(5-6):430–437
125. Modesti G, Zimmermann B, Börsch M, Herrmann A, Saalwächter K (2009) Diffusion in model networks as studied by NMR and fluorescence correlation spectroscopy. Macromolecules 42(13):4681–4689
126. Raccis R, Roskamp R, Hopp I, Menges B, Koynov K, Jonas U, Knoll W, Butt HJ, Fytas G (2011) Probing mobility and structural inhomogeneities in grafted hydrogel films by fluorescence correlation spectroscopy. Soft Matter 7(15):7042–7053
127. Michelman-Ribeiro A, Boukari H, Nossal R, Horkay F (2004) Structural changes in polymer gels probed by fluorescence correlation spectroscopy. Macromolecules 37(26):10212–10214
128. Wöll D, Uji-i H, Schnitzler T, Hotta J, Dedecker P, Herrmann A, De Schryver FC, Müllen K, Hofkens J (2008) Radical polymerization tracked by single molecule spectroscopy. Angew Chem Int Ed 47:783–787
129. Stempfle B, Dill M, Winterhalder M, Müllen K, Wöll D (2012) Single molecule diffusion and its heterogeneity during the bulk radical polymerization of styrene and methyl methacrylate. Polym Chem 3:2456–2463
130. Zustiak SP, Boukari H, Leach JB (2010) Solute diffusion and interactions in cross-linked poly (ethylene glycol) hydrogels studied by fluorescence correlation spectroscopy. Soft Matter 6 (15):3609–3618
131. Dell ZE, Schweizer KS (2014) Theory of localization and activated hopping of nanoparticles in cross-linked networks and entangled polymer melts. Macromolecules 47(1):405–414
132. Zhang R, Cherdhirankorn T, Graf K, Koynov K, Berger R (2008) Swelling of cross-linked polystyrene beads in toluene. Microelectron Eng 85(5–6):1261–1264
133. Pristinski D, Kozlovskaya V, Sukhishvili SA (2005) Fluorescence correlation spectroscopy studies of diffusion of a weak polyelectrolyte in aqueous solutions. J Chem Phys 122 (1):014907
134. van Rompaey E, Engelborghs Y, Sanders N, De Smedt C, Demeester J (2001) Interactions between oligonucleotides and cationic polymers investigated by fluorescence correlation spectroscopy. Pharm Res 18(7):928–936
135. Jia P, Yang Q, Gong Y, Zhao J (2012) Dynamic exchange of counterions of polystyrene sulfonate. J Chem Phys 136(8):084904
136. Kim B-S, Lebedeva OV, Koynov K, Gong H, Glasser G, Lieberwith I, Vinogradova OI (2005) Effect of organic solvent on the permeability and stiffness of polyelectrolyte multilayer microcapsules. Macromolecules 38(12):5214–5222
137. Wong JE, Müller CB, Laschewsky A, Richtering W (2007) Direct evidence of layer-by-layer assembly of polyelectrolyte multilayers on soft and porous temperature-sensitive PNiPAM microgel using fluorescence correlation spectroscopy. J Phys Chem B 111(29):8527–8531
138. Gianneli M, Beines PW, Roskamp RF, Koynov K, Fytas G, Knoll W (2007) Local and global dynamics of transient polymer networks and swollen gels anchored on solid surfaces. J Phys Chem C 111(35):13205–13211
139. Haraguchi K, Takehisa T (2002) Nanocomposite hydrogels: a unique organic–inorganic network structure with extraordinary mechanical, optical, and swelling/de-swelling properties. Adv Mater 14(16):1120–1124

140. Ferse B, Richter S, Eckert F, Kulkarni A, Papadakis CM, Arndt KF (2008) Gelation mechanism of poly(N-isopropylacrylamide)-clay nanocomposite hydrogels synthesized by photopolymerization. Langmuir 24(21):12627–12635
141. Stempfle B, Große A, Ferse B, Arndt K-F, Wöll D (2014) Anomalous diffusion in thermoresponsive polymer-clay composite hydrogels probed by widefield fluorescence microscopy. Langmuir. doi:10.1021/la503571j
142. Hink MA, Griep RA, Borst JW, van Hoek A, Eppink MHM, Schots A, Visser AJWG (2000) Structural dynamics of green fluorescent protein alone and fused with a single chain Fv protein. J Biol Chem 275(23):17556–17560
143. Lehmann S, Seiffert S, Richtering W (2012) Spatially resolved tracer diffusion in complex responsive hydrogels. J Am Chem Soc 134:15963–15969
144. Ebeling B, Eggers S, Hendrich M, Nitschke A, Vana P (2014) Flipping the pressure- and temperature-dependent cloud-point behavior in the cononsolvency system of poly (N-isopropylacrylamide) in water and ethanol. Macromolecules 47(4):1462–1469
145. Hofmann CH, Plamper FA, Scherzinger C, Hietala S, Richtering W (2013) Cononsolvency revisited: solvent entrapment by N-Isopropylacrylamide and N N-diethylacrylamide microgels in different water/methanol mixtures. Macromolecules 46(2):523–532
146. Kyriakos K, Philipp M, Adelsberger J, Jaksch S, Berezkin AV, Lugo DM, Richtering W, Grillo I, Miasnikova A, Laschewsky A, Müller-Buschbaum P, Papadakis CM (2014) Cononsolvency of water/methanol mixtures for PNIPAM and PS-b-PNIPAM: pathway of aggregate formation investigated using time-resolved SANS. Macromolecules 47 (19):6867–6879
147. Maccarrone S, Scherzinger C, Holderer O, Lindner P, Sharp M, Richtering W, Richter D (2014) Cononsolvency effects on the structure and dynamics of microgels. Macromolecules: 140820073721000. doi:10.1021/ma500954t
148. Tanaka F, Koga T, Kojima H, Winnik FM (2009) Temperature- and tension-induced coil – globule transition of poly(N-isopropylacrylamide) chains in water and mixed solvent of water/methanol. Macromolecules 42(4):1321–1330
149. Wang F, Shi Y, Luo S, Chen Y, Zhao J (2012) Conformational transition of poly (N-isopropylacrylamide) single chains in its cononsolvency process: a study by fluorescence correlation spectroscopy and scaling analysis. Macromolecules 45(22):9196–9204
150. Salzinger S, Huber S, Jaksch S, Busch P, Jordan R, Papadakis CM (2012) Aggregation behavior of thermo-responsive poly(2-oxazoline)s at the cloud point investigated by FCS and SANS. Colloid Polym Sci 290(5):385–400
151. Jee A-Y, Curtis-Fisk JL, Granick S (2014) Nanoparticle diffusion in methycellulose thermoreversible association polymer. Macromolecules 47(16):5793–5797
152. Fu Y, Ye F, Sanders WG, Collinson MM, Higgins DA (2006) Single molecule spectroscopy studies of diffusion in mesoporous silica thin films. J Phys Chem B 110(18):9164–9170
153. Sukhishvili SA, Chen Y, Müller JD, Gratton E, Schweizer KS, Granick S (2000) Materials science—diffusion of a polymer 'pancake'. Nature 406(6792):146–146
154. Zhao J, Granick S (2004) Polymer lateral diffusion at the solid – liquid interface. J Am Chem Soc 126(20):6242–6243
155. Zhao J, Granick S (2007) How polymer surface diffusion depends on surface coverage. Macromolecules 40(4):1243–1247
156. Pan X, Aw C, Du Y, Yu H, Wohland T (2006) Characterization of poly(acrylic acid) diffusion dynamics on the grafted surface of poly(ethylene terephthalate) films by fluorescence correlation spectroscopy. Biophys Rev Lett 1(4):1–9
157. Reznik C, Estillore N, Advincula RC, Landes CF (2009) Single molecule spectroscopy reveals heterogeneous transport mechanisms for molecular ions in a polyelectrolyte polymer brush. J Phys Chem B 113(44):14611–14618
158. Schuch H, Klingler J, Rossmanith P, Frechen T, Gerst M, Feldthusen J, Müller AHE (2000) Characterization of micelles of polyisobutylene-block-poly(methacrylic acid) in aqueous medium. Macromolecules 33(5):1734–1740

159. Nörenberg R, Klingler J, Horn D (1999) Study of the interactions between poly(vinyl pyrrolidone) and sodium dodecyl sulfate by fluorescence correlation spectroscopy. Angew Chem Int Ed 38(11):1626–1629
160. Bonné TB, Lüdtke K, Jordan R, Štěpánek P, Papadakis CM (2004) Aggregation behavior of amphiphilic poly(2-alkyl-2-oxazoline) diblock copolymers in aqueous solution studied by fluorescence correlation spectroscopy (vol 282, pg 833, 2004). Colloid Polym Sci 282 (12):1425–1425
161. Bonné TB, Papadakis CM, Lüdtke K, Jordan R (2007) Role of the tracer in characterizing the aggregation behavior of aqueous block copolymer solutions using fluorescence correlation spectroscopy. Colloid Polym Sci 285(5):491–497
162. Colombani O, Ruppel M, Schubert F, Zettl H, Pergushov DV, Müller AHE (2007) Synthesis of poly(n-butyl acrylate)-block-poly(acrylic acid) diblock copolymers by ATRP and their micellization in water. Macromolecules 40(12):4338–4350
163. Loos K, Böker A, Zettl H, Zhang M, Krausch G, Müller AHE (2005) Micellar aggregates of amylose-block-polystyrene rod – coil block copolymers in Water and THF. Macromolecules 38(3):873–879
164. Humpolíčková J, Procházka K, Hof M, Tuzar Z, Špírková M (2003) Fluorescence correlation spectroscopy using octadecylrhodamine B as a specific micelle-binding fluorescent tag; light scattering and tapping mode atomic force microscopy studies of amphiphilic water-soluble block copolymer micelles†,‡. Langmuir 19(10):4111–4119
165. Sedlacek O, Monnery BD, Filippov SK, Hoogenboom R, Hruby M (2012) Poly(2-Oxazoline) s—are they more advantageous for biomedical applications than other polymers? Macromol Rapid Commun 33(19):1648–1662
166. Okada Y, Tanaka F (2005) Cooperative hydration, chain collapse, and flat LCST behavior in aqueous poly(N-isopropylacrylamide) solutions. Macromolecules 38(10):4465–4471
167. Štěpánek M, Matějíček P, Humpolíčková J, Havránková J, Podhájecká K, Špírková M, Tuzar Z, Tsitsilianis C, Procházka K (2005) New insights on the solution behavior and self-assembly of polystyrene/poly(2-vinylpyridine) 'hairy' heteroarm star copolymers with highly asymmetric arms in polar organic and aqueous media. Polymer 46(23):10493–10505
168. Jurkiewicz P, Koňák Č, Šubr V, Hof M, Štěpánek P, Ulbrich K (2008) Investigation of nanoparticle coating by fluorescence correlation spectroscopy. Macromol Chem Phys 209 (14):1447–1453
169. Roe RJ (2000) Methods of X-Ray and neutron scattering in polymer science (Topics in polymer science). Oxford University Press, New York
170. Malo de Molina P, Appavou M-S, Gradzielski M (2014) Oil-in-water microemulsion droplets of TDMAO/decane interconnected by the telechelic C18-EO150-C18: clustering and network formation. Soft Matter 10(28):5072–5084
171. Papadakis CM, Košovan P, Richtering W, Wöll D (2014) Polymers in focus: fluorescence correlation spectroscopy. Colloid Polym Sci 292:2399–2411
172. Peter C, Kremer K (2009) Multiscale simulation of soft matter systems—from the atomistic to the coarse-grained level and back. Soft Matter 5(22):4357–4366

Index

K. Procházka (ed.), *Fluorescence Studies of Polymer Containing Systems*,
Springer Series on Fluorescence 16, DOI 10.1007/978-3-319-26788-3